HIGH-PRESSURE DIRECT-INJECTION OF NATURAL GAS WITH ENTRAINED DIESEL INTO A COMPRESSION-IGNITION ENGINE

by

BENJAMIN SCOTT BROWN

BASc., University of British Columbia, 2006

A THESIS SUBMITTED IN PARTIAL FULFILLMENT OF
THE REQUIREMENTS FOR THE DEGREE OF

MASTER OF APPLIED SCIENCE

in

THE FACULTY OF GRADUATE STUDIES

(Mechanical Engineering)

THE UNIVERSITY OF BRITISH COLUMBIA

(Vancouver)

August 2008

Abstract

The high-pressure direct-injection (HPDI) of natural gas in a compression ignition engine has the potential to reduce demand for petroleum derived fuels and significantly reduce the level of pollutants and greenhouse gases emitted from heavy duty transport vehicles. A new HPDI injector was tested where diesel is injected into a gas/diesel reservoir in the injector and the diesel and gas are then co-injected into the combustion chamber. In order to identify interactions between the diesel and gas in the reservoir, two different injector geometries were tested: prototypes A and B. Prototype B had reduced reservoir volume to increase gas velocity inside the injector.

A majority of the tests were conducted in a single-cylinder test engine derived from a Cummins ISX diesel engine. As prototype A was being modified to create Prototype B this test engine was moved to a larger test cell. After updating the electrical, mechanical, and safety systems, the test engine in the new test cell was found to run repeatably; however, emissions comparisons between both test cells was not possible due to different analyzers being used.

Single gas and double gas injections were conducted for both injector prototypes. The single gas injection tests found that increasing the diesel injection mass reduced the mass of gas injected. Increased diesel injection mass also shortened ignition delay, reduced unburned and partially burned fuel and increased NOx emissions. Holding the diesel injection mass constant and reducing the gas injection mass had the same effect as increasing diesel on ignition delay and gaseous emissions. If the diesel injection mass was kept constant and a second gas injection was added, the heat release due to the first injection decreased and the start of combustion was retarded. This appears to have occurred because some of the diesel was carried into the cylinder by the second injection and less diesel was available in the first injection to promote ignition.

Double gas injection tests were conducted where the load, speed, and combustion timing were controlled in order to determine how injector operation affects parameters such as knock intensity, and gaseous emissions. At lower diesel injection masses, retarded combustion timing led to shorter ignition delays and less intense knock and lower unburned fuel emissions at lower loads. Longer relative times between the diesel and gas injections had a similar effect as lower diesel injection mass, especially at advanced combustion timing. For these tests Prototype B exhibited shorter ignition delays but higher knock intensities than Prototype A.

Table of Contents

List of Tables

List of Figures

Nomenclature

2GEOI	:	2nd Gas End of Injection
2GPW	:	2nd Gas Pulse Width
2GSOI	:	2nd Gas Start of Injection
2RIT	:	2nd RIT (end of pilot to start of main)
A/D	:	Analog to digital
ANOVA	:	Analysis of Variance
ATDC	:	After Top Dead Centre
BDC	:	Bottom Dead Centre
Bsfc	:	brake specific fuel consumption
BTDC	:	Before Top Dead Centre
CA	:	Crank angle
CERC	:	Clean Energy Research Centre
CF	:	wet-to-dry conversion factor
CH_4	:	methane
CI	:	Compression Ignition
CLD	:	Chemiluminescent Detector
CO	:	Carbon Monoxide
CO2	:	Carbon Dioxide
COV	:	Co-efficient of Variation
CR	:	Compression Ratio
DAQ	:	Data Acquisition
DEOI	:	Diesel end of injection
Df	:	degrees of freedom
DIR	:	Diesel Return
DPW	:	Diesel Pulse Width
DSOI	:	Diesel Start of Injection
EGR	:	Exhaust Gas Recirculation
EQR	:	Equivalence Ratio
ESC 13	:	13 mode European Steady Cycle Test
FID	:	Flame Ionization Detector
FPGA	:	Field-Programmable Gate-Array
GEOI	:	Gas End of Injection
GHG	:	Greenhouse Gas
GIMEP	:	Gross Indicated Mean Effective Pressure
GLR	:	Gas-to-liquid Ratio (mass basis)
GLVR	:	Gas-to-liquid Volume Ratio
GPW	:	Gas Pulse Width
GSOI	:	Gas Start of Injection

HC	:	Hydrocarbon
HCCI	:	Homogenous Charge Compression Ignition
HPDI	:	High-Pressure Direct-Injection
HRR	:	Heat Release Rate
IHR	:	Integrated Heat Release
IVC	:	Inlet Valve Closing
MAT	:	Manifold Air Temperature
MCE	:	Main Combustion Event\
MS	:	Mean of Squares
NDIR	:	Non-dispersive infrared
NIMEP	:	Net Mean Effective Pressure
nmHC	:	non-methane Hydrocarbons
NO	:	Nitrogen Monoxide
NOx	:	Oxides of Nitrogen
NV	:	Needle Valve
oCA	:	degrees Crank Angle
OCS	:	Orbital Combustion System
P	:	Pressure
PCE	:	Pilot Combustion Event
PIDING	:	Pilot Ignited Direct Injection Natural Gas
PM	:	Particulate Matter
R	:	Gas Constant (for air)
RIT	:	Relative injection timing (end of pre-injection to start of pilot)
SCRE	:	Single Cylinder Research Engine
SI	:	Spark-ignited
SOC	:	Start of Combustion
SOL	:	Solenoid
SS	:	Sum of Squares
T	:	Temperature
TDC	:	Top dead centre
tHC	:	total hydrocarbons
UBC	:	University of British Columbia
uHC	:	Unburned Hydrocarbons
V	:	Volume
WP	:	Westport

Acknowledgements

I would like first like to acknowledge the mentorship of my supervisor, Dr. Steve Rogak, for expertly provided direction in helping me develop my skills as a researcher, and patiently helping me hone and polish this thesis.

This work could not have been completed without the excellent resources and experimental facilities at the University of British Columbia. I would like to thank especially Bob Parry for his endless work in maintaining the research engine and long hours in helping me with testing. Also, thanks to Gord Wright in his expertise and work in helping to re-install the electrical and control systems for the engine. Thanks to the previous researchers at UBC without whose work this thesis would not be possible. Thanks to Joey Mikawoz, Mike Marr, and Heather Jones. In particular, thanks to Gordon McTaggart-Cowan for knowing everything there is to know about the research engine, and for providing support and advice on several occasions.

I would also like to acknowledge both the financial and technical support from Westport Innovations. Issues that I had been struggling with for days were resolved through short conversations with individuals such as Sandeep Munshi, Al Welch, and Mike Wickstone. Thank you to Dr. Phil Hill who always provided support and encouragement. I'd also like to thank Koyo Inokoshi and Mike Baker for their help with the co-injector..

My thanks to my many fellow graduate students and the help and camaraderie they provided. In particular thanks to Nick Berger, Edward Chan, Chris Laforet, Andrew Mezo, Wu Ning,

James Saunders, Malcolm Sheild, and Michael Yeung. The collective experience and knowledge they provided was a crucial in ensuring my research continued to progress.

Lastly I would like to thank my parents for always encouraging me through my childhood and youth to strive to be the best I can and to follow my dreams. Lastly, thanks to my loving wife and eternal companion, Donna, for her unconditional love and support. Thank you, Donna, for providing an ear when it was needed, and for your loving care and support over throughout these last few years.

Chapter 1 - Introduction

Due to favorable fuel efficiency, power density, and reliability, diesel-fuelled compression-ignition (CI) engines power an overwhelming majority of heavy-duty vehicle applications. Heavy-duty vehicles (gross weight > 3856 kg) are used in areas such as public transportation, commercial goods transportation, construction, and waste disposal. Due the significant impacts of diesel engine exhaust on air quality, as well as rising petroleum prices, there is great interest in engine emissions and fuel economy. The use of natural gas as an alternative to petroleum derived diesel is also being investigated.

1.1 Current Issues Facing CI Engines

In terms of air quality and health one of the pollutants of most concern in diesel engines are oxides of nitrogen (NOx). NOx consists mainly of two components: nitrogen oxide (NO), and nitrogen dioxide (NO_2) (Seinfeld and Pandis 2006). Increased levels of NOx in ambient air cause irritation to the eyes, nose, mouth and lungs and lowers resistance to respiratory infection (US EPA 2008). However, NOx by themselves are of little concern. The "safe" levels of NOx as outlined by the US national ambient air quality standard (US NAAQS) is rarely exceeded in US and Canadian cities (Ontario MOE 2001). Secondary reactions involving NOx and unburned hydrocarbons (uHC), however, have contributed to increased levels of ground-level ozone and photochemical smog. For persons with existing respiratory issues, high levels of ozone have been shown to increase the hospitalization rate due to damage to the lung tissue. Atmospheric quantities of ozone as low as 80 parts per billion (80 ppb) have been shown to reduce lung function and increase susceptibility to respiratory

infections (US EPA 2008). In a study conducted on Canadian and international cities, 18 of 27 cities exceeded the one hour US NAAQS of 120 ppb (Ontario MOE 2001).

Particulate matter (PM) is another emission from the diesel-fuelled CI engines. From diesel fuelled engines, PM consists mostly of solids with some adsorbed organic compounds (Heywood 1988, 627). PM which is less than 2.5 microns ($PM_{2.5}$) in diameter are able to enter deep into the respiratory tract, agitating the lungs or entering directly into the blood stream. Short term exposures to $PM_{2.5}$ have been linked to increased heart attacks, asthma attacks and acute bronchitis.

Countries around the world have regulations to reduce the level of pollutants emitted from heavy-duty diesel engines. For example, Table 1.1 shows North American required reductions between 1988 to 2010 of uHC, NOx, and PM. The most significant pollutant reductions in the last 20 years have been the 2007-2010 emission standards. If engine manufacturers do not meet the required emissions standards then they must pay increasing non-conformance penalties which will either force the engine manufacturers to fix the non-compliant engines or stop distribution (US EPA 2002a).

With conventional diesel engines, meeting both NOx and $PM_{2.5}$ standards has been difficult due to the well-known NOx – PM tradeoff (Heywood 1988, 866). In order to meet the 2010 standards, exhaust aftertreatment devices will need to be installed. Ceramic particulate filters have been added to reduce the level of PM. Three-way catalytic converters used in stoichiometric spark-ignited (SI) engines cannot be used in lean burning diesel engines.

Table 1.1: Exhaust emissions standards for heavy-duty engines in the United States, g/bhp-hr (Dieselnet n.d.)

Year	uHC*	NOx	PM
1988	1.3	10.7	0.6
1990	1.3	6	0.6
1991	1.3	5	0.25
1994	1.3	5	0.1
1998	1.3	4	0.1
2004	0.5	2.5	0.1
2007	0.14**	0.2**	0.01
2010	0.14	0.2	0.01

* Non-methane hydrocarbons only
**Half of the engine sales must meet 2010 Emissions regulations and remainder must meet 2004 standards

Therefore, in order to reduce NOx, either a lean NOx trap or a NOx scrubber must be used. Two-way catalytic converters are used to simultaneously reduce CO and uHC emissions. However, all of these emission-control devices are expected to increase fuel consumption by 1-3%, add around $4000 to the cost of the engine, and add significant future maintenance and replacement costs to the engine (Schubert and Fable 2005; US EPA 2002b).

There is increasing pressure to reduce greenhouse gas (GHG) emissions from the transportation sector. Although CO_2 emissions from heavy-duty engines are not yet regulated, soot (the black body carbon component may contribute to global warming) is controlled through the health-motivated standards. Methane is a powerful GHG and it is regulated in Europe in natural gas engines to 1.1 g/kWh (Dieselnet n.d.).

Due to interactions between supply and demand, the price of petroleum-based fuel has been steadily increasing over the last two decades (EIA 2007). The total fuel costs over the life of the heavy-duty vehicle is one of the more significant life-cycle costs of the vehicle (Schubert and Fable 2001). In the past, global fuel prices have risen in response to wars, political

instability, natural disasters, or trade embargoes (EIA 2007). Demand is outpacing supply, which is contributing to higher fuel prices. Governments are therefore looking at ways to distribute risk through the use of non-petroleum based fuels for medium duty and heavy duty applications. Different fuels are being investigated and subsidized by governments both to reduce greenhouse gas emissions (GHGs) and provide viable alternatives to petroleum-derived diesel. For example in the US the "Energy Policy Act" was implemented in 2005 in order to reduce dependence on foreign oil and reduce greenhouse gases (US DOI 2005). It provides up to $32,000 in tax credits for purchasing heavy-duty natural gas, propane, or hybrid electric vehicles (US IRS 2005).

1.2 Natural Gas Use for Commercial Vehicles

Natural gas is a leading alternative fuel that can be used to simultaneously address climate change and energy demand issues from the use of petroleum-derived diesel in medium and heavy-duty vehicles. The main constituent, methane, has the lowest carbon-to-hydrogen ratio of any organic compound. Engines running primarily on natural gas have been shown to emit significantly lower GHGs provided that methane emissions are low (McTaggart-Cowan 2006a). Throughout the world, sources of natural gas are more distributed than petroleum (Radler 2006) and presently natural gas prices are lower than diesel. In addition, methane can be considered a renewable resource since it can be produced through anaerobic digestion of waste.

One of the ways to efficiently run heavy-duty engines on natural gas is to install a high pressure direct-injection (HPDI[1]) system developed by Westport Innovations Inc. For an HPDI engine, a small amount of diesel is required to initiate combustion of the natural gas jet. Not only is most of the diesel replaced (~95% by energy content) with natural gas, the engine-out NOx emissions have been shown to be reduced by 40% and the PM by 70%, without compromising performance or efficiency (Dumitrescu *et al.* 2000; Harrington *et al.* 2002).

Figure 1.1 shows the HPDI injector used to inject both diesel and natural gas. The inner (diesel) and outer (gas) injection systems are controlled separately by different solenoids, with the diesel fuel also acting as a hydraulic fluid in order to lift the injector needles. Gas and diesel can then be separately and independently injected through concentric injection systems. This injector is usually installed in an unmodified diesel engine.

To date, Westport has successfully installed its HPDI technology in off-road mining trucks near Queensland, Australia, transport trucks in Ontario, and shipping trucks in ports throughout California. In the San Francisco Bay area for example, HPDI fuelling systems have been successfully installed in 13 refuse-hauling trucks. Over 10 million km have been logged by this fleet (Westport Innovations 2008a).

---

[1] "HPDI" is a trademark of Westport Power Inc.

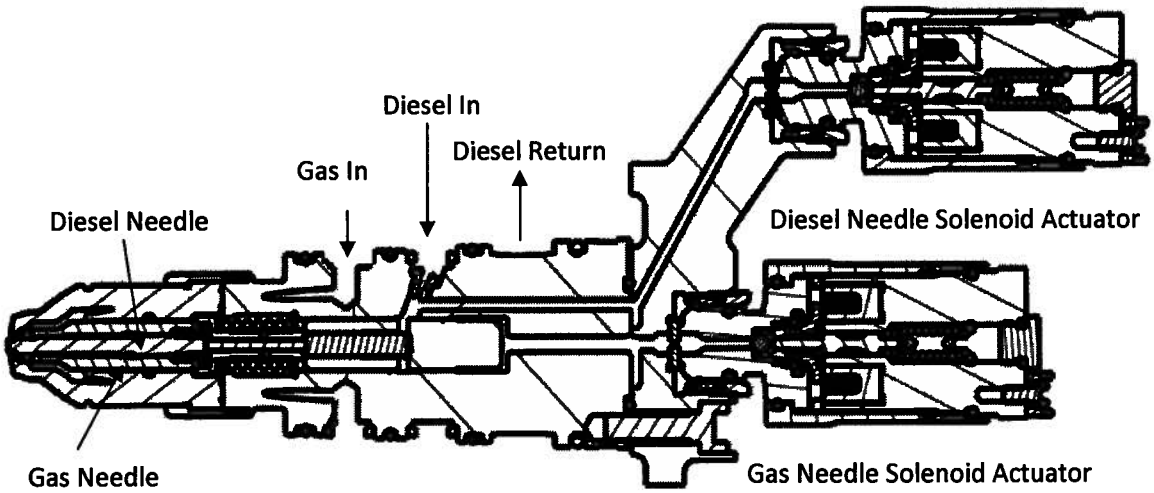

Figure 1.1: HPDI injector schematic

A new prototype HPDI injector has been devised where the pilot injection consists of a small amount of the pilot diesel co-injected with natural gas. In co-injection, gas-blast atomization is used to inject both diesel and natural gas through the same injection holes. Depending on how and when the diesel is introduced into the gas/diesel reservoir of the injector, the atomization process and subsequent combustion will be affected. This process is also affected by the number of injections per cycle. This "co-injector" design has potential to significantly improve on the simplicity and thus the cost of the HPDI injector. Since the diesel is entrained into the combustion chamber by the natural gas, the diesel injection system may not be needed. Significant material and manufacturing cost reductions may result. However, further study is required to characterize and optimize the injector.

1.3 Objectives and Scope

Ultimately, one needs to know whether the co-injector has similar or better performance than the current industry standard–the J36 Westport HPDI injector. However, the J36 (and associated control strategies) has been optimized over more than 15 years of research and development. This is the first thesis on this type of co-injector and it has not been previously established which parameters (ignition delay, combustion variability, knock intensity, etc.) set the boundaries of the operable region of the injector. Therefore, the goal of this thesis is to determine the parameters important to operation with only prelininary comparisons between the HPDI-J36 and the co-injector.

In addition, since the gas and diesel are injected into the combustion chamber as a mixture, another objective of this research is to better understand the gas/diesel interactions. These objectives are attained mostly through experiments conducted in a heavy-duty four stroke single-cylinder research engine with undiluted charge air during single and double gas injection operation as will be explained in Section 2.3. Also introduced in 3.1.7 are the two different co-injector geometries used in this study: Prototype A and Prototype B.

During this research, the test engine had to be moved. As a result, thousands of hours were spent reconnecting, redesigning, and testing the control and measurement systems. An additional objective of this thesis is to document the major changes to the usability and performance of the facility, particularly those that might affect comparisons between old and new measurements.

1.4 Thesis Structure

Chapter 1 provides background and motivation for studying HPDI co-injection and outlines the research objectives. Chapter 2 discusses prior work on two-phase injection and injection systems. Chapter 3 discusses the research engine as well as the injector flowbenches used for this research. Chapter 4 is divided into five sections which outline the testing procedure, single injection flow tests, double/single injection comparisons, and double injection emissions tests. Finally, a summary of the significant findings as well as recommendations for future work are discussed in Chapter 5.

Chapter 2 - Background

Numerous studies have been conducted to determine the benefits of using different natural gas engines such as stoichiometric, lean burn, or natural gas direct-injection for heavy-duty vehicles. Research on liquid/gas co-injection, however, has been limited. This chapter briefly describes the differences between types of heavy-duty natural gas engines and summarizes work that contributes to better understanding of the processes involved in two phase direct injection for internal combustion engines.

2.1 Current Natural Gas Technologies for Medium-Duty and Heavy-Duty Engines

Ideally, natural gas would replace the diesel in order to avoid the extra costs of an additional fuelling system. However, in order for natural gas to auto-ignite, the temperature needs to be over 1100-1200 K which would necessitate compression ratios exceeding 23:1 (Aggarwal and Assanis 1998). The high temperature needed would adversely affect the engine performance and emissions. Therefore, ignition is usually assisted through the use of a spark, a hot surface or a pilot injection. Currently, stoichiometric spark-ignited (SI) engines, lean burn SI engines, and pilot-ignited lean burn engines are the most prevalent in industry and will be the only alternatives to HPDI discussed.

2.1.1 Stoichiometric Spark-Ignited Natural Gas Engines

Stoichiometric spark-ignited natural gas engines can most economically meet the 2010 emissions standards (Chiu *et al.* 2007). Stoichiometric engines operate without excess fuel or oxygen, so the resulting exhaust emissions of CO and uHC are oxidized and the NOx are reduced over the three-way catalyst. The vehicle-out emissions can therefore be substantially reduced with commercially-proven exhaust treatment technologies. Premixed natural gas engines have exceptionally low emissions of PM (Faiz *et al.* 1996). The carbon-based particulate emissions from pre-mixed combustion are derived mostly from the engine oil (Faiz *et al.* 1996; Heywood 1988).

Because emission control technology is already well developed for these engines, the life cycle costs of stoichiometric SI natural gas engines have been found to be similar to if not better than projected life-cycle costs of a similar sized diesel-fuelled engine that require exhaust gas treatments (Schubert and Fable 2005).

Stoichiometric natural gas engines, however, have significant drawbacks that have prevented them from being more widely adopted. Since the air-fuel mixture needs to be kept relatively close to stoichiometric, the charge air needs to be metered as well as the fuel. At part load, the charge air is throttled, introducing significant pumping losses. Duggal *et al.* (2004) measured the performance of a diesel heavy-duty engine on the 13-mode European Steady Cycle (ESC 13), which can be compared with the measurements by Chiu *et al.* (2004) for a stoichiometric natural gas engine of similar size. Averaged over the 13 modes, the natural gas engine had 25% higher brake specific fuel consumption.

Current stoichiometric SI engines have significantly lower power and torque capabilities compared to a diesel fuelled engine. This is due, in part to lower volumetric efficiency due to the gaseous fuel displacing combustion air that could have been inducted into the combustion chamber. More importantly, there are design constraints that limit the maximum compression ratios to about 11:1 (Faiz *et al.* 1996; Chiu *et al.* 2004; Zhang *et al.* 1998). The factors that limit the maximum power and torque are engine knock and excessive exhaust temperatures (above 973 °C) (Zhang *et al.* 1998). Lower maximum temperatures are important to reduce mechanical and thermal wear to the engine components such as the gaskets, exhaust valves, cylinder heads, and turbochargers. Similarly, excessive and prolonged engine knock breaks down thermal boundary layers which can cause severe damage to the piston, piston rings, etc (Taylor 1985, 39; Heywood 1988, 456). Current production stoichiometric natural gas engines are limited to about 261 kW (350 hp) and 895–1356 nm (660–1000 lb-ft) of torque (Westport Innovations 2008b; Cummins n.d.), limiting their use to applications such as transit, and medium-duty vehicle applications.

2.1.2 Lean-Burn Spark-Ignited Natural Gas Engines

The torque and efficiency limits of stoichiometric SI engines can be addressed through the use of a lean combustion. Prior to increased restrictions on pollutant emissions, most natural gas-fuelled engines were lean burning engines. In lean burning engines, the excess combustion air lowers the exhaust temperature which reduces the engine-out NOx emissions and minimizes engine damage from thermal cycling. Slightly higher power and torque characteristics can be attained through the use of pre-mixed lean burning of natural gas since the maximum power and performance of the engine is not dependent on the maximum

cylinder temperature. Previous lean burn technologies were 10 – 20 percent more efficient than stoichiometric engines (Faiz *et al.* 1996), although still lower than the efficiency of a diesel engine.

Unlike stoichiometric engines, throttling is not necessary for lean burn SI engines at most operating points since these engines can operate stably at a wide range of equivalence ratios. Only at low load, where there were large cycle-to-cycle variation is throttling necessary to avoid bulk extinction during the expansion stroke. Since a leaner mixture is used, lower combustion temperatures allow higher compression ratios before the onset of knock.

The biggest drawback for lean-burn engines is that the exhaust treatment technologies are relatively immature. Lean combustion reduces engine-out NOx, but not enough to meet recent heavy-duty engine NOx regulations in many applications. Excess oxygen prevents NOx from being reduced on a three-way catalyst.

In addition, compared to stoichiometric natural gas engines, lean burn engines have higher levels of unburned fuel, most particularly methane. Methane emissions are important for two reasons. First, methane is a significant greenhouse gas which by mass is 21 times more powerful at warming the atmosphere than CO_2 (Foster *et al.* 2007). Second, the catalytic conversion efficiency for CH_4 is strongly dependent on temperature. Low exhaust temperatures common to lean burn engines (200 °C to 400 °C) lead to conversion efficiencies around 10 – 15% (Duggal *et al.* 2004).

2.1.3 Lean-Burn Pilot-Ignited Natural Gas Engines

Lean burn pilot-ignited natural gas engines are commonly referred to as "dual-fuel engines" (Srinivasan *et al.* 2006; Taylor 1985). Natural gas is introduced into the combustion chamber so that it will form a homogenous mixture with the combustion air. Instead of using a spark, a small amount of diesel (about 20% on an energy basis) is used to ignite the mixture (Srinivasan et *al.* 2006). Therefore, similar to SI engines the part load efficiency and maximum torque are limited. Potentially, more diesel could be used at these operating points; however, the engine-out emissions of NOx are observed to increase with increased diesel injection mass (Srinivasan *et al.* 2006).

2.2 High-Pressure Direct-Injection

High-pressure direct-injection (HPDI) natural gas engines provide diesel-like performance, reliability, and efficiency for both two stroke engines (Hodgins *et al.* 1996; Douville *et al.* 1998; Harrington *et al.* 2002) and four stroke engines (Dumitrescu *et al.* 2000; Duggal et al. 2004). Since HPDI engines inject all of the fuel near the end of the compression stroke, most of the fuel burns in a turbulent diffusion flame. Therefore, higher load capacities can be achieved since HPDI engines are not limited by the onset of knock. Compared to SI natural gas engines, higher compression ratios can be used (around 15-19:1 rather than around 11:1) and thus higher thermal efficiencies are observed in HPDI engines. The load is controlled by metering the fuel only; therefore, diesel-like efficiencies at part load are achievable.

While the performance and efficiency are similar to a diesel engine, the NOx, PM emissions are significantly lower. Duggal *et al.* (2004) summarized the performance of the HPDI

fuelling system in a Cummins ISX engine modified with a smaller compressor and intercooler. They reported that the installed HPDI system was able reduce NOx by 40% and the PM by 80%. Goudie *et al.* (2005) determined that at extremely high EGR rates (40% EGR) with an oxidation catalyst, the PM and NOx emissions were 0.36 g/bhp-hr and 0.04 g/bhp-hr respectively for an ESC 13 mode test cycle.

Similar to lean burn natural gas SI engines the exhaust aftertreatment options are immature and expensive. However, engine-out NOx are much closer to the 2010 emissions standards and therefore fewer exhaust treatments may be necessary. For example, with higher levels of EGR, the NOx emissions may be met and the PM can be filtered using a particulate filter (Williams 2007).

2.2.1 Ignition Delay in HPDI Engines

For any direct-injection compression-ignition engine, there is a time lag between the introduction of fuel into the chamber and combustion. When a cool liquid jet is introduced into the turbulent high-temperature high-pressure environment, numerous things happen before it burns. Cavitation and turbulence in the liquid jet cause it to disintegrate into smaller droplets (Adomeit *et al.* 2002; Rotondi *et al.* 2001) Aerodynamic forces will also cause droplet breakup as Kelvin-Helmholtz (sinusoidal) instabilities overcome surface tension and liquid viscosity (Rotondi *et al.* 2001; Lörcher and Mewes 2001). Due to the higher ambient temperature the droplets heat up and begin to evaporate. The gas from the surface diffuses outward and mixes with the surroundings to form a combustible mixture. Due to the high temperature and pressure, radicals then start to form in the mixture. Exothermic reactions occur, leading to exponentially more exothermic reactions.

The time from the introduction of the droplet to ignition is referred to as the ignition delay. It is composed of two parts: the physical delay and chemical delay. Physical Delay is the time it takes for the fuel to establish an ignitable mixture (Teng et al. 2003) consisting of physical phenomenon such as mixing, heating, and evaporation. Chemical delay is harder to predict due to the hundreds of possible chemical reactions that can take place simultaneously. Chemical delay is often calculated from empirical Arhennius-type relations:

$$\tau_{ig} = A \cdot \exp(E / RT) \cdot [Fuel]^{a} \cdot [Oxygen]^{b} \qquad (2.1)$$

Where A, a, and b are constants found experimentally (e.g. Shock tube, combustion bomb). Chemical delay for diesel fuel under normal operating conditions is less than 0.67 ms (Teng et al. 2003). Compared to the physical delay, chemical delay is usually considered to be much shorter since physical delay includes the slow processes of heat and mass transfer and evaporation (Teng et al. 2003; Sazhina 1999). The chemical and physical delay cannot simply be added up as chemical reactions can take place as the droplet is evaporating and mixing.

In addition to physical and chemical delay, there is a noticeable delay after the commanded pilot injection till the injector needle lifts. This is referred to as injection delay. This injection delay has been found to be around 0.5 – 0.7 ms for the J36 series HPDI injectors used for this work (Kostka 2008). Figure 2.1 shows the ignition delay broken down into injection delay, physical delay, and chemical delay.

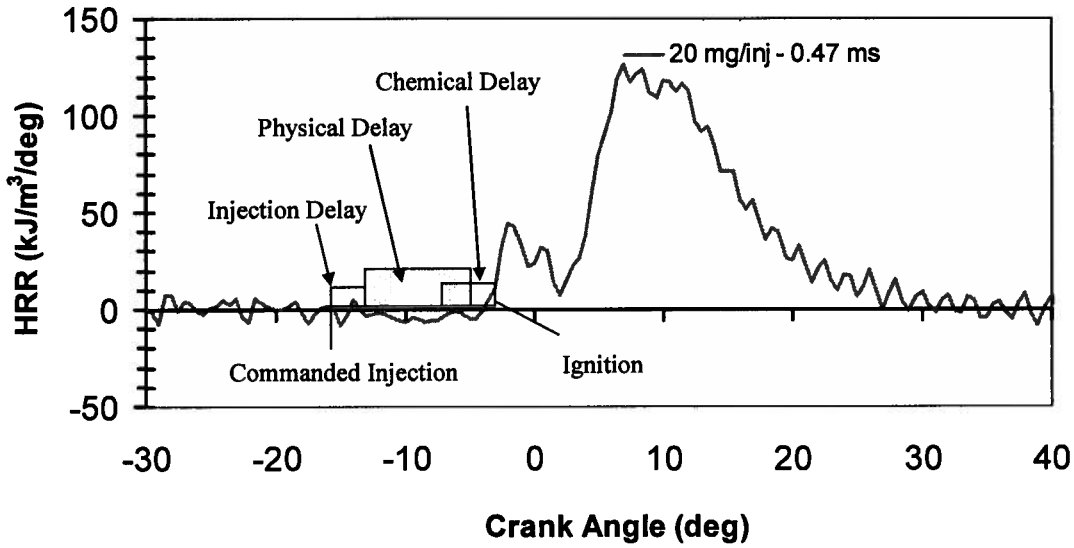

Figure 2.1: Injection delay, physical delay, and chemical delay for a typical heat releas rate (HRR) curve

2.3 Co-Injection

For the Westport HPDI injector, natural gas and diesel are separately injected into the combustion chamber as shown in Figure 2.2a. The HPDI co-injector was constructed from a J36-03 build HPDI injector by modifying the inner diesel injection system so that diesel is injected into the gas reservoir instead of directly into the combustion chamber, as shown in Figure 2.2b. This was done by plugging the needle tip and drilling holes through the gas needle. A more detailed description of the modifications needed to make Prototype A (the original co-injector concept) and Prototype B (Prototype A with an added sleeve in to change the geometry of the gas/diesel mixing chamber) can be found in Section 3.1.7.

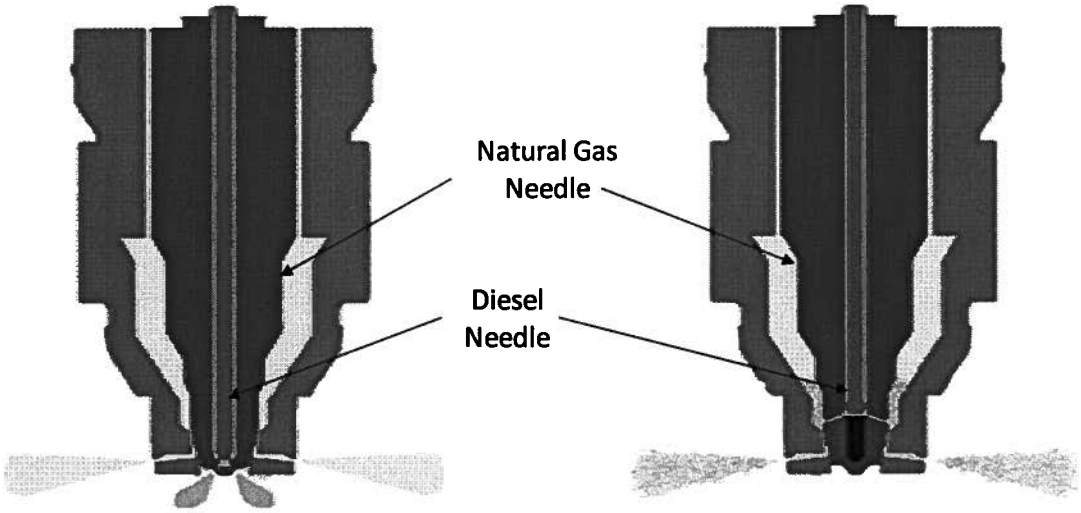

Figure 2.2: Injector nozzle schematic for HPDI injector operation and HPDI co-injector operation

The gas and diesel injections are also shown in Figure 2.2. Whereas the diesel and gas are injected separately with the HPDI injector, a gas/diesel two-phase mixture is injected with the HPDI co-injector.

2.3.1 Co-injector Operation

For the co-injector, three injections are needed for normal operation: the diesel pre-injection, the pilot gas injection, and the main gas injection. Figure 2.3 shows the three injections. During the pre-injection, the diesel injection needle lifts and diesel is injected into the common gas/diesel reservoir. For the J36-HPDI injector, the diesel injection is referred to as the pilot injection, since the diesel is directly injected into the combustion chamber and acts as the ignition source. For the HPDI co-injector, however, the pilot injection refers to the mixture of diesel and natural gas and is injected as the gas needle lifts. Shortly after the pilot injection, the gas needle lifts again and the main charge of natural gas is injected.

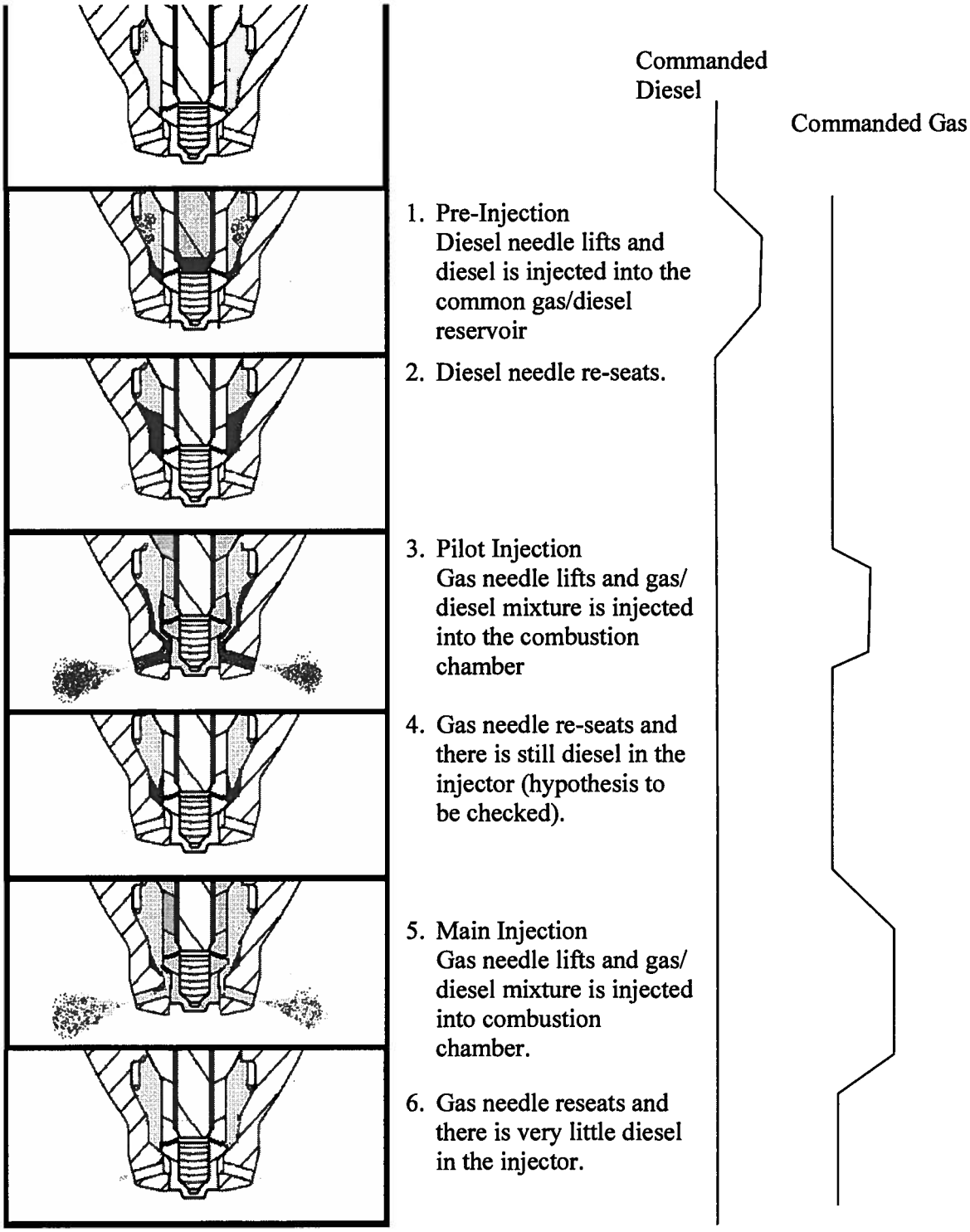

Figure 2.3: Injection sequence for normal double injection operation

For some cases at low load and low engine speed the co-injector may operate with a single gas injection. For this case, all of the diesel injected into the gas/diesel reservoir is injected during the pilot gas injection, unlike normal double gas injection operation where the injected diesel can potentially be divided between the two gas injections due to the gas and diesel mixing in the gas/diesel reservoir and liquid diesel sticking to the walls.

Prototype A (the original co-injector concept shown in Figures 2.2b and 2.3) has the following potential advantages over the Westport HPDI injector. Firstly, since the diesel is co-injected with the natural gas, there will be a natural gas jet for every diesel jet. With previous HPDI injectors the exhaust emissions were observed to cycle every two minutes, supposedly due to the diesel holes in the gas needle changing position as the gas needle rotated. HPDI injectors therefore have more diesel holes than required to ensure stable combustion, which implies that some of the gas jets are not optimally aligned with the pilot sprays (Dumitrescu *et al.* 2000; Ouellette *et al.* 1998).

Secondly, there will be overlap between the diesel and gas jets. McTaggart-Cowan found for the HPDI injector that when the gas was injected before or very shortly after the diesel injection significant reductions in PM were observed. He speculated that auto-ignition of a diesel-natural gas mixture may have occurred which led to substantial PM reductions which remained low independent of the EGR level (McTaggart-Cowan 2006a; McTaggart-Cowan *et al.* 2003).

Finally and most importantly, significant system cost reductions are potentially available with future models of the HPDI co-injector. Since diesel is injected into the gas/diesel reservoir instead of directly into the engine, the diesel injection system could potentially be

simplified substantially. The major costs of the HPDI injector include machining the injectors to tight tolerances to prevent diesel and gas leaks into the cylinder from around the injector needles and to allow separate passages for the diesel and natural gas. The cost reduction from one less injector needle, actuator, and injector driver per injector approaches the 50% cost reduction goal of this project, especially when the machining cost reductions are included. The design simplification would also allow a reduction in injector size, possibly making HPDI co-injection viable for light duty applications.

2.3.2 Previous Work at UBC on Co-injection

No previous work has been published on the operation of the HPDI co-injector prior to 2007. Engine tests by Jones and McTaggart-Cowan were distributed only as internal fact-sheets with very basic descriptions of the tests conducted and analysis of the results. Some of the key findings are described below.

In November 2005, Jones completed two test sets with Prototype A with single gas injections (Jones 2005a; Jones 2005b). More diesel was required to run Prototype A stably than the J36 injector, especially for starting the engine. Also, the co-injector produced higher CH_4 and CO emissions at low load. One of the most striking results of the single-injection tests was the presence of "ringing" (periodic pressure fluctuations over 3 bar–discussed in Section 3.2.5) at high diesel injection masses. Although the ignition delay was only slightly longer than for a typical HPDI injector, the energy injection rate from the co-injector was high since large quantities of fuel were injected prior to ignition. The solution proposed was to have a short "pilot" injection, followed by a "main" injection, as shown in Figure 2.3.

Later, Jones (2006) compared double injection tests of Prototype A with normal operation of the J36 injector at mid speed/low load, mid speed/high load, and high speed/high load which are similar to the ESC 13 test modes #7, #6, and #4 respectively (Dieselnet n.d.). Jones found at high loads that the HPDI co-injector had lower PM, less fuel consumption, and similar NOx, tHC, and CO emissions. Figures 2.4 and 2.5 show the PM and NOx for one case.

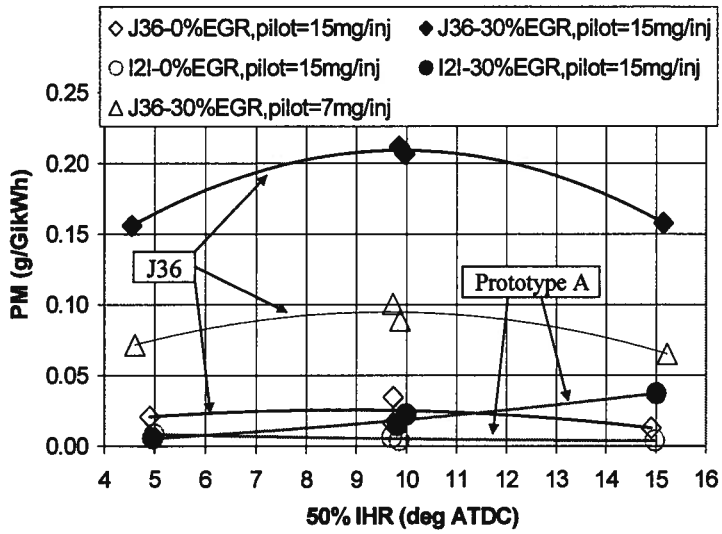

Figure 2.4: PM emissions for J36 and Co-injector Prototype A at 75% load and 1100 RPM (Jones 2006)

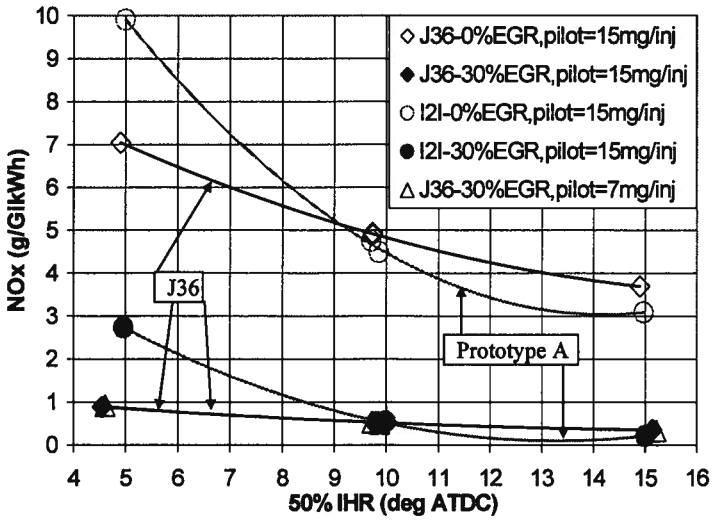

Figure 2.5: NOx emissions for J36 and Co-injector Prototype A at 75% load and 1100 RPM (Jones 2006)

These figures show significant improvements in the PM emissions for the HPDI co-injector compared with the original HPDI injector at high engine loads without significantly increasing the NOx. Jones also found that PM emissions could be reduced in the J36 HPDI injector by reducing the diesel injection mass. However, lower injection masses for Prototype A could not be tested at this point as diesel injection masses lower than 12 mg/inj led to misfiring of the engine. In addition, Jones found the tHC and CO emissions were significantly higher for the co-injector at low loads.

In continuation of the work done by Jones, McTaggart-Cowan (2006b) performed single injection tests to determine the best method for reducing the high levels of uHC at low loads. McTaggart-Cowan found that the high cycle-to-cycle variation can be substantially reduced by increasing the diesel flow rate, increasing the intake air pressure, or reducing the gas injection pressure. He suggested that the higher combustion variability and higher uHC emissions were due to a lower diesel/gas volume ratio by volume injected. He found, however, that the transition from single injection to double injection operation was sensitive to operating condition and that the introduction of the main injection had the potential to stop combustion due to the pilot injection. Further details of the test conditions and results from McTaggart-Cowan can be found in Chapter 4, since they are closely related to tests performed for this thesis. The full factsheets compiled by Jones (2006) and McTaggart-Cowan (2006b) can be found in Appendix D.

Optical studies of the co-injector Prototypes have also been conducted on Prototype A by Mikawoz (2005) and for Prototype B by Marr (2007). From the movies recorded of Prototype A by Mikawoz (2005), most of the Viscor (a replacement for diesel used for

injector calibration) appeared to be finely atomized and injected during the beginning of the injection. The work by Marr (2007) on Prototype B supported this observation as he found that the majority of the liquid is injected near the start of the injection. Figure 2.7 shows movie stills collected by Marr (2007).

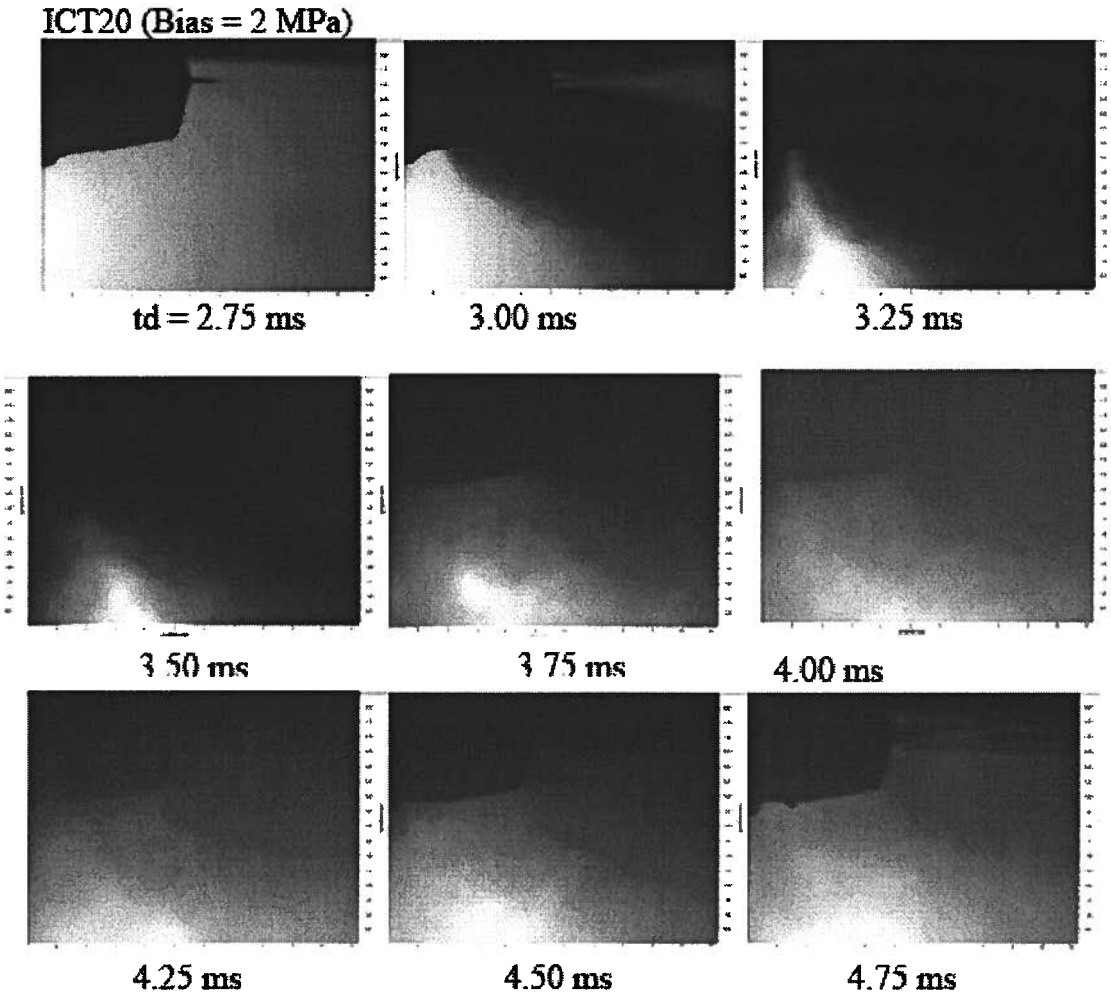

Figure 2.6: Movie stills of Prototype B with 2 MPa bias, 1.0 ms diesel pulse width, 1.95 gas pulse width (Marr 2007)

The diesel (shown as the dark jet) is injected around 0.5 ms after the start of injection. The time of maximum diesel flux was found to be relatively independent of bias pressure, diesel pulse width, and gas pulse widths (GPWs). From these preliminary tests, Marr also found

that for Prototype B, GPWs less than 1.5 ms restricted the Viscor injection volumes and that the co-injector seemed to reach steacy state almost immediately.

2.3.3 Patents and Studies on Gas/Liquid Co-injection

Injecting a gas/liquid mixture in internal combustion engines is not new. The first use of air to help atomize diesel was in 1893 with the original diesel engine (Stone 1999, 9). It wasn't until 1910 that it was replaced with the high pressure liquid jet injectors used today.

Currently, there are patents for improving atomization in SI engines (Kimmel and Dillon 2002) and for CI engines (Tarr et al. 1999) using gas-assist atomization for the liquid fuel. Fundamental studies conducted with these injectors are described below. Other patents have been disclosed which use natural gas as the primary fuel as well as the atomizing fluid for the igniter. For example, Hill *et al.* (1991) describe the use of natural gas to continuously atomize diesel using a pre-chamber. Similarly, Yang (2002) describes a dual fuel injector that uses natural gas to bring the diesel into the combustion chamber at injection pressures between 1.5 – 4.0 MPa. These devices sound similar in operation and purpose to the HPDI co-injector (patent pending); however, peer-reviewed studies related to direct-injection natural gas engines with entrained diesel cannot be found.

For SI engine applications, Orbital Engine Company produces an air-assisted direct fuel injection system referred to in the Orbital Combustion System (OCS). The OCS is used both for stratified charge and homogenous charge SI engines (Boretti *et al.* 2001). The OCS is similar to the HPDI Coinjector in that fuel is metered into the mixing chamber using an injector. In the case of the OCS, a conventional pencil stream port fuel injector is used

(Boretti *et al.* 2001). Cathcart and Zavier (2000) report the mass of fuel injected into the combustion chamber changes with time, and is dependent on the delay time between the pre-injection event and the direct injection event with a maximum flux around 1 ms with an injection pressure of 6.5 bar and a gasoline – air bias of 0.7 bar. For the OCS, the gas/liquid mass ratio (GLR) is 2 to 0.2 going from low load to high load (Houston and Cathcart 1998). Since the gas used for the HPDI co-injection is also a fuel, the GLR can be between 0.5 – 2.5 (McTaggart-Cowan 2006b). For low diesel injection masses the co-injector GLR can be as high as 3.5.

Although the OCS has similarities to the HPDI co-injector, there are fundamental differences between the two. Compared to diesel direct injection, fuel injection into the combustion chamber begins much earlier in the compression stroke (about 80° – 150° BTDC) in order to allow a stratified charge to form before the spark event. Relatively low injection pressures are therefore needed for the OCS (on the order of 6.5 bar) (Borretti *et al.* 2007; Houston and Cathcart 1998). Higher injection pressures are needed for direct-injection compression-ignition engines to inject the fuel near the end of the compression stroke. Perhaps most importantly, air is used as the atomizing gas instead of natural gas.

Fundamental studies have been published for a wide range of injection pressures, including diesel relevant injection pressures and conditions, using gas/liquid injection processes referred to as "effervescent atomization". The gas injected into the liquid is done in order to reduce the injection pressure needed to produce small liquid droplets. Therefore, work with effervescent atomization has concentrated on low GLRs. Sovani *et al.* (2001b) found that previous studies on effervescent atomization with diesel or a diesel substitute were conducted

at a GLR between 0 – 0.3. Still, the fundamental studies conducted by these workers are beneficial in attempting to understand the injection processes for the HPDI co-injector.

Roesler and Lefebvre (1988), Lörcher and Mewes (2001), and Chin and Lefebvre (1993) studied the internal flows of an effervescent atomizer. There are four flow regimes reported that may be applicable to the flow in the HPDI co-injector, namely, bubbly flow, plug flow, annular flow and dispersed flow. These are shown in Figure 2.6. Chin and Lefebvre (1993) reported that as the injection pressure increased, the range of the bubbly flow regime was extended to higher GLRs. For their tests at injection pressures of 8 bar, they reported that at GLRs greater than 0.4 the liquid (water) was completely broken up by the gas (air) and was dispersed as droplets in the atomizing gas. For a non-homogenous mixture of gas and liquid in the mixing reservoir, the flow will transition from one flow regime to the next, depending on the distribution of liquid.

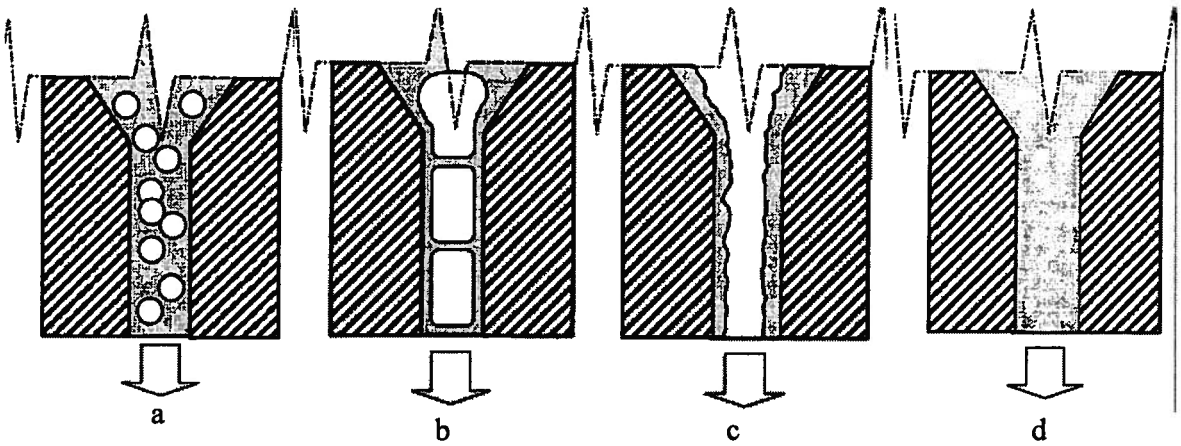

Figure 2.7: Four flow regimes expected in HPDI co-injector: a) bubbly flow, b) plug flow, c) annular flow, and d) dispersed flow

Liquid/gas injection has potential to reduce the droplet diameter in three ways. First, in two phase flow the speed of sound is lower (Sherstyuk 2000; Sovani *et al.* 2001) than for a pure

gas injection. This means that flow chokes at a much lower velocity, and therefore there will be a steep pressure jump across the minimum flow area. This steep pressure drop is beneficial in increasing atomization quality (Sovani *et al.* 2001). Good atomization of the fluid can result, even if there are large exit orifices, low injection rates, or low injection pressures (Sovani *et al.* 2001). Second, two-phase flow can effectively reduce the size of the orifice for the liquid. This can be seen in Figure 2.6c where the liquid is pushed to the outside of the orifice wall for annular flow. Finally, as the gas expands after the orifice, the rapidly expanding gas core will break the annular flow into smaller ligaments which will then form smaller droplets (Sovani *et al.* 2001).

In summary, gas-blast atomization is not new, and has been used before in direct injection engine applications. However, there have been no peer reviewed papers on its use as a way to deliver pilot diesel in a natural gas direct-injection engine. The preliminary work of Jones (2005a; 2005b; 2006) and McTaggart-Cowan (2006b) show that the relationship between the diesel injection mass and ignition is complex and requires further research. These studies concluded that double gas injection operation was required for most operating conditions. In comparison with the J36 over a range of operating conditions the co-injector exhibited lower PM emissions, especially when EGR was used. However, it was also found that work was needed in order to lower the CH_4 and CO emissions at low load as well as to reduce the dependence of operating condition on the diesel injection mass.

The objectives first explained in Section 1.3 can now be developed into the following four research objectives in order to forward the work done by McTaggart-Cowan and Jones:

1. For single-injection operation, determine how the gas injection mass changes in response to changes in the commanded gas injection duration and injected diesel mass.
2. For single-injection operation, determine the effect the relative amounts of gas and diesel have on exhaust emissions, combustion variability, and ignition delay.
3. For double-injection operation, observe how a second gas injection affects the amount of diesel injected into the combustion chamber during the first injection.
4. For double-injection operation, determine how injector geometry affects the injector operation and quantify the effect injector geometry has on emissions, combustion variability, knock, and ignition delay.

By addressing these four research objectives, the importance of the gas/diesel interactions on engine exhaust emissions and combustion variability can be better understood.

Chapter 3 – Apparatus and Procedures

3.1 Single-Cylinder Research Engine (SCRE)

The test engine used for this study is derived from a 400 hp 6-cylinder Cummins ISX engine modified to operate with one firing cylinder (2.5 L displacement, 137 mm bore, 169 mm stroke, 261.5 mm connecting rod). The other five working pistons were replaced with drilled-through pistons. On the deactivated cylinders, the intake and exhaust valves were bolted shut, and the rocker arms were removed (McTaggart-Cowan 2006a).

The SCRE can use several different pistons and air inlet systems. Due to scheduling constraints, several series of tests compare two injector variants for the 16.7:1 compression ratio (CR) enforcer piston. Several other test series compare the injector variants using a 15:1 CR piston insert with swirl plates at the intake valve.

The SCRE was run in two different locations. The tests in 2007-2008 were conducted after the engine had been moved from Kaiser 1180 to the Clean Energy Research Centre (CERC). The test cell setup prior to 2007 is described extensively by McTaggart-Cowan *et al.* (2004), McTaggart-Cowan (2006a), and Jones (2004). Since the modifications to the engine may have an impact on the operation of the engine, the engine setup in CERC will be described in detail, with any important changes from the previous system noted.

The engine speed is controlled by a General Electric eddy-current water-cooled dynamometer connected to the engine through a flexible spider coupling. At low loads, a Baldor 30 kW electric 'vector' drive motor will assist in overcoming the frictional losses of the non-firing cylinders. In Kaiser 1180 the vector drive was attached to the dynamometer using a belt

drive. Due to frequent belt failures, a flexible spider coupling connects the two in the CERC test cell.

The engine coolant thermostat has been bolted open to allow continuous flow of coolant through the engine. The cooling water is fed to the cooling tower through a flow control valve in order to control the coolant temperature from 77 to 80 °C.

3.1.1 Test Cell

In CERC, the SCRE has been mounted in a large temperature-controlled test cell as shown in Figure 3.1. This test cell is much larger than the previous test cell in Kaiser. Figure 3.2 shows a plan view of the components inside of the SCRE test cell with a summary of the components listed in Table 3.1.

The CERC installation allows the operator to monitor and operate the engine in a much safer manner than in Kaiser. A large shatterproof window allows the operator to safely monitor most of the components seated beside the Data Acquisition (DAQ)/Control Computer inside the engine control room. During operation the test cell is ventilated at a rate of 55 air changes per hour resulting in cell temperatures between 10 and 25°C as air is drawn across the test cell from the cell intake air duct to the air evacuation air duct (Veco 2004). The test cell CH_4 and CO detectors are integrated into the building shutdown controls.

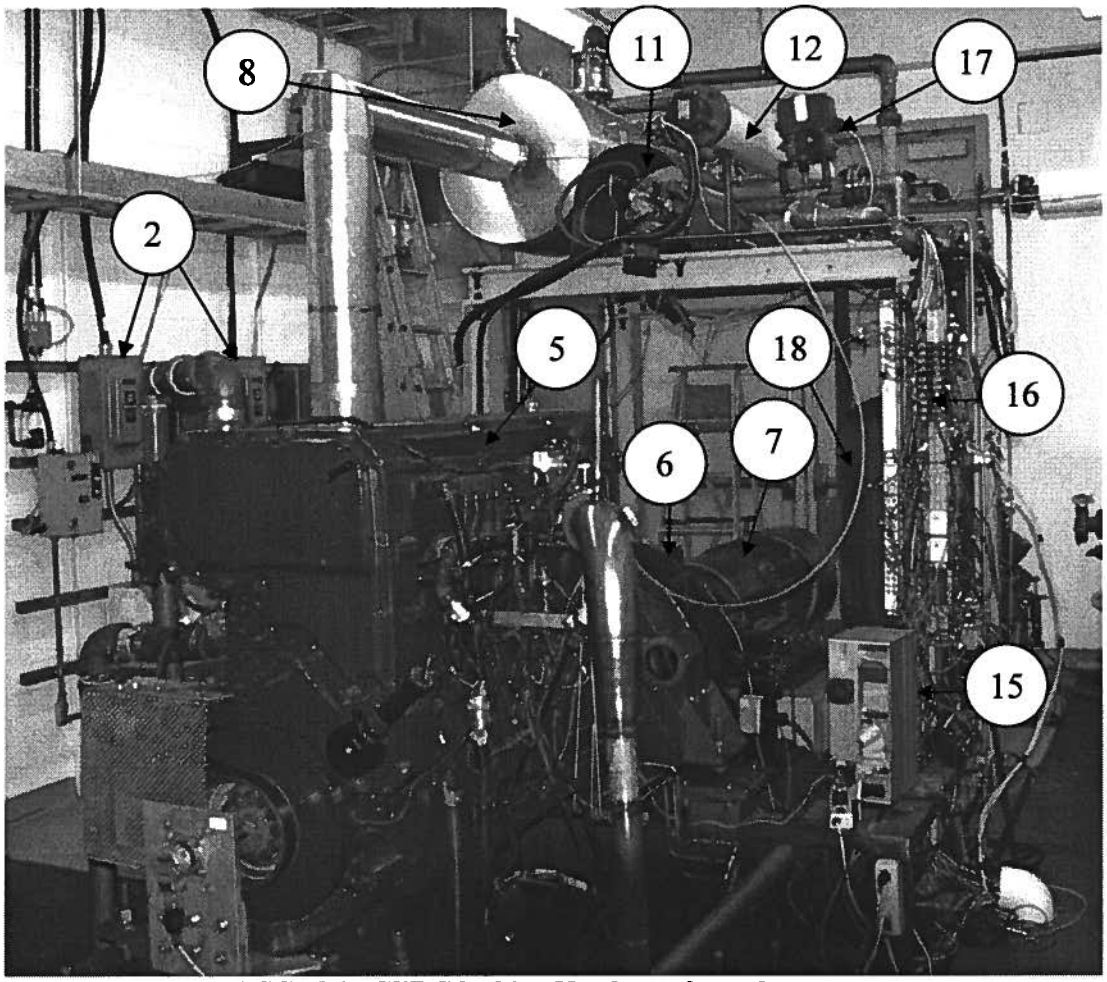

Figure 3.1: Installed SCRE in CERC looking Northeast from the entrance

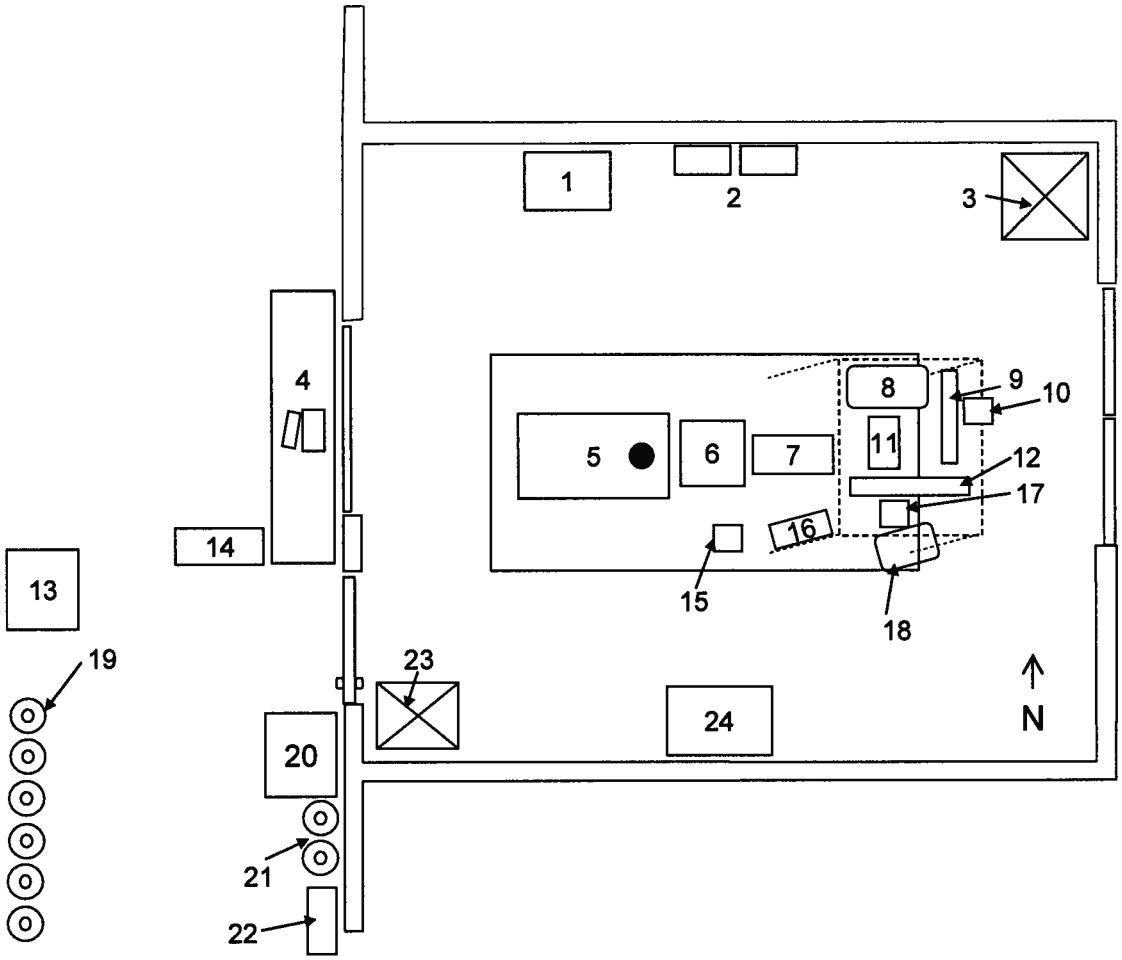

Figure 3.2: Test cell setup schematic

Table 3.1: List of Components inside CERC test cell

1	Cooling Tower	13	AVL Emissions Bench
2	Power Switches for CAH and Vector	14	Control Panel
3	Cell Intake Air Duct	15	Signal Multiplexer
4	DAQ/Control Computer	16	Temperature/Voltage Wiring Tree
5	Single Cylinder Research Engine	17	Charge Air Heater
6	Dynamometer	18	Intake Surge Tank
7	Vector Drive	19	Emissions Bench Calibration Gases
8	Exhaust Surge Tank	20	PM Dilution/Measuring System
9	EGR Cooler	21	PM Dilution Bottles
10	Back Pressure Valve	22	Vacuum Pump/Particulate Filters
11	High Pressure Diesel Pump	23	Cell Exhaust Air Duct
12	EGR Valve	24	Fuel Conditioning Module

3.1.2 Fuel Supply System

Figure 3.3 shows the flow diagram for the fuel supply system. The method of pressurizing and circulating the diesel is the same described by McTaggart-Cowan (2006a). The bias pressure (diesel – gas rail pressure) is usually set to around 0.80 MPa for the J36-HPDI injector in order to ensure that the gas does not leak into the diesel. This is accomplished through the use of a dome-loaded self-venting regulator, PCV-NG-500, which ensures constant bias pressure between the diesel and gas. For co-injector testing, the bias pressure needs to be much greater in order to inject 10-20 mg of diesel during the 5 ms maximum needle lift duration. In the tests conducted in 2006 and 2007 (in both test cells), the additional bias was created through the use of a high-pressure regulator installed on the natural gas line downstream of the dome-loaded regulator. However, the pressure fluctuations caused by gas injection may have been causing poor performance and/or deterioration of the regulator. Therefore, for the tests conducted in 2008, the high-pressure regulator was removed and the bias pressure at the injector was controlled by lowering the diesel pressure at the dome loaded regulator through the use of needle valves, (needle valves NV-DIR-620 and NV-DIR-630 in Figure 3.3).

The natural gas for CERC is supplied continuously at pressures up to 5000 psi from a dedicated gas line and is compressed by an integrated three-stage piston compressor. The Kaiser installation used separate multi-stage compression systems. In the event of an emergency or a rapid engine shutdown, two solenoid valves will shut off the gas supply to the test cell. These are shown as SOL-NG-400 and SOL-NG-401 in Figure 3.3.

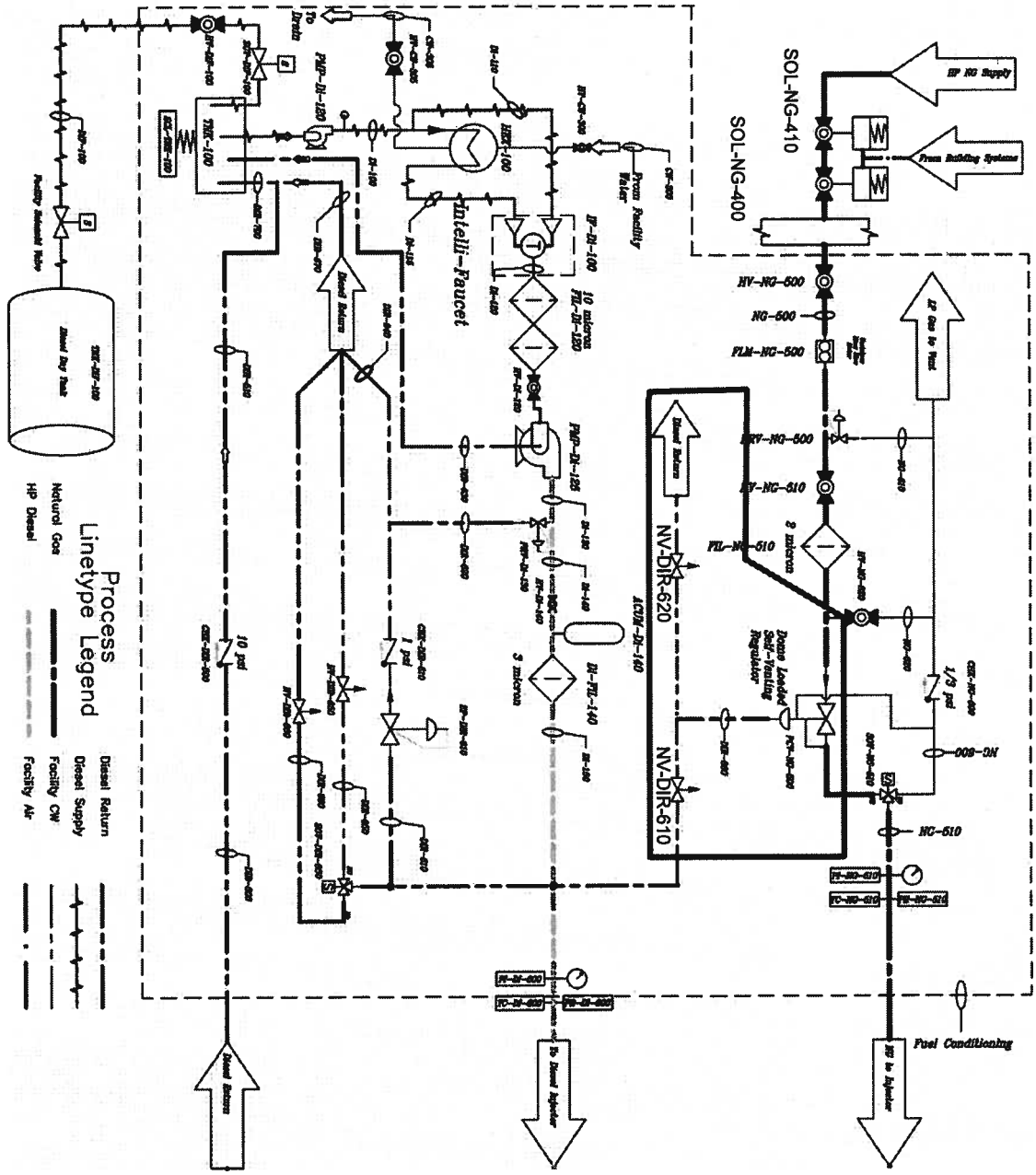

Figure 3.3: Diesel and natural gas process diagram with bias control loop using needle valves

3.1.3 Air Supply System

An oil-flooded screw-type compressor was used to supply the combustion air. A refrigerated dryer and low-pressure-drop filter were used to remove the water and oil from the intake air. For the tests in 2007 and 2008 automatic controls were installed for the intake air and exhaust back pressures. The back pressure can also be controlled manually with a motorized butterfly valve controlled through a ten-turn potentiometer. The temperature of the combustion air is controlled with a three-phase/20 amp/240V resistance heater to ± 2 °C.

A 90 L intake surge tank and an insulated 90 L insulated exhaust surge tank were used to dampen pressure fluctuations in the intake and exhaust lines. The surge tanks are located on a nearby platform. The pipe lengths and volumes between the surge tanks and the engine were similar in both installations. The intake surge tank is vertical to allow water condensation to drain from the system. Figure 3.4 shows the flow diagram for the air, exhaust, and cooling systems.

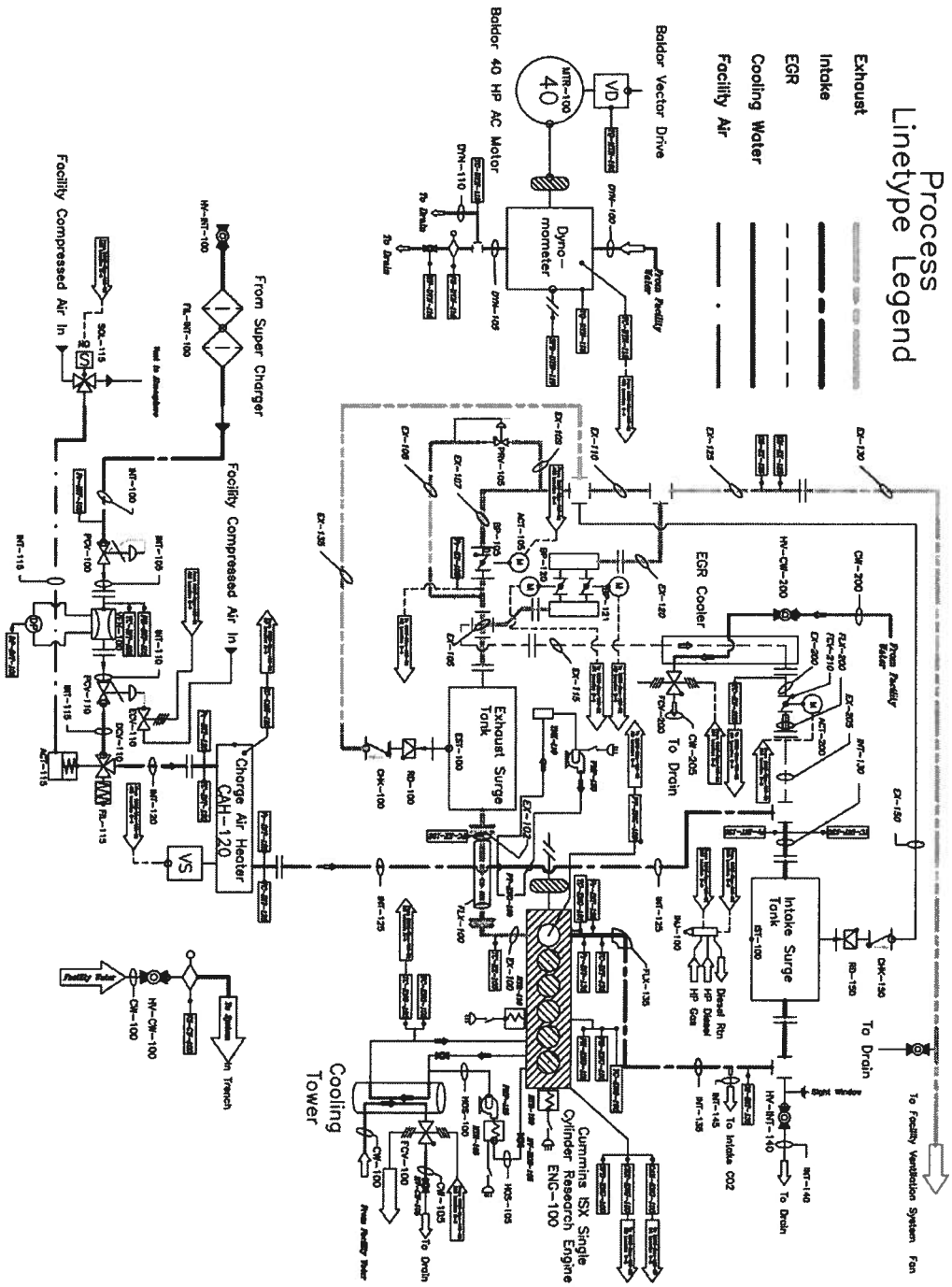

Figure 3.4: Process diagram for combustion air, facility air, and cooling water

3.1.4 Emissions Measurement and Calculations

As with the previous system, the gaseous emissions (O_2, CO_2, CO, CH_4, uHC, and NO_x) measurements are taken downstream of the exhaust surge tank in order to ensure homogeneity in the exhaust stream. The exhaust passes through a heated line and filter to arrive at the AVL Emissions Bench, CEB II, which has limit monitoring and automatic calibration. Inside the emissions bench the exhaust is split into two branches: the wet measurements and the dry measurements. On the wet side (water not removed) the CH_4, uHC, and NOx concentrations are measured. All other gases are measured as on the dry side. All emissions are measured according to SAE vehicle exhaust measurement standards (SAE 1993, 1995). Appendix A lists the stated accuracy and range for each analyzer.

The uHC and CH_4 are measured using a Flame Ionizing Detector (FID). In the emission bench used in 2006, only the uHC was measured in this fashion. A hydrogen flame inside a constant electric field ionizes organic carbon to produce a current proportional to the amount of carbon present (Pierburg 2002a). A portion of the sample is passed through a thermo-chemical converter which converts all non-methane hydrocarbons to CO_2 and water. The CH_4 concentration is measured through a second FID. The resulting currents are compared against the reference span gases of methane, and propane listed in Appendix A. During post-processing, the propane-equivalent measurement of the uHC is converted to a methane equivalent measurement by dividing by 3 (the carbon number ratio for propane to methane).

The NOx is measured using a chemiluminescent detector (CLD) which measures the light intensity of NO burning with ozone. To measure the NO_x concentration, NO_2 is first reduced NO using a thermo-catalytic converter. During the oxidation process, light is generated

between 600 and 1200 nm. Low absolute pressures are used to increase the probability of producing light and reduce the cross sensitivity from other components (Pierburg 2002b). The NO_x is multiplied by the K-NO_x correction factor which is used since the amount of NO formed in combustion is dependent on the humidity of the inlet air (SAE International 1995).

The remaining constituents need to be measured with the water removed. The amount of water in the exhaust (used for calculating the "wet" concentrations of O_2, CO_2, CO) is calculated assuming complete combustion of the fuel in air, minus the uHC, which is usually negligible. The following approach can then be used in converting the dry measurements to wet measurements (SAE 1995), starting with the stoichiometry,

$$CH_y = nO_2 + n(3.76N_2) + mH_2O \rightarrow CO_2 + \left(\frac{y}{2} + m\right)H_2O + xO_2 + n(3.76\,N_2) \quad (3.1)$$

In this equation, the variables y, n, and m, and x represent the atomic hydrogen-to-carbon ratio of the gas/diesel injection, the moles of oxygen in air to the engine, the moles of water in the combustion air, and the moles of excess oxygen (SAE 1995).

$$W = \frac{0.5y + (7.63 \times 10^{3}h)n - 2tHC_{C1}}{(4.76 + 7.63 \times 10^{3}h)n + 0.25y} \quad (3.2)$$

In this equation, h is the specific humidity expressed in terms of $g_{H20}/kg_{dry\ air}$. The conversion factor (CF) to convert the dry values is therefore

$$CF = 1 - W \quad (3.3)$$

Oxygen concentrations are measured using the paramagnetic properties of the gas (O_2 becomes magnetized when under an external magnetic field). The instrument consists of an

oxygen free gas enclosed in a dumbbell shaped body under a non-uniform magnetic field. The oxygen will migrate towards the magnetic field at one side of the dumbbell and the resulting higher pressure will cause the dumbbell to rotate. The voltage needed to keep the dumbbell horizontal is proportional to the oxygen concentration (ABB Automation 2001). The interference factor can be calculated by Equation 3.4 (SAE 1993).

$$\text{Interference} = 28.8 \times \%NO_x \times 0.01 + 0.623 \times \%CO_2 \times 0.01 \qquad (3.4)$$

Although other gases such as CO_2 and CO are weakly paramagnetic, and NO_x are diamagnetic (repelled by a magnetic field), the interference for the worst case (high CO_2 low NO_x) for this study was less than 0.03% (SAE 1993).

CO and CO_2 are measured with Non-Dispersive Infrared absorption (NDIR) instrumentation. Non-elemental gases will absorb discrete bands of infrared energy. The frequency of light absorbed depends directly on the type of gas. A light emitter of known frequencies and amplitudes goes through the sample gas and light is absorbed. Constant pressure columns of the reference gases are located at the other end which converts light absorption into volume change of a diaphragm (ABB Automation 2000).

At the beginning of each day that testing occurred, the emissions analyzers were re-calibrated using zero and span calibration gases. At the end of the day, the calibrations were checked to determine whether the calibration of the analyzers had changed.

In January 2008, problems were noted in the uHC measurements that eventually led to a complete servicing of the emissions bench. It was believed that this servicing did not affect any of the tests. This was checked by repeating an entire test series in June 2008.

Note that the old emissions bench in Kaiser was not frequently checked for linearization, nor did it have pressure and flow checks to ensure proper operation of the analyzers. After comparing repeatability points for the Kaiser and CERC installations, it was found that the two emissions systems might be significantly different (see Section 3.3).

3.1.5 Engine Speed, Temperature, and Flow Measurement

In both the CERC and Kaiser installations, Hall-Effect sensors are installed on the crank, cam, and dynamometer shaft in order to measure engine speed and position. The crank and cam sensor signals are conditioned and amplified at the sensor and sent to the controller. The dynamometer shaft sensor signal is sent to the Digalog Dynamometer Controller where it is conditioned, amplified, and used for engine speed control.

The fuel, intake and exhaust pressures are measured with strain gauge diaphragm pressure transducers. These transducers were re-calibrated when the engine was moved to the new test cell. Temperatures are measured with K-type thermocouples. Appendix B gives the instrument list and the expected accuracy of each updated from what was reported by McTaggart-Cowan (2006a).

The diesel fuel is kept in a small recirculation tank which was refilled as needed. The diesel flow rate is calculated gravimetrically by determining the change of the diesel mass in the recirculation tank over a sample time of 120 s or more (pail-and-scale). The natural gas mass flow rate is measured using a Micromotion Coriolis effect mass flow meter.

A UBC-built venturi meter is used for measuring airflow. With the current calibration, however, there is an offset in the carbon mass balance. This offset was assumed to be due to

a lower air-flow rate than expected. This may be caused by unresolved leaks in the intake air system as well as errors in the calibration of the venturi. Therefore, as described in Appendix C, the air flow rate was determined through the use of the carbon balance.

3.1.6 Engine Control, Monitoring, and Data Acquisition

In the test cell at CERC, most of the control and monitoring of the SCRE takes place in engine control room. A field-programmable gate-array (FPGA) is installed in the control computer with the ability to send and receive both analog and digital signals (NI 7831-R). A simplified information flow diagram is shown in Figure 3.5. The review of the shutdown logic and the operating procedures was a significant part of this thesis work over the winter of 2007/2008. Detailed process and instrument drawings and fault scenarios were prepared for approximately 6 hours of review meetings with Westport technical staff. The final operating procedures and Labview control logic are the result of this process. Details are given in the electronic appendix of this thesis (...rogak/sbrown/Thesis/Brown_Thesis.zip).

The information flow diagram shows data flow through the sensors, connection panels and multiplexers to the control computer. The multiplexers combine, amplify (for thermocouple measurements), and condition several analog signals for transmission through a single cable. The signals are converted to digital signals through a 12 bit Analog-to-Digital (A/D) card in the computer (PCI-MIO-16E-1). The SCXI 1001 chassis collects either "slow-speed" temperature and voltage signals at about 1 Hz, or "high-speed" voltage signals every ½ degree crank angle (^{o}CA).

Included on the FPGA board are -10V to 10V digital-to-analog converters. Since the FPGA operates at a clock speed of up to 40 MHz, it can be used for the high-speed control of fuel injection, a function previously taken care of by a Westport controller board. Similarly, the intake air selection, intake air pressure, exhaust back pressure, and coolant temperature are controlled by digital and analog control signals from the FPGA.

The remaining controls needed for engine operation are controlled manually through the control panel or regulators and valves in the test cell. The intake air heater, motorized back pressure valve, and engine speed and load are controlled at the control panel. Only control of the diesel pressure, diesel-gas bias pressure and intake venturi pressure require the regulator/valve to be manually opened or closed.

The control panel, the Labview control program and FPGA control program include safety logic. The integrated safety system is capable of monitoring the temperatures and pressures important to the functionality and safety of the test cell, warning the operator of unsafe conditions, and shutting down the engine as shutdown limits are reached. The shut down levels are set by the user. During a shutdown, the control computer decides that a shutdown is necessary and sends a 'software shutdown' signal to the FPGA. The FPGA then decides that a shutdown is necessary and sets all of the actuators to their default positions and sends a 'shutdown output' signal to shut down the remaining actuators. Similarly, a shutdown signal can be invoked through the FPGA board, the control panel, loss of power, or cooling water.

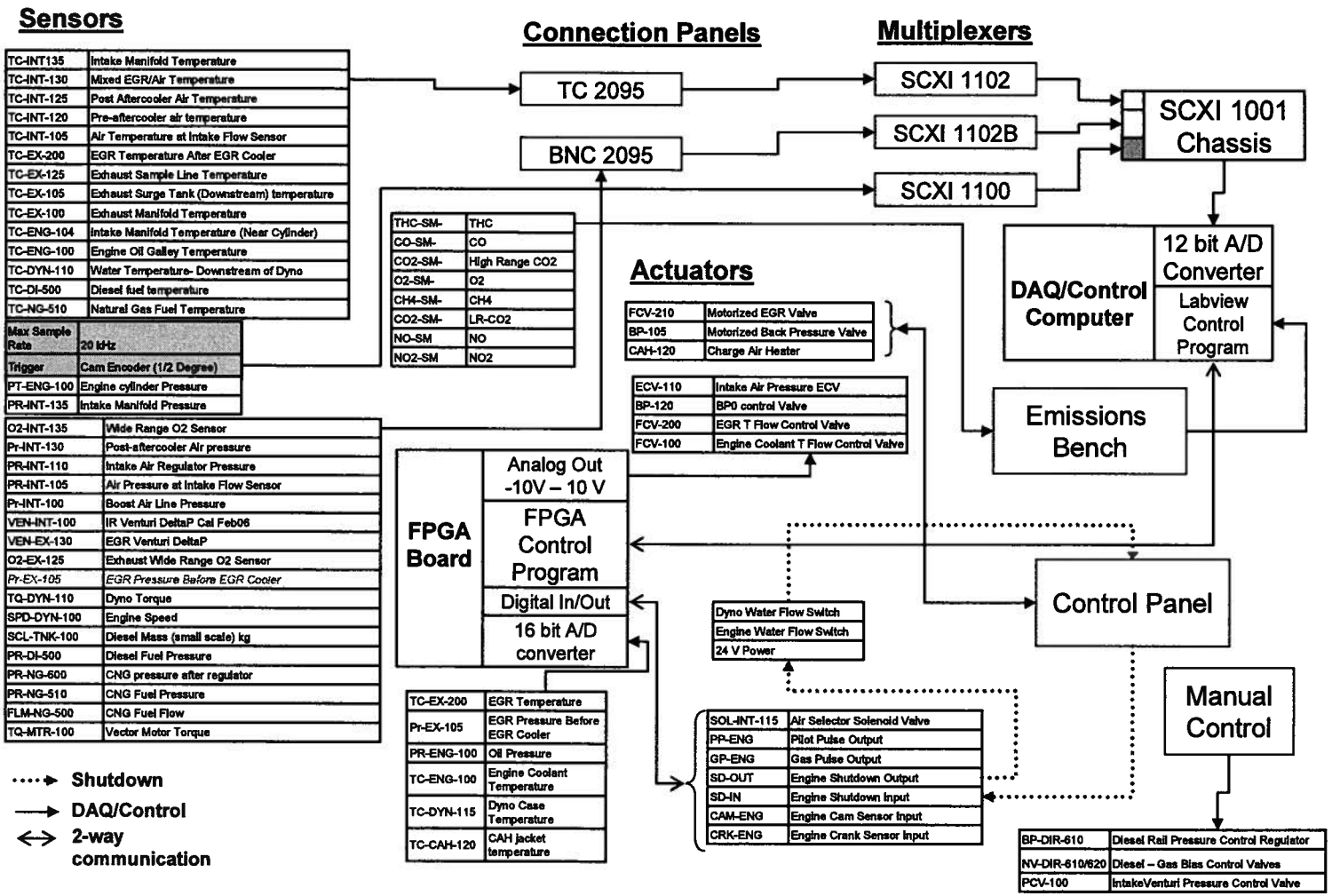

Figure 3.5: Data acquisition flow diagram

3.1.7 HPDI Co-Injector Operation

The co-injector injects diesel into the common gas/diesel reservoir through 7 holes of 0.17 mm diameter. As the diesel needle lifts, diesel is injected into the gas/diesel reservoir where it mixes with the gas. The amount of diesel injected depends on the bias pressure between the diesel and gas rail pressures and the injection duration. The gas diesel mixture is then injected into the combustion chamber during the pilot injection. The pilot injection usually lasts between 0.47 and 0.7 ms. Finally, in 0.3 to 1 ms after the pilot injection the main injection occurs. For high load applications, most of the gas is injected during the main injection with injection durations ranging from 0.8 – 1.1 ms.

Based on measured diesel flow rates and the commanded diesel needle opening time, the velocity of the fluid entering the gas/diesel reservoir ranges from 10 to 80 m/s. Based on the measured diesel – gas bias pressure and Bernoulli's equation, the maximum velocity should range from 45 to 88 m/s. Both estimation methods are crude and serve only to show that the diesel may move a significant distance inside the injector before the gas needle opens.

While the engine was being moved, the HPDI co-injector prototype was also being modified. In an attempt to improve the design of Prototype A (the original HPDI co-injector concept), the internal geometry was changed by adding a sleeve to create Prototype B. Figure 3.6 shows the modification that was made. The injector sleeve reduces the inner reservoir volume by 33%. It decreases the minimum annular area in the injector from 30 mm^2 to 10 mm^2, resulting in three times higher fluid velocity. In an attempt to keep the gas/diesel mixture near the injector tip, the annular area expands to 30 mm^2 near the diesel holes. This volume is about 35 mm^3, enough for 30 mg of diesel.

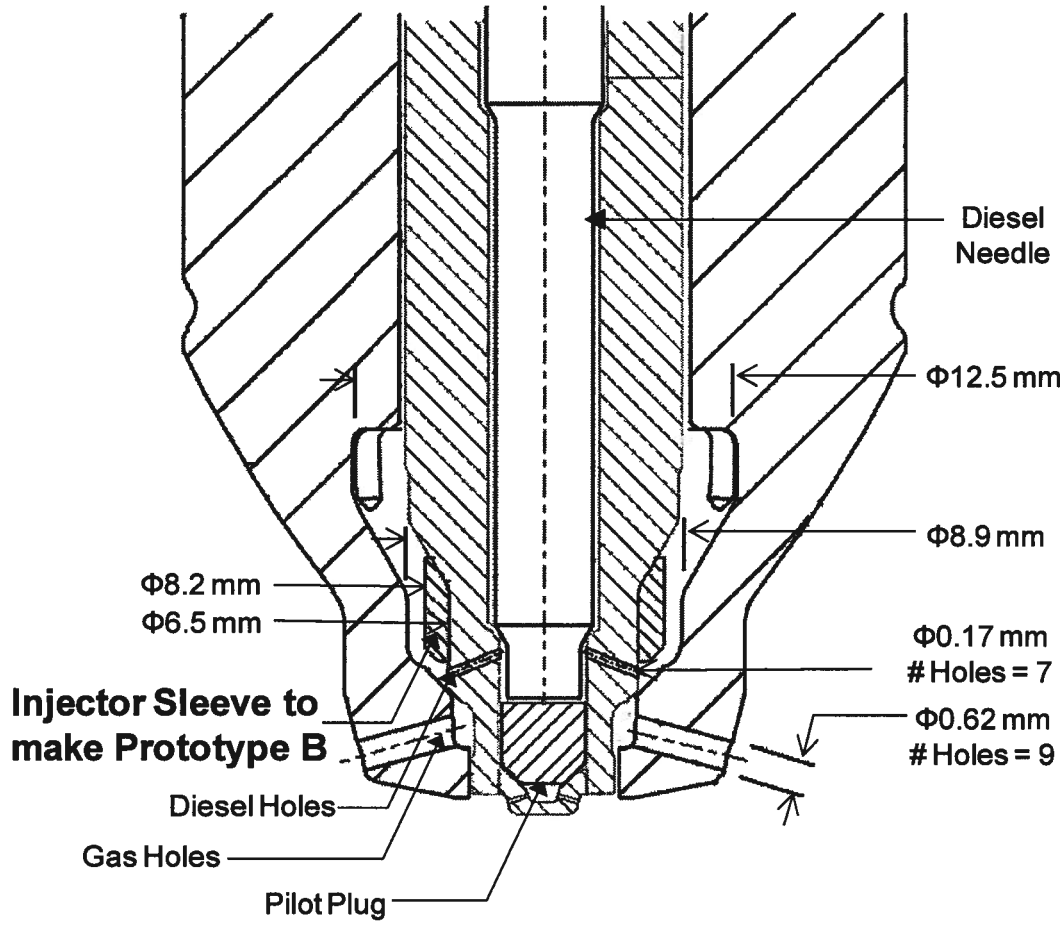

Figure 3.6: Geometry of a HPDI co-injector nozzle

3.1.8 Injection Command Parameters

The Westport Controller used in Kaiser was replaced with injection control using the FPGA board. For the Westport (WP) Controller, the commanded injections were based on timing of the commanded diesel end-of-injection (DEOI) to top dead centre (TDC), and the gas timings relative to end of the previous injection (Figure 3.7) TDC was calculated based on the 2 missing teeth in the crank signal at -60° after top dead centre (ATDC). The end of the pilot injection was then timed to end at a specified time before

TDC. The commanded first gas injection was then commanded to occur at a specified time after the end of the diesel pre-injection, referred to as the relative injection timing (RIT). Similarly, the commanded second gas was injected a short time after the end of the first injection, referred to as the second RIT (2RIT).

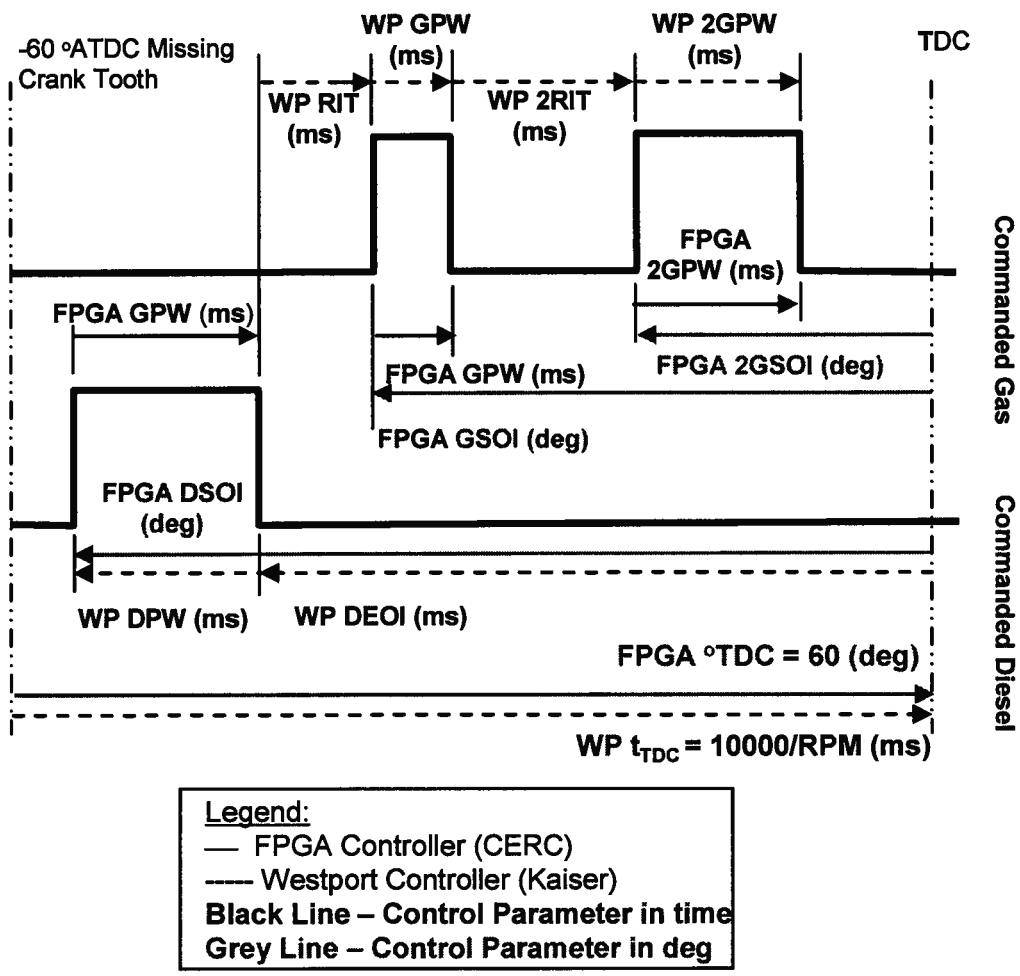

Figure 3.7: Commanded injection operation for the Westport Controller and FPGA controller

The FPGA control logic was based on absolute injection angles instead of the timing of the commanded pulse widths; therefore, the absolute injection angle is controlled. Whereas the original controller calculated the time until TDC from the two missing teeth

on the engine crank signal at -60° ATDC, the FPGA system reset the counters at -60° ATDC and then compared the crank angle to the commanded gas/diesel crank angle. An optical encoder attached to the flywheel provides ¼ degree resolution as a comparator. Because this comparison is reset at -60° ATDC, commanded injections that overlap this point will not operate properly.

The diesel start of injection (DSOI), gas start of injection (GSOI), and second gas start of injection (2GSOI) are specified in crank angle degrees after top dead centre (ATDC) of the power stroke. The diesel pulse width (DPW), gas pulse width (GPW), and second gas pulse width (2GPW) are specified in milliseconds (ms).

The differences between the Kaiser and CERC control systems make exact comparisons of repeatability points difficult. For the emission tests discussed in Section 4.5, the required injection angle to obtain a specified RIT for the first commanded gas injection is calculated and input into the Labview control program. Several methods were used to check the alignment of the rotational encoders and injection command timing, as described in W1-FAC-3788-ANYS (Appendix D).

3.2 Cylinder Pressure Measurements and Analysis

The cylinder pressure is used to determine heat release rates, indicated power, ignition delay, combustion variability, and knock intensity. These are the main parameters used to characterize combustion, so they warrant careful discussion.

3.2.1 Equipment Description

An AVL water-cooled QC33C piezoelectric transducer measures the in-cylinder pressure and a charge amplifier converts the signal from the transducer to a voltage. Because the piezoelectric transducer measures the change in pressure, the absolute pressure in the cylinder is modified so that it matches the pressure measured in the intake manifold near the time the intake valve closes (-180°ATDC). The intake manifold pressure is measured every ½ degree crank angle by a high speed strain-gauge pressure transducer. This procedure was used also in the Kaiser installation.

Piezoelectric pressure transducers should have factory-calibrated charge/pressure conversion factors, so that knowing the charge amplifier characteristics, no further calibration is needed. The practice in Kaiser (McTaggart-Cowan, 2008) was to choose the bar/volts factor in order to reconcile motoring curve behaviour with calibration experiments in a small constant volume chamber. Whether or not this procedure was optimal did not affect previous results, which were all done for a consistent pressure measurement procedure.

In January of 2008, it was necessary to replace the old charge amplifier (Kistler 503) with a model 504D Kistler charge amplifier. The overall bar/volt conversion was set to 2.850 bar/V to reconcile pressure traces from Kaiser and CERC for the same operating condition (previously set to 3.866 bar/V in Kaiser). Section 3.3 discusses this further.

In April 2008, the charge amplifier was replaced with the AVL model FlexIFEM. The QC33C piezoelectric pressure transducer was also replaced with a new QC33C pressure

transducer. This time the pressure/voltage conversion was set to 2.000 bar/V, consistent with the factory settings. The bar/V conversion factor was confirmed in the small constant volume chamber. The impact of these changes on data comparisons is discussed in Section 3.3.

Figure 3.8 shows a two representative indicated pressure vs. crank angle plots obtained in this study. In Section 3.2.5 the pressure fluctuations are analyzed.

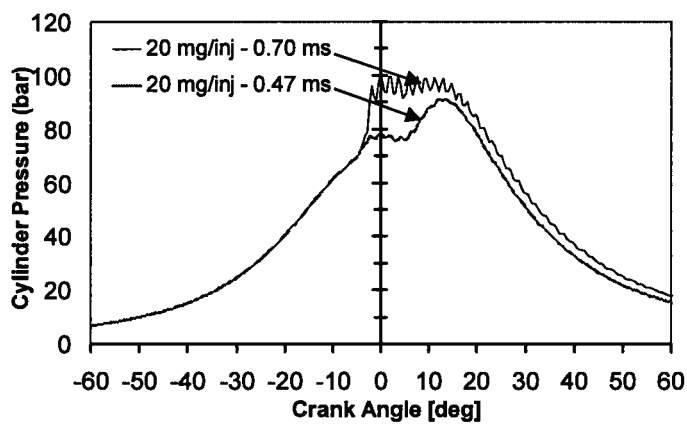

Figure 3.8: Sample indicated pressure curves for prototype B for two different pilot GPWs (1200 RPM, 24 MPa diesel rail pressure)

3.2.2 Indicated Mean Effective Pressure (IMEP) and Engine Variability

The indicated pressure curves can be used to determine the amount of work output from the engine. The net indicated mean effective pressure (NIMEP) is a measure of the indicated work output per unit of swept volume and can be expressed as the cyclic integral of work (P*dV*) for each of the four strokes (Sonntag *et al.* 2003).

$$NIMEP = \frac{\oint PdV}{swept\ volume} = \frac{\oint PdV_{comp,expansion,exhaust,intake}}{swept\ volume} \tag{3.5}$$

Small pressure differences at low cylinder pressures during the intake and exhaust strokes led to higher uncertainties in the pressure measurements during these strokes, which reduced the confidence in the NIMEP. For this reason, the gross indicated mean effective pressure (GIMEP), which takes into account only the compression and expansion stroke was used. GIMEP has been previously used in the SCRE (McTaggart-Cowan 2006; McTaggart-Cowan *et al.* 2006; Jones 2004, 2006) as well as by other workers (Boretti *et al.*2007; Cathcart and Zavier 2000; Cairns *et al.* 2006) as a measure for defining the engine output.

$$GIMEP = \frac{\int_{180}^{-180} PdV}{swept\ volume} \tag{3.6}$$

Since the pressure is measured every ½ °CA, the integral becomes a summation from bottom dead centre (BDC) of the compression stroke to BDC of the expansion stroke. Due to the encoder offset, the pressure is not recorded at BDC and therefore the volume V_0 at BDC is computed from the swept and clearance volumes, as shown in the following equation, assuming the pressure at BDC is the same as the first measured pressure, P_0.

$$\text{GIMEP} = \frac{\left(\frac{P_1 + P_0}{2}\right)\cdot\left(V_1 - \left(V_{swept} + V_{clearance}\right)\right) + \sum_{k=2}^{720}\left(\frac{P_k + P_{k-1}}{2}\right)\cdot\left(V_k - V_{k-1}\right)}{V_{swept}} \tag{3.7}$$

The coefficient of variation (COV; standard deviation/mean) of the mean effective pressure has been used widely for determination of the cyclic variability of the engine (Duggal et al. 2004; Cathcart and Zavier 2000; Boretti *et al.* 2007; McTaggart-Cowan *et al.* 2006; Zhang *et al.* 1998; McTaggart-Cowan 2006). The maximum acceptable COV

IMEP is usually between 3-6% (Zhang *et al.* 1998; Cathcart and Zavier 2000; Duggal et al. 2004).

3.2.3 Heat Release Rate

The in-cylinder pressure as a function of the engine crank angle can be used to determine the heat release rate (HRR). The heat release rate is an approximation of the amount of heat that would need to be added (due to the release of chemical energy) to the combustion cylinder to observe the measured in-cylinder pressure (Stone 1999, 547).

HRR during the power stroke is based on an air standard cycle which has the following assumptions (not considering the pumping work) (Sonntag *et al.* 2003, 410):

- A fixed mass of air is the working fluid through the entire cycle, and the air is always an ideal gas. Thus there are no inlet process and exhaust process.
- The combustion process is replaced by a process transferring heat from an external source.
- Air has a constant specific heat.

With these in mind, the HRR curve is usually only computed from -180 ° to 180 ° ATDC. Using the First Law of Thermodynamics for a closed volume (after the inlet valve closes and before the exhaust valve opens), the net heat release can be written (Stone 1999, 548):

$$\frac{dQ_{net}}{d\theta} = \frac{\gamma}{\gamma - 1} p \frac{dV}{d\theta} + \frac{\gamma}{\gamma - 1} V \frac{dp}{d\theta} \tag{3.8}$$

where γ is the constant specific heat ratio for the exhaust gas mixture (set at 1.30 for the diesel process) (Heywood 1988, 510).

The crevice regions of the combustion chamber at TDC are non-negligible and can make up a few percent of the clearance volume. The gas the crevice is cooler and denser and has properties much different from those in the rest of the cylinder (Heywood 1988, 509).

In some previous work, multi-zone HRR models which take into account heat transfer to the walls and combustion processes have been used (Hill and Douville 1997, Hill and McTaggart-Cowan 2005). For this study, the single zone heat release rate model was used since the more complicated versions of heat release are still approximations. Semi-quantitative comparisons of ignition delay, 50% IHR, and knock can still be drawn from the simpler HRR model. Figure 3.9 shows the unfiltered HRR curves derived from the pressure data of Figure 3.8.

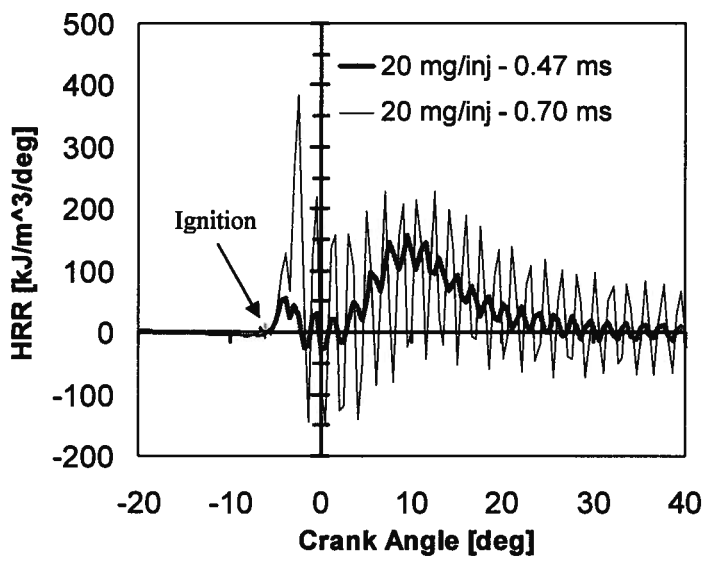

Figure 3.9: HRR curves for in-cylinder pressures shown in Figure 3.8

Note that in Figure 3.9 that the pressure fluctuations of Figure 3.8 are exacerbated on the HRR curves. In order to better calculate performance metrics such as ignition delay, the high frequency pressure fluctuations were filtered out using a low-pass Gaussian digital

filter. As discussed in Section 3.2.5, the cutoff frequency was chosen so that it would filter out any frequencies higher than 3.5 kHz.

3.2.4 Ignition Delay

As discussed in Chapter 2, the ignition delay is measured from the start of commanded injection to the start of combustion (SOC). The start of combustion is difficult to define (Stone 1999, 549). In previous work the start of combustion was defined as the 5% IHR (Asad and Zhang 2008, McTaggart-Cowan 2006b), rapid pressure rise (Donghui *et al.* 2004), the point where the indicated pressure trace separates from the motoring pressure trace (Srinivasan *et al.* 2006, Dumitrescu *et al.* 2000).

Stone recommends using the minimum of the IHR, or the first non-zero HRR (Stone 1999, 549) which is what was used by McTaggart-Cowan (2006a) and McTaggart-Cowan *et al.* (2006). For this study, the start of combustion (shown in Figure 3.9) was found as the intercept of the HRR curve of the first combustion event with the zero HRR axis. This intercept was calculated by finding the slope between 30 kJ/m^3/deg and 20 kJ/m^3/deg.

Figure 3.10 shows the ignition delay as defined by the 5% IHR plotted against the ignition delay defined by the first non-zero HRR for Test Series VIII-B2 tests (tests are described later in Section 4.5). Note that both calculation methods are correlated, with shorter ignition delays calculated from the 5% IHR typically longer by about 1 ms; larger ignition delays are in agreement.

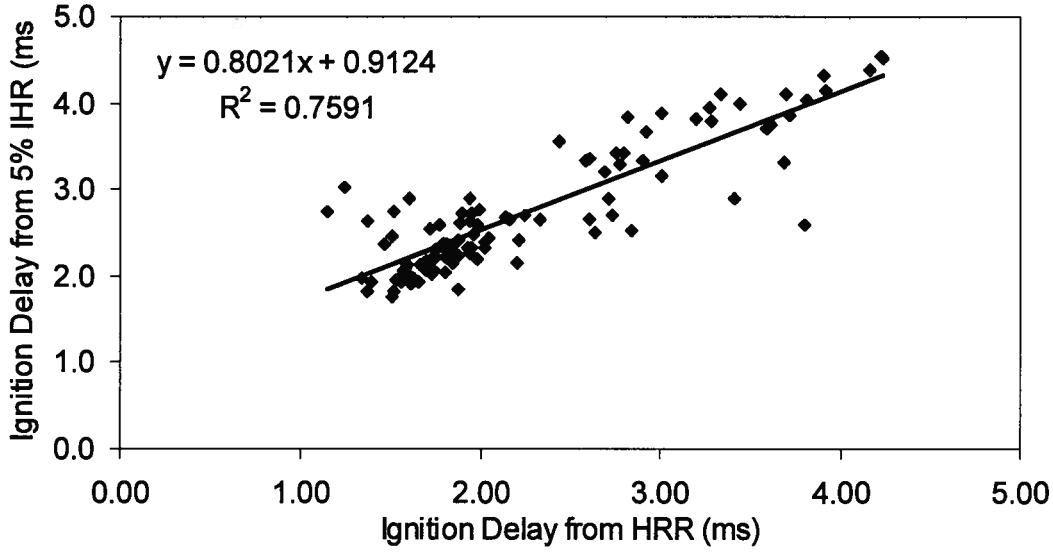

Figure 3.10: Comparison of ignition delay calculation methods

3.2.5 Knock

Heywood (1988, 505) describes combustion in a compression-ignition engine as a rapid premixed burning phase followed by a controlled burning phase. During the testing process, there were specific operating conditions where significant fluctuations were observed on the indicated pressure trace. The observed pressure fluctuations are due in part to the rapid energy release and subsequent pressure rise, shock wave and wave reflection off of the chamber walls during the premixed burning phase (Heywood 1988, 454; Taylor 1985, 95). The amount of engine noise and engine knock with the co-injector was greater in magnitude than that of a J36-HPDI injector where diesel and gas are injected separately. Although the exact cause of engine knock has not yet been ascertained, a possible cause could be a high initial injection rate of natural gas and diesel causing a larger proportion of fuel to burn during the premixed phase.

Knock intensity can be measured in two ways. First, the knock intensity can be attained by determining the maximum amplitude of the fluctuating portion of the indicated pressure curve (Heywood 1988, 455). Vibrations that are picked up by the pressure transducer are a combination of the structural vibration as a result of a rapid pressure rise and pressure waves in the cylinder (Christensen *et al.* 1998). The pressure fluctuations are due to the gas in the cylinder resonating at the first transverse mode acoustical frequency (Heywood 1988, 455). The first transverse mode acoustical frequency is defined as

$$f = \frac{ac}{\pi D} \tag{3.9}$$

where c is the speed of sound of the gas, a is a geometric constant (taken as 1.84 for this case), and D is the cylinder diameter (Eng 2002). The speed of sound will be dependent on the gas temperature. Given the pressure and volume data, the in-cylinder temperature can be approximated by the ideal gas law relation:

$$T_2 = \frac{P_2 V_2}{P_1 V_1} T_1 \tag{3.10}$$

Where the T_1 is the intake manifold temperature, V_1 and P_1 are the volume and pressure when the intake valve closes, and T_2, V_2, and P_2 are the temperature, volume and pressure right before ignition. The speed of sound of the compressed gas can then be calculated assuming a constant specific heat ratio by the relation $c = \sqrt{kRT}$, where R is the gas constant for air (287 J/kgK). For the test case, the first transverse mode frequency should

therefore be about 3.7 kHz, which is expected since the first mode frequency for engine cylinders is usually between 3 – 10 kHz (Heywood 1988).

Ideally, a bandpass filter set to the first transverse acoustical frequency would be put on the signal output with the maximum amplitude from each cycle representing the knock intensity (Heywood 1988, 455). For this study, since there was no filter installed, the frequency is found through a Fourier transformation of the raw in-cylinder pressure data to the frequency domain. Figure 3.11 shows that there was an experienced frequency between 3 and 4 kHz on a frequency domain plot.

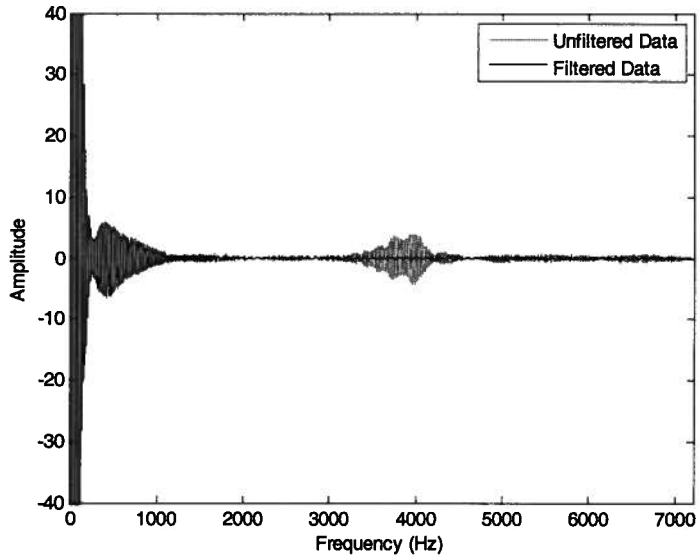

Figure 3.11: FFT of pressure data from Figure 3.8 for the high-knocking case (0.70 ms pilot GPW)

The knock intensity can be obtained by finding the maximum difference between the filtered and unfiltered indicated pressure curve for each of the 45 recorded cycles. Figure 3.12 shows the maximum amplitude of the fluctuations occurring for the high and low

knocking cases of Figure 3.8. The boundary between "normal" and "heavy" knock is not well defined. For this study, knock intensities over 300 kPa are considered heavy knock, consistent with a description by Heywood (1988, 455). Note that the knock intensity for high diesel, long pilot GPW duration is well above 300 kPa (3 bar), signifying that intense knocking is occurring.

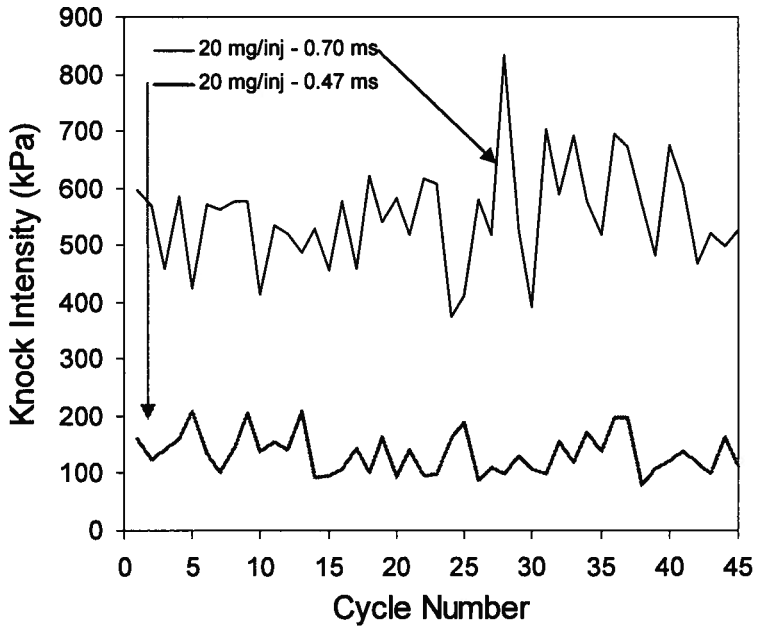

Figure 3.12: Knock intensity (maximum amplitude of difference between filtered and unfiltered pressure signal) for 45 cycles, pressures from Figure 3.8

Another way to report the level of knocking is to report the maximum rate of pressure rise (max dP/dCA). Shiga et al. (1988) related the maximum rate of pressure rise of a diesel engine to the knock intensity. They found that knock intensity increased with the square of the maximum rate of pressure rise. Usually, a maximum rate of pressure rise between 6-10 bar/deg is considered the stress limit for diesel engines (Christensen *et al.* 1998; Obert 1973, 589).

Figure 3.13 shows the relationship between knock intensity and the maximum rate of pressure rise. From these tests, there is appears to be a correlation between knock intensity and maximum rate of pressure rise. It appears that a 3 bar knock intensity corresponds to a maximum rate of pressure rise of 6 - 12 bar/deg, consistent with the recommendations for maximum rates of pressure rise made by Christensen *et al.* (1998) and Obert (1973).

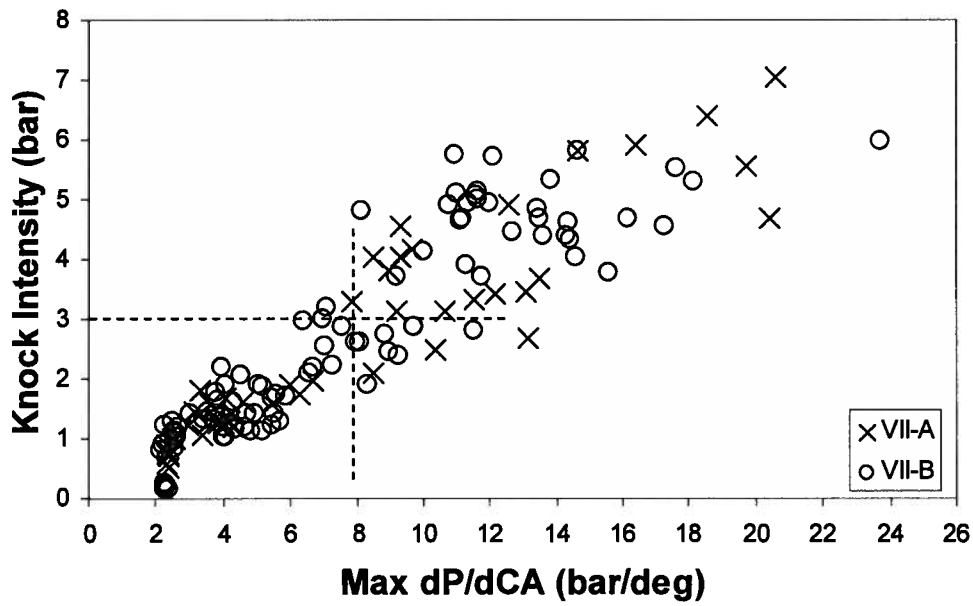

Figure 3.13: Knock intensity plotted vs. maximum rate of pressure rise (max dP/dCA). Test Series VII defined in Chapter 4.

The conventional detection method of engine knock, however, does not include information about the amount of energy released or the cylinder pressures and temperatures at the time of knock occurrence. Engine geometry and the pressure at which knock occurs are just as important as the knock intensity (Taylor 1985, 39; Fitton and Nates 1996). Specific cases of intense and prolonged engine knock without engine

damage has been previously reported (Christensen et al. 1998; Vressner *et al.* 2003, Taylor 1985, 39).

Damage due to knock can occur as the thermal boundary layer around the piston and cylinder walls breaks down due to the pressure waves inside the cylinder (Stone 1999, 74). Aluminum pistons are especially susceptible to melting or holing during engine knock due to the lower melting temperature of aluminium. Piston rings and lands can be broken due to the pressure waves. When a piston ring fails, it will likely score the internal combustion engine's piston liner. The high frequency mechanical vibrations can cause extra fatigue on engine components shortening their lives.

Damage in spark ignited engines due to knock is much more prevalent, since it usually occurs near stoichiometric conditions. A large amount of energy is therefore released. Note that for all of the cases considered, the maximum cylinder pressure for the SCRE is always below 150 bar and the exhaust temperature is below 600 °C.

There are no peer reviewed studies on damage due to knock in a pilot-ignited direct-injection natural gas engine. The closest studies found for similar sized engines were with natural gas homogenous charge compression ignition (HCCI).

Christensen et al. (1998) operated a similar sized engine, fuel, and boost pressure with significant knock occurring. This engine was operated as a homogenous charge compression ignition engine for short durations at 40 bar/deg and continuously at 15-20 bar/deg without any noticeable wear to the engine. Table 3.2 shows compares the geometries and temperatures of the engines. Note that for this study, the manifold temperatures were quite a bit lower.

Table 3.2: Engine Size Comparison Between Volvo TD100 (Christensen et al. 1998) and Cummins ISX (Duggal et al. 2004)

	Volvo TD100	Cummins ISX
Displacement (L)	1.6	2.5
Stroke (m)	0.14	0.17
Bore (m)	0.12	0.137
Connecting Rod (m)	0.26	0.26
Compression ratio	17.5	16.7
Boost Pressure (bar)	1	1
Manifold Temperature °C	100 -170	30
Fuel Tested	Natural Gas	Diesel/Natural Gas
Equivalence Ratio	0.33 – 0.4	0.3-0.55

It is important to note that the engine was running on a homogenous charge of natural gas at manifold temperatures higher than the controlled temperature of the SCRE in order to promote autoignition of the natural gas. This would lead to in-cylinder gas temperatures at TDC (without combustion) 350 – 450 K higher than the Cummins ISX. Christensen *et al.* (1998) found the peak cylinder temperatures to be up to 2000 K. Vressner et al. (2003) attribute the lack of damage to the low temperatures near the wall due to lean combustion. These peak temperatures would be similar in the SCRE at lower equivalence ratios. Figures 3.14 and 3.15 show the proportion of Test Series VII cases (described in Chapter 4) that exceed the 10 bar/deg limit by Obert (1973) and the 20 bar/deg limit by Christensen et al.(1998). Less than 1% of all of the tests run exceeded 20 bar/deg.

Both the 16.7:1 and 15:1 pistons were inspected after over 20 hours of operation with the co-injector, and there was no sign of damage to the pistons or rings. The valve train did not appear to be affected either. However, test conditions that exhibit heavy knock should

be avoided unless there are specific attributes of the co-injector that need to be observed at high diesel/high gas pilot injections.

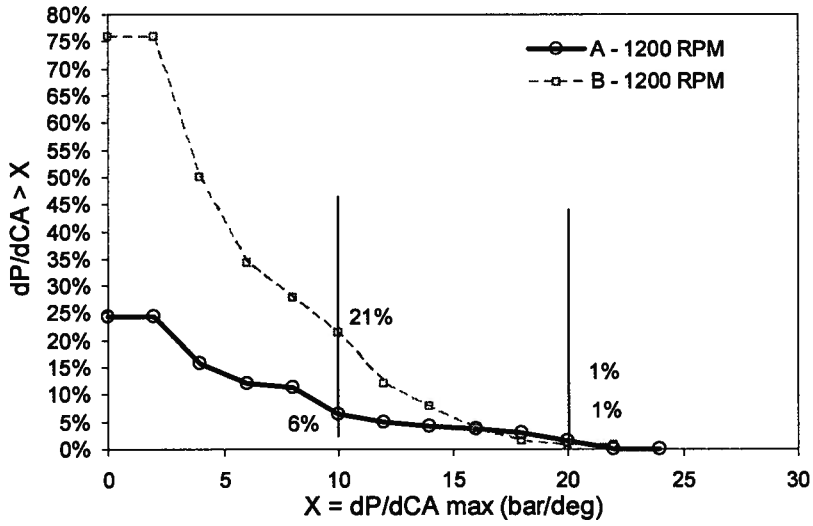

Figure 3.14: Distribution of maximum rate of pressure rise for Test Series VII-1200 RPM

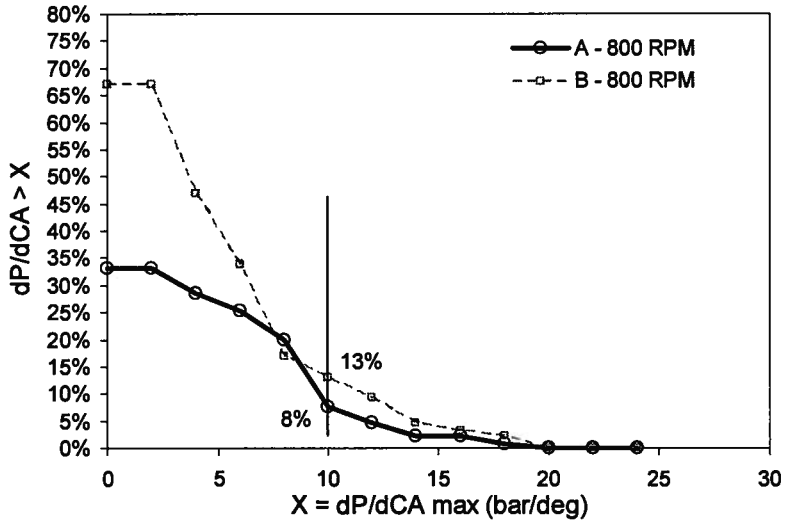

Figure 3.15: Distribution of maximum rate of pressure rise for Test Series VII-800 RPM

Lower diesel injection masses or shorter pilot gas injection durations can reduce the severity of diesel knock. Figures 3.9, 3.16, and 3.17 show that the fluctuations can effectively be reduced by reducing the pilot injection duration, reducing the diesel injection mass, or both. Lower diesel injection masses will prevent many cases which

would otherwise exhibit strong diesel knock. Chapter 4 results include more detail on the conditions that affect knock.

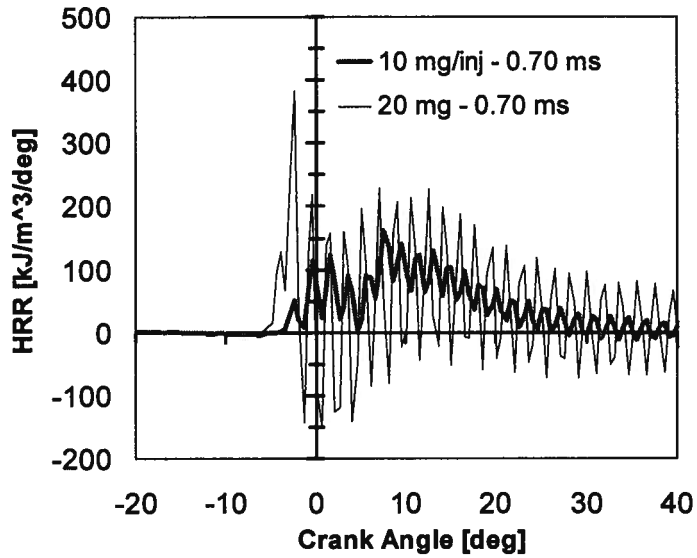

Figure 3.16: Reduction of Engine Knock by Reducing Diesel Injection Mass (Prototype B)

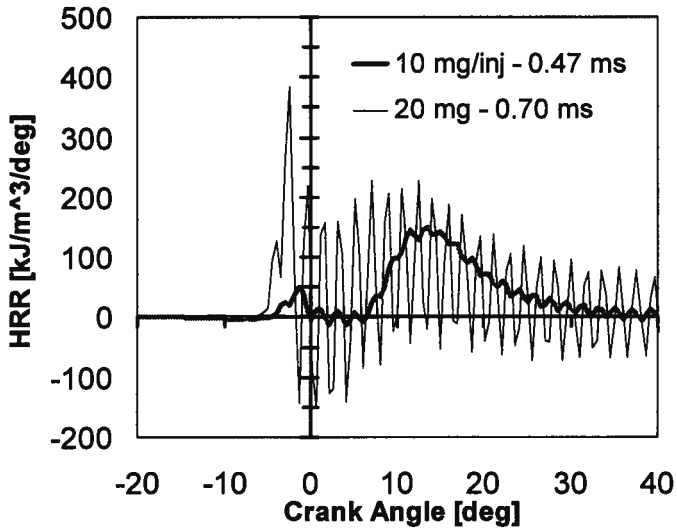

Figure 3.17: Reduction of Knock Intensity by Reducing Diesel Injection Mass and Pilot GPW (Prototype B)

3.3 Performance Comparisons for CERC and Kaiser Tests

In order to determine the long-term repeatability of the engine, a repeatability test was conducted in the engine to begin each day at oil temperatures of 95-100 °C. This was especially important with the Westport J36-008 HPDI injector, which has been used in benchmark testing since 2005. The indicated pressure and HRR curves shown in Figures 3.18 and 3.19 compare the recorded combustion for repeatability testing in CERC and in Kaiser with the J36-008 injector. Unfortunately, the tests conducted in February-March 2008 were conducted with heated intake air to 70°C. These points are therefore compared against bracketed temperatures (57°C and 81 °C) collected in May 2006. As mentioned in Section 3.2.1, the in-cylinder pressure measurements in 2005 were calibrated against a small volume pressure chamber. This method could not be used in the new test cell due to some leakage between the small volume pressure chamber and the transducer. Therefore, to continue on with the testing, the voltage-to-pressure conversion factor for the tests in 2008 was set so that the GIMEP was similar to that in 2005. Figures 3.18 and 3.19 show that for this condition, the peak pressure location and magnitude, and the HRR curves were comparable. These similarities indicate that even though GIMEP is similar between the 2005 and 2008 tests by design, engine operation is similar between both test cell locations.

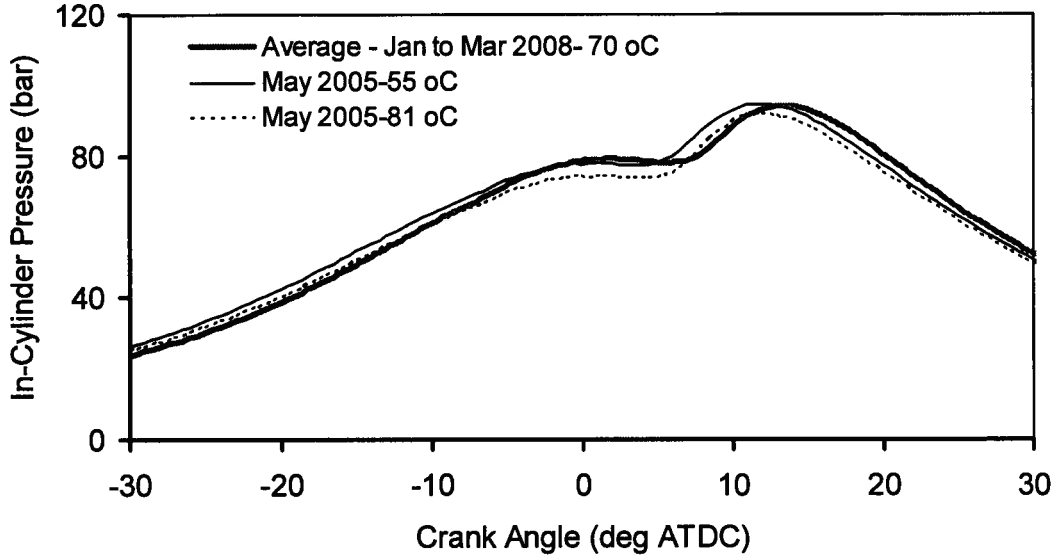

Figure 3.18: Comparison of in-cylinder pressure curves for SCRE setup in CERC(2008) and Kaiser(2005) for J36-008. 1200 RPM, 8 bar GIMEP, 0.40 EQR, 90 kPa MAP, 1.0 ms RIT, 16.7:1 CR

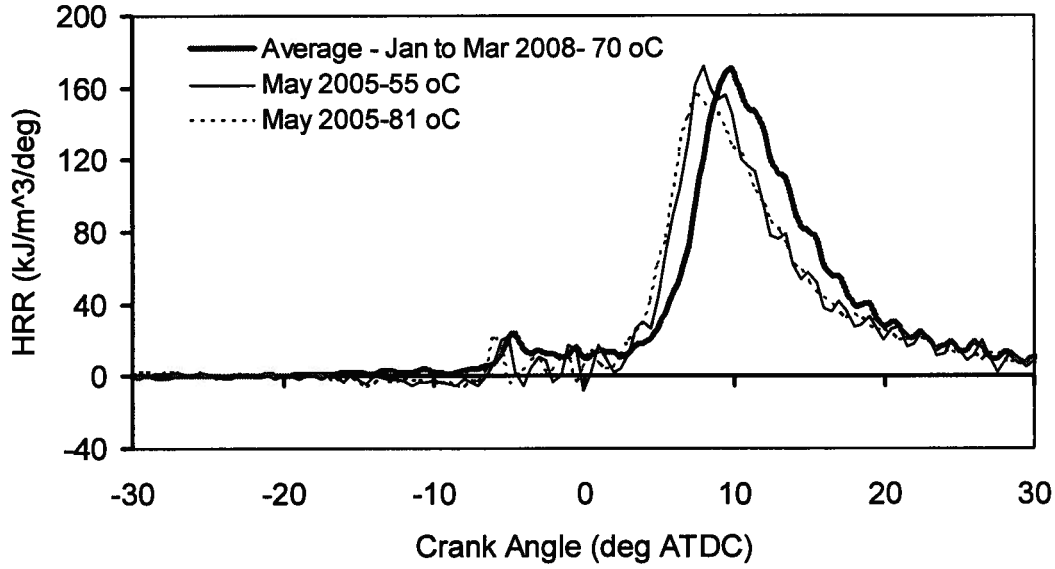

Figure 3.19: Comparison of Heat Release Rates for SCRE setup in CERC(2008) and Kaiser(2005) for J36-008. 1200 RPM, 8 bar GIMEP, 0.40 EQR, 90 kPa MAP, 1.0 ms RIT, 16.7:1 CR, Heated Intake Air

In June, 2008, further repeatability tests were conducted with the J36-008 with unheated air. These results were compared with the tests conducted in 2006 by Jones. Table 3.3

compares the CERC in June of 2008 measurements to those made at similar operating conditions in Kaiser in January of 2006.

As seen from the table, the intake manifold temperature was slightly lower in the CERC setup, which would be expected from the larger, more effectively ventilated test cell. Similarly, the electrical systems in the CERC test cell have been laid out to reduce the electrical noise in the signals. This could potentially reduce the calculated knock intensity.

Even with the controlled parameters in the CERC setup set to $\pm 5\%$ of the Kaiser setup, there were still significant differences in the emissions measurements. Most notably were the CO measurements where the Kaiser emissions were more than 100% higher than the CERC measurements. Similarly, the CH_4 emissions were lower in the CERC setup and the uHC were higher, which resulted in the non-methane hydrocarbons (nmHC) to be more than 100% lower in the Kaiser setup.

Table 3.3: Comparison of Performance Parameters Between CERC (2008) and Kaiser (2006) tests using J36-008 injector

	Number of Tests	3 2008 tests	3 2006 tests	% Change (2006 - 2008) /2008 x 100
Controlled Parameters	Engine Speed (RPM)	1206 +/- 4	1210 +/- 1	0.3%
	Gas Rail Pressure (MPa)	20.9 +/- 0.1	21.4 +/- 0.2	2.6%
	Air Flow (kg/hr)	143.0 +/- 0.4	142.8 +/- 0.9	-0.2%
	Exhaust Back Pressure (kPa)	79 +/- 7	76 +/- 7	-2.7%
	Diesel Injection Duration (ms)	0.65	0.65	
	Equivalence Ratio	0.394 +/- 0.007	0.408 +/- 0.004	3.7%
	GIMEP (bar)	8.33 +/- 0.27	8.48 +/- 0.03	1.8%
	50% IHR	10.4 +/- 0.3	10.0 +/- 0.1	-4.0%
Measured Parameters	Manifold air temperature (°C)	20.7 +/- 0.5	25.0 +/- 1.0	20%
	Manifold air pressure (kPag)	60.9 +/- 0.1	59.4 +/- 2.8	-2.4%
	Disel injection mass (mg/inj)	8.2 +/- 0.9	8.2 +/- 1.1	0.7%
	CNG injection mass (mg/inj.)	84.3 +/- 1.7	87.1 +/- 1.1	3.4%
	Peak Pressure (bar)	86.5 +/- 1.8	92.1 +/- 0.8	6.5%
	Knock Intensity (kPa)	108.2 +/- 6.4	145.5 +/- 7.4	34.5%
Emissions	CO (g/kg of fuel)	2.21 +/- 0.10	4.51 +/- 0.63	104%
	NOx (g/kg of fuel)	32.51 +/- 0.68	26.13 +/- 0.41	-20%
	CH4 (g/kg of fuel)	2.33 +/- 0.27	3.13 +/- 0.15	34%
	tHC (g/kg of fuel)	4.30 +/- 0.45	2.94 +/- 0.02	-32%
	CO2 (kg/kg of fuel)	2.63 +/- 0.01	2.44 +/- 0.04	-7.1%
	O2 (kg/kg of fuel)	5.10 +/- 0.15	4.99 +/- 0.04	-2.1%
Mass Balance Ratios	Carbon balance ratio	1.051 +/- 0.004	0.977 +/- 0.019	-7.1%
	Nitrogen balance ratio	1.00	1.00	
	Hydrogen balance ratio	1.00	1.00	
	Oxygen balance ratio	0.984 +/- 0.001	0.991 +/- 0.004	0.7%

For these tests the AVL charge amplifier was used with a pressure/voltage conversion factor of 2.000 bar/V. The indicated pressure and HRR in Figures 3.20and 3.21 compare the recorded combustion for similar operating points in CERC and in Kaiser for repeatability testing. Note that the measured in-cylinder pressures for the June-CERC tests were lower, probably due to pressure calibration errors in the Kaiser setup. It is likely that the uncertainty associated with the calibration of the pressure transducer/charge amplifier in the small constant-volume chamber was large.

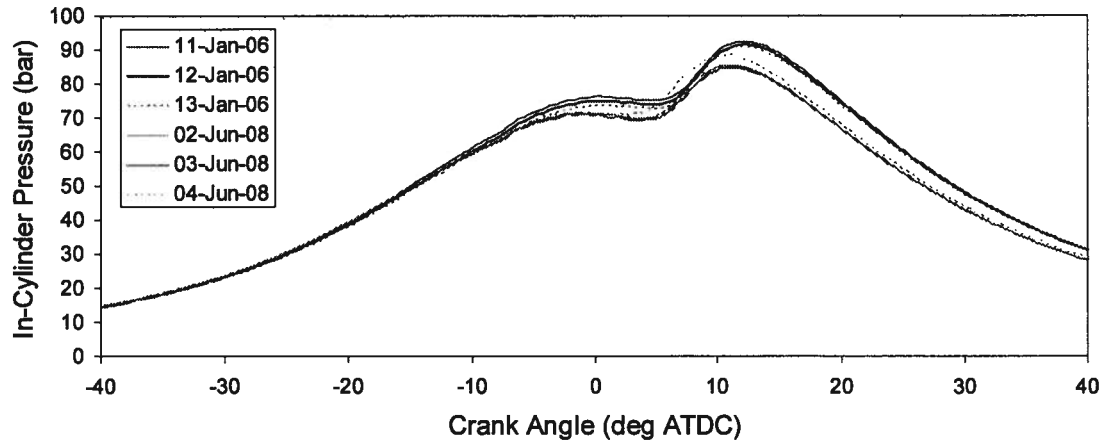

Figure 3.20: Comparison of In-Cylinder Pressure for SCRE setup in CERC(2008) and Kaiser(2005) for J36-008. Unheated Intake Air

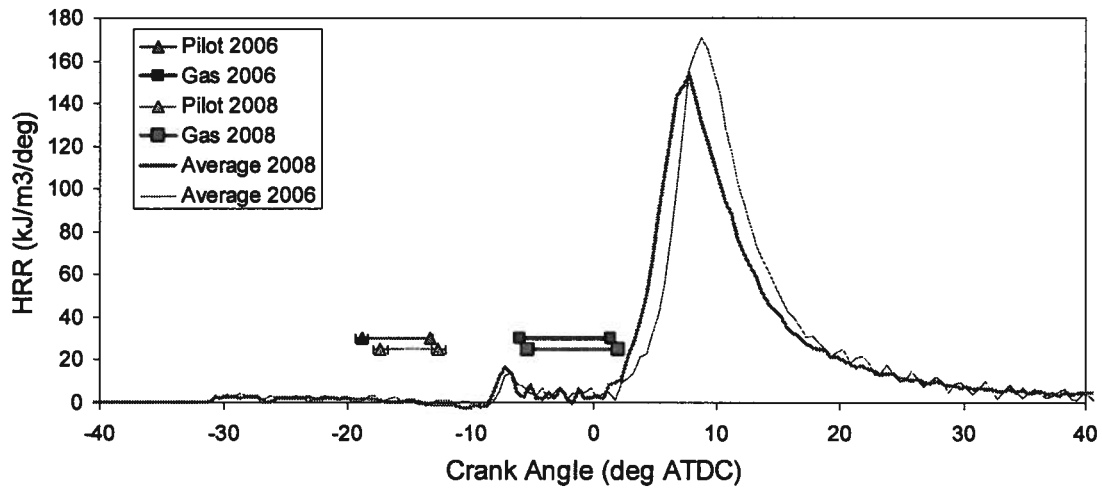

Figure 3.21: Comparison of In-Cylinder Pressure for SCRE setup in CERC(2008) and Kaiser(2005) for J36-008. Unheated Intake Air

These repeatability tests show that emission measurements from the two test cells cannot be compared quantitatively. Furthermore, the in-cylinder pressure is slightly different between the CERC tests after April 2008 and the other tests. Table 3.4 shows the implications of a larger or smaller conversion factor on the cylinder pressure measurements and analysis.

Table 3.4: Implications of 7.5% increased conversion factor

	Units	A	B	% change (A- B)/B
Conversion Factor	bar/V	2.151	2.000	7.5%
GIMEP	bar	8.8	8.2	7.5%
COV GIMEP	%	1.8	1.8	0.0%
Pcyl max	bar	92.1	85.8	7.4%
COV Pcyl max	%	0.7	0.7	0.1%
CA @ Pcyl max	oCA	13.3	13.3	0.0%
COV CA @ Pcyl max	%	4.6	4.6	0.0%
HRR max	kJ/m3/oCA	174.7	162.6	7.5%
dP/dCA max	bar/oCA	4.5	4.2	7.5%
Knock Intensity	bar	1.2	1.1	7.5%
IHR max	kj/m^3	1594.4	1496.9	6.5%
Start of Combustion	°CA	3.96	4.05	-2.2%
2% IHR	°CA	-6.6	-6.6	0.0%
5% IHR	°CA	2.4	2.9	-16.9%
10% IHR	°CA	5.4	5.4	0.0%
50% IHR	°CA	10.5	10.6	-0.8%
90% IHR	°CA	23.0	24.5	-6.1%
Combustion Duration (90% IHR - 5% IHR)	°CA	20.5	21.5	-4.7%

Parameters dependent on the pressure such as the GIMEP, maximum cylinder pressure, maximum rate of pressure rise, knock intensity, etc. change at the same rate as the pressure conversion factor. The COV GIMEP, the CA 50% IHR, the start of combustion, and the combustion duration are affected to a lesser degree. The parameters that are affected less represent robust parameters for analysis. Although the IHR appears to be affected by the choice of conversion factor, the ratio between two IHR (discussed in Section 4.4) also represents a robust measurement between Prototype A and Prototype B.

3.4 Injector Characterization Flowbenches

Two injector characterization flowbenches at Westport were used in this study. The BTR2 is used to check the quality of the all Westport injectors. This rig provides a static back pressure of 80 bar with a gas injection pressure of 16 MPa. Nitrogen is used as a substitute for CNG for these tests. Viscor® calibrating fluid is used instead of diesel because it has density and viscosity similar to diesel while being less of a fire hazard. For HPDI injectors, the liquid and gas injections can be tested separately; however with the co-injector prototype, only the gas flow response to commanded injection duration was tested. The EFS1 injector characterization flowbench has the ability to test up to 6 injectors simultaneously to determine injector-to-injector flow differences from a common rail. Injectors are installed in a modified engine head and the injectors can be tested against a static pressure of 60 bar simulating the engine cylinder pressure near the end of the compression stroke. For single injector testing, five blanks were installed in the EFS1. This EFS1 uses natural gas (rather than nitrogen), but the diesel was again replaced by Viscor. In order to determine the gas flow response to changes in commanded pulse width as well as changes in diesel injection mass, the mass flow rate of the diesel was measured gravimetrically (pail and scale), while a coriolis flow meter was used to measure the mass flow rate of the gas.

Chapter 4 –Results

4.1 Overview of Testing

Tests for this study were conducted so that the flow and combustion characteristics of two injector geometries could be compared. Table 4.1 shows the 8 different test series (I – VIII) used in this study as well as the engine location and engine setup for each test. Three of these test series (I, VII, and VIII) were repeated with Prototype A and Prototype B.

Flow characterization (I and II) of the prototypes was conducted at Westport Innovations (Section 4.2.1 and Section 4.2.2). All other test series (III – VIII) were conducted at UBC with different combinations of test cell location, piston geometry and injector geometry as shown in Table 4.1.

Series III, IV, and V were conducted in the engine using one injection per cycle, making it possible to determine the gas and diesel flow characteristics of each injector. Two series (VI and VII) compared single and double injection operation to determine the influence of the second injection on the first (pilot) injection. Finally, Series VIII examined the combustion variability, knock and emissions for a few standardized operating modes.

Table 4.1: Chronological Overview of Test Series

Test Series - Injector Prototype	Test Location, Apparatus	Start Date (dd-mm-yy)	End Date (dd-mm-yy)	Operator	# of Tests	# of Repeats	Total # tests	Compression Ratio	Charge Amplifier	Injections per Cycle
VIII-A	SCRE, Kaiser	09-01-06	13-01-06	HJ	9	6	15	16.7	Kist. 503	2
I-A	BTR2, Westport	09-03-06	09-03-06	KI	11	0	11	-	-	1
III-A	SCRE, Kaiser	21-03-06	22-03-06	GMC	43	0	43	15	Kist. 503	1
IV-A	SCRE, Kaiser	22-08-06	22-08-06	SB	10	0	10	15	Kist. 503	1
VI-A	SCRE, Kaiser	22-08-06	22-08-06	SB	18	0	18	15	Kist. 503	2
VII-A	SCRE, Kaiser	13-09-06	15-09-06	SB	16	14	30	15	Kist. 503	1,2
VII-B	SCRE, CERC	17-12-07	15-01-08	SB	40	37	77	15	Kist. 503	1,2
VIII-B	SCRE, CERC	22-02-08	26-02-08	SB	9	15	24	16.7	Kist. 504D	2
II-B	EFS1, Westport	29-02-08	11-03-08	KI	23	0	23	-	-	1
I-B	BTR2, Westport	27-03-08	27-03-08	KI	11	0	11	-	-	1
V-B	SCRE, CERC	13-06-08	13-06-08	SB	11	0	11	16.7	AVL FlexIFEM	1
VIII-B2	SCRE, CERC	09-06-08	13-06-08	SB	30	3	90	16.7	AVL FlexIFEM	2

* HJ = Heather Jones, KI = Koyo Inokoshi, SB = Scott Brown, GMC = Gord McTaggart-Cowan

4.2 Single Injection Flow Characterization

Five different tests were conducted with single injection operation: two at Westport Innovations on flow benches to characterize the gas flow (Test Series I and II) and three at UBC in the SCRE (Test Series III, IV, and V). The results from these tests are described hereafter.

4.2.1 Test Series I and II: Flowbench Tests at Westport Innovations

The BTR2 injector flow characterization rig was used for Test Series I for both injector prototypes. Table 4.2 shows the range of variables tested for both test series.

Table 4.2: Controlled Parameters for Test Series I and II: Westport Flowbenches BTR2 and EFS1

	Test Series I	Test Series II
Simultated Engine Speed (RPM)	1800	1200
Gas Rail Pressure (Mpa)	16	23
Diesel - Gas Bias Pressure (MPa)	0.5 - 0.8	1.2
Back Pressure (bar)	80	60
RIT (ms)	n/a	1
Gas	Nitrogen	Natural Gas
Liquid	Viscor	Viscor
GPW (ms)	0.5 - 3	0.45-0.7
DPW (ms)	0	0 - 2
# Tests / Prototype	11 for A & B	23 for B

Test Series I provides important information about the gas flow over a wide range of GPWs; however, this flow test does not provide adequate resolution in the area of interest (0.5 – 0.7 ms GPW), nor can it be used to determine the gas flow response to different diesel injection masses. In Series I (Figure 4.1) gas characterization tests were conducted in the BTR2 for both Prototypes A and B testing the gas injection separate from the diesel injection.

Prototype B (with the sleeve) exhibited 8 – 26% lower mass flow rates than Prototype A, depending on injection durations. At a gas pulse width (GPW) of 0.7 ms, the gas mass flow rate is 26% lower for Prototype B than it is for Prototype A. This reduction could be due to higher friction losses in the gas/diesel reservoir which would result in lower injection flows. The thick dashed lines in Figure 4.1 represent the acceptable injector-to-injector variability of Westport J-36 injectors. Both A and B were within these limits.

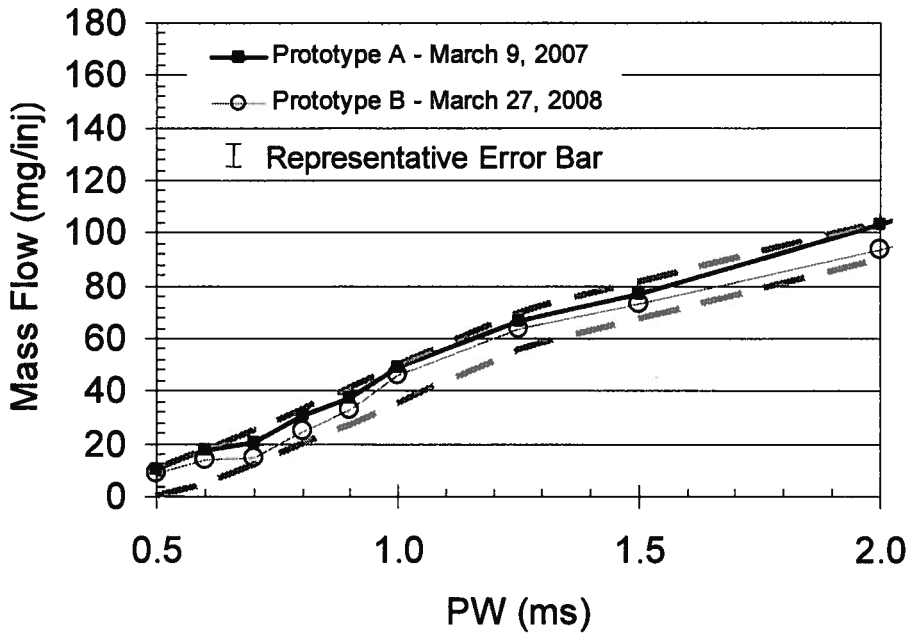

Figure 4.1: Gas injection mass as measured at Westport Innovations with only a gas injection

The EFS1 flowbench was used for Test Series II, in order to test the diesel and gas injections together. These were tested over a range of pilot GPWs and diesel injection masses common for normal operation. A full factorial test was conducted over 6 gas pulse widths (0.45 to 0.7 ms in 0.05 ms increments) and 4 diesel pulse widths (0 ms, 1 ms, 1.5 ms, and 2 ms) resulting in 23 data points (0.45 ms GPW w/ 0 ms DPW not tested). The diesel flow rate was calculated from the change of diesel mass for test durations between 10 and 20 minutes. The natural gas flow rates were averaged over 100 seconds at a collection rate of 1 Hz.

For the EFS1 flowbench, only Prototype B was tested. Figure 4.2 shows the results of the GPW sweeps with different diesel fuelling amounts.

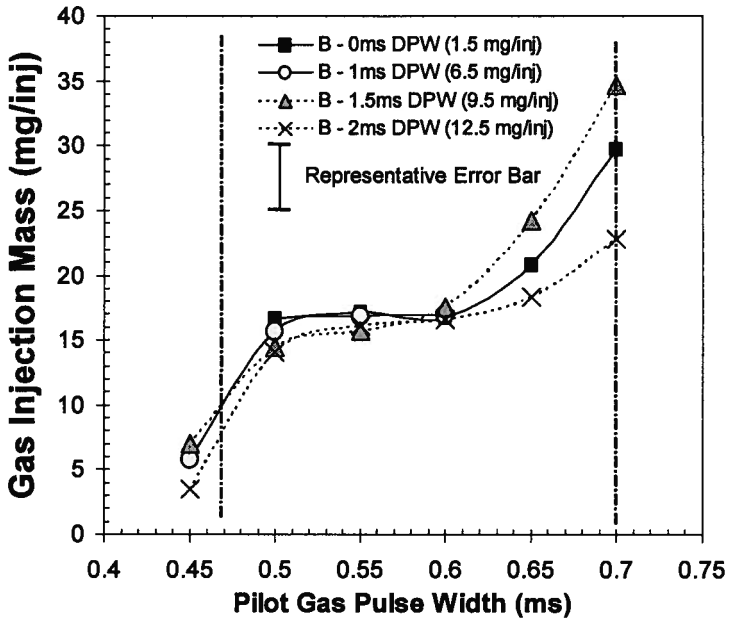

Figure 4.2: Gas injection mass as measured by the gas/diesel flowbench (EFS1) at Westport Innovations

For injection durations shorter than 0.5 ms, the gas injection mass drops off very quickly. For GPWs from 0.5 – 0.65 ms, the injection mass is, surprisingly, almost independent of the gas injection duration. The observed plateau in this test is likely not perfectly flat as shown but appears flat due to a quantization error. At pilot GPWs longer than 0.65 ms, the gas injection mass again increases. Because only one test was run at each condition, flow measurements were taken from SCRE experiments to check the trends.

4.2.2 Test Series III, IV, and V: Gas/Diesel Characterization of Single Injection Tests at UBC

Series III was performed by McTaggart-Cowan (2006) to determine the minimum diesel flow rate for low-load single-injection operation.. It is beneficial to study single injections to elucidate the behaviour of the pilot injection of normal double-injection operation. With

single injection operation, it is possible to estimate the gas and diesel masses for each injection from the averaged gas and diesel injection rate. With double injections, the distribution of masses among the two pulses is indeterminate. The single injection tests are shown in Table 4.3.

Table 4.3: Controlled parameters for Test Series III and IV: single injection tests in SCRE

	Prototype A												Prot. B	
Test Series	IIIa			IIIb					IIIc			IV	V	
Compression Ratio	15			15					15			15	16.7	
Gas Rail Pressure (MPa)	16.5			22.5					27.5			22.4	22.3	
Engine Speed (RPM)	800			800					800			800	800	
Diesel Rail Pressure (MPa)	18.5			24.7					29.5			24	24	
Pilot SOI (deg ATDC)	-10			-9.5					-7			-9	-8	
RIT (ms)	0.7			0.7					0.7			0.7	1	
MAT (°C)	unheated			unheated					unheated			70	56	
Test Point	1-4	5 - 8	9 - 11	12 - 15	16 - 19	20	21-23	24	25 - 28	29	30-32	1-6	7-10	1-10	11-14
Pilot GPW (ms)	0.75	0.75	0.75	0.7	0.7	0.6	0.6	0.5	0.6	0.6	0.6	0.65-min*	min* - 0.75	0.5 - 0.7	0.5 - 0.7
Diesel Injection Mass (mg/inj)	30	15	min*	30	min*	30	min*	min*	30	15	min*	17	23	22	15
Intake Manifold Pressure (kPa)	65 to 5	65 to 5	65 to 5	65 to 5	65 to 5	5	45 to 5	45	65 to 5	65	45 to 5	65	65	37	37

Test Series III was conducted at three different injection pressures whereas Series IV was conducted only at moderate injection pressures. Note that as the gas pressure increased, the pilot SOI was set to occur later and the pilot GPW is set to be shorter. This was done in an attempt to offset the effect of higher injection rates at higher injection pressures.

For these tests, the injection timings were chosen so that it would simulate the pilot injection for normal injection operation (McTaggart-Cowan 2006b). For Test Series III the intake air was unheated, resulting in temperature fluctuations in the intake manifold ranging from 20 to 30 °C. The intake air for Test Series IV, however, was heated to 70 °C.

Test Series V is a set of single-injection tests that was conducted with Prototype B, intended only to characterize flow as a function of commanded pulse width. The compression ratio was not the same for Test Series V as it was for Series III and IV, but the gas and diesel flow rates should be similar, at similar cylinder pressures. Assuming constant specific heat during compression of an ideal gas, the cylinder pressure, P_{tdc}, and the in-cylinder temperature, T_{tdc}, can be estimated using the compression ratio, CR, and the polytropic constant, n (Sonntag et al. 2003, 278). For these tests n was set to 1.35, which near both to the polytropic constant suggested by Heywood (1984, 385) and the constant found from the measured pressure rise during the compression stroke.

$$P_{tdc} = P_{bdc} \times (CR)^{n} \tag{4.1}$$

$$T_{tdc} = T_{bdc} (CR)^{n-1} \tag{4.2}$$

Dropping the MAP from 60 kPa (for Test Series IV case) to around 40 kPa keeps the peak cylinder pressures nearly constant. Similarly, a MAT of 56°C (329 K) will lead to similar in-cylinder temperatures close to that of the lower CR tests with a MAT of 70 °C.

For different injection pressures, pilot GPWs, injection masses and manifold pressures, the fuel specific emissions, combustion variability, and ignition delay were calculated. The diesel injection mass or pilot GPW "min*" refers to the minimum amount of diesel or gas necessary to maintain stable combustion and may change from test point to test point (as seen in Figure 4.3). The intake manifold pressure was changed in 20 kPa increments.

The importance of matching the in-cylinder pressures for injector comparisons can be seen in Figure 4.3. In this data from Test Series III conducted by McTaggart-Cowan and re-analyzed for this study, the amount of gas injected changes with manifold air pressure.

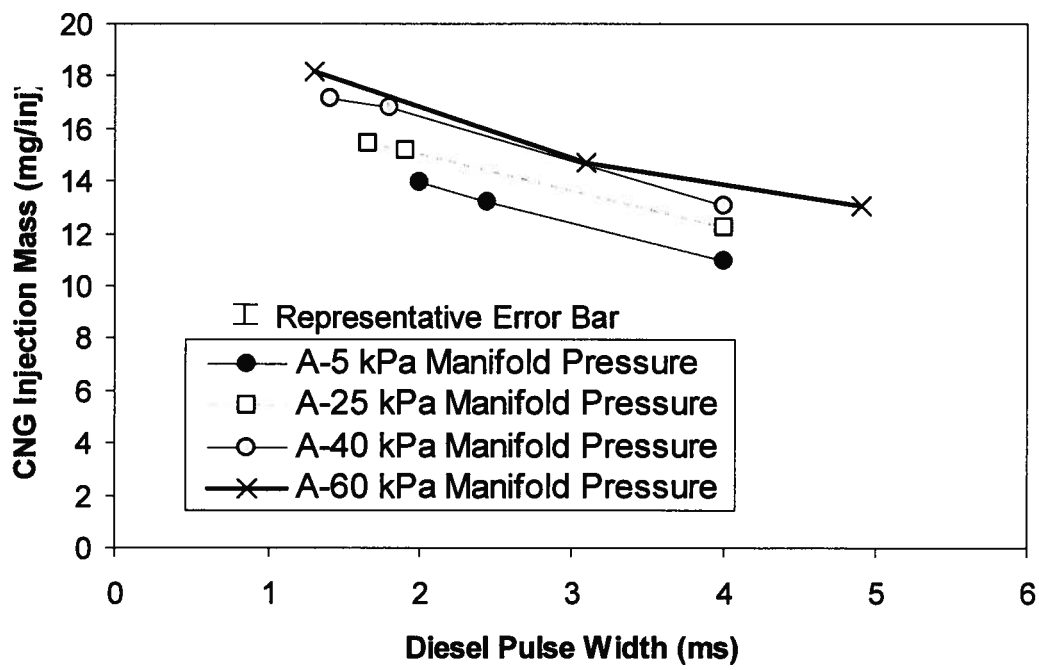

Figure 4.3: Changes in CNG injection mass with increased diesel injection mass at different manifold pressures (Test Series IIIa). 800 RPM, 16.5 MPa gas injection pressure, 0.75 ms GPW

Note that the minimum diesel pulse width is shorter for higher manifold air pressures. At the time of commanded injection, the diesel fuel used to hydraulically hold the injector needle closed is drained from the injector. Higher cylinder pressures may cause the opening force to overcome the closing force sooner so that the injector needle lifts sooner, leading to an earlier injection of the gas/diesel mixture. The actual injection duration (as opposed to the commanded duration) is increased (Jones 2005b; McTaggart Cowan 2006b). Also seen in this figure is the effect of diesel pulse width on the amount of gas injected. The gas injection mass decreases as the amount of diesel injected increases.

Figure 4.4 compares the gas injection mass rates of prototypes A (Series IV) and B (Series V). The gas flows are lower for Prototype B, consistent with the Westport BTR2 tests (Figure 4.1). Additional tests with Prototype B and the 16.7:1 piston and 60 kPa MAP produced flows that were higher than the Protype B flows of Figure 4.4 but lower than the Prototype A flows of Figure 4.4.

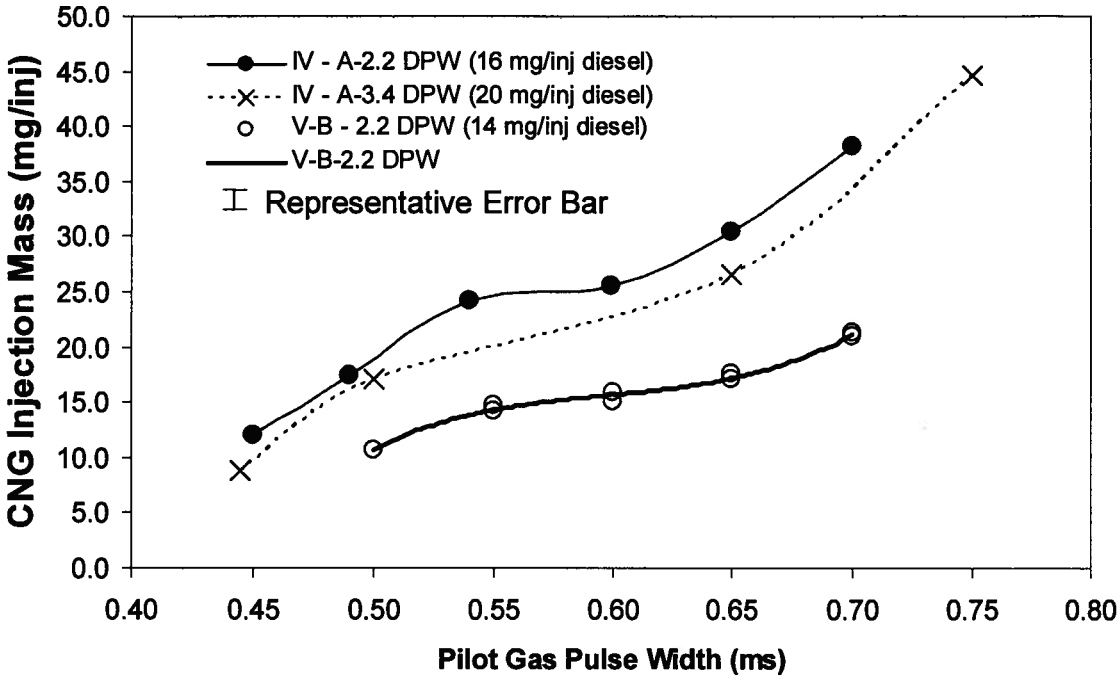

Figure 4.4: Comparison of Gas injection mass of Prototype A and Prototype B measured in the SCRE

Similar to BTR2 flowtests shown in Figure 4.2, the dependence of gas injection mass on pilot GPW is non-linear. For Prototypes A and B, the CNG injection mass decreased with increasing diesel injection mass for all GPWs. This behaviour makes sense, but contrasts with some of the Westport tests (see Figure 4.2).

4.3 Test Series III and IV: Single Injection Emissions and Combustion Characteristics for Prototype A

The series III and IV tests were conducted for a wide range of conditions and were not originally conceived as a systematic study of single-injection operation. Nevertheless, certain patterns emerge that will be useful in understanding the series VII and VIII double-injection experiments. Figures 4.5-4.7 show the ignition delay, COV GIMEP, and fuel

specific emissions plotted as a function of the gas/diesel volume ratio (GDVR), which is defined as

$$GDVR = \frac{\rho_{diesel}}{\rho_{gas}} \times \frac{m_{gas}}{m_{diesel}} \tag{4.3}$$

Where ρ is the fluid in-cylinder density at the time of injection and m is the mass injected. The natural gas density inside the combustion chamber is approximated by the peak cylinder pressure, and the start of combustion is approximated by the 5% IHR, consistent with the work done by McTaggart-Cowan (2006b). While one can't expect this ratio to characterize all aspects of the combustion, it is clear from the figures that the emissions and ignition delay converge towards low GDVRs, for a wide range of conditions. At high GDVRs, the combustion is apparently more sensitive to other factors that would require further study.

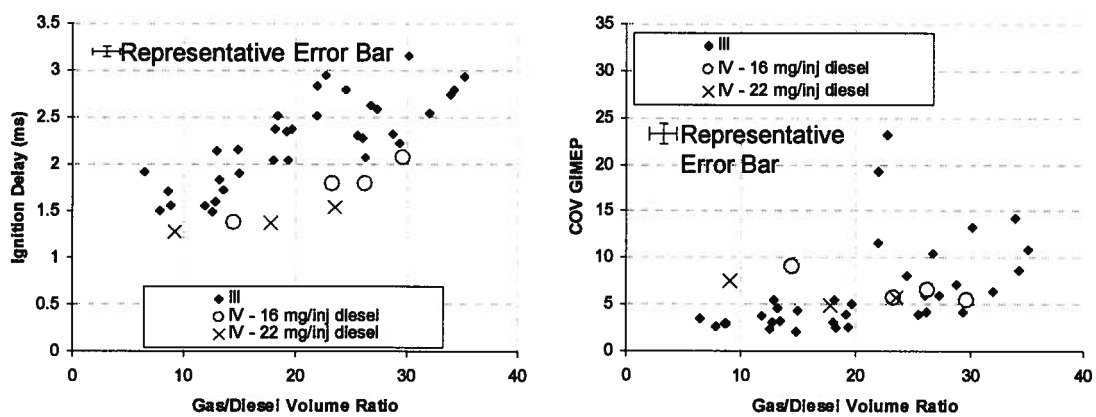

Figure 4.5: Ignition delay and COV GIMEP vs. gas/diesel volume ratio (Single Pulse)

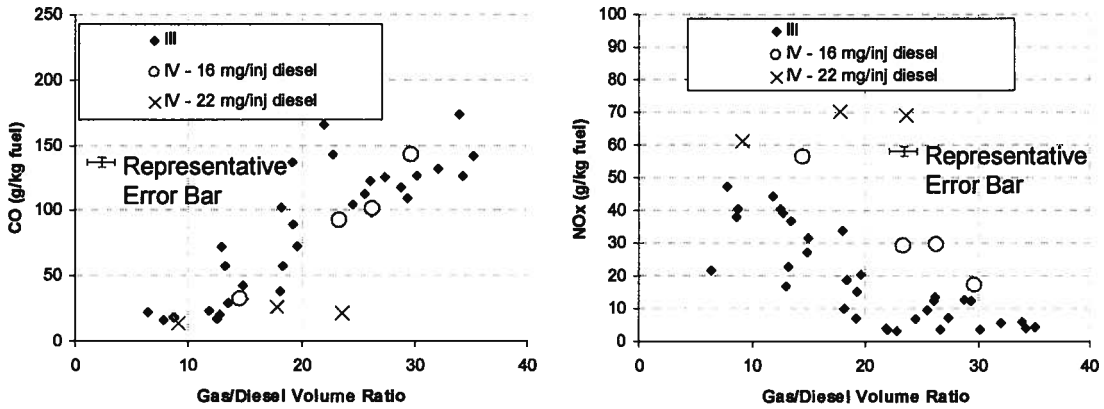

Figure 4.6: CO and NOx vs. gas/diesel volume ratio (Single Pulse)

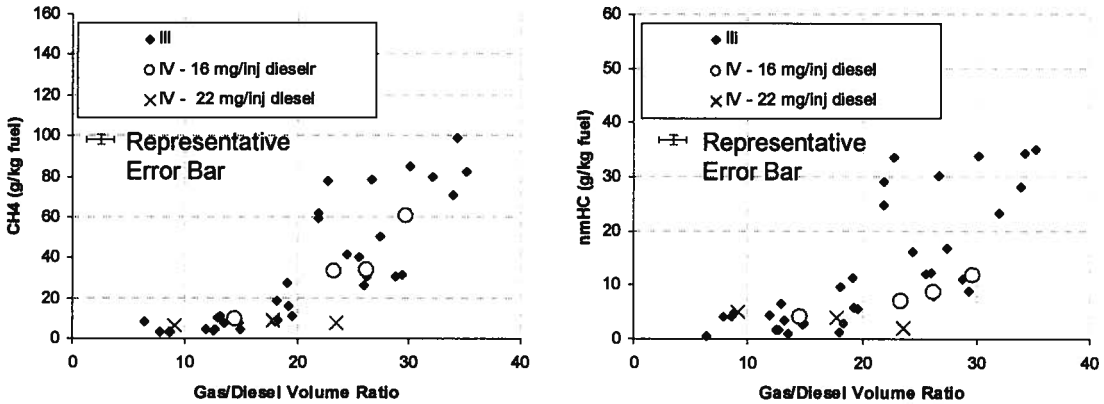

Figure 4.7: CH_4 and nmHC vs. gas/diesel volume ratio (Single Pulse)

The results of Test Series III and IV show that the observed correlations between emissions and GDVR might be related to the ignition delay (Figure 4.5). The smaller diesel quantities in Test Series III (i.e. larger gas/diesel volume ratios) resulted in the diesel being more dispersed throughout the gas so that the diesel would take more time to form an ignitable mixture with the air in the combustion chamber. Since the start of combustion was retarded and more variable this resulted in higher uHC. Similarly, increased gas injection mass in Test Series IV would also lead to less likelihood of having an ignitable mixture shortly after

the pilot injection. For single injection operation, the combustion stability did not appear to have a significant influence on emissions.

4.4 Test Series VI and VII: Pilot/Main Injection Interactions

Except at extremely low loads, the HPDI co-injector operates with double injections (both a diesel/gas pilot injection and a main gas injection). If the co-injector is to operate with lower diesel quantities, multiple injections are required at higher loads and speeds. Single injection operation at high speed would require high diesel mass injection rates to increase the likelihood of the injected diesel mixing with the combustion air to an ignitable mixture. However, as discussed in Section 2.3.2, lower diesel injection masses are desired in order to maintain an acceptable knock intensity level. Lower diesel injection rates require shorter gas pulse widths in order to maintain low gas/diesel volume ratios and thus acceptable combustion variability and uHC emissions. A main gas injection is therefore required after the primary pilot injection for high loads and/or engine speeds.

Also, for diesel fuelled engines, significant NOx emission reductions for similar PM emissions can be achieved with multiple injection operation (Nehmer and Reitz 1994; Ghaffarpour *et al.* 2006). The same amount of energy is being released over a longer period, resulting in cooler cylinder temperatures and thus lower NOx. PM emissions would also be also lower as the soot producing regions at the jet tips are broken down and restarted with the second injection (Nehmer and Reitz 1994; Ghaffarpour *et al.* 2006). Double gas injection operation for the HPDI co-injector could potentially have similar effects.

Two different tests (VI and VII) were conducted with double-injection operation. Series VI examined the effect of the second injection on the first injection for a wide range of operating conditions. The results were qualitatively very similar to those of Series VII. However, Series VI had fewer repeats at each condition, so the trends were less clear than in Series VII. Therefore, Series VI results were moved to Appendix B.

Test Series VII was conducted in order to determine the significance of the interactions between the pilot injection and the main injection. For this test series, three test modes were conducted for each test. First, the engine was run normally with a double gas injection. At this mode, the main injection followed shortly after the pilot injection in order to ensure stable engine speed and low uHC emissions. For the second mode, the pilot injection pressure, timing and duration were held constant. The high speed data was recorded immediately after removing the main injection. The thermal mass of the piston and cylinder allowed the wall temperatures, and therefore the diesel evaporation rates from the walls was expected to be similar. This procedure was repeated for the third mode, except instead of removing the main injection, the main injection was retarded to past 10 degrees after top dead centre (10° ATDC).

The in-cylinder pressure and temperatures were controlled through control of the intake air pressure and temperature, as well as the back pressure. Back pressures higher than 30 kPa above the intake would cause the exhaust gas residuals to exceed a mass fraction of 0.03 (McTaggart-Cowan 2003). For VII tests, the back pressure was set under the intake pressure to minimize the amount of residuals. If there were no injection-to-injection variations and the pilot injection was truly independent of the main injection, then the heat release duration,

timing, and magnitude during the pilot combustion event would also be the same regardless of whether there was a main injection present.

Table 4.4 summarizes the different points that were tested for Test Series VII at 1200 RPM. Similarly, Test Series VII at 800 RPM (Test points 1-24) is also discussed in Appendix B. The sample times, operating parameters and performance measurements for each test can be found in Appendix E.

For these tests, the diesel flow rates were controlled at two different levels: low flow and high flow. Low diesel flow rates were controlled to around 10 mg/inj and high diesel flow rates around 20 mg/inj. However, the exact control of the diesel flow rate was found to be time consuming. It appeared that fluctuations in the bias pressure and/or extra noise on the scale may have been a contributing factor. Therefore for VII Series tests, some control over the diesel injection mass was sacrificed for longer sample times in order to ensure accurate mass flow measurements. These tests were recorded from 180s to 300s. In addition, at moderate speeds, the pilot injection by itself was not sufficient to run the engine. In both locations for the SCRE, the engine speed was reduced by up to 12% at 1200 RPM when the main injection was removed. The implications of this are discussed in Section 4.4.1.

Table 4.4: Test Matrix for Test Series VII: Normal Double, and Retarded Double Injection Operation in SCRE for both Prototype A and Prototype B. Engine Speed: 1200 RPM, manifold temperature: 70 °C, MAP–90 kPa, exhaust pressure–50 kPa, 2RIT ~ 1.3 ms

Test Point	Diesel Rail Pressure (MPa)	Diesel Injection Mass (mg/inj)	Pilot Gas Pulse Width (ms)	Bias Pressure (Diesel - Gas) MPa	Pilot Start of Injection (deg ATDC)	# of Repeats Prototype A	# of Repeats Prototype B
25	18	Low	0.47	2.5	-17	0	0
26	18	Low	0.7	2.5	-17	0	1
27	18	High	0.47	2.5	-17	0	0
28	18	High	0.7	2.5	-17	0	0
29	24	Low	0.47	2.5	-17	6	1
30	24	Low	0.7	2.5	-17	3	3
31	24	High	0.47	2.5	-17	4	1
32	24	High	0.7	2.5	-17	3	4
33	28	Low	0.47	2.5	-17	0	3
34	28	Low	0.7	2.5	-17	0	3
35	28	High	0.47	2.5	-17	0	4
36	28	High	0.7	2.5	-17	0	4
37	18	Low	0.47	1.0	-17	0	3
38	18	Low	0.7	1.0	-17	0	3
39	18	High	0.47	1.0	-17	0	2
40	18	High	0.7	1.0	-17	0	2
41	24	Low	0.47	1.0	-17	1	1
42	24	Low	0.7	1.0	-17	0	1
43	24	High	0.47	1.0	-17	0	2
44	24	High	0.7	1.0	-17	0	1
			Total Number of Tests 1200 RPM			17	39

Unshaded regions in repetitions box: no data recorded.

For Series VII tests the diesel introduced during the pre-injection was assumed to be injected into the combustion chamber both during the pilot injection as well as the main injection. Sample Integrated Heat Release (IHR) and the Heat Release Rate (HRR) curves for the three operating modes are shown in Figure 4.8.

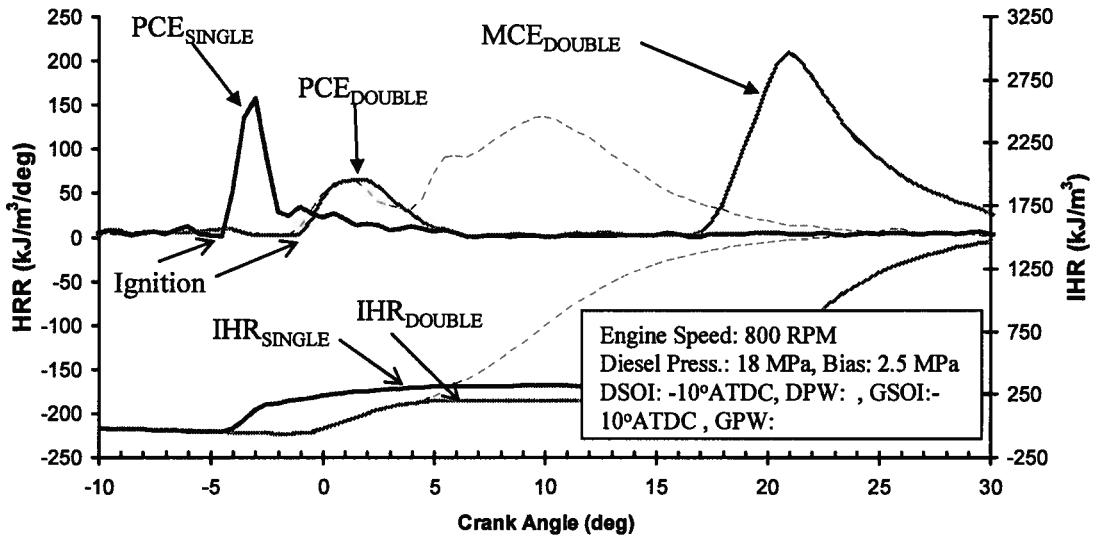

Figure 4.8: Representative HRR (Filtered) and IHR curves (Test Series VII-A- 4, 800 RPM, 22.0 mg/inj)

These curves are typical for the Series VII experiments. Note that for normal operation, two distinct combustion events were observed: the pilot combustion event (PCE) starting about -2° ADTC and the main combustion event (MCE) which starts about 4° ADTC. The MCE was greater in magnitude and longer in duration than the PCE. At lower diesel injection masses a lower magnitude PCE was observed.

Two combustion performance metrics used to quantitatively characterize the combustion performance are also displayed in Figure 4.8: the ignition delay and the IHR ratio. The ignition delay has been used previously and is defined in Section 3.1.6. Ignition was earlier for the PCE of the single injection mode (PCE_{SINGLE}) compared to PCE_{DOUBLE}. The

integrated heat release for single injection (IHR_{SINGLE}) and IHR_{DOUBLE} were found at the end of combustion of the PCE (crank angle where HRR<10 kJ/m^3/deg). Note in Figure 4.8 that the IHR_{SINGLE} was greater in magnitude than IHR_{DOUBLE} for the PCE, indicating that more heat was released during the PCE of the single injection mode. The IHR ratio is defined as $IHR_{DOUBLE}/IHR_{SINGLE}$.

As seen later in this section, for Series VII tests, the ignition delay was affected significantly by the diesel injection mass. The ignition delay for these tests is indicative of the ignitability of the fuel injected. Since the diesel is the fuel used for ignition is already finely atomized, shorter ignition delays may indicate that more diesel is available to mix with the combustion air early in the combustion cycle. The other factors affecting ignition delay for these test series are discussed briefly in Section 4.4.1.

The IHR ratio is a comparison of both the energy of fuel injected and the combustibility of the mixture through the compression and power stroke. At lower engine speeds, higher diesel injection masses, larger pilot GPWs, or higher pressures, higher IHR ratios were observed (see Appendix E/Appendix F). Ignition delay and IHR ratio may be correlated since a longer ignition delay may lead to over-leaning of the fuel before ignition. Also, longer ignition delays push the PCE further into the expansion stroke increasing the likelihood of bulk extinction. Therefore the longer ignition delays for double-injection operation may lead to a lower-magnitude PCE.

IHR ratios lower than one can mean a number of things. First, it may indicate that for double injection operation that less energy is released per unit of fuel injected for the same amount (or increased levels) of fuel injected during the pilot injection. It was previously thought that

the change in timing and magnitude of the HRR curves due to main injection addition was due to flame quenching and/or ignition delay from the addition of a cool turbulent jet during the main injection (Jones 2006). Note in Figure 4.9 the PCE_{DOUBLE} is nearly the same for the retarded and normal double injection. If there were adverse interactions between the PCE and the main injection, a significant difference would be observed with the PCE during normal double and retarded double injection operation. Low IHR ratios may also indicate that for double injection operation the same amount of energy is released per unit of fuel, but less fuel is injected. Without an accurate combined flow/combustion model, however, it is almost impossible to separate the importance of each factor.

The observed differences in the HRR traces might be explained by gas/diesel interactions inside the injector shown schematically in Section 2.3.1 (Figure 2.3). It is likely that the high diesel velocity (10-80 m/s) during the pre-injection distributes the diesel through the injection reservoir both as a thin film on the reservoir walls as well as droplets mixed with the gas. As the injector opens during the pilot injection, the gas/diesel mixture will be injected into the combustion chamber. Since the diesel pre-injection essentially occurs a full cycle before the main gas injection it is assumed that the removal of the main gas injection will not affect the mass of diesel injected. A portion of the diesel will be retained in the reservoir after the pilot injection, dependent on reservoir geometry and the distribution of the diesel in the reservoir. Marr (2007) observed that the injector achieved steady state almost instantaneously which was also observed when the main gas injection was removed.

The conceptual model is effective in explaining some of the observed differences between single and double injection operation. For single-injection operation, the retained diesel will

be injected with the following pilot injection and will therefore be a factor in reducing the ignition delay, since the added diesel will increase the likelihood of the diesel mixing with the combustion air. For double-injection operation, this diesel will be injected during the main injection where ignition has already occurred. Since more diesel is injected into the combustion chamber during the pilot gas injection, the IHR will be higher for the PCE which will reduce the IHR ratio.

4.4.1 Other Factors Affecting Ignition Delay and IHR ratio

For both prototypes the relative injection timing (RIT) between the end of the pre-injection to the beginning of the pilot injection was changed while the start of the pilot injection remained relatively the same. Prior to these tests, Jones (2006) found that the RIT had very little effect on the HRR or emissions. These tests, however, were not conducted over a wide range of RITs or diesel injection masses. Figure 4.9 shows the HRR curves for different RITs for Prototype A at a low diesel injection mass (between 10 – 15 mg/inj). It appears that the timing of the diesel injection into the gas/diesel reservoir makes a difference to the HRR curve. As seen in the HRR curves in Appendix F.2, at longer pilot GPWs and higher diesel injection masses, the difference is less evident. The RITs that result in the shortest ignition delay seem to be negative RITs and those close to 0. It is clear that although RIT may not affect the shape of the HRR (in some cases), it can affect the start of combustion. This is consistent with the conclusions of Jones (2006) as shown in Section 4.5.2.

Also of significance in Figure 4.9 are the diesel to pilot RITs of 1.10 ms, 1.25 ms, and 1.45 ms. These test points resulted in significantly higher CH_4 and uHC emissions. The diesel

injection mass for these cases was found to be significantly lower (around 10 mg/inj as opposed to 15 mg/inj as found in Appendix E.2).

The mechanism of how the RIT affects diesel injection mass and combustion is unclear. From Figure 4.9 it appears that the timing of the injection is important, which may indicate an optimal distribution of the diesel within the gas/diesel reservoir. Whether or not the RIT affects the needle opening time is also unclear. Additional testing is required to determine more conclusively the relationship between RIT and ignition.

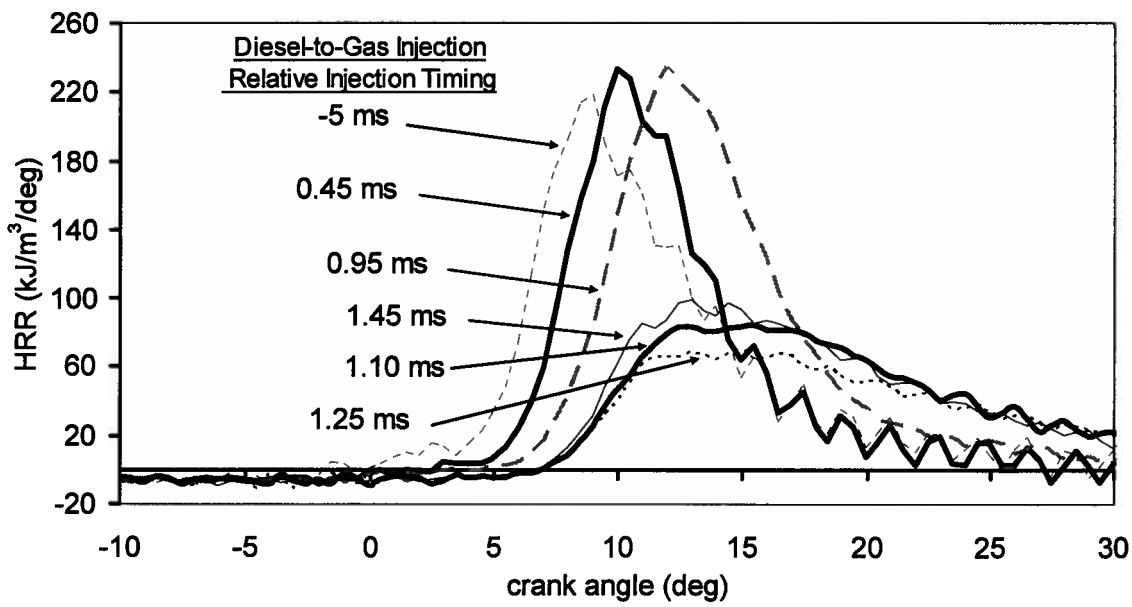

Figure 4.9: Comparison of HRR curves for different relative injection timing. Double injection tests at a low diesel injection mass (VII-A-29)

Pilot injection pressure, pilot timing, intake and exhaust air pressures, intake manifold temperature, and engine speed are relevant factors that affect ignition delay (Heywood 1988, 546). Although these parameters are controlled, as discussed in Section 3.3.4, perfect

control of these parameters is nearly impossible considering the variation in load applied during single and double injection operation and the difficulty in control of these parameters in the SCRE. In the absence of the main injection at 1200 RPM, the engine speed may fall by as much as 12% (150 rpm), due to the difficulty the dynamometer and electric drive motor have of instantaneously reacting to the change in fuelling. A reduction in engine speed would be expected to show lower IHR ratios since at lower engine speeds there is more time before the expansion stroke for combustion to occur, increasing the magnitude of PCE_{SINGLE}.

At lower engine speeds, less swirl changes the fuel evaporation rates as well as the mixing processes. In addition, lower peak compression temperatures will result from more heat lost per stroke (Heywood 1988, 546). At reduced engine speeds, longer ignition delays are therefore expected.

In comparing double to single injection in Test Series VII-A there is a possibility that lower engine speeds would result in shorter ignition delays. As mentioned in Section 3.2.1, the start of the pilot injection for Test Series VII-A occurs before TDC based on a measured time rather than measured crank angle; therefore, the actual crank angle the pilot injection begins will be closer to TDC at lower speeds. It is likely that the pilot injections closer to TDC will reduce the ignition delay, since the initial temperatures and pressures inside the combustion chamber are higher. The expected change in ignition delay due to higher in-cylinder pressures, however, would only partially explain the shorter ignition delays observed for single injection operation. Also, this change is only applicable to the high speed tests from Test Series VII-A since no significant speed change was observed at 800 RPM and the

injector control for Test Series VII-B ensured the pilot injection occurred at the same crank angle when the main injection was removed.

4.4.2 Comparison Between VII-A and VII-B: Injector Geometry Effects on Ignition Delay and IHR ratio, 1200 RPM

Figure 4.10 shows representative HRR curves for Prototype A at 1200 RPM, whereas Figure 4.11 shows the same for Prototype B. The vertical lines represent the start of commanded diesel pre-injection, pilot injection, and main injection (around -30, -17, -5 deg BTDC). Note that the main gas injection is later for higher pilot GPWs since the 2RIT is held constant.

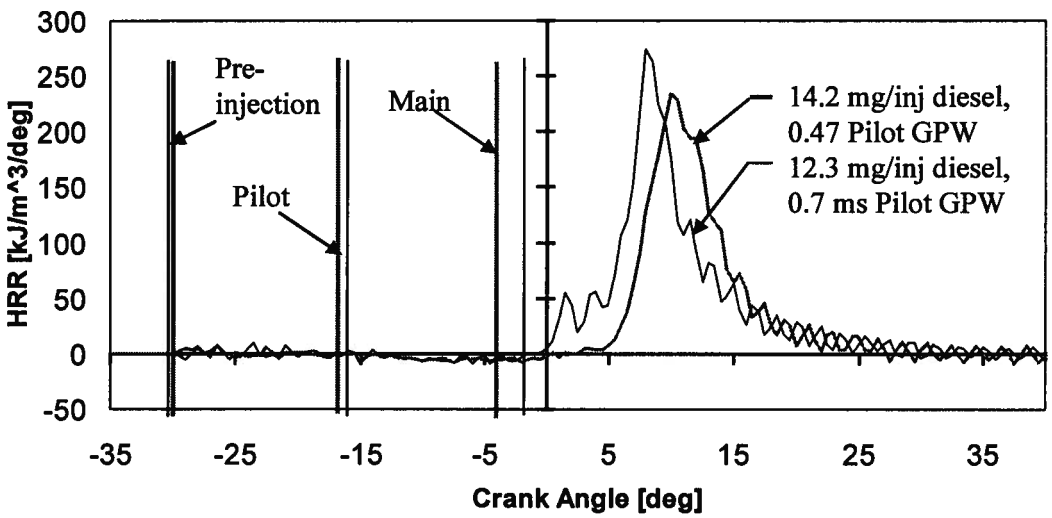

Figure 4.10: Unfiltered HRR curves for Prototype A at 24 MPa Diesel Rail Pressure (VII-A-29 and VII-A-30)

For Prototype A, longer GPWs resulted in an advanced start of combustion, whereas for Prototype B, the start of combustion was not dependent on the GPW. In addition for some of the low diesel injection masses and with short pilot GPWs, no significant PCE was observed for Prototype A. On the other hand a distinct PCE was observed for Prototype B for nearly

the same conditions. The absolute start of combustion was also observed to be sooner for Prototype B.

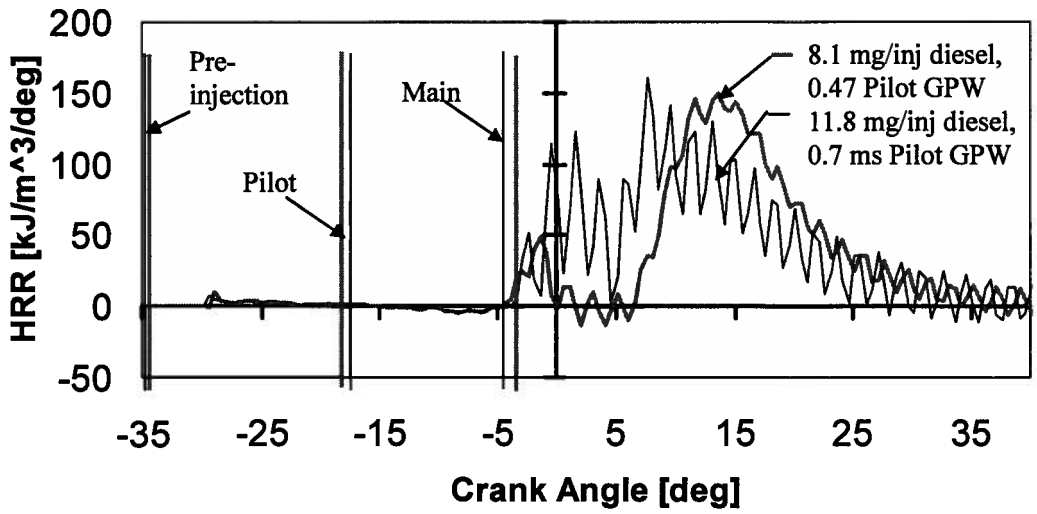

Figure 4.11: Unfiltered HRR curves for Prototype B at 24 MPa Diesel Rail Pressure (VII-B-29 and VII-B-30)

In order to determine whether the trends observed in Figures 4.10 and 4.11 hold true for different diesel injection masses, Figure 4.12 shows the measured ignition delay for both Prototype A and Prototype B at 1200 RPM and 24 MPa diesel rail pressure for different diesel injection masses. Since no difference was observed in ignition delay between the high and low bias cases, these are plotted on the same figure. Note that the test points with no measurable PCE have been identified with a "+", since the ignition delay is also dependent on the main injection timing for these cases. For these points, ignition delays greater than 3 ms were typical for Prototype A. For Prototype B, there was always a PCE present, even at low diesel injection masses.

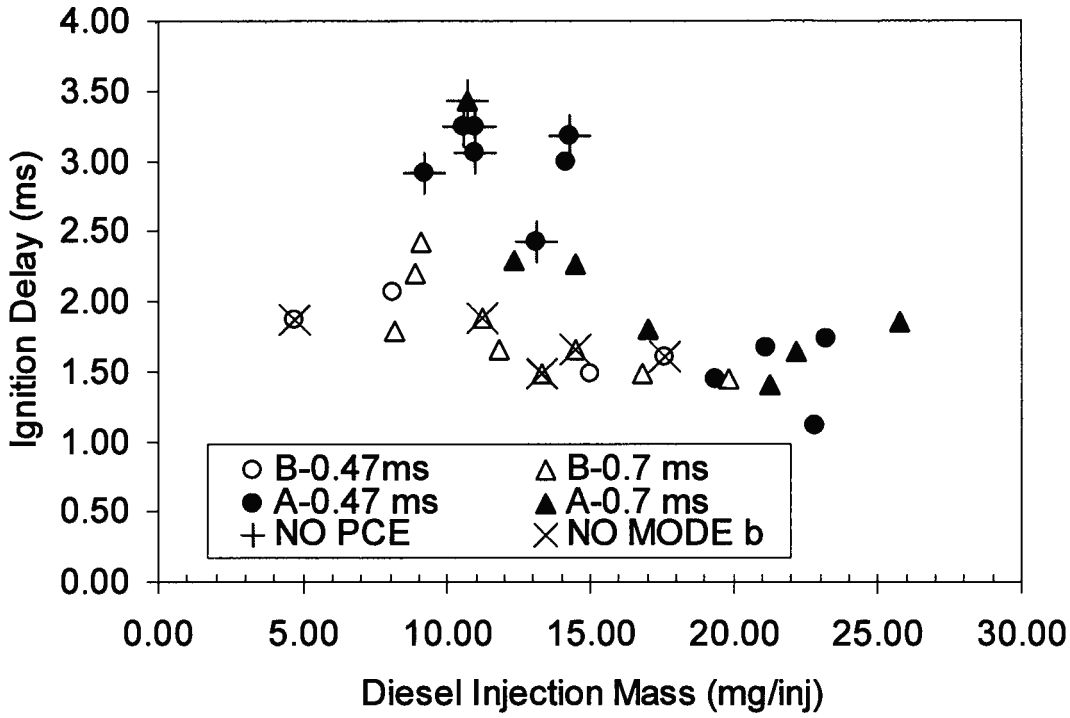

Figure 4.12: Ignition Delay comparisons between Prototype A and Prototype B at 1200 RPM, 24 MPa diesel rail pressure

Two observations can be made about the difference in ignition delay between Prototype A and Prototype B. First, the ignition delay for Prototype B is consistently shorter than the ignition delay for Prototype A, especially at lower diesel injection masses. At larger injection masses, it is unclear whether there is a difference in ignition delay between prototypes. Ignition delay for Prototype B is less dependent on the diesel injection mass and therefore, as the ignition delay increases for Prototype A, the ignition delay for prototype B stays around 2 ms. This indicates that for Prototype B, the fuel mixture is more ignitable.

Second, the minimum diesel needed for stable operation was observed to be significantly lower for Prototype B. For Prototype A, diesel injection masses under 12 mg/inj resulted in high COV GIMEP and methane emissions indicative of total or near-total mis-firing of the

engine. Similar engine variability was observed in Prototype B around 8 mg/inj. The fact that there was always an observed PCE for Prototype B, even if it was very small, may have had an influence on lower attainable diesel injection masses.

Figure 4.13 shows the knock intensity (defined in Section 3.2.4) plotted against diesel injection mass for both Prototype A and B. Although it appears that Prototype B has higher knock intensity than Prototype B, the difference is far less evident than the difference in ignition delay.

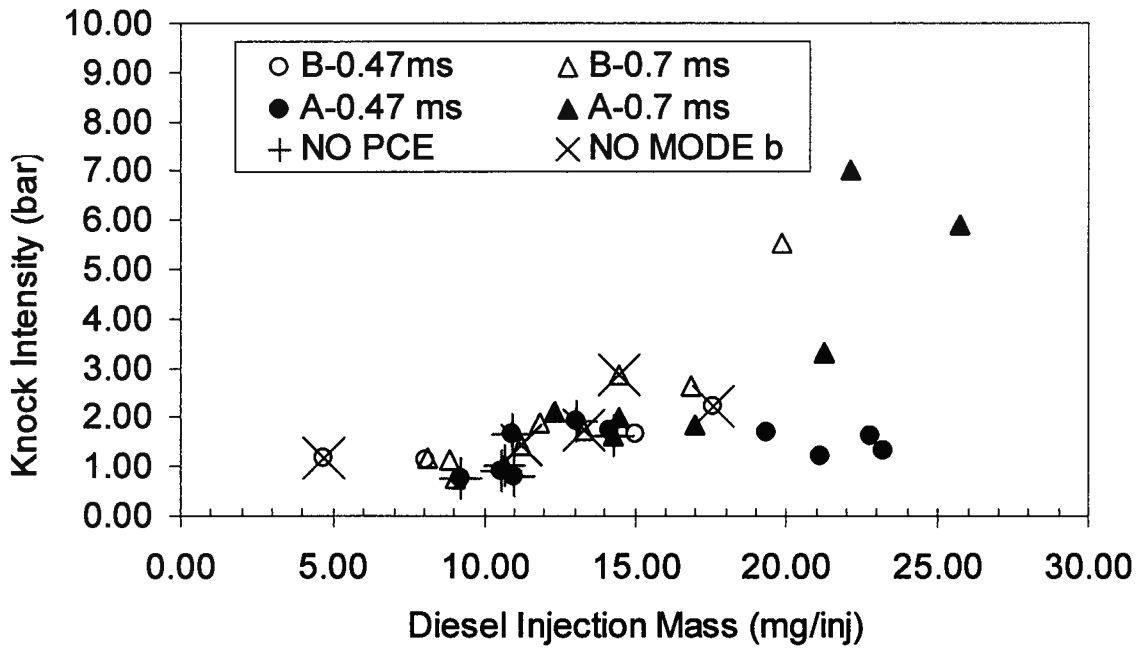

Figure 4.13: Knock Intensity comparisons between Prototype A and Prototype B at 1200 RPM, 24 MPa diesel rail pressure

For Prototype A there were many cases where a significant PCE was only observed with the main injection removed. For these cases, an IHR ratio of zero was assigned and plotted as "NO PCE". This does not mean that no fuel was injected during the pilot injection, rather

both diesel and gas were injected but not at a sufficient quantity to initiate combustion. Conversely, for some of the test cases for Test Series VII with Prototype B, there was no PCE present when the second injection was removed. These test points are indicated as "NO MODE b" tests in the Figures 4.12 to 4.14 (plotted with an "x"). At 1200 RPM, these test points were most often observed at low bias cases. Without injector visualization at low diesel-to-gas bias pressures, determining the source of injector variability is difficult.

Figure 4.14 shows the IHR ratio for Test Series VII for both Prototype A and Prototype B. Note that PCE_{SINGLE} was greater in magnitude for most cases than PCE_{DOUBLE}. For the same injector, the IHR ratio was closer to one at higher diesel injection masses and at longer pilot GPWs. At very low diesel injection masses, the IHR ratio is reduced as the ignition degraded and there was no observable PCE for all or some of the 45 cycles of recorded high-speed data. As the diesel mass increased, a lack of a significant PCE was less of an issue, but there still might have been diesel retained in the injector. If a specific amount of diesel was retained due to areas of low velocity or recirculation in the injector then the higher diesel injection masses would result in the observed higher IHR ratios since the fraction of diesel retained would be relatively less important. Similarly, longer pilot GPW durations would have higher IHR ratios since there would be more time to clear out the diesel and energy-wise the retained diesel would have less of an impact. There may also be a maximum amount of diesel which can be injected during the pilot injection (for a specific GPW). In this case, the IHR ratio would decrease as the diesel mass reaches its maximum. More measurements would be needed to determine the relative importance of each model.

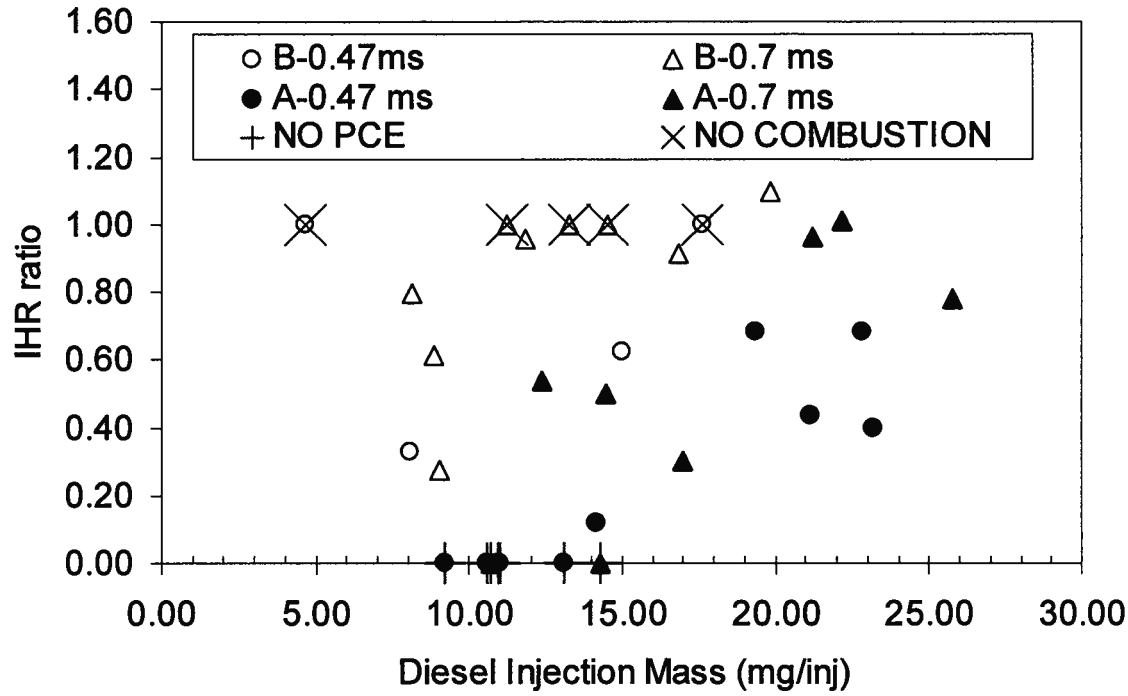

Figure 4.14: Ratio of heat released during the Pilot Combustion Event for Prototype A and Prototype B at 1200 RPM, 24 MPa diesel rail pressure

4.5 Test Series VIII: Emissions and Combustion for Multimode Timing Sweeps

The effects of double injection operation on combustion variability, emissions, ignition delay, and knock intensity were tested in the SCRE in Test Series VIII-A, VIII-B, and VIII-B2 (see Table 4.10) . These tests were conducted at three of the European Stationary Cycle (ESC 13) test modes (#7, #6, and #4) which are 30% load/1100 RPM, 75% load/1100 RPM, and 75% load/1400 RPM respectively. Test Series VIII-A was conducted by Jones (2006). Although the bias pressure was slightly lower for VIII-B and VIII-B2, the difference did not affect the operation of the injector since the diesel injection mass was held constant. The

exhaust manifold pressure would affect the residual fraction of exhaust gas retained in the cylinder and was therefore fixed to around 10 kPa (exhaust – intake pressure) for all tests.

As discussed in Section 3.2 the pre-injection could not overlap -60° ATDC in the CERC location since the comparators used for injection control are reset at this point. This is only important for the diesel pre-injections, since the fuel injection into the combustion chamber would not occur so early in the compression stroke. For Prototype B, the importance of pre-injection timing on emissions was investigated by changing the RIT.

Table 4.4 shows the four timing sweep test modes conducted for the three load/speed combinations. The baseline test mode consisted of nine test points (three timings for the three load/speed combinations) at a specified RIT, diesel injection mass, and pilot GPW. The RIT and diesel injection mass were then changed separately for an additional two test modes. Finally, the pilot GPW was changed from 0.7 ms to 0.6 ms for low speed/low load timing sweep. Shown also in Table 4.4 are the two tests conducted with Prototype B (B and B2) and the test conducted with Prototype A (A).

The measured values for the controlled parameters, combustion parameters, power specific emissions, and injection timing are tabulated in Appendix E and the indicated pressure and heat release rate curves are shown in Appendix F.

Table 4.5: Test matrix for Test Series VIII: double injection timing Sweeps for comparison of emissions in SCRE

Test Point	50% IHR (deg ATDC)	RIT (ms)	Engine Speed (RPM)	GIMEP (bar)	EQR	Diesel Injection Mass (mg/inj)	GPW (ms)	Repetitions A	B	B2
1	5	1	1100	6	0.3	15	0.7		2	5
2	10	1	1100	6	0.3	15	0.7		2	3
3	15	1	1100	6	0.3	15	0.7		1	4
4	5	1	1100	13	0.55	15	0.7	2	1	4
5	10	1	1100	13	0.55	15	0.7	6	2	4
6	15	1	1100	13	0.55	15	0.7	2		4
7	5	1	1400	13	0.55	15	0.7	1		3
8	10	1	1400	13	0.55	15	0.7	2		3
9	15	1	1400	13	0.55	15	0.7	1		3
10	5	-7.3	1100	6	0.3	15	0.7			3
11	10	-7.3	1100	6	0.3	15	0.7			3
12	15	-7.3	1100	6	0.3	15	0.7			3
13	5	-7.3	1100	13	0.55	15	0.7		2	3
14	10	-7.3	1100	13	0.55	15	0.7		2	3
15	15	-7.3	1100	13	0.55	15	0.7		2	3
16	5	-7.3	1400	13	0.55	15	0.7		6	2
17	10	-7.3	1400	13	0.55	15	0.7		6	3
18	15	-7.3	1400	13	0.55	15	0.7		5	3
19	5	1	1100	6	0.3	12	0.7			3
20	10	1	1100	6	0.3	12	0.7			3
21	15	1	1100	6	0.3	12	0.7			3
22	5	1	1100	13	0.55	12	0.7		3	3
23	10	1	1100	13	0.55	12	0.7		3	3
24	15	1	1100	13	0.55	12	0.7		3	3
25	5	1	1400	13	0.55	12	0.7		2	3
26	10	1	1400	13	0.55	12	0.7		1	3
27	15	1	1400	13	0.55	12	0.7			3
28	5	1	1100	6	0.3	15	0.6	1		3
29	10	1	1100	6	0.3	15	0.6	2		3
30	15	1	1100	6	0.3	15	0.6	1		3

4.5.1 Series VIII-B and VIII-B2: Effect of Operating Mode and Injection Parameters

In Section 4.4, the influence of the diesel pre-injection timing on combustion characteristics was briefly discussed. The influence of the RIT, diesel injection mass, and pilot GPW on emissions were not discussed for Test Series VII due to the intrinsic changes made to the load and equivalence ratio.

Figures 4.15 to 4.18 compare the combustion characteristics and power specific emissions for the four different test modes at low load/1100 RPM for the Test Series VIII-B and VIII-B2. Each figure compares the timing sweeps for the four test modes (baseline, -7.3 ms RIT, 12 mg/inj diesel, and 0.6 ms GPW). Similarly, Figures 4.19 to 4.22 and Figures 4.23 to 4.26 are comparisons at high load/1100 RPM and high load/1400 RPM respectively. Since the VIII tests were conducted at constant equivalence ratio and load, the response to different changes such as changes to the RIT, diesel injection mass, and pilot gas duration can be tested. Figures 4.15 to 4.26 show that the ignition delay is dependent on the diesel injection mass, that the effect of the diesel injection mass and relative injection timing are similar in many cases, that at low load the CH_4, tHC and CO emissions correlate strongly with the ignition delay, the NOx emissions were independent of diesel injection mass and relative injection timing, and that at higher loads the higher load test points have similar ignition delays but higher knock intensities.

First, the ignition delay gets shorter as the amount of diesel injected is increased. From Figure 4.15, the ignition delay was observed to be 3 ms for the low diesel injection mass (points 19-21) as opposed to 2 ms for the baseline (points 1-3). This trend was also observed in the Series VII tests (Figure 4.12). High load/1100 RPM (Figure 4.19), and high load/1400 RPM (Figure 4.23) also showed longer ignition delays for lower diesel injection masses, especially at advanced combustion timing. For a purely diesel fuelled engine, the amount of diesel injected (holding load constant) has little effect on ignition delay (Heywood 1988, 546). For the HPDI co-injector, the amount of diesel injected early in the injection cycle may play a critical role in the observed shorter ignition delay times for higher diesel injection masses. If more diesel were injected earlier during the injection process then this finely

atomized diesel would mix with the combustion air earlier leading to earlier combustion. As with the Series VII tests (Figure 4.12) the pilot GPW made little difference to ignition delay.

Second, increased RIT (as observed with a negative RIT) and reduced diesel injection mass had a similar effect on performance. From Figure 4.15, both increased RIT (VIII-B2 10-12) and lower diesel injection mass (VIII-B2 19 -21) had ignition delays longer than the baseline case (VIII-B2 1–3). This was more evident at advanced combustion timing. At high loads, the lack of a significant pilot combustion event at advanced combustion timing led to longer ignition delays and higher knock intensity, as some fuel which was injected during the pilot gas injection would potentially still be at the right combustible mixture at the time of ignition. Similar operation between longer RITs and lower diesel injection masses could both be related to the amount of diesel injected during the pilot gas injection. Longer dwell times between the diesel pre-injection and pilot gas injection mean that the diesel may be more distributed throughout the gas diesel reservoir, reducing the proportion that is available for ignition. Figures 4.16, Figure 4.20, and Figure 4.24 show that reduced diesel injection mass and increased RIT (negative RIT) had the same effect of reducing the knock intensity, especially at lower engine speeds.

Third, the CO, CH_4 and tHC emissions at low load/1100 RPM followed the ignition delay trends. Test modes with longer ignition delay resulted in higher CO, CH_4 and tHC emissions. It appears that at lower loads, longer ignition delay leads to overleaning of the fuel mixture which leads to higher CH_4 and tHC emissions.

At higher loads and higher engine speeds, there was little or no difference in these gaseous emissions, consistent with the tests by Jones (2006) which found the RIT made little

difference to the power specific emissions. At higher loads the CH_4 and tHC emissions are near the limits of detection (150 ppm and 230 ppm respectively) such that determining differences in emissions between test modes would be difficult.

Fourth, for Test Series VIII-B2, the advanced combustion timing was observed to increase the NOx emissions. Also, cases where there was no PCE (such as test points 22-24 in Figure 4.21 and test points 16-18 and 25-27 in Figure 4.25) NOx emissions were higher. NOx formation for non-EGR cases at constant speed and load should only be affected by the injection parameters (Heywood 1988, 863). NOx emissions were not affected by the RIT between the diesel and gas injections, diesel injection mass, or pilot GPW, indicative that the spray characteristics were not affected sufficiently to observe a difference in NOx emissions.

Finally, comparing the tests from low load/1100 RPM and high load/1100 RPM, the ignition delay is similar (Figure 4.15 vs. 4.19), but the knock intensity is greater (Figure 4.16 vs. Figure 4.20). Since the RIT is constant at 1 ms between tests, the pilot start of injection is advanced by about 2.5 degrees for the high load case. Based on the dependency of ignition delay on combustion timing, ignition delay should be longer for the higher load case due to an advanced pilot injection of 2 – 3 degrees. The similarity between the ignition delay and increase in knock intensity between low load and high load cases may be due to higher in-cylinder temperatures at higher loads. Hot walls and residuals would increase diesel evaporation rates and chemical reaction rates during both the ignition and premixed burn phases of combustion. This might explain why knock intensities increase even though ignition delay has not been extended due to the earlier injection.

Series VIII-B tests are also compared to VIII-B2 tests in Figures 4.15 to 4.26. Due to the variance in VIII-B tests, the NOx, CO, CH_4, and tHC emissions are for many modes similar to Test Series VIII-B2. Ignition was found to be similar for most cases; however, Test Series VIII-B2 showed longer ignition delays at advanced injection timing. In addition, at low load, the CO, CH_4 and uHC are predictably lower for VIII-B tests. The differences could be related more to variation in the controlled operating conditions rather than any variations in the injector. Since the airflow for Series VIII-B tests was based on an assumption that the airflow included unresolved air leaks (see Section 3.1.5) the intake pressure was slightly higher for VIII-B tests, resulting in earlier injector needle opening times. Since the air leaks have been resolved, engine control has been reasonably controllable over a wide range of injection timings and engine speeds.

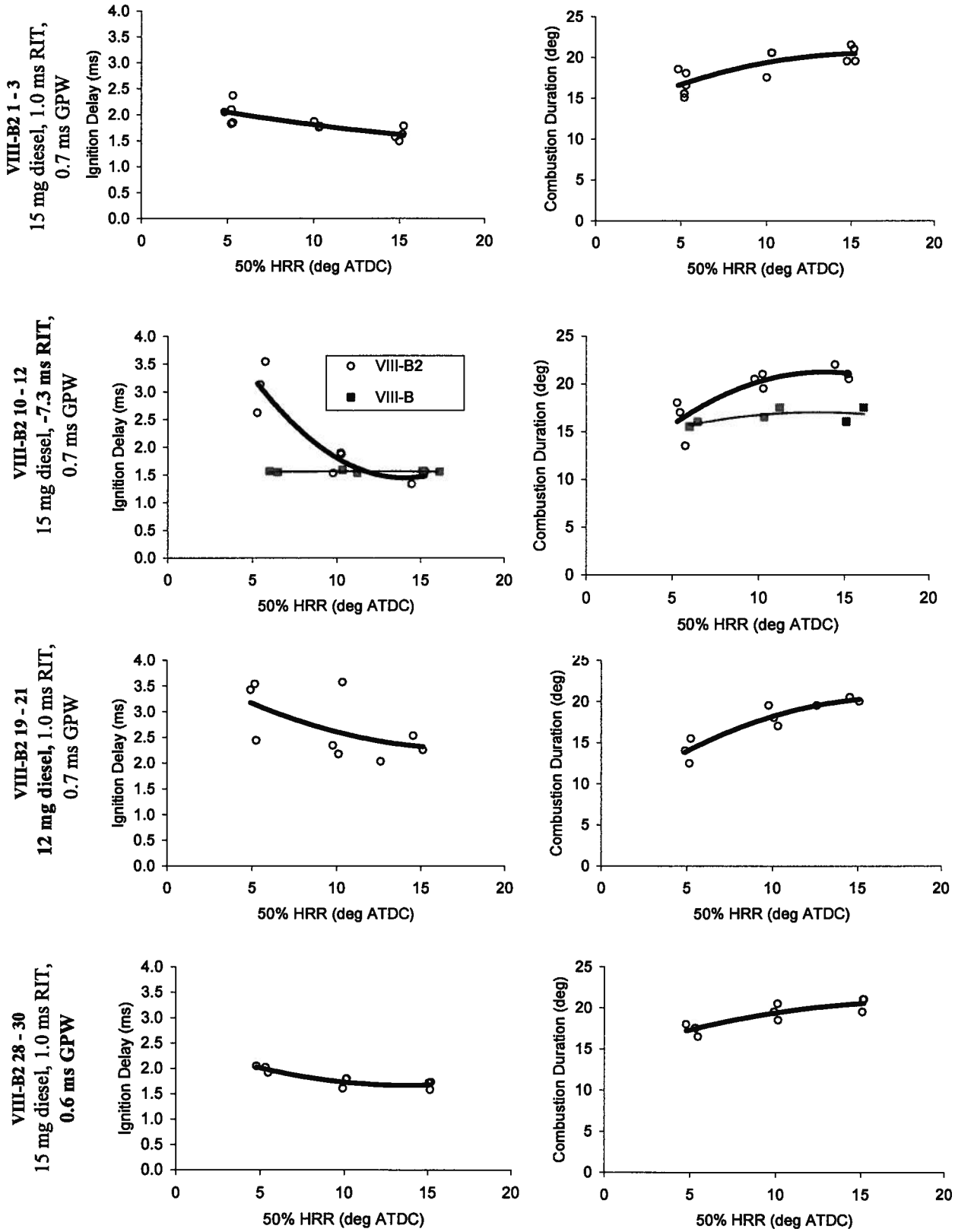

Figure 4.15: Ignition delay and combustion duration for 1100 RPM and 6 bar GIMEP

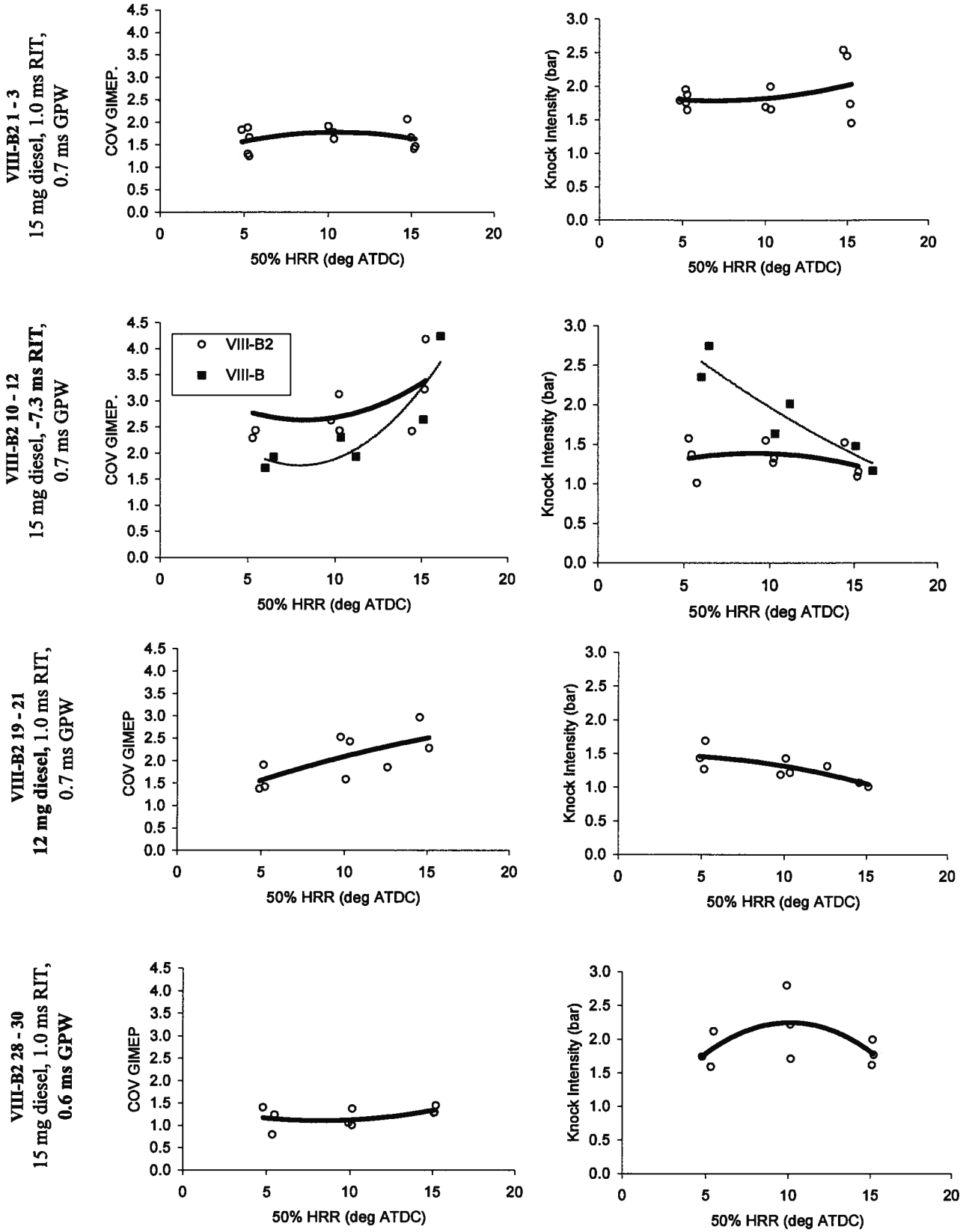

Figure 4.16: COV GIMEP and knock intensity for 1100 RPM and 6 bar GIMEP

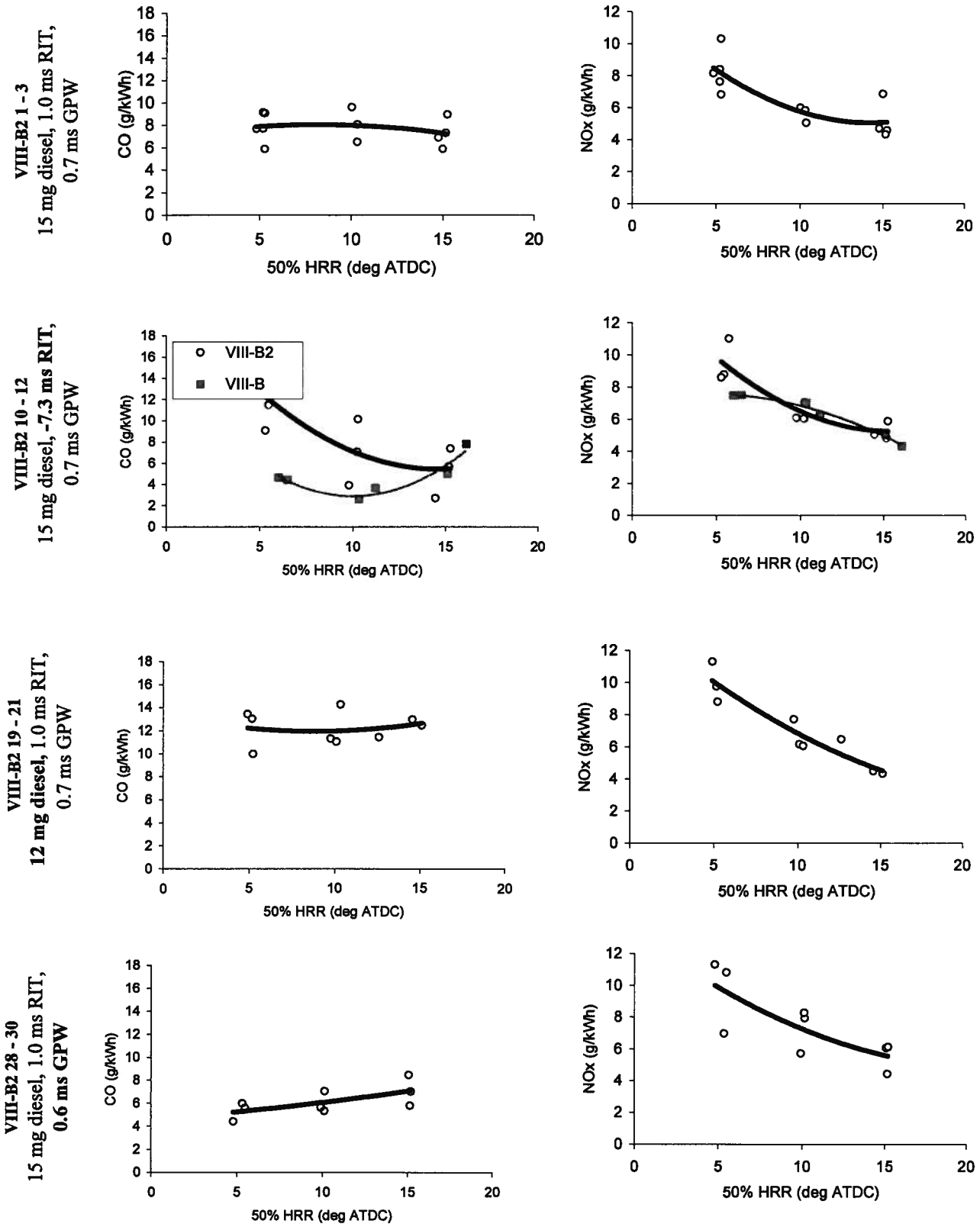

Figure 4.17: CO and NOx for 1100 RPM and 6 bar GIMEP

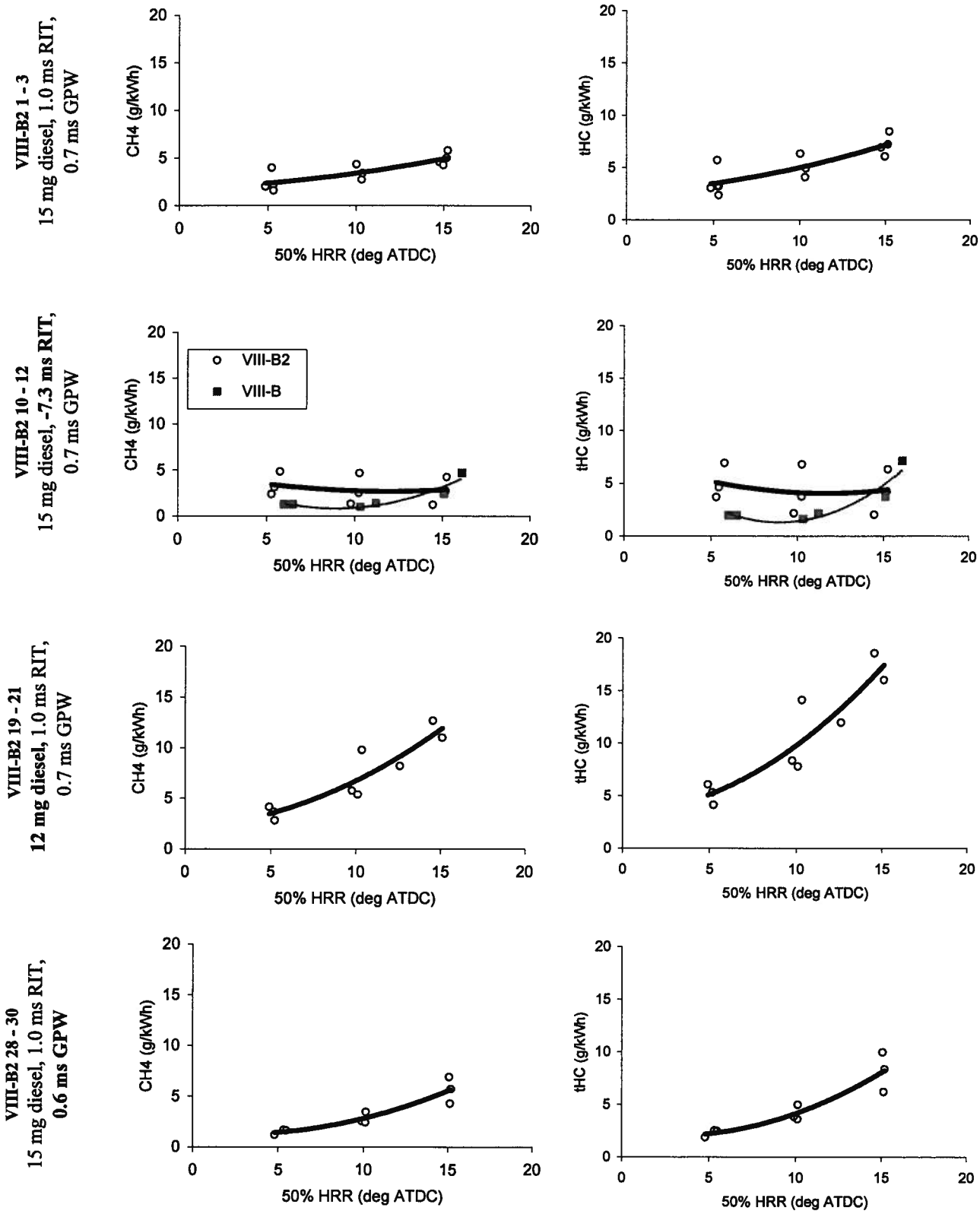

Figure 4.18: CH4 and tHC for 1100 RPM and 6 bar GIMEP

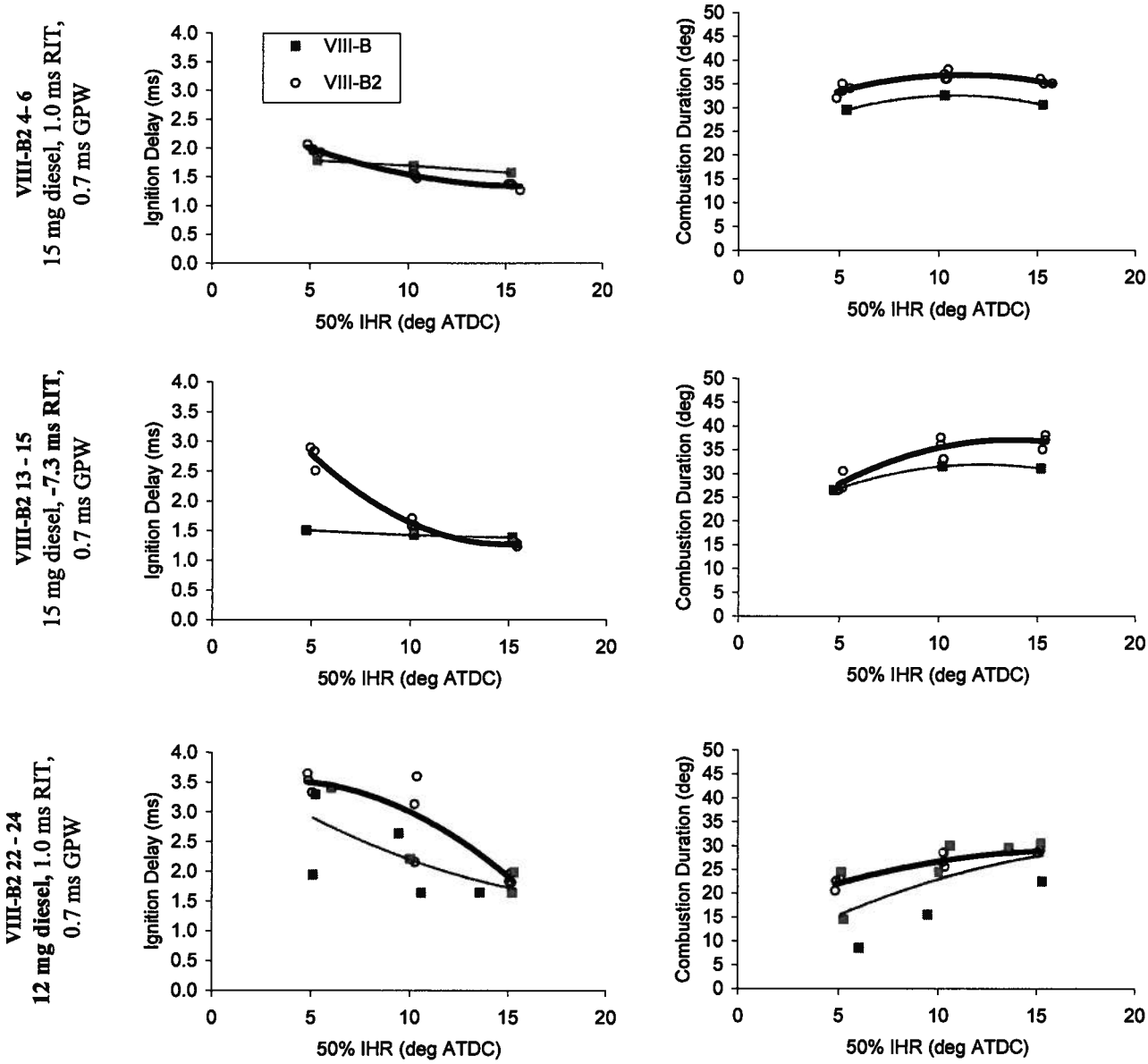

Figure 4.19: Ignition delay and combustion duration for 1100 RPM and 13 bar GIMEP

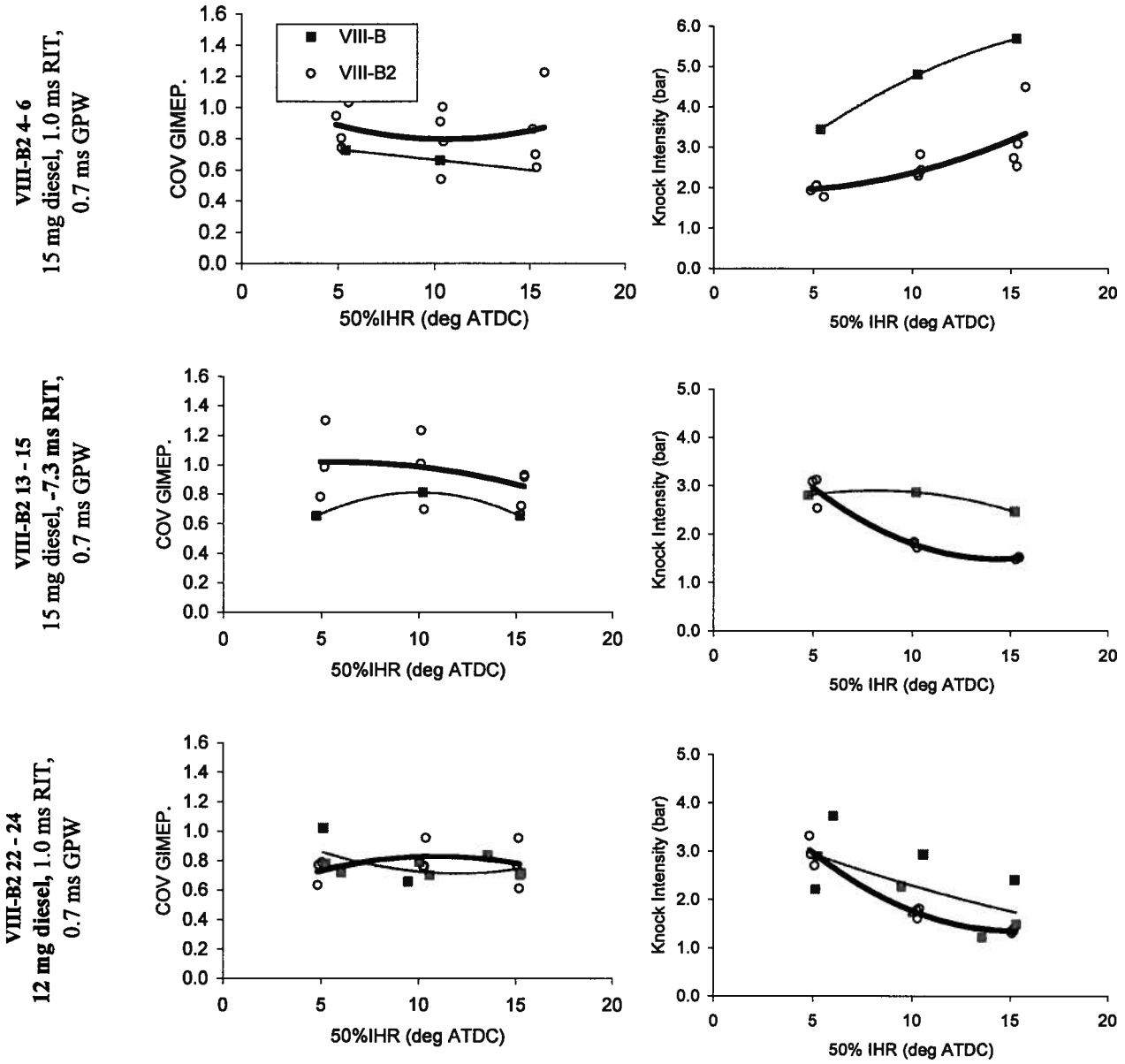

Figure 4.20: COV GIMEP and knock intensity for 1100 RPM and 13 bar GIMEP

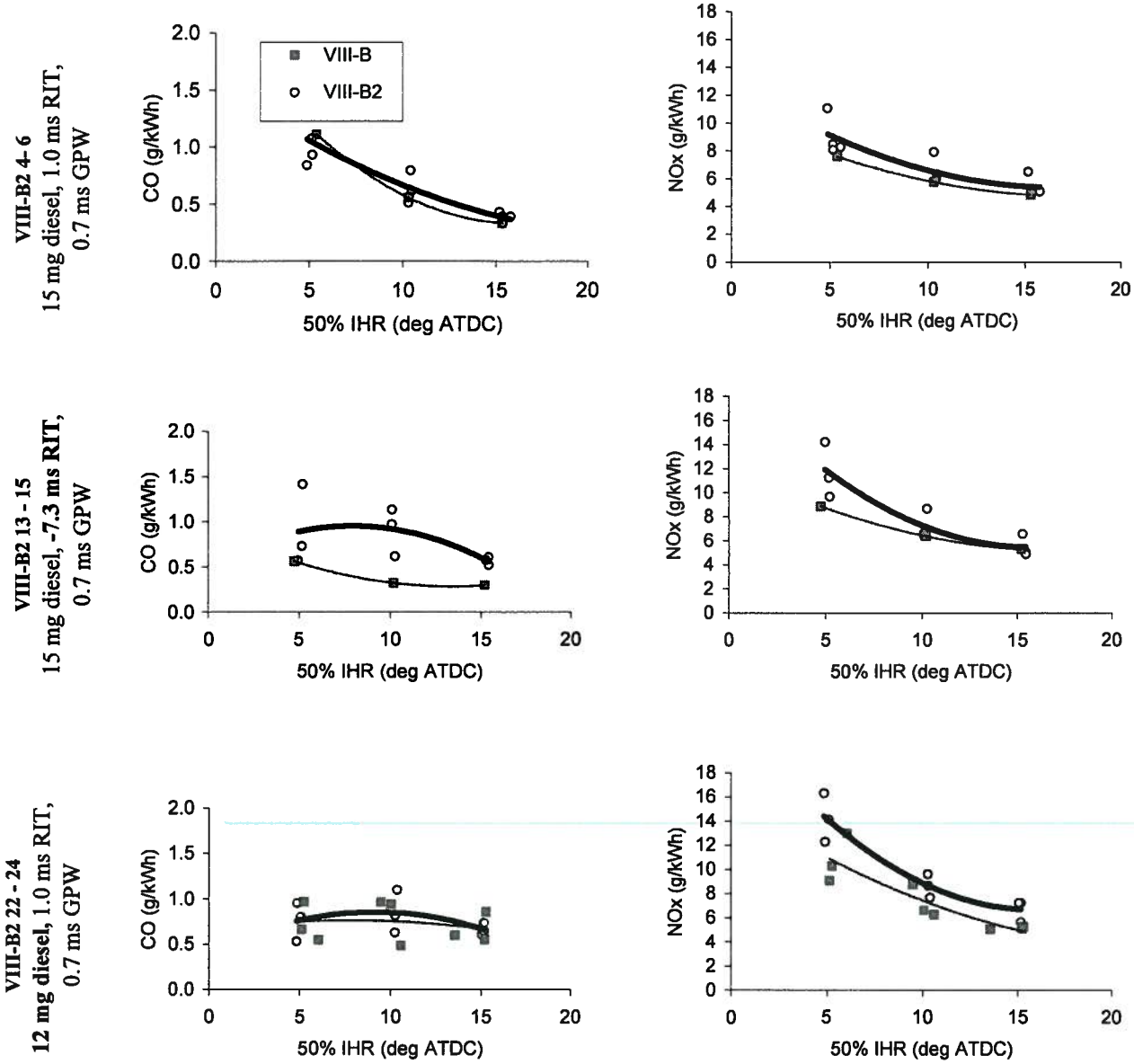

Figure 4.21: CO and NOx for 1100 RPM and 13 bar GIMEP

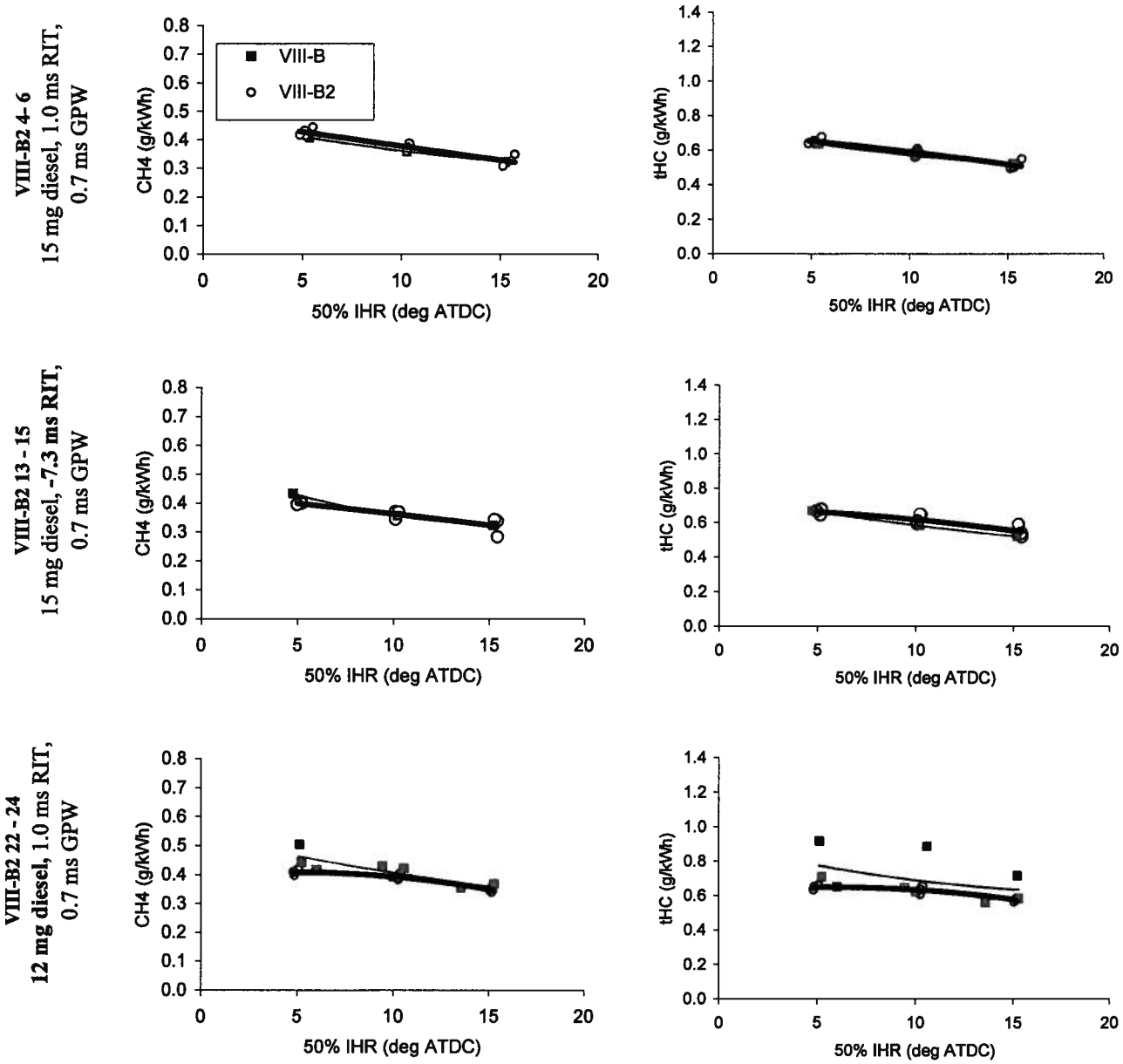

Figure 4.22: CH4 and tHC for 1100 RPM and 13 bar GIMEP

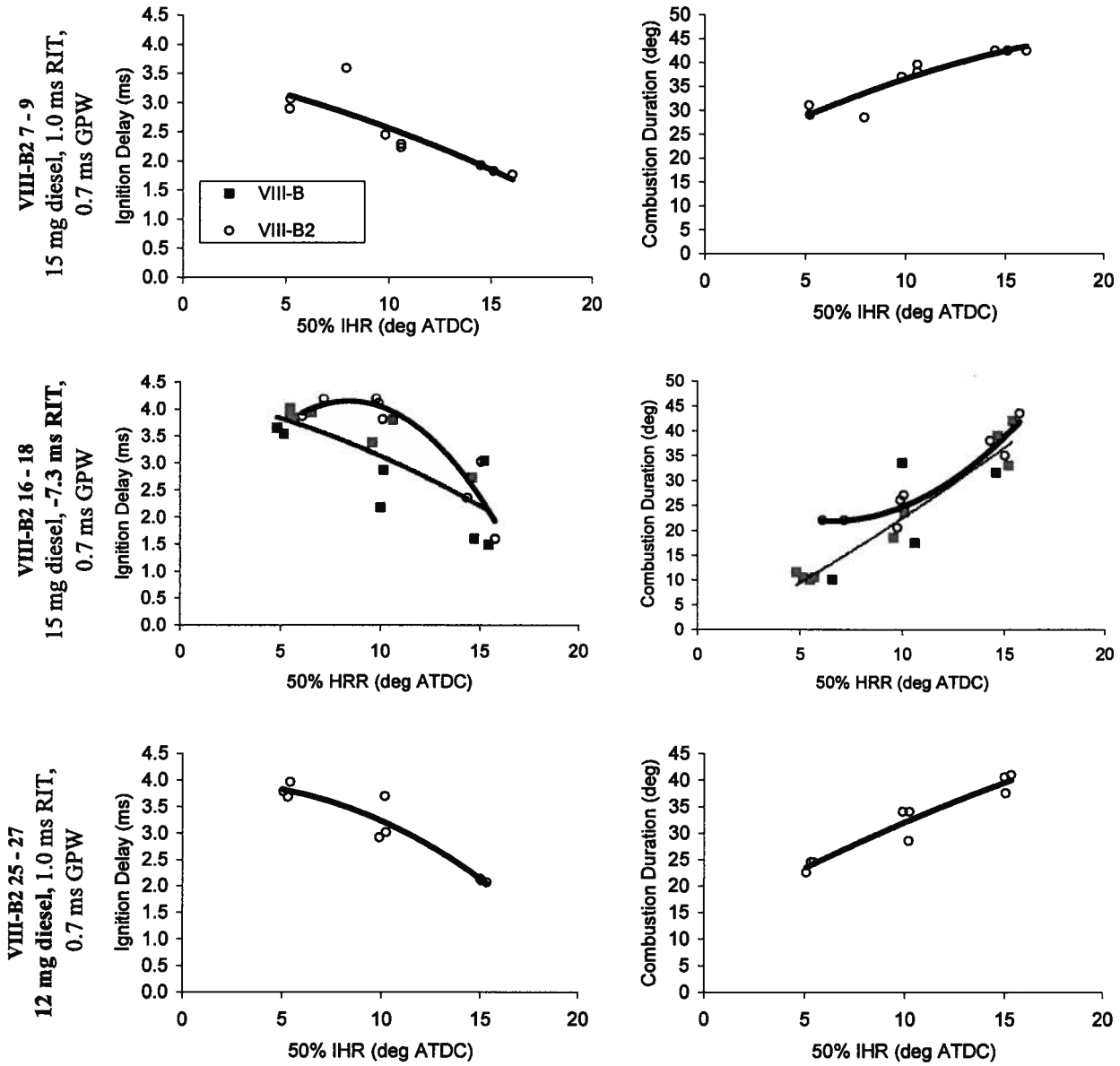

Figure 4.23: Ignition delay and combustion duration for 1400 RPM and 13 bar GIMEP

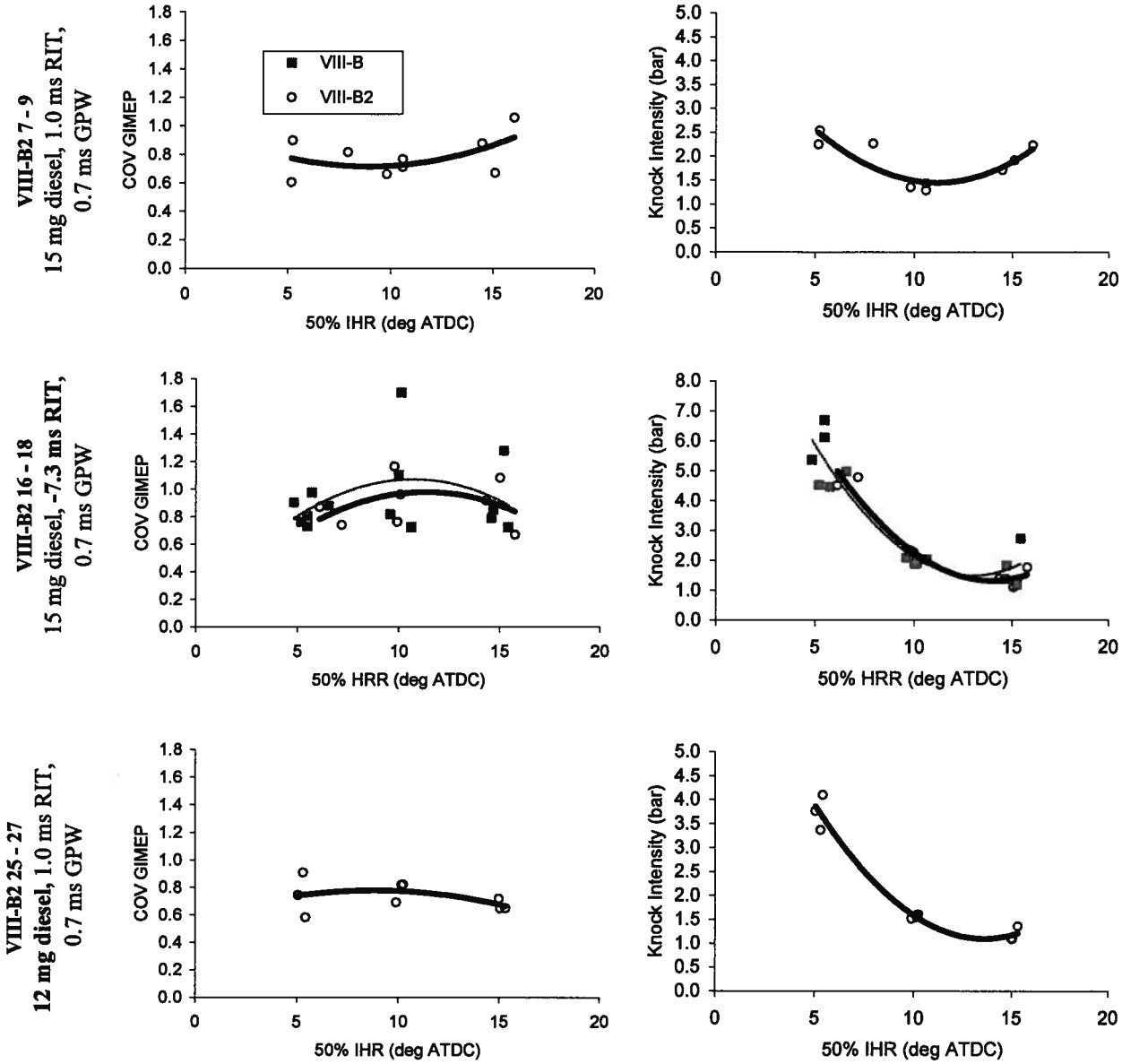

Figure 4.24: COV GIMEP and knock intensity for 1400 RPM and 13 bar GIMEP

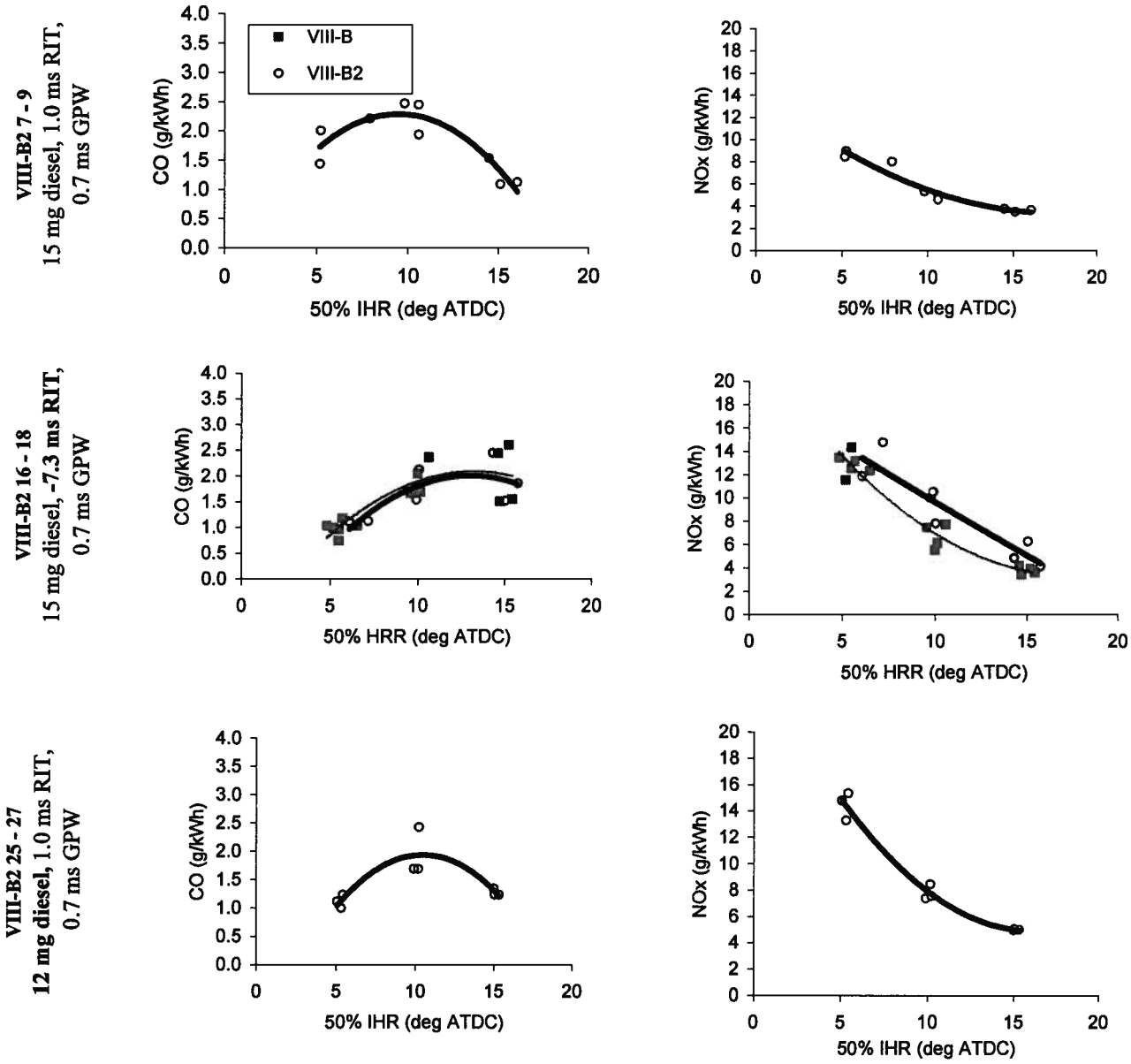

Figure 4.25: CO and NOx for 1400 RPM and 13 bar GIMEP

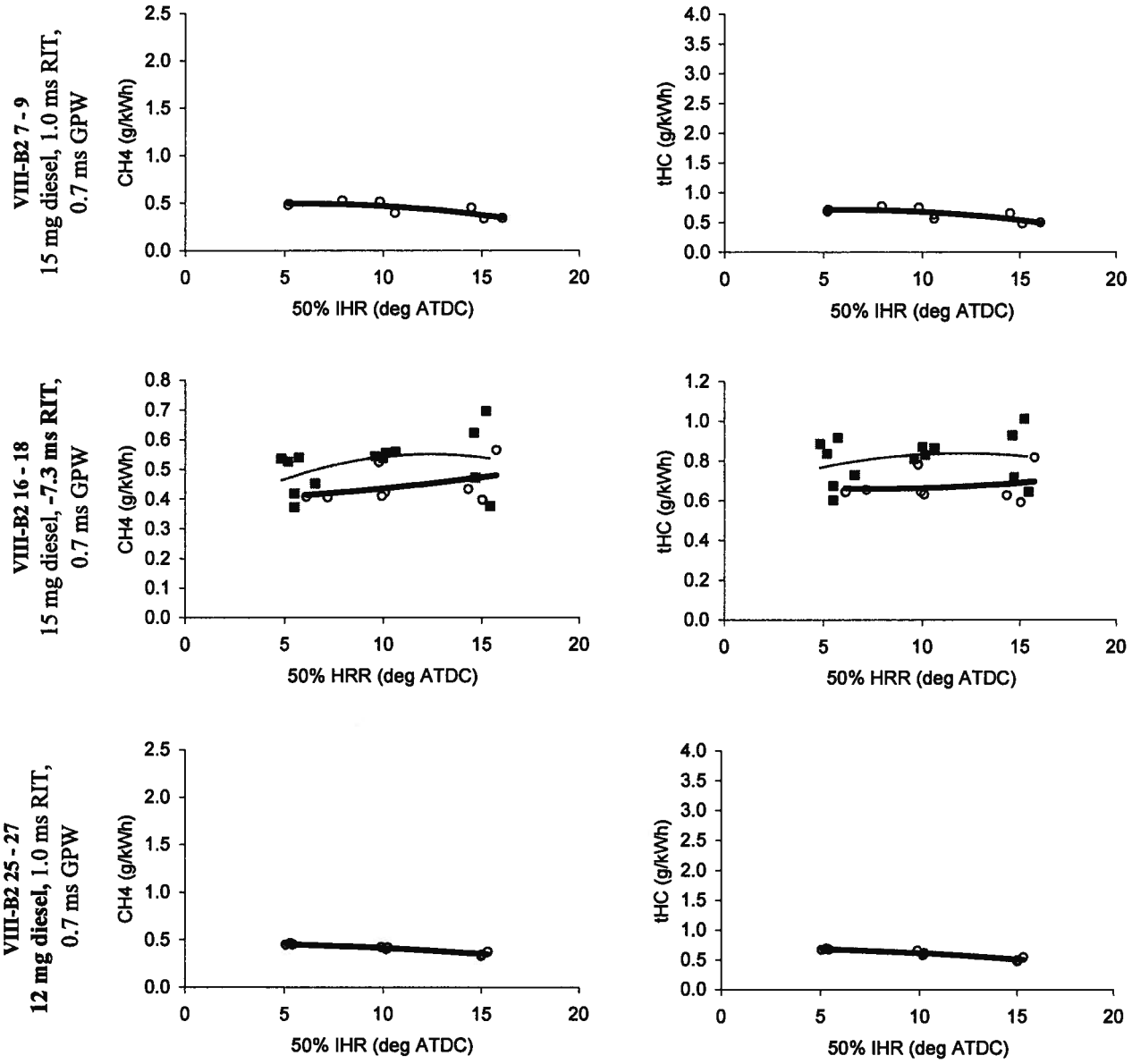

Figure 4.26: CH4 and tHC for 1400 RPM and 13 bar GIMEP

4.5.2 Series VIII-A and VIII-B Combustion Comparisons

As mentioned in Section 3.3, comparisons of the emissions between Prototype A and Prototype B are problematic, since each injector prototype was tested in a different location with different gaseous emissions analyzers. A discussion of the emission comparisons between Prototype A and Prototype B is discussed in Appendix B. The combustion parameters obtained from the high speed in-cylinder pressure data, however, should be easily compared.

Comparisons of ignition delay, combustion duration, COV GIMEP, and knock intensity between VIII-A, VIII-B, and VIII-B2 tests are shown in Figures 4.27 an 4.28 for the three different load/speed combinations.

Figure 4.27 shows that at low load/1100 RPM (0.6 ms pilot GPW), high load/1100 RPM, and high load/1400 RPM, Prototype B has a shorter ignition delay and longer combustion duration. Since the intake pressure and back pressure are similar for these cases, the difference in ignition delay is not related to the residual, but is indicative of the improved performance of Prototype B due to the inserted sleeve. The diesel injection mass was comparable between Prototype A and Prototype B, although the diesel flow rates were much more variant for VIII-A tests. The relative injection timing (RIT) was 1.0 ms compared to 0.3 ms for VIII-B2 tests. Since shorter RITs advances the start of combustion, the difference in ignition delay for VIII-B2 tests is actually more significant.

The primary purpose of the diesel is to promote ignition. Therefore the shorter measured ignition delay is indicative of better performance with the modified injector geometry, since

the diesel is being used more efficiently (less diesel is needed for the same operating point). In addition, at higher loads the added sleeve effectively increases the allowable fuelling rates (to allow stable combustion with acceptable knock) which extends the operating range of the injector, potentially allowing lower engine emissions through new operating strategies.

Figure 4.28 shows the combustion variability and knock intensity comparisons between Prototype A and Prototype B. At higher loads the difference in combustion variability and knock intensity between prototypes is less evident. At low load Prototype B has lower combustion variability but higher knock intensity. A similar knock intensity and combustion variability could be attained for Prototype A by increasing the amount of diesel injected; therefore, at low loads the range of operation of the injector seems be similar between injector prototypes, but shifted to lower diesel injection masses for Prototype B.

Figure 4.29 compares the ignition delay against knock intensity for all of the VIII tests. This figure shows the tradeoff between ignition delay and knock intensity over a wide range of loads, speeds, and combustion timings.

At ignition delays shorter than 2 ms the knock intensity increased substantially. The knock intensity for Prototype A appeared to increase at longer ignition delays (about 2.3 to 2.1 ms) compared to Prototype B (2.0 – 1.8 ms). Both Prototype A and B exhibited a small "tail" that didn't follow the ignition delay/knock intensity tradeoff curve. For Prototype B these were test points at lower diesel injection masses and retarded combustion timing (VIII-B2 24) which also had some of the shortest ignition delays. For Prototype A these points were mid-load with 50% IHR at 10°ATDC where the lowest knock intensity levels were recorded.

At ignition delays greater than 3.0 ms the knock increased as ignition delay was extended. These test points occurred mostly at advanced combustion timing which had small pilot combustion events.

The characteristics of the ignition delay/knock tradeoff curve show the same things that were observed in previous tests; namely, shorter ignition delays lead to higher knock intensity, when there is no pilot combustion event present the knock intensity increases, and lower diesel injection masses lead to lower magnitude knock intensity.

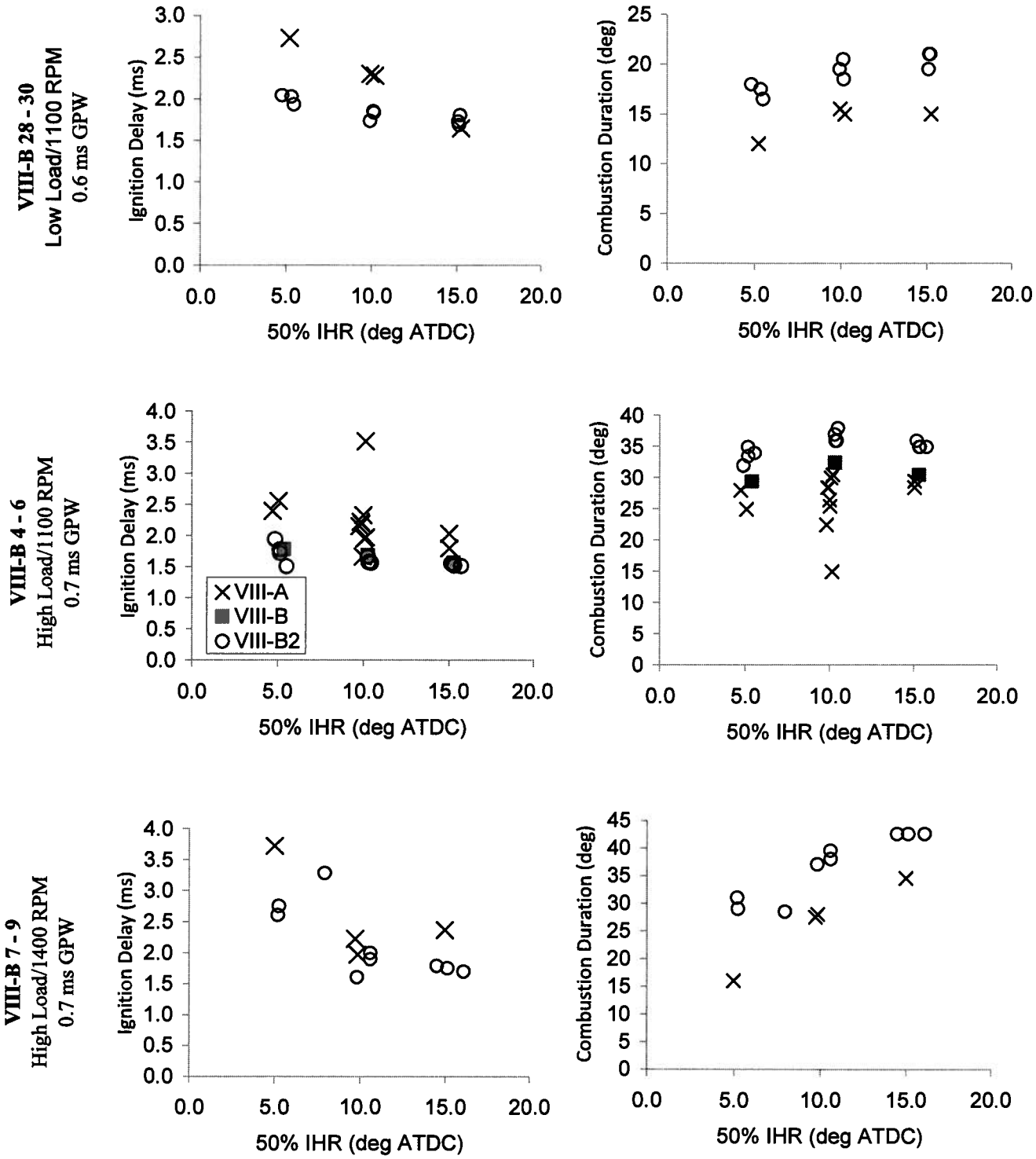

Figure 4.27: Ignition Delay and combustion duration for load/speed timing sweeps

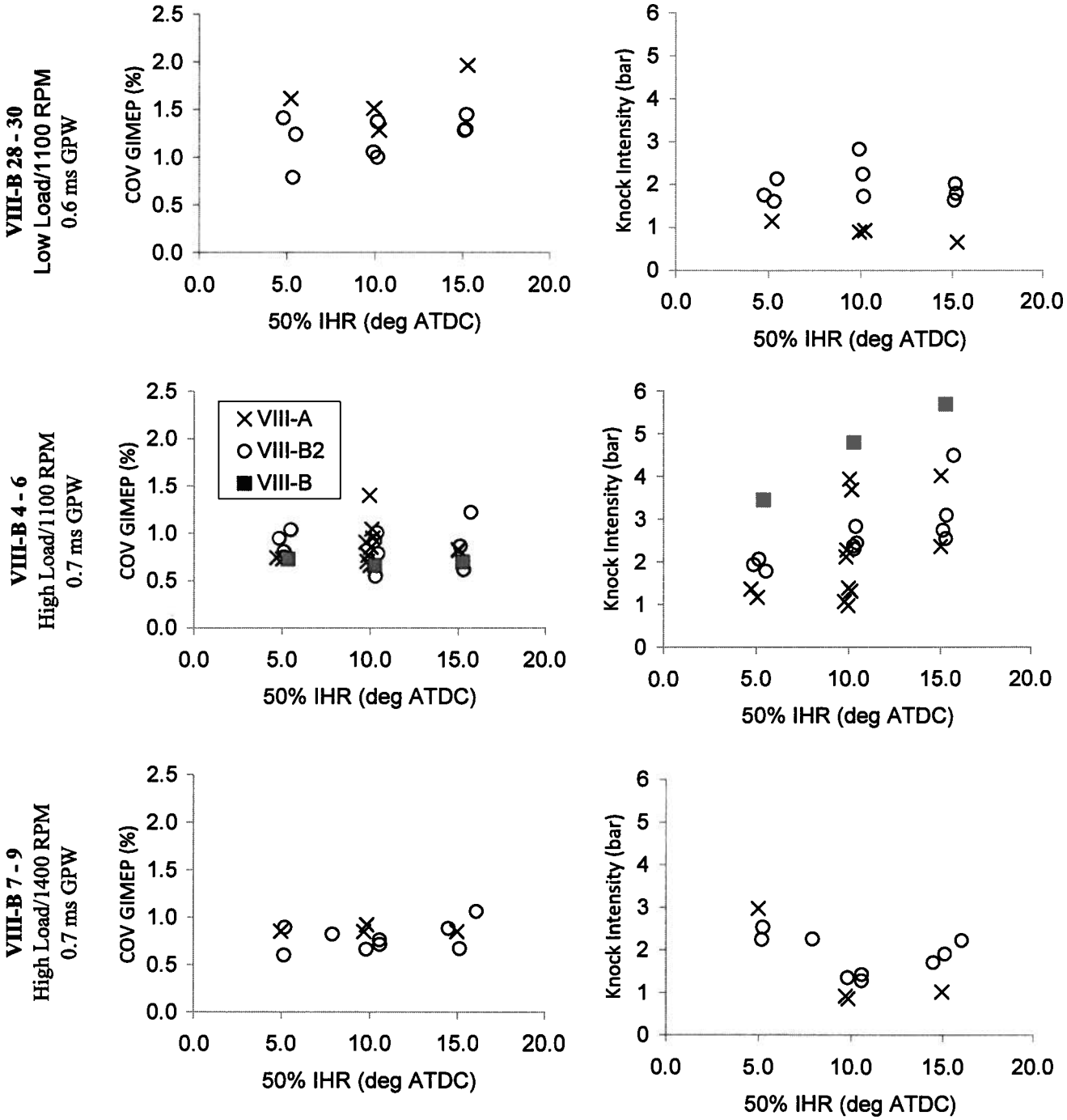

Figure 4.28: COV GIMEP and knock intensity for load/speed timing sweeps.

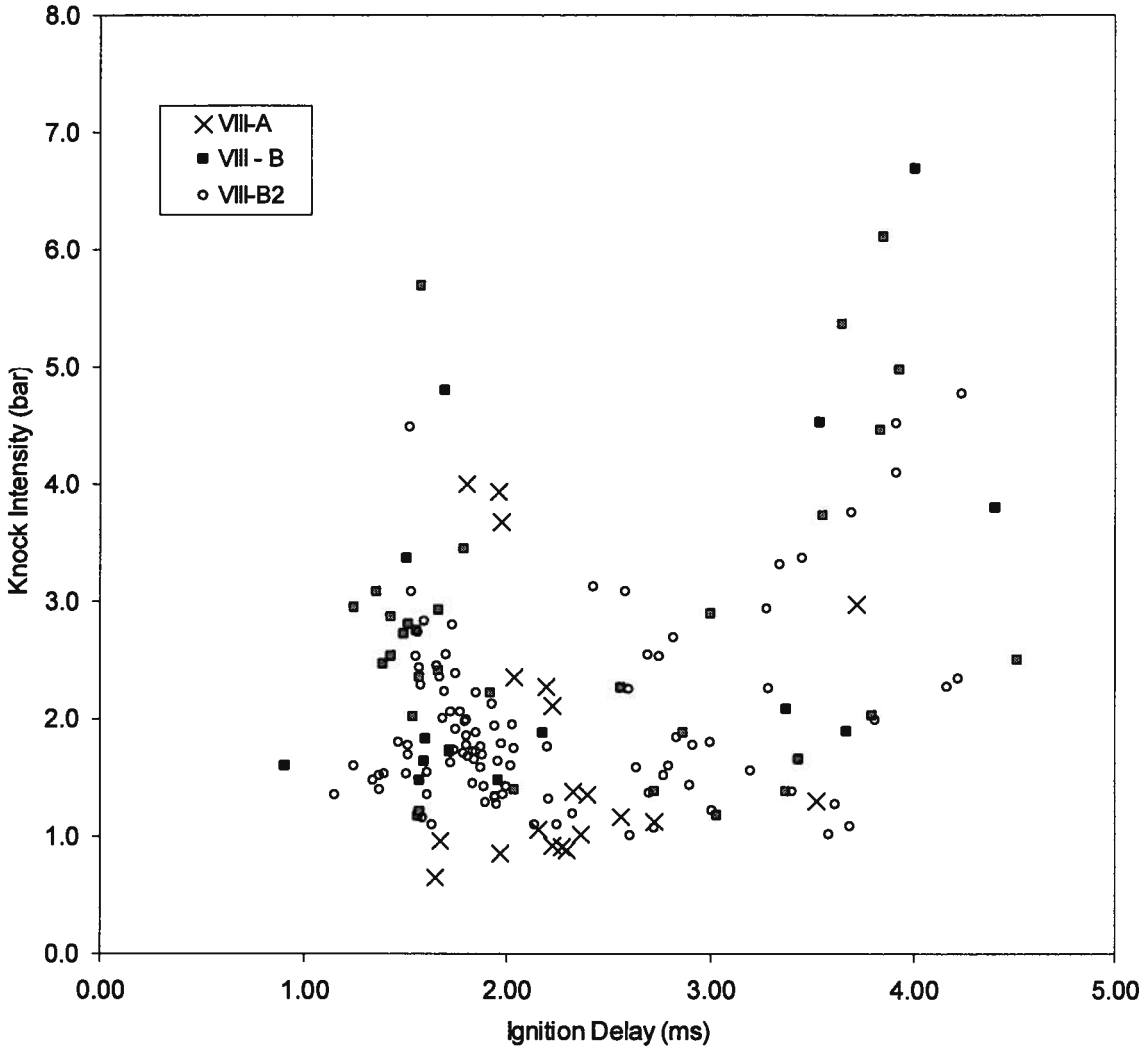

Figure 4.29: Knock Intensity/Ignition Delay Tradeoff Curve

Chapter 5: Conclusions and Recommendations

The objective of this research was to understand the interactions between the diesel and natural gas in an injector prototype and how these interactions affected the combustion performance and emissions of the engine. The fuel injector used was a high-pressure direct-injection natural gas injector where the pilot diesel was first mixed with the natural gas inside the injector and then co-injected with the gas into the combustion chamber.

The combustion performance of the injector was addressed through studies where the injector geometry and injector operation were varied. The geometry of the injector was modified by inserting a sleeve into the common gas/diesel reservoir.

While the injector was being modified, much work was also done in moving the single cylinder research engine (SCRE) from one location to another and comparing its operation. It was concluded that comparison of the emissions between the two test cells would be difficult due to different emission benches being used. Operation of the engine and the in-cylinder pressure, however, were observed to be similar in both test cells.

This chapter summarizes the general observations and conclusions made from the each of the tests conducted and recommends future work with HPDI co-injection. Similar to previous work this study concluded that for most operating conditions two gas injections were needed: the pilot gas injection and the main gas injection. Also, consistent with previous tests the relative amounts of gas and diesel injected during the pilot injection were important to engine performance. It was found that the main injection reduced the effectiveness of the pilot injection by scavenging diesel from the gas/diesel mixture in the injection reservoir,

lengthening ignition delay and requiring more diesel for stable operation. An added injector sleeve which increased fluid velocity in the gas/diesel reservoir and attempted to segregate the gas and diesel was found to reduce the amount of diesel needed for stable operation and reduce the ignition delay. In addition, it was determined the maximum allowable amount of diesel in the pilot injection was limited by engine knock (rapid energy release which causes high frequency in-cylinder pressure fluctuations)..

5.1 Injector Flow

From single-injection tests in the SCRE, the in-cylinder pressure was observed to have a significant effect on the gas injection rate. As the manifold air pressure (and thus the in-cylinder pressure at the time of injection) increased, the gas injection mass was also observed to increase. This had been noted previously by both McTaggart-Cowan (2006) and Jones (2006). Higher cylinder pressures may lift the injector needle earlier and hold open the needle longer thus increasing the gas injection mass. For a given injection pressure and gas pulse width, both the test engine and the Westport flow rigs showed that a 25% increase in diesel injection mass resulted in a 10 – 15 % reduction in gas injection mass. Also observed was that the gas injection response to commanded pulse width was non-linear. Between 0.5 and 0.6 ms commanded gas pulse width (GPW) durations, the change in gas injection rate was less steep. It is unclear whether this observation is caused by force balance on the injector needle or whether it was exclusive to the co-injector.

For both the Westport flow rigs and the SCRE, the difference in injector flow was measured for both co-injector prototypes. The sleeved injector (Prototype B) exhibited 8-25% lower gas injection masses than the unsleeved injector (Prototype A) for similar rail pressures,

cylinder pressures, and injection durations. Still, the measured gas flow rates for Prototype B were within an acceptable range of operation.

5.2 Ignition Delay and Heat Release Rate

For single injection operation, the ignition delay was shortened as more diesel or less gas was added. Ignition delay was strongly correlated with the ratio of gas to diesel on a volume basis at the time of injection. Over a wide range of equivalence ratios this relationship was found to be true whether the gas pulse width duration was held constant and the diesel injection mass was changed, or vice versa.

During normal injection operation, two gas injections were used resulting in a bi-modal heat release rate (HRR) curve comprised of the pilot combustion event and the main combustion event. Assuming the pilot gas injection and subsequent combustion were independent of the main injection then the HRR curve for single injection operation should have accurately represented the pilot combustion event for double injection operation. However, when the main injection was removed (keeping the pilot injection timing and duration unchanged), ignition delay was shorter and the magnitude of the heat released during the pilot combustion event was larger for both co-injector geometries. The difference was more apparent at lower diesel injection masses, and shorter injection durations. Injection pressure and bias pressure had a minor effect on the change in ignition delay.

The ignition delay was found to be most dependent on the diesel injection mass. Higher diesel injection masses led to shorter ignition delay times. Interestingly, increasing the relative injection timing (RIT) between the diesel injection (diesel injected into the gas/diesel

reservoir) and the gas injection (gas/diesel mixture injected into combustion chamber) had the same effect in many cases as lowering the diesel injection mass, especially at advanced combustion timing. This may be an indication of diesel distribution in the spray being dependent on the distribution of the diesel in the gas/diesel reservoir.

The added sleeve made a significant difference to the ignition delay and heat released during the pilot combustion event. Significantly shorter ignition delays were observed with the added sleeve consistently over different speeds and operating conditions. The difference in ignition delay was most evident at lower loads. In addition, for some cases with the unmodified co-injector (Prototype A), no significant pilot combustion event was observed until after the main injection was removed. With Prototype B, no such observations were made. Due to the increased pilot combustion heat release, the added sleeve also significantly reduced the amount of diesel needed for stable combustion. Up to 20% less diesel was needed for the modified co-injector to run the engine without misfiring.

5.3 Knock and Combustion Variability

For single injection operation (and the pilot injection for double injection operation) the minimum diesel and gas injection masses were limited by combustion variability as measured by the coefficient of variation of the gross indicated mean effective pressure (COV GIMEP). For single injection operation, the combustion variability increased as the diesel injection mass was reduced. The combustion variability could not be reduced by reducing the gas pulse width.

For double injection operation the combustion variability increased as the load was lessened or the combustion timing was retarded. At all other points tested the COV GIMEP remained relatively constant over all combustion timings for both injector prototypes. This indicated that when sufficient diesel was present for combustion, the sleeve did not positively or negatively affect combustion variability.

For single injection operation (and the pilot injection for double injection operation) the maximum diesel and gas injection masses were limited by the onset of heavy "knock". The indicated pressure curves (for both single and double injection operation) exhibited pressure fluctuations around 3-4 kHz which was found to be the first transverse mode acoustical frequency of the cylinder.

The relationship between knock intensity and ignition delay is complicated. For lower diesel injection masses (12 mg/inj) and high diesel injection masses (15 mg/inj) with longer RITs, knock intensity increased at longer ignition delays. Since knock intensity increased with increased pre-mixed combustion, the longer ignition delays lead to higher knock intensity levels. However, for higher diesel injection masses injected into the gas/diesel reservoir just prior to the gas injection, the knock intensity was reduced at later combustion timing.

In-cylinder temperature may have also been a factor in increased knock intensity. At higher loads (with accompanying higher cylinder and exhaust temperatures) the knock intensity was observed to increase, even though the ignition delay was held relatively constant. The higher temperatures may have caused faster reaction rates which would lead to higher rates of pressure rise.

At higher diesel injection masses, the knock intensity for the sleeved injector (Prototype B) was slightly higher, especially at lower engine speeds. However, at lower diesel injection masses and double injection tests with no significant pilot combustion event for Prototype A, the knock intensity was observed to be greater for Prototype A due to additional premixed combustion. For a given speed and load if the range of diesel injection masses were bracketed on one side by a significant pilot combustion event and on the other by knock intensity, then the injector sleeve moved this bracket towards lower diesel injection masses.

5.4 Emissions

For single injection operation, the fuel specific emissions of CO, and CH_4 from the engine could be reduced by either shortening the gas pulse width or increasing the amount of diesel injected, effectively lowering the ratio between the volume of natural gas and liquid diesel at cylinder pressures. This correlation was attributed to increased gas volumes adversely lowering the likelihood of the diesel mixing with the air to an ignitable state. Strong negative correlations were also observed between NOx emissions and the gas/diesel volume ratio.

For longer ignition delays, the injected fuel mixes past combustibility before ignition occurs which increases the amount of unburned and partially burned fuel emitted. For single injection operation and for double injection operation with a short second injection (low load cases), a large portion of unburned and partially burned fuel is not re-ingested by the flame. These emissions represent a substantial portion of the CH_4 and uHC emissions for low load and single injection operation. At higher loads (longer second injection) much of these emissions are re-ingested into the flame, which significantly lowers the uHC emissions.

Although the uHC and CH_4 emissions may be related to the ignition delay at higher loads, the emissions bench could not detect differences between the test modes.

Due to improvements made to the research engine, emissions between Prototype A and Prototype B could not be compared since the analyzers used to measure emissions in both cases were different. However, since the ignition delay was significantly shorter for Prototype B, one would expect the CH_4, uHC and CO emissions to be similarly lower at low load for Prototype B with little change in the NOx emissions.

5.5 Conceptual Model of Co-injection

A conceptual model based on the observations about injector flow, combustion characteristics, and emissions is as follows: diesel fuel is injected into the gas/diesel reservoir at high velocities such that during the pre-injection the diesel is distributed through the injection reservoir both as a thin film on the reservoir walls as well as droplets mixed with the gas. As the injector opens during the pilot injection, the gas/diesel mixture will be injected into the combustion chamber. Because diesel is injected with the gas, increased diesel injection mass will displace the natural gas.

A significant portion of the diesel will be retained in the reservoir after the pilot injection, depending on the reservoir geometry and the distribution of the diesel in the reservoir. For single-injection operation, the retained diesel will be injected with the following pilot injection and will therefore be a factor in reducing the ignition delay and increasing the magnitude of heat released. For double-injection operation, this diesel will be injected during the main injection, and is therefore unavailable as an ignition promoter.

In Prototype B, the added sleeve reduced the volume of the gas/diesel reservoir, resulting in higher fluid velocities inside the injector. These higher velocities could have sheared the diesel off of the walls more efficiently and swept the diesel out of the injector more quickly. In addition, the sleeve may help contain a higher concentration of diesel near the injector tip so that the highest concentration of diesel is injected near the beginning of the injection event. The finely atomized diesel introduced earlier in the injection event would have more time to mix to an ignitable mixture with the air, reducing the ignition delay and increasing the proportion of heat released during the pilot combustion event. Knock intensity may also increase with increased diesel concentrations, since higher concentrations of diesel may lead to more ignition sites for a faster burn.

5.6 Co-injector Operation and Co-injector Outlook

Since this is the first thesis on the HPDI co-injector, comparisons between the co-injector prototypes and the industry standard HPDI J36 are of interest. Table 5.1 outlines the similarities and differences in operation and performance between the injectors.

Overall, both Prototype A and Prototype B operated surprisingly well considering that very little has been done to optimize the geometry of the injector for mixed diesel/gas operation. At high load the engine out gaseous emissions were similar to the J36 injector with lower PM emissions which is probably due to better diesel atomization (Jones 2006).

Table 5.1: Injector comparisons between the HPDI-J36 and the co-injector

Injector Operation, Performance and Emissions Comparisons between J36 and Co-Injector		
1	Ability to reproduce a given operating condition with a fixed set of operating and injector parameters	Reproducibility similar to J36 IF fuel and cylinder pressures are identical, higher test-to-test variability at lower diesel injection masses. Additional variability due to extra control over gas to diesel bias pressure and relative effect of cylinder pressure.
2	Effect on emissions (general)	At high load, emissions will depend mainly on the main gas timing, equivalence ratio, and oxygen concentration. At low loads, the pilot injection has a larger effect and emissions can be quite different.
3	Effect on PM	Generally lower PM for the co-injector. For the J36, PM emissions depend strongly on the diesel pilot injection.
4	Effect on NOx	Lower NOx at low load. At high load similar NOx emissions.
5	Effect on uHC, CH4	Higher CH4 emissions at low load. At high load similar CH4 emissions
6	Combustion variability (COV	Slightly higher combustion variability.
7	Knock intensity	Variable, from levels similar to J36, to above 10 bar. Knock is controlled by the pilot gas injection duration and diesel injection masses
8	Sensitivity to diesel quantity	Higher sensitivity. Limited at low diesel quantites due to combustion variability/unburned fuel. Limited at high fuel quantities due to knock.
9	Sensitivity to engine speed	High sensitivity. More diesel is needed at higher engine speeds for stable operation.
10	Sensitivity to cylinder pressure	High sensitivity. Lower cylinder pressures (either lower boost or advanced injection timing) cause gas needle to lift later.
11	Engine Startup	Higher diesel quantities (20 - 30 mg/inj vs. 10 - 15 mg/inj for J36), and earlier injection timing (-14 deg ATDC vs. -8 deg ATDC for J36) needed to start.
12	Transient engine control	Unknown. Transient control currently could be limited by software. Transient control problems were identified with Co-injector A but not extensively described. No transient control problems have yet been identified for Prototype B.

There were, however, issues observed with the repeatability and combustion variability using the co-injector. Similar operating conditions are produced with the J36-HPDI injector for a given set of pulse width durations, injection pressures, and cylinder pressures. Repeatability with the co-injector is dependent on parameters such as combustion timing, diesel injection quantities and diesel injection timing relative to the gas injection. The operation of the J36 injector is less sensitive to differences in cylinder pressures and diesel quantities.

Most of these operational difficulties may be related to the ability to control the quantities of diesel and gas injected during the pilot injection. Unlike the J36-HPDI injector, co-injector

operation is highly sensitive to the amount of diesel injected during the pilot gas injection. Combustion variability increases at low diesel injection quantities and high knock increases at high diesel injection quantities. The added sleeve appears to widen the window of acceptable operation, especially at higher loads. Using shorter pilot gas injection durations is also an effective strategy in reducing sensitivity to diesel quantity; however, the current injector design limits the minimum achievable gas pulse width to 0.46 ms with recommended gas pulse widths above 0.6 ms. Shorter gas pulse widths are an issue with the current injector since cylinder pressure has a greater effect on gas injections especially at lower gas injection durations, making early combustion timing (before 5 ^{o}ATDC) troublesome.

Issues with engine startup (Jones 2005a, 2005b; McTaggart-Cowan 2006b) and transient operation (Jones 2005a) have been identified in previous works. However, these points do not currently seem to be an issue. Higher diesel quantities (~20 mg/inj) are needed to start the engine naturally aspirated. Sensitivity to changes in engine operating speed have not been observed with the current engine setup. It is unclear whether this is a result of the changes in the injection control or to the injector geometry.

For both Prototype B and future single-actuator injectors the injector design could be better optimized to increase repeatability and reduce the effect of cylinder pressure. Optimization of the injector should concentrate on better gas needle response at earlier injection timings and lower manifold pressures, more repeatable injector operation at shorter gas pulse widths, and internal injector geometries that prevent diesel from mixing excessively with the gas before the pilot gas injection.

5.7 Future Work

Future work on HPDI co-injectors (either the current Prototype B or future variants with a single actuator) could be broken down into the following categories: injector modeling, injector visualization, and engine tests.

Even though the conceptual model of the gas/diesel interactions adequately described the observations of improved combustion performance with the modified co-injector, it does not describe all of the observations made. The model does not adequately describe the effect of the relative injection timing (RIT) on ignition delay, knock intensity, or diesel injection mass. For longer RITs, diesel will be injected into the gas/diesel reservoir earlier and the gas/diesel bias pressure may also be changing which would affect the diesel injection rate. Whether this allows the diesel to be more dispersed in the natural gas, whether a large concentration of diesel still exists in the reservoir, and whether the diesel has absorbed a sufficient quantity of natural gas to cause flash atomization is unknown. In addition, during the injection of the gas diesel mixture, it is unclear whether the dispersed diesel effectively lowers the critical velocity of the fluid at the choking point or whether the diesel reduces the natural gas by replacement. Scaled models of a transparent injector would be a problem because it is unclear which of these phenomena is important. A mathematical model that addresses all of these phenomena would be beneficial in explaining the difference in combustion.

In addition to a more comprehensive model, the work started by Mikawoz (2005) and Marr (2006) in the injector visualization chamber should be continued. If similar operating points were conducted for Prototype A by Mikawoz and for Prototype B by Marr, these visualizations could be compared to determine whether there was any observable difference

between Prototype A and Prototype B. Further study should be done with Prototype B in order to quantify the effect of diesel injection mass and gas pulse width on the gas/diesel spray during double gas injection operation.

Improvements could be made to the single cylinder research engine in order to improve experiment quality and streamline testing time. The diesel flow rate which should be based only on the bias pressure (diesel – gas rail pressure) and the pre-injection pulse width was observed to be erratic for the same pulse width, both test to test and repetitions. Since engine performance with the co-injector is closely related to the amount of diesel injected, this significantly affected the repeatability of the injector. The source of the erratic diesel flow rate is unknown. As the single cylinder engine, diesel and natural gas supply systems, and ancillary sensors and analyzers are optimized, similar tests could be conducted in order to determine the source of these uncertainties.

In summary, with the understanding of the co-injector gained from this study, future work will concentrate on optimizing the co-injector for lower absolute hydrocarbon emissions as well as reducing the amount of diesel needed at higher engine speeds. This will be done both in the test engine as well as in a spray visualization chamber. Future work with HPDI co-injection will also involve new injector geometries. These prototypes will consist of a single injection system with the diesel injection mass controlled by the engine speed and the bias pressure.

References

EIA – Energy Information Administration
Ontario MOE – Ontario Ministry of the Environment
US DOI – U. S. Department of Interior
US EPA – U. S. Environmental Protection Agency
US IRS – U. S. Internal Revenue Service

ABB Automation. 2000. Advance Optima-Module Magnos 16 Service Manual. 43/24-1005-1 EN.

ABB Automation. 2001. Advance Optima-Module Magnos 16 Service Manual. 43/24-1001-1 EN.

Agarwal, Apoorva and Dennis N. Assanis. 1998. Multi-Dimensional Modeling of Natural Gas Ignition Under Compression Ignition Conditions Using Detailed Chemistry. *SAE Technical Paper* 980136.

Adomeit, P., O. Lang, R. Schulz and V. Weng. 2002. CFD Simulation of Diesel Injection and Combustion. *SAE Technical Paper* 2002-01-0945.

Ashgriz, N., R. Washburn, and T. Barbat. 1996. Segregation of drop size and velocity in jet impinging splash-plate atomizers. *Int. J. Heat and Fluid Flow* 17: 509-516.

Boretti, A.A. S.H. Jin, G. Zakis, M. J. Brear, W. Attard, H. Watson, H. Carlisle, and W. Bryce. 2007. Experimental and Numerical Study of an Air Assisted Fuel Injector for a D.I.S.I. Engine. *SAE Technical Paper* 2007-01-1415.

Cathcart, G. and C. Zavier. 2000. Fundamental Characteristics of an Air-Assisted Direct Injection Combustion System as Applied to 4-Stroke Automotive Gasoline Engines. *SAE Technical Paper* 2000-01-0256.

Chin J. S., Lefebvre A.H. 1993. Flow Regimes in Effervescent Atomization. *Atomization and Sprays* 3:463-75.

Chiu, J.P., J. Wegrzyn and K.E. Murphy. 2004. Low Emissions Class 8 Heavy-Duty On-Highway Natural Gas and Gasoline Engine. *SAE Technical Paper* 2004-01-2982.

Chiu, J. P., J.D. Taylor, C. Tai, T. Reppert, and L. Christensen. 2007. US 2010 Emissions Capable Camless Heavy-Duty On-Highway Natural Gas Engine. *SAE Technical Paper* 2007-01-1930.

Christensen, M. B. Johansson, P Amnéus, F. Mauss. 1998. Supercharged Homogenous Charge Compression Ignition. *SAE Technical Paper* 980787.

Cummins Southern Plains. 2008. ISL Engine. http://www.cummins-sp.com/engines/automotive/isl_engine.htm. Accessed May 21, 2008.

Cummins-Westport Inc. n.d. Specification sheets for B-gas, C-gas, and L-gas engines. Available from http://www.cumminswestport.com/products/index.php. Accessed May 06, 2008.

Dieselnet. n.d. Emission standards: Summary of worldwide diesel emission standards. Available from http://www.dieselnet.com/standards. Accessed July 10, 2008.

Douville B., P. Ouellette, A. Touchette, B. Ursu. 1998. Performance and Emissions of a Two-Stroke Engine Fueled Using High-Pressure Direct Injection of Natural Gas. *SAE Technical Paper* 981160.

Duggal, V.K., E.J. Lyford-Pike, J.F. Wright, M. Dunn, D. Goudie, and S. Munshi. 2004. Development of the High-Pressure Direct-Injected, Ultra Low-NOx Natural Gas Engine. NREL/SR-540-35911. http://www.nrel.gov/vehiclesandfuels/ngvtf/pdfs/35911.pdf. Accessed May 06, 2008.

Dumitrescu, S., P. G. Hill, G. Li, and P. Ouellette. 2000. Effects of Injection Changes on Efficiency and Emissions of a Diesel Engine Fueled by Direct Injection of Natural Gas. *SAE Technical Paper* 2000-01-1805.

Energy Information Administration. 2007. Annual oil market chronology Energy Data, Statistics and Analysis. Available from http://www.eia.doe.gov/emeu/cabs/AOMC/pdf.pdf. Accessed July 10, 2008.

Eng, J.A. 2002. Characterization of Pressure Waves in HCCI Combustion. *SAE Technical Paper* 2002-01-2859.

Faiz, A., C. S. Weaver, and M. P. Walsh. 1996. Air Pollution from Motor Vehicles: Standards and Technologies for Controlling Emissions. Washington D.C. World Bank. Available from http://elaw.org/assets/pdf/faizweaverwalsh.pdf. Accessed May 06, 2008.

Fitton, J.C., and R.J. Nates.1996. Knock Erosion in Spark-Ignition Engines. *SAE Technical Paper* 962102.

Forster, P., V. Ramaswamy, P. Artaxo, T. Berntsen, R. Betts, D.W. Fahey, J. Haywood, J. Lean, D.C. Lowe, G. Myhre, J. Nganga, R. Prinn,G. Raga, M. Schulz and R. Van Dorland. 2007. Changes in Atmospheric Constituents and in Radiative Forcing. In: Climate Change 2007: The Physical Science Basis. Contribution of Working Group I to the Fourth Assessment Report of the Intergovernmental Panel on Climate Change [Solomon, S., D. Qin, M. Manning, Z. Chen, M. Marquis, K.B. Averyt, M.Tignor and H.L. Miller (eds.)]. Cambridge University Press, Cambridge, United Kingdom and New York, NY, USA.

Ghaffarpour, M., Azarfam, M., and Noorpoor, A. 2006. Emissions reduction in Diesel Engines Using New Fuel Injection System. *JSME International Journal.* Series B, Vol. 49 (4): 1298 – 1306.

Goudie, D., M. Dunn, S.R. Munshi, E. Lyford-Pike, J. Wright, V. Duggal and M. Frailey. 2005. Development of a Compression Ignition Heavy Duty Pilot-Ignited Natural Gas Fuelled Engine for Low NOx Emissions. *SAE Technical Paper* 2005-01-2954.

Harrington, J., S. Munshi, C. Nedelcu, P. Ouellette, J. Thomson and S. Whitfield. 2002. Direct Injection of Natural Gas in a Heavy-Duty Diesel Engine. *SAE Technical Paper* 2002-01- 1630.

Heywood, J. B. 1988. *Internal Combustion Engine Fundamentals.* New York,NY: McGraw Hill. ISBN: 007028637X.

Hill, P. G., R. Pierik, and B.K. Hodgins. 1991. *Intensifier-injector for gaseous fuel for positive displacement engines.* Patent 5067467, filed 1991, and issued 11/26/1991. Available at http://www.freepatentsonline.com/5067467.html Accessed June 18, 2008.

Hill, P.G. and G.P. McTaggart-Cowan. 2005. Nitrogen Oxide Production in a Diesel Engine Fueled by Natural Gas. *SAE Technical Paper* 2005-01-1727.

Hodgins, K. B., Hill, P. G., Ouellete, P. and Hung, P. 1996. Directly injected natural gas fueling of diesel engines. *SAE Technical Paper* 961671.

Houston, Rodney and Geoffrey Cathcart. 1998. Combustion and Emissions Characteristics of Orbital's Combustion Process Applied to Multi-Cylinder Automotive Direct Injected 4-Stroke Engines. *SAE Technical Paper*. 980153.

Jones, H. L. 2004. Source and Characterization of Particulate Matter from a Pilot-Ignited Natural Gas Fuelled Engine. Master's Thesis, University of British Columbia.

Jones, Heather L. 2005a. *U1-FAC-091-TEST.* Engine Testing Results from First I2I-Coinjector Prototype. SCRE Project Factsheets.

Jones, H. L. 2005b. *U1-FAC-092-TEST.* Engine Testing Results from First I2I-Coinjector Prototype – 2nd Round of Testing. SCRE Project Factsheets.

Jones, H. L. 2006. *U1-FAC-093-TEST.* Engine testing results from first I2I-coinjector prototype – 3rd round of testing J36 comparison to I2I injector. SCRE Project Factsheets.

Jones, H.L., G.P. McTaggart-Cowan, S.N. Rogak, W.K. Bushe, S.R. Munshi and B.A. Buchholz. 2005. Source Apportionment of Particulate Matter from a Diesel Pilot-Ignited Natural Gas Fuelled Heavy Duty DI Engine. *SAE Technical Paper* 2005-01-2149.

Kimmel, J. A. and S. P. Dillon. 2002. *Air assist fuel injectors.* Patent United States Patent No. 6,484,700, filed 2000, and issued 11/26/2002. Available at http://www.freepatentsonline.com/6484700.html Accessed June 18, 2008.

Kostka, P. 2008. Email correspondence between UBC/Westport Innovations regarding J36 injector operation. April 24, 2008.

Li, G., P. Ouellette, S. Dumitrescu, and P.G. Hill. 1999. Optimization Study of Pilot-Ignited Natural Gas Direct-Injection in Diesel Engines. *SAE Technical Paper* 1999-01-3556. SAE Transactions, Journal of Fuels and Lubricants. 108(4).

Lörcher, M. and D. Mewes. 2001. Atomization of Liquids by Two-phase Gas-liquid Flow through a Plain-orifice Nozzle: Flow Regimes inside the Nozzle. *Chemical Engineering & Technology* 24(2): 167-172.

Marr, M. 2007. Experimental Imaging of Westport HPDI Fuel Injectors and Evaluation of the LaVision Droplet Sizing System. UBC Internal report. Available in electronic appendix of this thesis (...rogak/sbrown/Thesis/Brown_Thesis.zip).

McTaggart-Cowan, G.P. 2003. *U1-FAC-024-ANYS.* SCRE Project Factsheets.

McTaggart-Cowan, G. P. 2006a. Pollutant Formation in a Gaseous-Fuelled Direct Injection Engine. Doctorate Thesis, University of British Columbia.

McTaggart-Cowan G. P. 2006b. *U1-FAC-098-TEST.* SCRE Project Factsheets.

McTaggart-Cowan, G. P. 2008. Email correspondence regarding calibration of the charge amplifier. February 21, 2008.

McTaggart-Cowan, G.P., W.K. Bushe, S.N. Rogak, P.G. Hill and S.R. Munshi. 2003. Injection Parameter Effects on a Direct Injected, Pilot Ignited, Heavy Duty Natural Gas Engine with EGR. *SAE Technical Paper* 2003-01-3089. *SAE Transactions, Journal of Fuels and Lubricants.* 112(4):2103-2109.

McTaggart-Cowan, G.P., W.K. Bushe, P.G. Hill and S.R. Munshi. 2004a. A Supercharged Single- Cylinder Heavy-Duty Engine for High Pressure Direct Injection of Natural Gas. International Journal of Engine Research. 4(4):315-330.

McTaggart-Cowan, G.P., S.N. Rogak, P.G. Hill, W.K. Bushe and S.R. Munshi. 2004b. Effects of Operating Condition on Particulate Matter and Nitrogen Oxides Emissions from a Heavy- Duty Direct Injection Natural Gas Engine using Cooled Exhaust Gas Recirculation. *International Journal of Engine Research.* 5(6): 499-511.

McTaggart-Cowan, G.P., W.K. Bushe, S.N. Rogak, P.G. Hill and S.R. Munshi. 2004c. The Effects of Varying EGR Test Conditions on a Direct Injection of Natural Gas Heavy-Duty Engine with High EGR Levels. *SAE Technical Paper* 2004-01-2955. *SAE Transactions, Journal of Engines.* 113(3):1500-1509.

McTaggart-Cowan, G.P., W.K. Bushe, S.N. Rogak, P.G. Hill and S.R. Munshi. 2005. PM and NOx Reduction by Injection Parameter Alterations in a Direct Injected, Pilot Ignited, Heavy Duty Natural Gas Engine with EGR at Various Operating Conditions. *SAE Technical Paper* 2005-01-1733. *SAE Transactions, Journal of Engines.* 114(3).

Mikawoz, J. 2005. Movie of Prototype B.avi. Available in electronic appendix of this thesis (...rogak/sbrown/Thesis/Brown_Thesis.zip).

Nagasaka, Kenso, T. Takagi, K. Koyanagi, T. Yamauchi. 2000. The Development of a Fine Atomization Injector. *JSAE*, 21 (2000): 309-313.

Nehmer, D. and Reitz, R. Measurement of the effect of injection rate and split injections on diesel engine soot and NOx emissions. 1994. *SAE Technical Paper.* 940668.

Obert, Edward F. 1973. *Internal Combustion Engines and Air Pollution.* Intext Educational Publishers, Chapter 15. ISBN: 0700221832.

Ontario Ministry of the Environment. 2001. Air quality in Ontario 2001 Report. Available from http://www.ene.gov.on.ca/envision/techdocs/4521e.htm. Accessed May 5, 2008.

Ouellette, P., Douville, B., Hill, P. G. and Ursu, B. 1998. NOx reduction in a directly injected natural gas engine. *Proceedings of the 1998 Fall Technical Conference of the ASME, IC Engine Division, ICE* Vol. 31-3, Clymer, New York, September 1998.

Ouellette, P., P. Mtui and P.G. Hill. 1998. Numerical Simulations of Directly Injected Natural Gas and Pilot Diesel Fuel in a Two-Stroke Compression Ignition Engine. *SAE Technical Paper* 981400.

Pierburg Instruments. 2002a. Flame Ionization Detector (FID 4000). D.-No. 0.850929.0.1. 7-37.

Pierburg Instruments. 2002b. Chemiluminescence Detector (CLD 4000). D.-No. 0.850929.0.1, 7-85.

Roesler T.C., Lefebvre A.H.. Photographic Studies on Aerated Liquid Atomization, Combustion Fundamentals and Applications. 1988. *Proceedings of the Meeting of the Central States Section of the Combustion Institute,* Indianapolis, Indiana, Paper 3.

Radler, Marilyn. 2006. Oil production, reserves increase slightly in 2006. Oil & Gas Journal. Vol. 104.47 (December 18, 2006).

Rotondi, R., G. Bella, C. Grimaldi, and L. Postrioti. 2001. Atomization of High-Pressure Diesel Spray: Experimental Validation of a New Breakup Model. *SAE Technical Paper.* 2001-01-1070.

SAE International. 1993. Instrumentation and Techniques for Exhaust Gas Emissions measurement. *SAE Standard Works,* SAE 254.

SAE International. 1995.

Sazhin, S.S., W.A. Abdelghaffar, E.M. Sazhina, and M.R. Heikal. 2005. Models for droplet transient heating: Effects on droplet evaporation, ignition, and break-up. *International Journal of Thermal Sciences* 44:610–622.

Sazhina, E.M., S.S. Sazhin, M.R. Heikal, and C.J. Maroony. 1999. The Shell autoignition model: applications to gasoline and diesel fuels. Fuel 78 (1999) 389–401.

Schubert, R. K., and S. Fable. 2005. Comparative costs of 2010 heavy-duty diesel and natural gas technologies: Final report. TIAX LLC, Cupertino, California, 2005. Available from www.acurex.com/reports/HDDV_NGVCostComparisonFinalr3.pdf. Accessed May 6, 2008.

Seinfeld, J. H., and S. N. Pandis. 1998. *Atmospheric Chemistry and Physics: From Air Pollution to Climate Change*. 2nd ed. Hoboken, New Jersey: John Wiley & Sons. ISBN: 0471178152.

Sherstyuk, A.N. 2000. Speed of Sound in a Homogenous Liquid-Gas Mixture. *Chemical and Petroleum Engineering*, Vol 36, Nos. 5-6.

Shiga, S., H. Ehara, T. Karasawa, and T. Kurabayashi. 1988. Effect of Exhaust Gas Recircualation on Diesel Knock Intensity and its Mechanism. *Comb. and Flame.* Vol. 72, Issue 3, June 1988: 225 – 234.

Sonntag, R. E., C. Borgnakke, and G. J. Van Wylen. 2003. *Fundamentals of Thermodynamics.* 6th ed. New York, NY: John Wiley & Sons. ISBN: 0471152323.

Sovani, S. D. 2001. High Pressure Gas/Liquid Flow Inside an Effervescent Diesel Injector and its Effects on Spray Characteristics. Doctorate Thesis. Purdue University. Available at http://docs.lib.purdue.edu/dissertations/AAI3037642. Accessed May 06, 2008.

Sovani, S. D., P. E. Sojka, and A. H. Lefebvre. 2001a. Effervescent Atomization. *Progress in Energy and Combustion Science,* 27 (2001):483-521.

Sovani, S. D., J. D. Crofts, P. E. Sojka, J. P. Gore, and W. E. Eckerle. 2005. Structure and Steady-state Spray Performance of an Effervescent Diesel Injector. *Fuel 84* (2005): 1503-1514.

Srinivasan, K.K., S.R. Krishan, S.Singh, K.C. Midkiff, S.R. Bell, W. Gong, S.B. Fiveland, M. Willi. 2006. The Advanced Injection Low Pilot Ignited Natural Gas Engine: A Combustion Analysis. *Journal of Engineering for Gas Turbines and Power*, JANUARY 2006, Vol. 128, 213-218.

Stone, R. 1999. *Introduction to Internal Combustion Engines.* 3rd Ed. Society of Automotive Engineers. Warrendale, PA. ISBN: 0768004950.

Sullivan, G.D., J. Huang, T.X. Wang, W. K. Bushe and S.N. Rogak. 2005. Emissions Variability in Gaseous Fuel Direct Injection Compression Ignition Combustion. *SAE Technical Paper* 2005-01-0917.

Tarr, Y. J., L. D. Tikk, W.A. Eckerle, and L. L. Peters. *Effervescent Injector for Diesel Engines.* Patent 5884611, filed 1999, and issued 03/23/1999. Available at http://www.freepatentsonline.com/5884611.html (accessed June 19, 2008).

Taylor, C. F. 1985. *The Internal-Combustion Engine in Theory and Practice*. Vol. 2. Cambridge, Mass.: The M.I.T. Press. ISBN: 0262200511.

Teng, H., J. C. McCandless and J. B. Schneyeret. 2003. Compression Ignition Delay (Physical + Chemical) of Dimethyl Ether –An Alternative Fuel for Compression-Ignition Engines. *SAE Technical Paper* 2003-01-0759.

U.S. Department of Interior. 2005. Energy policy act of 2005. Available from http://www.doi.gov/iepa/EnergyPolicyActof2005.pdf. Accessed May 19, 2008.

U.S. Enviromental Protection Agency. 2002a. Non-conformance Penalties for Heavy-Duty Diesel Engines. Available from http://www.epa.gov/otaq/regs/hd-hwy/ncp/f02025.pdf. Accessed May 21, 2008.

U.S. Environmental Protection Agency. 2002b. Chapter 6: Estimated engine and equipment costs. Available from http://www.epa.gov/nonroad-diesel/2004fr/420r04007g.pdf. Accessed May 21, 2008.

U.S. Environmental Protection Agency. 2008. Six Common Air Pollutants. Available from http://www.epa.gov/air/urbanair. Accessed May 21, 2008.

U. S. Internal Revenue Service. 2005. Qualified alternative fuel motor vehicles and heavy hybrid vehicles. Available from http://www.irs.gov/businesses/article/0,,id=175456,00.html#14. Accessed June 06, 2008.

Veco. 2004. Emergency Shutdown Systems for the University of British Columbia.

Vressner, A., A. Lundin, M. Christensen, P. Tunestal, and B. Johannson. 2003. Pressure Oscillations during rapid HCCI combustion. *SAE Technical Paper*, 2003-01-3217.

Wannatong, Krisada, N. Akarapanyavit, S.Siengsanorh, and S. Chanchaona. 2007. Combustion and Knock Characteristics of Natural Gas Diesel Dual Fuel Engine. *SAE Technical Paper* 2007-01-2047.

Westport Innovations Inc. Direct Injection Natural Gas Demonstration Project. 2008a. Available from http://www.westport.com/pdf/WPT-AHD_HPDI_Fuel_System_MED0.pdf. Accessed May 21, 2008.

Westport Innovations Inc. Cummins NG Engine Goes Stoichiometric, with Added EGR Westport Power. 2008b. http://www.westport.com/news/view.php?table=tLArticle&id=108&return_to=media.php. Accessed May 06, 2008.

Yang, J. 2002. *Dual fuel compression ignition engine.* Patent 6427660, filed 2002, and issued 08/06/2002. Available at http://www.freepatentsonline.com/6427660.html (accessed June 19, 2008).

Zhang, F., K. Okamoto, S. Morimoto and F. Shoji. 1998. Methods of Increasing the BMEP (Power Output) for Natural Gas Spark Ignition Engines. *SAE Technical Paper*, 981385.

Zhang, J., D. Jiang, Z. Huang, T. Obokata, S. Shiga, M. Araki. 2005. Experimental Study on Flashing Atomization of Methane/Liquid Fuel Binary Mixtures. *Energy and Fuels*, 19 (2005): 2050-2055.

Zhang, J., D. Jiang, Z. Huang, X. Wang, and Q. Wei. 2006. Performance and Emissions of Direct Injection Diesel Engine Fuelled with Diesel Fuel Containing Dissolved Methane. *Energy and Fuels,* (2006) 20, 504-511.

APPENDICES

Appendix A- Instrumentation List

This section describes the equipment used for controlling the SCRE and for collecting the important pressures and temperatures. The capabilities of the data acquisition hardware is given in Table A.1 and A.2. The range and accuracy of the temperature, pressure, and flow sensors shown in Table A.3 – A.4 are given as well as the range and accuracy of the gaseous emissions analyzers. The following tables show the instruments used for the CERC setup. The instrumentation list for the previous setup (Kaiser) has previously been described by McTaggart-Cowan (2006a).

Table A. 1: Data acquisition cards

Data Acquisition							
Device	**Model Number**	**Manufacturer**	**DAQ Flow Diagram**	**Sampling Rate/Channel**	**Analog Input**	**Analog Output**	**Digital Input/Output**
DAQ Card	PCI-MIO-16E-1	National Instruments	12 Bit A/D Converter	1.25 MS/s	16 Channels - 12 bit (-10 to 10V, 0 - 10V)	2 Channels - 12 bit (-10V to 10V)	8 Channels, 0 ..5 V
FPGA	NI 7831-R	National Instruments	FPGA Board	750 kS/s	8 Channels - 16 bit (-10 to 10V)	8 Channels - 16 bit (-10V to 10V)	160 Lines

Table A. 2: Data aquisition hardware

Data Acquisition					
Device	**Model Number**	**Manufacturer**	**DAQ Flow Diagram**	**Range**	**Resolution**
12 Slot Modular Chassis	SCXI1001 / A6F0F0	National Instruments	SCXI 1101		
DAQ Card - Thermocouple (2 hz filter)	SCXI 1102	National Instruments	SCXI 1102	± 0.1 V	12 bit (.049 mV) ~1.2 deg C
DAQ Card - Voltage (200 hz filter)	SCXI 1102B	National Instruments	SCXI 1102B	± 10 V	12 bit (4.88 mV)
DAQ Card - Voltage (unfiltered)	SCXI 1100	National Instruments	SCXI 1100	± 10 V	12 bit (4.88 mV)

Table A 3:Pressure and temperature transducers

Sensor Description					
Device	**Model Number**	**Manufacturer**	**DAQ Flow Diagram**	**Range**	**Accuracy**
Gaseous Fuel Flow	CMF010P323 NC / 397665; Transmitter: RFT9739 / 7027956	Micromotion Coriolis force Sensor:	FLM-NG-500	0- 15 kg/hr	±0.5%FS (for > 0.8 kg/hr)
Liquid Fuel	Gravimetric Scale	A1-Scale	SCL-TNK-100	0 - 6 kg	±0.1 g
Air Flow		UBC Design & Constructed Subsonic Venturi		0 - 500 kg/hr	Estimated ±2% FS
Diff. Pressure	1705557	Omega Diaphragm PX2300-2DI /	VEN-INT-100	0-2 psi	±1% FS
All T	(most):KMQXL-125U-6	Omega k-type Thermocouple	TC-**	–200°C to 1250°C	±0.75% rdg
Abs.		Setra Strain Gage 209	PR-**	From 0 - 2 to 0 - 5000 psi	±0.25% FS
Wideband Oxygen Sensor (UEGO)	LZA03-E1	NGK Spark Plugs	O2-**	-15.3 to 15.6 % Excess Oxygen	
Torque		Artech Industries	TQ-DYN-110		±0.05% FS
Intake Manifold Pressure	15-1C02EZ1V5 GBAR/405	PCB Piezoresistive	PR-INT-135	0 - 6 bar	
In-Cylinder Pressure	QC33C / M184	AVL Piezoelectric	PT-ENG-100	0-200 bar	Linearity ±0.2%; sensitivity 28.41 pC/bar
Charge Amplifier	503/1033	Kistler			
Crank Angle	XH25D-ss-720-ABCZ/AA042876	BEI Optical Shaft Encoder	SPD-DYN-110		±0.5 deg

Table A. 4: Gaseous emissions analyzers

Species	Manufacturer	Model	Measuring Principle	Range
INT CO2	ABB	Uras 14 EGA	NDIR	0 - 5.0 % vol
CO2	ABB	Uras 14 EGA	NDIR	0 - 15% vol
O2	ABB	Magnos 106 EGA	Paramagnetic	0 - 22% vol
NOx	PIERBURG	CLD 4000 hhd	Chemiluminescent	0 - 2600 ppm
NO	PIERBURG	CLD 4000 hhd	Chemiluminescent	0-2600 ppm
CO	ABB	Uras 14 EGA	NDIR	0 - 2300 ppm
CH4	PIERBURG	FID 4000 hhd	FID	0 - 3900 ppm
uHC	PIERBURG	FID 4000 hhd	FID	0-1500 ppm

General Specifications

Repeatability	<1% FS
Noise (Peak-Peak)	<2% FS
Drift:	<2% FS/8h
Linearity	<2% of point between 15% and 100% of measuring range
	<1% FS

Appendix B: Results of Test Series VI and VIII-A not Discussed in Body

B.1 Test Series VI: Pilot/Main Injection Interactions

On the same day as the Series IV tests (single gas injection in Section 4.2.1 and 4.2.2), double gas injection tests were conducted (Test Series VI). Table B.1 shows the controlled parameters with the main gas injection commanded to start 1.3 ms after the end of the pilot injection. Again for these tests, min* refers to the minimum duration pilot GPW that can be used for stable operation which can be seen on Figure B.1.

Table B.1: Controlled Parameters and Test Matrix for Test Series VI: Double Injection Tests in SCRE - Effect of Diesel and Gas Injection Mass

Test Series	VI			
Gas Rail Pressure (MPa)	22.4			
Diesel Rail Pressure (MPa)	24			
Engine Speed (RPM)	800			
Pilot SOI (deg ATDC)	-9			
RIT (ms)	0.7			
MAT (°C)	70			
Test Point	1-4	15-19	20-23	25-28
Pre-injection DPW (ms)	2.2	3.4	2.2	1.9
Pilot GPW (ms)	0.7	0.75-min*	0.8-min*	0.65-min*
Main GPW (ms)	0.8-0.45	EQR = 0.4	EQR = 0.4	EQR = 0.4

These tests were conducted at constant equivalence ratio of 0.4. For Test Series VI, two assumptions were made in order to compare the double injection operation to single injection operation. First, the CNG injection mass during the pilot injection was assumed to be independent of the CNG injected during the main injection. It was assumed that

since there was about 150 ms (2 engine revolutions) between the end of the main injection and the beginning of the next pilot injection that the main injection could not affect the CNG pressure at the injector tip. Second, all the diesel was assumed to be injected into the combustion chamber during the pilot injection event and the diesel mass was dependent on the pre-injection DPW only.

If all the diesel was introduced into the combustion chamber during the pilot injection then the combustion characteristics of the pilot combustion event should be similar with or without a main injection. However, Figure 4.12 shows the contrary. Comparing single injection operation to double injection operation for the same pre-injection DPW, the ignition delay (the time between the start of the commanded Pilot injection to the start of combustion) is consistently longer for double injection operation at lower pilot GPWs. Note for double injection operation that at pilot GPWs below 0.45 ms, a significant increase in ignition delay was observed, indicating that there was not enough fuel injected during the pilot injection to initiate combustion.

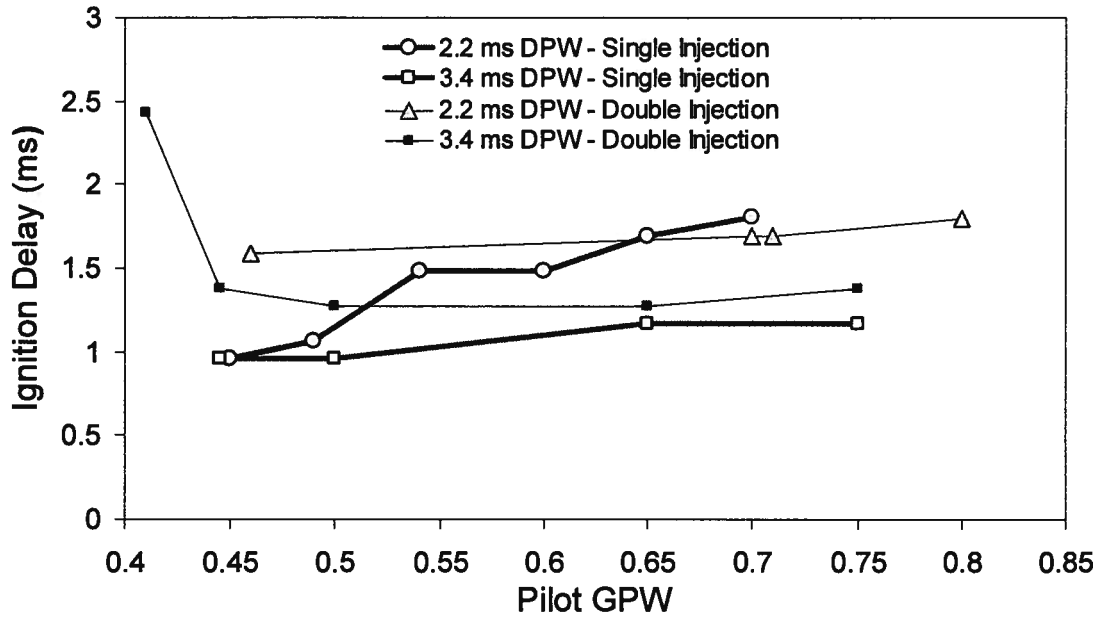

Figure B.1: Ignition delay for Single Injection vs. Double injection

Note that some of the variation between Prototype A and Prototype B could be due to test-to-test diesel mass fluctuations, since a higher gas/diesel volume ratio would result in longer ignition delays. Likewise, the longer ignition delay observed during double injection operation could be related to the gas/diesel injection interactions.

B.2 Comparison Between VII-A and VII-B: Injector Geometry Effects on Ignition Delay and IHR ratio, 800 RPM

Table B.2 summarizes the different points that were tested for Test Series VI at 800 RPM. The non-shaded regions represent regions where tests were not conducted. Note that for this test series, the tests conducted for Prototype A were much less broad. For Prototype A the relative injection timing (RIT) between the end of the pre-injection to the beginning of the pilot injection was changed while the start of the pilot injection remained relatively the same. Even when the diesel pre-injection occurred after the main

gas injection (the pre-injection occurred almost 2 revolutions before the pilot injection) there was very little difference in combustion.

Table B.2: Test Matrix for Test Series VII: Normal Double, and Retarded Double Injection Operation in SCRE for both Prototype A and Prototype B. Engine Speed-800 RPM, manifold temperature: 70 °C, MAP – 90 kPa, exhaust pressure – 50 kPa, 2RIT ~ 1.3 ms

Test Point	Diesel Pressure (Mpa)	Diesel Injection Mass (mg/inj)	Pilot Gas Pulse Width (ms)	Bias Pressure (Diesel - Gas) MPa	Pilot Start of Injection (deg ATDC)	Pre-injection to Pilot RIT for Prototype A (ms)	# of Repeats Prototype A	# of Repeats Prototype B
1	18	Low	0.47	2.5	-8	1.45, 3.45	3	1
2	18	Low	0.7	2.5	-8	-	0	1
3	18	High	0.47	2.5	-8	0.45	1	1
4	18	High	0.7	2.5	-8	0.45, 1.45	2	1
5	24	Low	0.47	2.5	-6.75	0.45	1	1
6	24	Low	0.7	2.5	-6.75	0.45	1	3
7	24	High	0.47	2.5	-6.75	0.45	2	1
8	24	High	0.7	2.5	-6.75	0.45	1	2
9	28	Low	0.47	2.5	-5	0.45	0	1
10	28	Low	0.7	2.5	-5	0.45	0	1
11	28	High	0.47	2.5	-5	0.45	2	1
12	28	High	0.7	2.5	-5	0.45	2	0
13	18	Low	0.47	1.0	-8	-	0	1
14	18	Low	0.7	1.0	-8	-	0	1
15	18	High	0.47	1.0	-8	-	0	1
16	18	High	0.7	1.0	-8	-	0	1
17	24	Low	0.47	1.0	-6.75	-	0	1
18	24	Low	0.7	1.0	-6.75	-	0	2
19	24	High	0.47	1.0	-6.75	-	0	2
20	24	High	0.7	1.0	-6.75	-	0	3
21	28	Low	0.47	1.0	-5	-	0	3
22	28	Low	0.7	1.0	-5	-	0	3
23	28	High	0.47	1.0	-5	-	0	2
24	28	High	0.7	1.0	-5	-	0	1
			Total Number of Tests 800 RPM				15	35

Unshaded regions in repetitions box: no data recorded.

In the new test cell setup (CERC), the engine speed was surprisingly difficult to control at engine speed of 800 RPM. At engine speeds lower than 850 RPM the dynamometer would intermittently cause the engine to stop. The issue was traced to the Hall Effect sensor gap on the dynamometer shaft or loose wiring between the dynamometer and the Digalog dynamometer controller. Therefore, all of the low speed engine tests for Prototype B for Test Series VII were conducted at 850 – 900 RPM.

Differences between Prototype A and B at 800 RPM were much less evident compared to 1200 RPM. This is due mostly to the range of pressures and flow rates tested without a significant number of repeats. Still, the comparisons were important for understanding the reasons significant differences were observed at higher engine speeds.

Figures B.2 shows the measured ignition delay between Prototype A and Prototype B at 18, 24, and 28 MPa diesel rail pressure respectively. At low injection pressures, differences in ignition delay were not observed. It was observed that at many points there was no PCE observed, resulting in longer ignition delay durations. At 24 MPa, however, Prototype B again shows shorter ignition delays. The uncertainty on the ignition delay is less than 0.1 ms. Similar to moderate pressures at 1200 RPM, there is little distinction between the ignition delay of the two injectors at high diesel fuelling rates. Finally, shorter ignition delays were again observed for Prototype B at 28 MPa.

Similar to 1200 RPM, the minimum diesel fuelling rate for stable combustion was lower for Prototype B than for Prototype A. The average minimum diesel fuelling rate was around 12-15 mg/inj for Prototype A and 5-10 mg/inj for Prototype B.

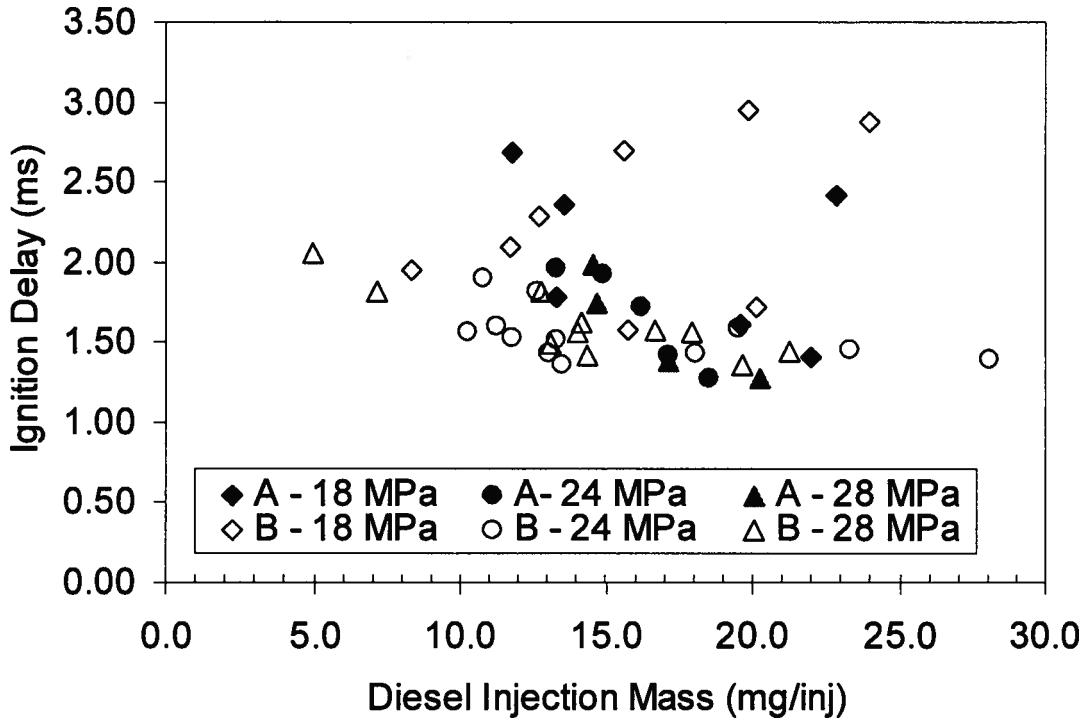

Figure B.2: Ignition Delay for VII-A and VII-B tests at 800 RPM

The trends observed for the IHR ratios between Prototype A and Prototype B at 800 RPM were not as evident as the VII-1200 RPM tests. As seen in Figure B.3, the IHR ratio varied widely. Still, there appears to be a shift to higher IHR ratios at higher diesel fuelling rates for both prototypes. Also, Prototype B appears to have a higher IHR ratio at moderate and high gas pressures. At lower injection pressures, the IHR ratio appeared to be slightly lower for Prototype B compared to Prototype A.

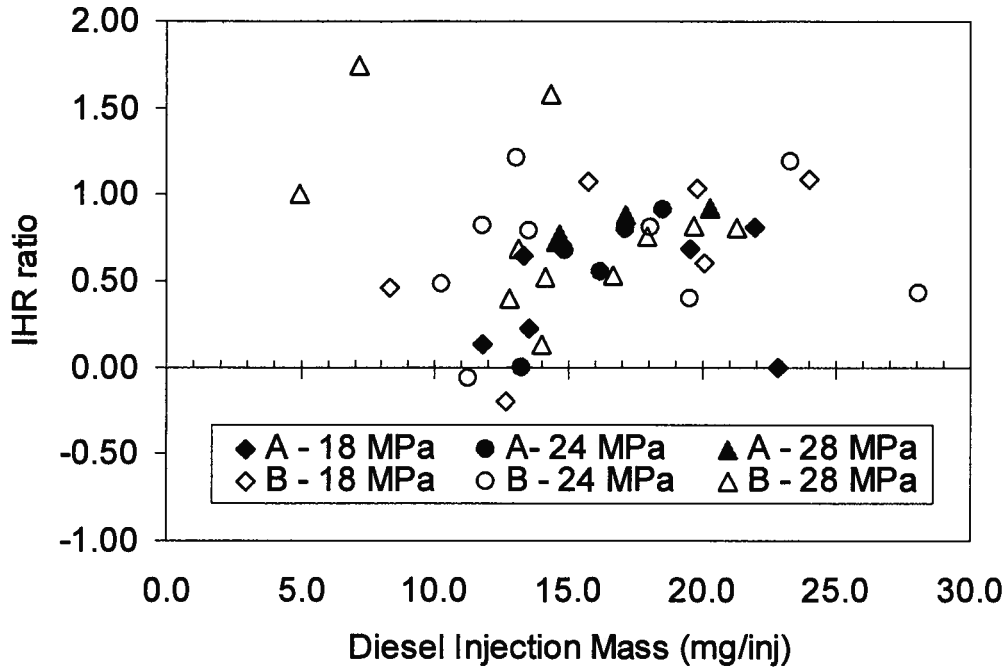

Figure B.3: IHR ratio for VII-A and VII-B tests at 800 RPM

Figure B.4 shows that the knock intensity between Prototypes A and B are similar. As with the ignition delay and IHR ratio, however, it was difficult to compare injector performance due to the lack of resolution with the VII-A tests. Knock intensity was observed to be slightly higher for the VII-B cases at 24 MPa rail pressure than both 28 MPa and 18 MPa test cases. This was different that what was observed for Prototype A, where higher knock intensities were observed at higher diesel rail pressures.

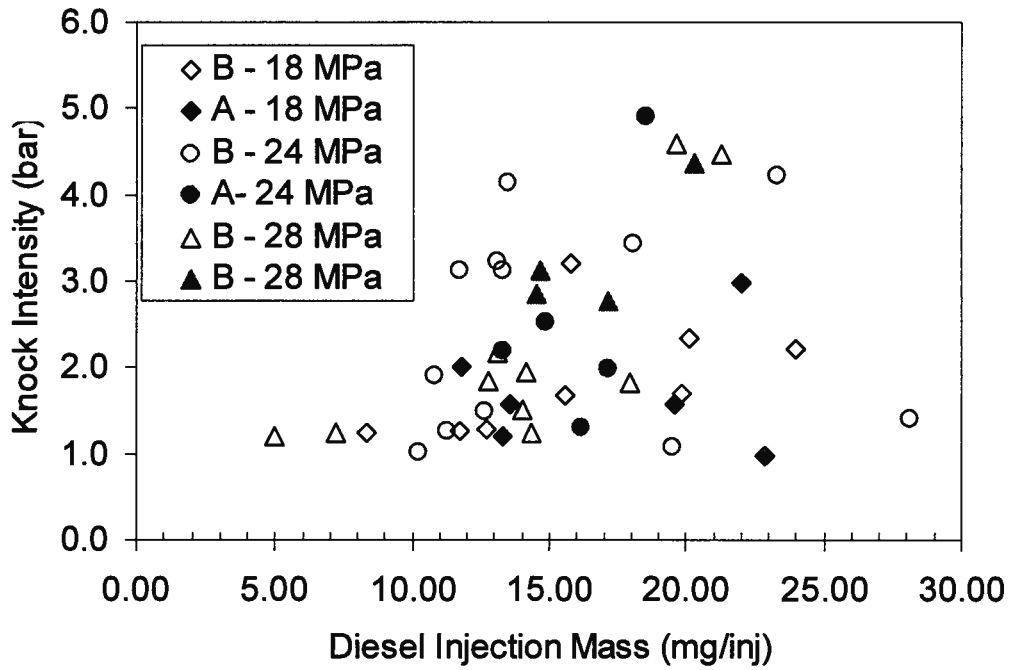

Figure B.4: Knock Intensity for VII-A and VII-B tests at 800 RPM

At both 800 RPM and 1200 RPM, diesel flow rate was shown to have the most significant influence on the pilot injection for all operating conditions. The lower the diesel flow rate, the greater the influence the second injection had on the first due to the second pulse scavenging some of the diesel from the nozzle plenum which had not been injected in the first pulse.

B.3 Test Series VIII: Double Injection Emissions and Combustion Characteristics

The objective for Test Series VIII was to compare ignition, combustion stability, and gaseous emissions between Prototype A and Prototype B for double injection operation. To compare emissions, timing sweeps at constant equivalence ratios and pilot fuelling rates were done. These tests were previously done for Prototype A by Jones (2006) at a CR of 16.7:1. Section 3.3.5 discusses the parameters that were held constant for this test series.

G.3.1 Analysis of Variance (ANOVA)

In order to determine the statistical significance of the injector type on the emissions and combustion stability, an Analysis of Variance (ANOVA) was performed. For ANOVA, the measured response (ignition delay, combustion stability, NOx emissions, etc) is related to the controlled parameters through the use of a block model. The block model used for these examples is presented in Equation B.1 (Hicks 1982, 252). In ANOVA, the hypothesis is that the treatment options τ_{ijk} are insignificant so that the each measured response Y_{ijkm} will consist only of its population mean μ, and a random error $\varepsilon_{m(ijk)}$.

$$Y_{ijkm} = \mu + \tau_{ijk} + \varepsilon_{m(ijk)} \tag{B.1}$$

The measured responses for this study were the ignition delay, the co-efficient of variation of the gross indicated mean effective pressure (COV GIMEP), and the power specific emission levels of CO, NOx, CH_4, uHC. The gross power and gross IMEP are used since the friction losses in the SCRE are not the same as in a heavy-duty engine with

six working cylinders. COV IMEP has been used in previous studies as a measure of combustion stability.

The treatments τ_{ijk} are the injector type (I_i), the 50% IHR (H_j), and the speed (S_k). The subscripts *i, j,* and *k* represent the different injector types, combustion timing, and speeds tested. Each possible combination of I, H, and S represent an observation cell which is repeated *m* times. These treatment terms plus the interaction terms are presented in Equation B.2.

$$Y_{ijkm} = \mu + R_m + I_i + H_j + S_k + I_iH_j + I_iS_k + H_jL_k + I_iH_jS_k + \varepsilon_{m(ijk)} \qquad \text{(B.2)}$$

Equation B.2 includes interaction terms which may contribute to observed differences between injectors. Second order interaction terms (I_iH_j, I_iS_k, etc) are usually negligible and third order interaction terms ($I_iH_jS_k$) are extremely rare. However, both second and third order interactions will be included in this analysis since significant second order interaction terms make interpreting the main effects more difficult (Hicks 1982, 94).

ANOVA is used since the sum of squares, SS_{total}, can be broken down into the sum of squares of the different treatments, interactions and error as shown in Equation B.3

$$SS_{total} = SS_I + SS_H + SS_S + SS_{I\times H} + SS_{I\times S} + SS_{H\times S} + SS_{I\times H\times S} + SS_{error} \qquad \text{(B.3)}$$

Each sum of squares is seen to be independent of the others and thus a Chi-squared distribution if divided by its degree-of-freedom (df) (Hicks 1982, 41); therefore, an F test can be employed.

G.3.2 Assumptions and Corrections for ANOVA

Although the complete factorial was completed for the test data, there were cases of missing repetitions, mostly for Prototype A. Equal number points are needed for a full factorial analysis in order to retain orthogonality (Hicks 1982, 73). For some observation cells only a single measurement was taken. In these cases, Hicks suggests replacing the missing observations with those that make the sum of the squares of the errors a minimum (Hicks 1982, 74). Each missing term can be solved for separately solving for SS_{error} over a wide range of that missing term and finding the minimum.

Also, it assumed that the treatment parameters are discrete. For the injector type this is evident since either Prototype A or B will be installed. The 50% IHR, the engine speed and the load, however are continuous and can vary widely in the SCRE. In this case, it is assumed that the change in the measured response due to the small change in H or L is much smaller than the random fluctuations, $\varepsilon_{m(ijk)}$.

Third, the Null Hypothesis of ANOVA is that all of the measurements are taken from a normal population with population mean μ and variance σ^2 (Devoire 2004, 689) The sample means for a specific combination of the treatment options is allowed to vary for each case, but the variance is assumed to be the same for all of the tests (Hicks 1982, 59). For these tests, the difference in variance was quickly checked for all of the measured responses through the use of the D_4 factor as described below (Hicks 1982, 60).

The D_4 factor test is usually used in quality control to check homogeneity of variance by determining for a given measured response whether all of the measured ranges of an observation cell (maximum Y_{ijkm} – minimum Y_{ijkm}) are less than $D_4\overline{R}$ where D_4 is 3.276 for a sample size of 2 and $\overline{R}$ is the average of all the measured ranges (Hicks 1982,

60). It was observed that for most of the cases, all of the ranges were within the threshold. The points outside the threshold were the CO, tHC, CH_4, and COV GIMEP for the low load, low speed, 50% IHR at 15°ATDC. Due to late cycle bulk flame extinction, the absolute magnitude of these measured responses was changing rapidly at a 50% IHR of 15°ATDC. Therefore, a 1 degree error in setting the timing contributed to the larger than normal variance measured for this observation cell.

Also, the measurements need to be repeatable and random (Hicks 1982, 59). This means that for a given I, H, and S, the measured response for any given set of treatment options needs to be pulled from the same normal distribution. The order of the observations in a block of tests should be completely random over all of the treatment parameters. As with previous experiments in the SCRE, the tests are randomized as much as possible without significantly increasing the test time (McTaggart-Cowan 2006a; Jones 2004). In this case, the three 50% IHR timings (10°, 5°, and 15° ATDC) were conducted sequentially.

Finally, the most important violation on randomization was testing Prototype A and B in two different test locations (Kaiser and CERC). Thus, there is no way to be sure that the differences attributed to the injector have no contribution from the engine installation.

Even though the variance in all of the tests was not completely equal, the treatment parameters were not discrete, and the observation cells were not in a completely random order, it was still useful to perform ANOVA in order to determine the significance of the treatment parameters. The Null Hypothesis is rejected at an α level of 0.01 (1 in 100 chance of identifying a significant effect when one is not present), as opposed to an α level of 0.05 used in previous work with the SCRE by McTaggart-Cowan (2006a). The

treatment factors and interactions that exhibit significant differences were examined further in an attempt to understand the reasons for the differences.

G.3.3 ANOVA Results

Table 4.1 gives the ANOVA for the three measured emissions and engine performance metric for fixed load/changing speed. As discussed in Section 3.3.6, an equivalent table for fixed speed/changing load is presented in Appendix B. The treatment variables and the interaction terms of the treatment variables in Equation 4.2 have been transposed into the table with the second column displaying the degrees of freedom (df) which is *i-1, j – 1,* etc. for the injector type, 50% IHR, etc. Although 3 tests were conducted for most of Test Series VIII-B, only the first two repetitions were used since most of the data points for Test Series VII-A had 2 or 1 repetitions.

Table B.3: ANOVA for Test Series VIII: fixed load/changing speed

	df	CO	Nox	uHC	CH_4	Ignition Delay (ms)	COV GIMEP
Injector (I)	*1*	2.9E-05	3.8E-04	1.3E-07	0.04	3.7E-04	0.60
50% IHR (H)	*2*	3.6E-05	1.0E-10	0.01	0.05	3.5E-05	0.77
Speed (S)	*1*	2.6E-11	1.00	2.7E-04	9.4E-04	1.4E-06	0.08
I x H	*2*	0.38	0.01	0.09	0.39	0.88	0.40
I x S	*1*	0.08	0.03	0.75	0.99	0.16	0.98
H x S	*2*	1.9E-06	6.4E-07	0.11	0.24	1.1E-03	0.77
I x H x S	*2*	0.91	0.57	0.18	0.58	0.31	0.60
Error	11						

The shaded regions represent those areas where the Null hypothesis (the measured response is independent of all treatments) is rejected at an α level of 0.01 (1 in 100 chance of identifying a significant effect when one is not present). The actual probability

is shown for these cases. Note that although the combustion timing and engine speed were observed to have significant impacts on the exhaust emissions and ignition delay, their significance will not be discussed.

As seen in Table B.3, the injector geometry was observed to have the greatest significance on ignition delay, CO, NOx, and uHC emissions. These differences will be discussed in the following section. There were no factors that significantly affected COV GIMEP, possibly since there was sufficient diesel used to avoid long ignition delays discussed in the earlier test series (VII).

Figures B.5 - B.7 show the ignition delay, combustion stability, and gaseous emissions plotted as a function of combustion timing. The difference in ignition delay due to injector geometry was found to be statistically significant at moderate engine speeds. Figure B.5 compares the ignition delay between Prototype A and Prototype B at 1100 RPM and 1400 RPM. At 1100 rpm, Prototype B exhibits ignition delays close to 1.6 ms, whereas Prototype A exhibits an ignition delay nearly a millisecond longer. At this speed, the combustion timing has little effect on ignition delay. At 1400 RPM there is little difference in ignition delay between Prototype A and B. At 1400 RPM there is a strong relationship between ignition delay and combustion timing with later timings exhibiting shorter ignition delays for both Prototype A and B. The amount of diesel injected at 1400 rpm may not be enough since the pilot combustion was not as significant at higher engine speeds. Figure B.5 also shows the difference in combustion stability between prototypes. As previously mentioned, the engine stability was similar for both prototypes due to sufficient diesel being used to ensure stable combustion.

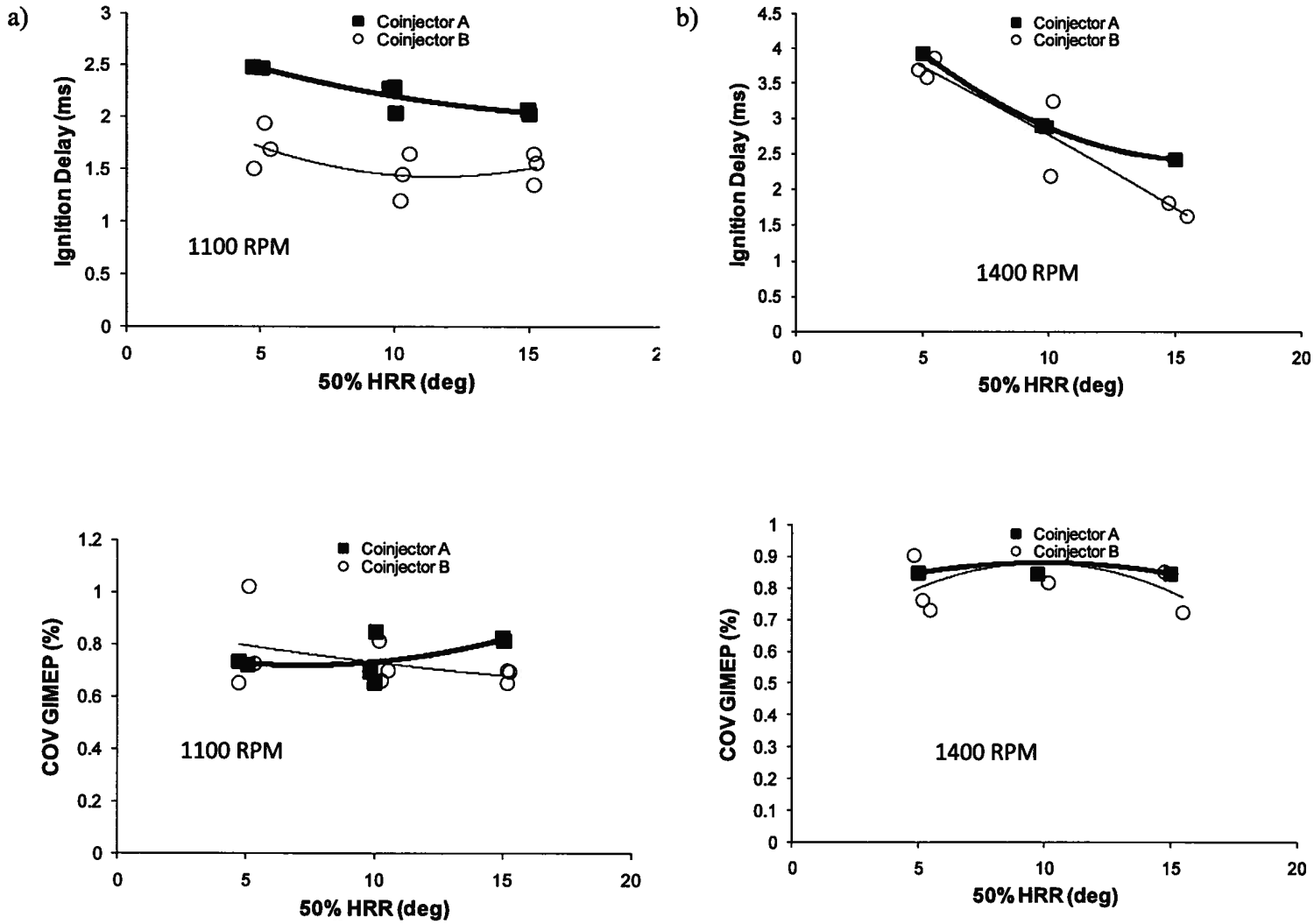

Figure B.5: Ignition delay and COV GIMEP for 13 bar GIMEP for a) 1100 RPM and b) 1400 RPM

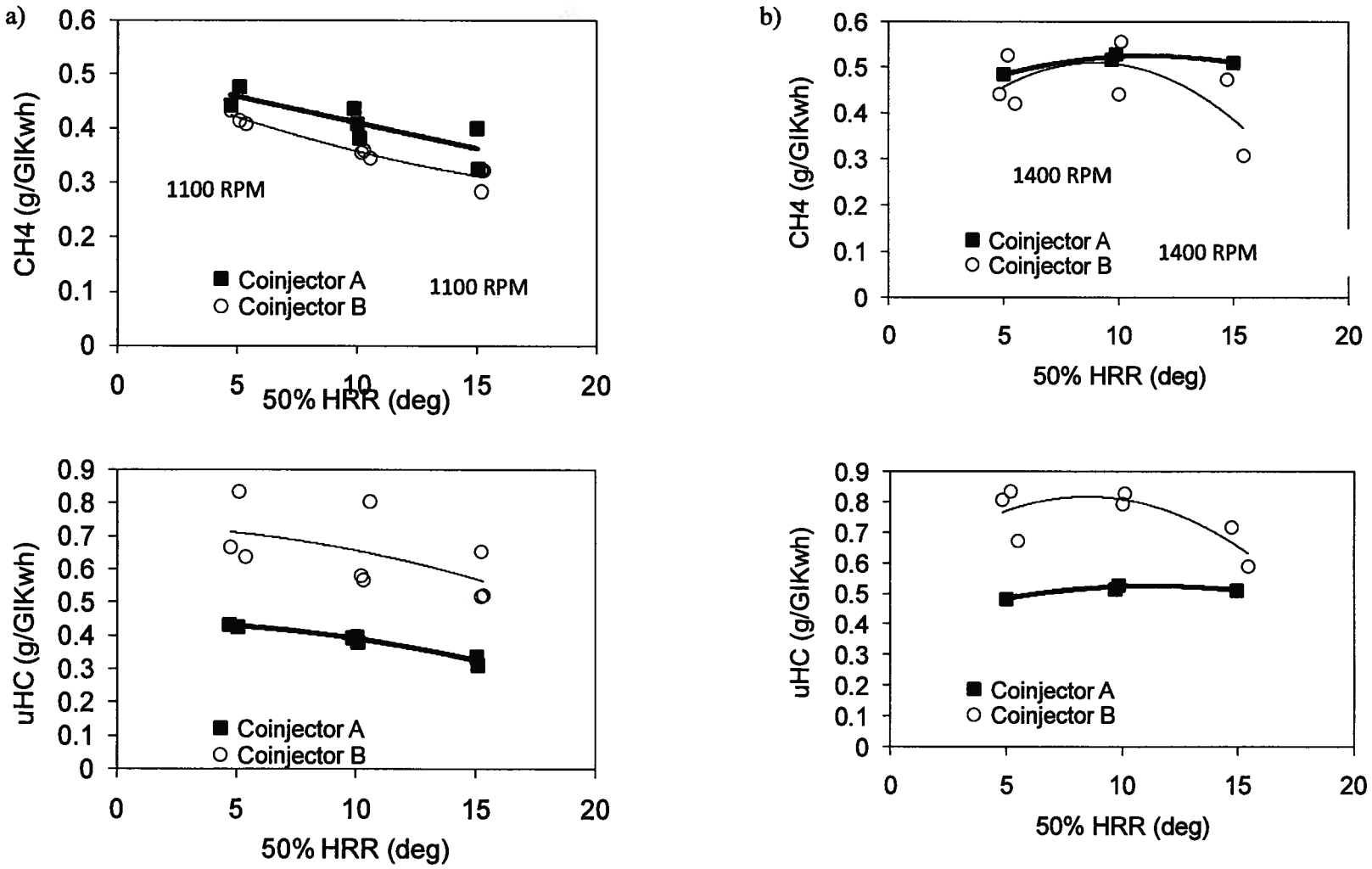

Figure B.6: CH_4 and uHC emissions for 13 bar GIMEP for a)1100 RPM and b) 1400 RPM.

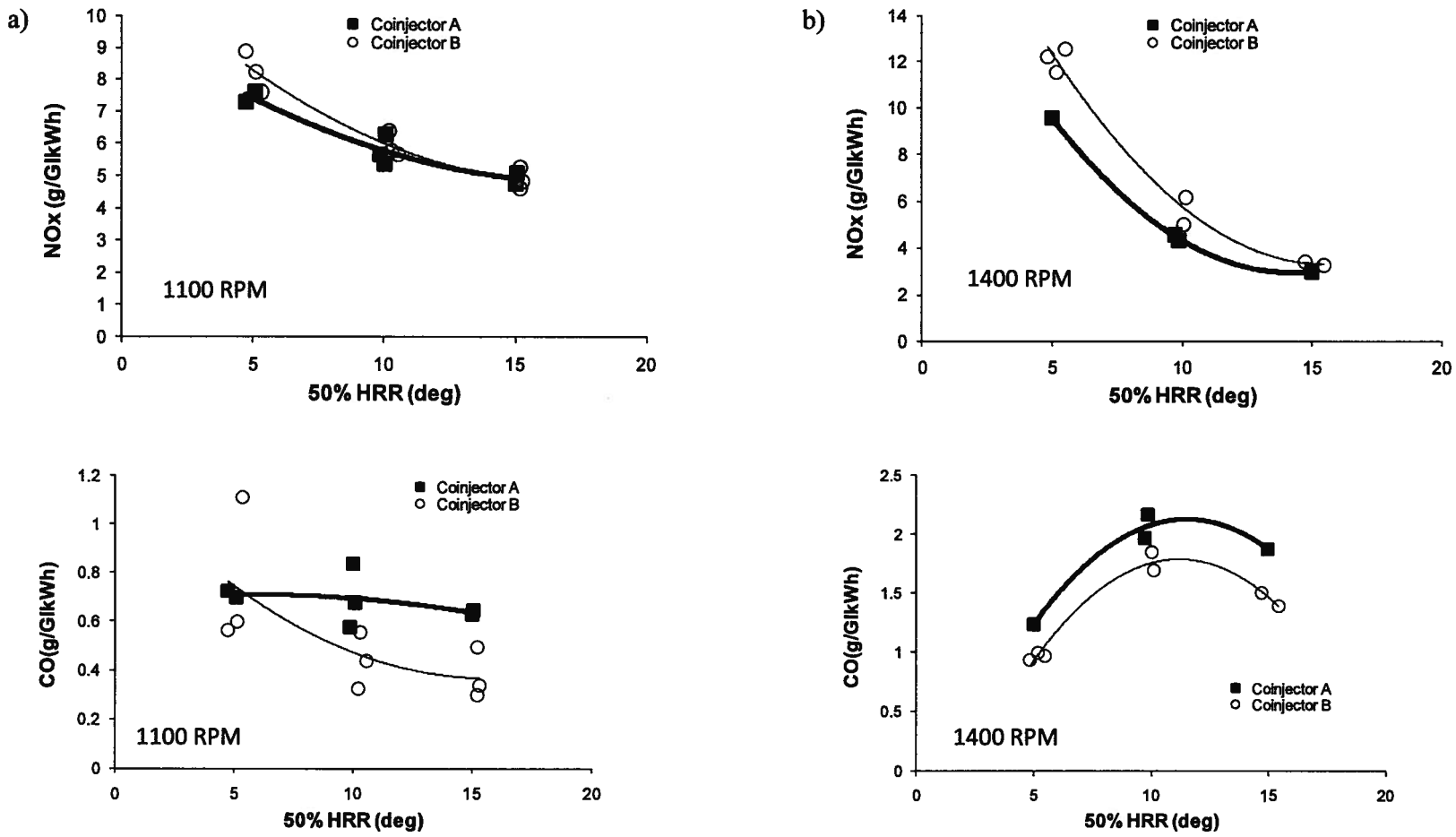

Figure B.7: NOx and CO emissions for 13 bar GIMEP for a)1100 RPM and b)1400 RPM

Figures B.6 shows the CH4 emissions and uHC emissions for the two different engine speeds. Although there were observed differences in engine stability and CH4 emissions between injectors, the difference was not statistically significant. The uHC however, measured significantly higher. The relatively higher uHC emissions was not expected for Prototype B since previous studies with the original HPDI injector have found that over 80% of the uHC emissions are unburned CH_4 (Dumitrescu et *al.* 2000; Duggal et *al.* 2004). More likely, there was a linearization error in either the CH4 or uHC emissions in one of the test cell setups.

The high uHC emissions are also suspect since the main causes for HC emissions in diesel engines fail to fully explain the observed differences in uHC emissions for the co-injectors. At moderate loads, there are three main mechanisms for hydrocarbon emissions in diesel engines: over-leaning due to long ignition delay times, under-mixing from low velocity fuel vapour introduced late in the combustion process from the injector sac volume, and late cycle bulk quenching (Heywood, . Hydrocarbon emissions due to over-leaning are correlated with ignition delay and should be lower for Prototype B. Similarly, the amount of low velocity fuel entering the combustion chamber late in the cycle should be nearly the same since the sac volume of the injector was not modified. Finally, the uHC emissions are seen to drop for later timings, as observed in Figure 4. If late cycle bulk quenching were important, higher uHC emissions should be observed for later injections.

Figures B.7 shows the NOx emissions and CO emissions for the two different engine speeds. NOx emissions are higher and CO emissions are lower at moderate speeds due to a shorter pilot GPW for Prototype A.

At moderate speeds and high speeds the CO emissions are consistently lower for Prototype B. NOx emissions appear to be similar for both Prototype A and Prototype B, except for at advanced combustion timing at high engine speeds where NOx emissions are higher for Prototype B.

It is important to understand the difference in ignition delay and combustion stability between Prototype A and Prototype B since these metrics may have an influence on some of the observed differences in emissions. Over-mixing of the fuel before ignition was not observed to be an issue since the shorter ignition delay times for Prototype B at 1100 RPM did not result in significantly lower CH_4 and uHC emissions. Shorter ignition delays for Prototype B indicated that there was more diesel in the pilot injection; therefore, more heat was released early in the combustion cycle lowering CO emissions and increasing NOx emissions.

In the equation B.2, S_k, which represents the speed in the constant speed/changing load case can be interchanged with the engine load (L_k) in the constant speed/changing load case.

This analysis was not included in the body of the thesis because different pilot injection durations were used between injectors, making it much more difficult to distinguish between the effects of the injector type and the effects of a shorter pilot GPW. Unfortunately, this negates any comparisons between Prototype A and Prototype B that could be done at low load for CO and NOx. The comparisons of COV GIMEP and ignition delay, however, should be fine since both were found to be independent of GPW (see Figures 4.9 and Figure 4.15 for COV GIMEP and ignition delay respectively).

Table B.4 shows the ANOVA results for the constant speed (1100 RPM), changing load (0.4 & 0.55 EQR) tests. Again, the injector geometry was observed to have a significant effect on the ignition delay, and power specific CO and NOx emissions. In addition, for the CO and NOx emissions there were load x injector interactions.

Table B.4: ANOVA for Test Series VIII: fixed speed/changing load

	df	CO	NOx	tHC	CH_4	Ignition Delay (ms)	COV GIMEP
Injector (I)	*1*	1.6E-05	2.0E-05	0.48	0.10	2.0E-08	0.02
50% IHR (H)	*2*	3.8E-04	1.3E-08	5.1E-04	1.8E-04	8.4E-04	0.04
Load (L)	*1*	1.8E-10	7.1E-05	4.6E-06	1.1E-06	5.0E-03	3.2E-06
I x H	*2*	0.58	0.61	0.95	0.49	0.06	0.41
I x L	*1*	3.8E-05	1.3E-03	0.90	0.15	0.17	0.02
H x L	*2*	3.3E-04	0.40	3.6E-04	1.1E-04	0.90	0.03
I x H x L	*2*	0.64	0.02	0.95	0.50	0.09	0.16
Error	11						

Figures B.8 – B.10 show the ignition delay, COV GIMEP, and power specific emissions at 30% Load/1100 RPM. As with higher speeds and loads, the ignition delay is significantly shorter for Prototype B. The COV GIMEP appears to be slightly higher for Prototype B, and the CH_4 a little lower. Longer pilot GPWs for Prototype B would allow for more early-cycle heat release which would lead to higher early-cycle cylinder temperatures. This could explain the higher NOx and lower CO emissions observed for Prototype B.

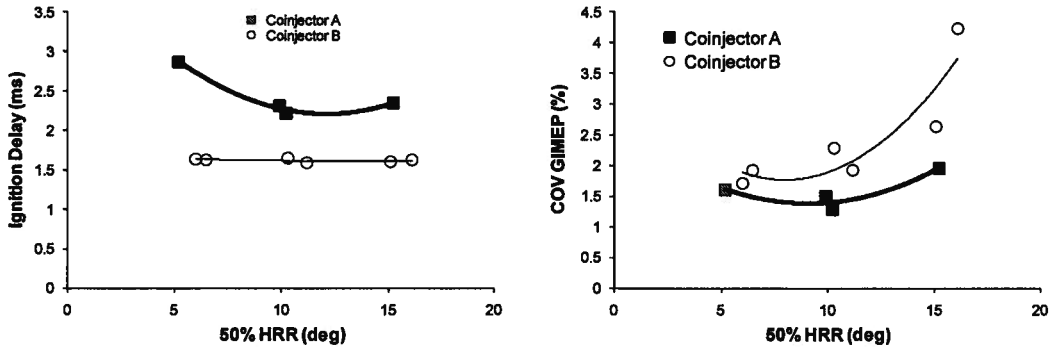

Figure B.8: Ignition delay and COV GIMEP for 6 bar GIMEP and 1100 RPM

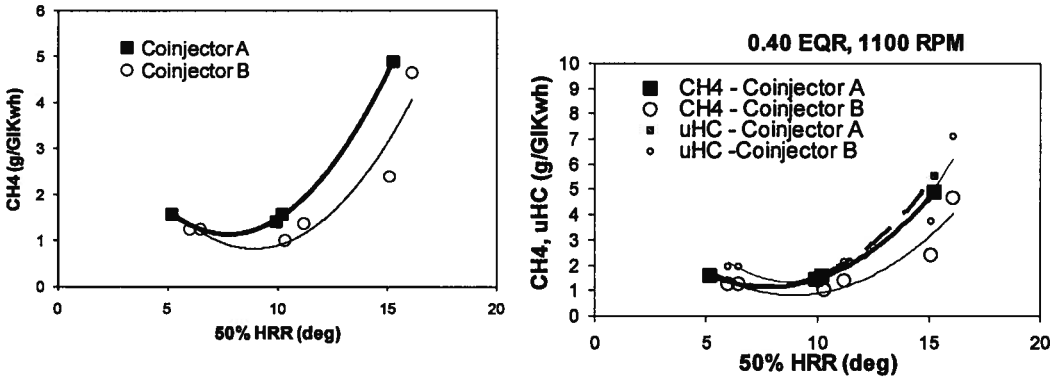

Figure B.9: CH4 and uHC emissions for 6 bar GIMEP and 1100 RPM

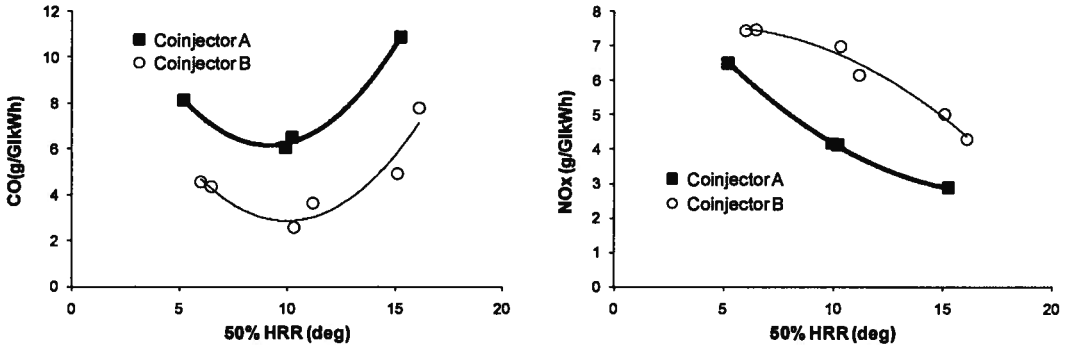

Figure B.10: NOx and CO emissions for 6 bar GIMEP for 1100 RPM

Appendix C: Carbon Balance and Airflow

In a perfect world, this section shouldn't exist. However, because of random and systematic error, mis-calibrated measurement devices, and human error, the measured and calculated values contain uncertainties.

Usually, the airflow rate is calculated through the use of a UBC built venturi. However, in this test engine, there have been problems getting a proper mass balance of Carbon. In addition, with the airflow measurement from the venturi, the volumetric efficiency was found to be greater than 1 for the SCRE, whereas it should be around 0.8 – 0.9.

The error in the Carbon balance indicates that there are one or more systematic errors from devices used to calculate the airflow. A systematic error is defined as an error that is independent of the number of measurements. Assuming that the emission bench analysers respond in a relatively linear fashion, systematic uncertainty should be minimized with these sensors as they are calibrated daily. The linearity CO2 and O2 passed linearization checks. While the diesel flow rate has large random fluctuations associated with it, there should be no systematic errors (unless of course there were a leak somewhere). This leaves the natural gas coriolis flow meter (systematic uncertainty may be due to residual strain in the strain gauge) or the airflow venturi (systematic error may be due to calibration).

For these tests, the error was assumed to come from the air flow reading. The other measurements that contribute to the mass balance of Carbon have been checked and so far, no systematic errors (offsets) have been found.

Therefore, in order to better approximate the airflow, an airflow was chosen so that the Carbon balance would be close to 1. Functionally, this is ignoring any measurements of airflow from the venturi and using the other measurements plus the First Law of Thermodynamics to solve for the airflow. Not only does this provide a more accurate measure of the airflow (assuming that there are no systematic errors in the other measurements), it also provides a more precise approximation of the airflow rate.

This can be shown through a study of the propagation of errors in the system. Instead of using the error propagation equation to determine the r.m.s of the airflow rate, Monte Carlo simulation is used. Since there are continual improvements to reduce both the random and systematic error in the system, the program can be quickly modified to reflect those changes.

Measured data was taken both from the old engine setup and the new engine setup. Assuming that the errors for each of the measurements were independent and Gaussian, a 10,000 Monte-Carlo simulation was run. Two simulations were run. The first was the airflow computed from the pressure drop through the venturi. For each run, a normally distributed measurement for the air line pressure, temperature, and venturi pressure drop were used to calculate air flow rate using the existing calculations for flow rate. Errors in the measurement of the venturi areas were not included at this point.

The calculated airflow based on the Carbon balance was done by taking normally distributed Gaussian distributions for the intake (airflow, intake CO2, CNG, and Diesel) and the exhaust (O2, CO2, CO, NOx, and tHC) to calculate the C balance. The standard deviations were assumed to be the variation of the measurement over the sample time. The airflow was then

changed by multiplying it by a correction factor until the C balance was equal to 1 ± 1E-6. The resulting histograms can be seen in Figures C.1a and C.1b.

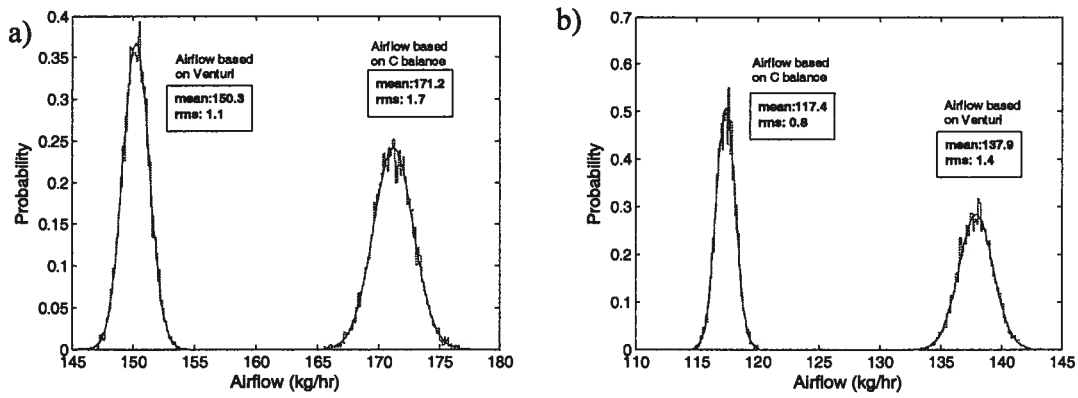

Figure C. 1: Comparison of Airflow Calculations in a) Kaiser, and b) CERC

Two important observations should be made about Figures C.1a and C.1b. First, that there is a systematic error in one or more of the measurements observed as a shift in the mean calculated air flow rates. Air leakage in the intake air system or piston blow-by may cause air flow rates as measured by the venturi to be higher than expected. Similarly, inaccurate measurements for the diesel flow rate, poor linearization of the O_2 emissions could cause high or low air flow readings using the Carbon ratio.

Second, there is still improvements that can be made in the CERC setup to reduce error, as seen by comparing the rms values between Figures C.1a and C.1b, shown in Table C.1. For both test locations, most of the error comes from the natural gas flow measurement, the CO_2 and the Diesel. However, in CERC, there are significant contributions from the uHC and the CO. A smaller bottle of span gas should help for the CO measurement.

Table C.1: Specific measurements contribution to Airflow Uncertainty (Carbon Balance)

	Kaiser	CERC
CO2 Error (kg/hr)	0.4	0.8
O2, CO, NOx Error (kg/hr)	0.0	0.0
CO	0.0	0.4
uHC Error (kg/hr)	0.0	0.2
CNG Error (kg/hr)	***2.1***	***1.0***
Diesel Error (kg/hr)	0.2	0.2
Total Error (kg/hr)	**1.7**	**1.4**

The measurement of the diesel mass has accumulated errors coming from two points. First errors are introduced due to the fluctuations in the actual mass of the diesel mass measured in the scale. This is caused by the re-circulating diesel. Diesel pressure fluctuations will cause flow fluctuations into the measuring tank. Electrical noise and vibration may also be a factor. The second source of error is the mode of digitizing the diesel mass. The 4 – 20 mA signal from the scale is first converted into a 1 – 5 V signal and then to a 12 bit number on a scale from 0-10V. For the scale maximum range of 4 kg this would result in a resolution of 2g per bit.

Similarly, Table C.2 shows the contributions of the specific measurements for the Airflow. Note that the Venturi pressure, and the airline pressure have the largest contributions for both sets. Not shown here are the contributions of uncertainty in the flow areas or Cv, which is used in the calculations. Depending on the uncertainty, these factors can have significant effects (up to 1.5 kg/hr error).

Table C. 2: Specific measurements contribution to Airflow Uncertainty (Venturi)

	Kaiser	CERC
Venturi dP Error (kg/hr)	0.8	1.0
Airline T Error (kg/hr)	0.0	0.2
Airline P Error (kg/hr)	0.6	0.7
Total	1.0	1.2

The pressure variations at the intake pressure are slightly larger for the new system, due partly to the fact that the air pressure is being regulated. Hysteresis in the pressure regulator introduces some random error.

From this analysis, the use of the Carbon Balance as an additional measure can give accurate approximations of a specific value, if there is a systematic error present. For example, for this study, it was used to measure the airflow rate.

Appendix D: Factsheets

The Factsheets are as follows:

- U1-FAC-093-TEST - Heather Jones
- U1-FAC-098-Test – Gord McTaggart-Cowan
- W1-FAC-3788-ANYS – Phil Hill

Engine Testing Results from First I2I-Coinjector Prototype – 3rd Round of Testing J36 Comparison to I2I Injector

Objectives

1. Compare the emissions using the I2I injector versus a J36 injector over a range of operating conditions
2. Study the effect of pilot injection mass on emissions and combustion stability with the J36 and I2I injector.
3. Establish that the timing of the pilot pulse for the I2I injector does not need to be strictly controlled.

Test Matrix

Basically three main speed/load conditions were tested: 30% and 1100rpm, 75% load and 1100rpm, and 75% load and 1500rpm. Each of these main conditions were tested with 30% EGR and without EGR. At each condition a timing sweep was done by setting the power at mid-timing (50% IHR at 10 degrees ATDC) and then the fuel flow rate was held constant during the sweep. Hence the GIMEP changed slightly during the timing sweep but the fuel and air flows stayed relatively constant.

All of the tests were completed with a fixed pilot fuelling of 15mg/injection. In addition, at 1100rpm and 75% load the pilot quantity was increased to 20mg/injection and a timing sweep was done for both injectors and the J36 was also tested with a lower pilot quantity of 7-8mg/injection (low pilot fuelling not possible with the I2I injector due to combustion instability). At 1100rpm and 75% load, the relative timing of the pilot pulse (PSEP) was varied with respect to the gas fuelling so that the pilot pulse was well ahead of the first gas pulse until it was after the second gas pulse. Table 1 shows the testing matrix and Table 2 shows the controlled parameters during testing.

Table 1: Test matrix

	GIMEP = 6bar, 1100rpm	GIMEP = 13bar, 1100rpm	GIMEP = 13bar, 1500rpm
0% EGR	50% IHR @ 5, 10, 15 degrees	50% IHR @ 5, 10, 15 deg. Pilot quantity 15, 20mg/inj* PSEP (I2I only) -5, -1, 0.3, 1ms**	50% IHR @ 5, 10, 15 degrees
30% EGR	50% IHR @ 5, 10, 15 degrees	50% IHR @ 5, 10, 15 deg. Pilot quantity 15, PSEP (I2I only) -5, -1, 0.3, 1ms**	50% IHR @ 5, 10, 15 degrees

* Timing sweep done with each quantity
** Done only at mid-timing (50%IHR at 10deg.)

The gas injection pressure was fixed to 21MPa for both injectors. The I2I injector had a diesel rail pressure of approximately 23.6MPa during testing. A bias of 2.6MPa worked well in the past so this was fixed. The exhaust back pressure was fixed to approximately 10kPa over the intake pressure so that the residual fraction in the cylinder and the exhaust temperature remained relatively constant during each timing sweep and from injector to injector. The I2I injector was run only with pulsed gas injection. The first gas pulse width was fixed to 0.6ms at

low load and 0.7ms at high load and the second gas pulse was used to control the power output. The second gas pulse was timed to occur 1.5ms after the end of the first gas pulse (shown in the last set of tests to be a good setting, refer to U1-FAC-092-TEST).

The overall equivalence ratio was fixed during this testing. The oxygen in the recirculated exhaust gas was included in this calculation so that when power is fixed, the intake manifold pressure will be higher to achieve the desired oxygen level (similar to supplemental EGR).

Table 2: Fixed Parameters

GRP	21 MPa
I2I injector Bias	2.6 MPa
Exhaust BP (without EGR)	10kPa over intake
Overall equivalence ratio (based upon oxygen/fuel)	0.3 at low load, 0.55 at high load
CNG flow	Fixed during timing sweep
Pilot timing (PSEP)	0.3ms
Pilot fuelling	15 mg/inj
I2I first gas pulse width	0.6ms (low load), 0.7ms (high load)
I2I 2nd Gas pulse timing	start 1.5ms after end of first gas pulse

Results

1. EMISSIONS

GIMEP = 6bar, 1100rpm

Figures 1.1, 1.2, 1.3, and 1.4 show the power specific hydrocarbon, nitrogen oxide, particulate matter, and carbon monoxide emissions respectively at low load and 1100rpm. Operation with the I2I injector produces much higher hydrocarbon and carbon monoxide emissions than the J36 at this low load condition. However, the NO_x and particulate matter emissions are significantly lower with the I2I injector. It was not possible to get to the earliest timing of a 50% IHR at 5 degrees with the I2I injector due to combustion instability at this low load condition. The reason for this is unknown.

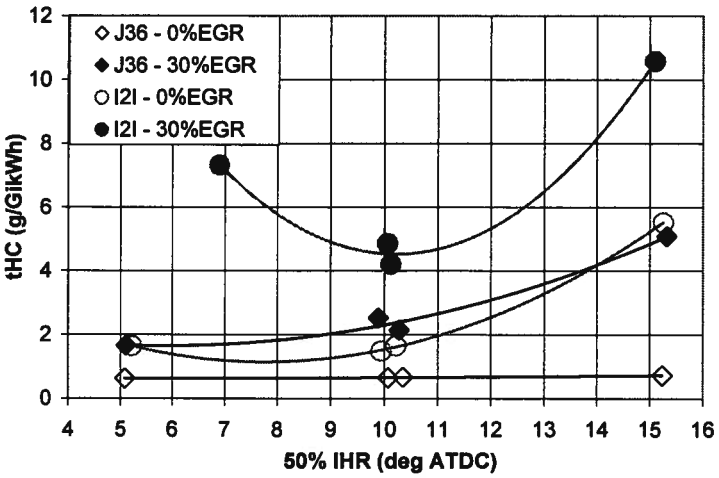

Figure 1.1: tHC emissions at low load and mid-speed

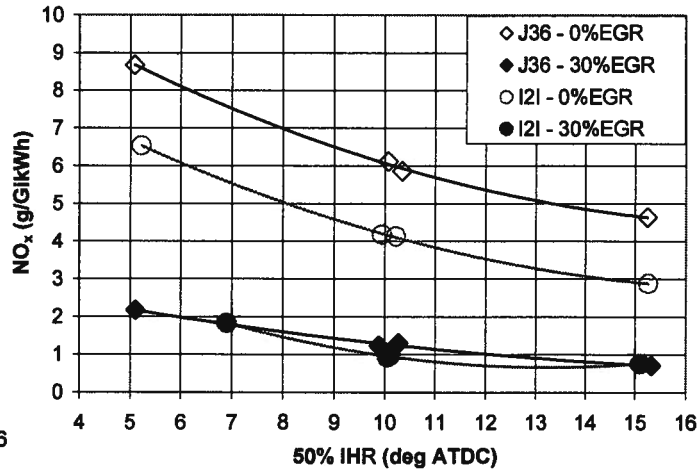

Figure 1.2: NOx emissions at low load and mid-speed

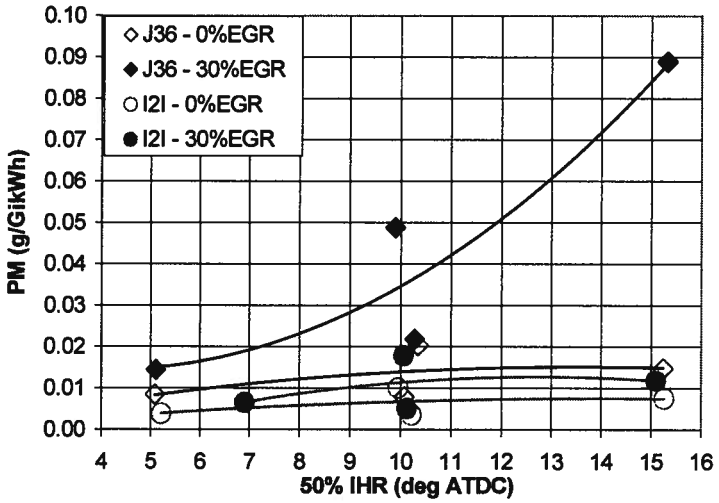

Figure 1.3: PM emissions at low load and mid-speed

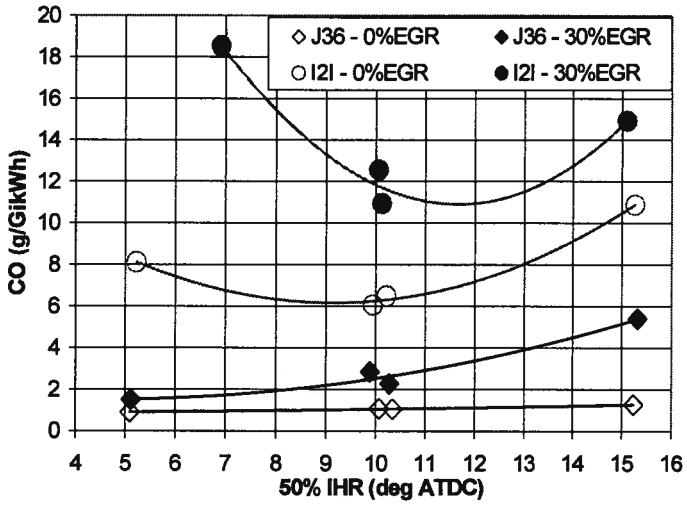

Figure 1.4: CO emissions at low load and mid-speed

GIMEP = 13bar, 1100rpm

Figures 1.5, 1.6, 1.7, and 1.8 show the power specific hydrocarbon, nitrogen oxide, particulate matter, and carbon monoxide emissions respectively at 75% load and 1100rpm. Generally, the two injectors are very comparable at this operating condition. The I2I injector gives slightly higher hydrocarbon emissions and lower particulate matter emissions that the J36 injector but the nitrogen oxide and carbon monoxide emissions are very close.

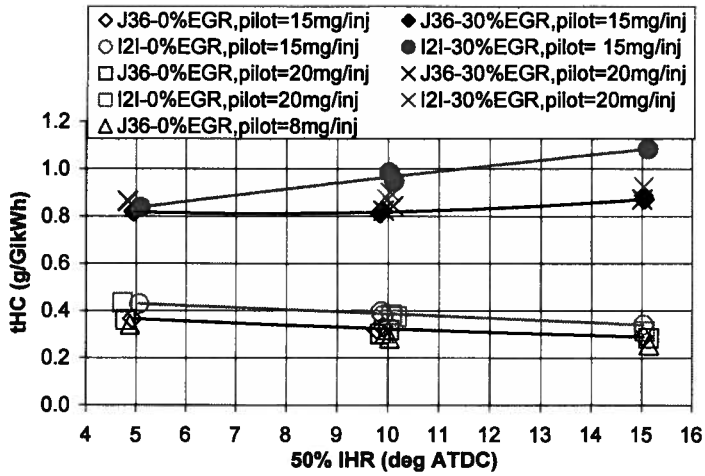

Figure 1.5: tHC emissions at 75% load and mid-speed

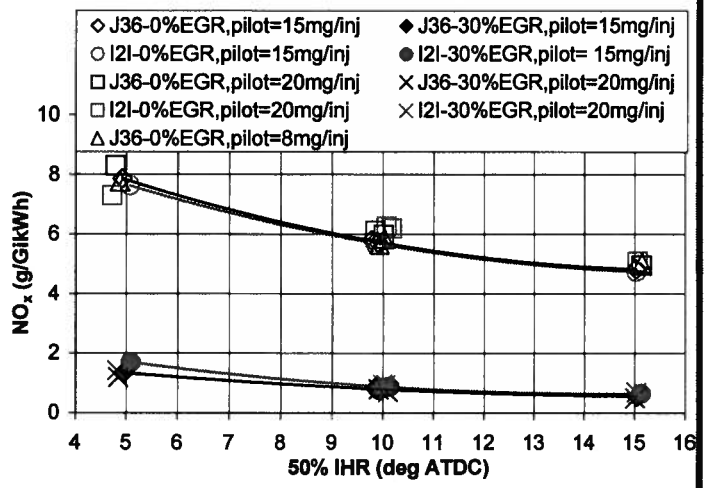

Figure 1.6: NOx emissions at 75% load and mid-speed

The effect of pilot fuelling amount on emissions can be seen in these figures as well. The J36 injector suffers higher particulate matter and carbon monoxide emissions with more diesel pilot added. Interestingly, more pilot fuelling with the I2I injector does not cause higher carbon monoxide emissions, only higher particulate emissions. It was not possible to decrease the pilot fuelling to 8mg/injection with the I2I injector due to combustion instability.

The better atomization in the I2I injector really shows here with the lower particulate matter emissions with this injector.

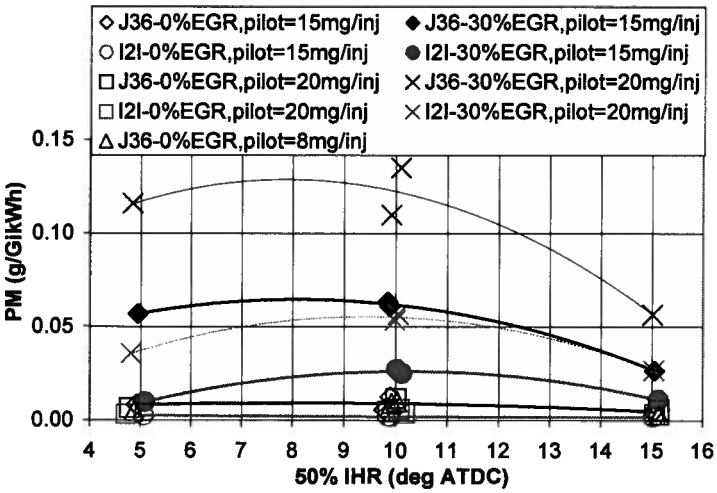

Figure 1.7: PM emissions at 75% load and mid-speed

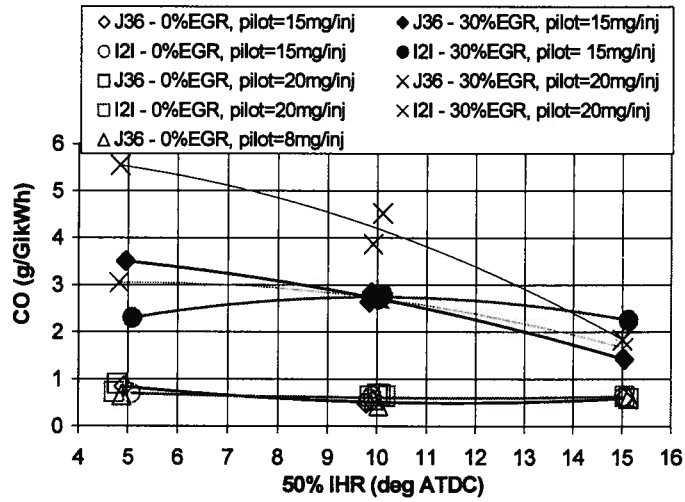

Figure 1.8: CO emissions at 75% load and mid-speed

GIMEP = 13bar, 1500rpm

Figures 1.9, 1.10, 1.11, and 1.12 show the power specific hydrocarbon, nitrogen oxide, particulate matter, and carbon monoxide emissions respectively at 75% load and 1500rpm. Generally, the hydrocarbon emissions are higher with the I2I injector and the particulate matter emissions lower. At this operating condition the effect of combustion timing has a much more dramatic effect with the I2I injector than the J36 injector. Hydrocarbon

emissions at 30% EGR are lower at early timing with the I2I injector and then much higher at late timings where as with the J36, hydrocarbon emissions are relatively constant over the timing sweep. Similarly, NO_x emissions with the I2I injector are more strongly affected by timing; early timing gives much higher NO_x than the J36 and later timing gives slightly lower NO_x.

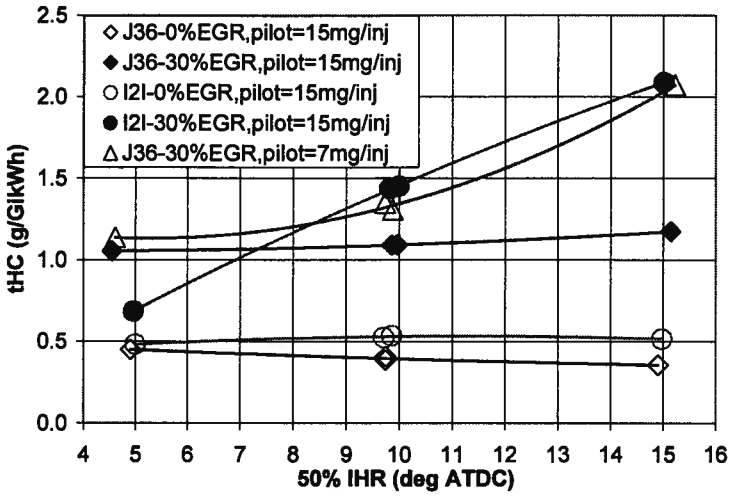

Figure 1.9: tHC emissions at 75% load and high speed

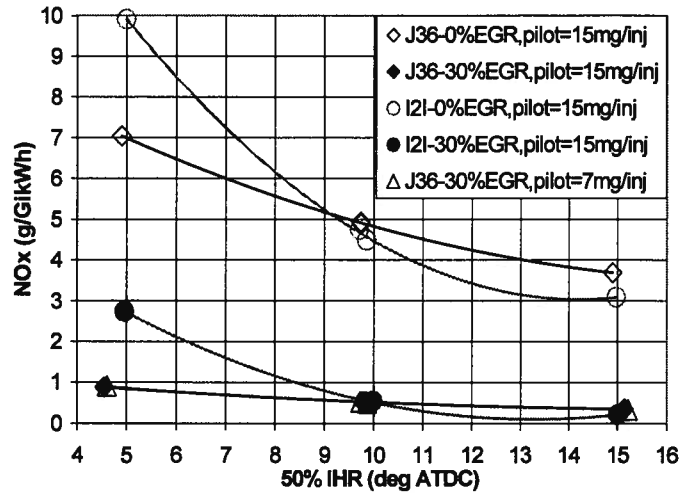

Figure 1.10: NO_x emissions at 75% load and high speed

Carbon monoxide emissions also follow a much different pattern with the I2I injector compared with the J36. At early timing the carbon monoxide emissions are approximately 3 times lower with the I2I and then quickly rise to levels higher than with the J36 after mid-timing.

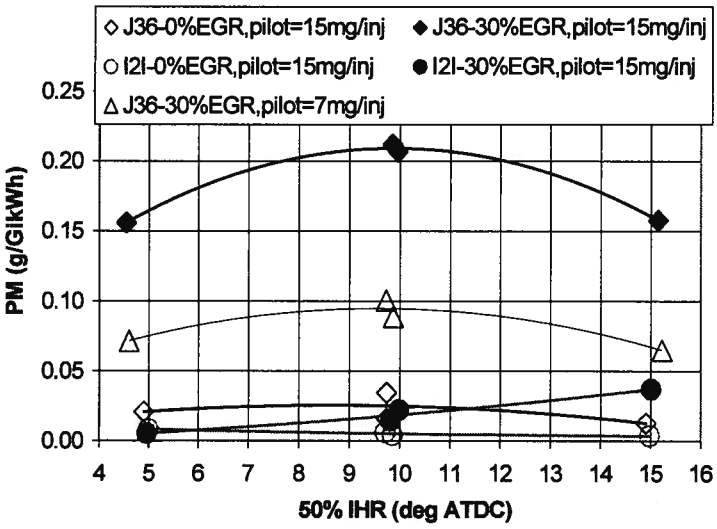

Figure 1.11: PM emissions at 75% load and high speed

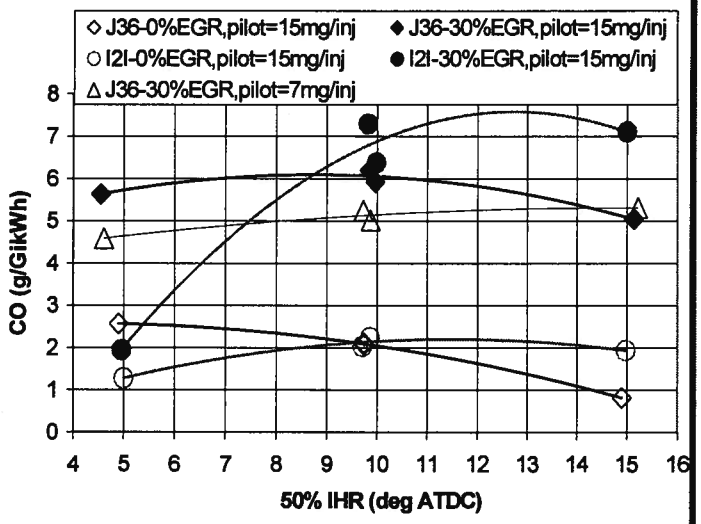

Figure 1.12: CO emissions at 75% load and high speed

Particulate matter emissions consistently lower with the I2I injector. At high load with EGR, particulate matter emissions significantly increase with the J36 injector. Lower pilot fuelling is definitely key to decreasing these particulate emissions in the J36 injector. Figure 1.11 shows that a decrease in diesel pilot fuelling of 50% decreases particulate emissions by more than 50%.

2. FUEL CONSUMPTION

The fuel consumption is shown in Figure 2.1. At high load the 2 injectors have very similar fuel consumption and in fact at high load the I2I injector may have slightly better efficiency. However, at low load with EGR the I2I injector has very poor efficiency. It causes a fuel consumption of approximately 5-7% higher at early and mid timings and over 10% higher at late timing. The cause of the extremely poor operation of the I2I injector at low load with EGR is unknown but it seems to be related to the cylinder pressure. The cylinder pressure was much higher with EGR during these tests since we fixed power output and the overall equivalence ratio (similar to supplemental EGR).

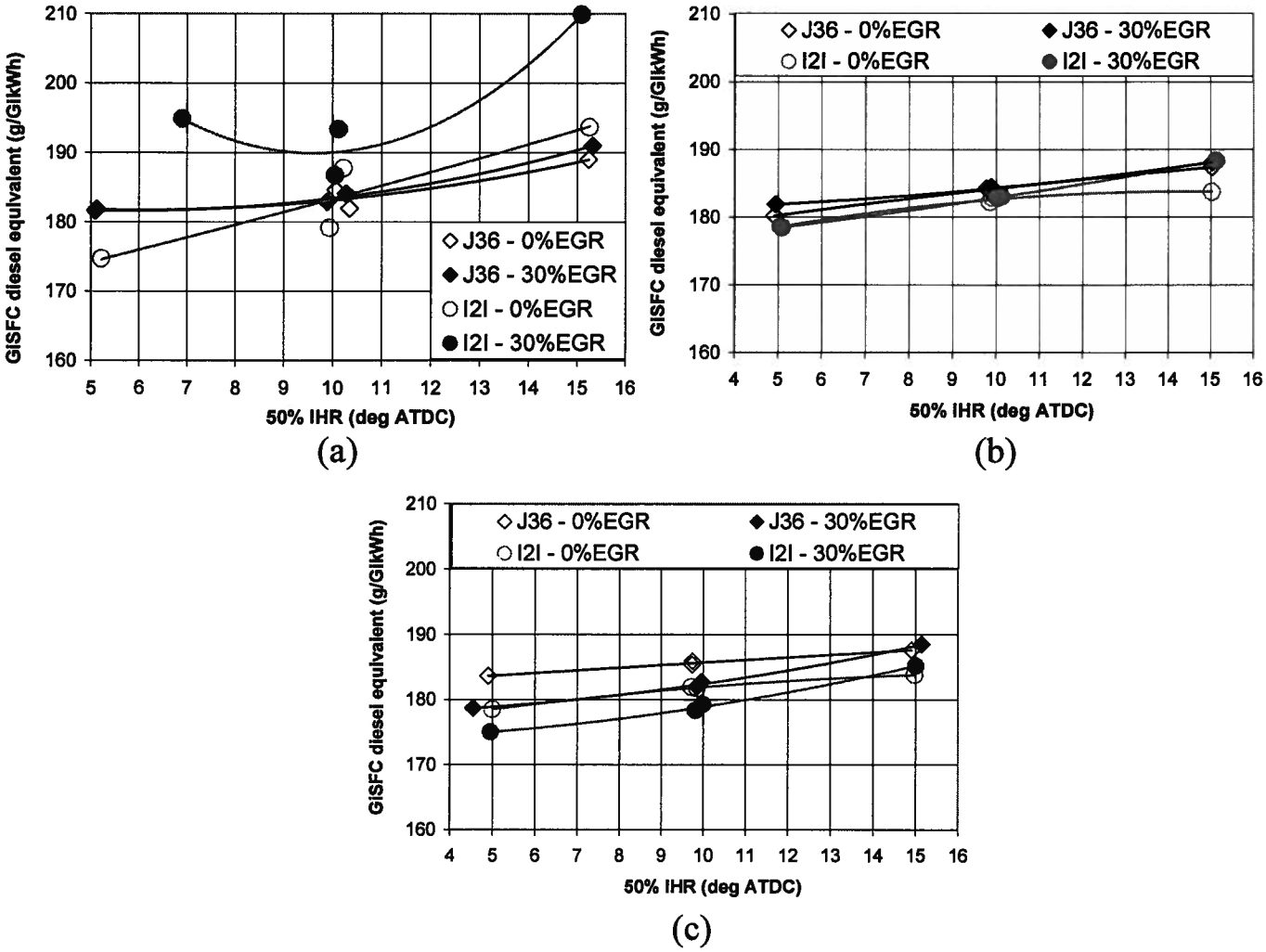

Figure 2.1: Fuel consumption at (a) low load, 1100rpm, (b) 75% load, 1100rpm, and (c) 75% load, 1500rpm

3. PILOT TIMING – I2I INJECTOR

The hypothesis was that a pilot pulse before the first gas pulse would be equivalent to a pilot pulse occurring after the second gas pulse in terms of operation. This is because the diesel is injected out of the gas sac so until the gas needle opens there is no diesel injection into the cylinder. To test this out the end of the pilot pulse was varied from 1 and 0.3 ms before the start of the first gas pulse to 1 and 5 ms after the start of the first gas pulse.

We will call the time between the end of the pilot pulse to the start of the first gas pulse the "pilot separation" (PSEP).

Table 3.1 shows the power specific emissions for each of the variations in PSEP. The top of the column contains a picture showing where the pilot pulse is located in relation to the gas pulses. The pilot timing varied from before the gas pulse to after the second gas pulse. Due to limitations of the controller, the pilot pulse could not be moved further back than –5ms. So to get the pilot pulse to occur after the second gas pulse, the timing between the two gas pulses had to be shortened (case 'd') otherwise the time between the gas pulses was fixed at 1.5ms.

Table 3.1: Emissions as a result of changing the pilot separation (PSEP) – time between the end of pilot pulse and the start of the first gas pulse.

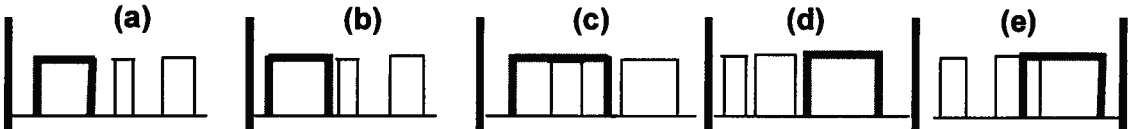

	(a)	(b)	(c)	(d)	(e)
PSEP (ms)	1	0.3	-1	**-5***	5
CO (g/Gikwh)	0.87	0.63	0.94	0.77	1.29
NOx (g/GikWh)	5.6	5.7	6.3	5.8	8.1
tHC (g/GikWh)	0.41	0.38	0.43	0.43	0.51
PM (g/GikWh)	0.008	0.002	0.003	0.004	0.002

Gas pulses
Pilot pulse
*** 2nd gas pulse was moved closer to the first so that the pilot pulse occurred after the second gas pulse as we could not set a pilot pulse of less than -5ms on the controller**

Generally, all pilot timings give approximately the same emissions except for case 'e' where the pilot is injected while the gas needle is open on the 2nd gas pulse. Figure 3.1 shows the corresponding pressure traces and heat release curves (averaged from 45 cycles). Basically all of the conditions run in the engine but case 'e' produces a sharp heat release likely because the pilot is igniting a pre-mixed gas mixture similar to HCCI combustion. Basically, as long as the pilot fuel is injected while a gas needle is closed the injector will behave the same.

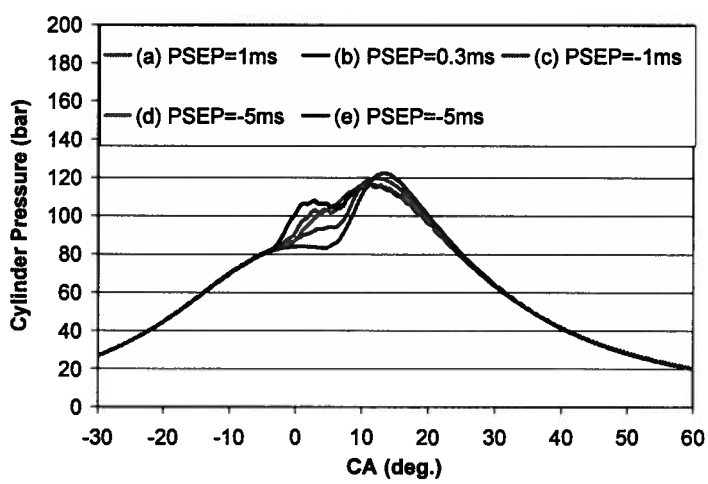

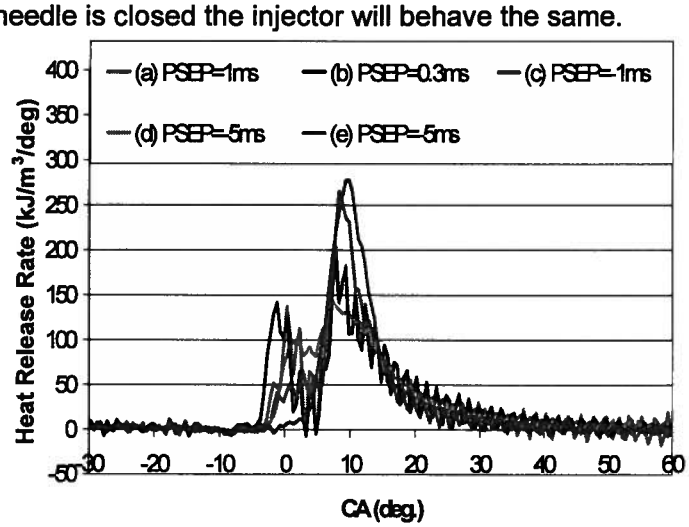

Figure 3.1: Cylinder pressure and heat release as the PSEP is varied (timing between end of pilot pulse and start of gas pulse)

4. COMBUSTION STABILITY

Figures 4.1 through 4.6 show the coefficients of variance of GIMEP and of maximum cylinder pressure for each of the operating conditions. The COV of P_{max} at the late timing in Figure 4.2 must be disregarded as it is the maximum pressure is due to compression at this condition and not due to combustion. The combustion stability is comparable between the two injectors with the exception of two conditions; low load with 30% EGR and with high pilot fuelling. At low load with 30% EGR the COV of GIMEP and P_{max} is up around 3.5% under the worst case (early timing). It was at this condition that high hydrocarbon emissions were also found. Figure 4.4 shows the COV of P_{max} up around 3% with high pilot fuelling.

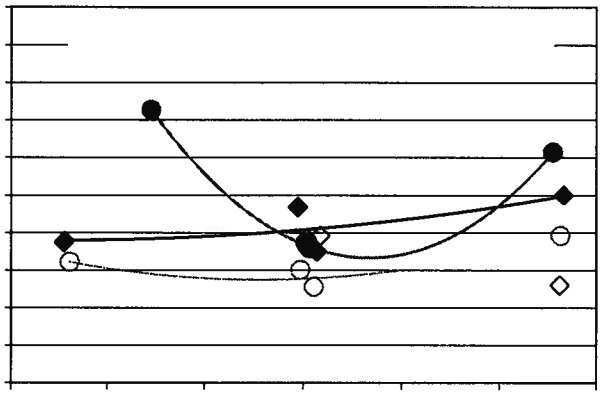

Figure 4.1: COV of GIMEP at low load and 1100rpm

Figure 4.2: COV of P_{max} at low load and 1100rpm

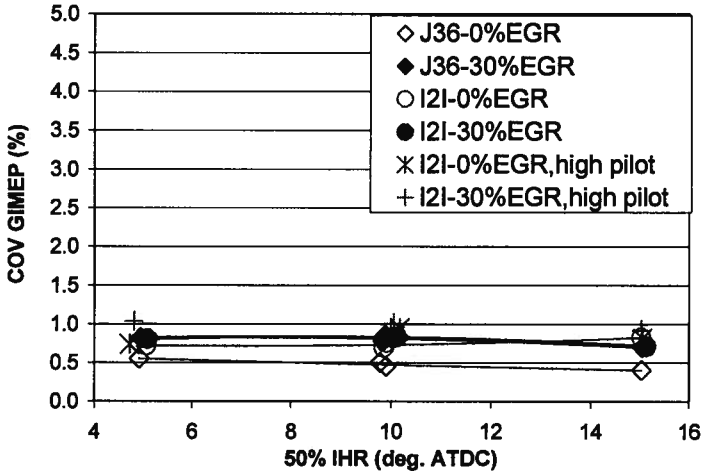

Figure 4.3: COV of GIMEP at 75% load and 1100rpm

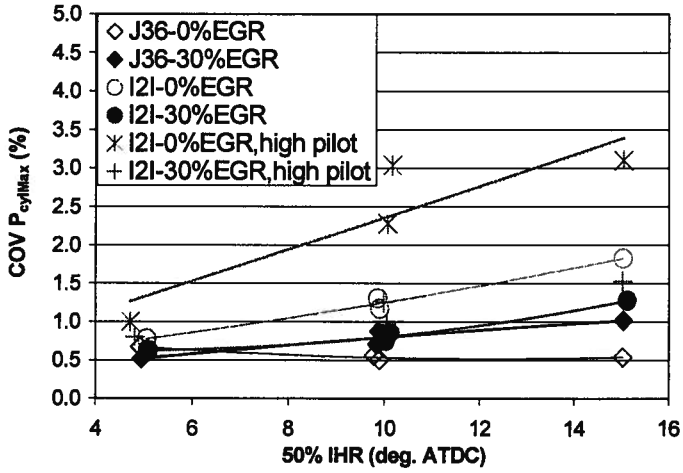

Figure 4.4: COV of P_{max} at 75% load and 1100rpm

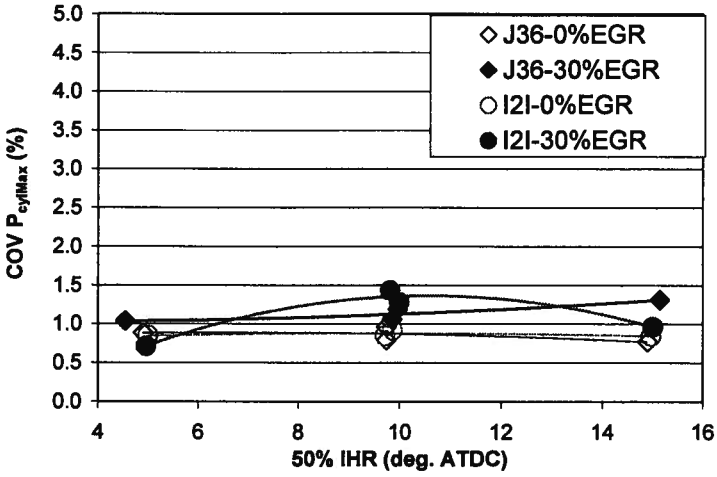

Figure 4.5: COV of GIMEP at 75% load and 1500rpm

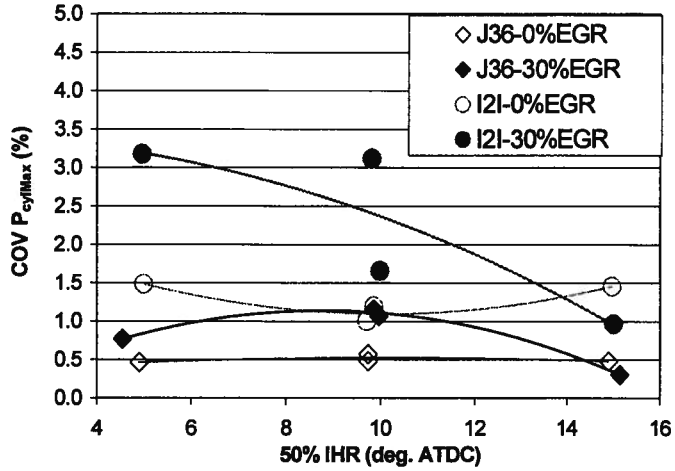

Figure 4.6: COV of Pmax at 75% load and 1500rpm

5. EFFECT OF PILOT FUELLING AMOUNT ON COMBUSTION

Figure 5.1 shows the effect of pilot fuelling on the J36 injector at 75% load, 1100rpm and no EGR (averages of 45 cycles). Basically as the pilot is increased the initial heat release moves earlier and releases more heat. However, the ignition delay is slightly longer with more pilot fuelling.

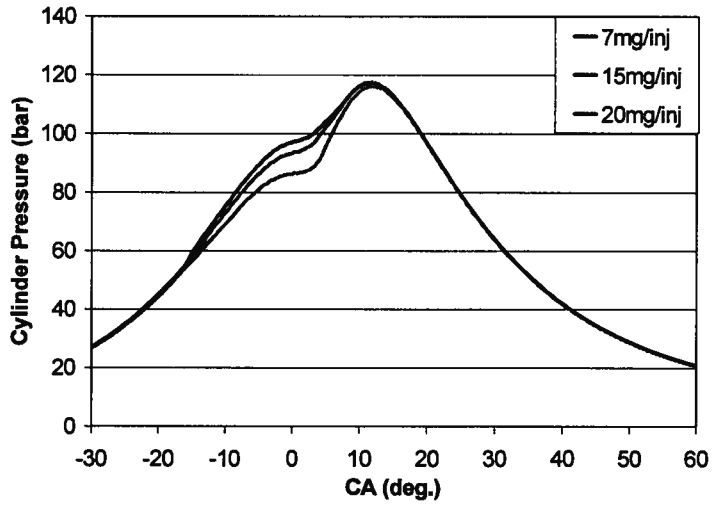

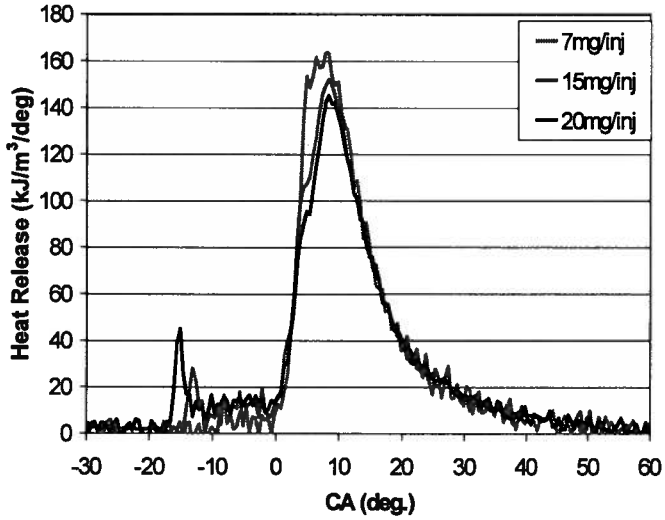

Figure 5.1: Pressure trace and heat release rate of J36 injector without EGR, 1100rpm, GIMEP=13bar

Figure 5.2 shows the pressure trace and heat release of the I2I injector under the same operating condition (45-cycle average). The I2I injector needs more pilot fuelling than the J36 so 7mg/injection was not possible. The injector runs well with 15mg/injection but as the pilot fuelling is increased to 20mg/injection there is some kind of "ringing" within the cylinder, this is evident in the large fluctuations seen in the pressure trace and heat release curve. It is unclear why this happens.

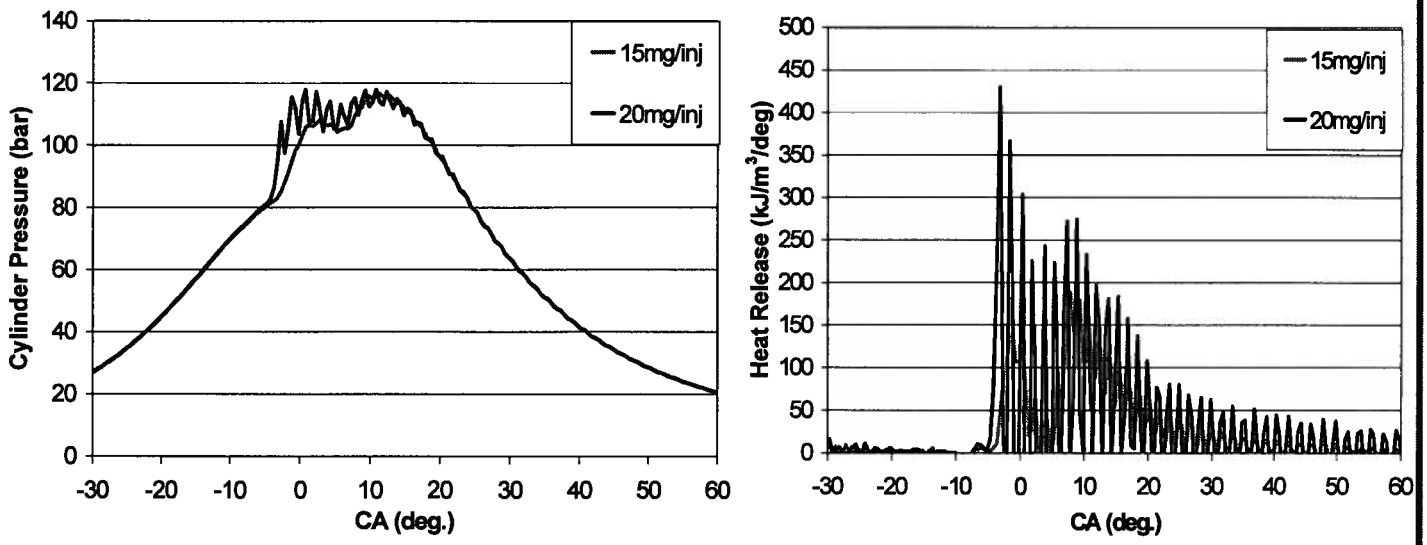

Figure 5.2: Pressure trace and heat release rate of I2I injector without EGR, 1100rpm, GIMEP=13bar

Conclusions

1. The I2I injector gives emissions levels comparable to that of a J36 under most of the tested operating conditions with the exception of low load where the hydrocarbon and carbon monoxide emission were excessive.
2. The I2I injector in general always gives lower particulate matter. This is likely due to the better diesel atomization with this injector.
3. Timing of the pilot injection is not very sensitive. As long as the gas needle is closed when the pilot is injected into the gas sac, the emissions are very similar.
4. Higher and lower pilot fuelling amounts prove to be troublesome with the I2I injector. High pilot fuelling produces a "ringing" in the cylinder and the injector does not run with low pilot fuelling (less than about 12mg/injection).

Recommendations

Basically the I2I injector has proven to have promise as a potentially low cost alternative to the J36 injector. Much more work needs to be done to redesign the injector so that the performance is better under all operating conditions. It is recommended that work be continued on the development of this injector.

Alternative Fuels Group
Department of Mechanical Engineering, University of British Columbia
2324 Main Mall, Vancouver, B.C. V6T 1Z4

SCRE Project

Key Question:

Can the I2I injector run at low load, and is there a minimum diesel pilot flow-rate under these conditions?

Method:

The prototype I2I injector was run at UBC's SCRE facility. The operating condition chosen was to test the low-load operation of the injector. To provide a baseline operating condition, the engine was operated at 800 RPM, 8.5 bar GIMEP with an intake manifold pressure of 65 kPa (g). A single pilot injection preceded a 2-stage gas injection process. The durations of the diesel pulse and the first gas pulse were semi-arbitrarily set for the lowest first gas pulse which retained stable operation. Timing was set for the mid-point of the heat-release rate (50%IHR) at 10°ATDC. For the low-load tests, the 2nd injection event was terminated, while the timing and duration of the 1st gas pulse was held constant. The diesel end-of-injection timing was held constant, but the duration was adjusted to provide the desired quantity of diesel. The manifold pressure was then reduced in 20kPa increments from 65 to 5 kPa (g). At each manifold pressure, three pilot flows were tested – 30 mg/inj, 20 mg/inj, and a 'minimum' which was selected as being the lowest pilot flow at which there was no evidence of the engine misfiring (for a number of conditions, this minimum was at, or above, 20 mg/inj). This third parameter was somewhat subjective, and the stability at this condition varied with the different test conditions. This procedure was carried out at 16.5, 22.5, and 27.5 MPa gas rail pressure (18.5, 24.5, and 29.5 diesel rail pressure). The testing was not randomized, with the 22.5 MPa testing carried out on 21/03/06 and the other two on 22/03/06. The manifold pressures were tested sequentially at each injection pressure. Uncertainties relating to this testing include the standard uncertainties relating to testing on the SCRE, as well as:

i) testing durations (3-4 minutes) were the minimum which have been shown to provide stable diesel mass flow measurements. Errors in this flow rate, in particular at low pilot flow conditions, were substantial

ii) operation of the engine at low-load tends to result in many instruments (including the gas and air flow-rates) being closer to their limits-of-detection, and as a result the uncertainty in their readings tend to increase.

The baseline injection parameters used in this testing are given in the table below:

Gas Rail Pressure	16.5	22.5	27.5
Diesel Rail Pressure	18.5	24.7	29.5
Gas SOI (°CA)	-10	-9.5	-7
Gas PW (baseline, ms)	0.75	0.7	0.6
Pilot EOI (baseline, °CA)	-13	-13	-10

Parameters not included in the table, but held constant for all tests included the manifold air temperature (~28°C), the end of pilot-first gas pulse separation (0.7 ms), EGR level (0).

Discussion:

The first objective of this testing was to determine whether the I2I injector was capable of running stably at low loads. In particular, concern had been raised based on previous testing that the injector would not function at near-atmospheric conditions. The coefficient of variation (COV) of the GIMEP under minimum and high diesel pilot flows are shown in Figures 1&2. Also shown in Figure 1 is the COV of GIMEP for the low injection pressure at a diesel pilot of ~20 mg/inj, which is roughly equivalent to the 'low' pilot flows at each of the higher injection pressures. These results indicate that while high variability in the combustion may occur at low pilot flows, increasing the pilot flow will substantially reduce this variability. The pilot flow rates corresponding to these low flows are shown in Figure 3. As can be seen, the high variability at the lowest injection pressure is attributed to the low pilot flow rate. By increasing the flow (to approximately 20 mg/inj), a substantial reduction in combustion variability is achieved. In general, observation of the plots suggests that lower manifold pressures result in higher combustion instability for a given diesel pilot flow. That lower pilot flows were achievable with the low injection pressure case may be due to the lower gas flow at this condition, as shown in Figure 4. This suggests that an important parameter may be the ratio of diesel pilot to gas (in the first pulse). However, further testing is required to investigate this hypothesis in more detail.

While emissions measurements were not a major objective of this work, including the HC and NOx emissions provides further insight into the combustion stability. In general, high hydrocarbons (in this case) can be attributed to high combustion variability, whereas high NO_x will indicate more stable, earlier, and more rapid combustion. Figures 5&6 show the HC emissions, with 5 for the 'low' pilot flow conditions and 6 for the 'high' pilot flow case. The equivalent NO_x emissions are shown in figures 7&8. The results agree with the previous assessment that the higher pilot flow results in much hotter, more stable combustion. This leads to high NO_x but low HC emissions.

AUTHOR:	G.P. McTaggart-Cowan	DATE
DOCUMENT NUMBER:	U1-FAC-098-Test	06-03-23
KEYWORDS:	I2I injector; low load	

The in-cylinder pressure traces tend to support these results. The pressure trace and heat-release rate for the low and high pilot flows for the low and high injection pressures at the low and high manifold pressures are shown. At the low injection pressure, the high pilot flow induces such a rapid heat-release (approaching detonation conditions) that 'ringing' of the in-cylinder pressure measurement is observed. This effect has been observed previously with this injector, and appears to occur for those cases with very high rate-of-increase of the in-cylinder pressure during the initial combustion event. Whether the ringing is actual pressure waves in the combustion chamber or is a mechanical or electrical effect in the pressure transducer is unknown. Similar ringing is observed at the other high-pilot conditions except for the low manifold pressure, high rail pressure case. It would appear that in this case, the initial rate of heat release is somewhat lower and as a result the pressure rise is not as rapid.

At the lower diesel flow rates, the ignition process appears to more closely resemble that of conventional HPDI combustion. Under certain conditions, there even appears to be an early first-stage combustion, followed by the main combustion event (for example, in the high injection pressure, low manifold pressure case). However, the duration between the initial and main heat releases are relatively short. Even at this condition (where ringing is not observed) the higher pilot flow can be seen to substantially increase the combustion rate. These results suggest that, at low load, the higher pilot flow is substantially increasing the initial heat-release rate of the premixed combustion phase. Due to the low load condition, the combustion is occurring primarily in the premixed phase. For the lower diesel quantities, the ignition delay is substantially increased and the peak heat-release rate is reduced. As the diesel flow gets very low (as shown in Figure 9), the overall combustion rate is greatly impaired. This is most likely due to the relatively small quantity of diesel (relative to the natural gas mass). It is likely that this small diesel quantity is more dispersed within the natural gas, impairing the ignition process. With the longer delay, the ignition also becomes more variable, resulting in some cycles with very long ignition delays (the limiting value which is approached is cycles where no ignition occurs: however, for the test points here, the conditions were selected to attempt to avoid such misfiring cycles).

The effect of the relative amounts of diesel and gas (in the first injection) are shown in Figures 10-13. The effects of both the mass and the volume ratio are shown, with the COV IMEP, tHC, CO and NOx emissions as outcomes. The diesel volume was calculated assuming incompressible fluid at a density of 848 kg/m^3. The gas density was estimated using the ideal gas law at the peak cylinder pressure and at ambient temperature. While this calculation is questionable (the injection process occurs before peak pressure; the gas will certainly be at a higher temperature than ambient when injected), however it is representative of the volume of gas injected per cycle. The relative volume of gas is shown to have a very significant influence on combustion stability and emissions. As expected, increases in the volume ratio (more gas to diesel) resulted in higher combustion variability, higher unburned fuel and CO emissions, and lower NOx emissions. The role of the mass ratio can be seen to be substantially less significant, with no clear trends in NOx or combustion stability, and only very rough trends in CO and unburned fuel. The correlation coefficients are given in the table below:

Parameter	COV GIMEP	tHC	CO	NOx
ρ*(Volume Ratio)*	0.669	0.824	0.877	-0.770
ρ*(Mass Ratio)*	0.406	0.585	0.63	-0.486

It should also be noted that the cross-correlation (Volume ratio – mass ratio) is also strong, as would be expected, with an ρ-value of 0.87. Given this strong cross-correlation, it is very significant that all the outputs are much more strongly correlated with the volume ratio than with the mass ratio, indicating that it is the relative volumes of the two fuels which are most significant.

Conclusions:

1) The I2I injector was shown to run successfully at low load conditions down to ambient manifold pressures. The engine was also started under normal (naturally-aspirated) conditions without undue problems.
2) A lower diesel mass limit of around 10-20 mg/inj was identified for most operating conditions. This depended on the amount of gas being injected, the manifold pressure, and the injection pressure. In general:
   a) the lower the manifold pressure, the more diesel was required
   b) the higher the injection pressure, the more diesel was required
   c) the more gas was injected (in the first pulse) the more diesel was required
3) The relative volumes of the diesel and gas (1st pulse) injections had a strong influence on combustion stability and emissions, with larger volumes of gas reducing stability and increasing HC and CO emissions.
4) This suggests that it may be possible to minimize diesel consumption by reducing the natural gas in the first gas pulse. Further power may be developed by increasing the duration of the 2nd pulse.
5) Transition from single gas pulse to double gas pulse operation proved to be sensitive to operating condition, with the potential for even very late 2nd injections (as much as 3 ms after the first pulse) still being sufficient to stop the combustion event. This is thought to be a result of injector dynamics.

Recommendations:

1) No attempt was made to optimize the injection process for low-load operation. Adjustments to the pilot-gas separation time, the absolute timing of the injection, or the diesel-gas rail bias could have substantial impacts on the overall combustion system, and hence require further investigation.
2) The response of the prototype injector to the specified commands was not always well understood. Further testing of the injector, either in the UBC spray rig or on the Westport rate tube, could provide more information regarding the injector's actual performance.
3) Pressure pulsations in the gas rail were observed to be significant. It would be interesting to study the effect of the double-pulse injection behaviour on the rail pressure with a high-pressure, high-speed transducer. This could provide important information for both the I2I and conventional HPDI programs.

Figures:

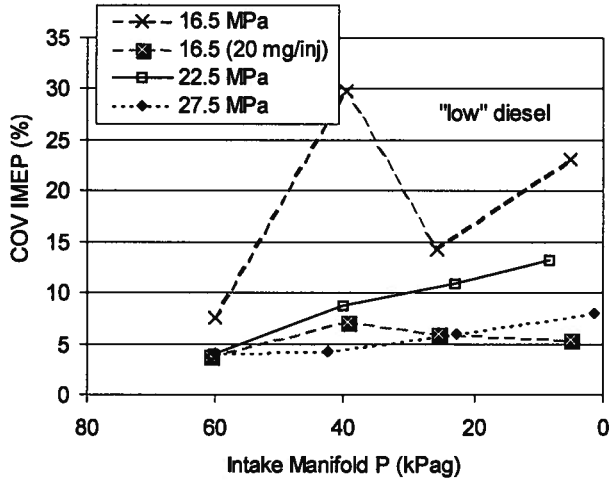

Fig. 1: COV GIMEP at various injection pressures over a range of manifold pressures at 'low' diesel pilot flow (<20mg/inj)

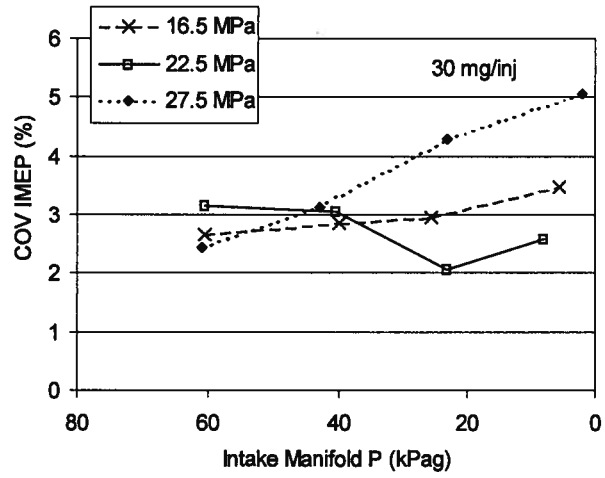

Fig. 2: COV GIMEP at various injection pressures over a range of manifold pressures at 'high' diesel pilot flow (~30mg/inj)

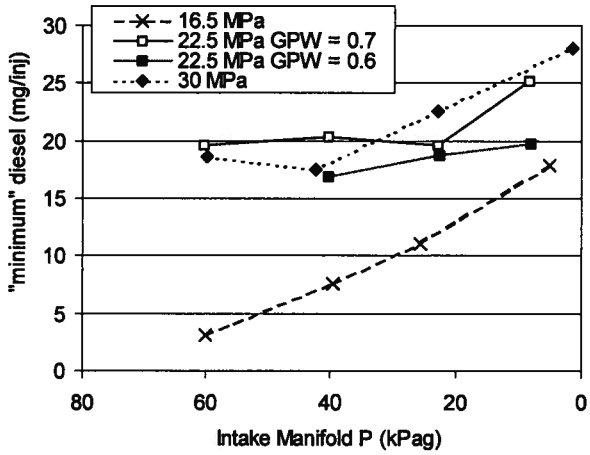

Fig. 3: "Minimum" diesel injection mass for the various injection and manifold pressure conditions. "Minimum" semi-arbitrary selection as point at which engine was not completely misfiring

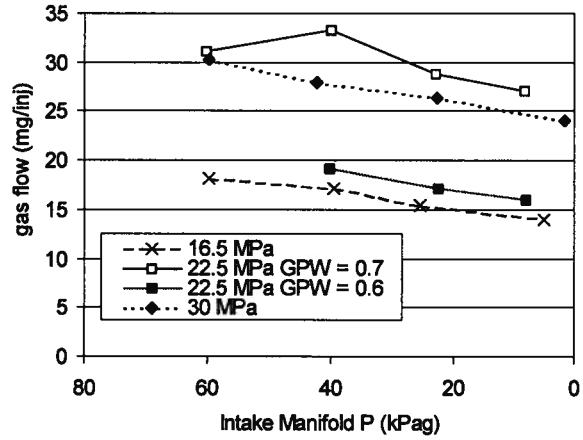

Fig. 4: Gas injection mass corresponding to diesel flows indicated in figure 3.

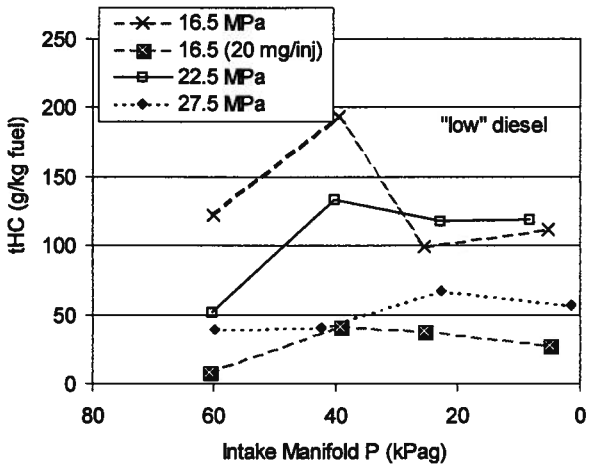

Fig. 5: HC emissions for 'minimum' diesel pilot flows

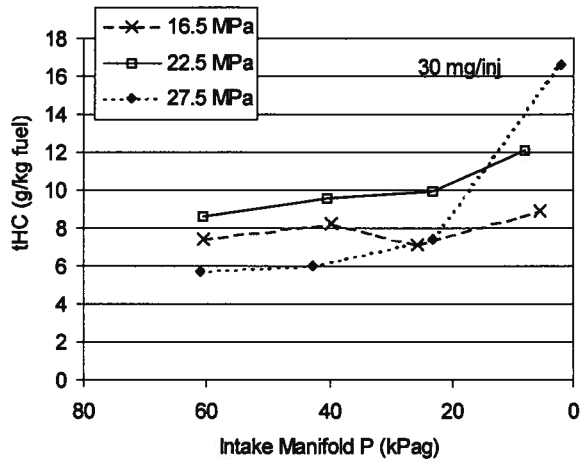

Fig. 6: HC emissions for 'high' diesel pilot flow

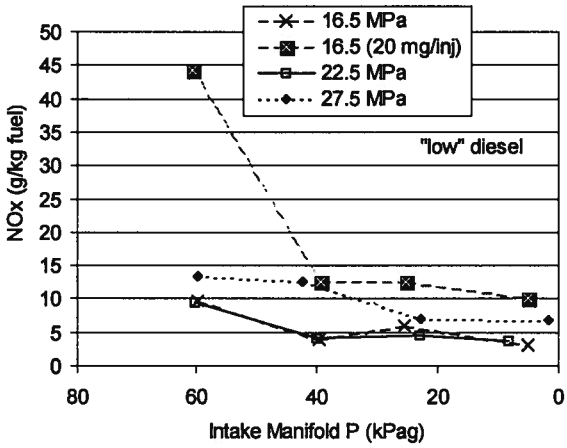

Fig. 7: NOx emissions for 'minimum' diesel pilot flows

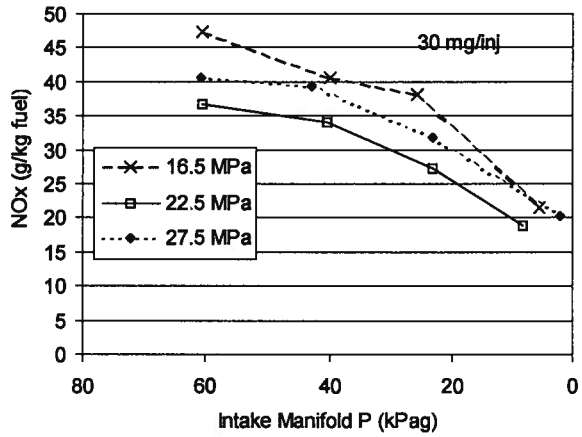

Fig. 8: NOx emissions for 'high' diesel pilot flow

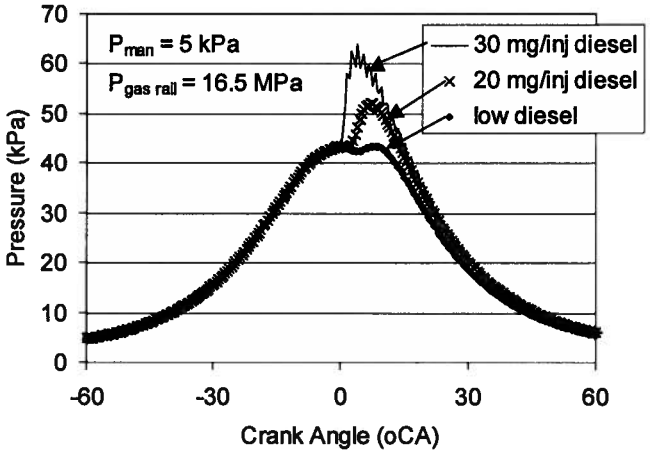

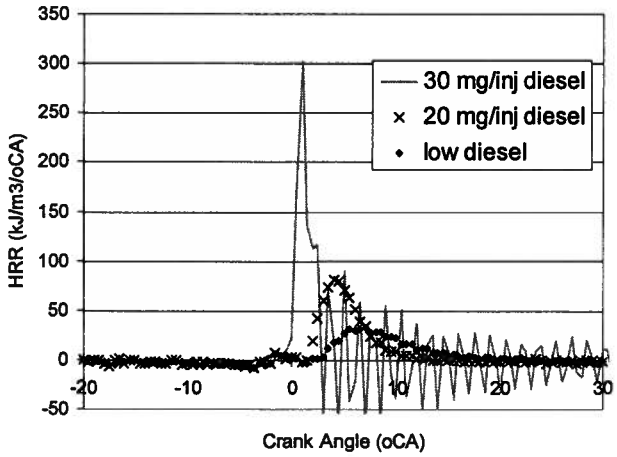

Fig. 9: P and HRR for low manifold pressure, low rail pressure.

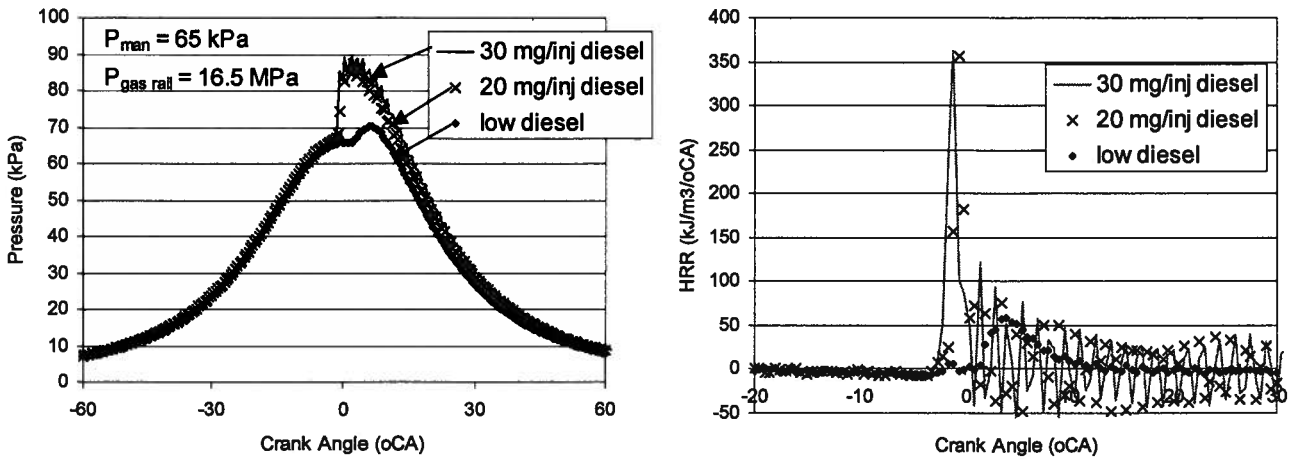

Fig. 10: P and HRR for high manifold pressure, low rail pressure.

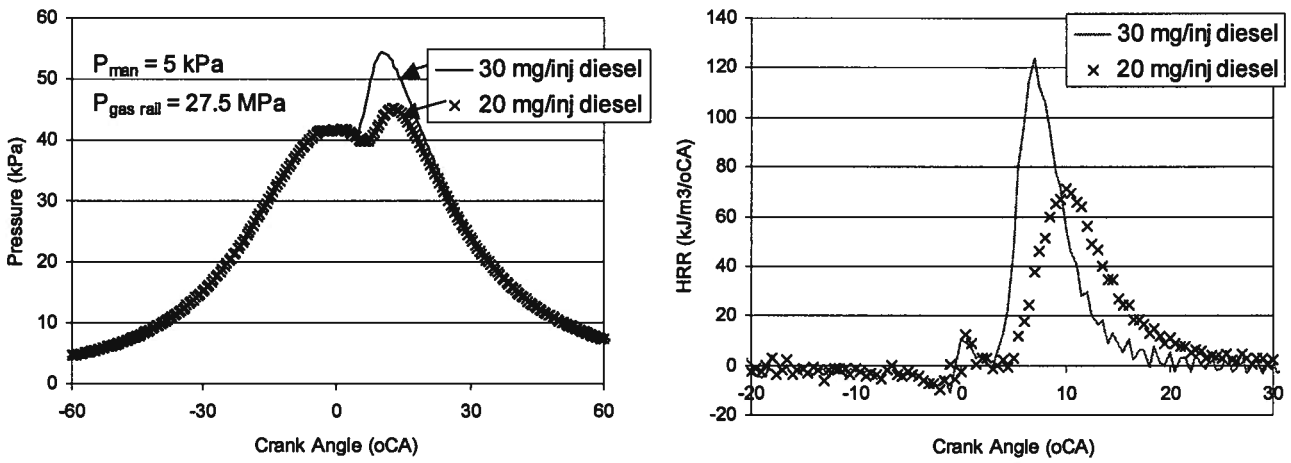

Fig. 11: P and HRR for low manifold pressure, high rail pressure.

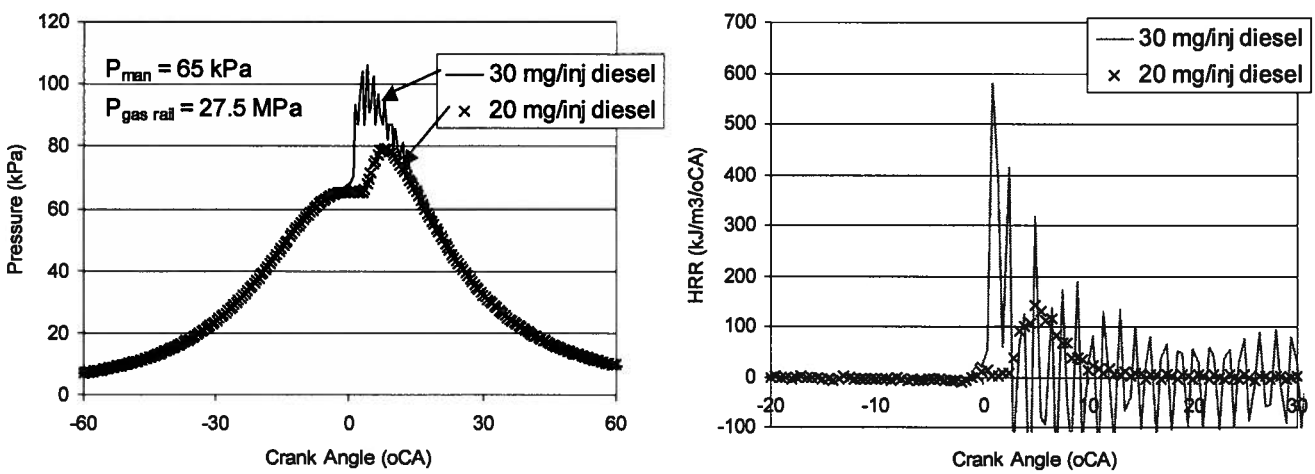

Fig. 12: P and HRR for high manifold pressure, high rail pressure.

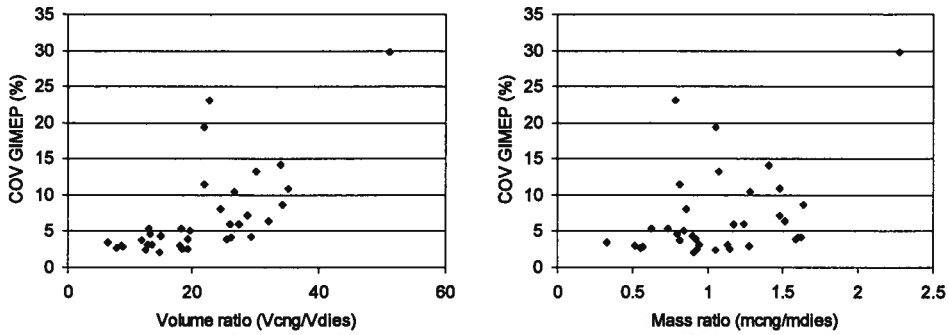

Fig. 13: COV GIMEP, for all points vs. volume and mass pilot-gas ratios.

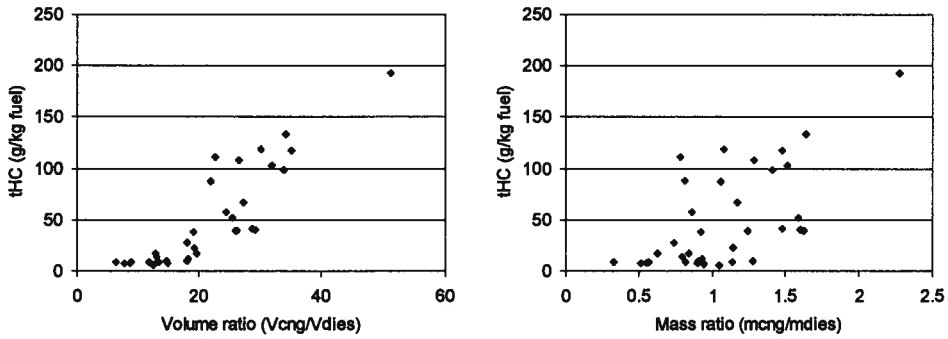

Fig. 14: tHC emissions, for all points vs. volume and mass pilot-gas ratios.

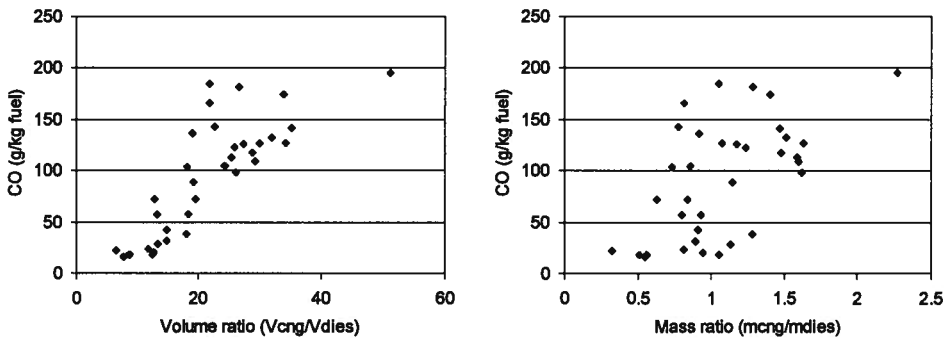

Fig. 15: CO emissions, for all points vs. volume and mass pilot-gas ratios.

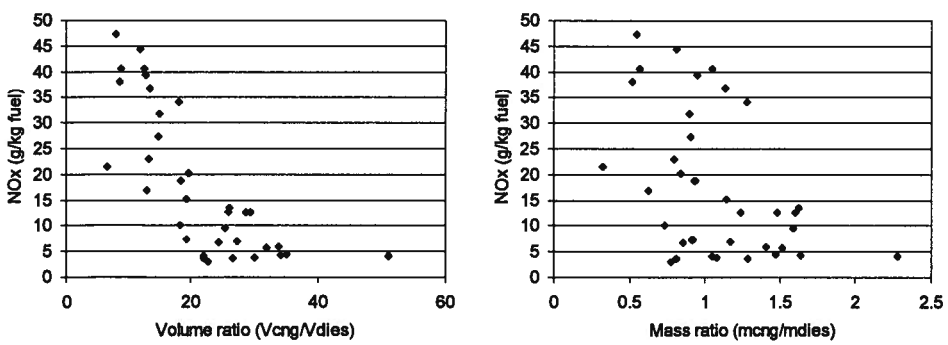

Fig. 16: NO_x emissions, for all points vs. volume and mass pilot-gas ratios.

Appendix B.3 – SCRE Timing Factsheet

This appendix (pp. 190 – 196) has not been included because of copyright restrictions. It contained the following information:

- **Documentation on the calibration of the optical shaft sensor to TDC**
- **What crank angle offset should be used for the SCRE in calculations with the indicated pressure curve**

This factsheet is available upon request. Hill, P.G. SCRE Timing Checks, W1-FAC-3788-ANYS, Westport Innovations Factsheet. December 2007.

[Original document missing pages 191-196]

Appendix E: Emissions Spreadsheets

The Emissions Spreadsheets are organized as follows:

- Appendix E.1 – VII-A tests at 800 RPM
- Appendix E.2 – VII-A tests at 1200 RPM
- Appendix E.3 – VII-B tests at 800 RPM
- Appendix E.4 – VII-B tests at 1200 RPM
- Appendix E.5 – VIII-A tests
- Appendix E.6 – VIII-B tests
- Appendix E.7 – VIII-B2 tests

On the emissions bench the top section has the test series number, test name, and date and time. The date and time format is in the same format that can be used to find the raw "slow" data files. For example, test series VII-A-1 has one test name "31-16-10-47". The raw data for this file can be found in the electronic appendix (...rogak/sbrown/Thesis/Brown_Thesis/) under the filename "VII-A-800/slow07-09-13-14.24.14.csv".

For VII series tests, the test files are organized first by injection pressure, then by pilot gas pulse width duration, then by diesel injection mass. The pressure traces and heat release rate plots for specific test points for Figures 4.8 to 4.14 can be found most easily through the diesel fuelling rate. These heat release figures with the accompanying "b" and "c" test modes can be found in Appendix F.1 to Appendix F.4.

For test series VIII tests, the emissions spreadsheets are organized by mode number.

figure #	31	34	37	30	27	40	8	11	1	12
Test Series - #	VII-A-1	VII-A-1	VII-A-1	VII-A-3	VII-A-4	VII-A-4	VII-A-5	VII-A-6	VII-A-7	VII-A-7
Test Name	31-16-10-47a	34-16-10-47-145GRIT a	37-16-10-47-345GRIT a	28-16-20-47a	25-16-20-70a	40-16-20-70-345GRIT a	07-12-47a	10-12-70a	01-20-47a	10-12-70a2
Date/Time	07-09-13 14.24.14	07-09-13 14.33.35	07-09-13 14.41.55	07-09-13 14.15.29	07-09-13 14.04.33	07-09-13 14.52.54	07-09-13 11.13.47	07-09-13 11.24.49	07-09-13 10.47.16	07-09-13 13.00.19
Ignition Delay (ms)	1.78	2.36	2.68	2.42	1.41	1.62	1.72	1.96	1.42	1.92
Knock (bar)	1.2	1.6	2.0	1.0	3.0	1.6	1.3	2.2	2.0	2.5
IHR (kJ/m3)	1614	1573	1570	1604	1574	1544	1604	1640	1613	1594
IHR Ratio	0.65	0.22	0.13	0.00	0.80	0.68	0.55	0.00	0.80	0.67
Engine Spd. (rpm)	807	807	807	803	803	807	798	792	804	793
MAT (°C)	71	71	71	71	71	71	70	73	63	69
MAP (kPag)	92.6	92.6	92.7	93.0	92.8	92.4	94.9	95.6	94.6	93.2
CNG Press. (MPa)	17.8	17.8	17.8	17.8	17.8	17.8	24.3	24.3	24.3	24.5
Diesel Press. (MPa)	20.1	20.0	20.0	20.0	19.9	19.9	27.0	27.0	27.0	27.5
Exhaust Press. (kPa)	57.2	56.2	56.5	56.1	55.9	56.9	45.4	45.3	47.0	50.7
Corr. Air flow (kg/hr)	114	114	114	114	114	114	115	114	117	113
Airflow (kg/hr)	99	99	99	99	99	99	100	99	102	99
Diesel inj. (mg/inj)	13.3	13.6	11.8	22.9	22.0	19.6	16.2	13.3	17.2	14.9
CNG flow (kg/hr)	2.30	2.23	2.23	2.11	2.07	2.03	2.26	2.30	2.17	2.24
CO (ppm-dry)	77	99	104	64	59	64	83	145	77	199
CO2 (%-dry)	4.21	4.13	4.13	4.29	4.25	4.16	4.26	4.32	4.26	4.23
NOx (ppm-dry)	1061	1104	1155	1083	1095	1024	1114	1126	1077	1097
O2 (%-dry)	13.68	13.83	13.83	13.70	13.75	13.93	13.60	13.49	13.67	13.66
CH4 (ppm-dry, C1)	126	125	125	118	127	125	126	135	126	139
tHC (ppm_{wet}, C1)	119	118	119	114	122	123	116	125	116	130
Exhaust T. (°C)	335	327	329	336	331	327	323	326	319	326
Pk. press. (bar)	101.7	101.5	103.3	100.5	113.2	104.1	108.2	104.3	100.0	108.0
CA@Pk. press. (bar)	13.6	13.3	13.1	13.4	12.9	13.3	11.1	13.9	13.2	13.3
Gross IMEP (bar)	8.47	8.52	8.26	8.33	8.56	8.25	8.64	8.44	8.13	8.66
EQR	0.38	0.37	0.37	0.39	0.38	0.36	0.38	0.38	0.37	0.38
5% IHR (deg)	4.4	2.9	5.9	-1.1	5.9	6.9	0.9	5.4	0.9	4.9
10% IHR (deg)	5.4	4.4	6.9	-0.1	6.9	7.4	1.4	6.4	2.9	5.4
50% IHR (deg)	10.0	9.8	9.6	9.8	9.5	10.2	8.9	10.0	9.7	9.6
90% IHR (deg)	17.0	17.0	16.0	17.0	12.5	15.5	15.5	15.5	17.0	15.0
COV GIMEP	1.2	1.5	1.3	1.3	2.3	1.2	2.3	2.5	1.4	2.0
DSOI (deg)	-19.2	-24.0	-33.7	-26.3	-26.3	-41.0	-14.4	-14.3	-18.3	-13.6
DEOI (deg)	-11.9	-16.7	-26.4	-11.9	-11.9	-26.4	-8.9	-8.8	-9.0	-8.9
GSOI (deg)	-9.7	-9.7	-9.7	-9.7	-9.7	-9.7	-6.8	-6.7	-6.8	-6.7
GEOI (deg)	-6.3	-6.3	-6.3	-7.3	-6.3	-6.3	-4.5	-3.4	-4.5	-3.4
2GSOI (deg)	0.0	0.0	12.3	-1.0	12.2	0.0	1.7	14.9	1.7	2.8
2GEOI (deg)	4.6	0.0	16.9	3.5	17.3	4.0	1.7	19.8	6.7	7.1
Comments										

figure #	5	15	18	21	24
Test Series - #	VII-A-8	VII-A-11	VII-A-11	VII-A-12	VII-A-12
Test Name	04-20-70a	13-28-20-47a	16-28-20-47a	19-28-20-70a	22-28-20-70a
Date/Time	07-09-13-10.59.04	07-09-13-13.19.38	07-09-13-13.28.27	07-09-13-13.36.23	07-09-13-13.45.55
Ignition Delay (ms)	1.27	1.74	1.27	1.38	1.99
Knock (bar)	4.9	3.1	4.4	2.8	2.8
IHR (kJ/m3)	1619	1540	1622	1747	1640
IHR Ratio	0.91	0.77	0.92	0.88	0.73
Engine Spd. (rpm)	799	798	797	799	802
MAT (°C)	74	71	69	69	70
MAP (kPag)	95.8	93.8	93.8	93.3	93.1
CNG Press. (MPa)	24.3	29.5	29.5	29.4	29.4
Diesel Press. (MPa)	27.0	32.1	32.1	32.1	32.1
Exhaust Press. (kPa)	45.3	53.3	54.4	55.6	56.0
Corr. Air flow (kg/hr)	114	113	113	113	114
Airflow (kg/hr)	99	99	98	99	99
Diesel inj. (mg/inj)	18.6	14.7	20.3	17.2	14.5
CNG flow (kg/hr)	2.22	2.17	2.18	2.34	2.30
CO (ppm-dry)	72	210	85	150	395
CO2 (%-dry)	4.46	4.13	4.35	4.58	4.15
NOx (ppm-dry)	1237	1117	1093	1217	1199
O2 (%-dry)	13.34	13.83	13.54	13.14	13.74
CH4 (ppm-dry, C1)	129	135	120	137	215
tHC (ppm_{wet}, C1)	119	126	111	128	198
Exhaust T. (°C)	329	323	333	350	332
Pk. press. (bar)	104.0	107.1	106.9	105.1	111.7
CA@Pk. press. (bar)	13.7	13.6	13.1	13.9	13.1
Gross IMEP (bar)	8.53	8.35	8.03	8.48	9.29
EQR	0.39	0.37	0.39	0.40	0.39
5% IHR (deg)	2.4	5.9	6.4	3.9	4.4
10% IHR (deg)	3.9	6.9	7.4	4.4	4.9
50% IHR (deg)	10.0	10.0	9.9	10.2	8.4
90% IHR (deg)	16.0	14.5	14.0	16.0	15.0
COV GIMEP	2.4	5.1	2.4	3.3	2.5
DSOI (deg)	-18.2	-12.7	-15.1	-15.1	-14.2
DEOI (deg)	-8.9	-7.5	-6.0	-6.0	-8.9
GSOI (deg)	-6.8	-5.3	-3.9	-3.9	-6.8
GEOI (deg)	-3.4	-3.1	-1.6	-0.5	-3.4
2GSOI (deg)	2.8	3.2	16.8	5.7	2.8
2GEOI (deg)	7.1	3.2	21.1	10.7	2.8
Comments					

Figure #	36	39	37	30	12	15	47	4	18	1	7	24
Test Series - #	VII-A-31	VII-A-31	VII-A-31	VII-A-31	VII-A-29	VII-A-29	VII-A-41	VII-A-29	VII-A-29	VII-A-29	VII-A-29	VII-A-30
Test Name	01-20-47a	01-20-47-045a	02-20-47a	05-20-47-345a	31-10-47-125a	34-10-47-110a	12-10-47a-LB	20-10-47-145a	10-10-47a	20-10-47-045a	26-10-47-095a	17-10-70-345a
Date/Time	07-09-15-10.28.08	07-09-14-10.44.24	07-09-15-10.34.52	07-09-14-10.58.31	07-09-14-12.15.28	07-09-14-12.26.24	07-09-15-11.27.50	07-09-14-11.57.40	07-09-15-11.05.54	07-09-14-11.46.52	07-09-14-12.05.15	07-09-14-11.31.48
Ignition Delay (ms)	1.45	1.67	1.12	1.73	2.91	3.24	3.06	3.25	2.43	2.99	3.18	3.43
IHR (kJ/m3)	275	1669	1827	1670	1073	1220	1804	1265	1690	1536	1783	1613
Knock (bar)	1.7	1.2	1.6	1.3	0.7	0.9	1.6	0.8	1.9	1.7	1.6	1.0
IHR Ratio	0.68	0.44	0.68	0.40	**0.00**	**0.00**	**0.00**	**0.00**	**0.00**	**0.12**	**0.00**	**0.00**
Engine Spd. (rpm)	1196	1206	1199	1195	1184	1193	1195	1178	1195	1211	1210	1196
MAT (°C)	71	51	68	71	70	70	70	70	70	70	70	72
MAP (kPag)	95.0	95.2	94.8	98.8	98.4	97.8	94.1	99.1	94.3	96.4	96.7	97.9
CNG Press. (MPa)	24.0	24.1	23.8	23.9	24.0	24.0	22.3	24.0	24.0	24.0	23.9	24.0
Diesel Press. (MPa)	26.3	26.6	26.1	26.3	26.3	26.3	23.1	26.4	26.3	26.4	26.2	26.4
Exhaust Press. (kPa)	48.1	55.0	50.6	55.3	54.9	54.8	52.6	54.0	53.4	54.5	56.7	57.7
Corr. Air flow (kg/hr)	170	178	170	172	171	172	168	171	168	172	172	171
Airflow (kg/hr)	147	155	148	150	148	149	146	148	146	150	150	149
Diesel inj. (mg/inj)	19.4	21.1	22.8	23.2	9.2	10.6	11.0	11.0	13.1	14.2	14.3	10.7
CNG flow (kg/hr)	2.58	3.22	3.79	3.23	3.25	3.29	3.80	3.22	3.44	3.25	3.76	3.51
CO (ppm-dry)	126	86	103	90	1240	1199	230	1233	188	183	177	954
CO2 (%-dry)	3.98	4.49	5.52	4.65	3.24	3.48	5.04	3.22	4.72	4.22	4.82	4.15
NOx (ppm-dry)	816	1222	1111	1379	613	445	1218	719	1118	1449	1628	967
O2 (%-dry)	14.20	13.32	11.59	12.97	14.84	14.45	12.06	14.91	12.67	13.43	12.31	13.44
CH4 (ppm-dry, C1)	160	154	147	150	4919	4952	208	4420	169	182	185	2560
tHC (ppm_{wet}, C1)	167	163	150	155	3951	3950	198	3950	163	192	227	2180
Exhaust T. (°C)	321	363	423	378	314	336	406	312	382	357	403	377
Pk. press. (bar)	96.0	97.3	100.1	98.2	76.0	76.5	94.7	78.3	100.4	95.5	93.9	78.4
CA@Pk. press. (bar)	11.1	13.2	13.1	13.0	2.2	3.5	16.4	5.0	13.8	14.5	16.8	7.9
Gross IMEP (bar)	7.21	8.84	9.87	8.89	5.50	6.28	9.49	6.55	9.07	8.09	9.34	8.26
EQR	0.32	0.37	0.45	0.39	0.35	0.36	0.42	0.35	0.39	0.37	0.42	0.38
5% IHR (deg)	-5.1	-0.1	-4.6	1.4	11.0	11.0	8.0	10.5	5.5	7.4	8.9	10.5
10% IHR (deg)	-3.6	3.4	-2.1	4.4	12.0	12.0	8.5	11.5	6.5	7.9	9.4	11.5
50% IHR (deg)	7.9	10.1	10.0	10.0	19.1	18.3	12.6	17.3	10.1	11.1	13.2	17.5
90% IHR (deg)	16.0	19.0	20.5	19.0	33.5	31.5	20.0	29.5	18.0	17.0	20.0	28.0
COV GIMEP	2.9	4.0	2.2	2.8	48.7	37.2	1.6	33.5	2.3	2.3	2.0	9.1
DSOI (deg)	16.1	-42.0	16.2	-63.1	-34.8	-34.0	16.1	-36.0	16.1	-29.8	-33.4	-51.0
DEOI (deg)	19.0	-20.3	19.1	-41.6	-25.6	-24.7	19.0	-26.9	19.0	-20.3	-24.0	-41.6
GSOI (deg)	-16.9	-17.0	-16.9	-16.8	-16.7	-16.8	-16.9	-16.6	-16.9	-17.1	-17.1	-16.9
GEOI (deg)	-13.5	-13.6	-13.5	-13.5	-13.4	-13.5	-13.5	-13.3	-13.5	-13.7	-13.7	-11.8
2GSOI (deg)	-4.2	-4.2	-4.2	-4.2	-4.1	-4.2	-4.2	-4.1	-4.2	-4.2	-4.2	-2.5
2GEOI (deg)	3.3	3.3	3.3	3.3	3.3	3.3	3.3	3.3	3.3	3.3	3.3	5.0
Comments												

Figure #	21	28	26	33	45	42	10	11
Test Series - #	VII-A-30	VII-A-30	VII-A-30	VII-A-31	VII-A-32	VII-A-32	VII-A-29	VII-A-29
Test Name	14-10-70-045a	08-10-70a	06-10-70a	08-20-47-345a	04-20-70a	11-20-70-045a	29-10-095a2 47-095a2	30-10-47-
Date/Time	07-09-14 11.23.44	07-09-15 10.57.47	07-09-15 10.52.22	07-09-14 11.05.40	07-09-15 10.40.52	07-09-14 11.13.22	07-09-14 12.10.22	07-09-14 12.12.34
Ignition Delay (ms)	2.30	2.26	1.81	1.86	1.41	1.65	3.26	3.16
IHR (kJ/m3)	1706	2135	2224	1907	646	614	1601	1607
Knock (bar)	2.1	2.0	1.8	5.9	3.3	7.0	1.3	1.4
IHR Ratio	0.54	0.50	0.30	0.78	0.96	**1.01**	0.00	0.00
Engine Spd. (rpm)	1210	1197	1198	1194	1198	1194	1201	1202
MAT (°C)	71	71	73	71	70	71	70	70
MAP (kPag)	96.9	94.8	95.0	98.6	94.5	98.2	96.9	96.3
CNG Press. (MPa)	24.1	23.8	23.8	23.9	23.6	23.9	24.0	24.0
Diesel Press. (MPa)	26.6	26.1	26.1	26.3	25.8	26.3	26.3	26.3
Exhaust Press. (kPa)	58.7	54.3	53.3	55.3	53.1	57.5	55.2	54.4
Corr. Air flow (kg/hr)	172	167	167	170	168	170	172	171
Airflow (kg/hr)	149	145	146	148	146	148	149	148
Diesel inj. (mg/inj)	12.3	14.5	17.0	25.8	21.2	22.1	11.5	30.8
CNG flow (kg/hr)	3.64	4.60	4.78	3.91	4.90	3.86	3.34	3.41
CO (ppm-dry)	239	259	187	80	186	73	438	353
CO2 (%-dry)	4.64	6.28	6.64	5.57	7.01	5.50	4.26	4.28
NOx (ppm-dry)	1573	1268	1139	1682	1223	1773	1261	1388
O2 (%-dry)	12.72	10.02	9.44	11.35	8.96	11.44	13.28	13.25
CH4 (ppm-dry, C1)	181	165	134	143	108	136	682	353
tHC (ppm_{wet}, C1)	180	161	134	148	114	139	467	377
Exhaust T. (°C)	384	478	499	433	518	429	366	366
Pk. press. (bar)	106.4	106.4	105.0	112.9	108.2	114.5	86.5	90.2
CA@Pk. press. (bar)	12.4	13.9	12.4	7.1	2.0	3.1	15.3	15.4
Gross IMEP (bar)	9.28	11.55	12.14	10.51	12.41	10.23	8.28	8.36
EQR	0.40	0.51	0.54	0.47	0.56	0.46	0.37	0.44
5% IHR (deg)	3.4	4.5	-0.1	-2.6	-5.6	-4.1	8.9	8.4
10% IHR (deg)	4.9	6.0	1.5	-2.1	-4.6	-4.1	9.4	8.9
50% IHR (deg)	8.9	10.8	10.8	7.4	11.0	7.6	13.7	12.9
90% IHR (deg)	17.0	22.5	26.0	22.0	27.5	21.0	20.5	19.5
COV GIMEP	2.5	1.7	1.1	2.7	1.2	1.8	3.4	3.9
DSOI (deg)	-29.8	16.2	16.2	-63.0	16.2	-41.5	-33.1	-33.2
DEOI (deg)	-20.3	19.0	19.0	-41.6	19.1	-20.1	-23.8	-23.8
GSOI (deg)	-17.1	-16.9	-16.9	-16.8	-16.9	-16.8	-16.9	-17.0
GEOI (deg)	-12.0	-11.8	-11.9	-11.8	-11.9	-11.8	-13.5	-13.6
2GSOI (deg)	-2.5	-2.5	-2.5	-2.5	-2.5	-2.5	-4.2	-4.2
2GEOI (deg)	5.0	5.0	5.0	4.9	5.0	4.9	3.3	3.3
Comments							VOID	VOID

Figure #	7	1	63	60	10	69	4	66	25	79	82	22
Test Series - #	VII-B-3	VII-B-1	VII-B-15	VII-B-13	VII-B-4	VII-B-16	VII-B-2	VII-B-15	VII-B-7	VII-B-19	VII-B-19	VII-B-7
Test Name	18-20-47a	18-10-47a	18-20-48LBa	18-10-52LBa	18-20-70a	18-20-70LBa	18-10-70a	18-10-70LBa	24-20-47a	24-20-47LBa1	24-20-47LBa	24-20-47a
Date/Time	07-12-19 18.24.10	07-12-19 17.52.34	07-12-19 16.37.14	07-12-19 17.16.38	07-12-19 18.11.25	07-12-19 16.53.09	07-12-19 18.03.53	07-12-19 17.04.36	07-12-19 19.00.50	07-12-19 15.30.44	07-12-19 15.47.14	07-12-19 12.21.56
Ignition Delay (ms)	2.87	2.95	2.70	2.28	1.73	1.58	1.95	2.10	1.59	1.43	1.52	1.39
Knock (bar)	2.2	1.7	1.7	1.3	2.3	3.2	1.2	1.3	1.1	3.2	3.1	1.4
IHR (kJ/m3)	837	833	1211	1097	1041	1489	970	1335	934	1551	1522	103
IHR Ratio	1.1	1.0	4.0	-0.2	0.6	1.1	0.5	8.9	0.4	1.2	6.7	0.4
Engine Spd. (rpm)	883	878	872	877	879	866	881	872	879	869	870	801
MAT (°C)	60	60	61	61	60	60	60	61	61	60	60	61
MAP (kPag)	93.6	93.8	95.6	92.7	93.5	93.9	92.8	92.5	93.7	96.2	95.5	95.3
CNG Press. (MPa)	17.4	17.2	17.5	17.3	17.4	17.3	17.4	17.5	23.3	23.0	23.2	23.3
Diesel Press. (MPa)	18.3	18.3	18.3	18.3	18.3	18.3	18.3	18.3	24.3	24.1	24.1	24.1
Exhaust Press. (kPa)	57.7	55.9	51.2	49.0	58.4	50.8	57.0	50.0	58.2	50.7	51.1	60.8
Corr. Air flow (kg/hr)	135	134	135	133	135	133	133	132	135	134	134	125
Airflow (kg/hr)	117	117	117	116	117	116	116	115	117	117	116	109
Diesel flow (kg/hr)	0.64	0.52	0.41	0.33	0.53	0.41	0.22	0.31	0.52	0.34	0.35	0.67
Diesel inj. (mg/inj)	23.97	19.85	15.61	12.68	20.11	15.77	8.31	11.75	19.54	13.07	13.31	28.08
CNG flow (kg/hr)	0.97	1.00	1.77	1.64	1.30	2.19	1.42	2.07	1.21	2.33	2.28	1.57
CO (ppm-dry)	267	308	150	126	46	35	217	172	62	31	31	26
CO2 (%-dry)	2.62	2.53	3.45	3.14	3.21	4.37	2.84	3.76	2.82	4.49	4.37	4.01
NOx (ppm-dry)	562	500	812	626	547	992	485	863	461	1067	1060	915
O2 (%-dry)	16.54	16.66	14.88	15.40	15.54	13.32	15.93	14.22	16.11	13.06	13.28	14.17
CH4 (ppm-dry, C1)	252	255	174	147	126	133	173	150	153	137	137	67
tHC (ppm_{wet}, C1)	122	123	77	64	61	57	86	64	63	62	59	59
Exhaust T. (°C)	210	206	270	250	248	320	232	289	229	326	318	294
Pk. press. (bar)	77.0	74.2	84.7	81.3	77.5	88.4	77.2	86.2	76.3	79.6	91.2	87.5
CA @ Pk. press. (bar)	14.1	14.5	14.7	13.6	7.8	13.6	13.0	14.3	13.4	5.0	14.9	14.2
Gross IMEP (bar)	4.36	4.29	6.46	5.84	5.63	8.17	5.17	7.23	4.96	10.86	8.45	7.48
EQR	0.22	0.21	0.31	0.28	0.26	0.37	0.24	0.35	0.24	0.38	0.38	0.33
5% IHR (deg)	9.1	9.6	8.6	7.1	2.1	2.1	4.6	6.6	4.1	3.1	2.6	1.6
10% IHR (deg)	9.6	10.1	9.1	8.1	2.6	2.6	6.1	7.6	7.1	16.6	3.6	6.1
50% IHR (deg)	11.3	11.9	11.4	10.5	10.6	10.3	10.4	10.8	10.6	21.1	11.0	10.6
90% IHR (deg)	14.1	15.1	15.6	15.6	18.1	17.6	16.6	16.1	16.1	29.1	17.1	16.6
COV GIMEP	4.2	8.7	9.9	10.9	4.1	10.0	7.7	9.9	3.9	7.6	15.4	4.3
DSOI (deg)	-31.0	-29.0	-41.0	-32.0	-31.0	-41.0	-22.0	-32.0	-24.0	-39.0	-40.0	-31.0
DEOI (deg)	-15.1	-15.3	-14.8	-15.2	-15.2	-15.0	-15.7	-15.3	-13.4	-12.9	-13.9	-14.7
GSOI (deg)	-8.0	-8.0	-8.0	-8.0	-8.0	-8.0	-8.0	-8.0	-6.8	-6.8	-6.8	-6.8
GEOI (deg)	-5.5	-5.5	-5.5	-5.3	-4.3	-4.4	-4.3	-4.3	-4.3	-4.3	-4.3	-4.5
2GSOI (deg)	-2.8	-2.5	-1.4	-1.8	-1.3	-1.3	-1.3	-1.3	0.0	-0.3	-0.8	0.0
2GEOI (deg)	3.6	3.8	4.9	4.6	5.1	5.0	5.1	5.0	5.3	5.5	5.0	5.3
Comments												

Figure #	72	13	75	33	19	95	86	28	16	92	85	51
Test Series - #	VII-B-17	VII-B-5	VII-B-18	VII-B-8	VII-B-6	VII-B-24	VII-B-22	VII-B-8	VII-B-6	VII-B-23	VII-B-21	VII-B-11
Test Name	24-10-47LBa	24-10-47a	24-10-70LBa-15.10.40	24-20-70a-15.10.00	24-10-70a-15.10.20	24-20-70LBa	24-10-70LBa	24-20-70a	24-10-70a	29-20-47LBa1	29-10-47LBa	29-20-47a1
Date/Time	07-12-19-15.41.12	07-12-19-12.06.51	08-01-15-10.38.13	08-01-15-10.00.24	08-01-15-10.21.06	07-12-19-15.56.08	07-12-19-16.06.40	07-12-19-12.30.46	07-12-19-11.59.45	07-12-19-15.09.17	07-12-19-14.26.00	07-12-17-17.29.49
Ignition Delay (ms)	1.82	1.57	1.60	1.44	1.60	1.45	1.91	1.36	1.53	1.81	2.06	1.57
Knock (bar)	1.5	1.0	1.3	3.4	1.3	4.2	1.9	4.1	3.1	1.2	1.2	1.8
IHR (kJ/m3)	1383	88	1360	1547	1244	2080	1849	1847	1427	1482	1573	1624
IHR Ratio	2.9	0.5	1.0	0.8	-0.1	1.2	20.3	0.8	0.8	1.7	1.0	0.8
Engine Spd. (rpm)	871	813	849	847	853	845	866	806	801	868	793	805
MAT (°C)	60	60	59	59	59	61	61	62	59	60	61	60
MAP (kPag)	95.3	94.0	92.1	92.7	92.0	97.6	95.2	94.6	94.1	96.6	94.2	46.9
CNG Press. (MPa)	23.2	23.1	23.3	22.5	23.1	22.9	23.2	23.3	23.4	28.7	28.7	28.4
Diesel Press. (MPa)	24.1	24.2	24.3	24.4	24.5	24.1	24.1	24.1	24.2	29.6	29.6	29.7
Exhaust Press. (kPa)	50.4	49.3	51.5	53.2	52.1	53.7	55.4	66.6	50.2	50.7	50.3	38.7
Corr. Air flow (kg/hr)	133	126	137	138	138	130	131	124	125	133	125	260
Airflow (kg/hr)	116	110	119	120	120	113	114	108	109	116	109	226
Diesel flow (kg/hr)	0.33	0.25	4.02	0.46	0.29	0.59	0.28	0.33	0.28	0.19	0.12	0.43
Diesel inj. (mg/inj)	12.62	10.25	157.72	18.08	11.26	23.30	10.79	13.52	11.76	7.18	4.98	17.96
CNG flow (kg/hr)	2.14	1.19	2.05	2.23	1.92	3.18	2.90	2.47	1.87	2.29	2.28	2.29
CO (ppm-dry)	67	68	480	53	812	37	128	37	84	570	829	14
CO2 (%-dry)	3.88	2.82	3.85	4.56	3.51	6.16	5.15	5.45	4.10	4.10	4.24	1.64
NOx (ppm-dry)	887	469	870	1096	661	1659	1689	1462	1001	924	884	527
O2 (%-dry)	14.02	16.10	14.22	13.14	14.71	10.14	11.72	11.48	13.80	13.60	13.22	17.98
CH4 (ppm-dry, C1)	137	75	302	105	833	110	127	60	79	346	1148	27
tHC (ppm_{wet}, C1)	61	65	153	57	390	48	55	55	69	160	509	16
Exhaust T. (°C)	295	224	291	325	277	417	371	380	295	313	328	426
Pk. press. (bar)	89.8	75.8	87.9	91.0	87.9	104.0	103.6	96.5	91.3	81.4	83.1	89.2
CA @ Pk. press. (bar)	14.0	13.9	14.5	13.6	14.5	14.3	14.8	14.9	13.3	17.5	16.3	12.0
Gross IMEP (bar)	7.50	5.08	7.29	8.36	7.29	11.60	10.15	10.35	7.85	7.91	8.45	7.44
EQR	0.36	0.22	0.78	0.37	0.31	0.56	0.47	0.43	0.33	0.36	0.37	0.20
5% IHR (deg)	6.6	3.1	5.6	3.1	5.6	1.6	7.1	1.6	2.6	9.6	9.6	3.1
10% IHR (deg)	7.6	7.1	7.1	3.6	7.1	2.1	8.1	1.6	3.1	10.6	10.6	3.6
50% IHR (deg)	10.3	11.0	10.7	10.2	10.7	10.1	11.0	10.8	9.8	14.0	13.8	10.7
90% IHR (deg)	15.6	16.1	15.6	17.1	15.6	19.6	15.6	18.6	15.6	19.1	19.1	16.6
COV GIMEP	12.9	7.1	2.5	1.4	2.5	12.0	7.8	3.4	5.7	12.0	9.4	3.2
DSOI (deg)	-30.0	-22.0	14.0	-30.0	14.0	-39.0	-30.0	-25.0	-21.0	-37.0	-33.0	-35.0
DEOI (deg)	-13.3	-13.7	22.7	-12.2	19.1	-13.7	-13.4	-12.4	-12.8	-16.2	-11.6	-20.5
GSOI (deg)	-6.8	-6.8	-6.8	-6.0	-6.8	-6.8	-6.8	-6.8	-6.8	-5.0	-5.0	-6.8
GEOI (deg)	-4.3	-4.5	-3.2	-2.4	-3.2	-3.2	-3.1	-3.4	-3.4	-2.6	-2.8	-4.5
2GSOI (deg)	-0.8	1.8	0.0	2.0	0.0	0.5	-1.0	1.5	2.0	2.5	2.5	2.0
2GEOI (deg)	5.0	6.2	4.6	6.6	4.6	6.1	4.7	6.8	6.3	6.7	6.3	6.3
Comments			VOID									

Figure #	54	39	36	48	89	57	45	42
Test Series - #	VII-B-11	VII-B-9	VII-B-9	VII-B-10	VII-B-22	VII-B-12	VII-B-10	VII-B-10
Test Name	29-20-47a	29-10-47a	29-10-47a1	29-10-70a-15.10.59	29-10-70LBa-15.11.25	29-20-70a	29-10-70a	29-10-70a
Date/Time	07-12-19 13.12.24	07-12-19 13.24.57	07-12-17 16.25.10	08-01-15 10.59.33	08-01-15 11.25.23	07-12-19 13.05.10	07-12-19 13.33.15	07-12-17 16.45.15
Ignition Delay (ms)	1.45	1.57	1.49	1.56	1.42	1.36	1.62	1.81
Knock (bar)	4.5		2.2	1.5	1.2	4.6	2.0	1.8
IHR (kJ/m3)	1355	1069	1460	1700	1300	1866	1385	1761
IHR Ratio	0.8	0.5	0.7	0.1	1.6	0.8	0.5	0.4
Engine Spd. (rpm)	818	825	812	909	869	809	819	803
MAT (°C)	63	63	64	59	60	63	63	61
MAP (kPag)	94.6	95.1	95.0	96.0	95.8	96.0	95.4	104.4
CNG Press. (MPa)	29.0	28.7	28.8	26.9	28.0	28.9	28.9	29.2
Diesel Press. (MPa)	29.7	29.7	30.0	29.3	29.3	29.6	29.7	29.9
Exhaust Press. (kPa)	53.4	49.3	49.5	64.8	64.5	60.1	49.9	49.4
Corr. Air flow (kg/hr)	126	127	127	148	141	124	126	127
Airflow (kg/hr)	109	110	110	129	123	108	109	110
Diesel flow (kg/hr)	0.52	0.41	0.32	0.38	0.37	0.48	0.35	0.31
Diesel inj. (mg/inj)	21.28	16.66	13.12	14.03	14.35	19.68	14.16	12.78
CNG flow (kg/hr)	1.71	1.37	2.04	2.67	3.09	2.52	1.87	2.50
CO (ppm-dry)	60	317	152	318	212	37	564	477
CO2 (%-dry)	4.08	3.11	4.01	4.68	5.56	5.59	3.91	4.71
NOx (ppm-dry)	961	644	1076	1171	1631	1681	1008	1501
O2 (%-dry)	13.92	15.49	13.86	12.82	11.23	11.22	14.01	12.50
CH4 (ppm-dry, C1)	130	222	113	199	134	109	310	236
tHC (ppm_{wet}, C1)	62	103	59	101	72	55	144	120
Exhaust T. (°C)	295	241	296	349	396	381	290	338
Pk. press. (bar)	89.2	83.8	83.8	93.2	71.1	104.7	92.6	92.6
CA @ Pk. press. (bar)	12.0	13.0	13.0	16.2	14.6	7.2	14.0	14.0
Gross IMEP (bar)	7.44	5.71	5.71	9.34	7.35	5.28	7.54	7.54
EQR	0.34	0.27	0.36	0.40	0.47	0.46	0.34	0.43
5% IHR (deg)	3.1	5.1	5.1	7.1	4.6	2.6	5.6	5.6
10% IHR (deg)	3.6	5.6	5.6	8.6	5.6	2.6	6.6	6.6
50% IHR (deg)	10.7	10.3	10.3	12.4	10.9	3.8	10.4	10.4
90% IHR (deg)	16.6	14.1	14.1	17.6	18.1	6.1	14.1	14.1
COV GIMEP	3.2	3.8	3.8	2.0	1.9	5.3	5.1	5.1
DSOI (deg)	-21.0	-16.0	-30.0	19.0	18.0	-21.0	-16.0	-30.0
DEOI (deg)	-10.2	-11.5	-21.7	22.8	27.9	-10.3	-11.6	-22.3
GSOI (deg)	-5.0	-5.0	-6.8	-5.0	-5.0	-5.0	-5.0	-6.8
GEOI (deg)	-2.7	-2.7	-4.5	-1.2	-1.3	-1.6	-1.6	-3.4
2GSOI (deg)	3.0	1.8	1.0	1.0	2.0	4.3	1.3	1.0
2GEOI (deg)	6.9	5.7	4.9	5.9	6.7	8.2	5.2	4.9
Comments								

Figure #	80	74	77	92	95	83	86	89	1	98	101	104
Test Series - #	VII-B-37	VII-B-37	VII-B-37	VII-B-39	VII-B-39	VII-B-38	VII-B-38	VII-B-38	VII-B-26	VII-B-40	VII-B-40	VII-B-41
Test Name	18-10-47LBa-18-13.40.53	18-10-47LBa-18-12.47	18-10-47LBa-aftera	18-20-47LBa	18-20-47LBa	18-10-70LBa	18-10-70LBa	18-10-70LBa-14.13.43	18-10-70a-14.13.25	18-20-70LBa	18-20-70LBa	24-10-47LBa
Date/Time	07-12-18-13.38.49	07-12-18-12.44.49	07-12-18-13.07.38	07-12-18-12.20.33	07-12-18-13.54.14	07-12-18-13.20.48	07-12-18-14.19.50	08-01-14-13.43.24	08-01-14-13.23.40	07-12-18-12.30.17	07-12-18-14.05.28	07-12-18-11.14.55
Ignition Delay (ms)	3.29	3.07	2.88	2.77	3.17	2.07	2.13	1.62	1.75	1.72	1.67	1.86
IHR (kJ/m3)	1622	1506	1592	2233	1689	1807	1864	847	1494	1782	1812	1956
Knock (bar)	1.21	2.22	1.41	2.44	2.40	1.23	1.30	0.69	0.56	4.99	4.95	1.14
IHR Ratio	**6.39**	**14.18**	**66.81**	**85.50**	**0.12**	**9.85**	**7.92**	2.48	0.68	0.95	0.85	**1.00**
Engine Spd. (rpm)	1194	1193	1194	1200	1193	1198	1200	1202	1213	1197	1199	1206
MAT (°C)	65	65	65	66	65	65	65	66	66	66	65	66
MAP (kPag)	94.3	94.3	95.0	93.4	95.0	95.7	95.6	96.4	91.3	95.4	93.8	94.8
CNG Press. (MPa)	17.8	17.8	17.5	17.7	17.7	17.7	17.6	16.9	16.9	17.5	17.4	23.8
Diesel Press. (MPa)	18.6	18.7	18.7	18.7	18.6	18.7	18.6	17.9	17.9	18.7	18.5	24.7
Exhaust Press. (kPa)	48.6	50.0	49.0	56.8	49.0	51.9	52.8	58.2	61.7	54.3	50.6	60.3
Corr. Air flow (kg/hr)	161	160	160	159	162	160	161	177	173	162	162	157
Airflow (kg/hr)	179	178	178	177	180	178	179	197	192	180	180	175
Diesel flow (kg/hr)	0.28	0.42	0.48	0.50	0.57	0.29	0.31	0.36	0.36	0.48	0.58	0.17
Diesel inj.(mg/inj)	7.79	11.61	13.53	13.85	15.89	7.97	8.73	9.91	10.00	13.40	16.15	4.69
CNG flow (kg/hr)	3.57	3.21	3.29	5.08	3.59	4.15	4.32	1.81	3.32	3.81	3.89	4.48
CO (ppm-dry)	349	434	47	124	89	133	107	185	112	46	45	46
CO2 (%-dry)	4.66	4.30	4.67	6.98	4.96	5.35	5.60	2.63	4.50	5.50	5.68	5.80
NOx (ppm-dry)	1337	1060	958	1174	1316	1019	1013	324	531	1000	1002	1452
O2 (%-dry)	12.56	13.24	12.74	8.60	12.18	11.35	10.96	16.34	13.02	11.32	11.05	10.54
CH4 (ppm-dry, C1)	371	631	109	59	117	124	113	178	149	102	100	107
tHC (ppm_{wet}, C1)	187	271	60	33	62	63	59	95	80	54	56	57
Exhaust T. (°C)	372	354	367	519	384	415	431	239	377	422	430	442
Pk. press. (bar)	86.3	93.6	88.8	99.5	95.9	94.6	95.2	73.8	73.5	93.9	94.2	102.9
CA@Pk. press. (bar)	15.4	14.5	13.7	12.5	14.5	12.8	12.5	12.0	9.8	9.4	10.7	12.9
Gross IMEP (bar)	8.75	8.29	8.77	12.49	9.25	10.16	10.47	4.70	8.15	9.98	10.26	11.02
EQR	-0.63	0.47	0.37	0.63	0.47	0.61	0.40	0.29	0.51	0.16	0.37	0.21
5% IHR (deg)	8.6	7.6	6.1	5.1	8.1	2.1	1.6	5.1	5.1	-3.9	-3.9	0.6
10% IHR (deg)	9.6	8.1	6.6	5.6	8.6	4.6	4.1	5.6	6.1	-2.9	-2.9	3.1
50% IHR (deg)	13.3	11.0	11.0	11.2	11.4	10.3	10.4	11.0	16.1	10.8	10.7	9.4
90% IHR (deg)	19.6	16.1	20.1	26.1	18.1	21.6	22.6	20.1	26.6	23.1	23.1	19.1
COV GIMEP	6.1	3.8	4.2	4.1	5.5	3.3	3.6	2.2	2.4	5.1	3.8	4.0
DSOI (deg)	-59.8	-59.0	22.0	-59.0	-59.8	-44.0	-44.5	18.0	23.0	-59.0	-59.8	-42.0
DEOI (deg)	-32.5	-30.4	41.0	-23.0	-24.0	-26.8	-27.2	31.0	27.4	-23.1	-23.8	-26.1
GSOI (deg)	-17.0	-17.0	-17.0	-17.0	-17.0	-17.0	-17.0	-9.0	-10.0	-17.0	-17.0	-17.0
GEOI (deg)	-13.6	-13.6	-13.6	-13.6	-13.6	-12.0	-12.0	-4.0	-3.4	-12.0	-12.0	-13.6
2GSOI (deg)	-10.0	-8.0	-6.5	-9.0	-7.5	-6.2	-6.9	-2.0	-1.0	-6.5	-7.2	-7.0
2GEOI (deg)	0.2	1.3	2.8	5.4	2.7	3.1	3.4	4.5	8.5	2.8	3.1	1.3
Comments												

Figure #	4	14	113	20	26	11	107	7	10	116	23	29
Test Series - #	VII-B-29	VII-B-31	VII-B-43	VII-B-32	VII-B-32	VII-B-30	VII-B-42	VII-B-30	VII-B-30	VII-B-44	VII-B-32	VII-B-32
Test Name	24-10-47a	24-20-47a1	24-20-47LBa2	24-20-70a1	24-20-70a1	24-10-70a-15.9.30	24-10-70LBa	24-10-70a	24-10-70a-14.13.00	24-20-70LBa	24-20-70a1	24-20-70a
Date/Time	07-12-18 10.44.16	07-12-17 14.15.33	07-12-18 11.54.30	07-12-17 14.33.10	07-12-17 14.50.56	08-01-15 09.29.20	07-12-18 11.31.33	07-12-18 10.52.35	08-01-14 13.01.47	07-12-18 11.42.01	07-12-17 14.42.15	07-12-18 10.59.11
Ignition Delay (ms)	2.07	1.49	1.61	1.79	2.20	2.42	1.88	1.66	1.49	1.65	1.48	1.44
IHR (kJ/m3)	120	219	160	1624	1599	1443	2386	1997	1579	2438	1819	613
Knock (bar)	1.11	1.63	2.21	1.15	1.13	0.73	1.40	1.87	1.70	2.82	2.61	5.51
IHR Ratio	0.33	0.62	**1.00**	0.79	0.61	0.27	**1.00**	0.95	**1.00**	**1.00**	0.91	1.10
Engine Spd. (rpm)	1210	1209	1197	1209	1221	1204	1206	1220	1214	1201	1211	1216
MAT (°C)	64	59	66	65	65	63	65	64	65	65	65	65
MAP (kPag)	93.4	94.2	95.7	92.3	93.1	93.1	93.6	93.3	93.4	96.4	92.8	94.2
CNG Press. (MPa)	23.9	23.8	22.8	23.2	23.3	23.3	23.3	23.6	23.1	22.9	23.2	23.2
Diesel Press. (MPa)	24.7	24.6	23.9	24.1	24.3	24.5	24.2	24.4	24.0	23.8	24.1	24.1
Exhaust Press. (kPa)	57.8	53.5	54.0	53.3	60.4	55.3	64.8	59.1	61.3	58.1	53.3	55.8
Corr. Air flow (kg/hr)	156	161	161	157	159	168	157	158	176	160	159	160
Airflow (kg/hr)	174	179	179	174	176	187	174	175	195	177	177	177
Diesel flow (kg/hr)	0.29	1.37	0.63	0.29	0.32	0.33	0.41	0.43	0.48	0.52	0.61	0.72
Diesel inj.(mg/inj)	8.09	15.00	17.62	8.12	8.85	9.04	11.24	11.83	13.29	14.51	16.84	19.84
CNG flow (kg/hr)	4.07	3.11	4.24	3.41	4.40	3.35	5.63	4.45	3.39	5.71	3.51	3.81
CO (ppm-dry)	45	36	54	71	52	595	195	89	171	201	267	49
CO2 (%-dry)	5.63	4.83	5.96	4.56	6.37	4.35	7.48	6.04	4.73	7.63	4.63	5.45
NOx (ppm-dry)	917	953	1281	969	1241	785	1350	1132	889	1284	1015	1263
O2 (%-dry)	11.00	12.62	10.47	12.80	9.83	13.22	7.57	10.25	12.65	7.41	12.66	11.40
CH4 (ppm-dry, C1)	103	118	98	129	99	475	68	118	175	51	192	129
tHC (ppm_{wet}, C1)	61	71	52	71	59	236	39	68	90	31	104	75
Exhaust T. (°C)	439	367	450	363	473	357	549	457	376	555	363	408
Pk. press. (bar)	81.9	91.3	98.7	92.1	101.1	72.0	106.3	97.1	87.4	107.6	94.0	100.7
CA@Pk. press. (bar)	17.8	14.0	14.2	13.5	2.7	8.2	12.7	12.4	12.4	10.7	13.9	5.8
Gross IMEP (bar)	10.29	9.01	11.09	8.79	11.35	7.75	13.39	11.18	8.72	13.72	8.92	10.24
EQR	-0.28	0.23	0.41	0.19	0.23	0.52	0.30	0.42	0.28	0.32	0.46	0.47
5% IHR (deg)	-1.4	-3.9	-3.4	3.6	-4.4	10.6	0.1	-1.4	2.6	-3.4	2.1	-3.9
10% IHR (deg)	8.6	4.1	3.6	5.6	-3.4	11.6	2.6	0.1	3.6	-2.4	5.1	-2.9
50% IHR (deg)	14.8	10.6	10.8	10.3	10.4	16.4	10.4	10.5	10.9	10.4	10.6	8.6
90% IHR (deg)	24.6	19.6	21.1	18.6	24.1	24.6	24.6	22.6	20.1	26.1	18.1	20.1
COV GIMEP	3.8	3.7	4.2	2.0	3.3	6.6	4.0	3.0	4.8	4.2	2.8	1.5
DSOI (deg)	-35.5	20.0	-58.0	60.0	60.0	-42.0	-42.0	-35.5	18.0	-55.0	60.0	-45.0
DEOI (deg)	-27.9	41.0	-22.1	77.4	78.3	-21.1	-26.1	-27.8	39.9	-26.2	77.9	-15.8
GSOI (deg)	-17.0	-17.0	-17.0	-15.9	-17.0	-10.0	-17.0	-17.0	-10.0	-17.0	-15.9	-15.9
GEOI (deg)	-13.6	-13.6	-13.6	-12.5	-11.9	-4.9	-11.9	-11.9	-4.9	-12.0	-10.8	-10.8
2GSOI (deg)	-1.5	-6.0	-5.5	-5.5	-4.7	-2.0	-4.3	-4.5	-2.0	-4.3	-5.0	-5.0
2GEOI (deg)	6.8	2.3	2.8	2.5	3.7	4.5	4.1	3.9	4.6	4.0	2.6	2.7
Comments									(109,110)			

Figure #	32	35	38	41	44	47	50	53	56	59	62	65
Test Series - #	VII-B-33	VII-B-33	VII-B-33	VII-B-34	VII-B-34	VII-B-34	VII-B-35	VII-B-35	VII-B-35	VII-B-36	VII-B-36	VII-B-36
Test Name	28-10-47a	28-10-47a	28-10-47a	28-10-70a	28-10-70a	28-10-70a	28-20-47a	28-20-47a	28-20-47a	28-20-70a	28-20-70a	28-20-70a
Date/Time	07-12-18 15.25.44	07-12-18 16.14.00	07-12-19 10.30.59	07-12-18 15.37.06	07-12-18 16.07.00	07-12-19 10.43.15	07-12-18 15.13.55	07-12-18 15.53.16	07-12-19 10.14.25	07-12-18 15.02.09	07-12-18 16.00.14	07-12-19 10.05.50
Ignition Delay (ms)	1.75	1.70	1.58	1.76	1.79	1.71	1.64	1.56	1.53	1.71	1.57	1.53
IHR (kJ/m3)	1486	1506	952	1888	1972	1584	1533	472	1097	2116	951	1649
Knock (bar)	1.69	1.75	2.98	1.41	1.42	1.79	1.91	4.67	4.92	2.20	3.79	4.61
IHR Ratio	0.63	0.60	0.55	0.81	0.87	0.82	0.74	0.82	0.96	0.98	0.95	0.84
Engine Spd. (rpm)	1194	1197	1201	1199	1201	1207	1192	1196	1200	1200	1203	1204
MAT (°C)	65	65	66	65	65	66	65	65	64	65	65	62
MAP (kPag)	94.1	93.3	94.9	95.1	94.1	92.4	95.2	94.3	94.5	94.7	94.7	95.0
CNG Press. (MPa)	29.0	29.4	28.5	28.6	29.0	28.6	29.2	29.2	28.7	28.9	29.1	28.4
Diesel Press. (MPa)	29.9	30.0	29.5	29.8	29.9	29.4	29.9	29.8	29.5	29.8	29.7	29.5
Exhaust Press. (kPa)	46.8	47.5	52.2	50.2	51.2	68.9	49.6	47.5	55.2	54.7	51.1	59.3
Corr. Air flow (kg/hr)	157	156	163	158	156	159	158	157	161	156	157	164
Airflow (kg/hr)	174	174	181	176	173	177	175	175	179	174	175	182
Diesel flow (kg/hr)	0.34	0.41	0.76	0.44	0.48	0.72	0.56	0.66	0.57	0.55	0.57	0.72
Diesel inj.(mg/inj)	9.48	11.37	21.15	12.29	13.34	19.92	15.70	18.44	15.87	15.17	15.91	19.85
CNG flow (kg/hr)	3.06	3.08	1.90	4.13	4.23	3.30	3.20	3.21	2.01	4.68	4.53	3.23
CO (ppm-dry)	209	194	345	289	278	446	149	74	105	107	53	66
CO2 (%-dry)	4.28	4.35	3.05	5.54	5.79	4.74	4.55	4.72	3.52	6.44	6.41	5.02
NOx (ppm-dry)	832	844	433	1126	1151	893	882	990	612	1232	1464	919
O2 (%-dry)	13.37	13.28	15.67	11.12	10.69	12.55	12.94	12.71	14.94	9.58	9.72	12.27
CH4 (ppm-dry, C1)	148	144	170	178	178	299	138	125	97	127	112	76
tHC (ppm_{wet}, C1)	77	74	108	90	89	161	72	66	71	67	60	63
Exhaust T. (°C)	338	342	259	417	433	385	356	362	284	473	465	384
Pk. press. (bar)	90.2	90.5	75.5	99.8	100.1	87.1	90.6	93.5	85.3	107.6	115.2	95.9
CA@Pk. press. (bar)	13.2	13.1	14.0	13.2	13.2	15.6	13.4	2.0	7.8	5.6	2.5	8.8
Gross IMEP (bar)	8.19	8.35	5.27	10.60	11.11	8.63	8.52	8.84	6.18	11.88	11.68	8.89
EQR	0.38	0.49	0.16	0.41	0.44	0.44	0.39	0.65	-0.02	0.69	0.66	0.50
5% IHR (deg)	-1.4	-1.4	6.1	-0.9	-0.9	6.1	-1.9	-4.9	4.1	-2.9	-4.9	4.1
10% IHR (deg)	0.6	0.1	6.6	1.1	1.1	7.1	-0.9	-3.4	4.6	-1.4	-3.4	4.6
50% IHR (deg)	10.4	10.4	12.7	10.2	10.4	12.5	10.6	10.7	11.6	10.2	10.9	13.2
90% IHR (deg)	17.6	17.6	19.1	19.1	20.1	19.1	18.1	18.1	20.6	22.1	23.1	24.1
COV GIMEP	2.5	1.8	5.6	2.4	2.0	4.6	3.1	2.5	6.5	4.3	2.4	8.5
DSOI (deg)	-32.0	-33.0	-29.0	-32.0	-38.0	-28.0	-40.0	-38.0	-38.0	-40.0	-38.0	-38.0
DEOI (deg)	-27.2	-28.0	-18.6	-27.3	-33.0	-17.9	-33.3	-27.2	-18.6	-33.2	-27.2	-18.5
GSOI (deg)	-17.0	-17.0	-8.0	-17.0	-17.0	-8.0	-17.0	-17.0	-8.0	-17.0	-17.0	-8.0
GEOI (deg)	-13.6	-13.6	-4.6	-12.0	-12.0	-2.9	-13.6	-13.6	-4.6	-12.0	-11.9	-2.9
2GSOI (deg)	-1.3	-1.3	0.0	-0.3	0.3	1.0	-0.8	-0.5	0.0	1.0	1.8	4.0
2GEOI (deg)	3.8	3.8	5.8	4.8	5.3	6.8	4.3	4.5	5.8	6.0	6.8	9.8
Comments												

Figure #	71	68
Test Series - #	VII-B-36	VII-B-36
Test Name	29-20-47a-14.12.40	29-20-70a-14.12.27
Date/Time	08-01-14-12.40.47	08-01-14-12.28.18
Ignition Delay (ms)	1.53	1.46
IHR (kJ/m3)	1690	1082
Knock (bar)	4.91	4.48
IHR Ratio	0.86	0.96
Engine Spd. (rpm)	1194	1201
MAT (°C)	65	63
MAP (kPag)	96.1	96.6
CNG Press. (MPa)	28.5	28.2
Diesel Press. (MPa)	29.4	29.3
Exhaust Press. (kPa)	61.2	63.1
Corr. Air flow (kg/hr)	177	177
Airflow (kg/hr)	197	197
Diesel flow (kg/hr)	0.54	0.61
Diesel inj.(mg/inj)	15.02	17.05
CNG flow (kg/hr)	3.38	4.29
CO (ppm-dry)	80	51
CO2 (%-dry)	4.88	6.07
NOx (ppm-dry)	945	1166
O2 (%-dry)	12.48	10.39
CH4 (ppm-dry, C1)	121	95
tHC (ppm_{wet}, C1)	65	61
Exhaust T. (°C)	378	454
Pk. press. (bar)	91.1	106.9
CA@Pk. press. (bar)	10.4	8.9
Gross IMEP (bar)	9.30	11.02
EQR	10.00	-5.50
5% IHR (deg)	4.1	3.6
10% IHR (deg)	5.1	4.1
50% IHR (deg)	11.8	9.1
90% IHR (deg)	20.6	27.1
COV GIMEP	5.2	5.5
DSOI (deg)	-53.0	-54.0
DEOI (deg)	-17.9	-20.1
GSOI (deg)	-8.0	-8.0
GEOI (deg)	-4.6	-3.0
2GSOI (deg)	0.0	9.0
2GEOI (deg)	6.4	13.3
Comments		0.391366857

Figure #	1	2	3	4	5	6	7	8	9	10	11	12
Test Series - #	VIII-A-4	VIII-A-4	VIII-A-5	VIII-A-5	VIII-A-5	VIII-A-5	VIII-A-5	VIII-A-5	VIII-A-5	VIII-A-5	VIII-A-6	VIII-A-6
Test Name	I2I-3-6	I2I-3-11	I2I-3-5	I2I-3-8	I2I-3-9	I2I-3-12	I2I-3-17	I2I-3-18	I2I-3-19	I2I-3-20	I2I-3-7	I2I-3-10
Date/Time	06-01-09 15.39.41	06-01-10 10.24.33	06-01-09 15.31.40	06-01-09 15.56.48	06-01-10 09.52.51	06-01-10 10.33.31	06-01-10 10.54.58	06-01-10 11.08.15	06-01-10 11.30.19	06-01-10 11.40.46	06-01-09 15.49.23	06-01-10 10.10.04
Ignition Delay (ms)	2.56	2.40	2.23	2.20	1.96	1.98	2.33	2.15	3.52	1.67	2.03	1.80
IHR (kJ/m3)	1431	1431	1455	1415	1449	1439	1430	1444	1514	1446	1508	1466
Knock (bar)	1.2	1.4	2.1	2.3	3.9	3.7	1.4	1.1	1.3	1.0	2.4	4.0
Comb. Dur. (deg)	25.0	28.0	28.5	28.5	30.0	30.5	25.5	22.5	15.0	26.5	28.5	29.5
Engine Spd. (rpm)	1103	1097	1103	1104	1099	1097	1097	1097	1098	1098	1102	1097
MAT (°C)	25	27	25	26	25	27	27	27	27	27	25	26
MAP (kPag)	83.7	86.6	83.5	83.5	86.9	86.7	86.1	86.1	85.2	85.3	83.8	86.7
CNG Press. (MPa)	21.0	21.0	21.0	21.0	21.0	21.0	21.0	21.0	21.0	21.0	21.0	21.0
Diesel Press. (MPa)	23.4	23.7	23.4	23.5	23.6	23.7	23.8	23.5	23.4	23.4	23.5	23.7
Exhaust Press. (kPa)	97.9	99.3	97.4	93.6	94.9	99.4	100.3	100.2	98.5	99.0	101.6	101.4
Corr. Air flow (kg/hr)	147	147	147	147	148	147	147	147	147	146	146	147
Disel inj.(mg/inj)	13.8	19.9	14.5	14.9	23.1	22.1	16.3	14.2	18.4	18.9	11.9	21.2
CNG flow (kg/hr)	4.36	4.18	4.34	4.32	4.18	4.22	4.25	4.32	4.14	4.26	4.33	4.19
CO (ppm-dry)	0.70	0.72	0.57	0.63	0.67	0.64	0.84	0.91	1.24	0.75	0.63	0.64
CO2 (%-dry)	0.44	0.45	0.45	0.45	0.46	0.46	0.45	0.45	0.45	0.45	0.46	0.47
NOx (ppm-dry)	7.60	7.28	5.64	5.70	6.25	6.18	5.36	6.09	7.83	5.56	4.73	5.07
O2 (%-dry)	0.50	0.51	0.51	0.51	0.52	0.51	0.53	0.52	0.53	0.50	0.52	0.53
CH4 (ppm-dry, C1)	0.48	0.44	0.44	0.44	0.38	0.38	0.41	0.43	0.45	0.36	0.40	0.32
tHC (ppm_{wet}, C1)	0.43	0.43	0.40	0.38	0.38	0.37	0.40	0.42	0.49	0.41	0.34	0.31
Exhaust T. (°C)	472	470	483	481	473	480	476	475	468	492	499	488
Pk. press. (bar)	138.5	138.5	117.7	117.3	120.1	120.1	117.0	120.6	124.5	117.1	104.3	116.1
CA@Pk. press. (bar)	10.7	10.4	13.5	13.4	5.7	5.0	13.9	14.3	15.5	13.5	7.5	6.0
Gross IMEP (bar)	13.28	13.13	13.03	12.95	12.94	12.92	12.95	13.03	12.84	13.10	12.69	12.63
EQR	0.55	0.55	0.55	0.55	0.56	0.56	0.55	0.55	0.54	0.56	0.54	0.56
5% IHR (deg)	-5.2	-7.2	-2.7	-2.7	-4.2	-4.2	-1.2	-0.2	4.3	-0.2	1.3	0.3
10% IHR (deg)	-3.7	-6.2	-1.7	-1.7	-3.7	-3.7	-0.2	2.3	5.8	0.8	2.3	0.8
50% IHR (deg)	5.1	4.7	9.9	9.9	10.1	**10.2**	10.0	9.8	10.1	10.0	15.0	**15.1**
90% IHR (deg)	19.8	20.8	25.8	25.8	25.8	26.3	24.3	22.3	19.3	26.3	29.8	29.8
COV GIMEP	0.7	0.7	0.7	0.8	0.8	0.9	0.7	0.9	1.0	1.4	0.8	0.8
DSOI (ms)	-5.9	-6.5	-5.1	-5.1	-5.6	-5.5	-5.7	-3.8	-0.7	0.7	-4.3	-4.7
DPW (ms)	2.1	2.6	2.1	2.1	2.7	2.5	1.9	2.0	2.5	2.5	2.1	2.6
RIT (ms)	0.3	0.3	0.3	0.3	0.3	0.3	1.0	-1.0	-5.0	-5.0	0.3	0.3
GPW (ms)	0.7	0.7	0.7	0.7	0.7	0.7	0.7	0.7	0.7	0.7	0.7	0.7
2RIT (ms)	1.50	1.50	0.50	1.50	1.50	1.50	1.50	1.50	1.50	1.50	1.50	1.50
2GPW (ms)	1.08	0.73	1.27	1.05	1.08	0.69	1.07	1.06	1.12	1.11	1.14	0.70
Comments									VOID			

13	14	15	16	17	18	19	20
VIII-A-7	VIII-A-8	VIII-A-8	VIII-A-9	VIII-A-28	VIII-A-29	VIII-A-29	VIII-A-30
I2I-3-14	I2I-3-13	I2I-3-16	I2I-3-15	I2I-3-3	I2I-3-1	I2I-3-4	I2I-3-2
06-01-10 12.22.10	06-01-10 12.11.20	06-01-10 12.38.21	06-01-10 12.30.00	06-01-09 15.07.29	06-01-09 14.46.26	06-01-09 15.15.25	06-01-09 14.57.03
3.72	2.22	1.97	2.36	2.73	2.30	2.28	1.65
1417	1412	1408	1445	696	713	704	687
3.0	0.9	0.9	1.0	1.1	0.9	0.9	0.6
16.0	27.5	28.0	34.5	12.0	15.5	15.0	15.0
1508	1505	1505	1501	1104	1104	1104	1102
31	31	32	31	24	24	24	24
96.9	97.0	96.6	96.6	52.2	52.6	52.0	52.5
21.0	21.0	21.0	21.0	21.0	21.0	21.0	21.0
23.2	23.2	23.1	23.2	23.7	23.7	23.7	23.7
111.4	112.3	113.9	113.5	64.6	64.4	65.0	64.8
198	198	198	198	124	124	124	124
16.8	15.3	13.9	11.3	12.4	13.9	16.6	15.2
5.87	5.87	5.86	5.87	1.76	1.79	1.79	1.76
1.23	1.96	2.16	1.87	8.12	6.06	6.49	10.87
0.42	0.44	0.44	0.45	0.46	0.46	0.47	0.47
9.56	4.58	4.33	2.98	6.51	4.16	4.11	2.87
0.50	0.52	0.52	0.54	1.43	1.41	1.43	1.56
0.48	0.52	0.53	0.51	1.57	1.42	1.57	4.89
0.47	0.51	0.52	0.50	1.64	1.48	1.65	5.52
496	521	525	540	290	302	302	306
157.2	120.1	118.3	100.3	97.4	82.2	80.9	67.9
10.0	13.9	13.9	6.6	10.2	14.2	14.6	2.7
13.36	12.99	12.88	12.58	6.05	6.11	6.02	5.66
0.56	0.56	0.55	0.54	0.29	0.30	0.31	0.30
-1.7	-1.7	-1.7	-1.2	-2.2	0.8	0.8	5.8
0.3	1.3	0.8	0.8	0.3	1.8	2.3	7.3
5.0	9.7	9.9	15.0	5.2	9.9	10.2	15.3
14.3	25.8	26.3	33.3	9.8	16.3	15.8	20.8
0.8	0.8	0.9	0.8	1.6	1.5	1.3	2.0
-6.4	-5.6	-5.6	-5.0	-5.6	-4.7	-4.6	-4.0
2.0	2.0	2.0	2.0	2.1	2.1	2.1	2.1
0.3	0.3	0.3	0.3	0.3	0.3	0.3	0.3
0.7	0.7	0.7	0.7	0.6	0.6	0.6	0.6
1.50	1.50	1.50	1.50	1.50	1.50	1.50	1.50
1.11	1.06	1.06	1.05	1.10	0.69	1.08	1.09

Figure #	1	2	3	4	5	6	7	8	9	10	11	12
Test Series - #	VIII-B-10	VIII-B-10	VIII-B-11	VIII-B-11	VIII-B-12	VIII-B-12	VIII-B-4	VIII-B-5	VIII-B-6	VIII-B-13	VIII-B-13	VIII-B-14
Test Name	E-1B	E-1D	E-1A	E-1E	E-1C	E-1F	D-1D	D-1E	D-1F	13-15-05-55-13	D-1B	11-15-10-55-13
Date/Time	08-02-25 14.45.40	08-02-25 16.55.19	08-02-25 14.34.08	08-02-25 17.03.04	08-02-25 14.50.56	08-02-25 17.08.27	08-02-26 18.07.45	08-02-26 18.15.28	08-02-26 18.22.52	08-02-22 21.06.52	08-02-25 13.32.05	08-02-22 20.54.47
Ignition Delay (ms)	1.55	1.56	1.59	1.53	1.56	1.57	1.78	1.69	1.57	1.35	1.51	1.50
IHR (kJ/m3)	1018	1055	1046	1065	948	959	2204	2239	2302	1466	2143	1461
Knock (bar)	2.7	2.4	1.6	2.0	1.2	1.5	3.4	4.8	5.7	3.1	2.8	3.4
Comb. Dur. (deg)	16.0	15.5	16.5	17.5	17.5	16.0	29.5	32.5	30.5	20.0	26.5	25.0
Engine Spd. (rpm)	1104	1102	1103	1100	1104	1082	1098	1096	1096	1114	1094	1113
MAT (°C)	49	50	49	50	49	50	47	47	47	49	48	50
MAP (kPag)	77.6	72.5	77.7	72.0	77.8	73.1	112.6	112.5	112.7	87.3	112.6	86.9
CNG Press. (MPa)	21.8	22.3	21.9	22.3	21.9	22.0	21.0	20.8	20.9	20.5	21.9	20.3
Diesel Press. (MPa)	23.9	24.2	24.1	24.2	23.9	24.2	23.1	23.1	23.1	22.1	24.0	22.1
Exhaust Press. (kPa)	72.3	58.5	71.7	58.0	71.3	55.3	107.1	107.9	108.3	71.4	100.4	72.7
Corr. Air flow (kg/hr)	130	126	131	126	131	125	151	151	152	135	152	135
Airflow (kg/hr)	143	139	144	138	144	138	166	166	167	148	167	148
Diesel inj. (mg/inj)	13.4	12.7	14.1	13.0	12.6	14.9	14.4	15.5	15.0	17.0	11.4	17.2
CNG flow (kg/hr)	1.74	1.78	1.75	1.82	1.70	1.56	4.27	4.26	4.28	2.60	4.08	2.68
CO (g/kW-hr)	4.37	4.59	2.58	3.62	7.81	4.94	1.11	0.56	0.34	1.84	0.56	1.00
CO2 (kg/kW-hr)	0.49	0.48	0.48	0.48	0.49	0.50	0.45	0.46	0.47	0.50	0.45	0.53
NOx (g/kW-hr)	7.48	7.46	6.99	6.17	4.29	5.02	7.59	5.76	4.83	10.07	8.87	7.26
O2 (kg/kW-hr)	1.64	1.49	1.59	1.46	1.82	1.75	0.55	0.56	0.57	1.07	0.59	1.05
CH4 (g/kW-hr)	1.24	1.25	1.00	1.38	4.66	2.40	0.41	0.36	0.32	0.73	0.43	0.63
tHC (g/kW-hr,C1)	1.96	1.95	1.61	2.13	7.12	3.73	0.64	0.57	0.52	1.24	0.67	1.04
Exhaust T. (°C)	280	286	286	298	282	278	466	475	485	352	446	377
Pk. press. (bar)	99.1	99.4	90.7	90.4	78.7	77.6	143.8	123.4	119.0	118.0	146.4	100.8
CA@Pk. press. (bar)	4.2	9.8	7.1	7.1	8.9	10.5	9.2	11.0	4.7	9.4	9.1	2.8
Gross IMEP (bar)	5.72	5.99	5.92	6.05	5.30	5.36	12.94	12.89	12.59	8.39	12.62	8.34
EQR	0.28	0.29	0.28	0.30	0.27	0.27	0.53	0.53	0.53	0.39	0.49	0.40
5% IHR (deg)	-4.1	-4.1	0.9	0.9	5.4	5.9	-7.6	-5.1	0.4	-8.1	-8.1	-4.6
10% IHR (deg)	-3.1	-3.1	1.9	1.4	6.4	6.4	-6.6	-4.6	0.4	-6.1	-6.1	-3.1
50% IHR (deg)	6.5	6.0	10.3	11.2	16.1	15.1	5.4	10.3	15.3	5.1	4.8	10.5
90% IHR (deg)	12.0	11.5	17.5	18.5	23.0	22.0	22.0	27.5	31.0	12.0	18.5	20.5
COV GIMEP	1.9	1.7	2.3	1.9	4.2	2.6	0.7	0.7	0.7	1.3	0.7	1.5
DSOI (ms)	3.0	2.7	3.8	3.6	4.4	4.3	-6.4	-5.8	-4.8	2.9	2.7	3.8
DPW (ms)	2.1	2.3	2.1	2.3	2.1	2.3	2.1	2.0	2.0	3.0	2.0	3.0
RIT (ms)	-7.6	-7.6	-7.6	-7.6	-7.6	-7.6	1.0	1.0	1.0	-9.2	-8.0	-9.2
GPW (ms)	0.7	0.7	0.7	0.7	0.7	0.7	0.7	0.7	0.7	0.7	0.7	0.7
2RIT (ms)	1.46	1.40	1.33	1.39	1.50	1.34	1.41	1.62	1.36	1.50	1.41	1.49
2GPW (ms)	0.54	0.57	0.54	0.56	0.54	0.56	1.20	1.14	1.17	0.86	1.04	0.86
Comments												VOID

Figure #	13	14	15	16	17	18	19	20	21	22	23	24
Test Series - #	VIII-B-14	VIII-B-15	VIII-B-15	VIII-B-16	VIII-B-16	VIII-B-16	VIII-B-16	VIII-B-16	VIII-B-16	VIII-B-17	VIII-B-17	VIII-B-17
Test Name	D-1A	12-15-05-55-13	D-1C	06-08-05-55-13	10-15-05-55-13	B-1B	C-1B	B-1D	C-1D	08-15-10-55-13	B-1A	C-1A
Date/Time	08-02-25 13.24.24	08-02-22 21.00.04	08-02-25 13.37.52	08-02-22 19.39.15	08-02-22 20.15.57	08-02-25 12.23.52	08-02-25 15.32.10	08-02-25 16.10.15	08-02-26 19.00.25	08-02-22 19.59.07	08-02-25 12.03.47	08-02-25 15.26.43
Ignition Delay (ms)	1.43	1.43	1.38	3.84	3.65	3.93	3.54	4.01	3.85	2.18	4.51	2.87
IHR (kJ/m3)	2235	1467	2341	2132	2143	2166	2091	2193	2137	2171	2220	2203
Knock (bar)	2.9	2.5	2.5	4.5	5.4	5.0	4.5	6.7	6.1	1.9	2.5	1.9
Comb. Dur. (deg)	31.5	24.0	31.0	10.5	11.5	10.0	10.5	10.0	10.0	33.5	14.5	23.5
Engine Spd. (rpm)	1094	1111	1094	1505	1513	1507	1511	1515	1513	1508	1505	1510
MAT (°C)	48	50	48	52	53	51	52	53	51	53	51	51
MAP (kPag)	112.4	87.0	112.6	148.4	144.3	148.1	148.0	147.8	139.2	148.1	144.5	147.1
CNG Press. (MPa)	21.7	20.4	22.0	20.6	20.7	21.3	21.4	21.6	21.1	20.6	21.4	21.5
Diesel Press. (MPa)	23.9	22.1	23.9	22.1	22.1	23.6	23.6	23.6	23.3	22.1	23.6	23.6
Exhaust Press. (kPa)	98.2	72.3	100.2	113.2	112.8	130.7	131.5	133.8	110.6	118.5	166.3	127.7
Corr. Air flow (kg/hr)	152	135	152	203	199	205	205	204	197	203	200	205
Airflow (kg/hr)	167	148	167	223	219	225	225	224	216	223	220	225
Diesel inj. (mg/inj)	18.4	15.5	11.8	16.3	14.3	15.2	18.2	15.3	17.8	14.0	14.8	17.9
CNG flow (kg/hr)	4.18	2.61	4.33	5.34	5.37	5.37	5.28	5.58	5.52	5.66	5.64	5.67
CO (g/kW-hr)	0.32	1.18	0.30	1.18	1.04	1.04	1.00	0.75	0.97	2.05	3.69	1.70
CO2 (kg/kW-hr)	0.46	0.53	0.47	0.47	0.47	0.43	0.44	0.44	0.45	0.49	0.43	0.44
NOx (g/kW-hr)	6.39	5.71	5.27	13.18	13.50	12.37	11.52	14.33	12.56	5.54	7.90	6.16
O2 (kg/kW-hr)	0.57	1.11	0.55	0.67	0.62	0.61	0.62	0.58	0.54	0.60	0.55	0.56
CH4 (g/kW-hr)	0.36	0.63	0.32	0.54	0.54	0.45	0.53	0.37	0.42	0.54	1.48	0.56
tHC (g/kW-hr,C1)	0.58	1.14	0.52	0.92	0.89	0.73	0.84	0.60	0.67	0.87	2.18	0.83
Exhaust T. (°C)	466	377	484	454	464	460	461	470	479	510	525	503
Pk. press. (bar)	122.6	95.1	118.2	156.8	161.4	156.1	158.7	164.3	160.0	122.8	128.1	127.4
CA@Pk. press. (bar)	11.2	6.1	4.8	10.1	9.1	10.9	9.4	9.9	9.6	12.5	15.2	13.7
Gross IMEP (bar)	12.80	8.11	12.90	12.36	12.52	12.46	12.26	12.59	12.47	12.80	12.85	12.88
EQR	0.53	0.39	0.52	0.50	0.51	0.50	0.50	0.51	0.54	0.52	0.53	0.53
5% IHR (deg)	-5.6	0.4	-1.1	-1.1	-2.6	-0.1	-1.6	-0.6	-1.1	-6.6	3.4	-0.6
10% IHR (deg)	-4.6	1.4	-0.1	0.4	-0.6	1.4	-0.1	0.9	0.4	-0.1	4.9	3.9
50% IHR (deg)	10.2	15.4	15.2	5.7	4.8	6.6	5.2	5.5	5.5	10.0	10.6	10.1
90% IHR (deg)	26.0	24.5	30.0	9.4	8.9	9.9	8.9	9.4	8.9	27.0	18.0	23.0
COV GIMEP	0.8	1.5	0.7	1.0	0.9	0.9	0.8	0.8	0.7	1.1	1.7	0.8
DSOI (ms)	3.4	4.6	4.2	2.7	2.1	2.3	1.7	1.6	1.0	3.1	2.2	2.3
DPW (ms)	2.0	3.0	2.0	2.3	2.8	1.5	1.9	1.6	1.8	2.8	1.4	1.9
RIT (ms)	-8.0	-9.2	-8.0	-9.2	-9.1	-8.0	-7.6	-7.6	-7.1	-9.1	-8.0	-7.6
GPW (ms)	0.7	0.7	0.7	0.7	0.7	0.7	0.7	0.7	0.7	0.7	0.7	0.7
2RIT (ms)	1.41	1.48	1.41	1.51	1.54	1.40	1.45	1.39	1.52	1.47	1.76	1.45
2GPW (ms)	1.04	0.86	1.04	1.08	1.05	1.14	1.08	1.15	1.19	1.05	1.11	1.08
Comments		VOID		VOID								

Figure #	25	26	27	28	29	30	31	32	33	34	35	36
Test Series - #	VIII-B-17	VIII-B-17	VIII-B-17	VIII-B-18	VIII-B-18	VIII-B-18	VIII-B-18	VIII-B-18	VIII-B-22	VIII-B-22	VIII-B-22	VIII-B-23
Test Name	B-1E	C-1D2	C-1E	09-15-13-15-55-20.07.12	B-1C	C-1C	B-1F	C-1F	02-08-13-05-55-18.36.20	A-1B	A-1D	01-08-13-10-55-18.30.40
Date/Time	08-02-25-16.16.40	08-02-26-19.09.51	08-02-26-19.20.30	08-02-22-	08-02-25-12.30.33	08-02-25-15.38.47	08-02-25-16.24.08	08-02-26-19.30.18	08-02-22-18.36.20	08-02-25-14.01.36	08-02-26-17.31.07	08-02-22-18.30.40
Ignition Delay (ms)	3.38	4.40	3.79	1.49	2.72	1.60	3.04	3.37	1.91	3.55	3.00	1.66
IHR (kJ/m3)	2202	2177	2201	2250	2314	2288	2256	2181	2160	2215	2172	2267
Knock (bar)	2.1	3.8	2.0	2.7	1.4	1.8	1.2	1.4	2.2	3.7	2.9	2.9
Comb. Dur. (deg)	18.5	13.5	17.5	42.0	31.5	39.0	33.0	30.0	24.5	8.5	14.5	30.0
Engine Spd. (rpm)	1515	1511	1516	1512	1507	1509	1515	1515	1096	1097	1098	1095
MAT (°C)	53	52	52	53	52	52	53	52	47	48	47	47
MAP (kPag)	146.7	138.7	138.7	144.6	147.5	147.4	146.9	138.4	112.5	112.7	108.9	112.0
CNG Press. (MPa)	21.4	21.5	21.3	20.7	21.5	21.6	21.7	21.6	20.7	21.8	21.0	20.6
Diesel Press. (MPa)	23.7	23.5	23.5	22.1	23.6	23.6	23.7	23.5	22.2	23.9	23.2	22.2
Exhaust Press. (kPa)	128.3	110.6	113.7	118.6	129.6	129.2	133.7	116.3	113.4	100.8	98.4	116.8
Corr. Air flow (kg/hr)	205	197	198	200	206	205	205	197	151	152	148	150
Airflow (kg/hr)	225	217	217	220	226	226	226	217	166	167	163	165
Diesel inj. (mg/inj)	16.5	16.3	16.5	14.0	15.8	17.5	14.2	15.5	6.3	6.9	8.9	8.6
CNG flow (kg/hr)	5.72	5.35	5.71	5.97	5.97	5.83	5.78	5.67	4.24	4.33	4.31	4.35
CO (g/kW-hr)	1.66	3.63	2.36	1.54	2.44	1.51	2.60	3.22	0.66	0.55	0.97	0.48
CO2 (kg/kW-hr)	0.44	0.43	0.44	0.51	0.45	0.46	0.45	0.46	0.50	0.44	0.44	0.50
NOx (g/kW-hr)	7.47	9.05	7.75	3.62	4.20	3.45	3.96	4.26	9.08	13.00	10.27	6.26
O2 (kg/kW-hr)	0.55	0.57	0.51	0.56	0.53	0.54	0.57	0.54	0.65	0.58	0.55	0.60
CH4 (g/kW-hr)	0.54	2.24	0.56	0.38	0.62	0.47	0.70	0.81	0.50	0.41	0.44	0.42
tHC (g/kW-hr,C1)	0.81	3.44	0.86	0.65	0.93	0.72	1.01	1.17	0.92	0.65	0.71	0.88
Exhaust T. (°C)	504	474	515	554	539	537	535	538	459	435	443	486
Pk. press. (bar)	131.8	140.5	124.1	110.9	105.4	106.6	101.8	98.7	142.3	159.0	152.2	120.5
CA@Pk. press. (bar)	13.8	13.3	15.1	3.1	16.8	3.4	14.4	15.2	9.5	10.1	9.3	11.8
Gross IMEP (bar)	12.93	12.38	12.90	12.65	13.01	12.85	12.56	12.24	12.51	12.78	12.81	12.91
EQR	0.53	0.52	0.55	0.56	0.55	0.54	0.53	0.54	0.50	0.51	0.53	0.52
5% IHR (deg)	1.9	0.4	2.4	-6.1	0.9	-4.6	-0.1	1.9	-6.6	1.4	-0.1	-3.6
10% IHR (deg)	3.9	1.9	4.4	-3.6	7.4	-1.1	8.4	8.4	-4.6	2.4	1.4	-3.1
50% IHR (deg)	9.6	8.0	10.6	15.4	14.6	14.7	15.2	15.3	5.1	6.0	5.2	10.6
90% IHR (deg)	20.5	14.0	20.0	36.0	32.5	34.5	33.0	32.0	18.0	9.9	14.5	26.5
COV GIMEP	0.9	0.7	1.0	0.7	0.8	0.9	1.3	1.5	1.0	0.7	0.8	0.7
DSOI (ms)	2.4	0.8	1.5	3.7	3.6	3.0	3.1	2.4	-5.9	3.0	-5.6	-5.1
DPW (ms)	1.6	1.7	1.7	2.8	1.5	1.9	1.6	1.7	2.2	0.9	0.9	2.2
RIT (ms)	-7.6	-7.1	-7.1	-9.1	-8.0	-7.6	-7.6	-7.1	0.3	-7.6	1.0	0.3
GPW (ms)	0.7	0.7	0.7	0.7	0.7	0.7	0.7	0.7	0.7	0.7	0.7	0.7
2RIT (ms)	1.39	1.50	1.56	1.48	1.40	1.45	1.53	1.56	1.40	1.34	1.54	1.40
2GPW (ms)	1.11	1.14	1.15	1.05	1.14	1.08	1.04	1.07	1.12	1.14	1.22	1.12
Comments												

Figure #	37	38	39	40	41	42	43	44	45	46	47
Test Series - #	VIII-B-23	VIII-B-23	VIII-B-24	VIII-B-24	VIII-B-24	VIII-B-25	VIII-B-25	VIII-B-26	33	VIII-B-35	VIII-B-36
Test Name	A-1A	A-1E	03-08-15-55-13	A-1C	A-1F	05-08-10-55-13	B-1A2	07-08-15-55-13	SLOW LOW CO	REP-08-02-26	REP-08-02-28
Date/Time	08-02-25 13.57.54	08-02-26 17.44.29	08-02-22 18.42.43	08-02-25 14.07.17	08-02-26 17.50.08	08-02-22 19.24.15	08-02-25 12.17.06	08-02-22 19.47.07	08-02-25 13.47.19	08-02-26 17.03.31	08-02-25 11.11.26
Ignition Delay (ms)	2.56	1.72	1.66	1.57	1.96	3.44	3.67	2.04	1.24	0.91	1.71
IHR (kJ/m3)	2242	2243	2442	2401	2359	2232	2210	2325	2394	1487	1527
Knock (bar)	2.3	1.7	2.4	1.2	1.5	1.6	1.9	1.4	2.94	1.59	1.72
Comb. Dur. (deg)	15.5	24.5	30.5	29.5	22.5	18.5	16.5	36.5	16	18.0	16.5
Engine Spd. (rpm)	1096	1096	1095	1095	1094	1505	1507	1507	1095	1188	1201
MAT (°C)	47	47	47	48	47	51	51	52	48	48	46
MAP (kPag)	112.5	107.5	112.6	112.5	107.7	148.2	147.4	148.2	112.2	99.1	99.9
CNG Press. (MPa)	21.9	21.1	20.8	21.7	21.0	20.8	21.5	20.8	21.7	21.2	21.4
Diesel Press. (MPa)	23.9	23.2	22.2	23.9	23.2	22.2	23.6	22.1	23.9	23.2	23.8
Exhaust Press. (kPa)	99.1	102.0	114.2	98.7	103.3	115.7	127.0	119.3	96.6	88.1	85.5
Corr. Air flow (kg/hr)	153	147	151	152	147	203	205	203	153	150	152
Airflow (kg/hr)	168	161	166	167	161	224	225	224	168	165	167
Diesel inj. (mg/inj)	7.4	9.6	7.0	11.0	10.7	13.1	13.7	11.1	11.4	12.4	13.3
CNG flow (kg/hr)	4.37	4.50	4.65	4.57	4.51	5.87	5.72	6.14	3.91	3.06	3.17
CO (g/kW-hr)	0.96	0.94	0.55	0.60	0.85	2.58	2.10	2.18	1.73	5.99	3.96
CO2 (kg/kW-hr)	0.45	0.46	0.51	0.45	0.46	0.48	0.44	0.50	0.40	0.45	0.46
NOx (g/kW-hr)	8.75	6.61	5.10	5.06	5.25	7.32	7.92	3.96	5.81	5.95	6.67
O2 (kg/kW-hr)	0.57	0.51	0.55	0.52	0.51	0.59	0.56	0.56	0.64	1.01	0.98
CH4 (g/kW-hr)	0.43	0.39	0.35	0.35	0.37	0.68	0.61	0.51	0.61	2.08	1.16
tHC (g/kW-hr,C1)	0.65	0.62	0.72	0.56	0.58	1.13	0.92	0.87	0.90	3.04	1.79
Exhaust T. (°C)	456	483	515	489	499	509	497	550	428	365	367
Pk. press. (bar)	134.5	124.8	110.7	111.4	103.6	124.0	126.7	103.3	134.5	102.2	107.5
CA@Pk. press. (bar)	13.1	13.3	5.4	15.0	18.0	14.9	14.6	15.5	13.1	13.8	12.8
Gross IMEP (bar)	12.92	12.98	13.35	13.36	13.00	12.97	12.87	13.01	12.92	8.53	8.65
EQR	0.51	0.55	0.55	0.55	0.56	0.53	0.52	0.55	0.47	0.39	0.40
5% IHR (deg)	3.9	0.4	-0.1	-0.1	6.9	2.9	2.9	-2.6	3.9	-0.6	-0.6
10% IHR (deg)	4.9	4.4	1.4	2.9	10.5	4.9	4.4	2.9	4.9	1.9	1.9
50% IHR (deg)	9.5	10.0	15.2	13.6	15.3	10.7	10.3	14.7	9.5	10.5	9.4
90% IHR (deg)	19.5	25.0	30.5	29.5	29.5	21.5	19.5	34.0	19.5	17.5	16.0
COV GIMEP	0.7	0.8	0.7	0.8	0.7	1.1	1.3	0.9	0.8	2.0	1.3
DSOI (ms)	3.8	-4.8	-4.5	4.6	-4.0	3.4	2.9	4.0	3.6	-5.3	-5.3
DPW (ms)	0.9	0.9	2.2	0.9	0.9	2.3	1.5	2.3	1.0	1.5	1.5
RIT (ms)	-7.6	1.0	0.3	-7.6	1.0	-9.3	-8.0	-9.1	-7.0	1.0	1.0
GPW (ms)	0.7	0.7	0.7	0.7	0.7	0.7	0.7	0.7	0.7	0.7	0.7
2RIT (ms)	1.34	1.55	1.48	1.33	1.44	1.51	1.40	1.50	1.25	1.64	1.42
2GPW (ms)	1.14	1.22	1.12	1.14	1.22	1.08	1.14	1.08	1.04	0.86	0.92
Comments										VOID	VOID

Figure #	1	2	3	4	5	6	7	8	9	10	11	12
Test Series - #	VIII-B2-1	VIII-B2-1	VIII-B2-1	VIII-B2-1	VIII-B2-1	VIII-B2-2	VIII-B2-2	VIII-B2-2	VIII-B2-3	VIII-B2-3	VIII-B2-3	VIII-B2-3
Test Name	VIII-1A	VIII-1	VIII-1B	VIII-1D	VIII-1D2	VIII-2A	VIII-2	VIII-2B	VIII-3A	VIII-3	VIII-3B	VIII-3D
Date/Time	08-06-09-12.14.42	08-06-11-09.25.32	08-06-11-15.00.33	08-06-12-12.01.07	08-06-12-12.40.51	08-06-09-12.03.28	08-06-11-09.20.26	08-06-11-15.11.08	08-06-09-12.27.00	08-06-11-09.31.41	08-06-11-15.27.00	08-06-12-12.28.00
Ignition Delay (ms)	1.98	2.03	1.95	1.87	1.85	1.80	1.88	1.84	1.70	1.83	1.74	1.65
IHR (kJ/m3)	1090	1084	1113	1083	1237	446	1040	469	420	378	483	540
Knock (bar)	1.8	1.9	1.6	1.8	1.9	2.0	1.7	1.7	2.5	1.4	1.7	2.4
Comb Dur. (deg)	18.5	15.5	16.5	15.0	18.0	20.5	17.5	20.5	19.5	19.5	21.0	21.5
Engine Spd. (rpm)	1103	1096	1092	1105	1103	1103	1096	1091	1100	1095	1091	1100
MAT (°C)	51	51	53	54	53	50	51	53	51	51	53	53
MAP (kPag)	48.8	40.7	47.6	46.4	61.6	49.0	40.6	47.4	48.7	40.3	47.5	62.3
CNG Press. (MPa)	21.0	21.1	21.1	21.3	21.1	21.1	21.4	21.1	21.0	21.3	21.2	21.1
Diesel Press. (MPa)	23.3	23.6	23.6	23.5	23.4	23.3	23.6	23.6	23.4	23.6	23.6	23.4
Exhaust Press. (kPa)	67.7	53.7	64.1	67.8	78.1	68.7	54.4	64.4	68.5	54.7	65.2	95.3
Corr. Air flow (kg/hr)	127	121	125	126	139	127	121	125	127	120	126	139
Airflow (kg/hr)	127	121	125	126	139	127	121	125	127	120	126	139
Diesel inj. (mg/inj)	14.2	14.4	15.3	14.2	14.6	14.1	14.3	14.6	14.5	14.0	15.3	14.8
CNG flow (kg/hr)	1.80	1.73	1.78	1.86	2.03	1.87	1.79	1.81	1.79	1.84	1.86	2.07
CO (g/kW-hr)	7.66	7.70	9.05	9.13	5.86	6.49	9.61	8.07	6.87	8.92	7.30	5.87
CO2 (kg/kW-hr)	0.48	0.48	0.48	0.50	0.47	0.48	0.48	0.49	0.49	0.49	0.50	0.50
NOx (g/kW-hr)	8.13	8.38	6.82	7.63	10.30	5.82	5.97	5.04	4.67	4.55	4.30	6.83
O2 (kg/kW-hr)	1.48	1.41	1.45	1.49	1.42	1.44	1.44	1.48	1.56	1.44	1.48	1.50
CH4 (g/kW-hr)	1.97	2.15	2.18	3.96	1.59	2.71	4.33	3.41	4.58	5.79	4.99	4.24
tHC (g/kW-hr,C1)	1.97	2.15	2.18	3.96	1.59	2.71	4.33	3.41	4.58	5.79	4.99	4.24
Exhaust T. (°C)	294	291	293	309	299	308	302	302	307	316	315	323
Pk. press. (bar)	92.7	89.3	92.9	89.4	101.6	78.6	75.6	80.2	75.3	67.3	75.7	85.0
CA@Pk. press. (bar)	8.6	9.0	9.0	8.9	9.0	8.2	13.0	4.2	6.1	6.3	6.6	6.2
Gross IMEP (bar)	6.00	5.96	6.09	5.87	6.82	6.14	5.86	5.99	5.78	5.82	5.95	6.48
EQR	0.30	0.51	0.30	0.31	0.30	0.30	0.56	0.30	0.30	0.55	0.31	0.31
5% IHR (deg)	-7.6	-5.1	-5.6	-4.6	-6.6	-3.6	-1.1	-3.6	1.5	1.9	1.0	0.5
10% IHR (deg)	-5.6	-4.1	-3.6	-3.1	-5.1	-2.1	-0.1	-2.6	2.0	2.9	1.5	1.5
50% IHR (deg)	4.9	5.2	5.3	5.2	5.3	10.3	10.0	10.4	14.8	15.3	15.2	15.0
90% IHR (deg)	11.0	10.5	11.0	10.5	11.5	17.0	16.5	17.0	21.0	21.5	22.0	22.0
COV GIMEP	1.8	1.3	1.2	1.3	1.7	1.8	1.9	1.6	2.1	1.5	1.4	1.7
DSOI (ms)	-5.9	-5.8	-6.3	-5.2	-5.8	-5.1	-5.0	-5.4	-4.4	-4.6	-4.6	-4.5
DPW (ms)	1.6	1.6	1.7	1.7	1.7	1.6	1.6	1.7	1.6	1.6	1.7	1.7
RIT (ms)	1.0	1.0	1.0	1.0	1.0	1.0	1.0	1.0	1.0	1.0	1.0	1.0
GPW (ms)	0.7	0.7	0.7	0.7	0.7	0.7	0.7	0.7	0.7	0.7	0.7	0.7
2RIT (ms)	1.65	1.47	1.90	1.63	1.49	1.73	1.47	1.91	1.66	1.78	1.83	1.73
2GPW (ms)	0.74	0.78	0.73	0.70	0.76	0.71	0.74	0.70	0.71	0.74	0.72	0.72
Comments												

Figure #	13	14	15	16	17	18	19	20	21	22	23	24
Test Series - #	VIII-B2-4	VIII-B2-4	VIII-B2-4	VIII-B2-4	VIII-B2-5	VIII-B2-5	VIII-B2-5	VIII-B2-5	VIII-B2-6	VIII-B2-6	VIII-B2-6	VIII-B2-6
Test Name	VIII-4A	VIII-4	VIII-4B	VIII-4D	VIII-5A	VIII-5	VIII-5B	VIII-5D	VIII-6A	VIII-6	VIII-6B	VIII-6D
Date/Time	08-06-10-10.28.00	08-06-11-09.50.00	08-06-11-16.05.00	08-06-12-11.14.00	08-06-10-10.19.00	08-06-11-09.43.00	08-06-11-15.55.00	08-06-12-11.05.00	08-06-10-10.37.00	08-06-11-09.55.00	08-06-11-16.16.00	08-06-12-11.33.00
Ignition Delay (ms)	1.51	1.77	1.72	1.94	1.59	1.56	1.58	1.67	1.52	1.55	1.52	1.56
IHR (kJ/m3)	2192	2193	2265	2148	550	565	546	540	582	621	578	582
Knock (bar)	1.8	2.0	2.1	1.9	2.8	2.4	2.3	2.4	4.5	2.5	3.1	2.7
Comb Dur. (deg)	34.0	35.0	33.5	32.0	36.0	38.0	36.0	37.0	35.0	35.0	35.0	36.0
Engine Spd. (rpm)	1101	1085	1079	1097	1099	1084	1078	1094	1097	1083	1076	1093
MAT (°C)	48	50	52	53	48	50	52	54	48	50	52	53
MAP (kPag)	87.1	71.4	74.5	68.3	87.0	71.6	73.6	70.8	87.1	70.8	74.8	73.1
CNG Press. (MPa)	21.1	21.3	21.0	21.0	21.1	21.3	20.9	21.0	21.1	21.3	21.0	21.0
Diesel Press. (MPa)	23.4	23.6	23.4	23.4	23.4	23.7	23.4	23.4	23.4	23.6	23.5	23.3
Exhaust Press. (kPa)	101.5	104.3	98.7	84.3	99.3	102.7	95.1	86.0	103.6	81.4	90.1	92.1
Corr. Air flow (kg/hr)	159	143	144	142	159	143	144	144	158	143	145	146
Airflow (kg/hr)	159	143	144	142	159	143	144	144	158	143	145	146
Diesel inj. (mg/inj)	15.1	16.0	15.8	15.2	14.9	15.7	16.1	15.2	15.2	15.7	15.5	14.9
CNG flow (kg/hr)	4.22	4.16	4.23	4.12	4.27	4.17	4.21	4.22	4.31	4.29	4.25	4.33
CO (g/kW-hr)	1.37	1.07	0.93	0.84	0.79	0.62	0.57	0.51	0.39	0.39	0.33	0.43
CO2 (kg/kW-hr)	0.47	0.46	0.47	0.47	0.47	0.47	0.48	0.48	0.49	0.48	0.48	0.48
NOx (g/kW-hr)	8.27	8.47	8.07	11.04	5.92	6.31	5.81	7.93	5.04	5.26	4.92	6.48
O2 (kg/kW-hr)	0.59	0.48	0.47	0.48	0.59	0.48	0.48	0.48	0.59	0.47	0.49	0.47
CH4 (g/kW-hr)	0.44	0.43	0.41	0.42	0.39	0.38	0.37	0.36	0.35	0.32	0.32	0.31
tHC (g/kW-hr,C1)	0.44	0.43	0.41	0.42	0.39	0.38	0.37	0.36	0.35	0.32	0.32	0.31
Exhaust T. (°C)	450	486	488	480	463	497	497	496	480	500	504	513
Pk. press. (bar)	135.3	131.5	133.8	128.6	115.7	110.3	111.8	110.2	105.3	96.6	98.0	97.5
CA@Pk. press. (bar)	9.3	9.3	9.2	9.2	12.4	12.6	12.4	12.4	3.4	4.4	3.8	3.4
Gross IMEP (bar)	12.95	13.13	13.30	12.76	12.90	12.92	13.02	12.84	12.56	12.98	12.96	13.01
EQR	0.55	0.54	0.55	0.55	0.31	0.56	0.55	0.55	0.50	0.50	0.55	0.56
5% IHR (deg)	-8.6	-7.1	-7.6	-7.6	-6.1	-5.6	-5.6	-6.1	-1.1	-1.1	-1.6	-2.6
10% IHR (deg)	-5.1	-4.1	-4.6	-4.6	-4.1	-3.6	-3.6	-4.1	-0.6	-0.1	-0.1	-1.1
50% IHR (deg)	5.5	5.2	5.2	4.9	10.4	10.5	10.3	10.3	15.8	15.3	15.4	15.2
90% IHR (deg)	25.5	28.0	26.0	24.5	30.0	32.5	30.5	31.0	34.0	34.0	33.5	33.5
COV GIMEP	1.0	0.8	0.7	0.9	1.0	0.8	0.5	0.9	1.2	0.7	0.6	0.9
DSOI (ms)	-6.2	-6.2	-6.2	-6.3	-5.5	-5.5	-5.4	-5.5	-4.5	-4.7	-4.7	-4.8
DPW (ms)	1.5	1.6	1.5	1.5	1.5	1.6	1.5	1.5	1.5	1.6	1.5	1.5
RIT (ms)	1.0	1.0	1.0	1.0	1.0	1.0	1.0	1.0	1.0	1.0	1.0	1.0
GPW (ms)	0.7	0.7	0.7	0.7	0.7	0.7	0.7	0.7	0.7	0.7	0.7	0.7
2RIT (ms)	1.64	1.59	1.59	1.64	1.65	1.59	1.59	1.66	1.40	1.60	1.60	1.66
2GPW (ms)	1.27	1.24	1.33	1.28	1.23	1.22	1.28	1.26	1.26	1.23	1.27	1.27
Comments												

Figure #	25	26	27	28	29	30	31	32	33	34	35	36
Test Series - #	VIII-B2-7	VIII-B2-7	VIII-B2-7	VIII-B2-8	VIII-B2-8	VIII-B2-8	VIII-B2-9	VIII-B2-9	VIII-B2-9	VIII-B2-10	VIII-B2-10	VIII-B2-10
Test Name	VIII-7A	VIII-7	VIII-7B	VIII-8A	VIII-8	VIII-8B	VIII-9A	VIII-9	VIII-9B	VIII-10A	VIII-10	VIII-10B
Date/Time	08-06-10-12.14.00	08-06-11-10.21.00	08-06-11-16.46.00	08-06-10-12.07.00	08-06-11-10.12.00	08-06-11-16.37.00	08-06-10-12.26.00	08-06-11-10.26.00	08-06-11-16.56.00	08-06-09-12.48.39	08-06-11-12.00.01	08-06-12-13.04.33
Ignition Delay (ms)	3.28	2.75	2.61	1.60	1.99	1.89	1.79	1.69	1.75	2.64	2.71	3.59
IHR (kJ/m3)	2237	2210	2227	2211	2177	2243	514	521	497	1100	1082	1039
Knock (bar)	2.3	2.5	2.2	1.3	1.4	1.3	1.7	2.2	1.9	1.6	1.4	1.0
Comb Dur. (deg)	28.5	29.0	31.0	37.0	38.0	39.5	42.5	42.5	42.5	18.0	17.0	13.5
Engine Spd. (rpm)	1405	1401	1402	1405	1402	1400	1406	1400	1399	1102	1102	1107
MAT (°C)	53	54	56	53	54	56	54	55	57	51	53	54
MAP (kPag)	112.2	96.4	97.9	112.2	96.2	98.4	111.4	96.3	98.2	48.7	44.4	45.4
CNG Press. (MPa)	21.2	21.1	20.9	21.1	21.1	20.8	21.2	21.0	20.8	21.0	21.0	21.2
Diesel Press. (MPa)	23.3	23.3	23.3	23.2	20.4	23.2	23.2	23.3	23.2	23.4	23.4	23.5
Exhaust Press. (kPa)	125.4	113.1	111.8	123.4	111.6	115.7	120.1	114.1	112.6	61.9	56.1	56.9
Corr. Air flow (kg/hr)	201	185	185	202	185	187	201	185	185	127	123	125
Airflow (kg/hr)	201	185	185	202	185	187	201	185	185	127	123	125
Diesel inj. (mg/inj)	14.5	14.5	14.5	14.7	14.7	14.5	14.0	15.2	14.8	15.4	16.0	14.8
CNG flow (kg/hr)	5.43	5.37	5.47	5.44	5.43	5.57	5.49	5.46	5.56	1.78	1.78	1.76
CO (g/kW-hr)	2.20	2.00	1.43	2.46	2.44	1.93	1.53	1.12	1.09	9.08	11.48	15.86
CO2 (kg/kW-hr)	0.45	0.45	0.46	0.46	0.47	0.47	0.47	0.48	0.49	0.48	0.48	0.48
NOx (g/kW-hr)	8.01	8.97	8.45	5.32	5.00	4.60	3.73	3.63	3.48	8.60	8.78	11.02
O2 (kg/kW-hr)	0.58	0.49	0.48	0.59	0.50	0.48	0.59	0.50	0.48	1.46	1.44	1.54
CH4 (g/kW-hr)	0.52	0.49	0.48	0.51	0.43	0.39	0.45	0.34	0.33	2.37	3.10	4.83
tHC (g/kW-hr,C1)	0.52	0.49	0.48	0.51	0.43	0.39	0.45	0.34	0.33	2.37	3.10	4.83
Exhaust T. (°C)	492	514	521	505	540	553	523	557	564	292	294	283
Pk. press. (bar)	132.9	135.8	135.5	118.8	109.9	111.7	100.5	96.5	95.5	91.4	88.6	84.7
CA@Pk. press. (bar)	11.7	9.0	9.0	12.1	12.9	12.1	5.1	2.9	5.1	9.2	9.6	9.8
Gross IMEP (bar)	13.13	13.08	13.20	12.92	12.75	13.05	12.73	12.54	12.73	6.07	5.98	5.72
EQR	0.55	0.55	0.55	0.55	0.55	0.56	0.50	0.50	0.56	0.30	0.31	0.30
5% IHR (deg)	-3.1	-4.6	-4.6	-5.6	-5.1	-5.1	-5.1	-4.6	-5.6	-6.6	-4.6	-0.1
10% IHR (deg)	2.0	-0.6	-0.6	-0.1	-0.6	0.5	-2.6	-2.1	-3.1	-2.6	-0.1	1.4
50% IHR (deg)	7.9	5.2	5.2	9.8	10.6	10.6	14.5	16.1	15.1	5.3	5.5	5.8
90% IHR (deg)	25.5	24.5	26.5	31.5	33.0	34.5	37.5	38.0	37.0	11.5	12.5	13.5
COV GIMEP	0.8	0.9	0.6	0.7	0.7	0.8	0.9	1.1	0.7	2.3	2.4	3.6
DSOI (ms)	-7.0	-6.7	-6.5	-6.4	-6.1	-5.9	-5.8	-5.4	-5.5	2.3	2.2	2.0
DPW (ms)	1.9	1.7	1.6	1.9	1.7	1.6	1.9	1.7	1.6	1.6	1.5	1.6
RIT (ms)	1.0	1.0	1.0	1.0	1.0	1.0	1.0	1.0	1.0	-7.3	-7.3	-7.3
GPW (ms)	0.7	0.7	0.7	0.7	0.7	0.7	0.7	0.7	0.7	0.7	0.7	0.7
2RIT (ms)	1.91	1.54	1.42	1.67	1.59	1.45	1.67	1.60	1.66	1.66	1.71	1.51
2GPW (ms)	1.28	1.36	1.47	1.28	1.34	1.46	1.25	1.32	1.38	0.74	0.76	0.80
Comments												

Figure #	37	38	39	40	41	42	43	44	45	46	47	48
Test Series - #	VIII-B2-11	VIII-B2-11	VIII-B2-11	VIII-B2-12	VIII-B2-12	VIII-B2-12-B	VIII-B2-13	VIII-B2-13	VIII-B2-13	VIII-B2-14	VIII-B2-14	VIII-B2-14
Test Name	VIII-11A	VIII-11A	VIII-11B	VIII-12A	VIII-12B	VIII-12	VIII-13A	VIII-13	VIII-13B	VIII-14A	VIII-14	VIII-14B
Date/Time	08-06-09-12.41.01	08-06-11-11.53.21	08-06-12-12.56.42	08-06-09-12.58.01	08-06-12-13.12.02	08-06-11-12.05.27	08-06-09-13.25.22	08-06-11-11.15.32	08-06-12-13.27.06	08-06-09-13.16.48	08-06-11-11.08.07	08-06-12-13.21.04
Ignition Delay (ms)	1.61	1.95	1.94	1.50	1.58	1.62	2.69	2.43	2.59	2.84	1.47	1.85
IHR (kJ/m3)	431	1075	1065	460	363	1059	2191	2199	2227	339	2238	2236
Knock (bar)	1.5	1.3	1.3	1.5	1.2	1.1	2.5	3.1	3.1	1.8	1.8	1.7
Comb Dur. (deg)	20.5	21.0	19.5	22.0	20.5	21.0	30.5	27.0	26.5	37.5	36.0	33.0
Engine Spd. (rpm)	1101	1100	1102	1101	1105	1101	1094	1101	1096	1093	1100	1096
MAT (°C)	51	53	54	51	54	53	50	53	53	50	53	52
MAP (kPag)	49.1	44.9	44.0	49.0	45.3	44.6	71.7	73.7	70.9	71.7	73.4	70.5
CNG Press. (MPa)	20.9	20.9	21.2	20.9	21.2	21.1	20.9	21.2	21.0	20.9	21.1	21.0
Diesel Press. (MPa)	23.4	23.4	23.5	23.5	23.5	23.5	23.3	23.5	23.3	23.3	23.5	23.3
Exhaust Press. (kPa)	67.8	57.6	54.9	62.6	58.6	56.5	83.5	99.6	84.4	83.8	100.4	87.0
Corr. Air flow (kg/hr)	127	124	124	127	125	124	144	145	144	144	145	144
Airflow (kg/hr)	127	124	124	127	125	124	144	145	144	144	145	144
Diesel inj. (mg/inj)	16.0	16.0	15.0	16.1	14.8	15.6	16.6	16.2	16.3	16.7	15.8	16.5
CNG flow (kg/hr)	1.71	1.82	1.77	1.76	1.76	1.83	4.24	4.22	4.21	4.24	4.26	4.22
CO (g/kW-hr)	3.88	7.04	10.15	2.69	7.37	5.66	1.41	0.73	0.57	1.13	0.97	0.62
CO2 (kg/kW-hr)	0.49	0.49	0.48	0.49	0.51	0.50	0.48	0.47	0.47	0.48	0.48	0.48
NOx (g/kW-hr)	6.07	6.03	7.02	5.03	5.86	4.80	9.66	11.24	14.21	6.39	6.62	8.67
O2 (kg/kW-hr)	1.53	1.40	1.47	1.47	1.57	1.44	0.46	0.48	0.46	0.47	0.48	0.48
CH4 (g/kW-hr)	1.30	2.51	4.63	1.21	4.23	2.71	0.40	0.40	0.39	0.34	0.37	0.37
tHC (g/kW-hr,C1)	1.30	2.51	4.63	1.21	4.23	2.71	0.40	0.40	0.39	0.34	0.37	0.37
Exhaust T. (°C)	300	309	298	309	309	320	481	481	472	496	505	493
Pk. press. (bar)	78.8	76.7	76.6	77.3	68.6	68.2	132.9	139.0	138.1	111.9	113.8	112.2
CA@Pk. press. (bar)	6.1	13.3	13.3	5.9	6.6	6.9	9.1	8.7	8.9	12.6	12.5	13.2
Gross IMEP (bar)	5.90	6.09	5.94	6.06	5.60	5.92	12.98	12.95	13.16	12.89	12.87	12.88
EQR	0.29	0.31	0.30	0.30	0.30	0.31	0.29	0.55	0.55	0.56	0.56	0.56
5% IHR (deg)	-3.6	-2.1	-2.1	0.4	2.4	2.4	-5.1	-2.1	-3.6	-5.6	-4.6	-4.6
10% IHR (deg)	-2.6	-0.1	-0.1	1.4	3.4	3.9	-0.1	-0.1	-0.1	3.4	1.9	2.9
50% IHR (deg)	9.8	10.2	10.3	14.5	15.3	15.2	5.2	5.2	5.0	10.1	10.1	10.3
90% IHR (deg)	17.0	19.0	17.5	22.5	23.0	23.5	25.5	25.0	23.0	32.0	31.5	28.5
COV GIMEP	2.6	3.1	2.4	2.4	4.2	3.2	1.3	1.0	0.8	1.2	1.0	0.7
DSOI (ms)	3.3	3.2	3.1	4.1	4.0	4.2	1.8	2.0	1.8	2.4	2.8	2.7
DPW (ms)	1.6	1.5	1.6	1.6	1.6	1.5	1.5	1.4	1.6	1.5	1.4	1.6
RIT (ms)	-7.3	-7.3	-7.3	-7.3	-7.3	-7.3	-7.3	-7.3	-7.3	-7.3	-7.3	-7.3
GPW (ms)	0.7	0.7	0.7	0.7	0.7	0.7	0.7	0.7	0.7	0.7	0.7	0.7
2RIT (ms)	1.59	1.70	1.65	1.47	1.51	1.48	1.71	1.54	1.51	1.86	1.57	1.51
2GPW (ms)	0.73	0.73	0.72	0.79	0.75	0.76	1.33	1.30	1.39	1.26	1.27	1.35
Comments												

Figure #	49	50	51	52	53	54	55	56	57	58	59	60
Test Series - #	VIII-B2-15	VIII-B2-15	VIII-B2-15	VIII-B2-16	VIII-B2-16	VIII-B2-17	VIII-B2-17	VIII-B2-17	VIII-B2-18	VIII-B2-18	VIII-B2-18	VIII-B2-19
Test Name	VIII-15A	VIII-15	VIII-15B	VIII-16	VIII-16B	VIII-17A	VIII-17	VIII-17B	VIII-18A	VIII-18	VIII-18B	VIII-19
Date/Time	08-06-09 13.34.11	08-06-11 11.29.06	08-06-12 13.32.19	08-06-11 10.45.46	08-06-12 14.09.48	08-06-10 11.30.50	08-06-11 10.40.31	08-06-12 14.00.04	08-06-10 12.32.36	08-06-11 10.51.25	08-06-12 14.16.48	08-06-11 12.30.28
Ignition Delay (ms)	1.37	1.39	1.34	3.92	4.24	4.22	3.82	4.17	2.20	3.41	3.68	1.51
IHR (kJ/m3)	488	454	414	2218	2215	2278	2194	2202	356	2206	2263	1087
Knock (bar)	1.5	1.5	1.5	4.5	4.8	2.3	2.0	2.3	1.8	1.4	1.1	1.7
Comb Dur. (deg)	38.0	37.0	35.0	22.0	22.0	20.5	27.0	26.0	43.5	38.0	35.0	15.5
Engine Spd. (rpm)	1092	1099	1094	1401	1399	1402	1401	1398	1405	1401	1396	1103
MAT (°C)	50	52	53	55	58	53	55	57	54	56	58	53
MAP (kPag)	71.6	72.3	70.4	95.5	90.1	111.4	95.3	90.8	111.1	95.3	90.6	44.9
CNG Press. (MPa)	20.9	21.2	21.0	21.2	20.9	21.1	21.2	20.9	21.2	21.2	20.9	20.9
Diesel Press. (MPa)	23.4	23.5	23.3	23.4	23.4	22.6	23.4	23.4	23.2	23.4	23.4	23.5
Exhaust Press. (kPa)	84.0	99.3	86.8	109.9	100.0	126.7	110.4	103.9	120.1	106.4	100.7	55.6
Corr. Air flow (kg/hr)	144	144	143	183	178	200	183	179	200	183	179	124
Airflow (kg/hr)	144	144	143	183	178	200	183	179	200	183	179	124
Diesel inj. (mg/inj)	16.9	16.4	16.8	17.9	17.9	16.0	17.5	17.0	18.3	17.1	16.5	13.9
CNG flow (kg/hr)	4.26	4.23	4.21	5.22	5.31	5.30	5.31	5.33	5.32	5.46	5.42	1.84
CO (g/kW-hr)	0.52	0.61	0.57	1.11	1.12	1.66	2.13	1.54	1.86	2.44	1.51	9.98
CO2 (kg/kW-hr)	0.50	0.48	0.49	0.45	0.47	0.46	0.47	0.47	0.48	0.49	0.48	0.47
NOx (g/kW-hr)	4.87	5.03	6.56	11.87	14.75	10.04	7.83	10.54	4.14	4.88	6.25	8.79
O2 (kg/kW-hr)	0.48	0.49	0.49	0.48	0.44	0.58	0.48	0.45	0.60	0.48	0.45	1.44
CH4 (g/kW-hr)	0.28	0.34	0.34	0.41	0.40	0.52	0.42	0.41	0.56	0.43	0.40	2.79
tHC (g/kW-hr,C1)	0.28	0.34	0.34	0.41	0.40	0.52	0.42	0.41	0.56	0.43	0.40	2.79
Exhaust T. (°C)	513	515	509	501	514	490	530	532	523	558	559	292
Pk. press. (bar)	91.6	92.7	91.0	142.7	137.9	126.8	116.3	118.8	95.9	96.1	92.9	91.4
CA@Pk. press. (bar)	4.7	12.4	17.0	10.1	11.2	14.2	14.1	14.0	8.1	16.5	17.1	8.8
Gross IMEP (bar)	12.64	12.68	12.60	13.07	13.04	13.09	12.95	12.96	12.54	12.68	12.80	6.01
EQR	0.29	0.55	0.56	0.56	0.57	0.55	0.56	0.56	0.55	0.51	0.57	0.31
5% IHR (deg)	-3.1	-2.6	-2.6	-1.6	-0.1	1.9	1.4	1.9	-7.1	-2.1	0.9	-4.1
10% IHR (deg)	-1.1	0.4	0.9	0.4	1.9	3.9	3.4	3.9	6.9	6.4	6.9	-1.1
50% IHR (deg)	15.4	15.4	15.3	6.1	7.2	9.8	10.1	9.9	15.8	14.3	15.1	5.2
90% IHR (deg)	35.0	34.5	32.5	20.5	22.0	22.5	28.5	28.0	36.5	36.0	36.0	11.5
COV GIMEP	0.9	0.9	0.7	0.9	0.7	1.2	1.0	0.8	0.7	0.9	1.1	1.4
DSOI (ms)	3.5	3.6	3.4	1.4	1.3	1.7	1.8	1.7	2.5	2.6	2.6	-5.6
DPW (ms)	1.5	1.4	1.6	1.6	1.5	1.3	1.6	1.5	1.9	1.6	1.5	1.2
RIT (ms)	-7.3	-7.3	-7.3	-7.3	-7.3	-7.3	-7.3	-7.3	-7.3	-7.3	-7.3	1.0
GPW (ms)	0.7	0.7	0.7	0.7	0.7	0.7	0.7	0.7	0.7	0.7	0.7	0.7
2RIT (ms)	1.59	1.65	1.65	1.70	1.88	1.76	1.70	1.88	1.69	1.58	1.64	1.53
2GPW (ms)	1.29	1.21	1.29	1.35	1.47	1.37	1.35	1.49	1.25	1.35	1.40	0.85
Comments												

Figure #	61	62	63	64	65	66	67	68	69	70	71	72
Test Series - #	VIII-B2-19	VIII-B2-19	VIII-B2-20	VIII-B2-20	VIII-B2-20	VIII-B2-21	VIII-B2-21A	VIII-B2-21B	VIII-B2-22	VIII-B2-22	VIII-B2-22	VIII-B2-23
Test Name	VIII-19A	VIII-19C	VIII-20	VIII-20A	VIII-20B	VIII-21	VIII-21A	VIII-21B	VIII-22	VIII-22B	VIII-22B	VIII-23
Date/Time	08-06-11 13.29.46	08-06-13 10.04.38	08-06-11 12.24.17	08-06-11 13.20.59	08-06-13 09.45.40	08-06-11 12.37.40	08-06-11 13.37.07	08-06-13 10.18.02	08-06-11 12.58.05	08-06-12 15.29.36	08-06-13 10.50.48	08-06-11 12.52.05
Ignition Delay (ms)	3.62	2.90	1.88	3.01	2.33	2.61	2.73	2.21	3.28	3.34	2.82	3.00
IHR (kJ/m3)	1133	1118	1041	1067	1062	990	1052	308	2204	2213	2198	2245
Knock (bar)	1.3	1.4	1.4	1.2	1.2	1.0	1.1	1.3	2.9	3.3	2.7	1.8
Comb Dur. (deg)	12.5	14.0	18.0	17.0	19.5	20.0	20.5	19.5	22.5	20.5	23.0	25.5
Engine Spd. (rpm)	1095	1098	1101	1094	1098	1092	1091	1098	1101	1096	1108	1099
MAT (°C)	53	52	53	53	52	53	52	52	52	54	52	51
MAP (kPag)	52.8	51.4	43.7	52.8	51.3	45.0	51.9	51.4	70.3	71.2	71.2	70.0
CNG Press. (MPa)	21.0	21.0	21.1	21.1	20.9	21.1	21.2	20.9	20.8	21.1	20.9	20.9
Diesel Press. (MPa)	23.6	23.4	23.5	23.6	23.5	23.5	23.6	23.4	23.3	23.5	23.3	23.4
Exhaust Press. (kPa)	10.9	68.6	55.0	11.3	80.7	56.3	10.9	69.9	29.1	81.4	94.4	28.6
Corr. Air flow (kg/hr)	132	130	123	133	130	124	132	130	146	144	145	146
Airflow (kg/hr)	132	130	123	133	130	124	132	130	146	144	145	146
Diesel inj. (mg/inj)	12.2	12.1	12.3	11.6	12.8	12.0	11.8	12.2	12.4	11.7	12.0	11.9
CNG flow (kg/hr)	1.90	1.96	1.88	2.02	1.91	1.88	2.03	1.93	4.32	4.33	4.32	4.33
CO (g/kW-hr)	13.02	13.44	11.06	14.27	11.31	12.45	12.96	11.43	0.95	0.53	0.80	1.09
CO2 (kg/kW-hr)	0.45	0.47	0.48	0.47	0.48	0.49	0.48	0.49	0.46	0.47	0.46	0.46
NOx (g/kW-hr)	9.75	11.29	6.15	6.04	7.69	4.33	4.49	6.45	12.27	16.30	14.14	7.65
O2 (kg/kW-hr)	1.52	1.50	1.47	1.59	1.55	1.60	1.62	1.62	0.49	0.48	0.48	0.50
CH4 (g/kW-hr)	3.66	4.15	5.36	9.75	5.73	10.97	12.64	8.16	0.40	0.41	0.42	0.40
tHC (g/kW-hr,C1)	3.66	4.15	5.36	9.75	5.73	10.97	12.64	8.16	0.40	0.41	0.42	0.40
Exhaust T. (°C)	243	290	303	258	303	307	268	301	432	467	476	451
Pk. press. (bar)	93.3	94.0	77.0	79.2	80.0	64.7	68.6	71.8	139.9	141.2	137.0	113.6
CA@Pk. press. (bar)	9.1	8.9	12.9	13.3	12.9	3.9	5.4	8.5	8.9	8.7	8.9	13.5
Gross IMEP (bar)	6.25	6.09	5.85	6.01	5.94	5.54	5.88	5.74	13.03	12.94	12.87	12.89
EQR	0.29	0.30	0.31	0.30	0.30	0.31	0.31	0.30	0.55	0.55	0.55	0.54
5% IHR (deg)	-0.1	-2.6	-0.1	1.4	-2.1	4.4	3.9	0.4	-0.6	-0.6	-1.1	2.9
10% IHR (deg)	1.4	0.9	2.4	5.9	0.9	6.9	7.9	2.4	0.9	0.9	0.9	5.4
50% IHR (deg)	5.2	4.9	10.1	10.3	9.8	15.1	14.6	12.6	4.9	4.8	5.1	10.4
90% IHR (deg)	12.5	11.5	18.0	18.5	17.5	24.5	24.5	20.0	22.0	20.0	22.0	28.5
COV GIMEP	1.9	1.4	1.6	2.4	2.5	2.3	3.0	1.8	0.8	0.6	0.8	1.0
DSOI (ms)	-5.9	-5.9	-4.8	-5.0	-5.2	-4.2	-4.2	-4.6	-5.8	-6.0	-5.9	-5.2
DPW (ms)	1.1	1.2	1.2	1.0	1.2	1.2	1.1	1.2	0.8	0.8	0.9	0.8
RIT (ms)	1.0	1.0	1.0	1.0	1.0	1.0	1.0	1.0	1.0	1.0	1.0	1.0
GPW (ms)	0.7	0.7	0.7	0.7	0.7	0.7	0.7	0.7	0.7	0.7	0.7	0.7
2RIT (ms)	1.49	1.65	1.54	1.75	1.81	1.57	1.54	1.65	1.59	1.78	1.67	1.90
2GPW (ms)	0.88	0.83	0.78	0.79	0.78	0.78	0.82	0.77	1.41	1.35	1.36	1.35
Comments												

Figure #	73	74	75	76	77	78	79	80	81	82	83	84
Test Series - #	VIII-B2-23	VIII-B2-23	VIII-B2-24	VIII-B2-24	VIII-B2-24	VIII-B2-25	VIII-B2-25	VIII-B2-25	VIII-B2-26	VIII-B2-26	VIII-B2-26	VIII-B2-27
Test Name	VIII-23B	VIII-23B	VIII-24	VIII-24B	VIII-24B	VIII-25	VIII-25B	VIII-25B	VIII-26	VIII-26B	VIII-26B	VIII-27
Date/Time	08-06-12 15.23.29	08-06-13 10.37.29	08-06-11 13.04.55	08-06-12 15.35.37	08-06-13 11.01.17	08-06-12 10.25.44	08-06-12 14.31.46	08-06-13 11.40.48	08-06-12 10.16.58	08-06-12 14.26.45	08-06-13 11.33.23	08-06-12 10.47.25
Ignition Delay (ms)	2.92	1.24	1.94	1.15	1.37	3.45	3.69	3.91	2.77	3.20	2.80	2.25
IHR (kJ/m3)	2224	2243	2293	2242	2242	2223	2173	2213	2221	2207	2193	399
Knock (bar)	1.8	1.6	1.3	1.3	1.4	3.4	3.8	4.1	1.5	1.6	1.6	1.1
Comb Dur. (deg)	26.5	28.5	29.0	28.5	29.0	24.5	22.5	24.5	34.0	28.5	34.0	40.5
Engine Spd. (rpm)	1096	1105	1098	1095	1100	1399	1397	1400	1398	1396	1399	1394
MAT (°C)	54	52	52	54	52	55	58	57	55	58	56	56
MAP (kPag)	70.5	71.0	69.8	70.5	70.9	91.7	94.8	96.0	91.5	94.1	96.4	98.5
CNG Press. (MPa)	21.1	20.9	20.8	21.1	20.9	20.9	20.9	20.9	20.8	21.0	20.9	20.9
Diesel Press. (MPa)	23.5	23.3	23.4	23.5	23.3	23.2	23.4	23.2	22.2	23.4	23.2	23.2
Exhaust Press. (kPa)	84.6	84.0	29.3	83.1	84.9	113.4	121.4	108.1	106.3	120.6	109.1	115.3
Corr. Air flow (kg/hr)	143	146	146	144	144	181	182	184	182	181	185	187
Airflow (kg/hr)	143	146	146	144	144	181	182	184	182	181	185	187
Diesel inj. (mg/inj)	12.0	11.6	12.4	11.9	11.6	13.3	12.6	12.2	13.4	12.4	12.6	13.3
CNG flow (kg/hr)	4.28	4.36	4.38	4.30	4.31	5.43	5.33	5.47	5.46	5.51	5.56	5.65
CO (g/kW-hr)	0.62	0.81	0.73	0.60	0.64	0.99	1.11	1.23	1.69	1.69	2.42	1.34
CO2 (kg/kW-hr)	0.47	0.47	0.48	0.49	0.48	0.46	0.46	0.45	0.47	0.47	0.47	0.49
NOx (g/kW-hr)	9.62	8.65	5.64	7.23	7.23	13.26	14.77	15.34	7.36	8.43	7.53	4.93
O2 (kg/kW-hr)	0.49	0.48	0.50	0.50	0.50	0.46	0.49	0.48	0.47	0.47	0.49	0.48
CH4 (g/kW-hr)	0.39	0.38	0.34	0.35	0.35	0.46	0.44	0.45	0.42	0.40	0.42	0.33
tHC (g/kW-hr,C1)	0.39	0.38	0.34	0.35	0.35	0.46	0.44	0.45	0.42	0.40	0.42	0.33
Exhaust T. (°C)	486	491	474	503	501	517	510	502	543	545	536	562
Pk. press. (bar)	113.0	112.2	92.4	91.8	91.6	139.7	144.1	146.1	113.5	114.7	114.4	95.3
CA@Pk. press. (bar)	13.5	13.2	17.6	17.6	17.7	9.3	8.9	9.3	12.7	13.6	13.2	16.0
Gross IMEP (bar)	12.78	12.92	12.66	12.42	12.41	13.12	12.86	13.12	12.94	12.91	12.93	12.89
EQR	0.55	0.55	0.55	0.55	0.55	0.56	0.54	0.55	0.56	0.56	0.55	0.56
5% IHR (deg)	0.4	-0.1	3.4	2.4	1.9	-1.6	-1.6	-1.1	-2.1	0.9	-1.1	-3.6
10% IHR (deg)	5.4	4.4	8.9	7.4	7.4	0.4	0.4	0.9	3.4	4.4	3.9	1.9
50% IHR (deg)	10.3	10.3	15.2	15.1	15.2	5.3	5.1	5.4	9.9	10.2	10.2	15.0
90% IHR (deg)	27.0	28.5	32.5	31.0	31.0	23.0	21.0	23.5	32.0	29.5	33.0	37.0
COV GIMEP	0.8	0.8	1.0	0.8	0.6	0.9	0.7	0.6	0.7	0.8	0.8	0.7
DSOI (ms)	-5.4	-5.0	-4.2	-4.2	-4.3	-6.6	-6.4	-6.8	-5.9	-5.8	-5.9	-5.5
DPW (ms)	0.8	0.9	0.8	0.8	0.9	1.4	1.2	1.4	1.4	1.2	1.4	1.4
RIT (ms)	1.0	1.0	1.0	1.0	1.0	1.0	1.0	1.0	1.0	1.0	1.0	1.0
GPW (ms)	0.7	0.7	0.7	0.7	0.7	0.7	0.7	0.7	0.7	0.7	0.7	0.7
2RIT (ms)	2.09	1.53	1.56	1.67	1.59	1.58	1.59	1.74	1.58	1.72	1.63	1.77
2GPW (ms)	1.28	1.34	1.36	1.24	1.29	1.45	1.40	1.30	1.42	1.36	1.30	1.42
Comments												

Figure #	85	86	87	88	89	90	91	92	93	94	95	96
Test Series - #	VIII-B2-27	VIII-B2-27	VIII-B2-28	VIII-B2-28	VIII-B2-28	VIII-B2-29	VIII-B2-29	VIII-B2-29	VIII-B2-30	VIII-B2-30	VIII-B2-30	REP-08-06-09
Test Name	VIII-27B	VIII-27B	VIII-28	VIII-28B	VIII-28B	VIII-29	VIII-29B	VIII-29B	VIII-30	VIII-30B	VIII-30B	REP-08-06-09
Date/Time	08-06-12-14.36.57	08-06-13-11.47.09	08-06-11-14.31.07	08-06-12-15.03.27	08-06-13-12.28.31	08-06-11-14.20.12	08-06-12-14.55.45	08-06-13-12.21.13	08-06-11-14.45.01	08-06-12-15.10.28	08-06-13-12.35.56	08-06-09-11.17.05
Ignition Delay (ms)	2.14	1.98	2.02	1.93	2.04	1.73	1.83	1.85	1.69	1.73	1.80	1.79
IHR (kJ/m3)	387	410	1101	1080	1108	426	1038	369	444	343	336	1499
Knock (bar)	1.1	1.4	1.6	2.1	1.7	2.8	1.7	2.2	2.0	1.6	1.8	2.0
Comb Dur. (deg)	37.5	41.0	17.5	16.5	18.0	19.5	18.5	20.5	21.0	19.5	21.0	27.5
Engine Spd. (rpm)	1395	1399	1093	1106	1103	1091	1105	1102	1090	1102	1101	1210
MAT (°C)	58	57	53	56	55	53	56	55	53	56	54	50
MAP (kPag)	94.2	95.4	47.7	44.4	48.9	48.1	45.1	49.6	49.9	44.7	49.0	58.8
CNG Press. (MPa)	21.0	20.9	21.0	21.2	20.9	21.1	21.4	21.0	21.1	21.4	21.0	21.0
Diesel Press. (MPa)	23.4	23.2	23.6	23.6	23.5	23.6	23.6	23.5	23.6	23.6	23.5	23.3
Exhaust Press. (kPa)	119.4	109.0	63.8	64.0	65.1	64.5	63.6	66.1	66.8	64.0	63.3	84.7
Corr. Air flow (kg/hr)	182	184	125	124	128	126	124	128	127	124	128	142
Airflow (kg/hr)	182	184	125	124	128	126	124	128	127	124	128	142
Diesel inj. (mg/inj)	12.3	12.1	15.8	14.8	14.6	15.5	13.7	13.5	15.5	13.6	14.4	13.8
CNG flow (kg/hr)	5.54	5.50	1.69	1.79	1.87	1.77	1.80	1.87	1.84	1.84	1.86	3.03
CO (g/kW-hr)	1.23	1.23	5.99	5.58	4.44	5.62	7.05	5.33	5.80	8.47	7.03	2.19
CO2 (kg/kW-hr)	0.48	0.48	0.47	0.49	0.49	0.50	0.49	0.49	0.49	0.50	0.50	0.48
NOx (g/kW-hr)	5.01	4.97	6.97	10.80	11.31	5.71	7.92	8.26	4.41	6.03	6.12	5.93
O2 (kg/kW-hr)	0.48	0.50	1.49	1.43	1.43	1.51	1.48	1.48	1.47	1.53	1.57	0.86
CH4 (g/kW-hr)	0.34	0.33	1.66	1.62	1.12	2.55	3.44	2.28	4.30	6.90	5.39	0.64
tHC (g/kW-hr,C1)	0.34	0.33	1.66	1.62	1.12	2.55	3.44	2.28	4.30	6.90	5.39	0.64
Exhaust T. (°C)	566	551	287	302	299	299	307	305	311	317	310	409
Pk. press. (bar)	92.7	91.9	92.2	90.1	93.2	80.8	76.9	79.4	78.3	67.3	70.8	90.5
CA@Pk. press. (bar)	16.4	16.4	8.9	9.1	8.5	3.9	13.2	12.6	5.4	6.6	6.4	12.9
Gross IMEP (bar)	12.59	12.52	6.03	5.94	6.17	5.91	5.84	6.04	6.09	5.66	5.76	8.64
EQR	0.56	0.55	0.29	0.30	0.30	0.30	0.30	0.30	0.30	0.31	0.30	0.41
5% IHR (deg)	-1.6	-2.6	-6.1	-4.1	-5.6	-3.1	-0.6	-1.6	0.4	2.9	2.4	-3.1
10% IHR (deg)	3.9	3.4	-4.6	-3.6	-4.6	-2.1	0.4	-1.1	0.9	4.4	2.9	-1.1
50% IHR (deg)	15.1	15.3	5.3	5.5	4.8	9.9	10.2	10.1	15.1	15.1	15.2	9.9
90% IHR (deg)	36.0	38.5	11.5	12.5	12.5	16.5	18.0	19.0	21.5	22.5	23.5	24.5
COV GIMEP	0.6	0.6	0.8	1.2	1.4	1.1	1.4	1.0	1.3	1.3	1.4	1.8
DSOI (ms)	-5.0	-5.2	-5.9	-5.5	-5.7	-5.2	-4.9	-4.8	-4.7	-4.3	-4.2	-5.2
DPW (ms)	1.2	1.4	1.7	1.5	1.4	1.7	1.5	1.4	1.7	1.5	1.4	1.5
RIT (ms)	1.0	1.0	1.0	1.0	1.0	1.0	1.0	1.0	1.0	1.0	1.0	1.0
GPW (ms)	0.7	0.7	0.6	0.6	0.6	0.6	0.6	0.6	0.6	0.6	0.6	0.7
2RIT (ms)	1.54	1.63	1.73	1.32	1.53	1.74	1.47	1.54	1.97	1.56	1.69	1.41
2GPW (ms)	1.35	1.24	0.74	0.85	0.90	0.72	0.76	0.82	0.76	0.79	0.80	0.98
Comments												

Figure #	97	98	99	100	101	102	103	104
Test Series - #	REP-08-06-10	REP-08-06-11	REP-08-06-12	REP-08-06-13	VIII-B2-1	VIII-B2-11	VIII-B2-19	VIII-B2-27
Test Name	REP-08-06-10	REP-08-06-11	REP-08-06-12	REP-08-06-13	VIII-1D	VIII-11	VIII-19B	VIII-27
Date/Time	08-06-10 10.03.04	08-06-11 09.01.13	08-06-12 09.52.04	08-06-13 09.21.47	08-06-12 12.13.00	08-06-11 11.44.00	08-06-13 09.58.00	
Ignition Delay (ms)	1.75	1.80	1.81	1.87	2.16	1.96	3.72	3.81
IHR (kJ/m3)	418	1545	1514	1541	1078	1061	1037	
Knock (bar)	2.4	1.9	1.7	1.6	1.7	1.2	1.1	0.8
Comb Dur. (deg)	27.5	26.5	25.5	26.5	15.0	19.5	14.5	40.5
Engine Spd. (rpm)	1202	1197	1204	1202	1106	1099	1097	1394
MAT (°C)	48	50	52	51	54	53	52	56
MAP (kPag)	75.0	59.0	56.9	58.1	40.6	44.3	51.7	98.9
CNG Press. (MPa)	20.9	21.0	21.0	21.0	21.2	21.5	21.0	20.8
Diesel Press. (MPa)	23.1	16.0	23.4	23.3	23.5	23.7	23.5	23.2
Exhaust Press. (kPa)	87.1	81.1	84.8	91.2	58.5	54.4	71.0	113.6
Corr. Air flow (kg/hr)	159	143	143	143	121	123	130	188
Airflow (kg/hr)	159	143	143	143	121	123	130	188
Diesel inj. (mg/inj)	14.2	#####	13.6	13.6	14.5	14.6	11.7	13.3
CNG flow (kg/hr)	3.09	3.05	2.99	3.01	1.76	1.84	1.94	5.58
CO (g/kW-hr)	2.11	672.59	2.86	2.67	9.53	10.98	16.95	1.27
CO2 (kg/kW-hr)	0.47	158.49	0.48	0.47	0.48	0.48	0.48	0.48
NOx (g/kW-hr)	5.86	23.59	7.96	8.35	10.16	5.75	10.51	4.59
O2 (kg/kW-hr)	1.00	287.13	0.88	0.86	1.42	1.44	1.60	0.50
CH4 (g/kW-hr)	0.75	#####	0.79	0.78	2.38	4.79	7.36	0.34
tHC (g/kW-hr,C1)	0.75	#####	0.79	0.78	2.38	4.79	7.36	0.34
Exhaust T. (°C)	374	401	404	404	299	305	287	557
Pk. press. (bar)	96.3	91.6	90.5	92.5	89.4	76.5	85.7	95.3
CA@Pk. press. (bar)	12.9	13.2	13.3	12.7	8.9	13.0	9.8	16.0
Gross IMEP (bar)	8.87	8.84	8.64	8.80	5.87	5.97	5.80	12.89
EQR	0.31	0.55	0.41	0.41	0.31	0.31	0.30	0.55
5% IHR (deg)	-3.6	-2.6	-3.6	-3.6	-4.6	-1.1	0.9	-3.6
10% IHR (deg)	-3.1	-0.6	-1.1	-1.6	-3.1	0.9	2.4	1.9
50% IHR (deg)	10.0	10.2	10.1	9.6	5.2	10.3	6.7	15.0
90% IHR (deg)	24.0	24.0	22.0	23.0	10.5	18.5	15.5	37.0
COV GIMEP	1.9	0.8	1.6	1.4	1.3	4.1	4.7	0.7
DSOI (ms)	-5.2	-5.2	-5.4	-5.4	-6.0	3.2	-5.9	-5.4
DPW (ms)	1.5	1.5	1.5	1.5	1.7	1.5	1.2	1.4
RIT (ms)	1.0	1.0	1.0	1.0	1.0	-7.3	1.0	1.0
GPW (ms)	0.7	0.7	0.7	0.7	0.7	0.7	0.7	0.7
2RIT (ms)	1.38	1.33	1.57	1.51	1.70	1.70	1.66	1.77
2GPW (ms)	1.00	1.02	0.95	0.98	0.71	0.69	0.80	1.40
Comments		VOID			VOID	VOID	VOID	VOID

Appendix F.1- Test Series VII-A-800 RPM Pressure and HRR Curves

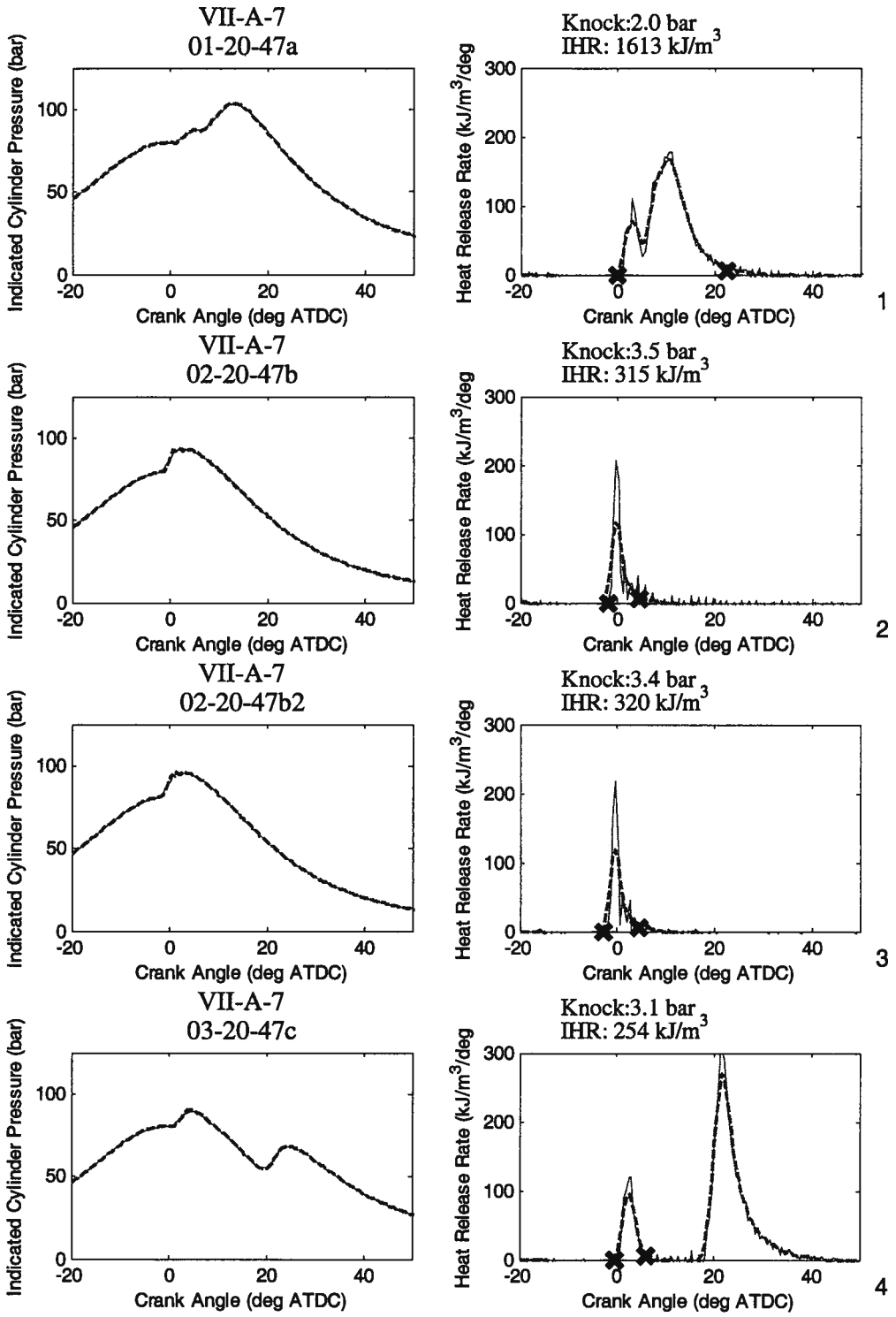

Figures F.1.1 to F.1.4 : Diesel flowrate: 17.2 mg/inj
IHR_{ratio}: 0.80 Knock Ratio: 0.92 Ignition Offset: 2.41 deg

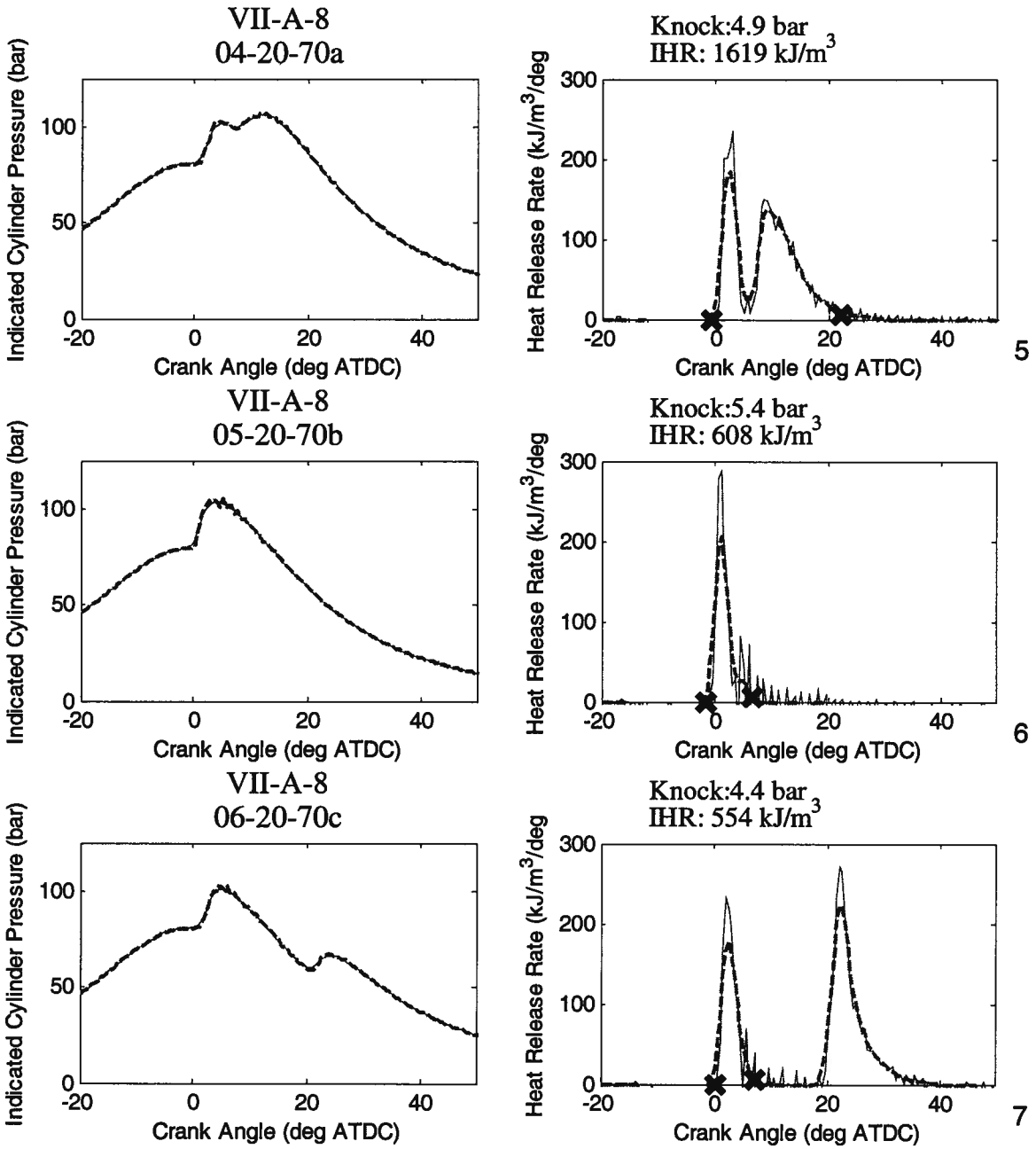

Figures F.1.5 to F.1.7 : Diesel flowrate: 18.6 mg/inj
IHR_{ratio}: 0.91 Knock Ratio: 0.81 Ignition Offset: 1.73 deg

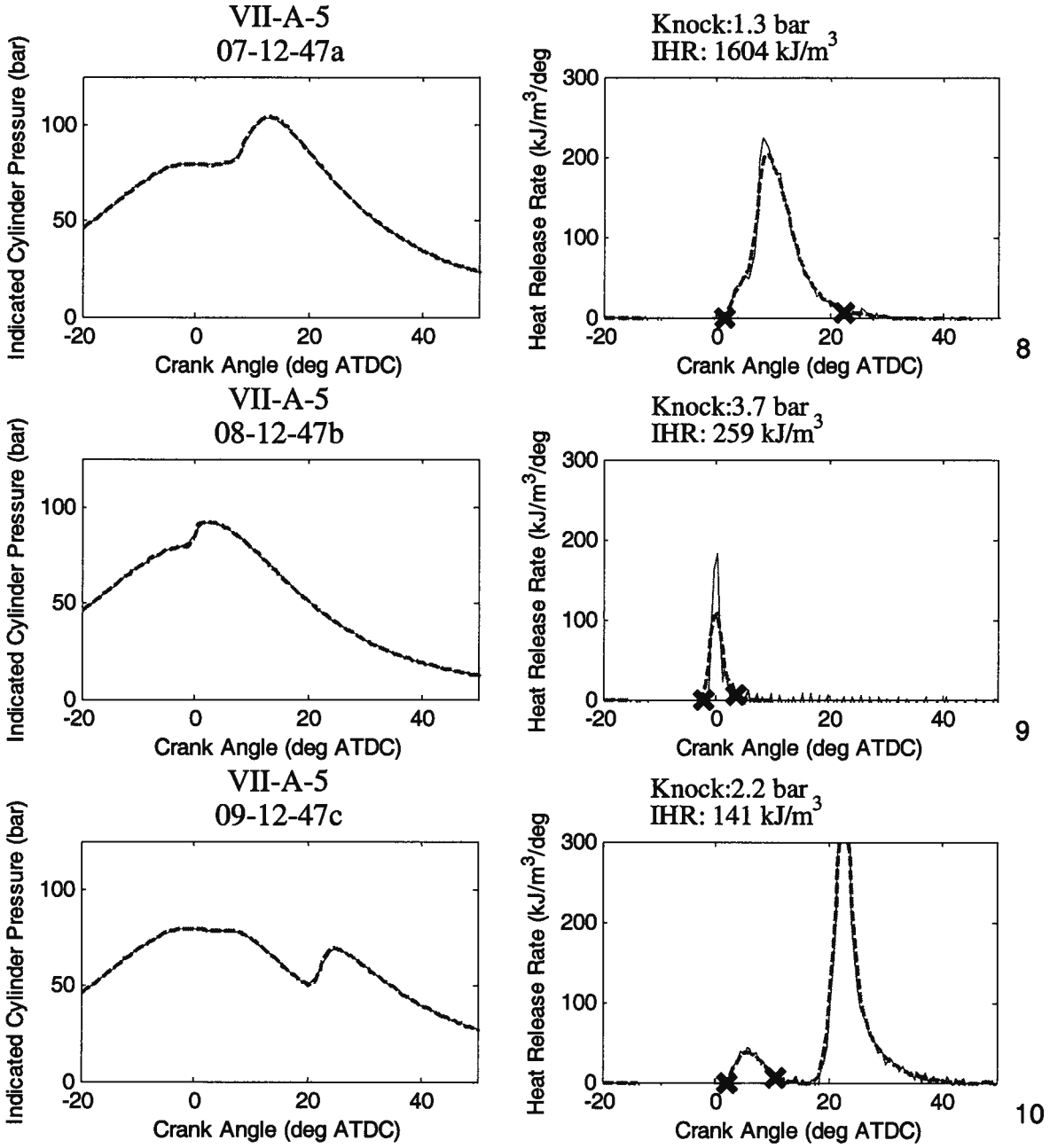

Figures F.1.8 to F.1.10 : Diesel flowrate: 16.2 mg/inj
IHR_{ratio}: 0.55 Knock Ratio: 0.58 Ignition Offset: 4.22 deg

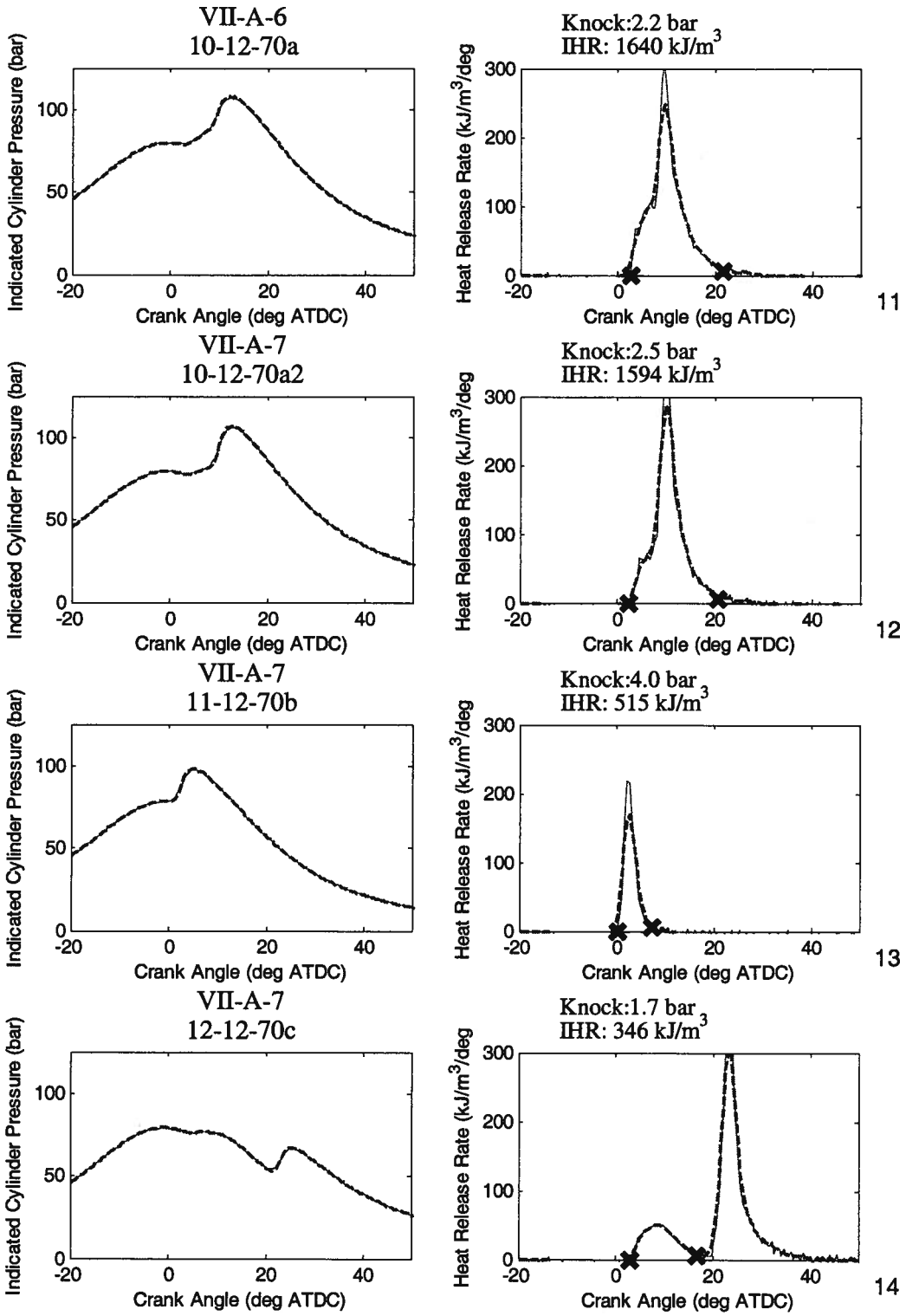

Figures F.1.12 to F.1.14 : Diesel flowrate: 14.9 mg/inj
IHR_{ratio}: 0.67 Knock Ratio: 0.42 Ignition Offset: 2.91 deg

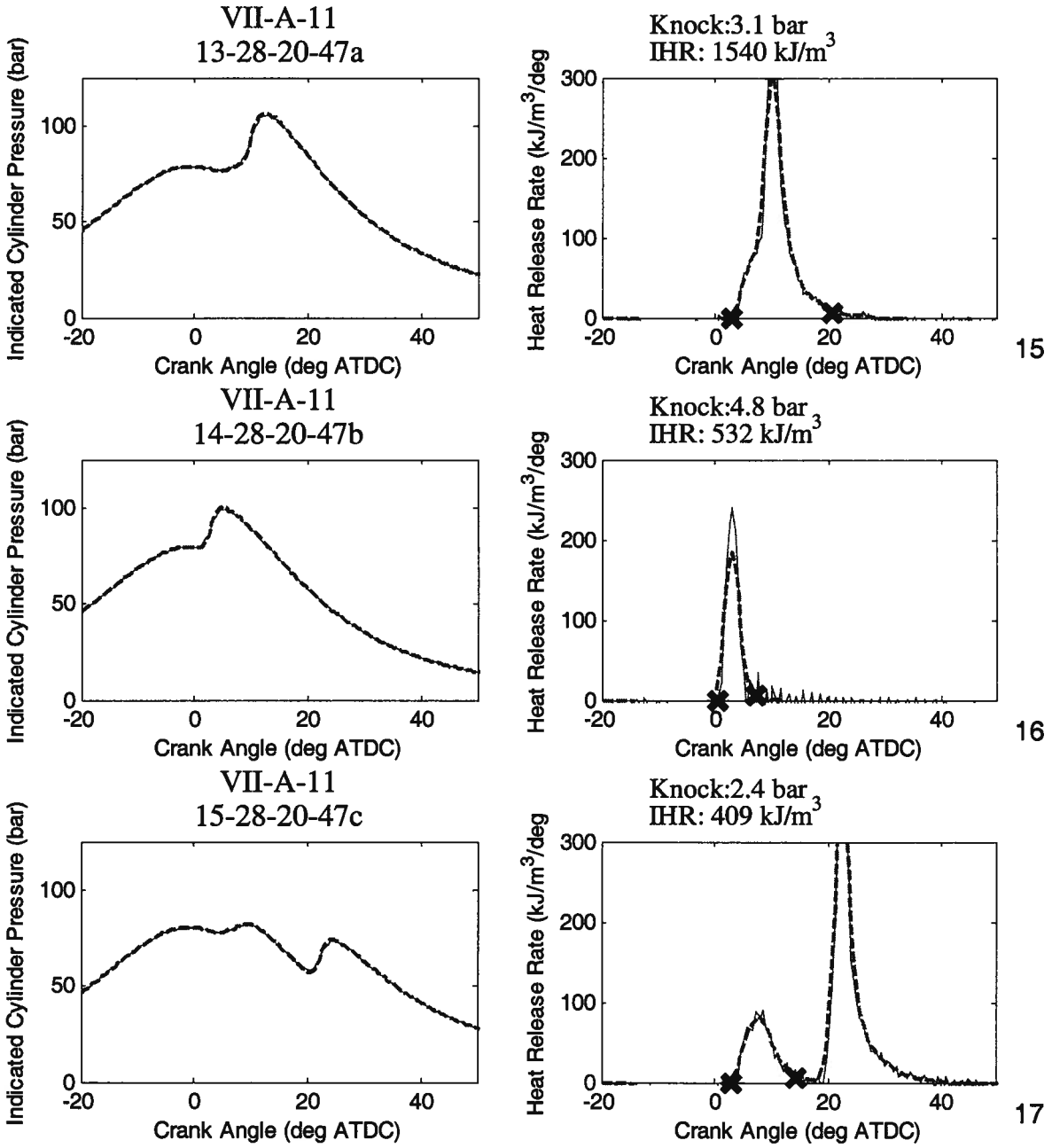

Figures F.1.15 to F.1.17 : Diesel flowrate: 14.7 mg/inj
IHR_{ratio}: 0.77 Knock Ratio: 0.51 Ignition Offset: 2.45 deg

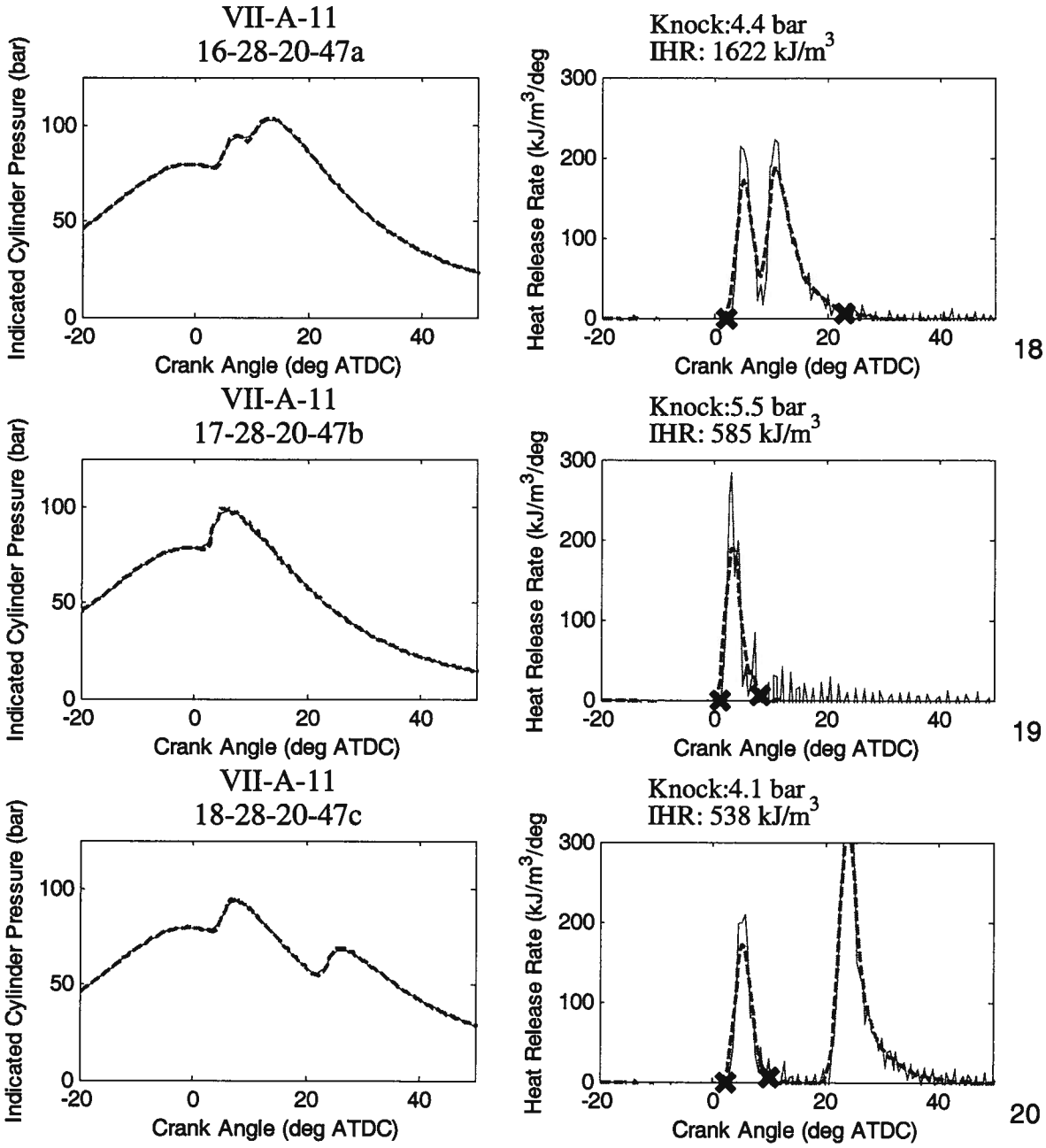

Figures F.1.18 to F.1.20 : Diesel flowrate: 20.3 mg/inj
IHR_{ratio}: 0.92 Knock Ratio: 0.75 Ignition Offset: 1.13 deg

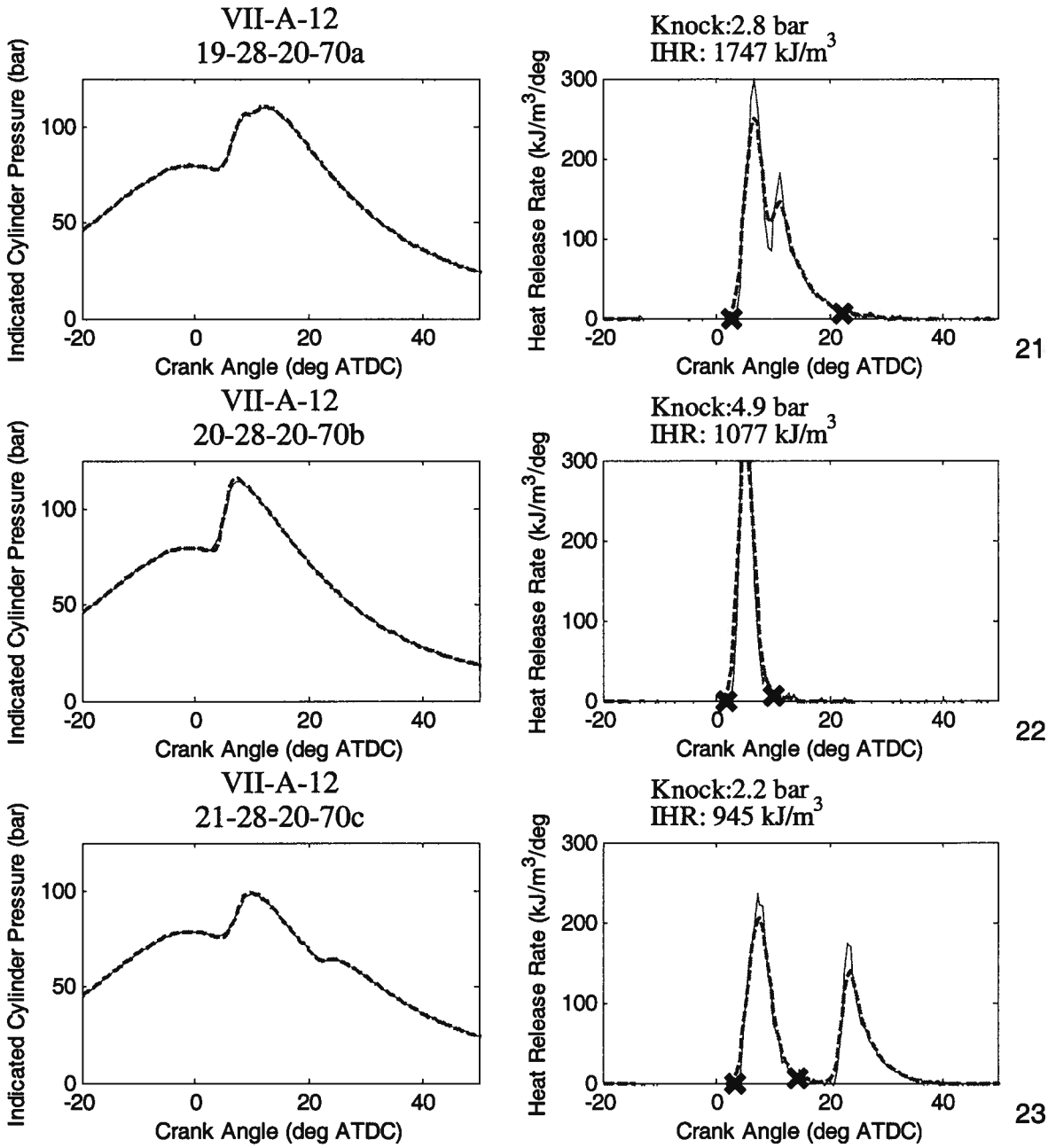

Figures F.1.21 to F.1.23 : Diesel flowrate: 17.2 mg/inj
IHR_{ratio}: 0.88 Knock Ratio: 0.45 Ignition Offset: 1.39 deg

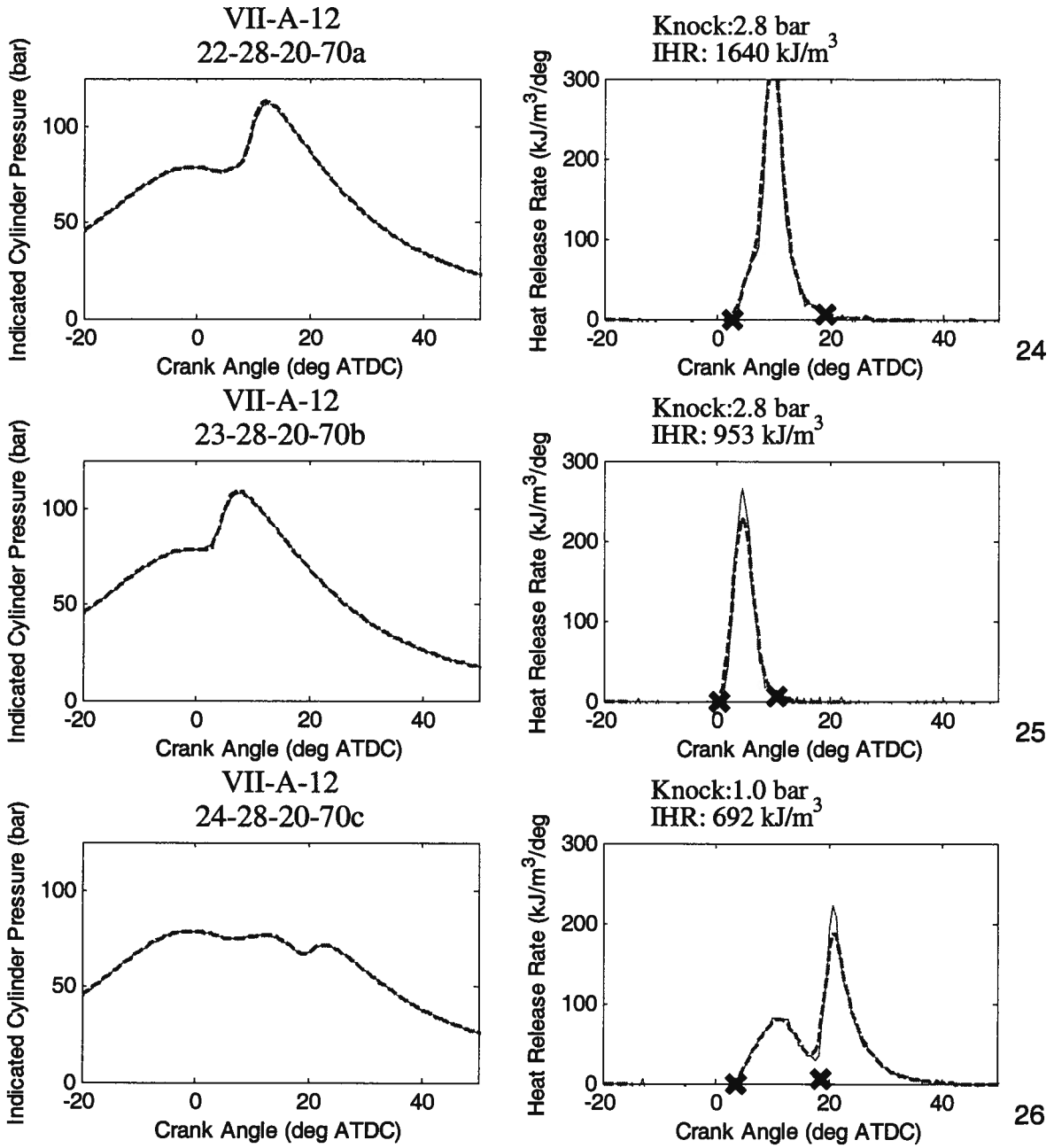

Figures F.1.24 to F.1.26 : Diesel flowrate: 14.5 mg/inj
IHR_{ratio}: 0.73 Knock Ratio: 0.34 Ignition Offset: 2.84 deg

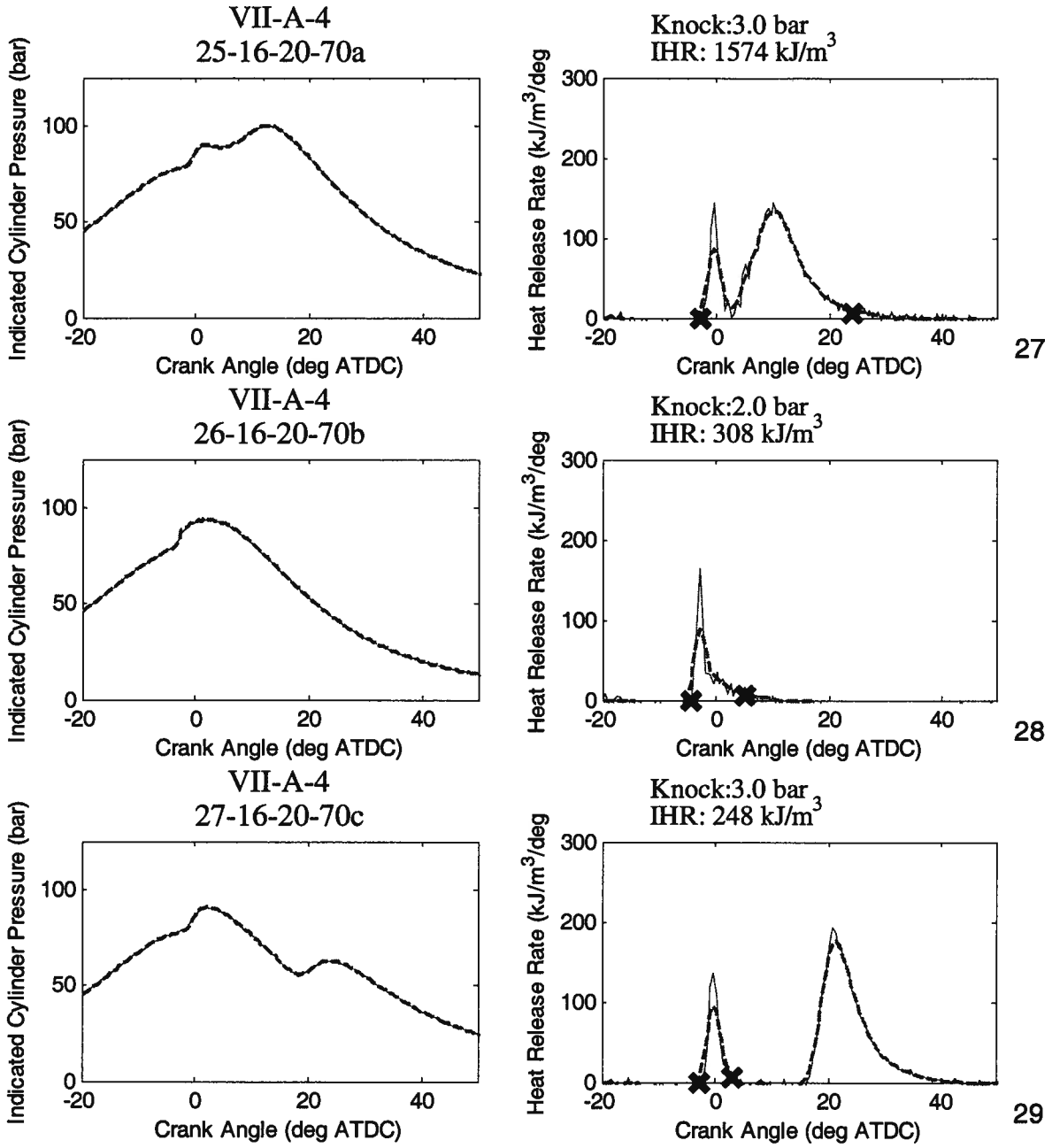

Figures F.1.27 to F.1.29 : Diesel flowrate: 22.0 mg/inj
IHR_{ratio}: 0.80 Knock Ratio: 1.48 Ignition Offset: 1.55 deg

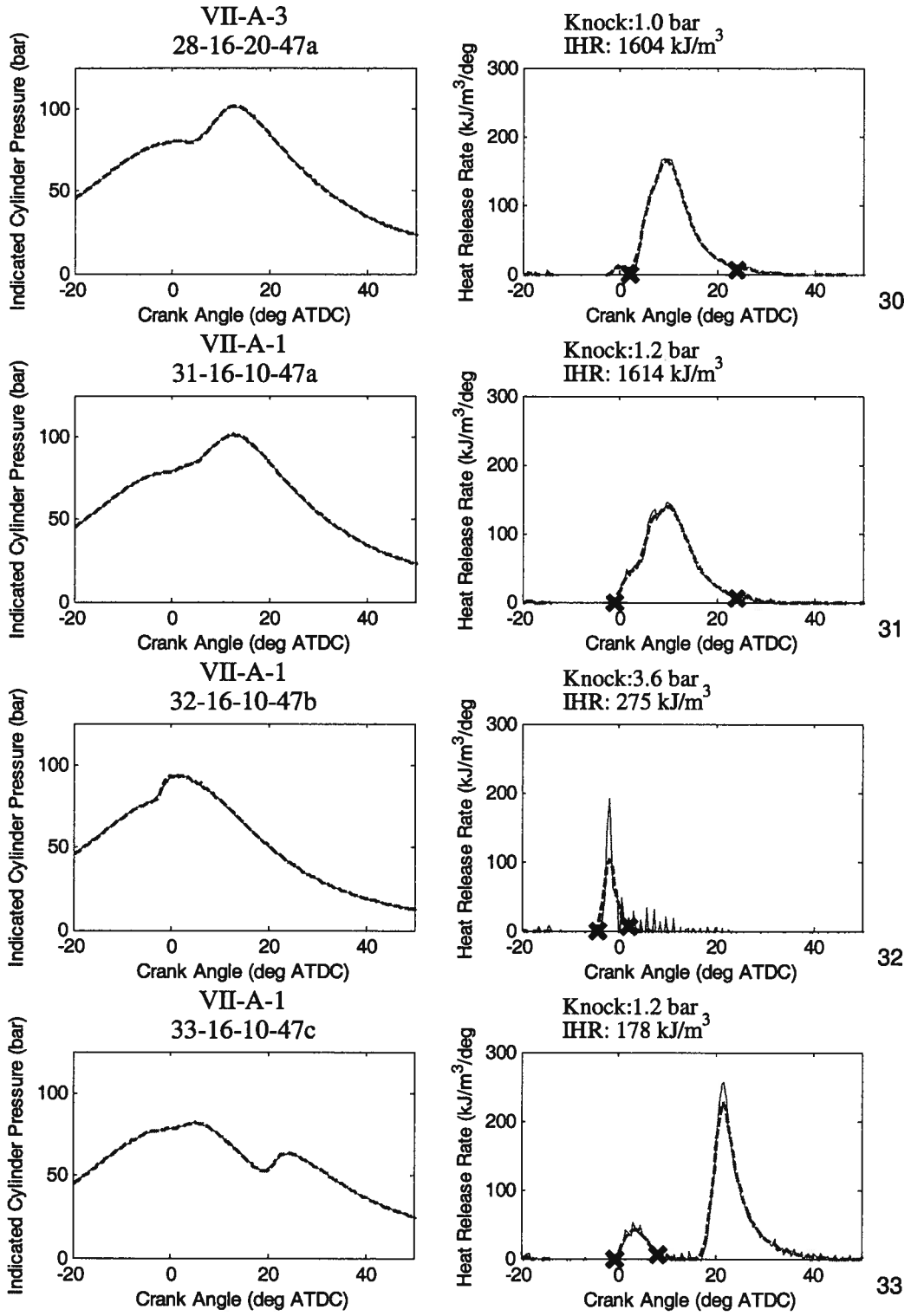

Figures F.1.31 to F.1.33 : Diesel flowrate: 13.3 mg/inj
IHR_{ratio}: 0.65 Knock Ratio: 0.33 Ignition Offset: 3.67 deg

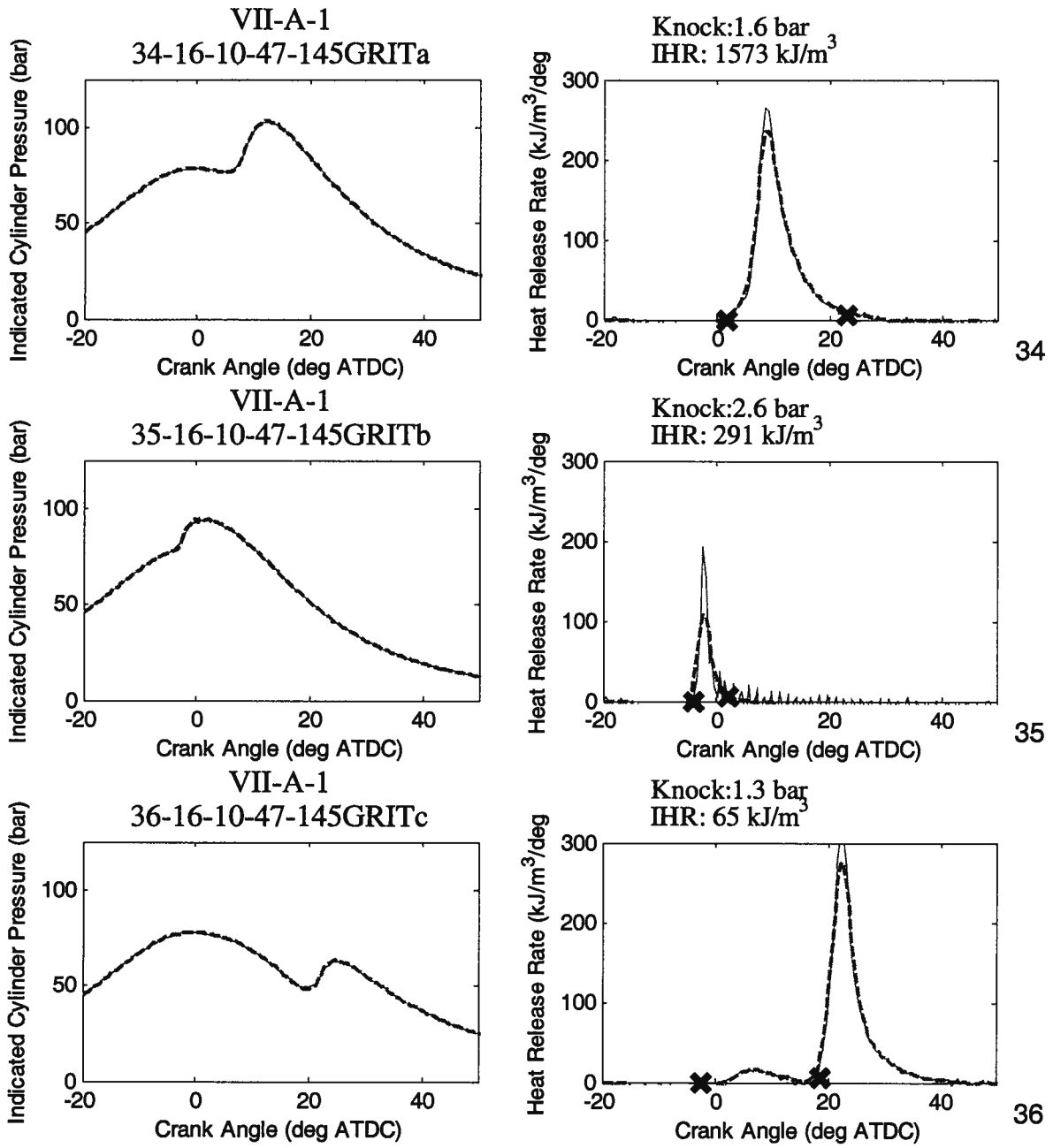

Figures F.1.34 to F.1.36 : Diesel flowrate: 13.6 mg/inj
IHR_{ratio}: 0.22 Knock Ratio: 0.51 Ignition Offset: 1.44 deg

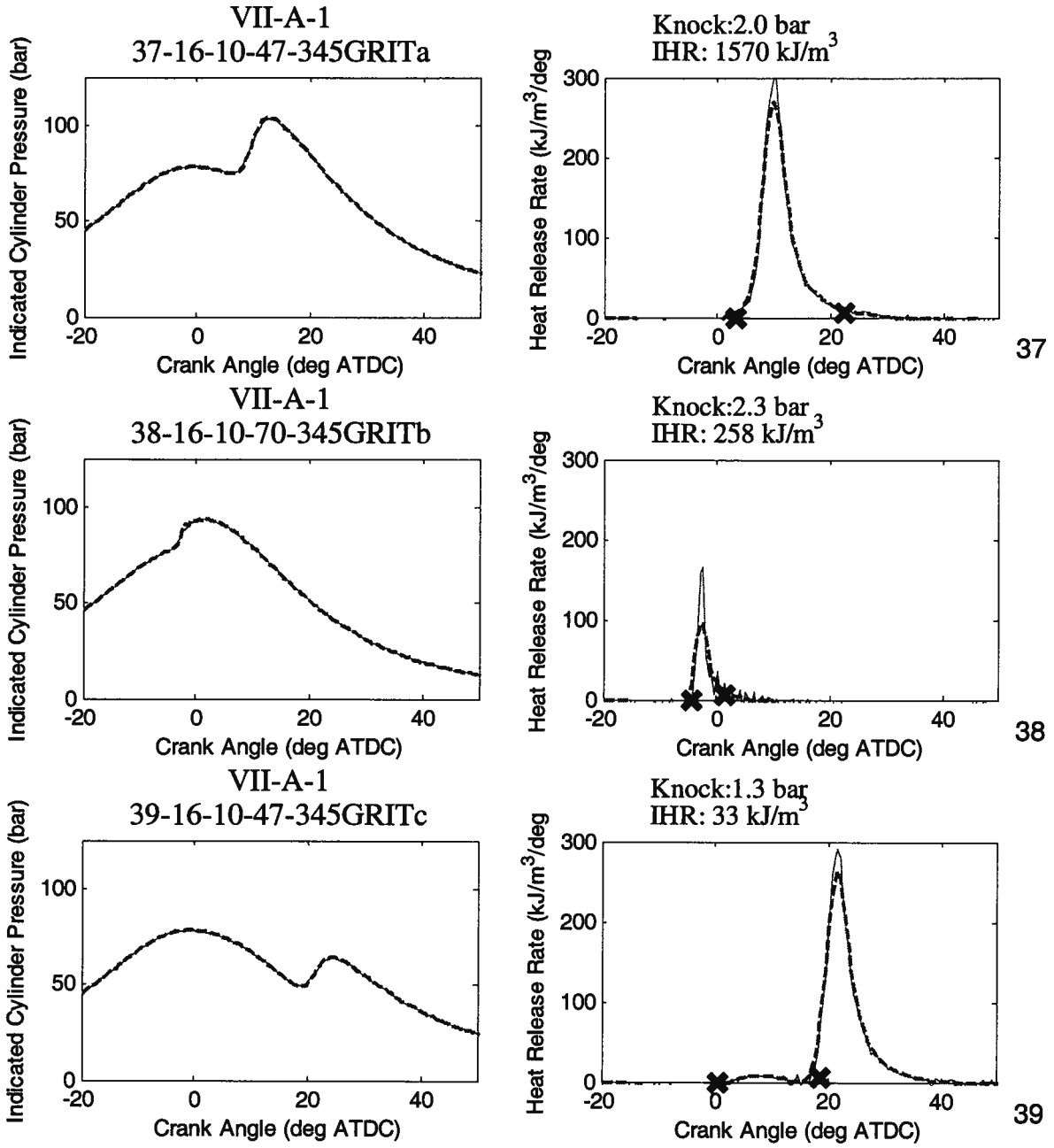

Figures F.1.37 to F.1.39 : Diesel flowrate: 11.8 mg/inj
IHR_{ratio}: 0.13 Knock Ratio: 0.59 Ignition Offset: 4.90 deg

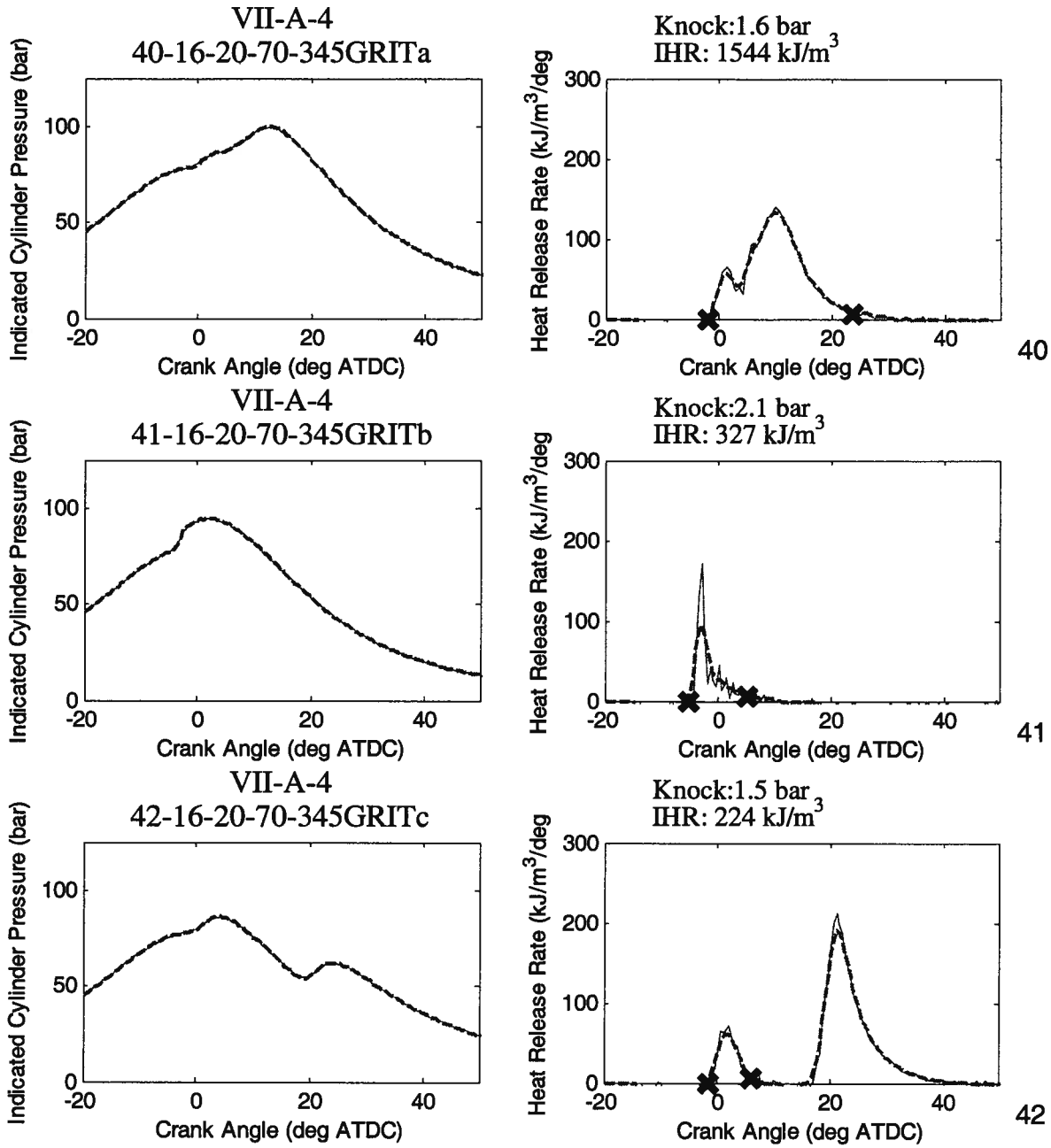

Figures F.1.40 to F.1.42 : Diesel flowrate: 19.6 mg/inj
IHR_{ratio}: 0.68 Knock Ratio: 0.74 Ignition Offset: 3.70 deg

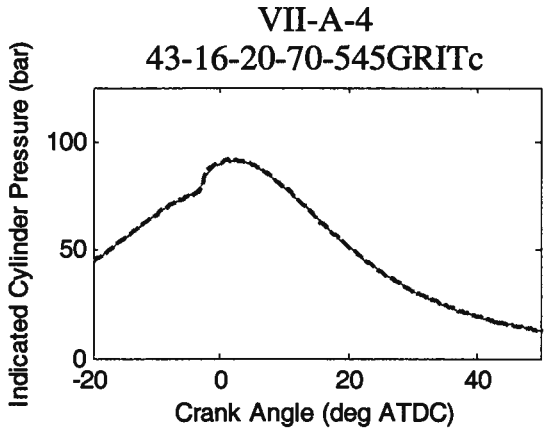
VII-A-4
43-16-20-70-545GRITc
Indicated Cylinder Pressure (bar)
100
50
0
-20
0
20
40
Crank Angle (deg ATDC)

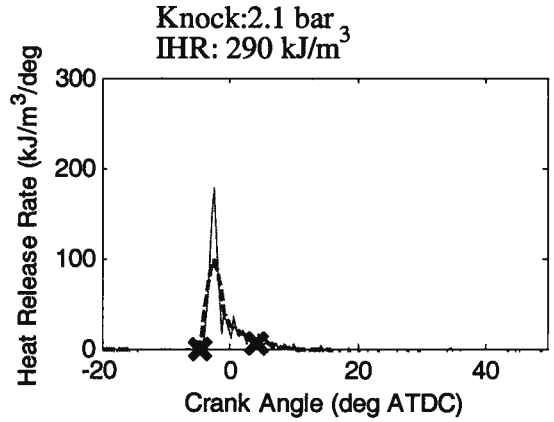
Knock:2.1 bar
IHR: 290 kJ/m3
Heat Release Rate (kJ/m3/deg
300
200
100
0
-20
0
20
40
Crank Angle (deg ATDC)

43

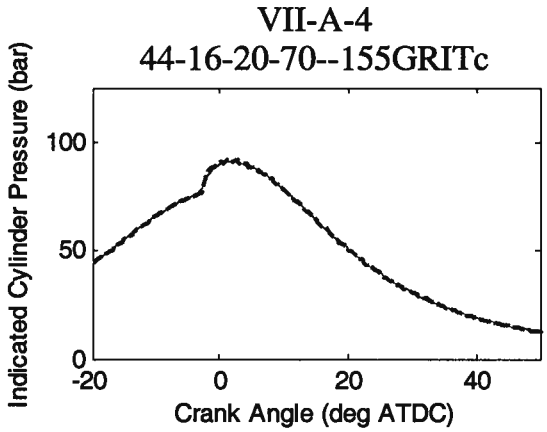
VII-A-4
44-16-20-70--155GRITc
Indicated Cylinder Pressure (bar)
100
50
0
-20
0
20
40
Crank Angle (deg ATDC)

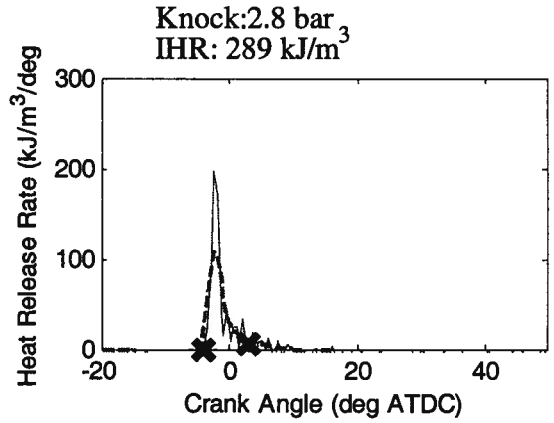
Knock:2.8 bar
IHR: 289 kJ/m3
Heat Release Rate (kJ/m3/deg
300
200
100
0
-20
0
20
40
Crank Angle (deg ATDC)

44

Appendix F.2- Test Series VII-A-1200 RPM Pressure and HRR Curves

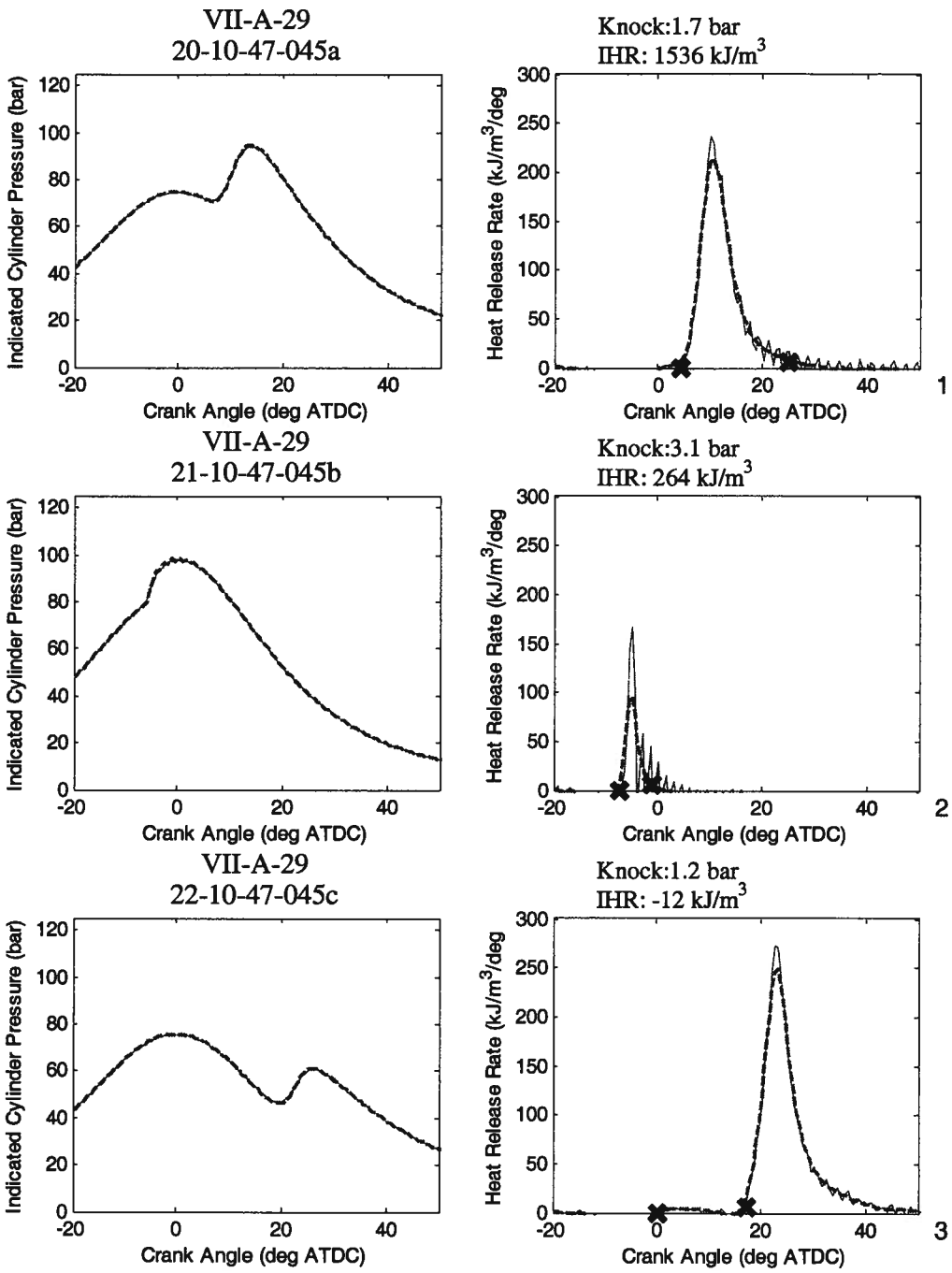

Figures F.2.1 to F.2.3 : Diesel flowrate: 14.2 mg/inj
IHR_{ratio}: -0.05 Knock Ratio: 0.38 Ignition Offset: 7.39 deg

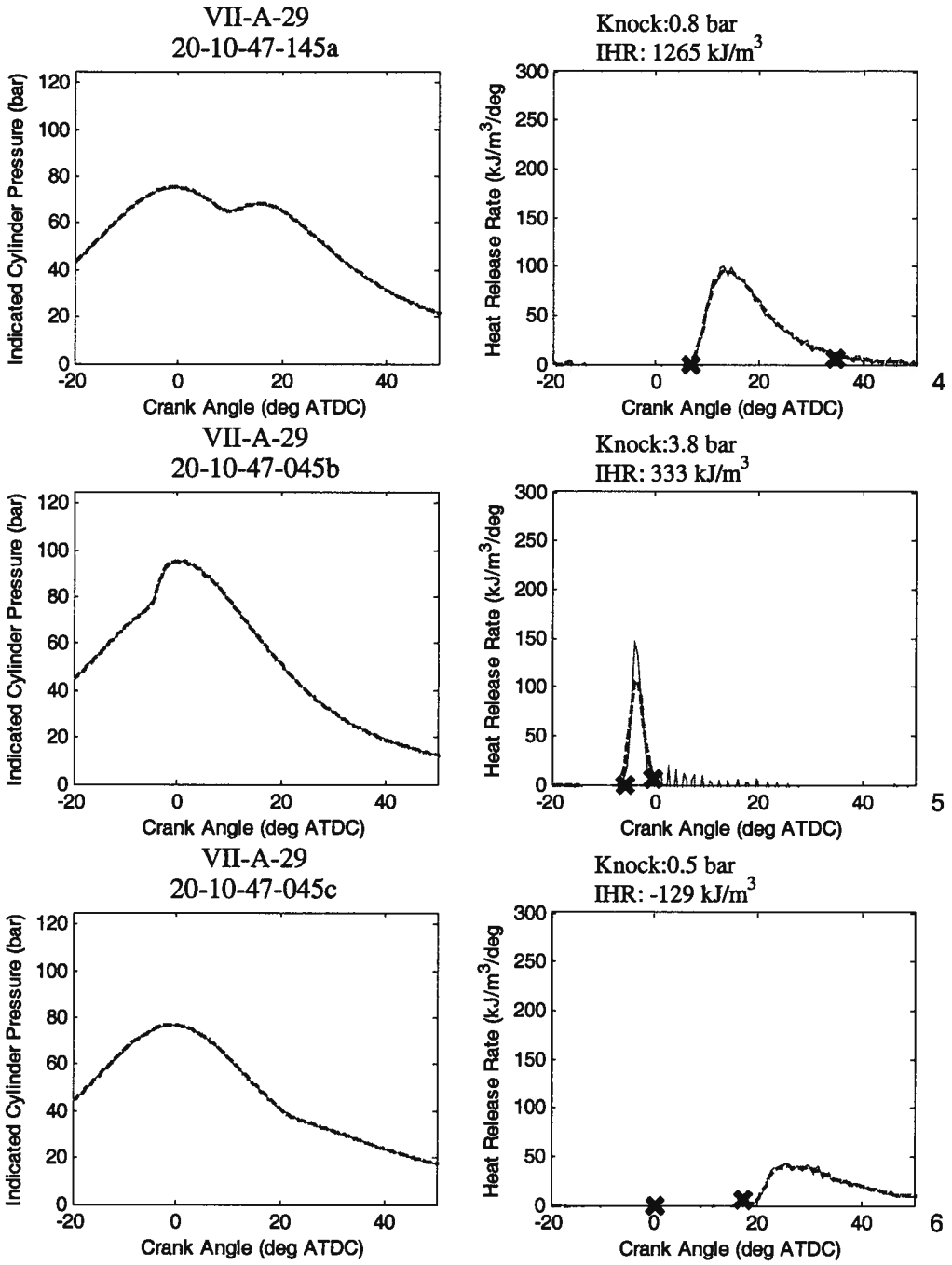

Figures F.2.4 to F.2.6 : Diesel flowrate: 11.0 mg/inj
IHR_{ratio}: -0.39 Knock Ratio: 0.14 Ignition Offset: 6.00 deg

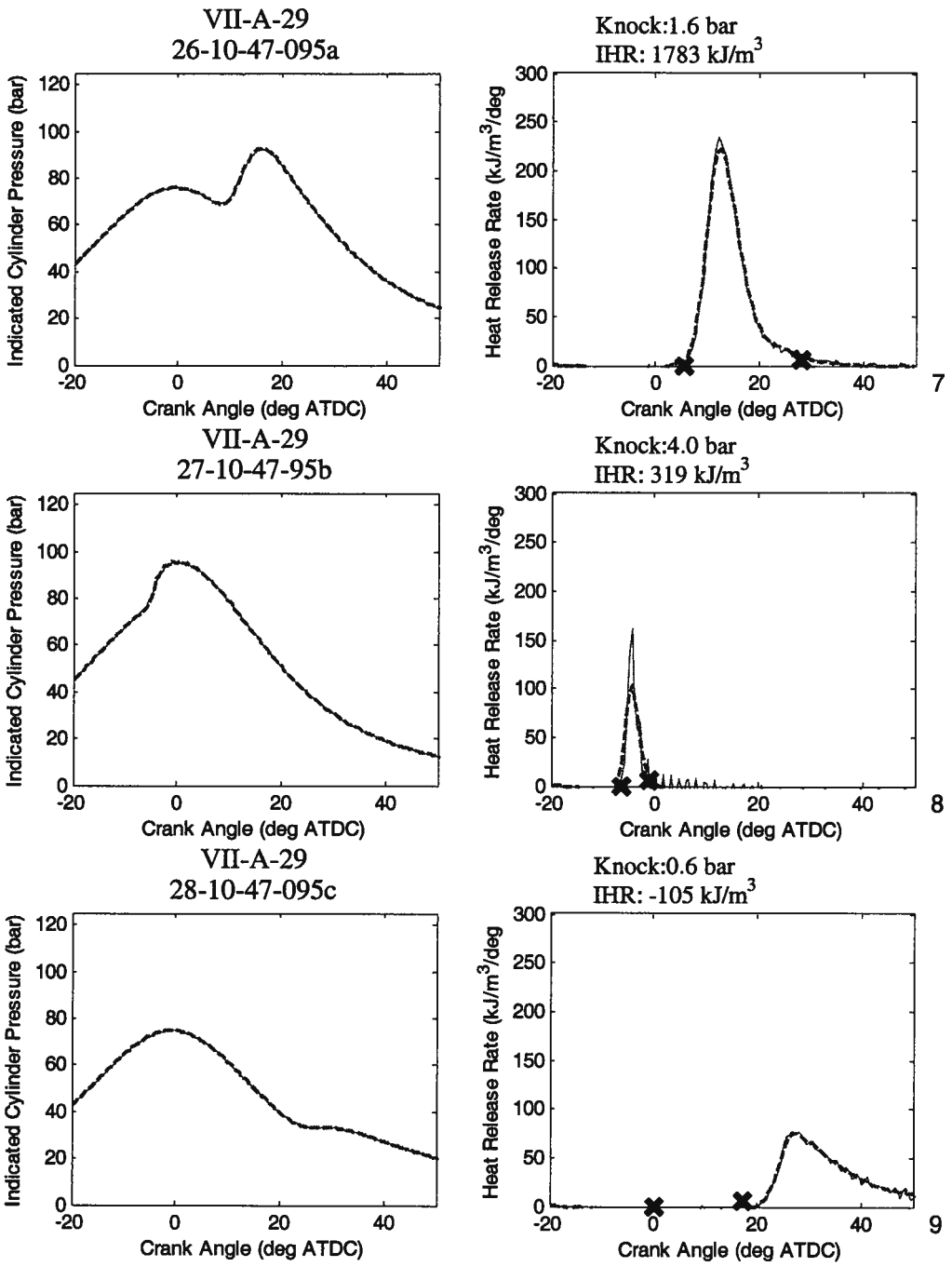

Figures F.2.7 to F.2.9 : Diesel flowrate: 14.3 mg/inj
IHR_{ratio}: -0.33 Knock Ratio: 0.14 Ignition Offset: 6.50 deg

VII-A-29
29-10-47-095a2

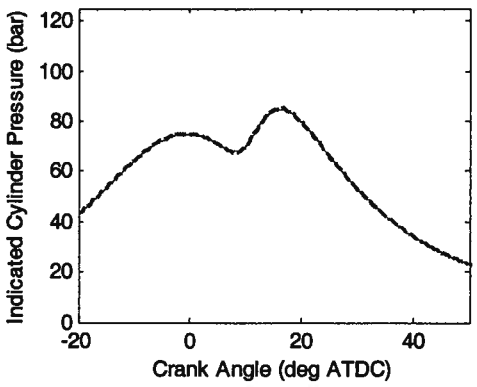

Knock:1.3 bar
IHR: 1601 kJ/m^3

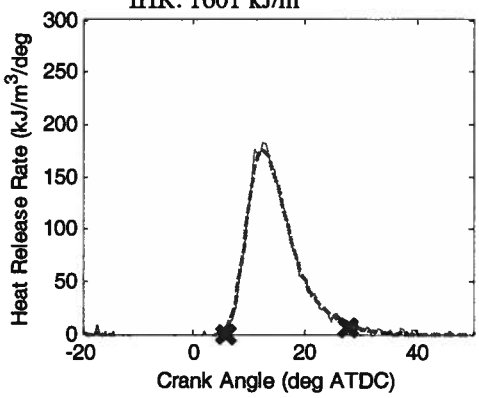

10

VII-A-29
30-10-47-095a2

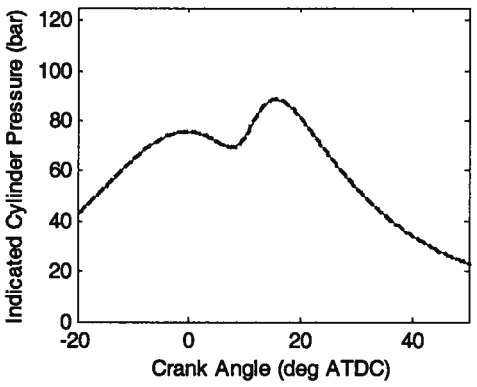

Knock:1.4 bar
IHR: 1607 kJ/m^3

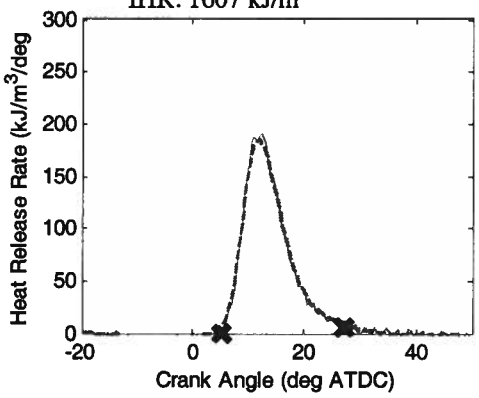

11

VII-A-29
31-10-47-125a

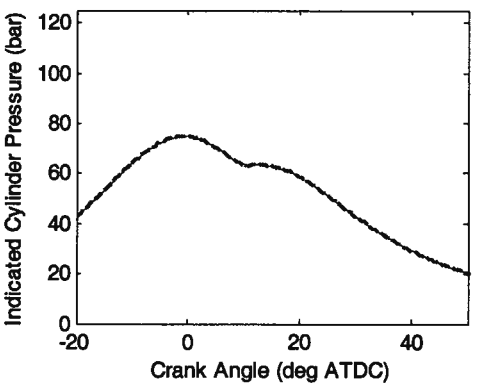

Knock:0.7 bar
IHR: 1073 kJ/m^3

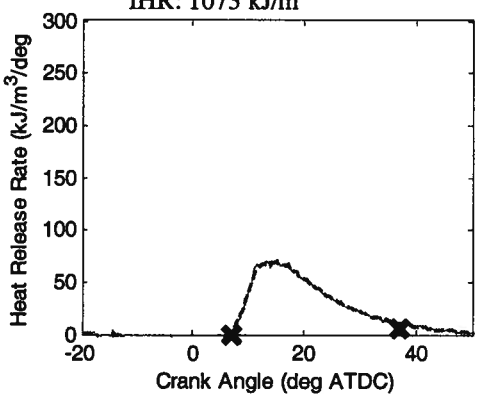

12

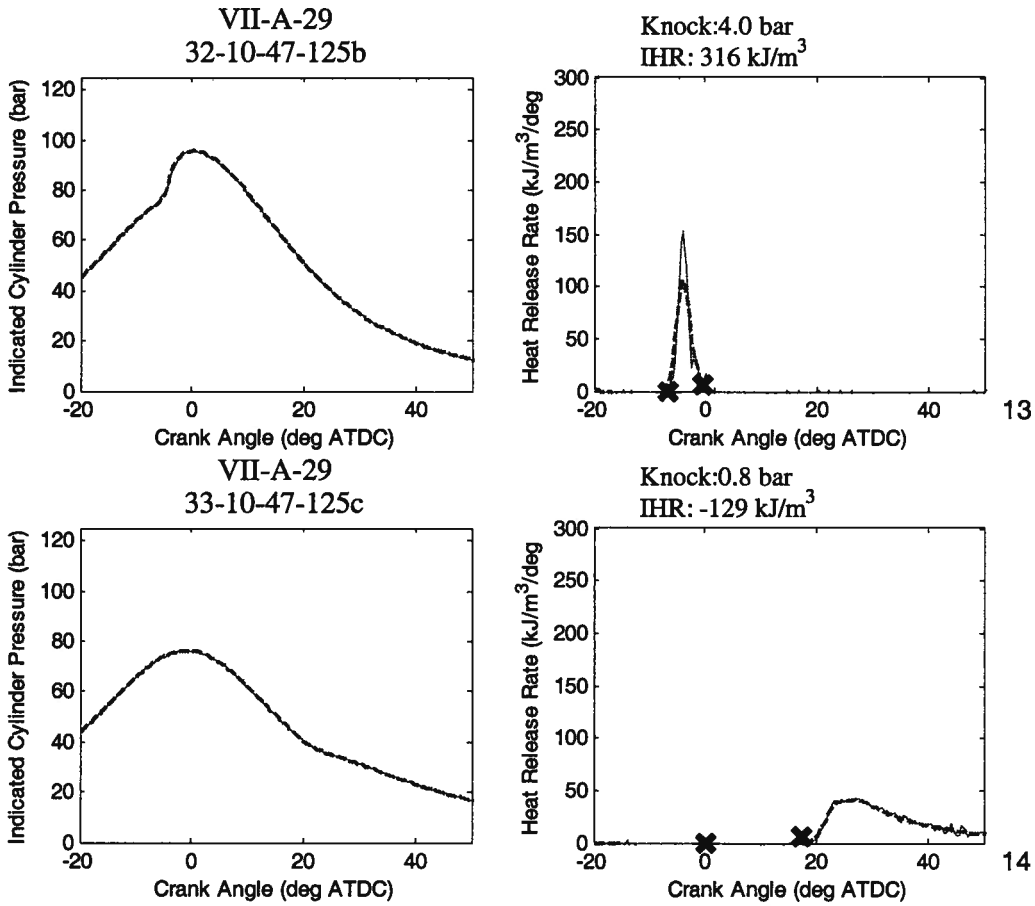

Figures F.2.10 to F.2.14 : Diesel flowrate: 11.5 mg/inj
IHR_{ratio}: -0.41 Knock Ratio: 0.19 Ignition Offset: 6.87 deg

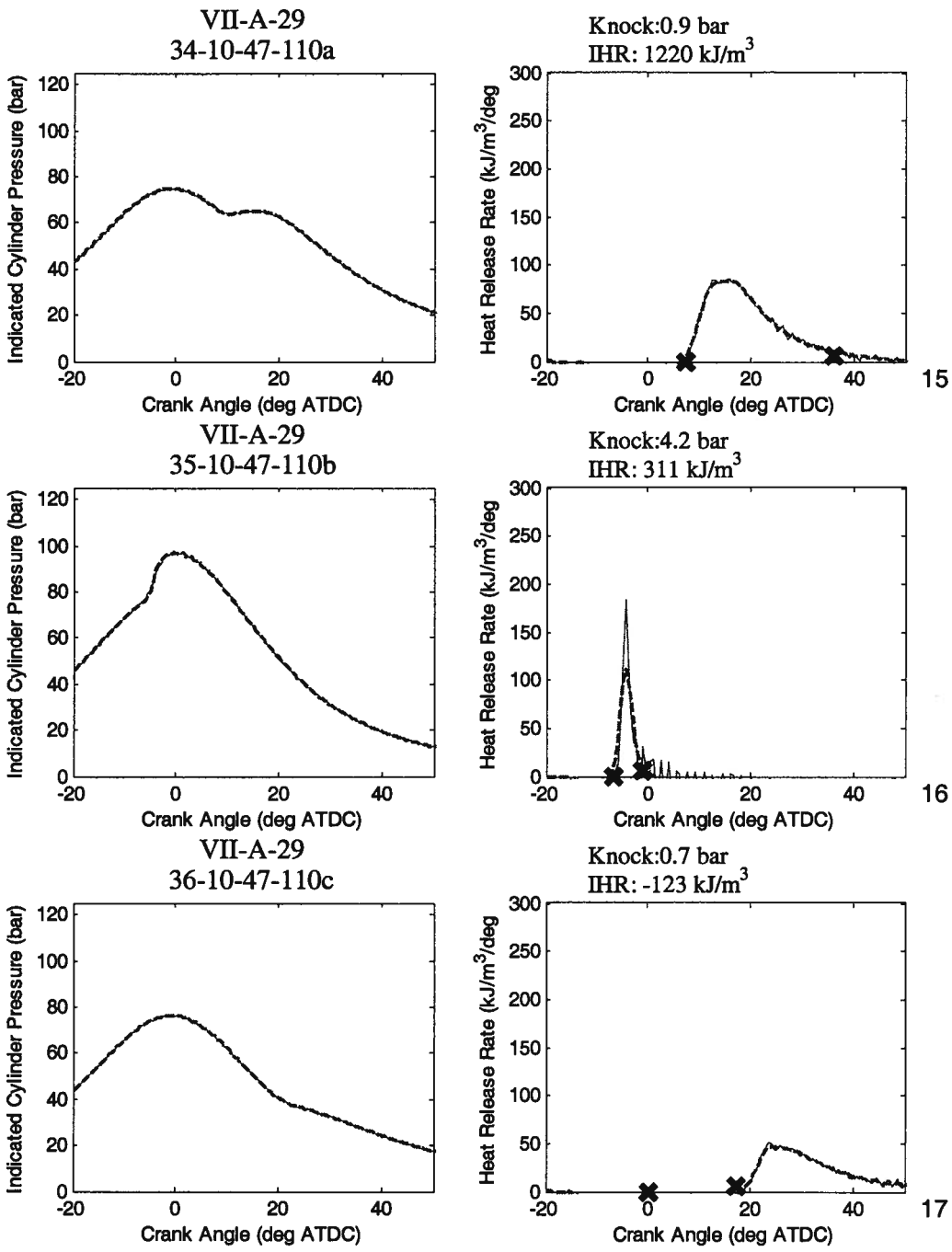

Figures F.2.15 to F.2.17 : Diesel flowrate: 10.6 mg/inj
IHR_{ratio}: -0.40 Knock Ratio: 0.17 Ignition Offset: 6.88 deg

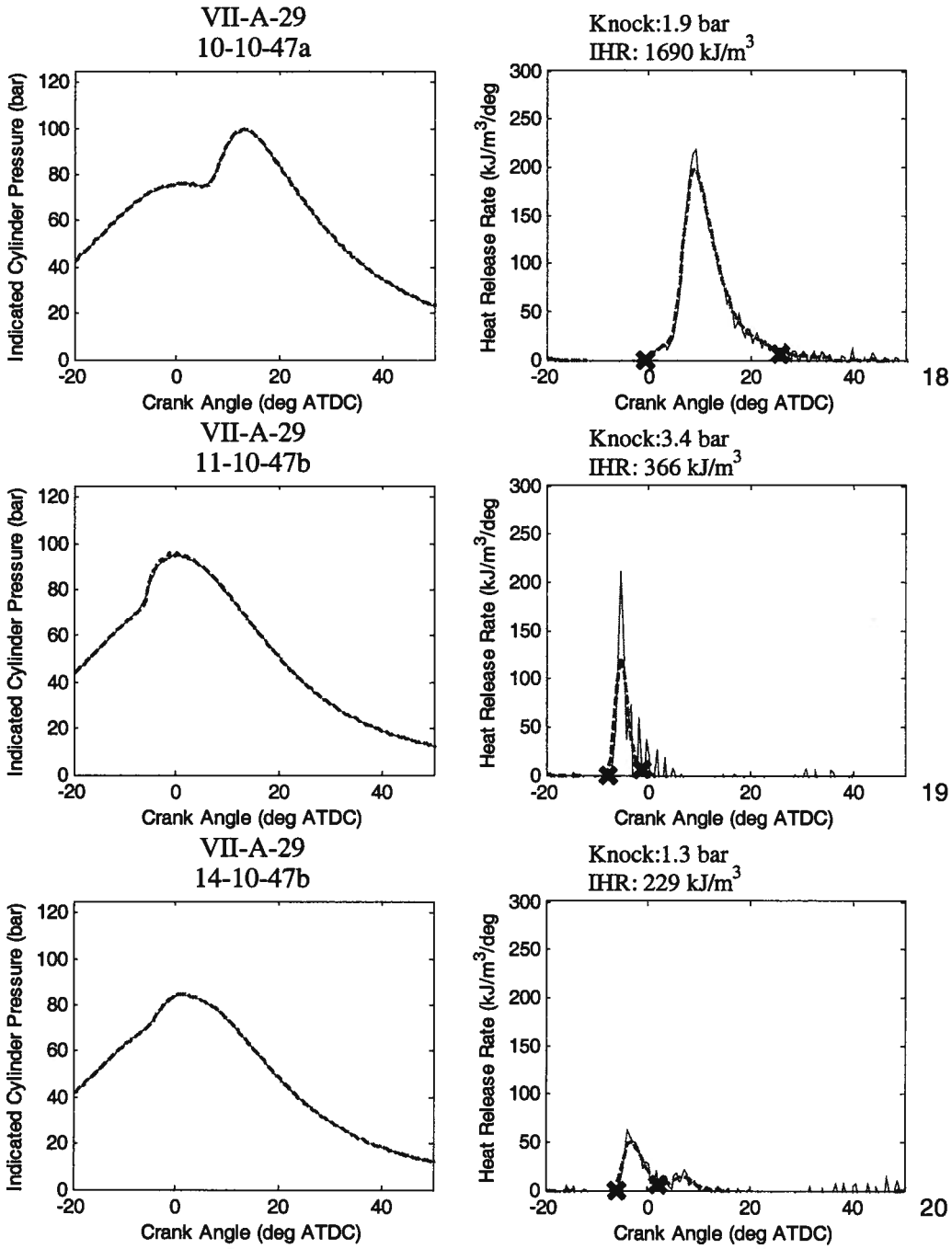

Figures F.2.18 to F.2.20 : Diesel flowrate: 3.4 mg/inj

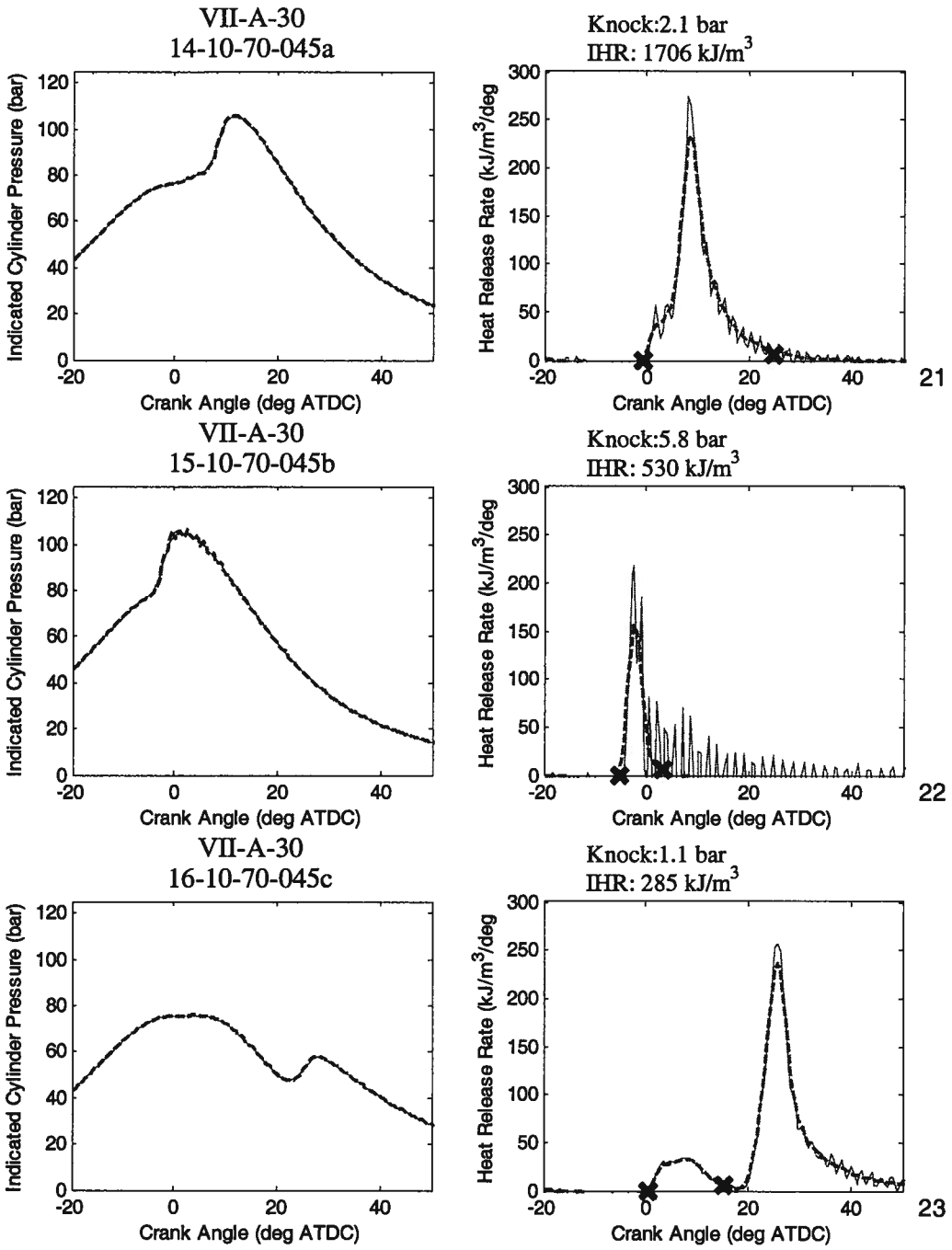

Figures F.2.21 to F.2.23 : Diesel flowrate: 12.3 mg/inj
IHR_{ratio}: 0.54 Knock Ratio: 0.19 Ignition Offset: 5.81 deg

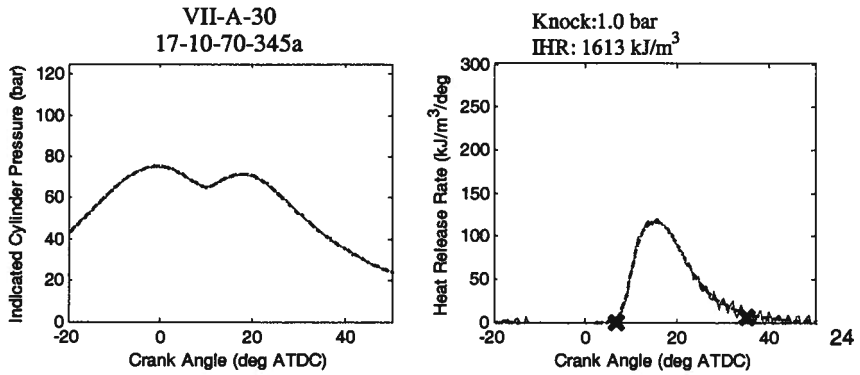

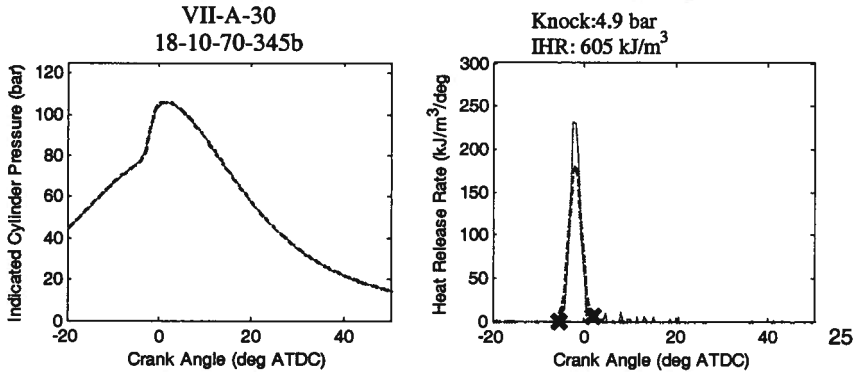

Figures F.2.24 to F.2.25 : Diesel flowrate: 10.7 mg/inj

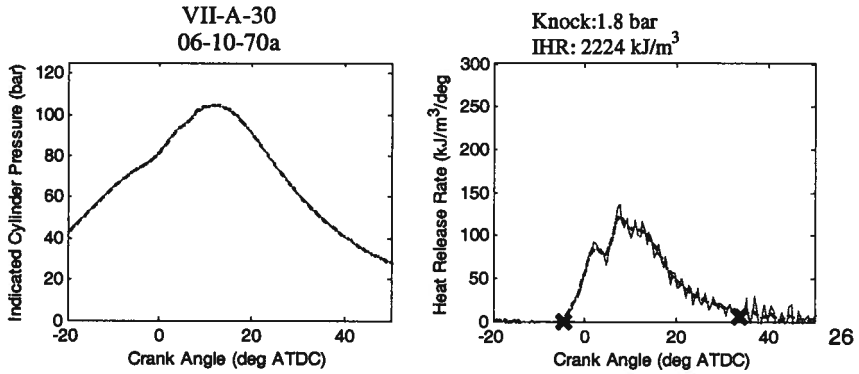

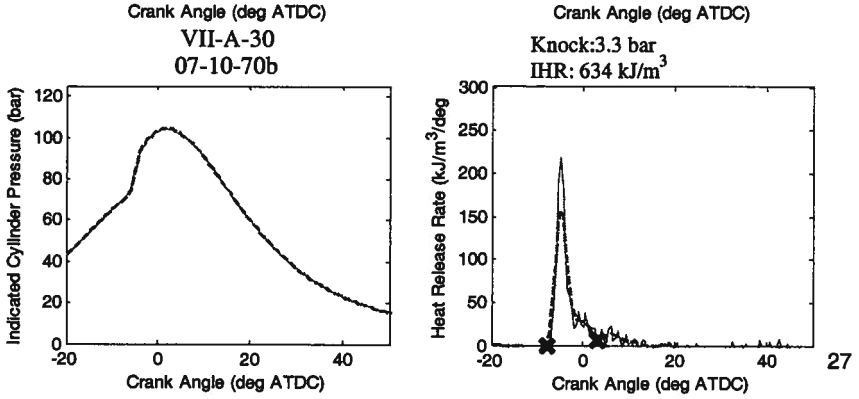

Figures F.2.26 to F.2.27 : Diesel flowrate: 17.0 mg/inj

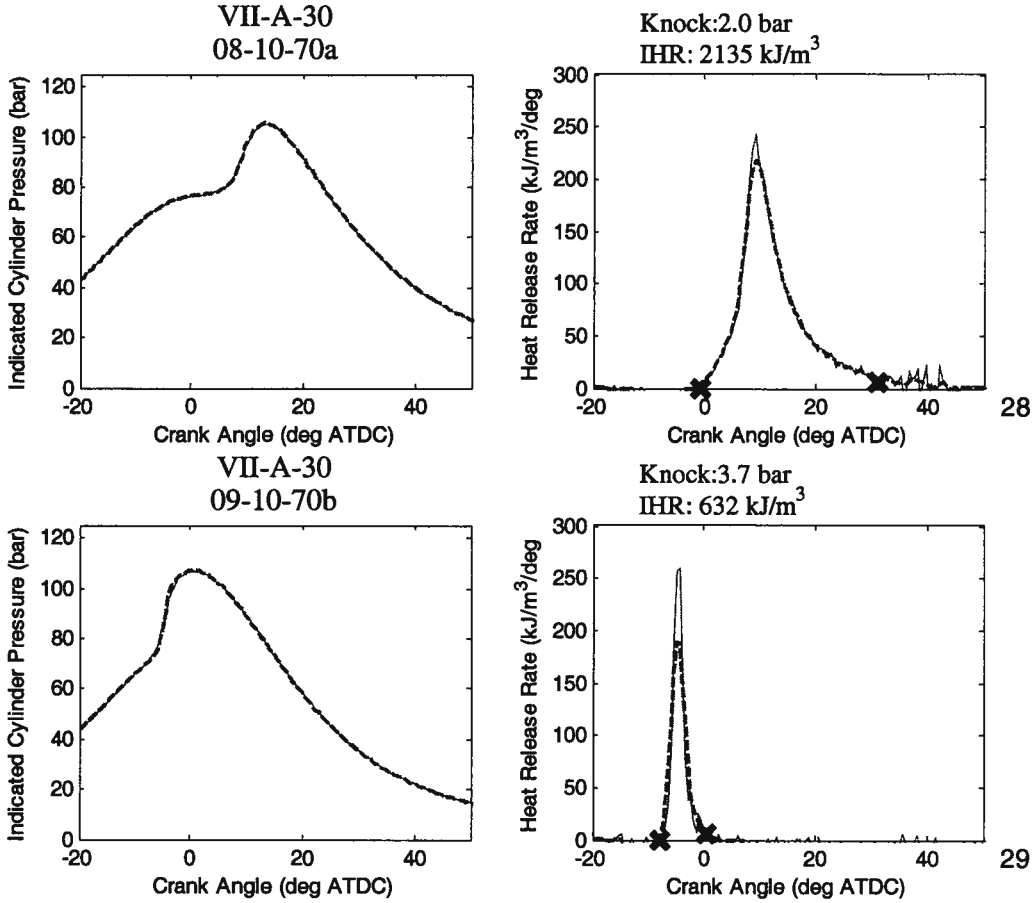

Figures F.2.28 to F.2.29 : Diesel flowrate: 14.5 mg/inj

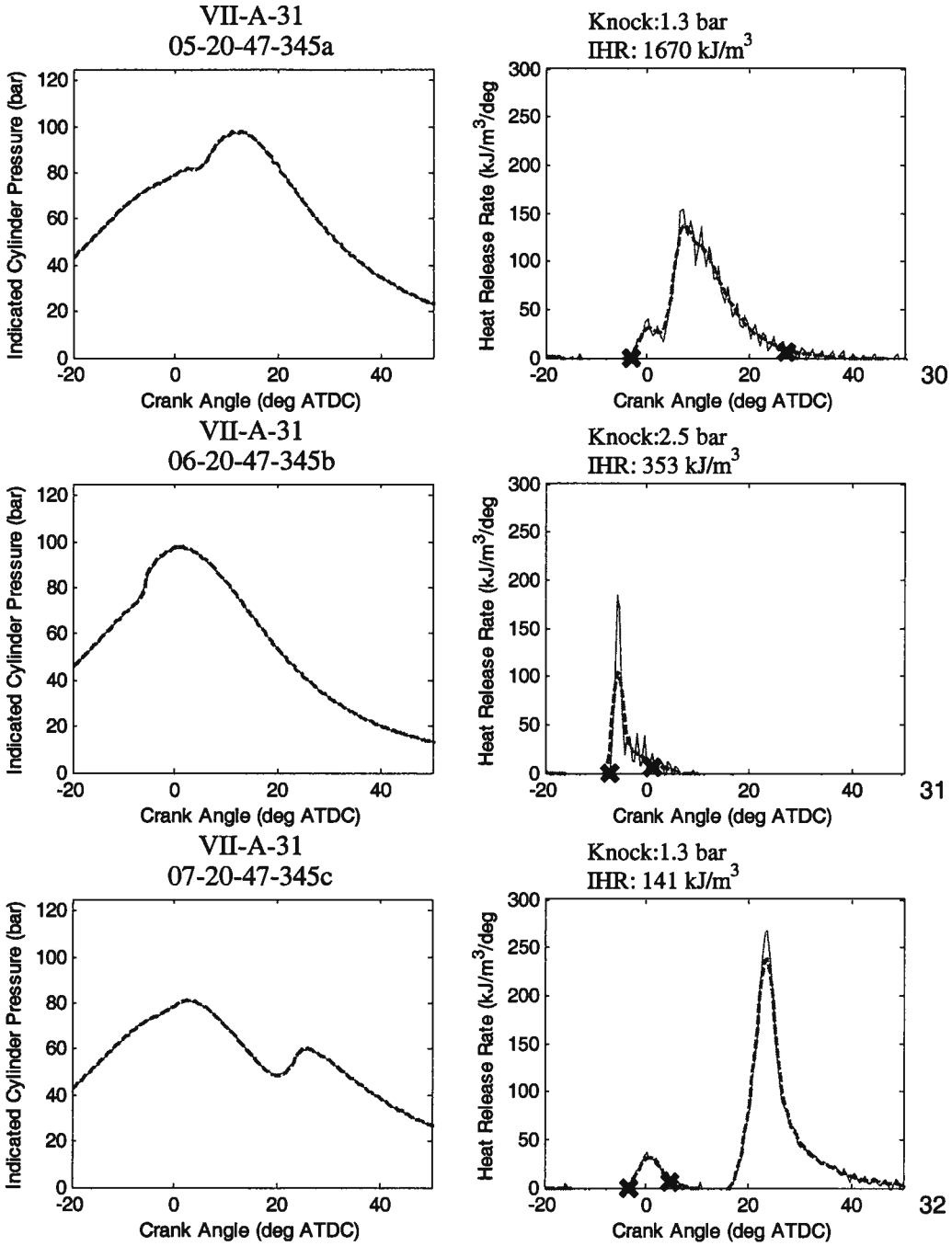

Figures F.2.30 to F.2.32 : Diesel flowrate: 23.2 mg/inj
IHR_{ratio}: 0.40 Knock Ratio: 0.51 Ignition Offset: 3.93 deg

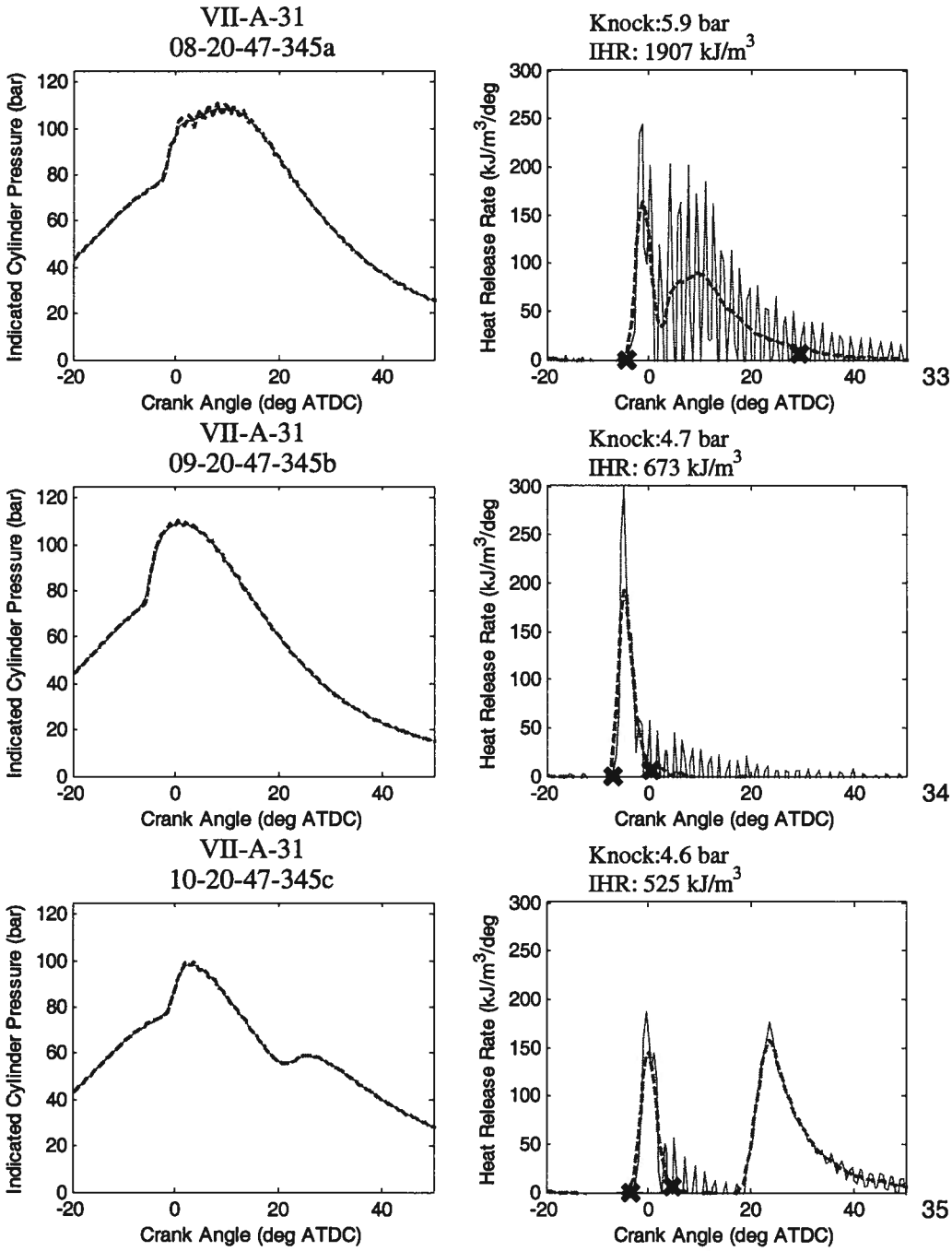

Figures F.2.33 to F.2.35 : Diesel flowrate: 25.8 mg/inj
IHR_{ratio}: 0.78 Knock Ratio: 0.98 Ignition Offset: 3.53 deg

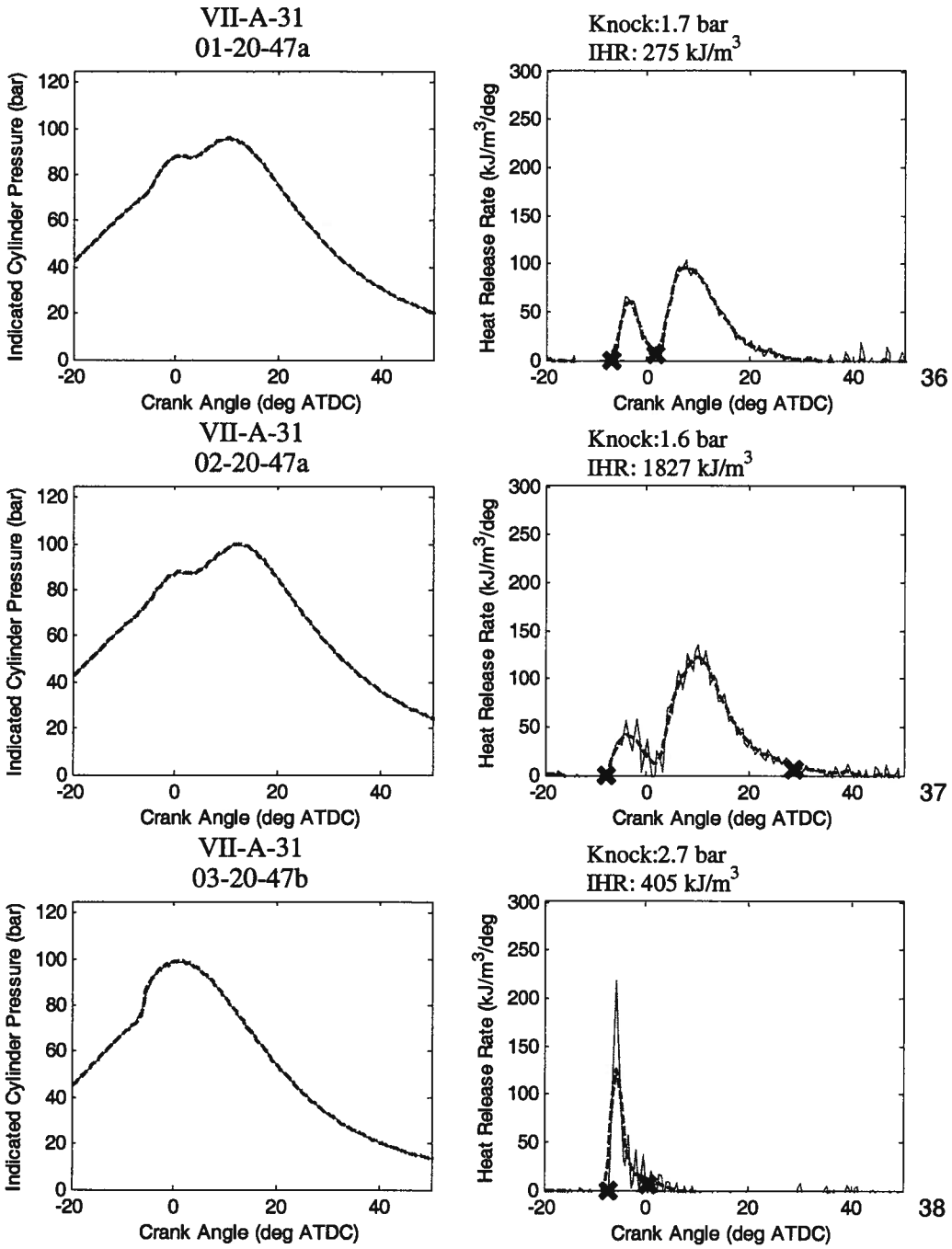

Figures F.2.36 to F.2.38 : Diesel flowrate: 19.4 mg/inj
IHR_{ratio}: 0.68 Knock Ratio: 0.60 Ignition Offset: -0.48 deg

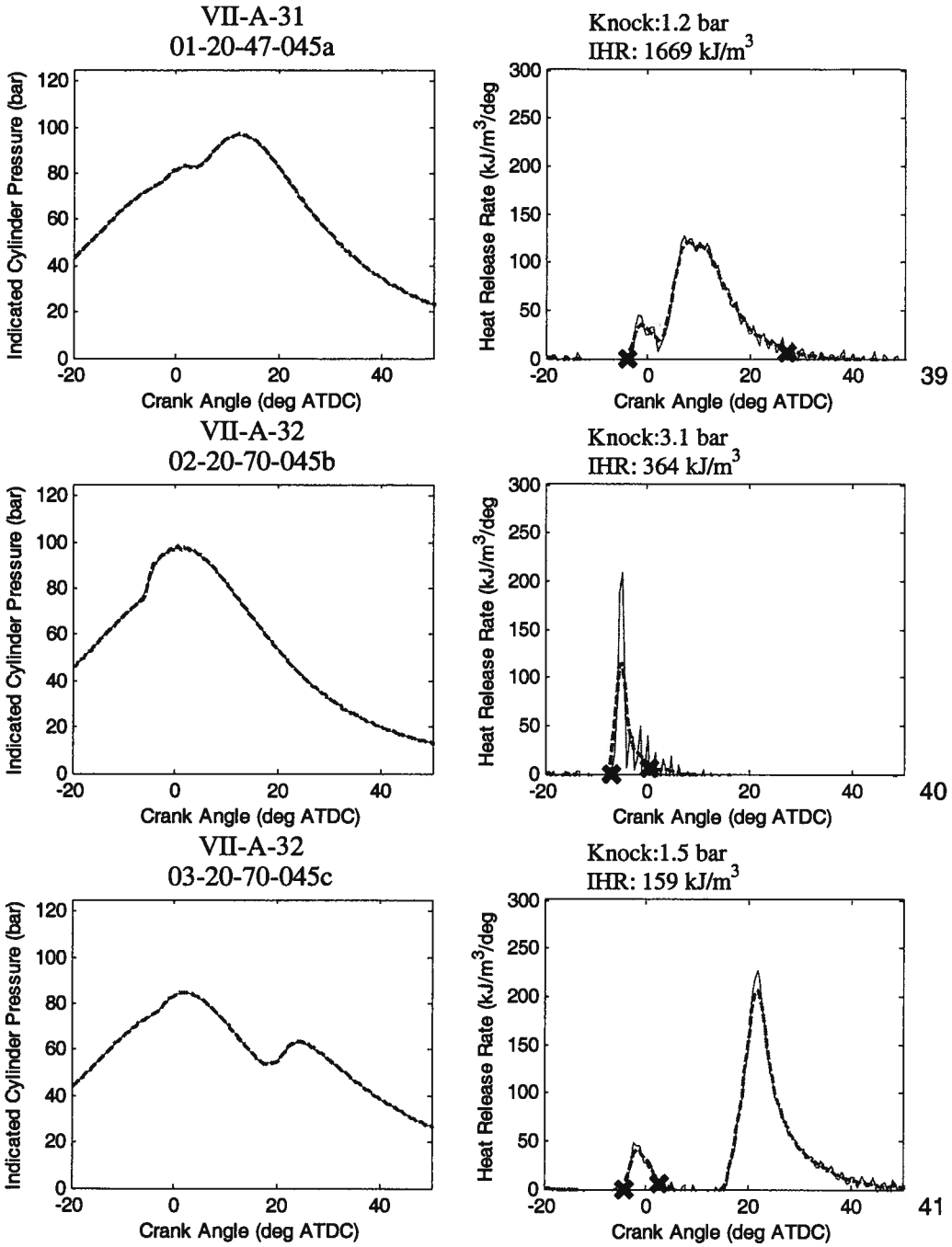

Figures F.2.39 to F.2.41 : Diesel flowrate: 21.1 mg/inj
IHR_{ratio}: 0.44 Knock Ratio: 0.47 Ignition Offset: 2.56 deg

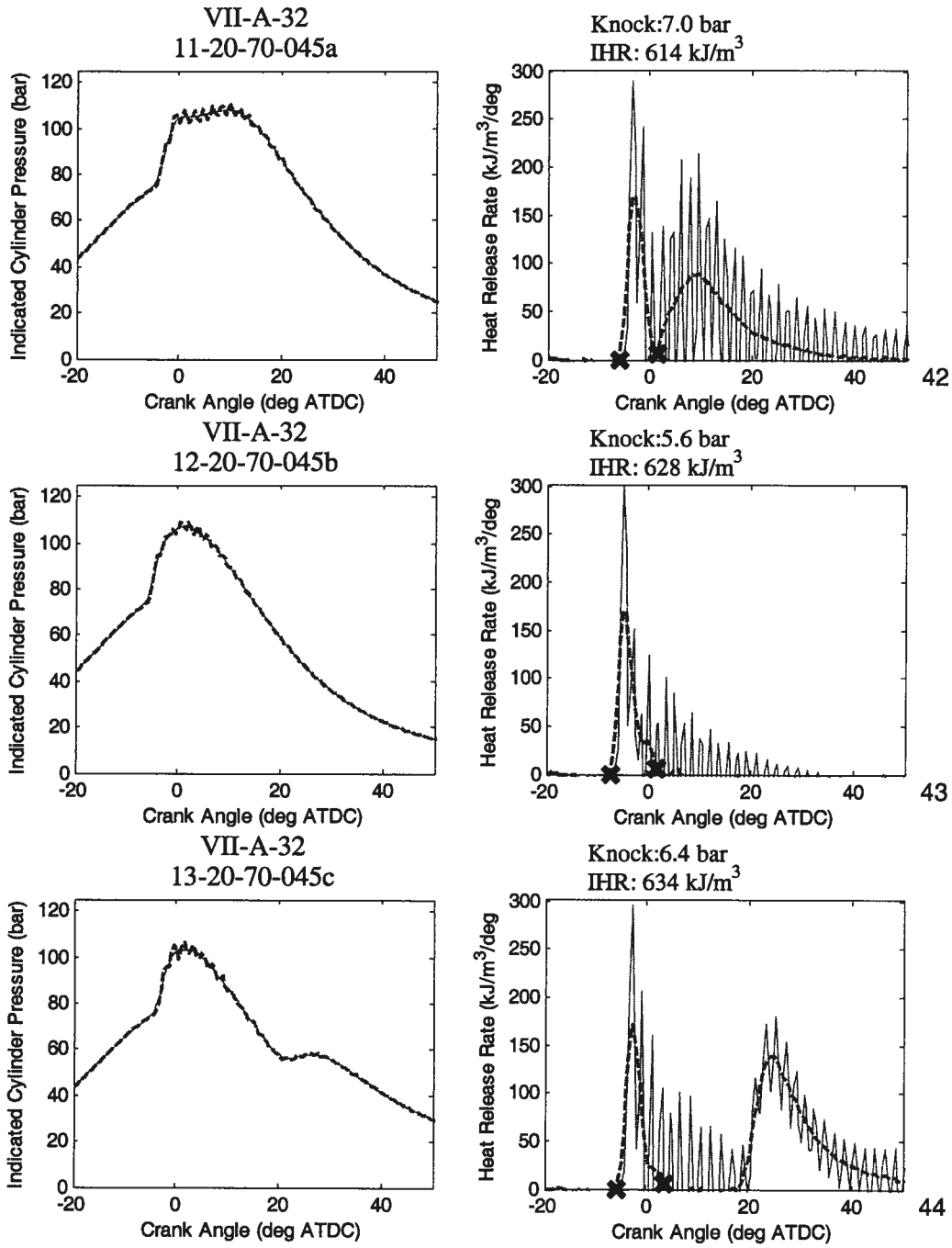

Figures F.2.42 to F.2.44 : Diesel flowrate: 22.1 mg/inj
IHR_{ratio}: 1.01 Knock Ratio: 1.15 Ignition Offset: 1.46 deg

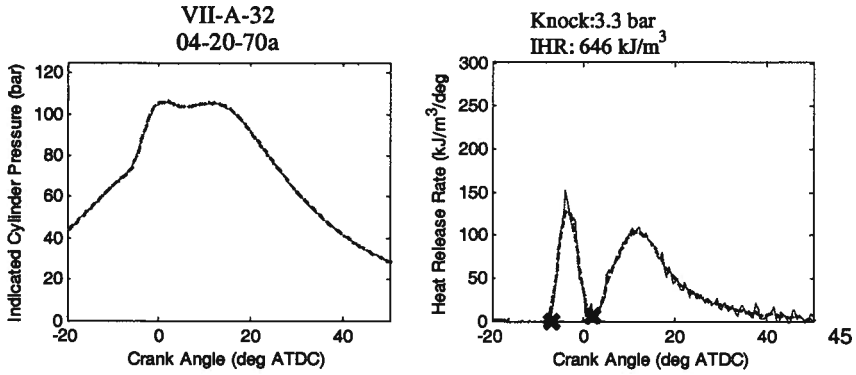

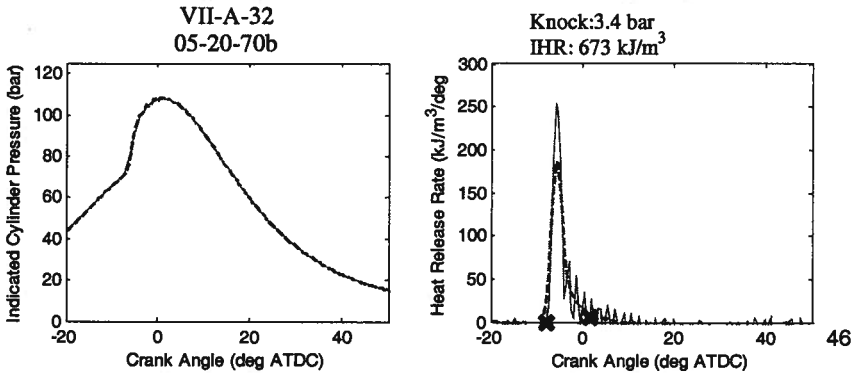

Figures F.2.45 to F.2.46 : Diesel flowrate: 21.2 mg/inj
IHR_{ratio}: 0.96 Knock Ratio: 0.95 Ignition Offset: 1.00 deg

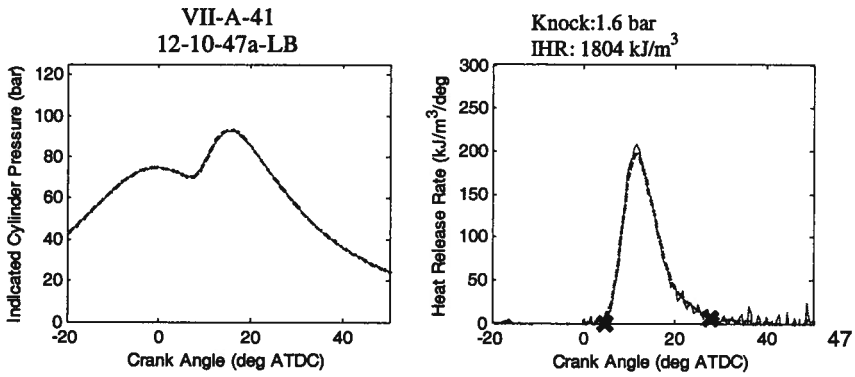

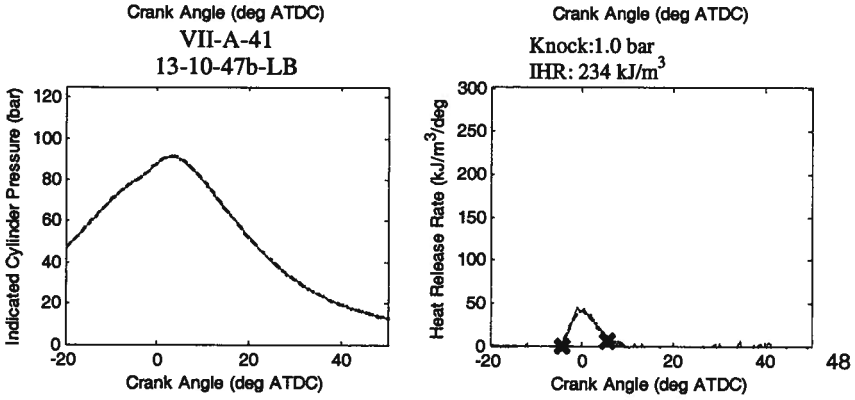

Figures F.2.47 to F.2.48 : Diesel flowrate: 11.0 mg/inj

Appendix F.3- Test Series VII-B-800 RPM Pressure and HRR Curves

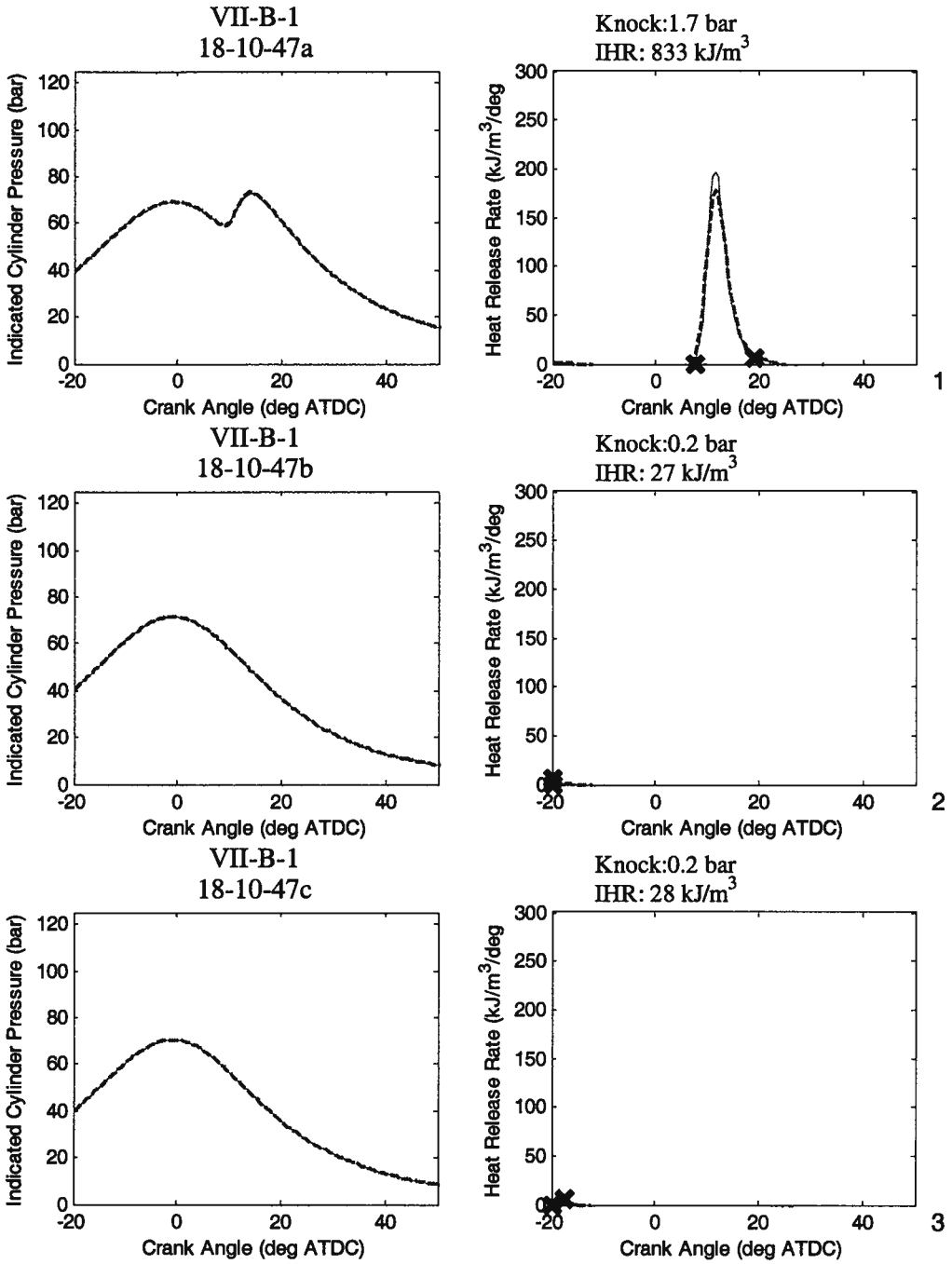

Figures F.3.1 to F.3.3 : Diesel flowrate: 19.9 mg/inj
IHR_{ratio}: 1.04 Knock Ratio: 0.93 Ignition Offset: 0.00 deg

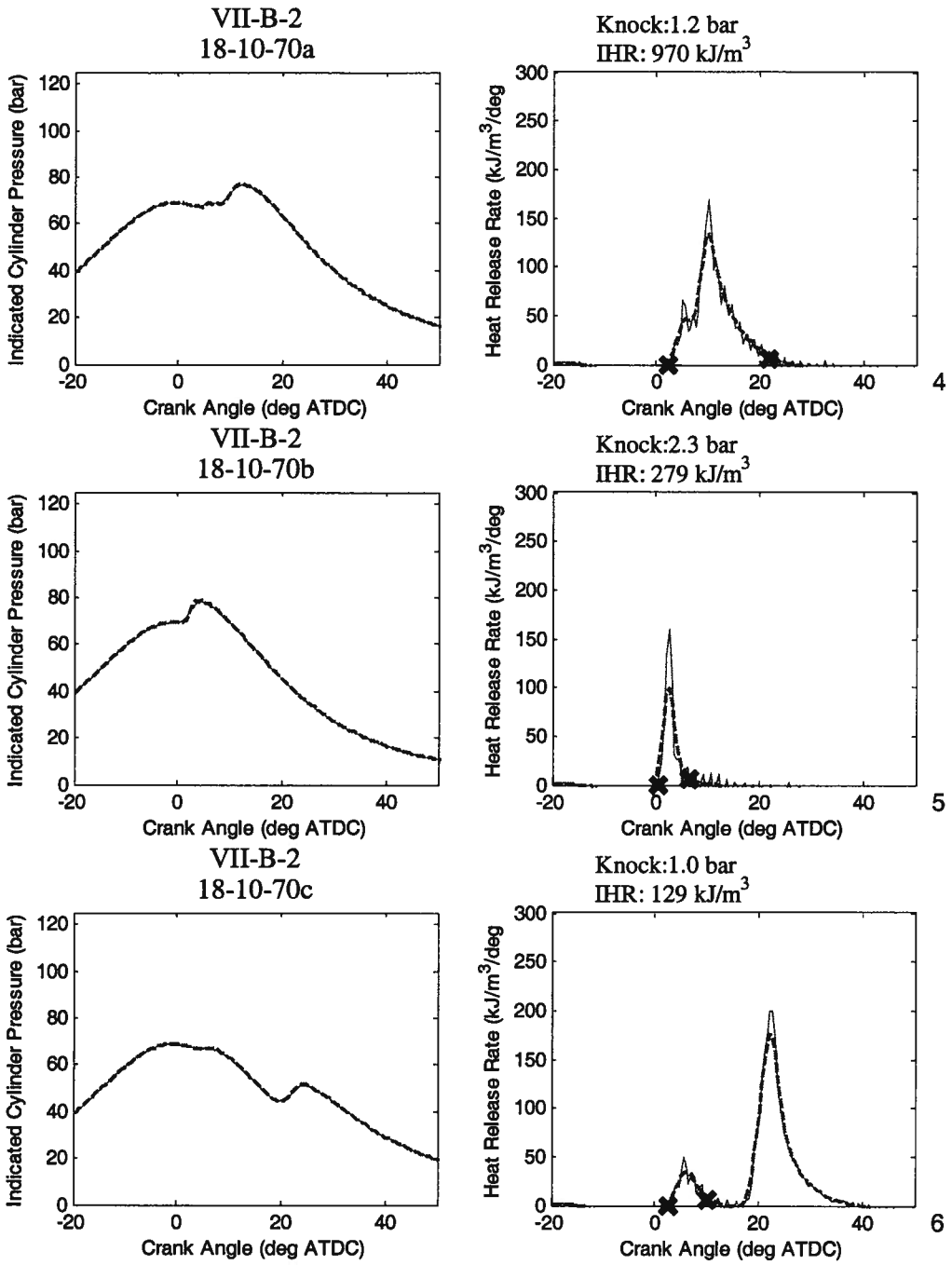

Figures F.3.4 to F.3.6 : Diesel flowrate: 8.3 mg/inj
IHR_{ratio}: 0.46 Knock Ratio: 0.42 Ignition Offset: 2.09 deg

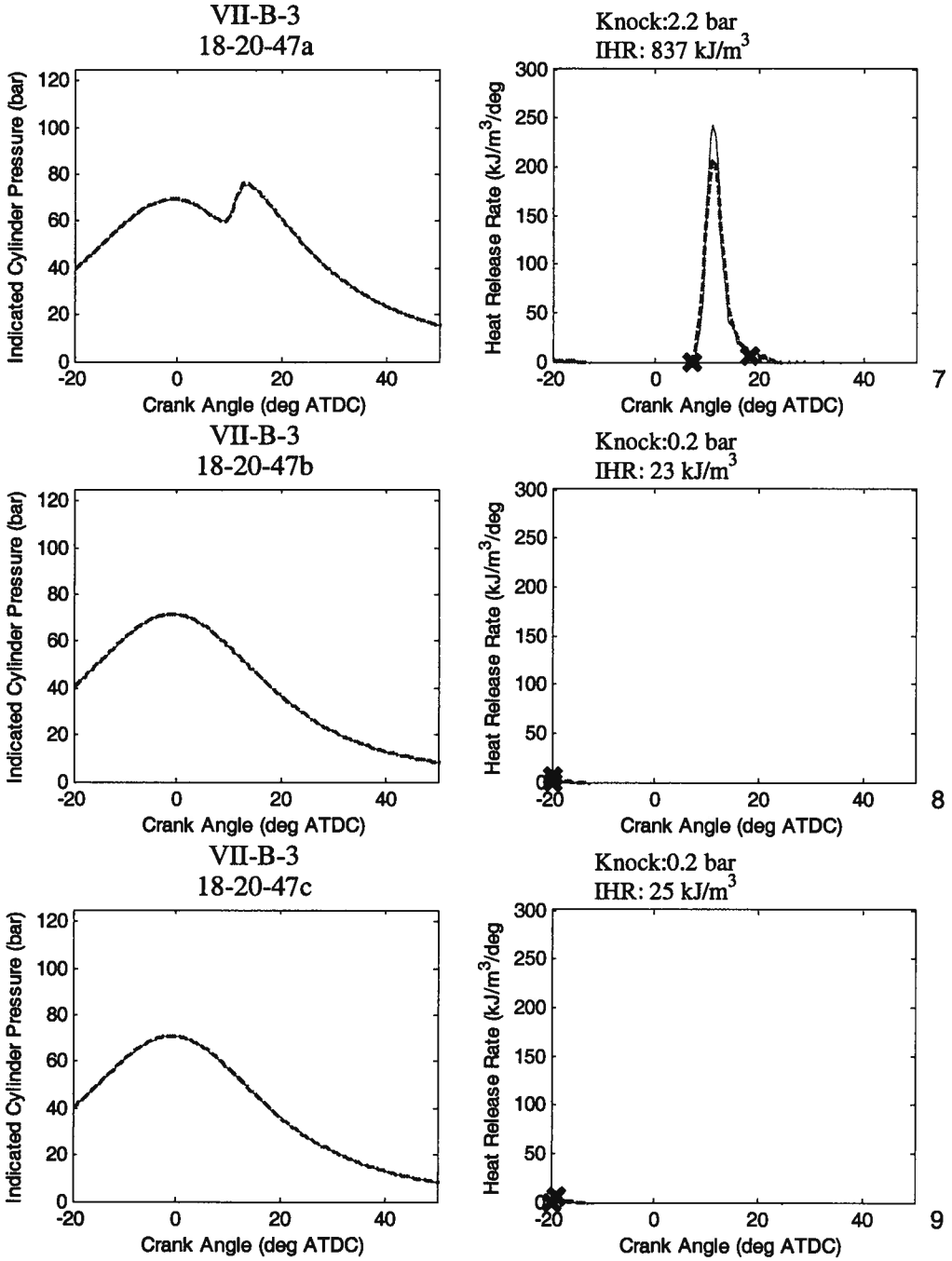

Figures F.3.7 to F.3.9 : Diesel flowrate: 24.0 mg/inj
IHR_{ratio}: 1.08 Knock Ratio: 1.01 Ignition Offset: 0.00 deg

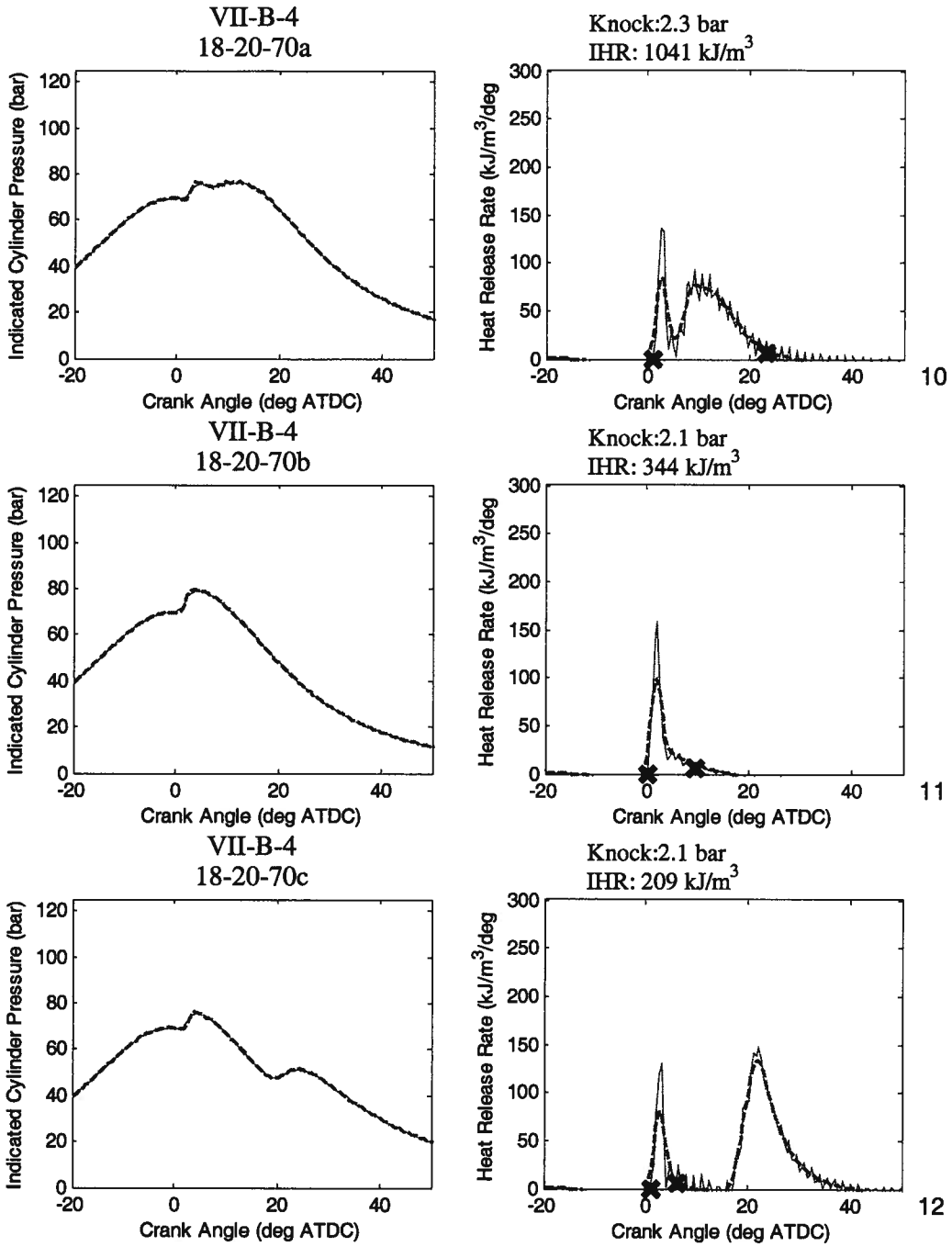

Figures F.3.10 to F.3.12 : Diesel flowrate: 20.1 mg/inj
IHR_{ratio}: 0.61 Knock Ratio: 1.00 Ignition Offset: 1.00 deg

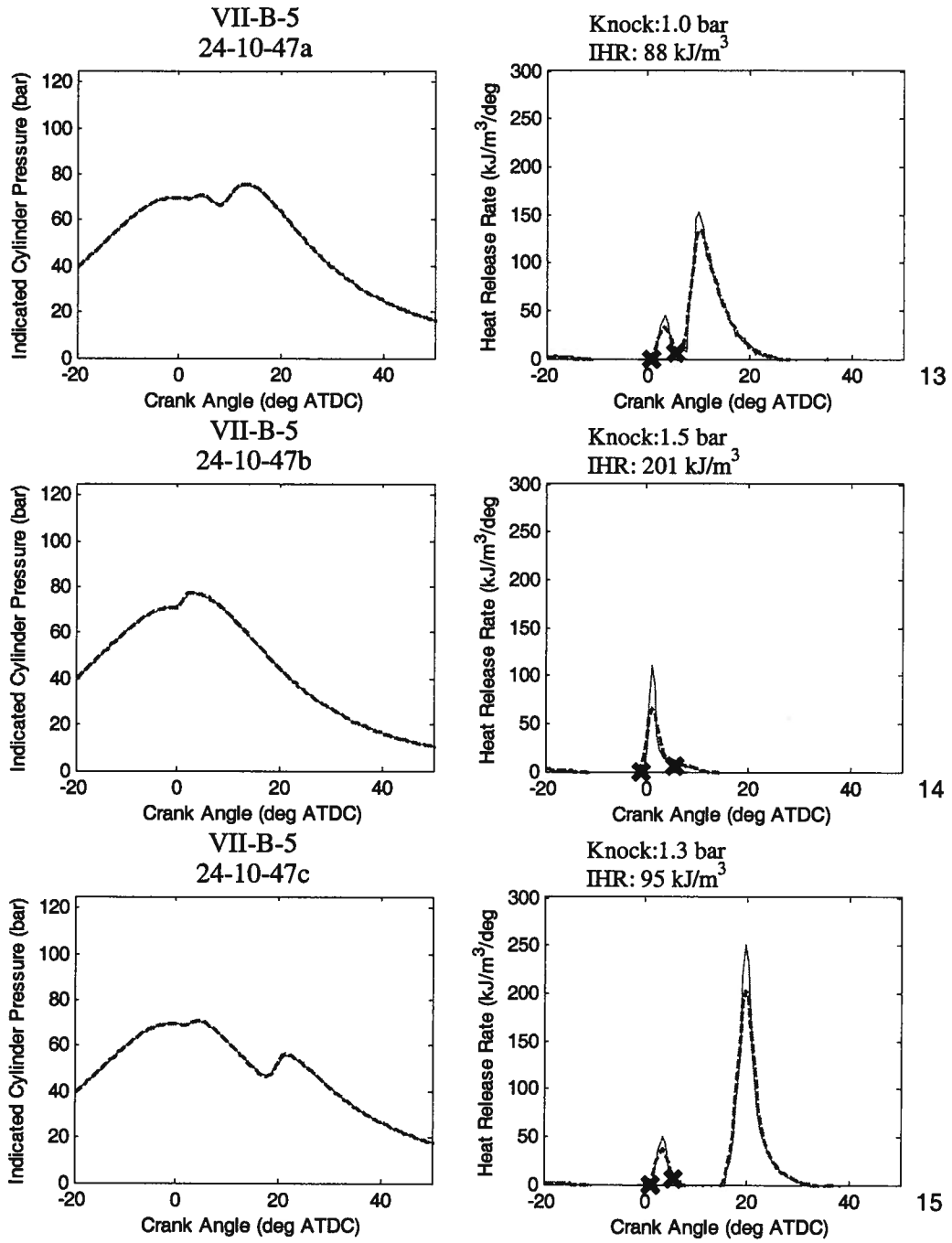

Figures F.3.13 to F.3.15 : Diesel flowrate: 10.2 mg/inj
IHR_{ratio}: 0.47 Knock Ratio: 0.86 Ignition Offset: 1.83 deg

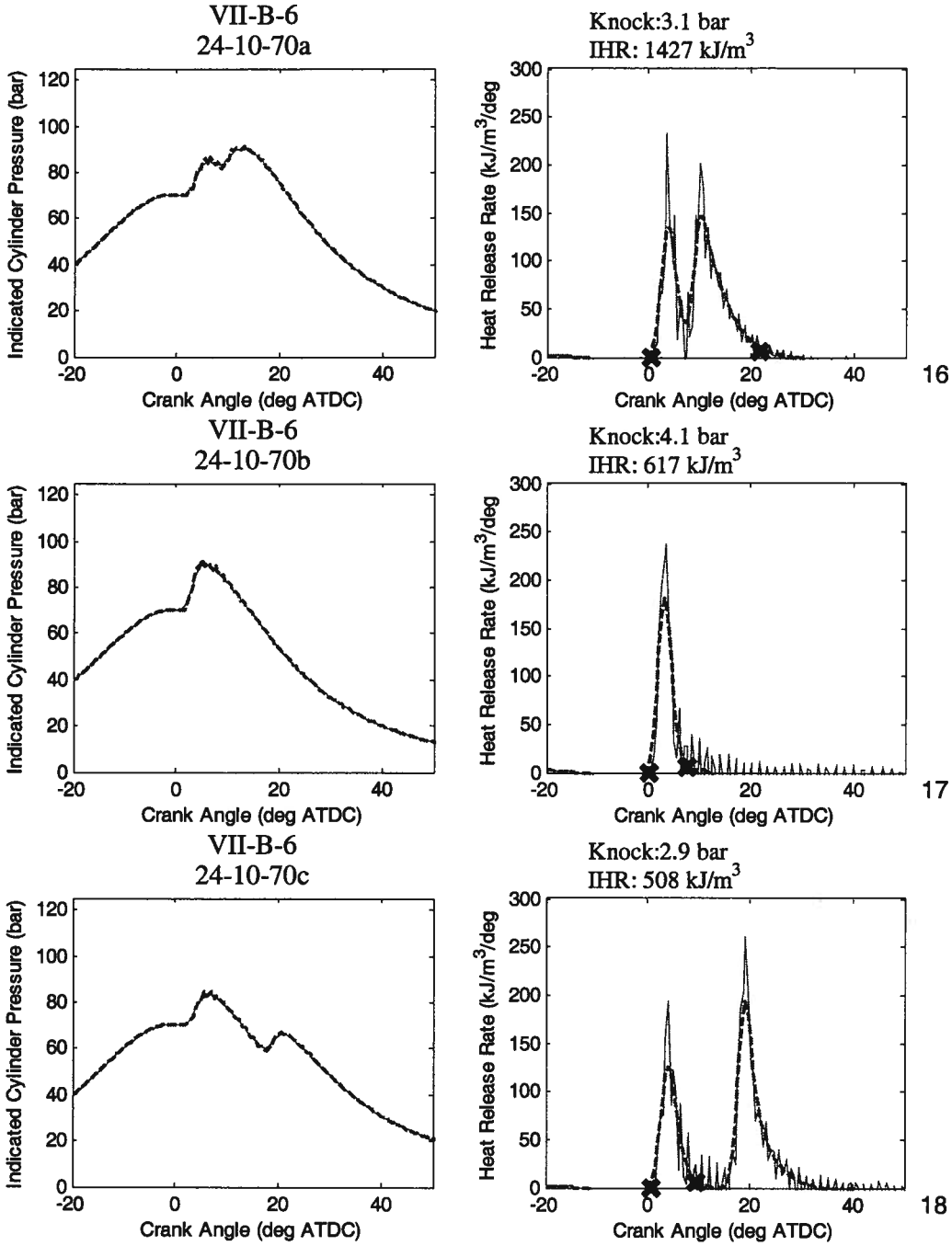

Figures F.3.16 to F.3.18 : Diesel flowrate: 11.8 mg/inj
IHR_{ratio}: 0.82 Knock Ratio: 0.71 Ignition Offset: 0.42 deg

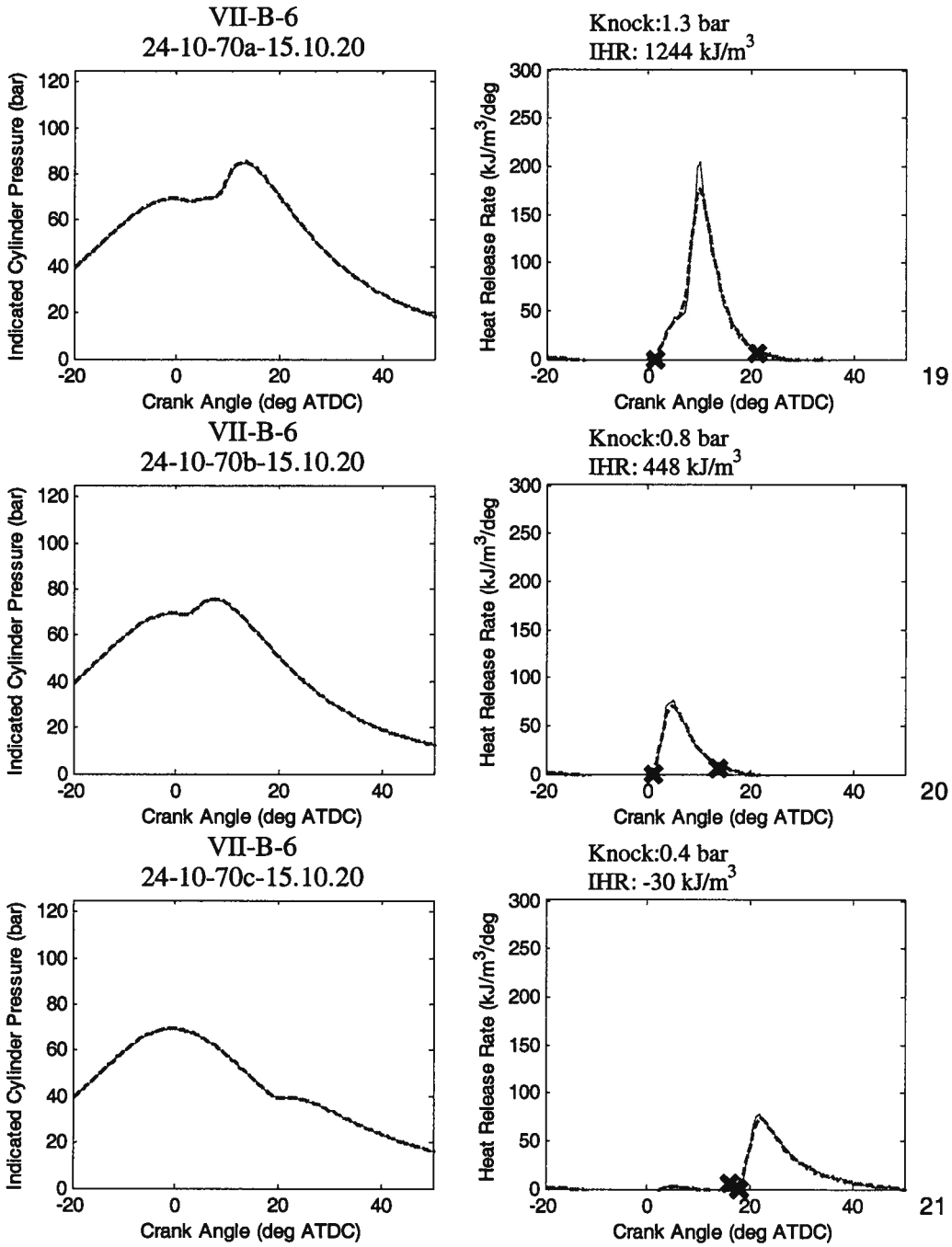

Figures F.3.19 to F.3.21 : Diesel flowrate: 11.3 mg/inj
IHR_{ratio}: -0.07 Knock Ratio: 0.42 Ignition Offset: 16.71 deg

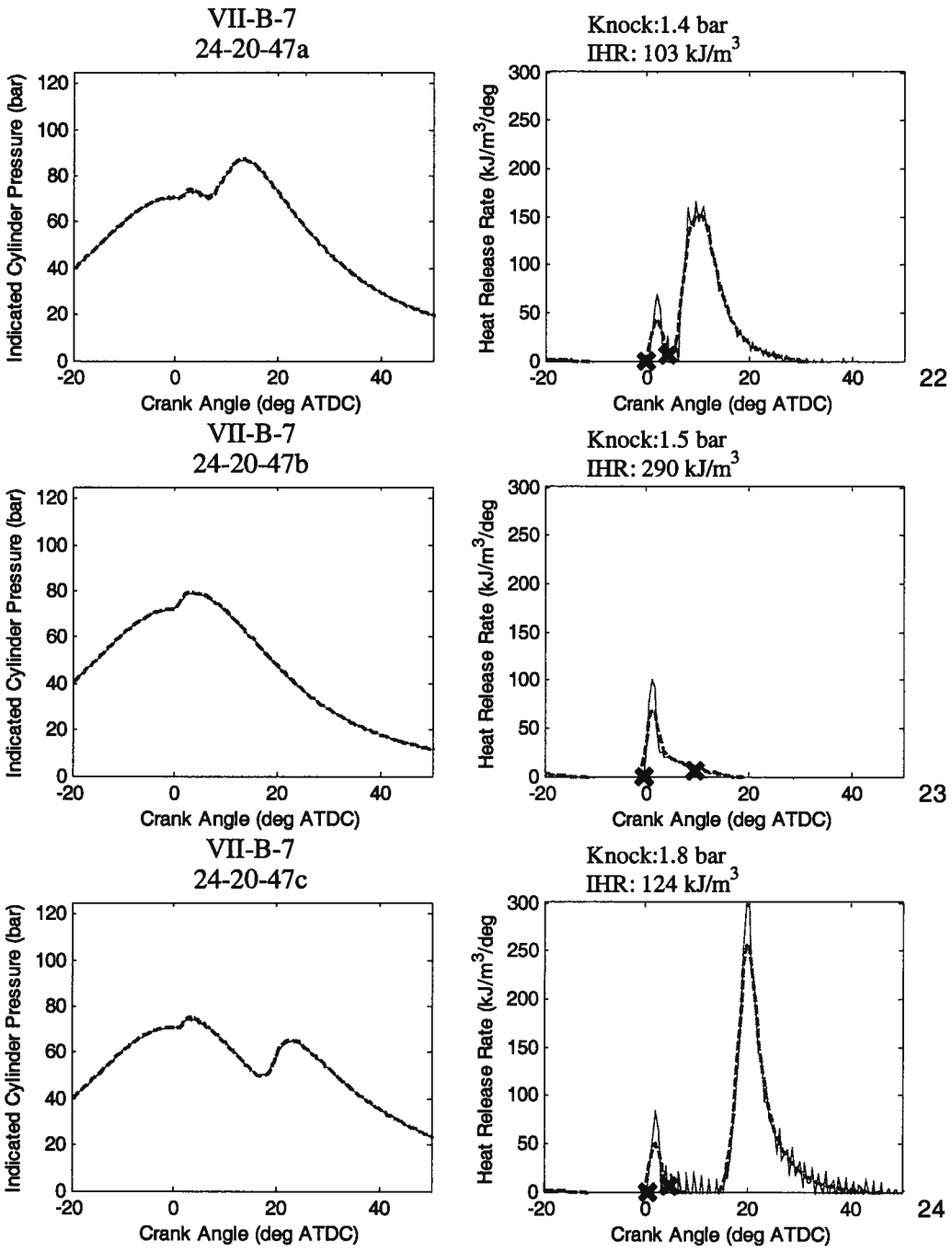

Figures F.3.22 to F.3.24 : Diesel flowrate: 28.1 mg/inj
IHR_{ratio}: 0.43 Knock Ratio: 1.24 Ignition Offset: 1.00 deg

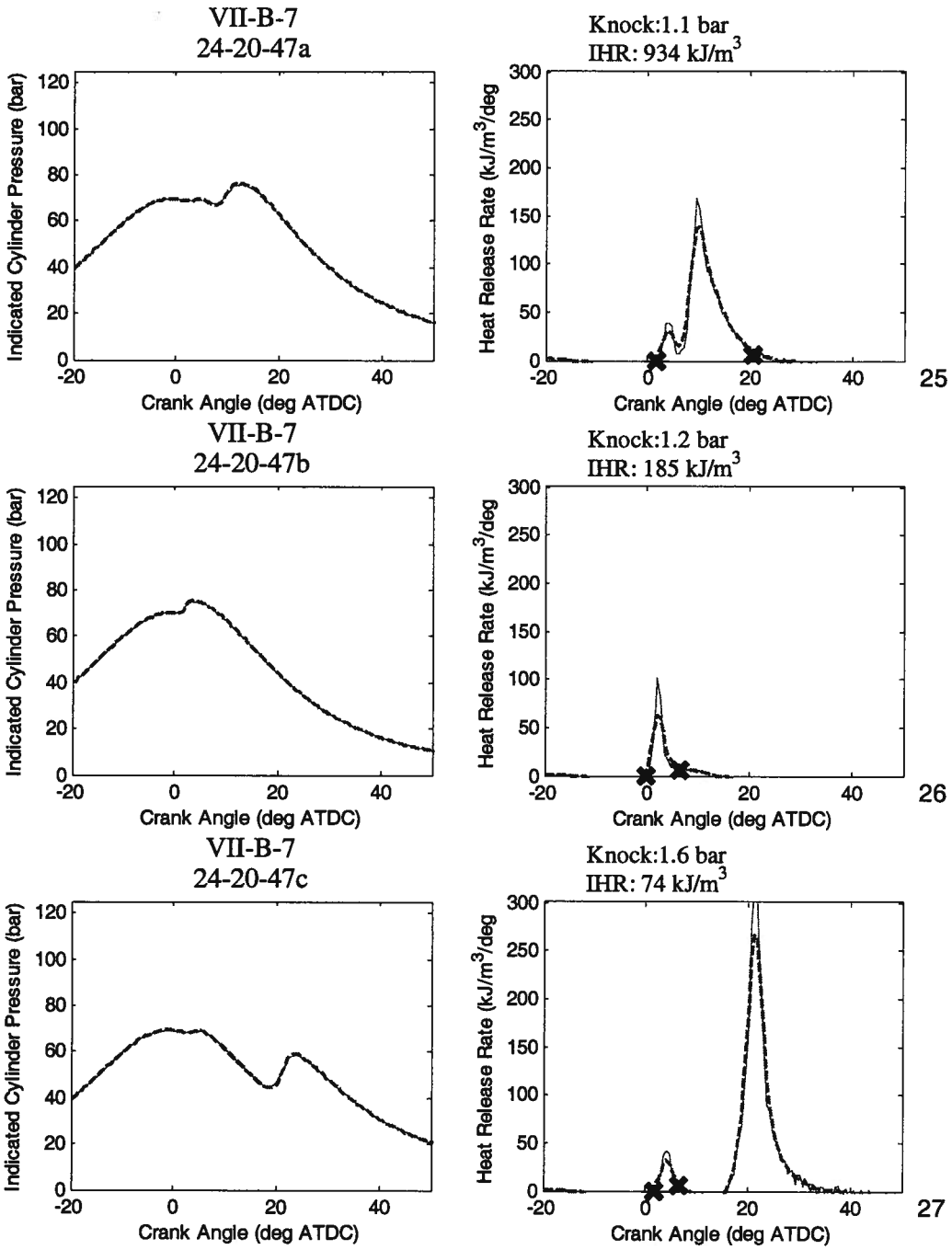

Figures F.3.25 to F.3.27 : Diesel flowrate: 19.5 mg/inj
IHR_{ratio}: 0.40 Knock Ratio: 1.27 Ignition Offset: 1.68 deg

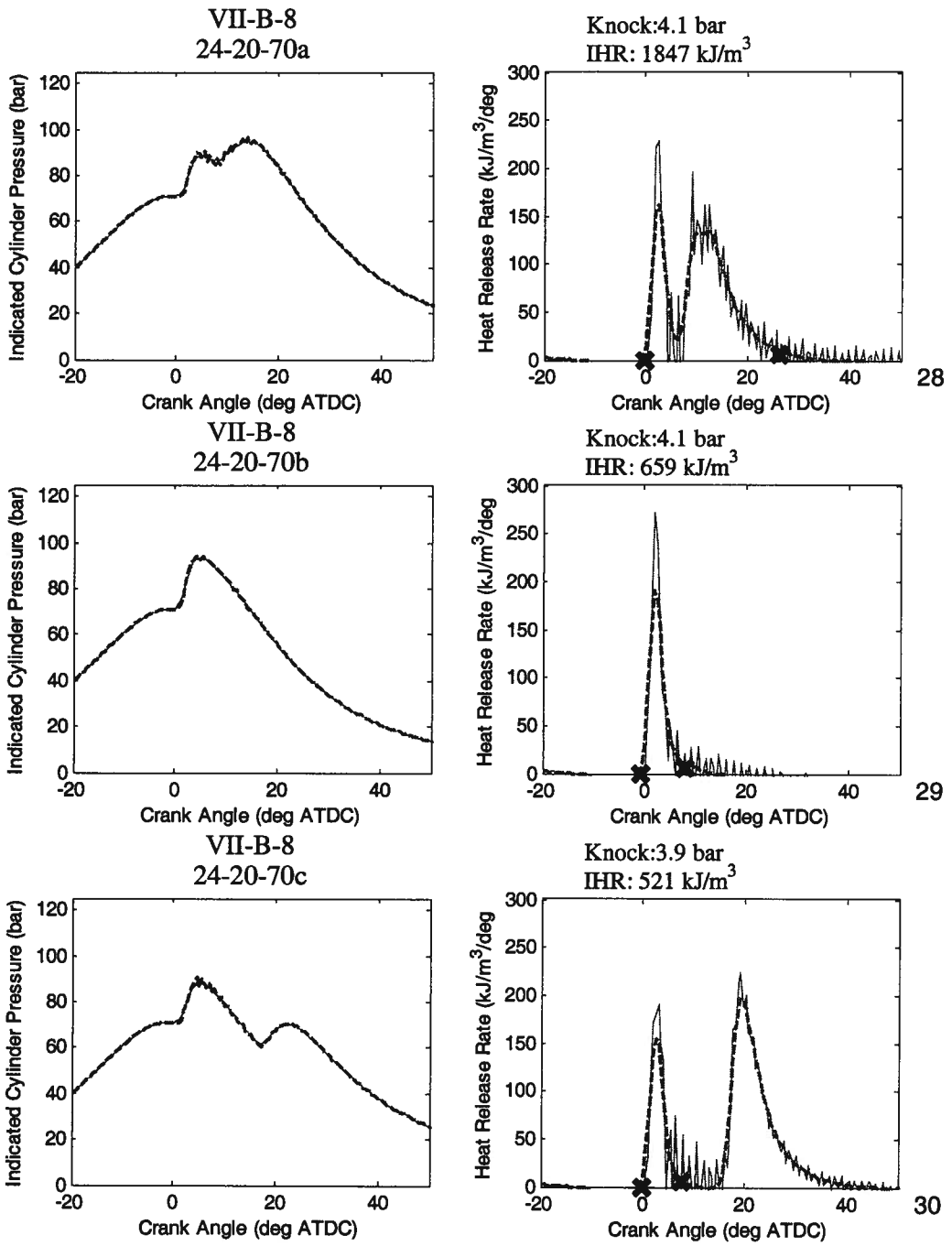

Figures F.3.28 to F.3.30 : Diesel flowrate: 13.5 mg/inj
IHR_{ratio}: 0.79 Knock Ratio: 0.94 Ignition Offset: 0.47 deg

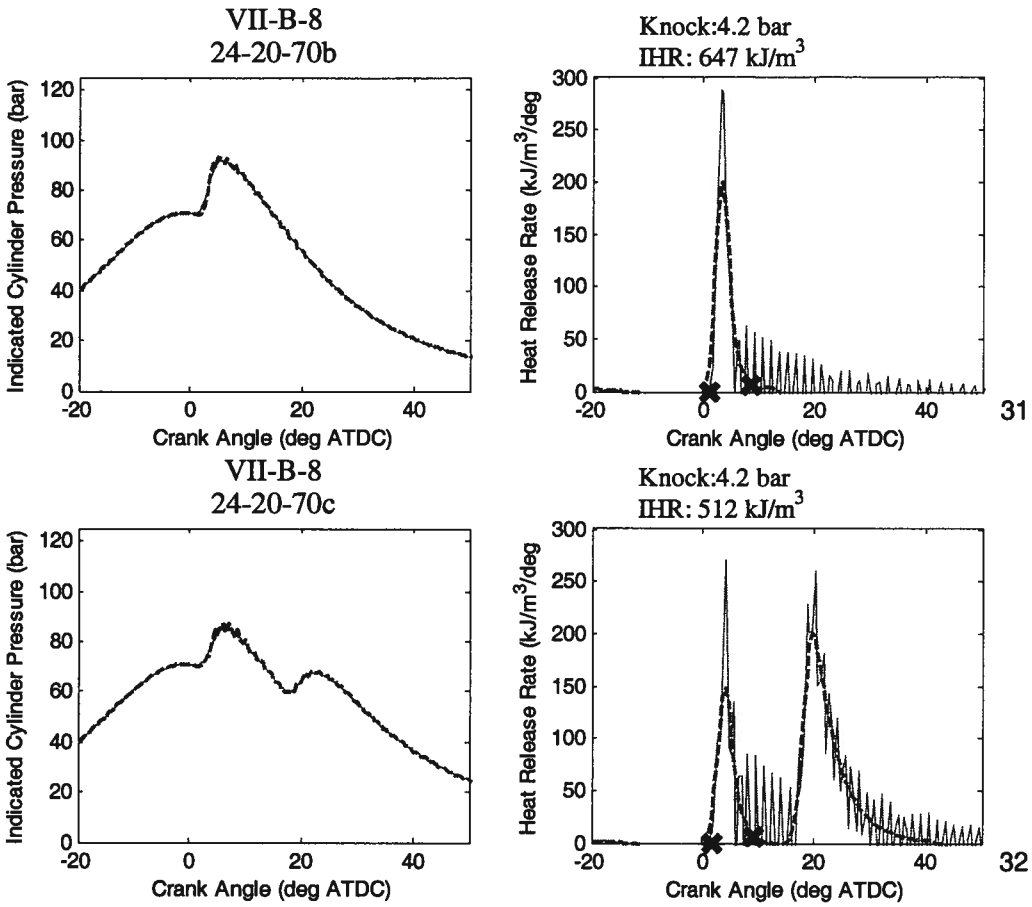

Figures F.3.31 to F.3.32 : Diesel flowrate: 20.1 mg/inj
IHR_{ratio}: 0.79 Knock Ratio: 1.00 Ignition Offset: 0.50 deg

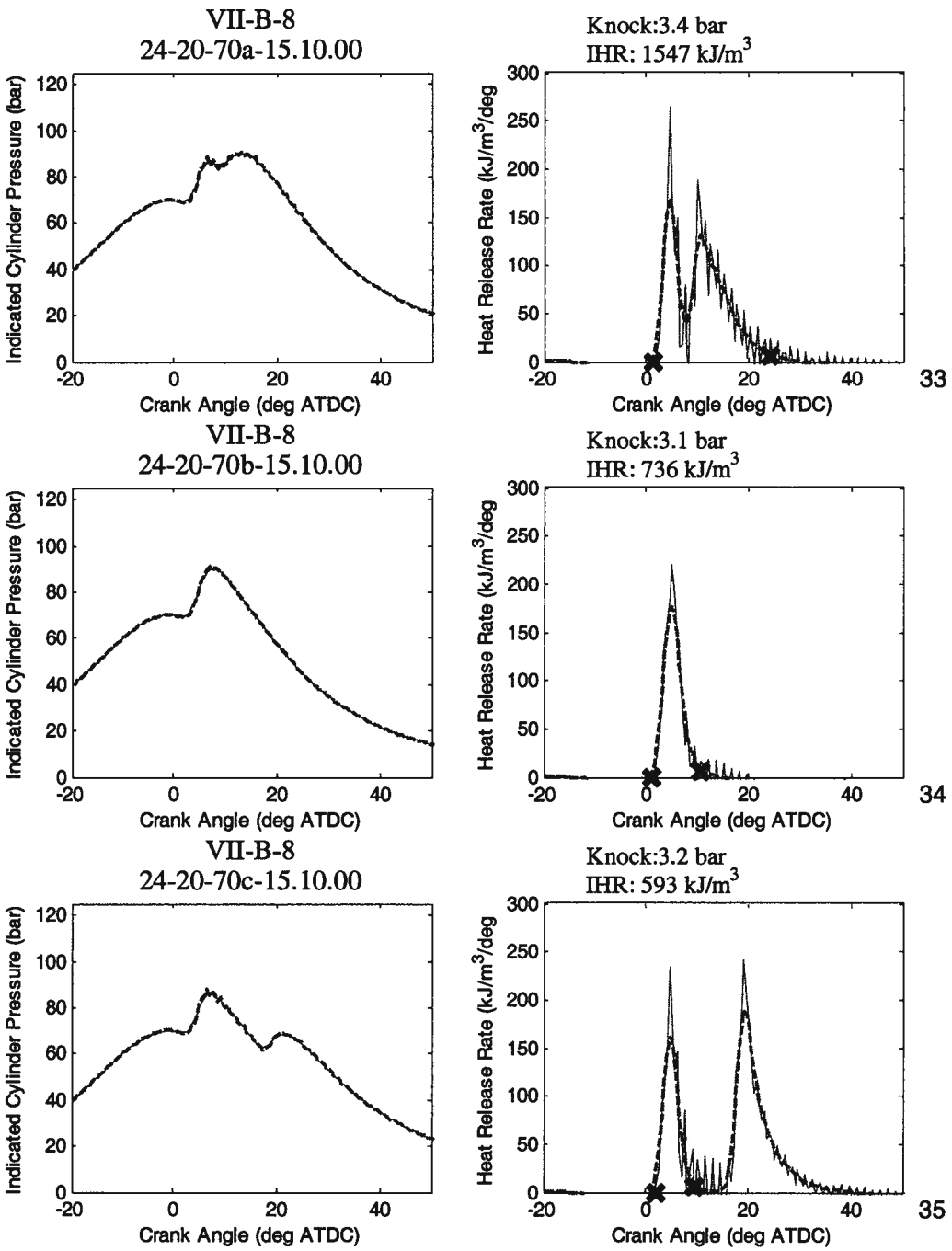

Figures F.3.33 to F.3.35 : Diesel flowrate: 18.1 mg/inj
IHR_{ratio}: 0.81 Knock Ratio: 1.03 Ignition Offset: 0.88 deg

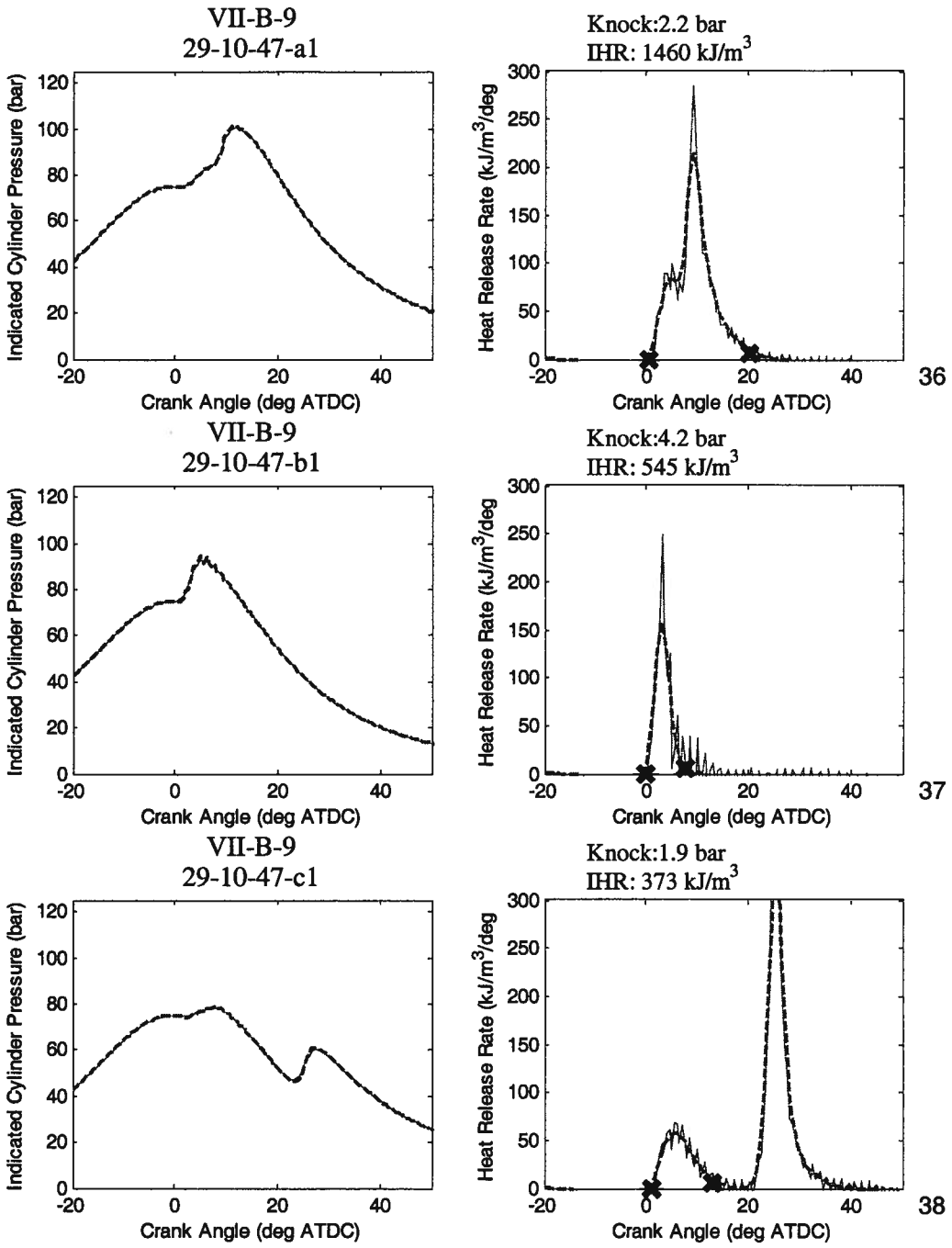

Figures F.3.36 to F.3.38 : Diesel flowrate: 13.1 mg/inj
IHR_{ratio}: 0.69 Knock Ratio: 0.46 Ignition Offset: 1.30 deg

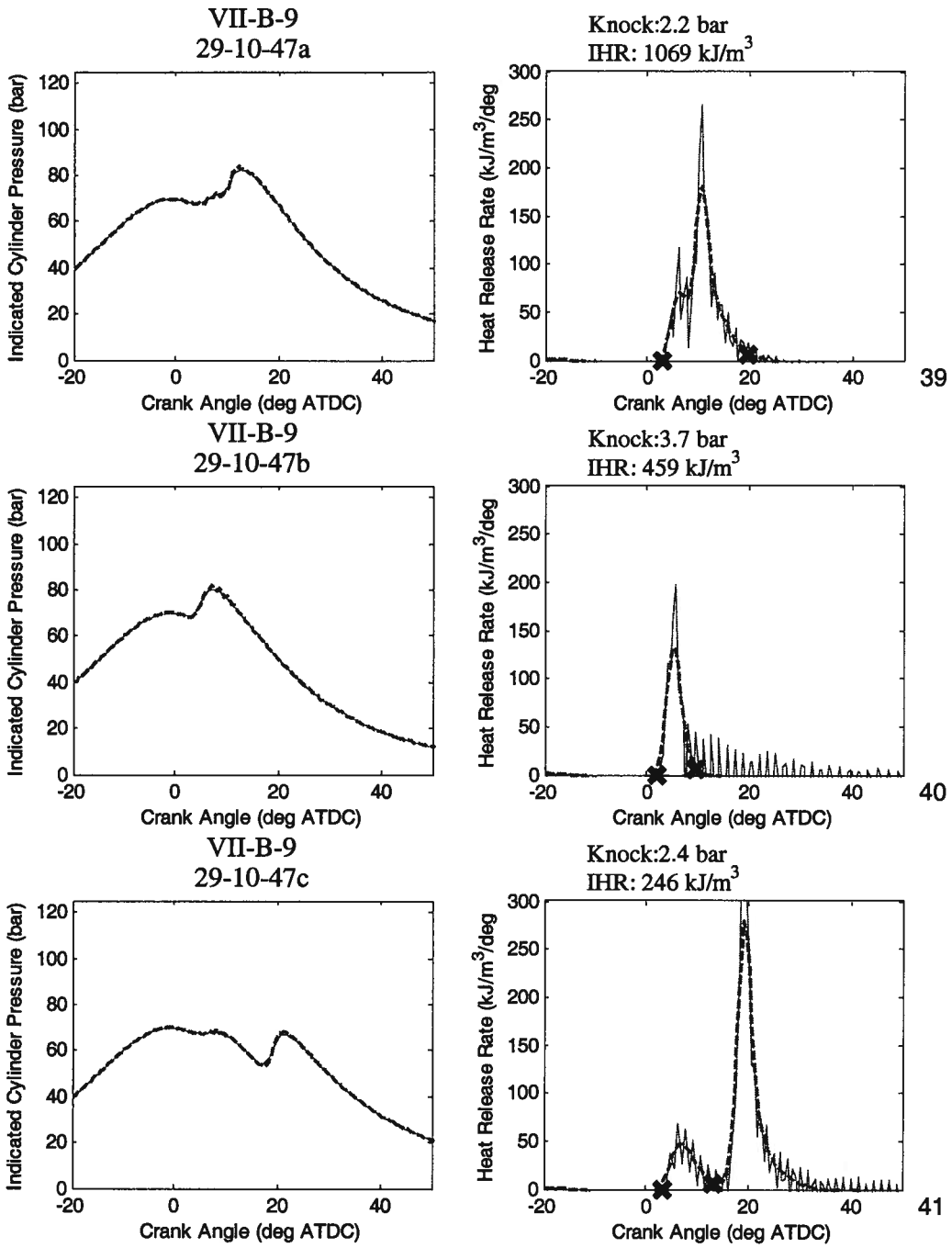

Figures F.3.39 to F.3.41 : Diesel flowrate: 16.7 mg/inj
IHR_{ratio}: 0.54 Knock Ratio: 0.65 Ignition Offset: 0.96 deg

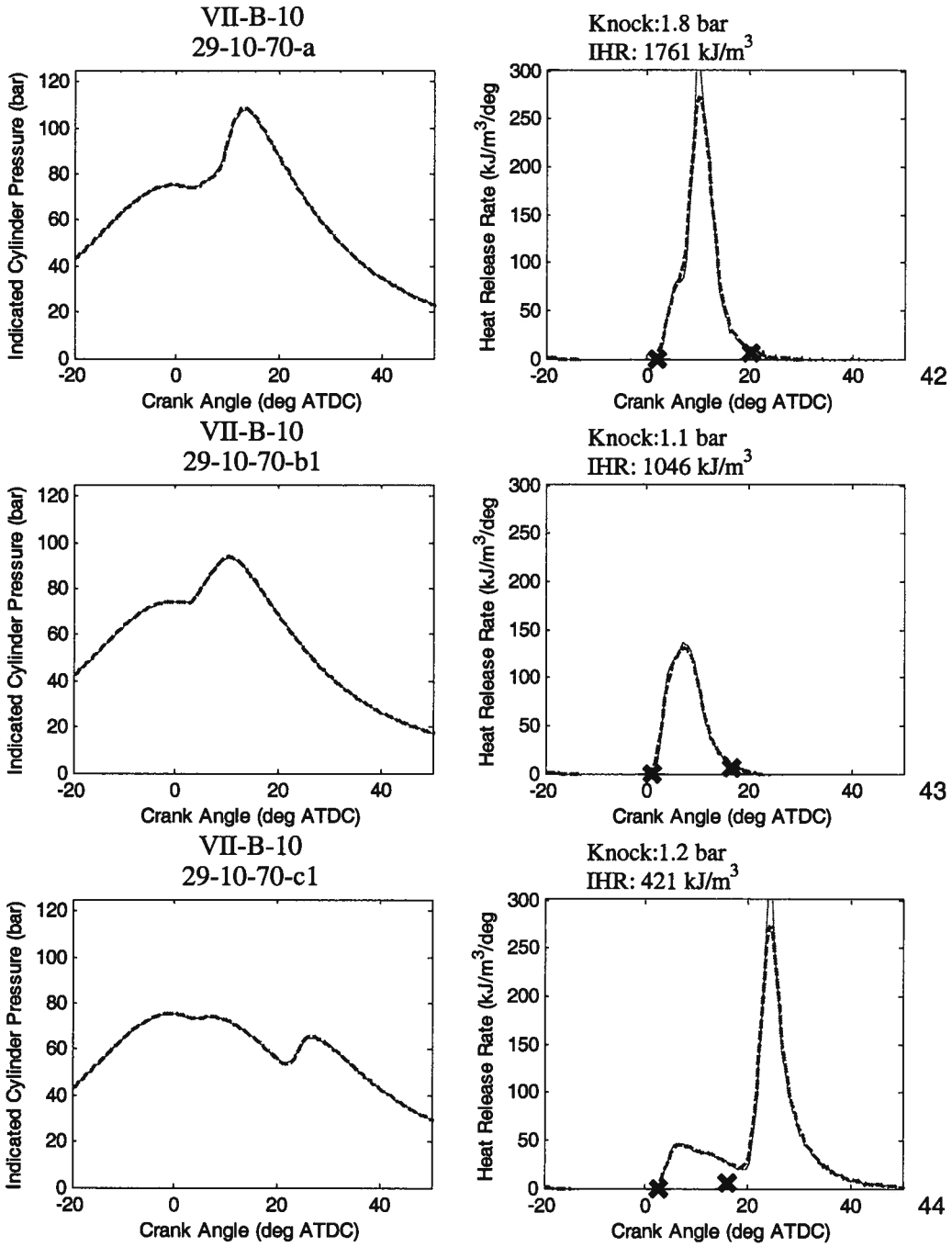

Figures F.3.42 to F.3.44 : Diesel flowrate: 12.8 mg/inj
IHR_{ratio}: 0.40 Knock Ratio: 1.10 Ignition Offset: 1.31 deg

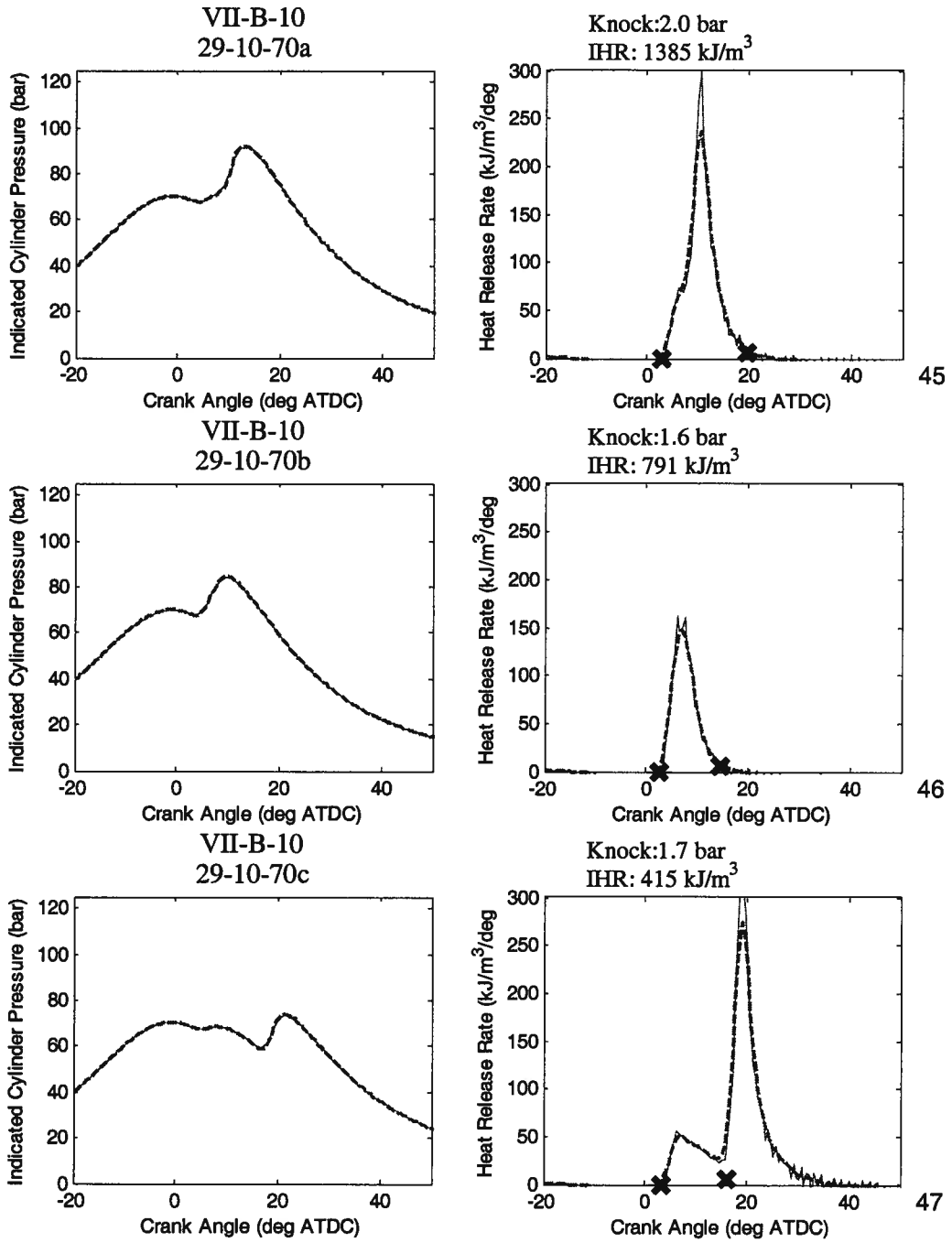

Figures F.3.45 to F.3.47 : Diesel flowrate: 14.2 mg/inj
IHR_{ratio}: 0.52 Knock Ratio: 1.05 Ignition Offset: 0.69 deg

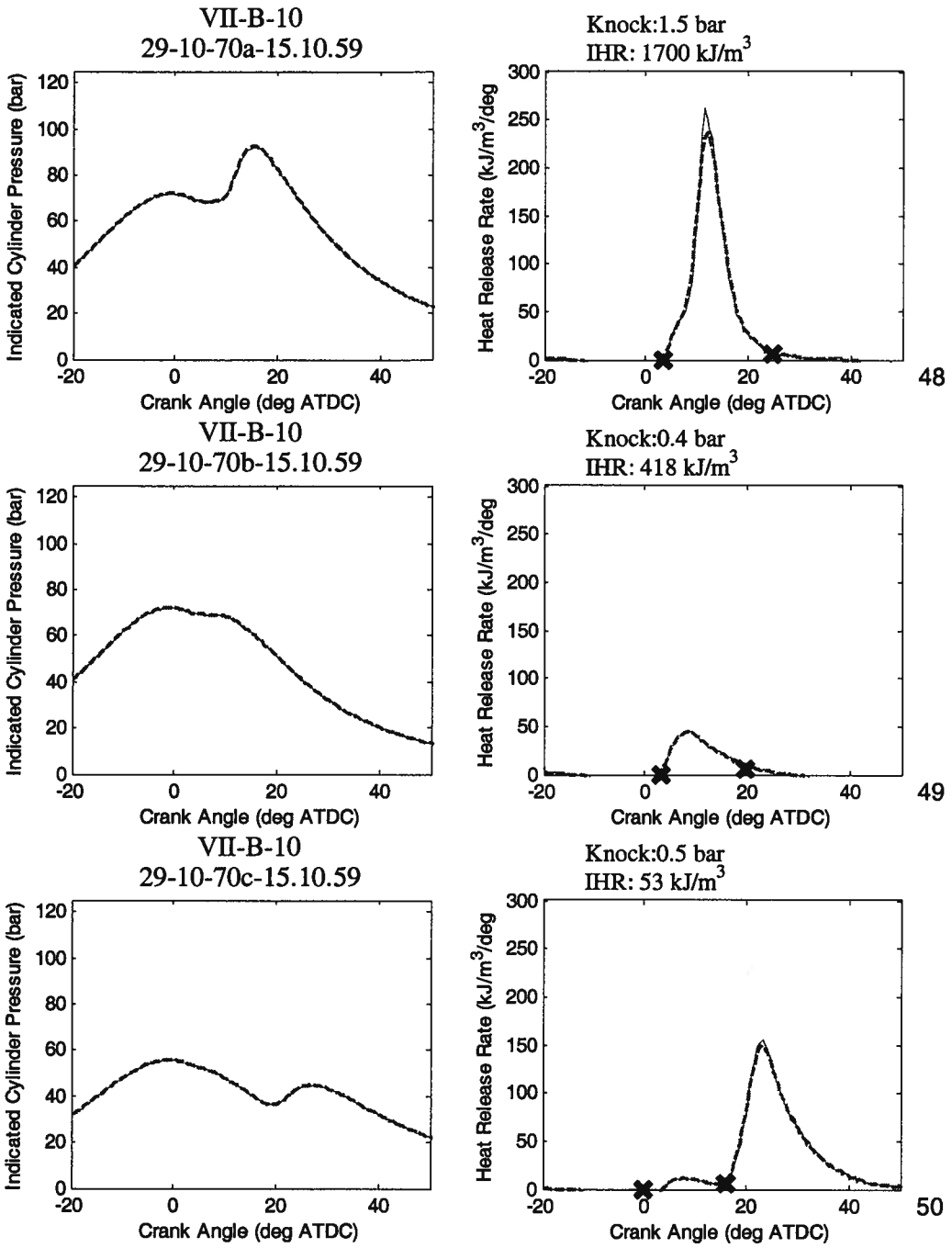

Figures F.3.48 to F.3.50 : Diesel flowrate: 14.0 mg/inj
IHR_{ratio}: 0.13 Knock Ratio: 1.26 Ignition Offset: -3.37 deg

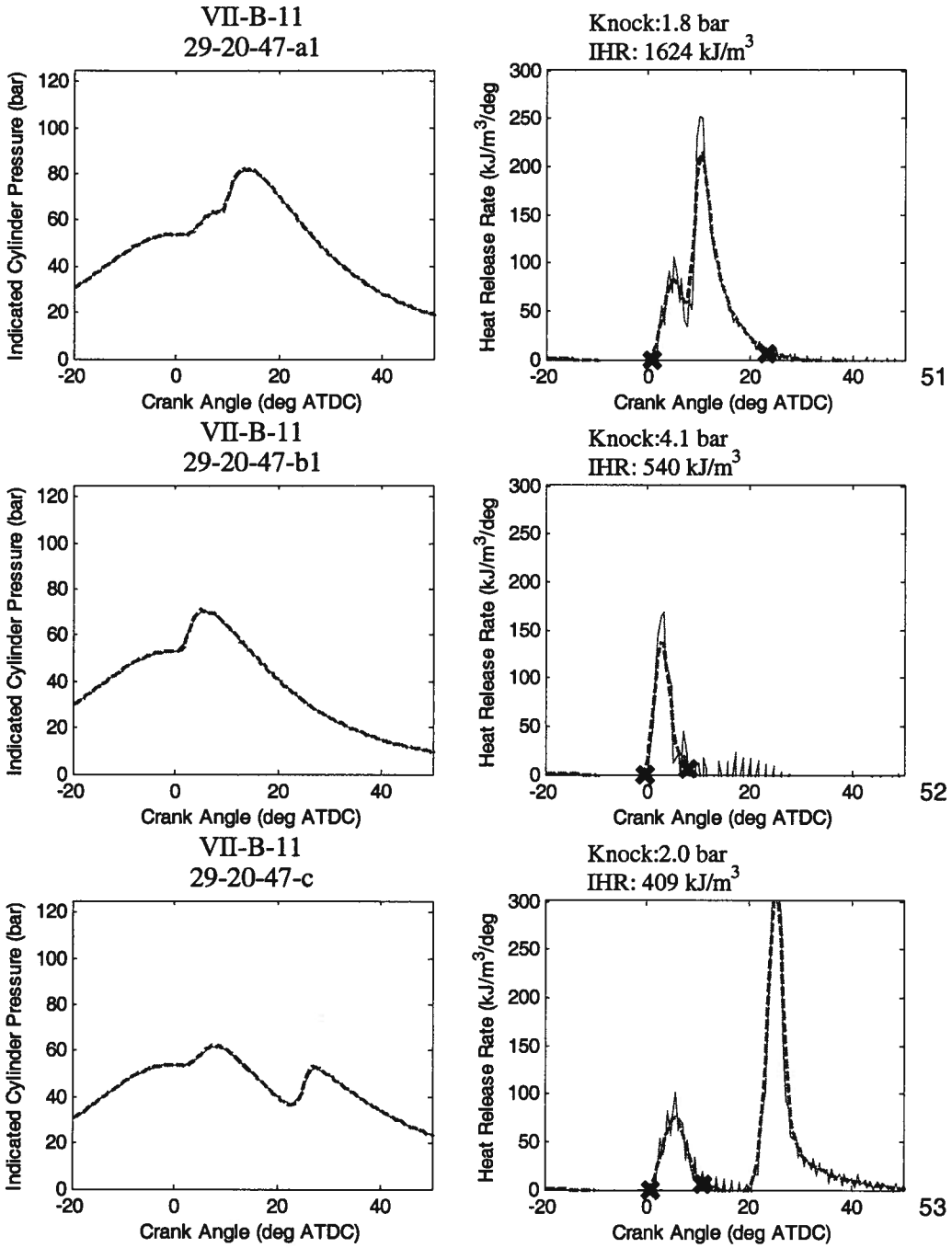

Figures F.3.51 to F.3.53 : Diesel flowrate: 18.0 mg/inj
IHR_{ratio}: 0.76 Knock Ratio: 0.50 Ignition Offset: 1.18 deg

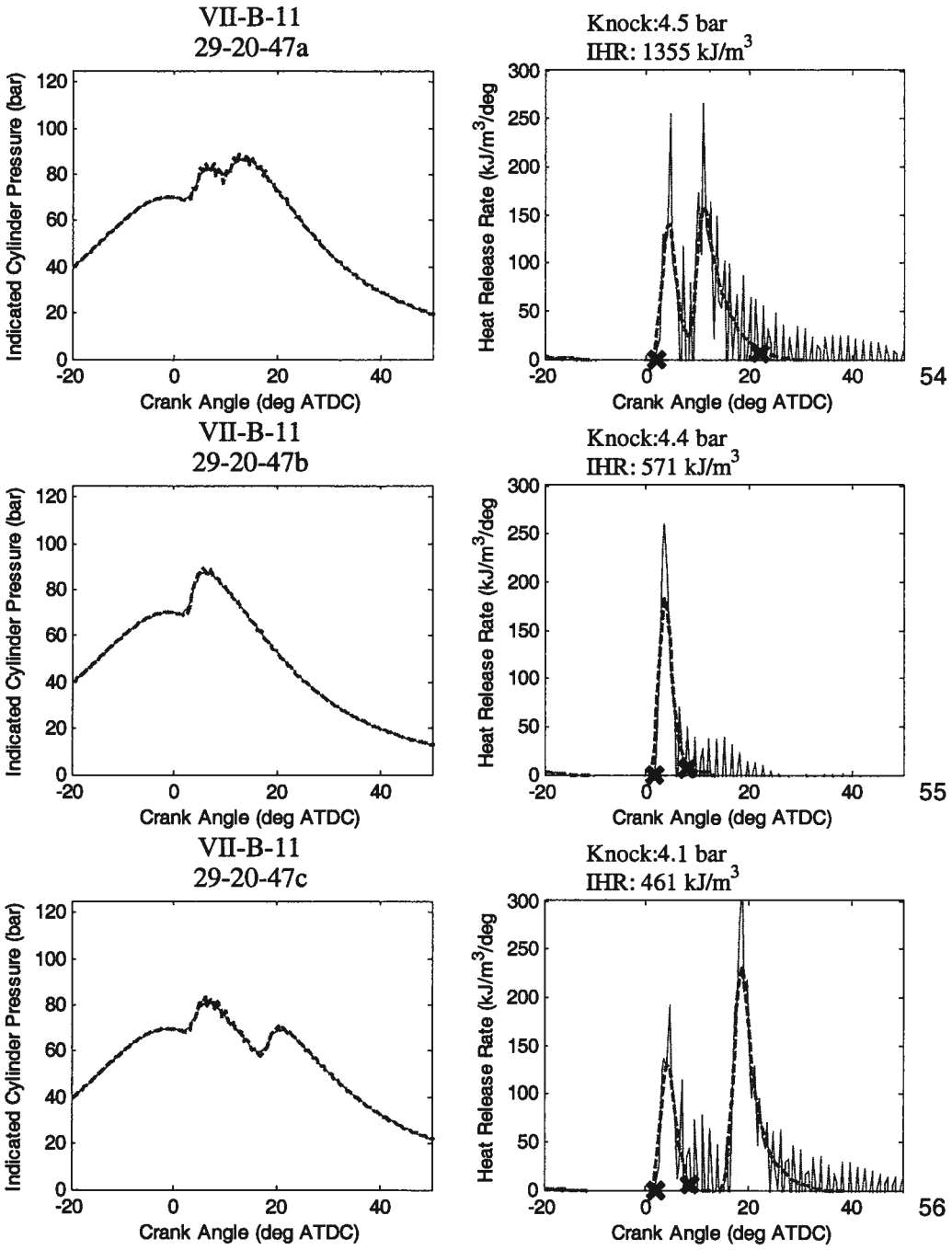

Figures F.3.54 to F.3.56 : Diesel flowrate: 21.3 mg/inj
IHR_{ratio}: 0.81 Knock Ratio: 0.93 Ignition Offset: 0.50 deg

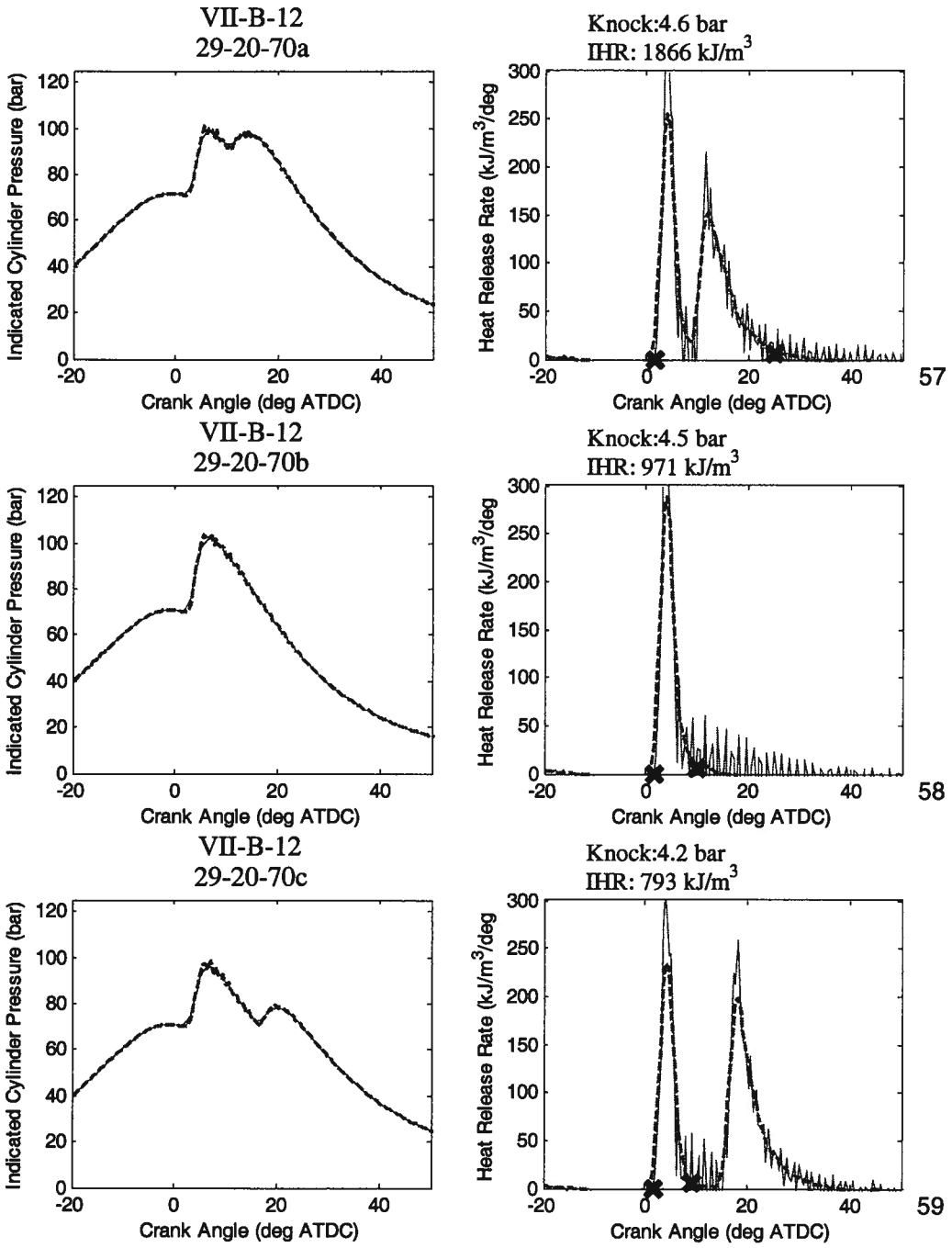

Figures F.3.57 to F.3.59 : Diesel flowrate: 19.7 mg/inj
IHR_{ratio}: 0.82 Knock Ratio: 0.93 Ignition Offset: 0.00 deg

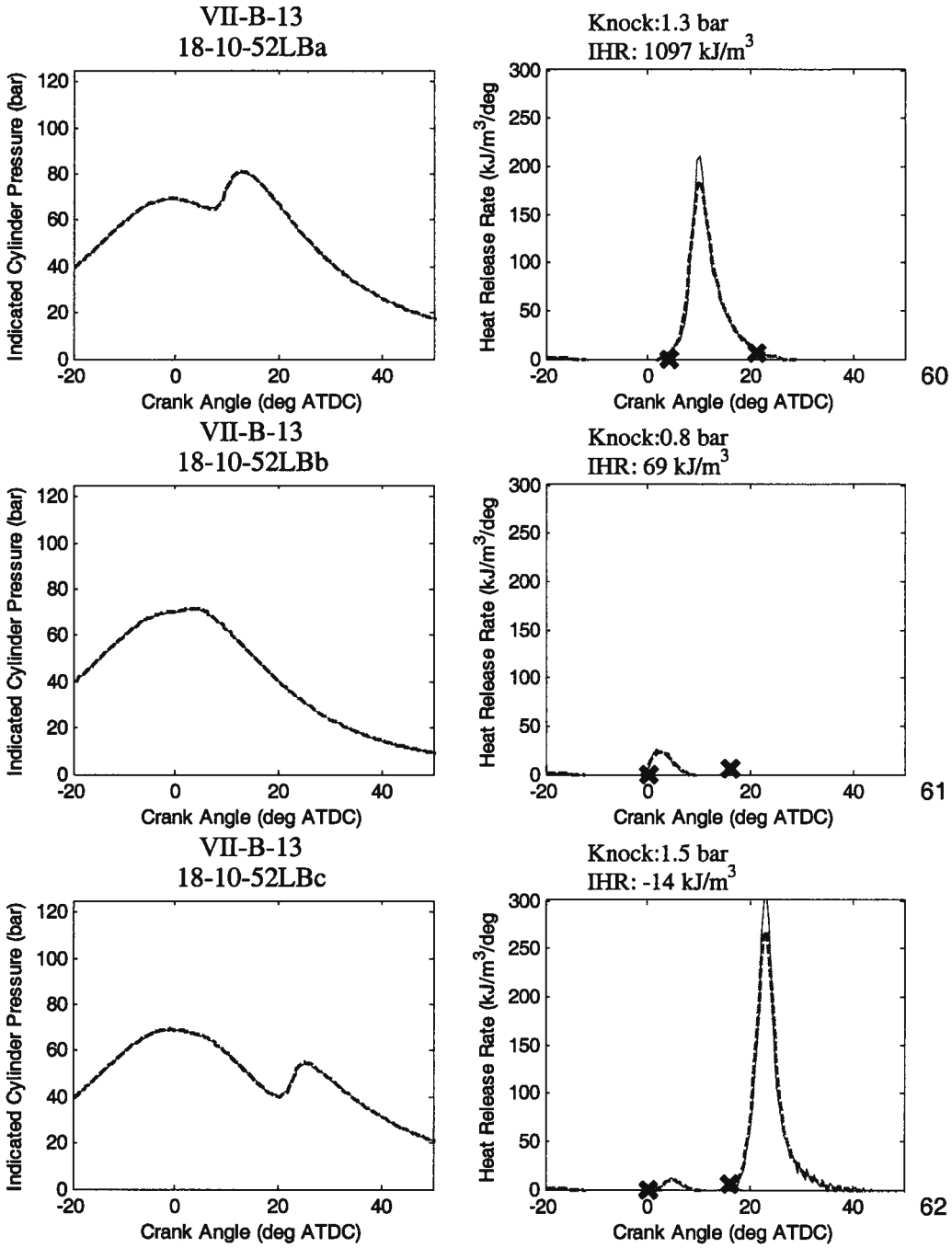

Figures F.3.60 to F.3.62 : Diesel flowrate: 12.7 mg/inj
IHR_{ratio}: -0.20 Knock Ratio: 1.89 Ignition Offset: 0.00 deg

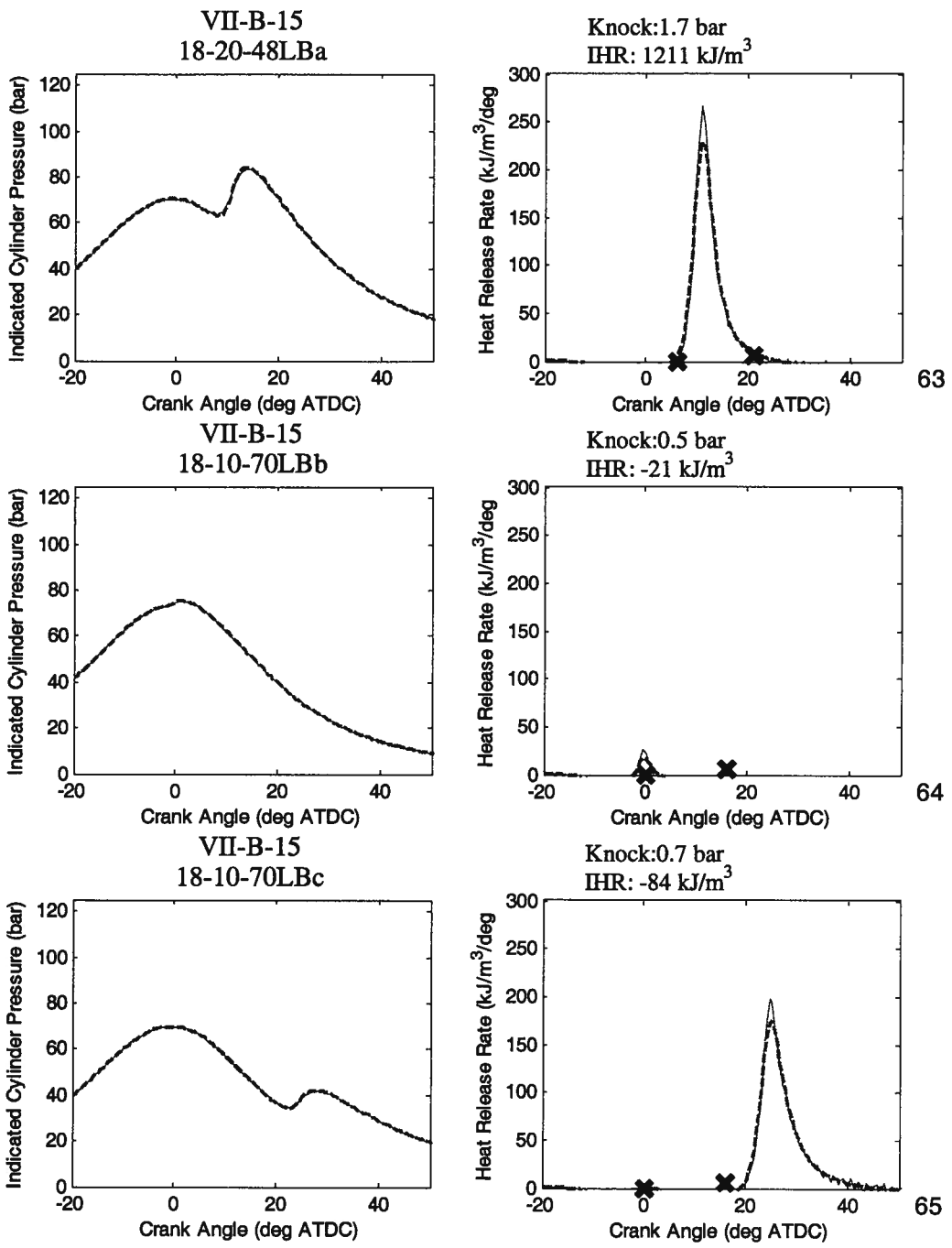

Figures F.3.63 to F.3.65 : Diesel flowrate: 15.6 mg/inj
IHR_{ratio}: 3.99 Knock Ratio: 1.44 Ignition Offset: 0.00 deg

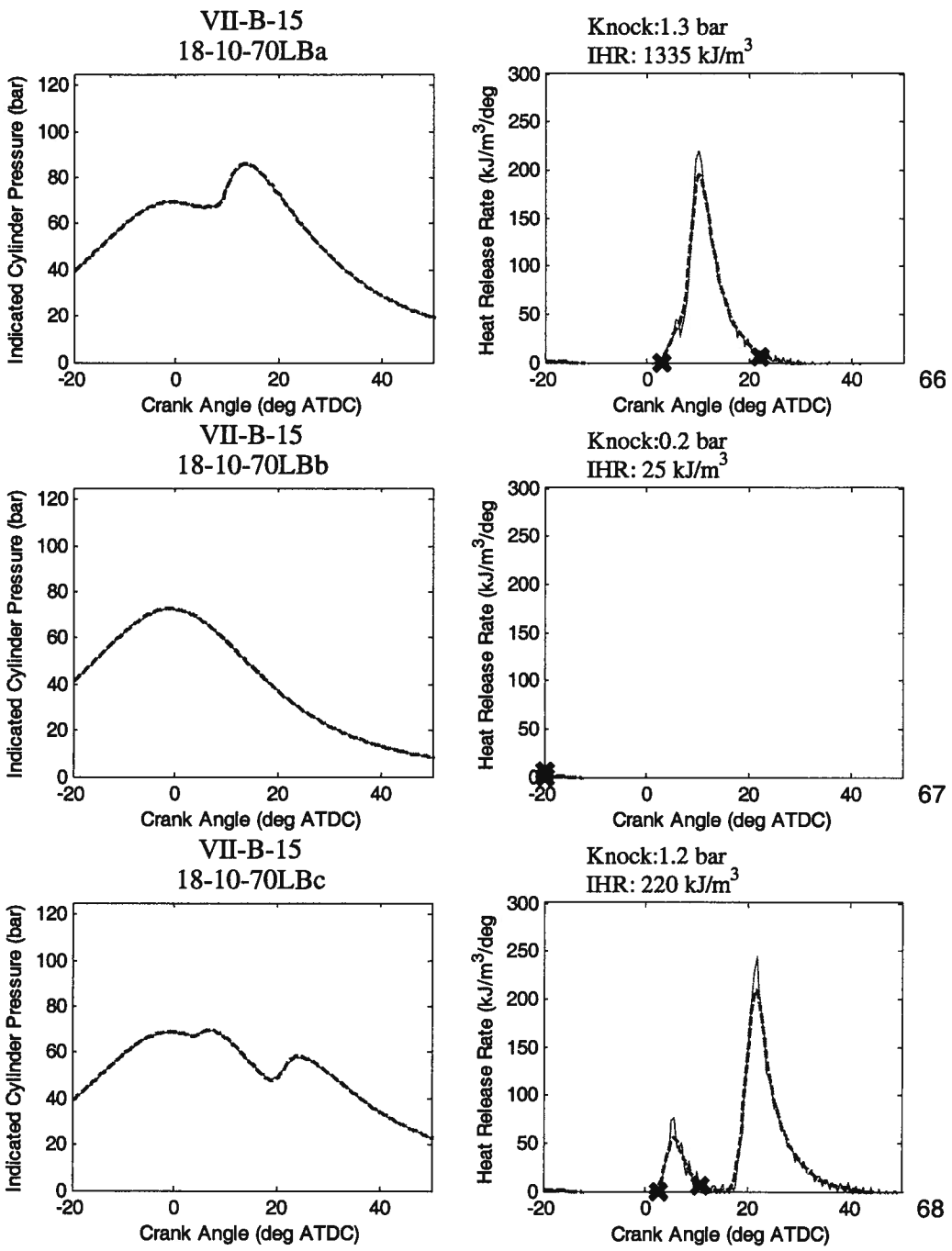

Figures F.3.66 to F.3.68 : Diesel flowrate: 11.8 mg/inj
IHR_{ratio}: 8.91 Knock Ratio: 7.69 Ignition Offset: 22.49 deg

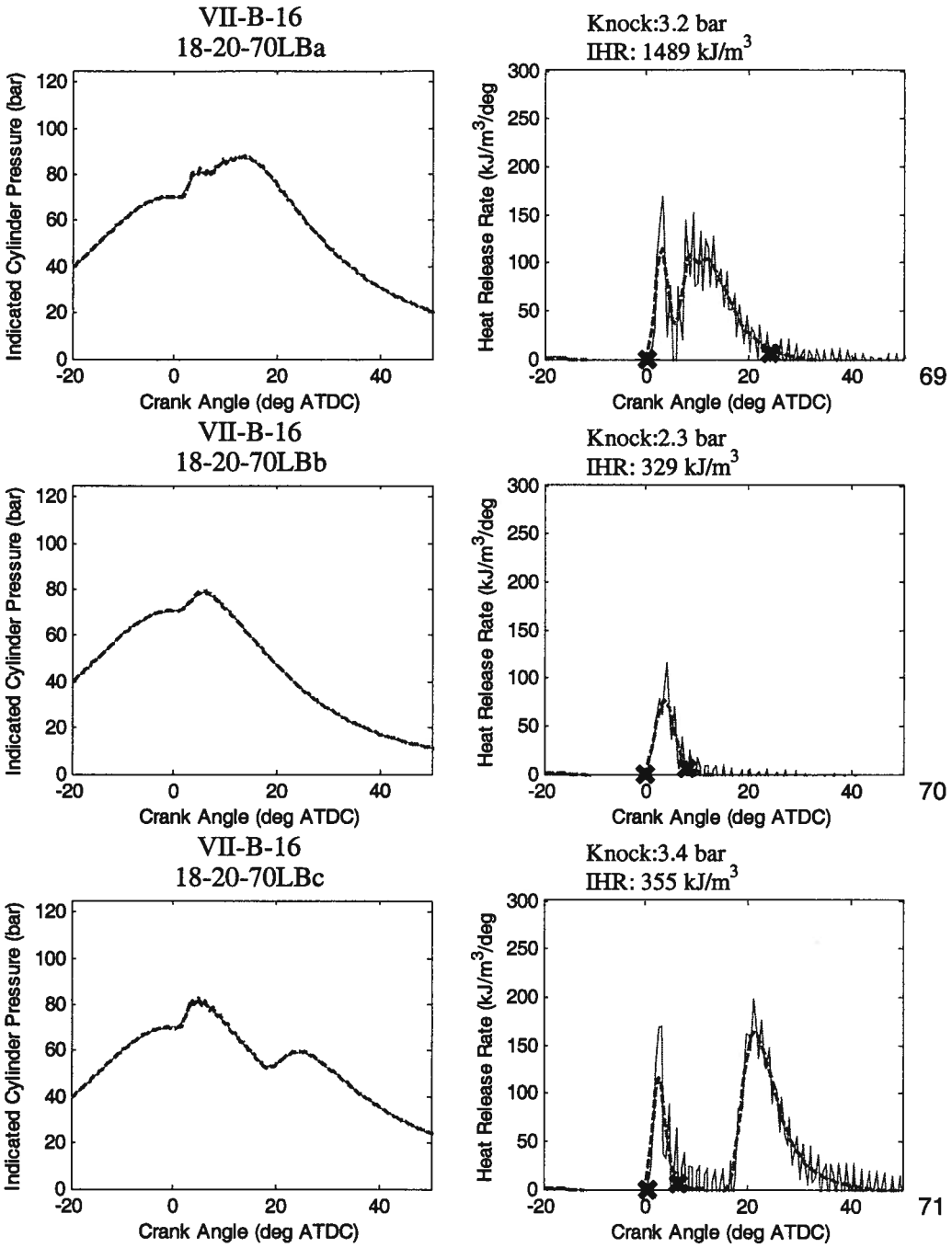

Figures F.3.69 to F.3.71 : Diesel flowrate: 15.8 mg/inj
IHR_{ratio}: 1.08 Knock Ratio: 1.48 Ignition Offset: 0.59 deg

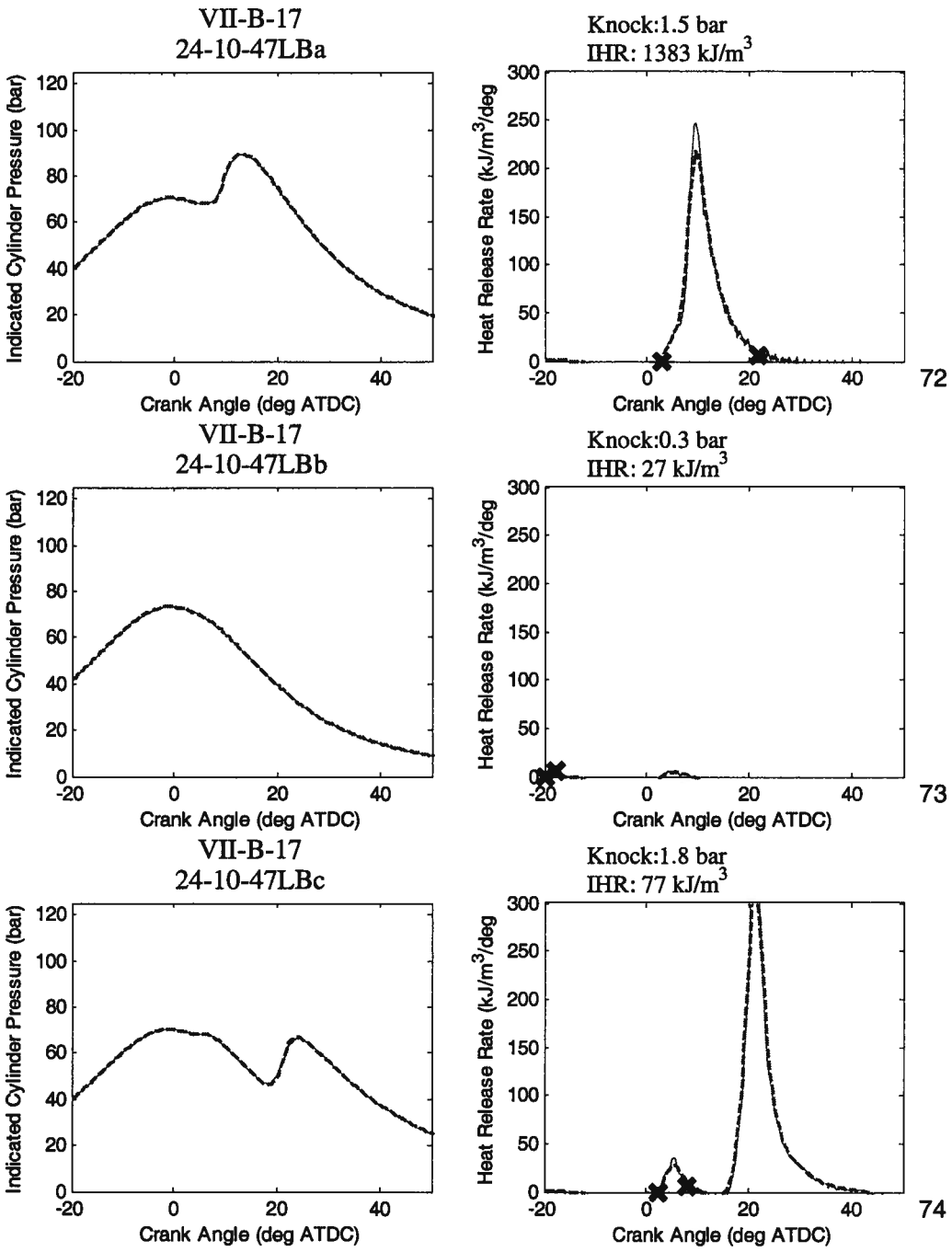

Figures F.3.72 to F.3.74 : Diesel flowrate: 12.6 mg/inj
IHR_{ratio}: 2.90 Knock Ratio: 6.25 Ignition Offset: 22.40 deg

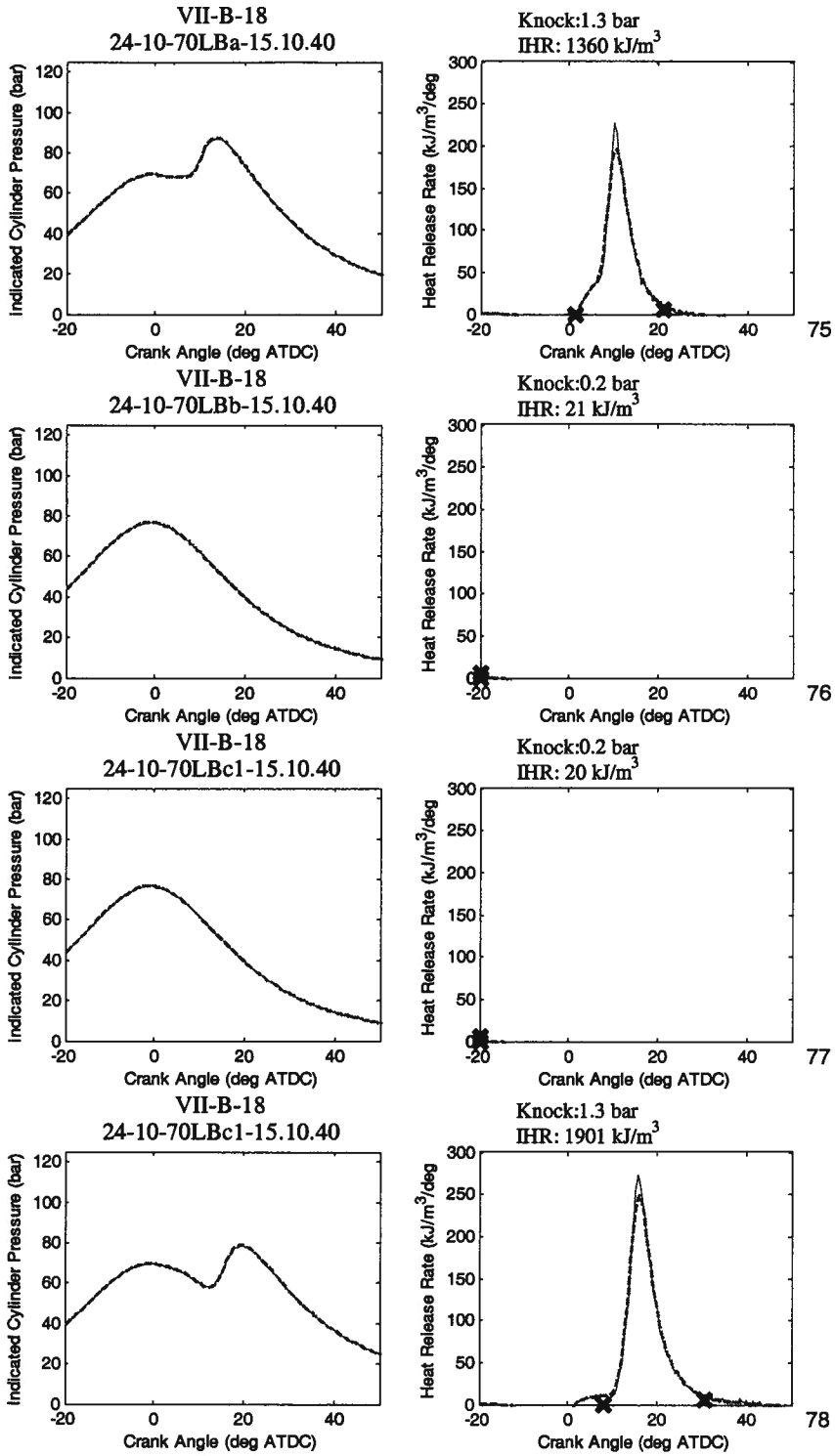

Figures F.3.76 to F.3.78 : Diesel flowrate: 19.2 mg/inj
IHR_{ratio}: 93.02 Knock Ratio: 7.34 Ignition Offset: 27.94 deg

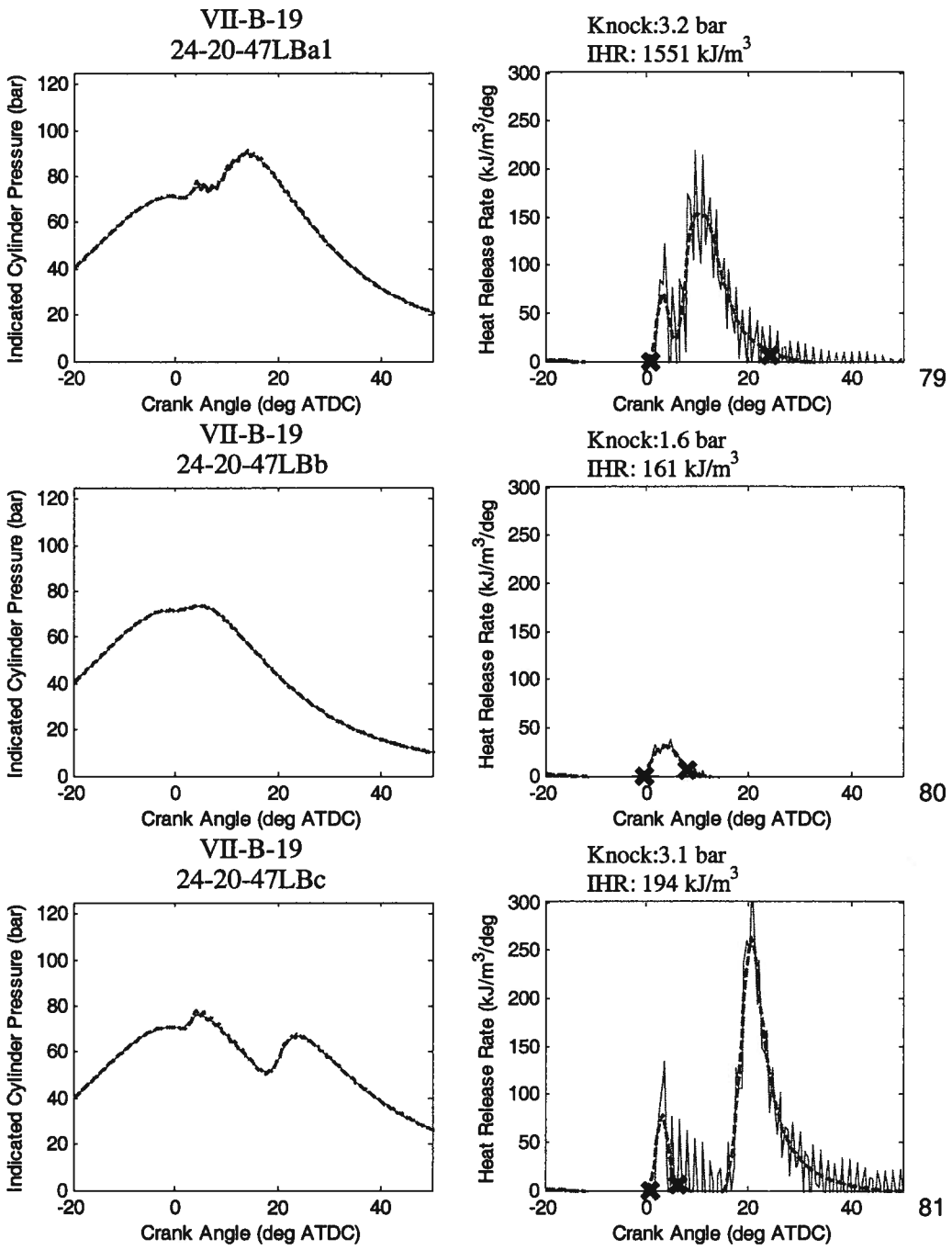

Figures F.3.79 to F.3.81 : Diesel flowrate: 13.1 mg/inj
IHR_{ratio}: 1.20 Knock Ratio: 1.93 Ignition Offset: 1.09 deg

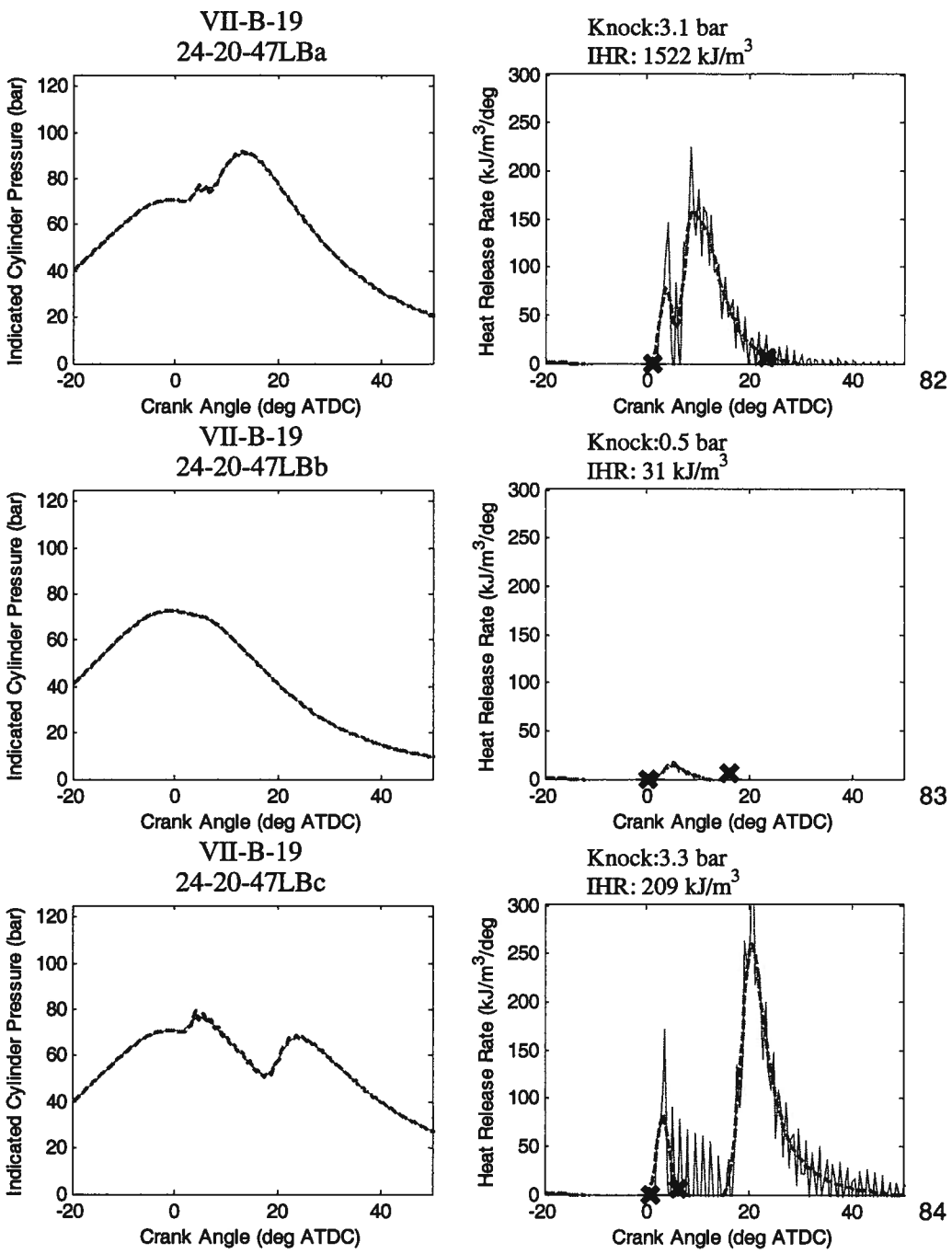

Figures F.3.82 to F.3.84 : Diesel flowrate: 13.3 mg/inj
IHR_{ratio}: 6.67 Knock Ratio: 6.24 Ignition Offset: 0.56 deg

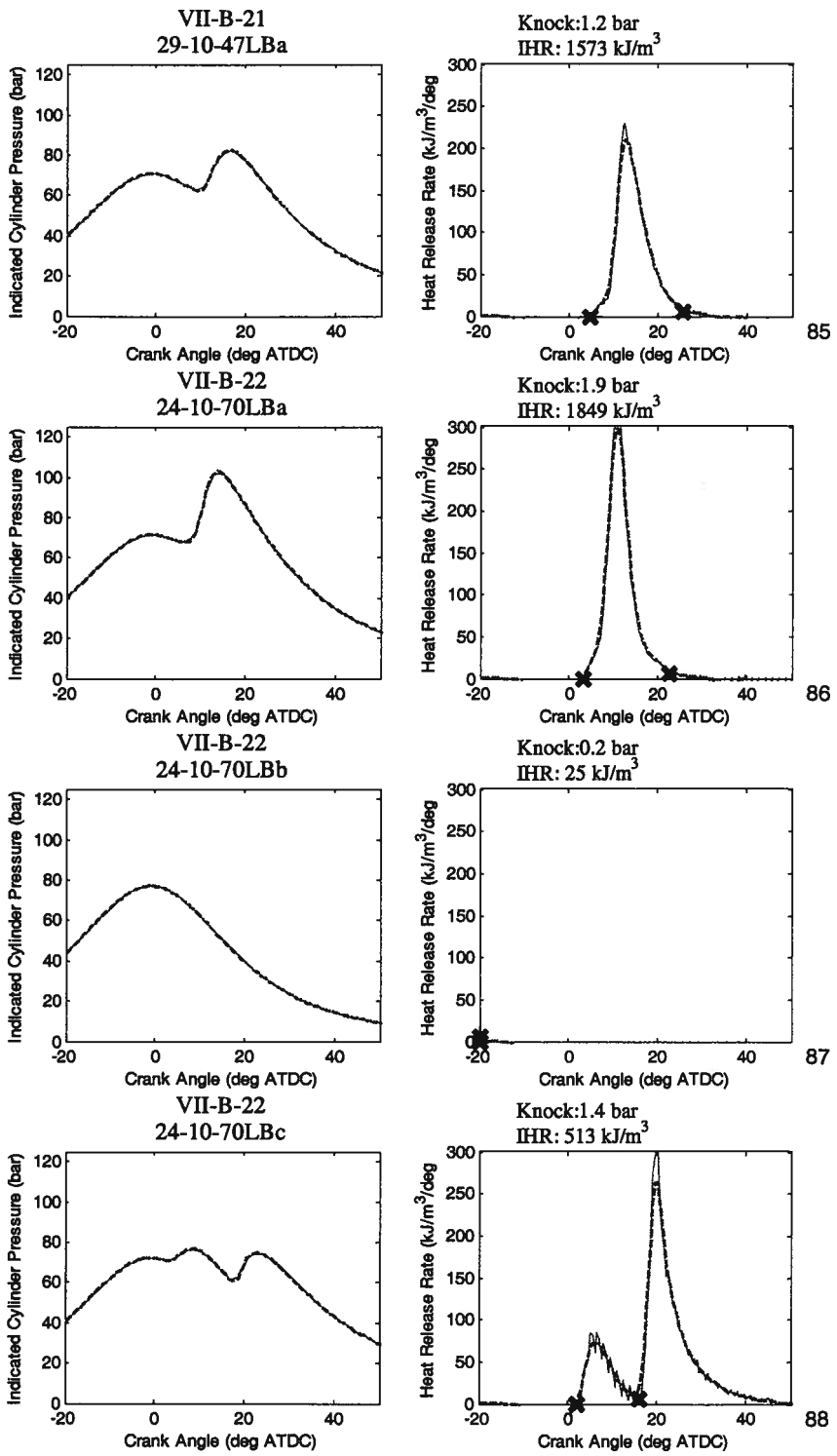

Figures F.3.86 to F.3.88 : Diesel flowrate: 10.8 mg/inj
IHR_{ratio}: 20.29 Knock Ratio: 7.58 Ignition Offset: 22.01 deg

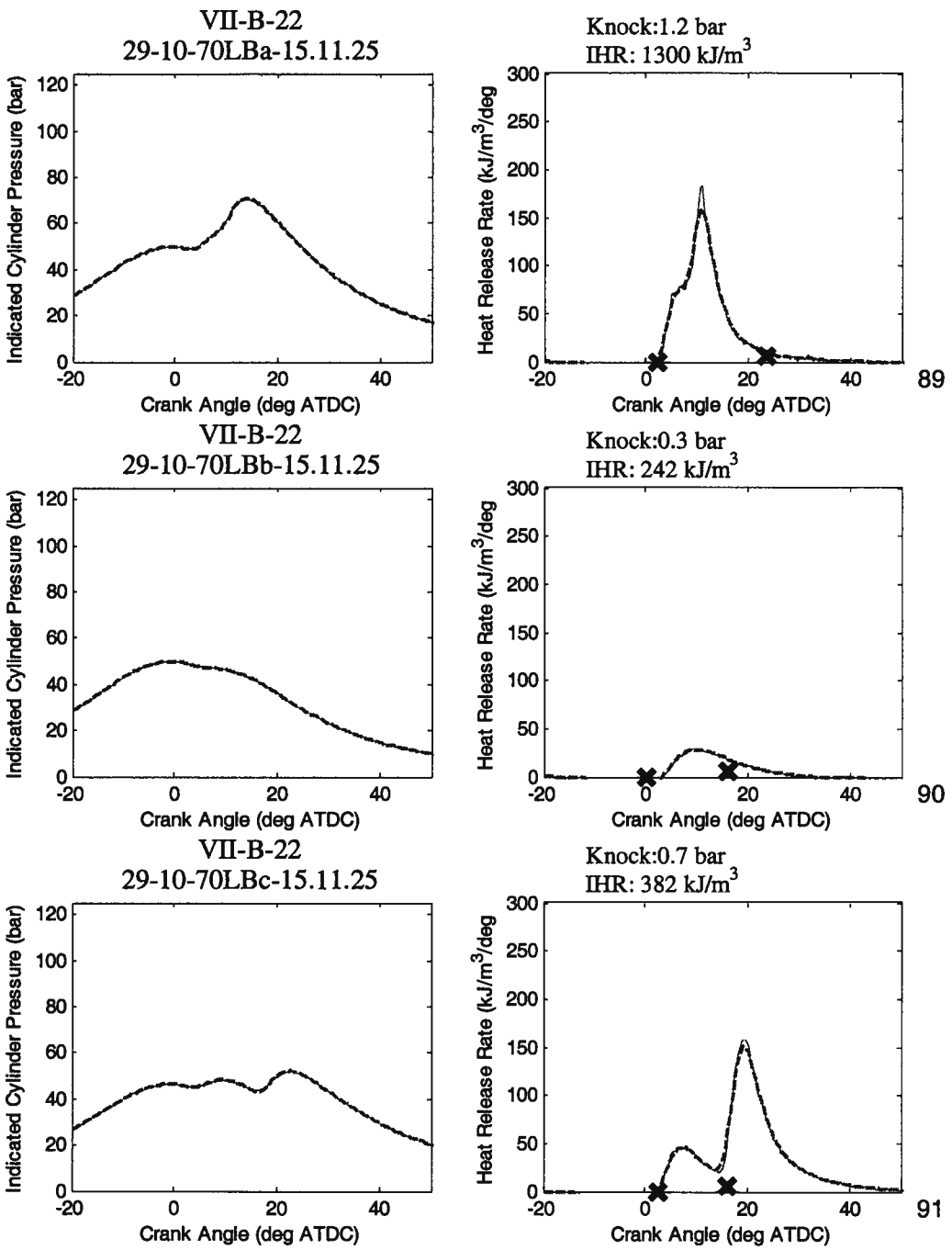

Figures F.3.89 to F.3.91 : Diesel flowrate: 14.3 mg/inj
IHR_{ratio}: 1.58 Knock Ratio: 2.60 Ignition Offset: 2.53 deg

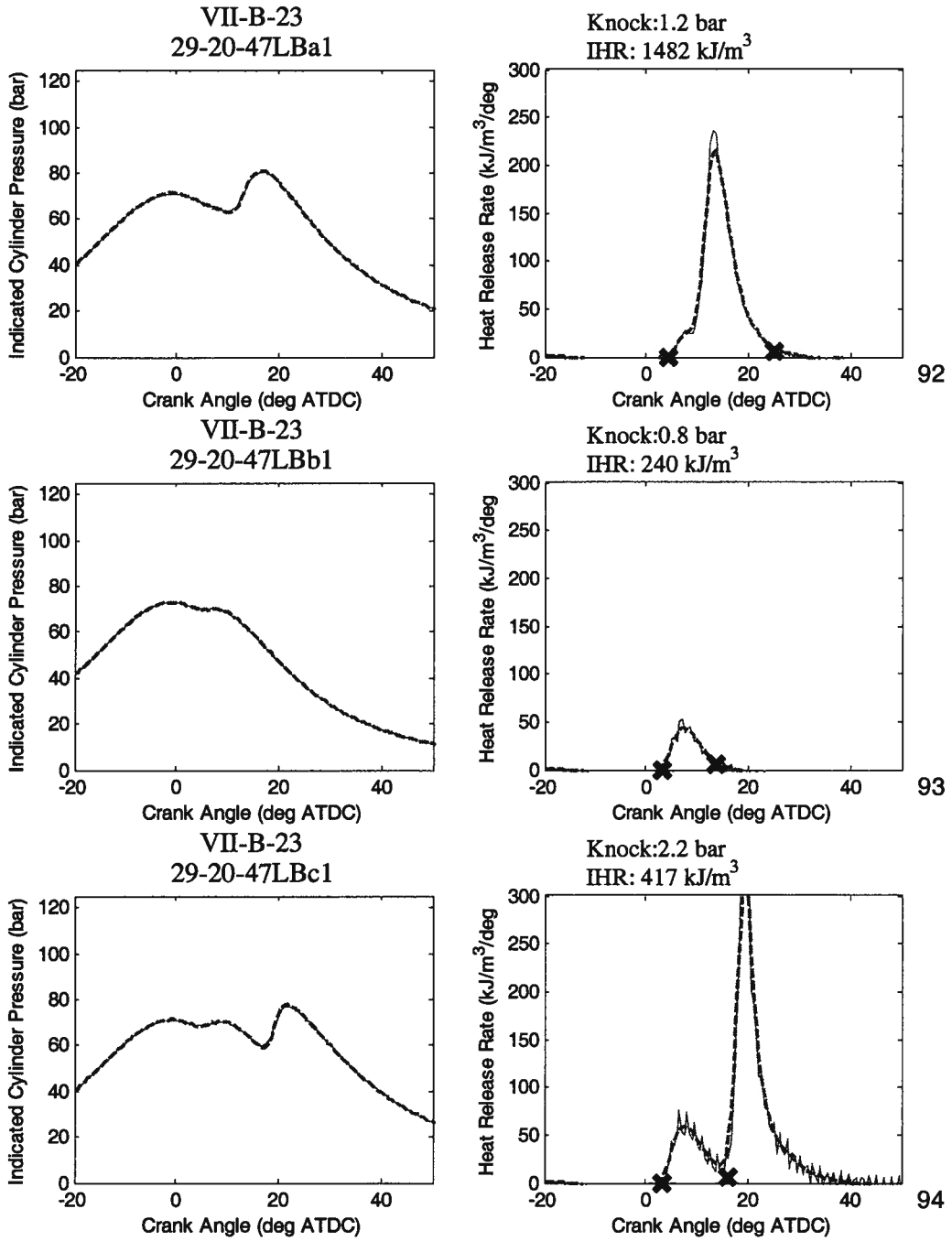

Figures F.3.92 to F.3.94 : Diesel flowrate: 7.2 mg/inj
IHR_{ratio}: 1.74 Knock Ratio: 2.74 Ignition Offset: 0.08 deg

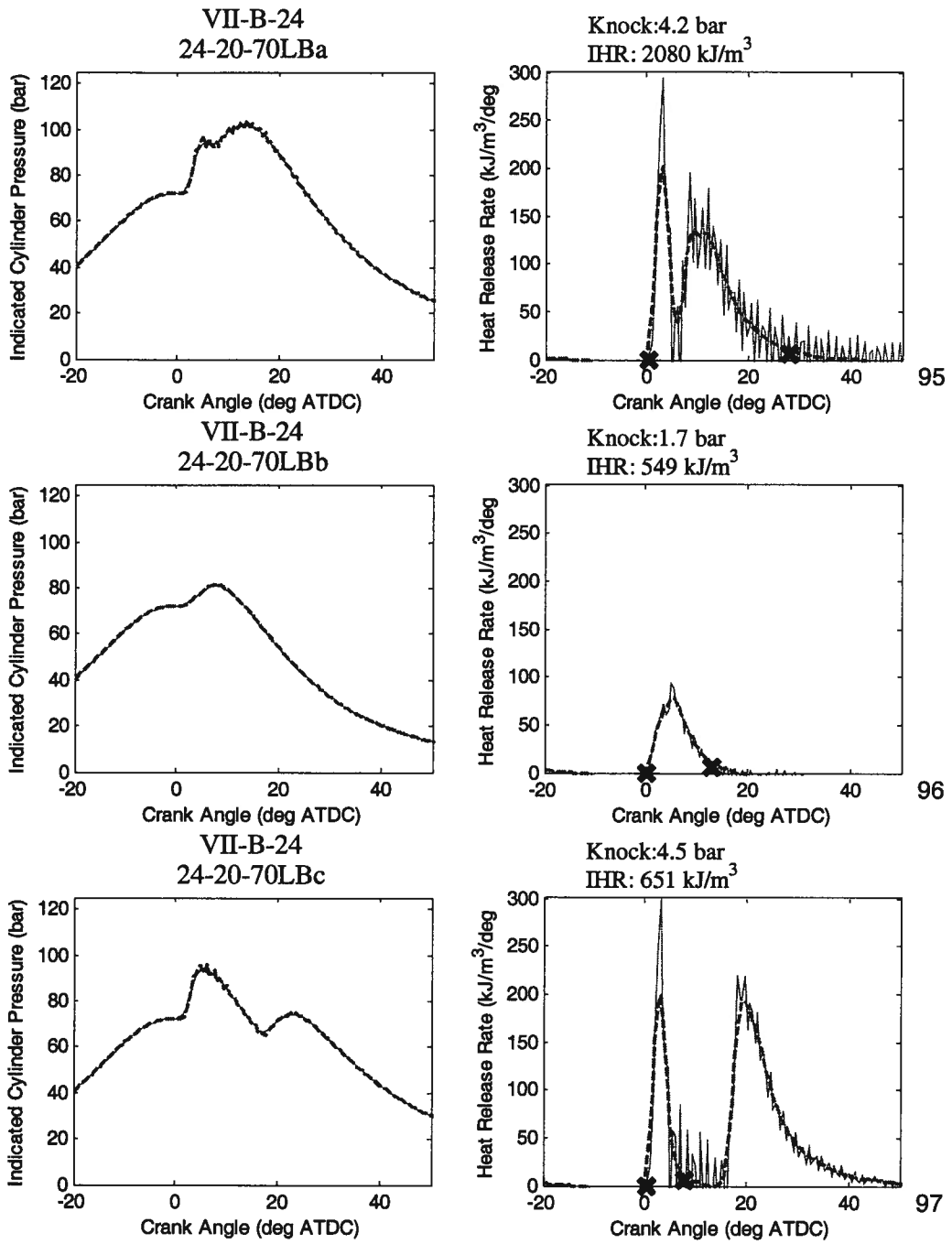

Figures F.3.95 to F.3.97 : Diesel flowrate: 23.3 mg/inj
IHR_{ratio}: 1.19 Knock Ratio: 2.68 Ignition Offset: 0.30 deg

Appendix F.4- Test Series VII-B-1200 RPM Pressure and HRR Curves

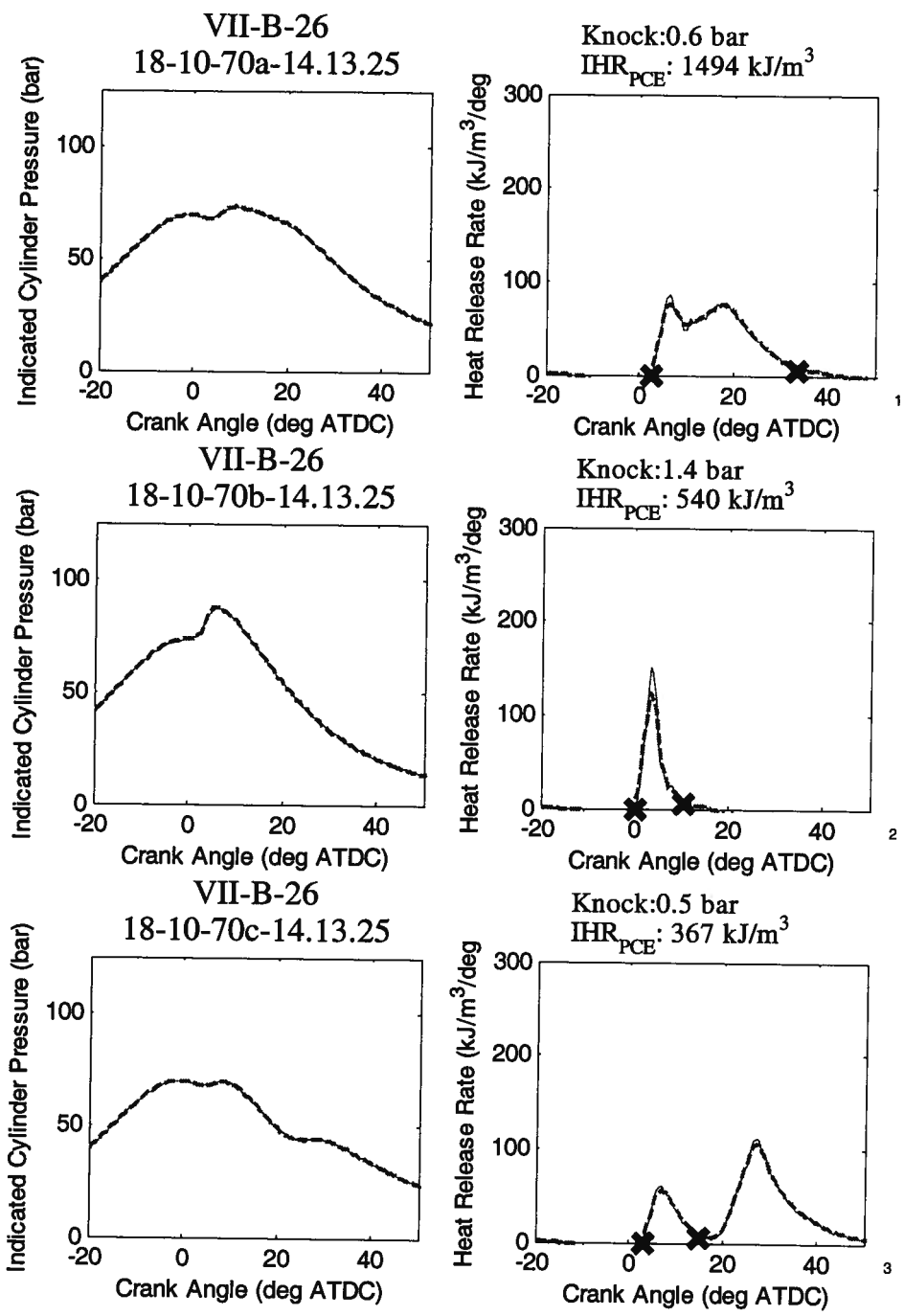

Figures E.4.1 to E.4.3 : Diesel flowrate: 10.0 mg/inj
IHR$_{ratio}$: 0.68 Knock Ratio: 0.32 Ignition Offset: 2.78 deg

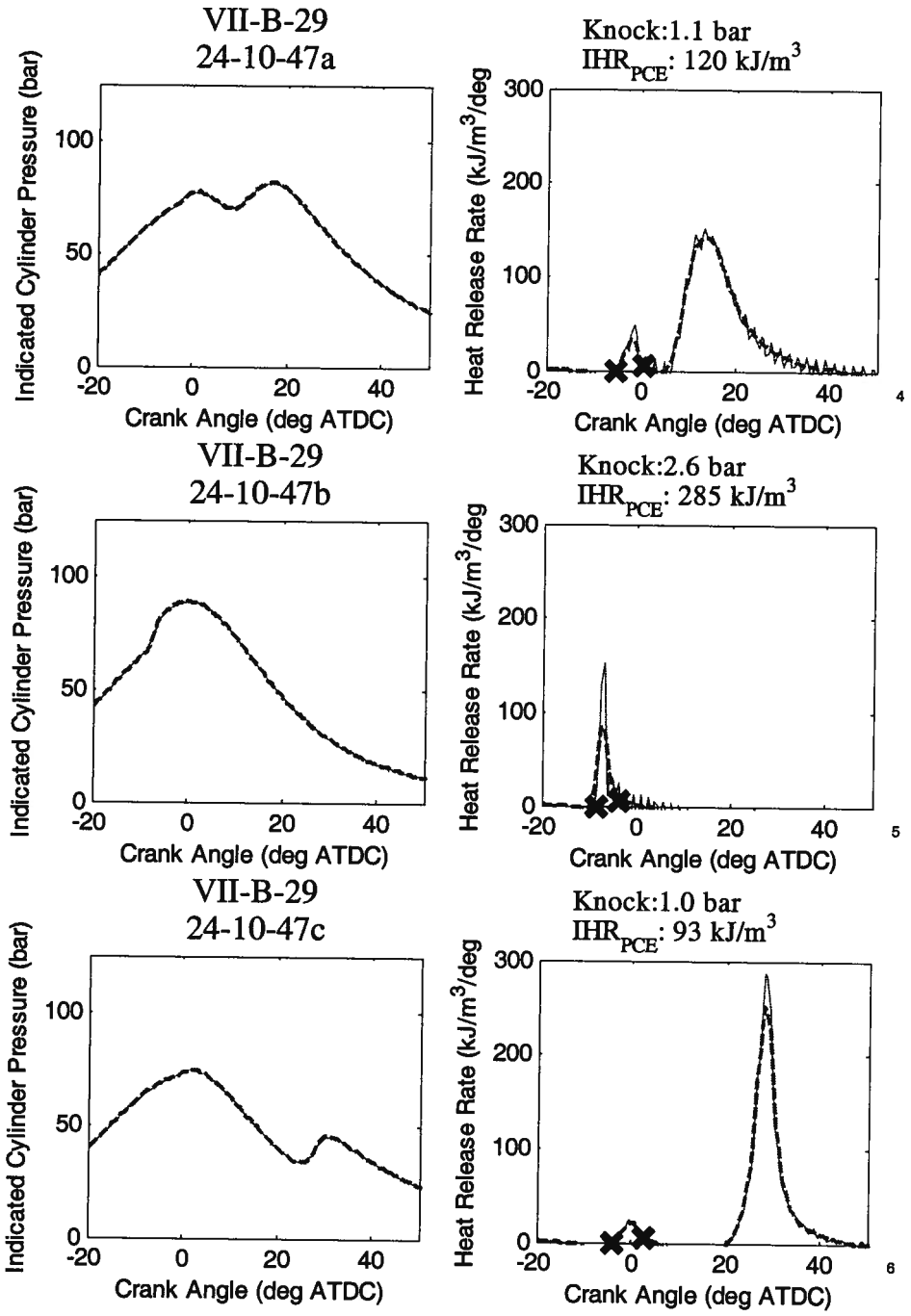

Figures E.4.4 to E.4.6 : Diesel flowrate: 8.1 mg/inj
IHR$_{ratio}$: 0.33 Knock Ratio: 0.40 Ignition Offset: 4.59 deg

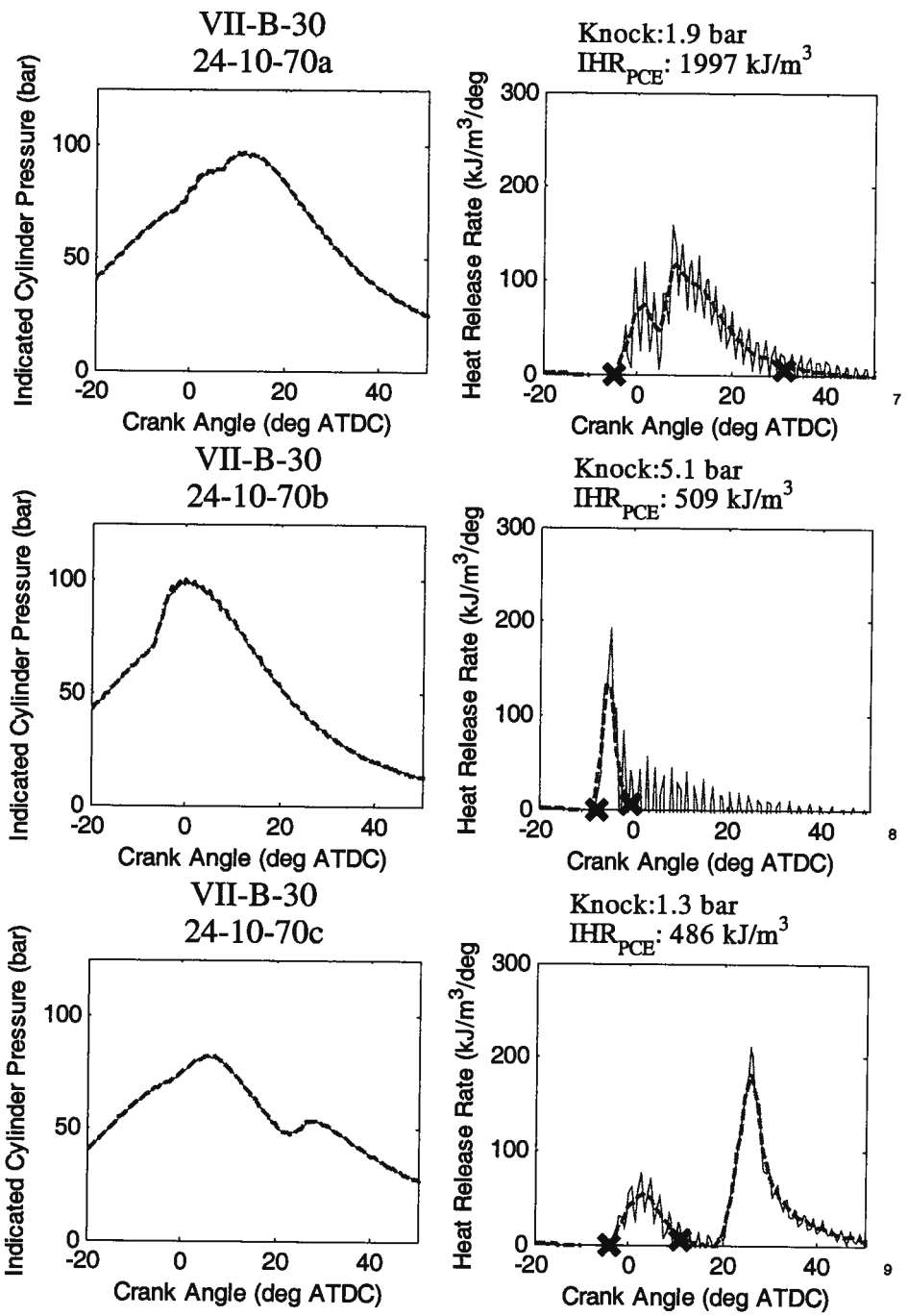

Figures E.4.7 to E.4.9 : Diesel flowrate: 11.8 mg/inj
IHR$_{ratio}$: 0.95 Knock Ratio: 0.25 Ignition Offset: 3.42 deg

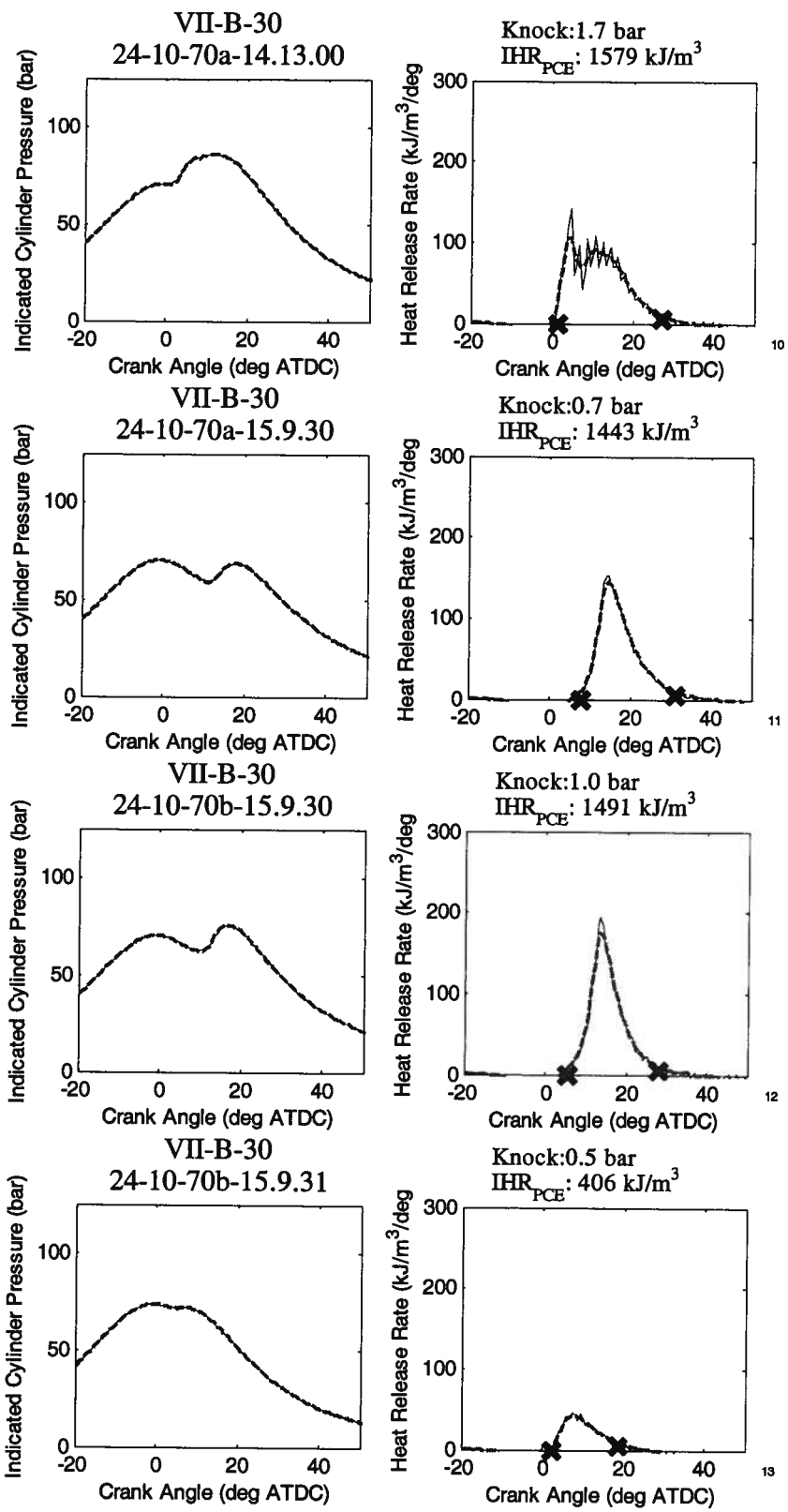

Figures F.10 to F.14: Diesel flowrate: 9.0 mg/inj

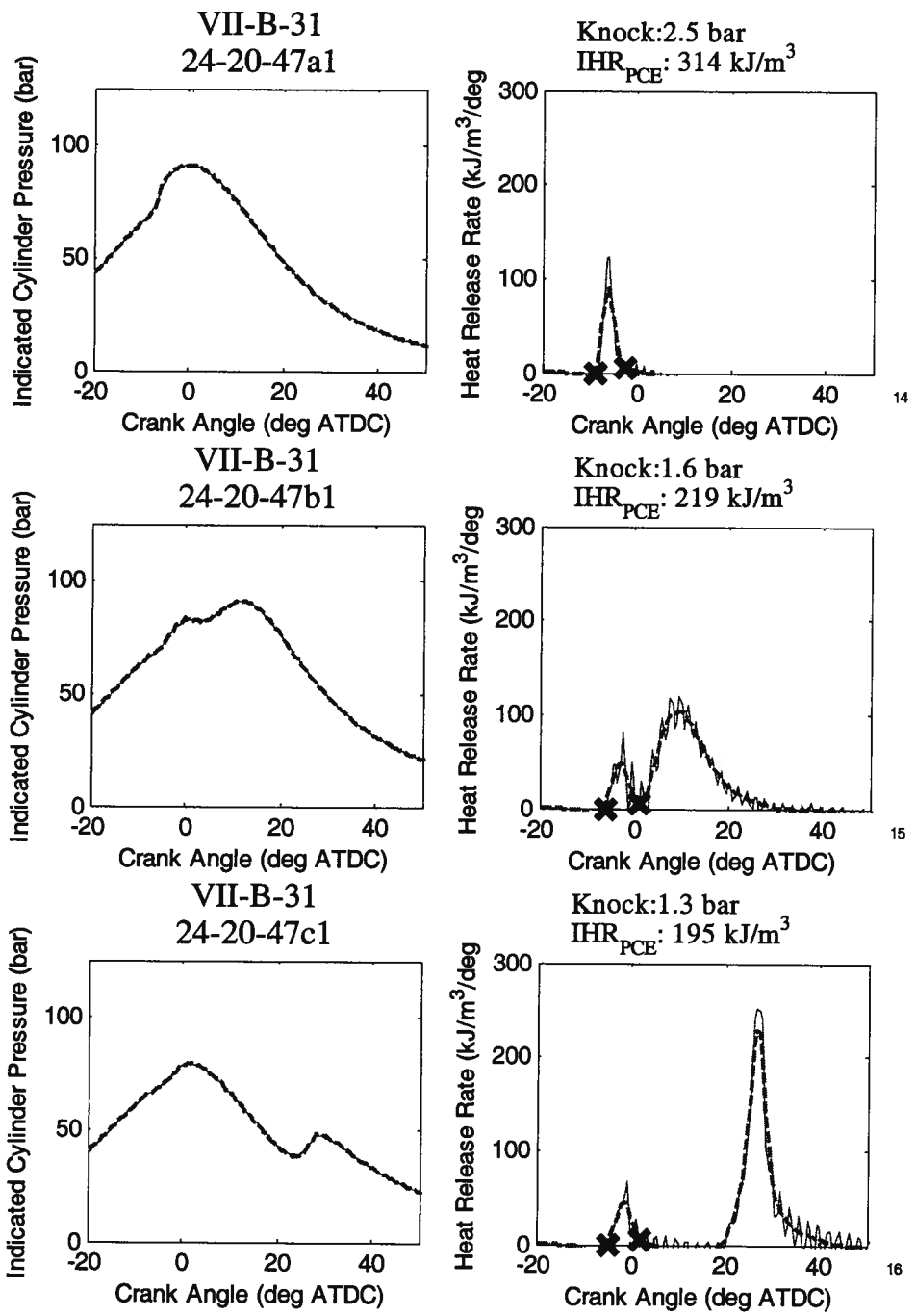

Figures E.4.14 to E.4.16 : Diesel flowrate: 37.9 mg/inj
IHR$_{ratio}$: 0.89 Knock Ratio: 0.81 Ignition Offset: 1.18 deg

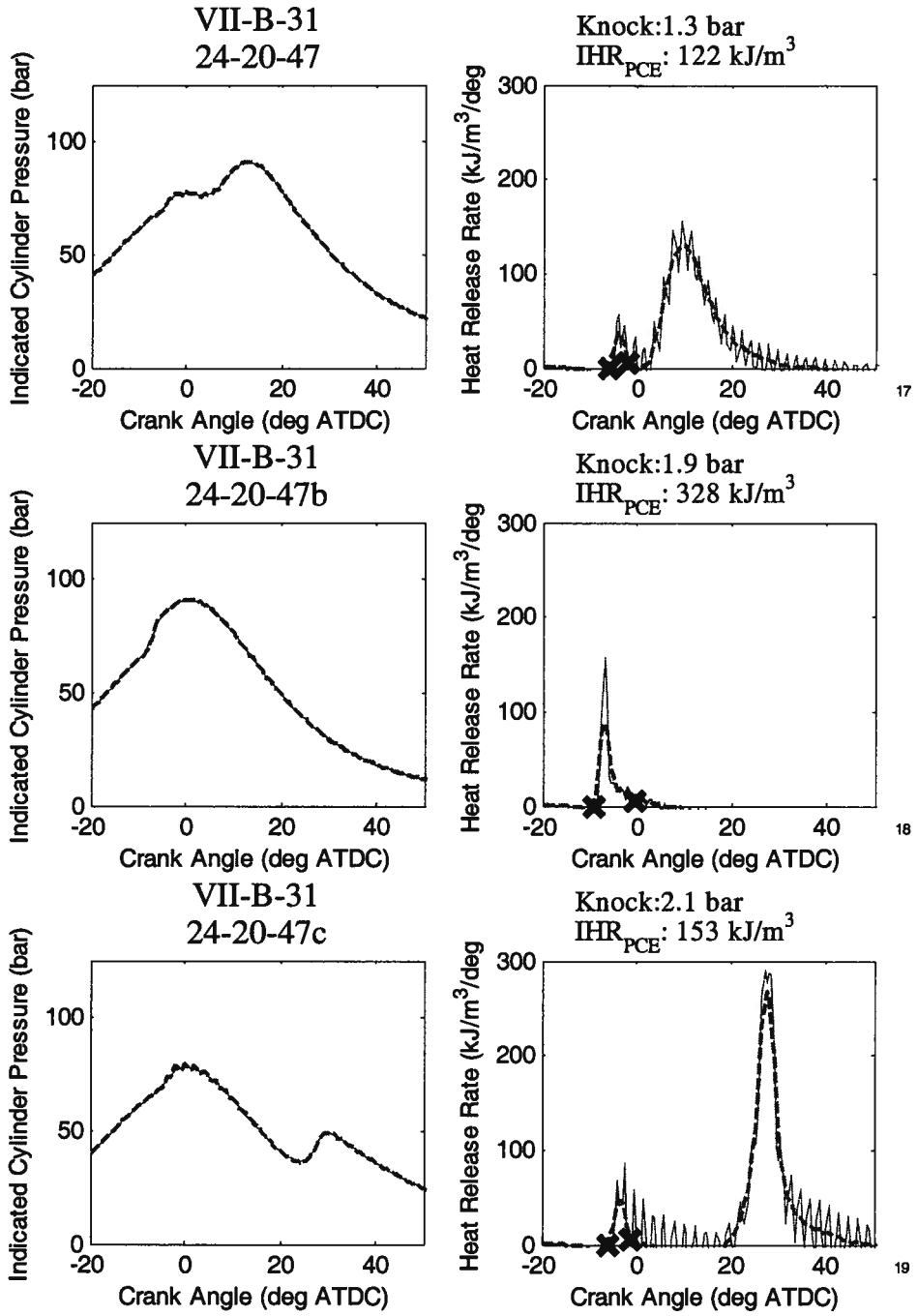

Figures E.4.17 to E.4.19 : Diesel flowrate: 20.4 mg/inj
IHR_{ratio}: 0.47 Knock Ratio: 1.07 Ignition Offset: 3.31 deg

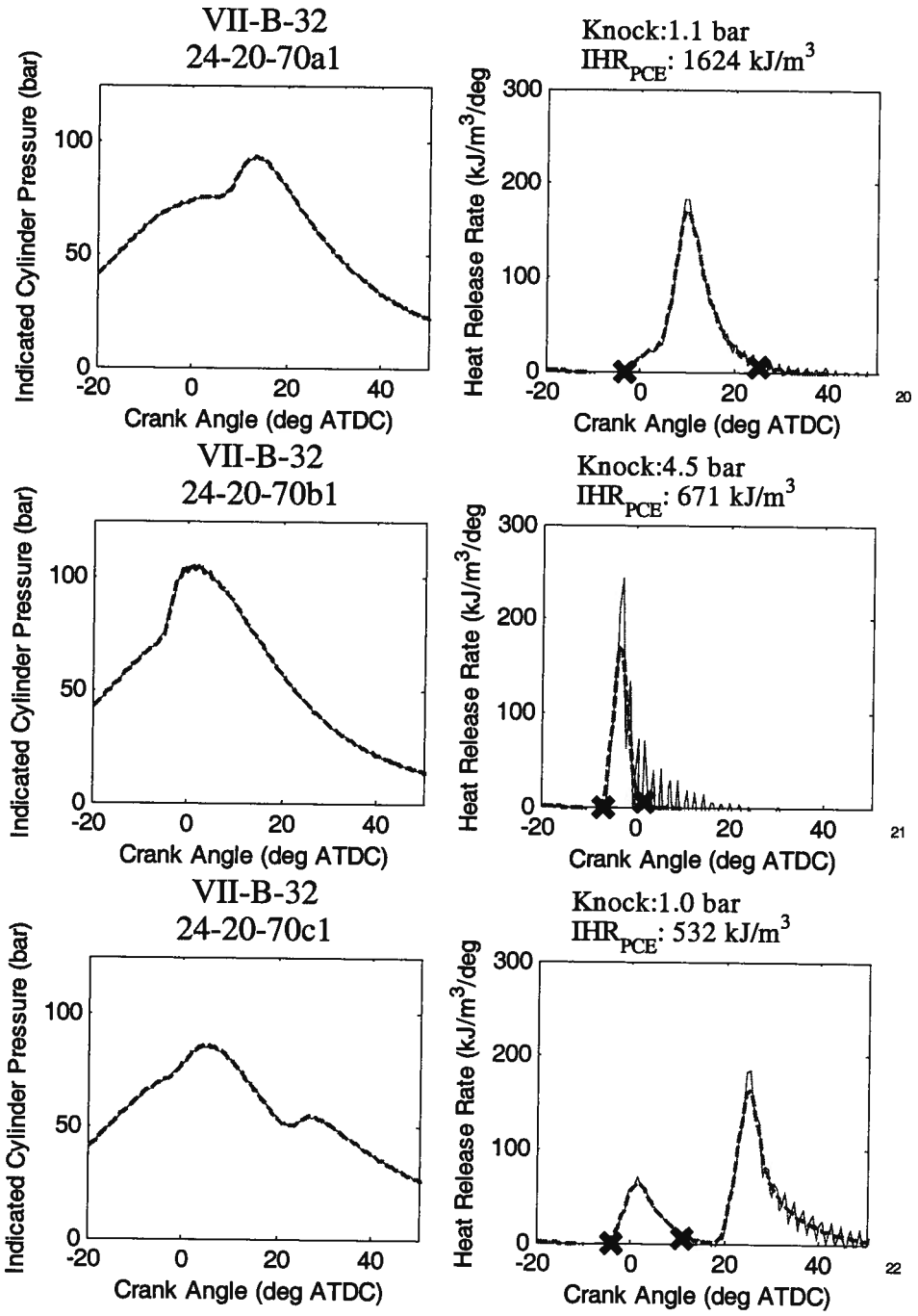

Figures E.4.20 to E.4.22 : Diesel flowrate: 8.1 mg/inj
IHR_{ratio}: 0.79 Knock Ratio: 0.23 Ignition Offset: 2.07 deg

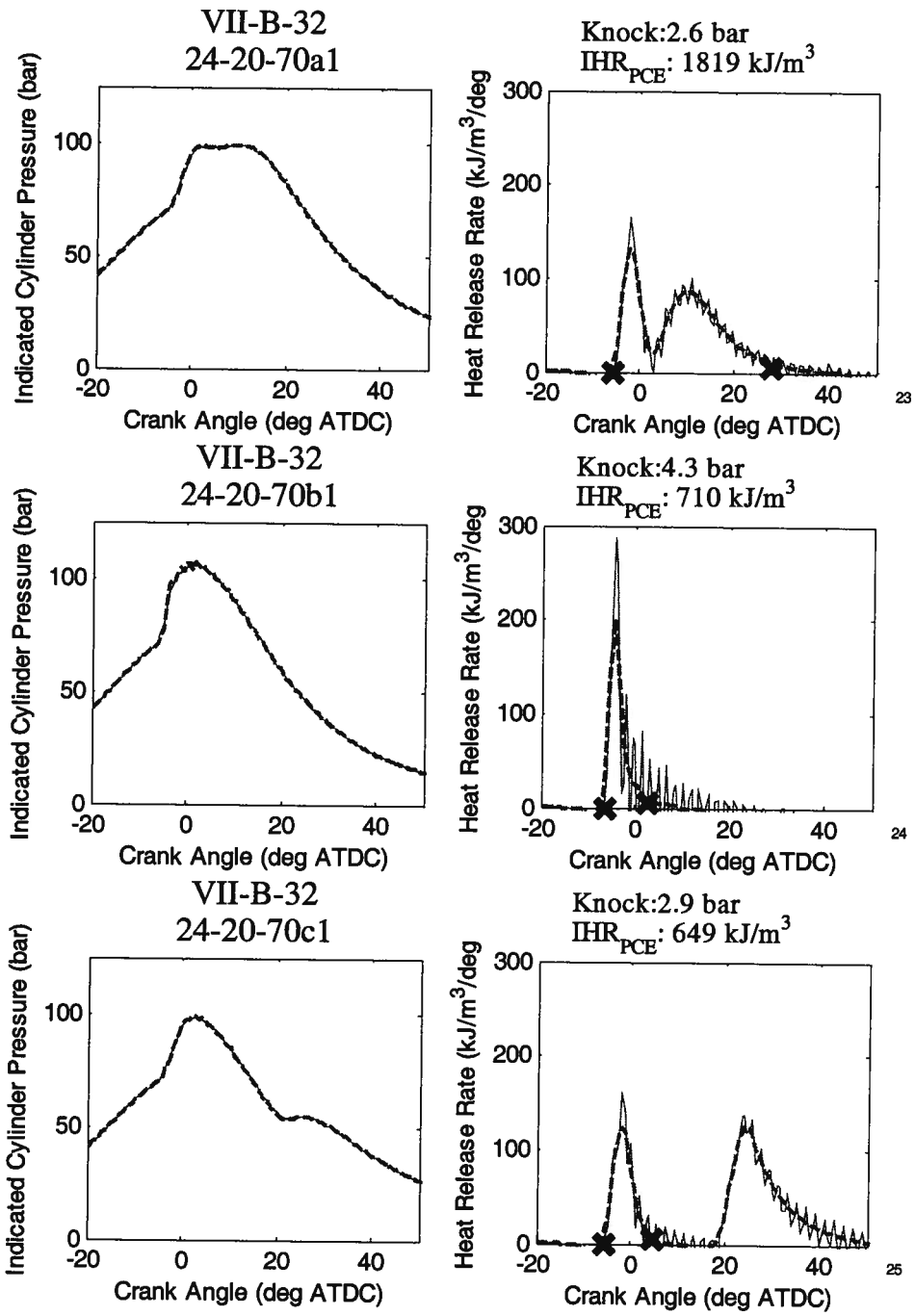

Figures E.4.23 to E.4.25 : Diesel flowrate: 16.8 mg/inj
IHR$_{ratio}$: 0.91 Knock Ratio: 0.66 Ignition Offset: 0.74 deg

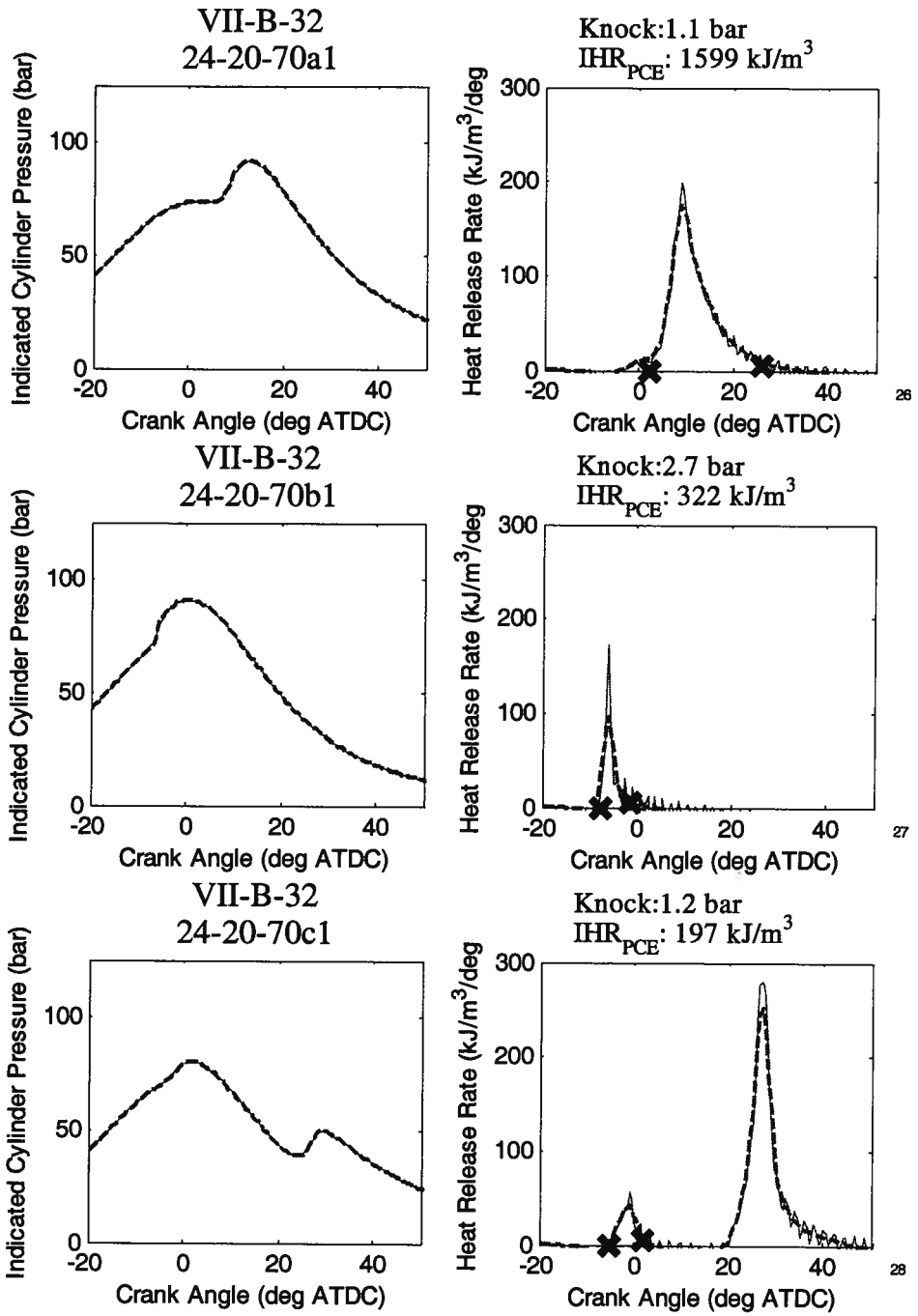

Figures E.4.26 to E.4.28 : Diesel flowrate: 8.9 mg/inj
IHR_{ratio}: 0.61 Knock Ratio: 0.43 Ignition Offset: 2.34 deg

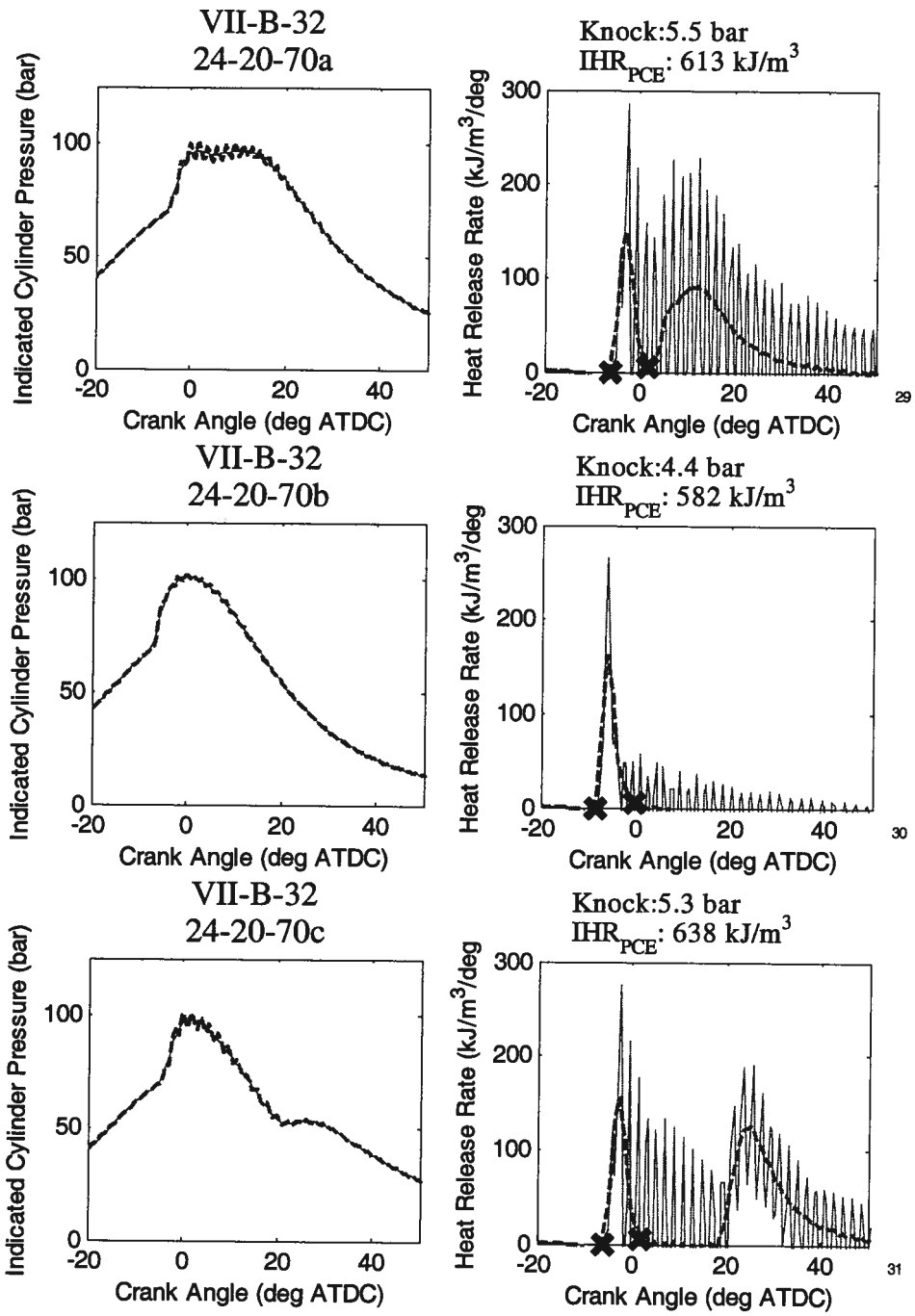

Figures E.4.29 to E.4.31 : Diesel flowrate: 19.8 mg/inj
IHR_{ratio}: 1.10 Knock Ratio: 1.21 Ignition Offset: 2.36 deg

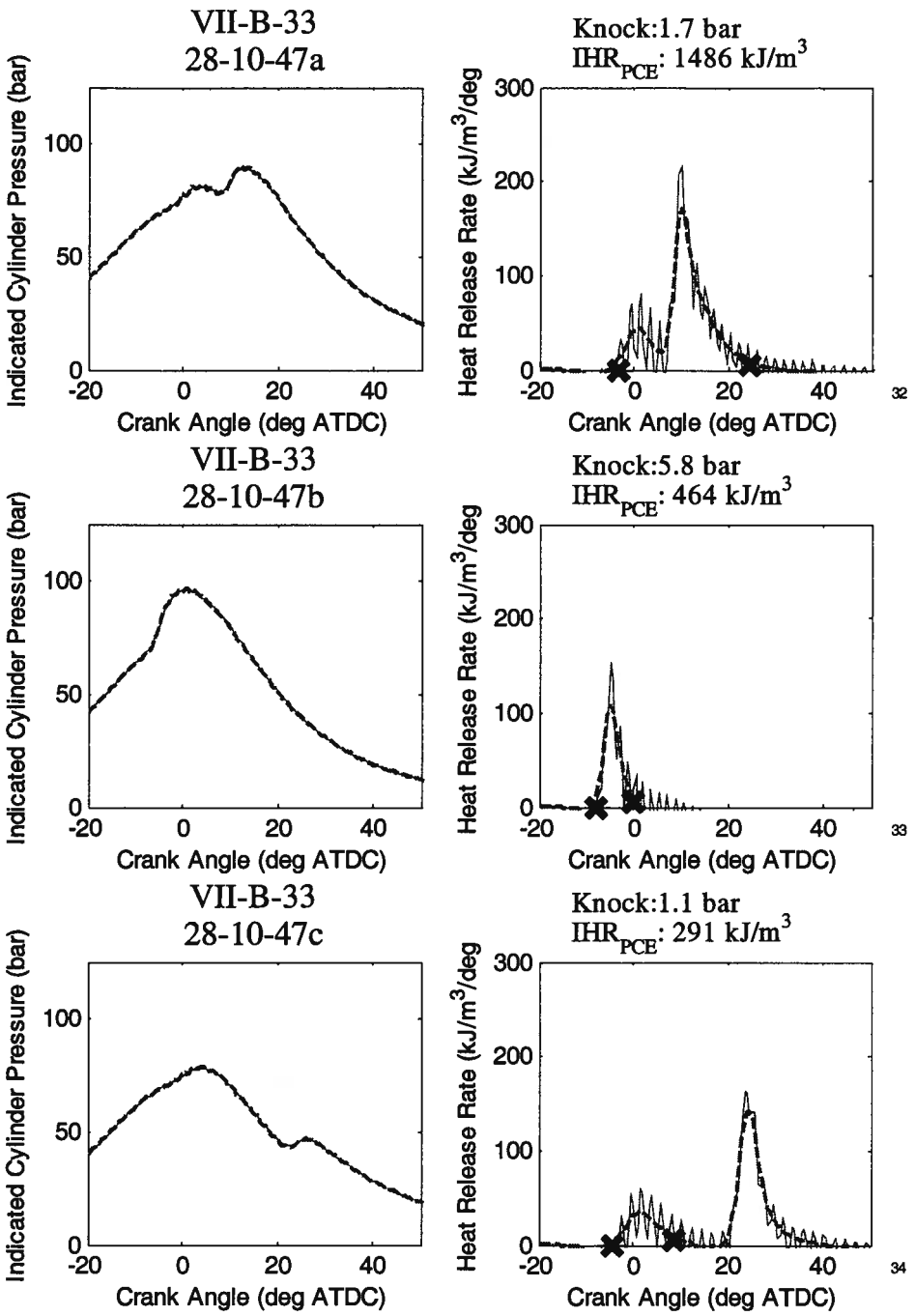

Figures E.4.32 to E.4.34 : Diesel flowrate: 9.5 mg/inj
IHR_{ratio}: 0.63 Knock Ratio: 0.20 Ignition Offset: 3.54 deg

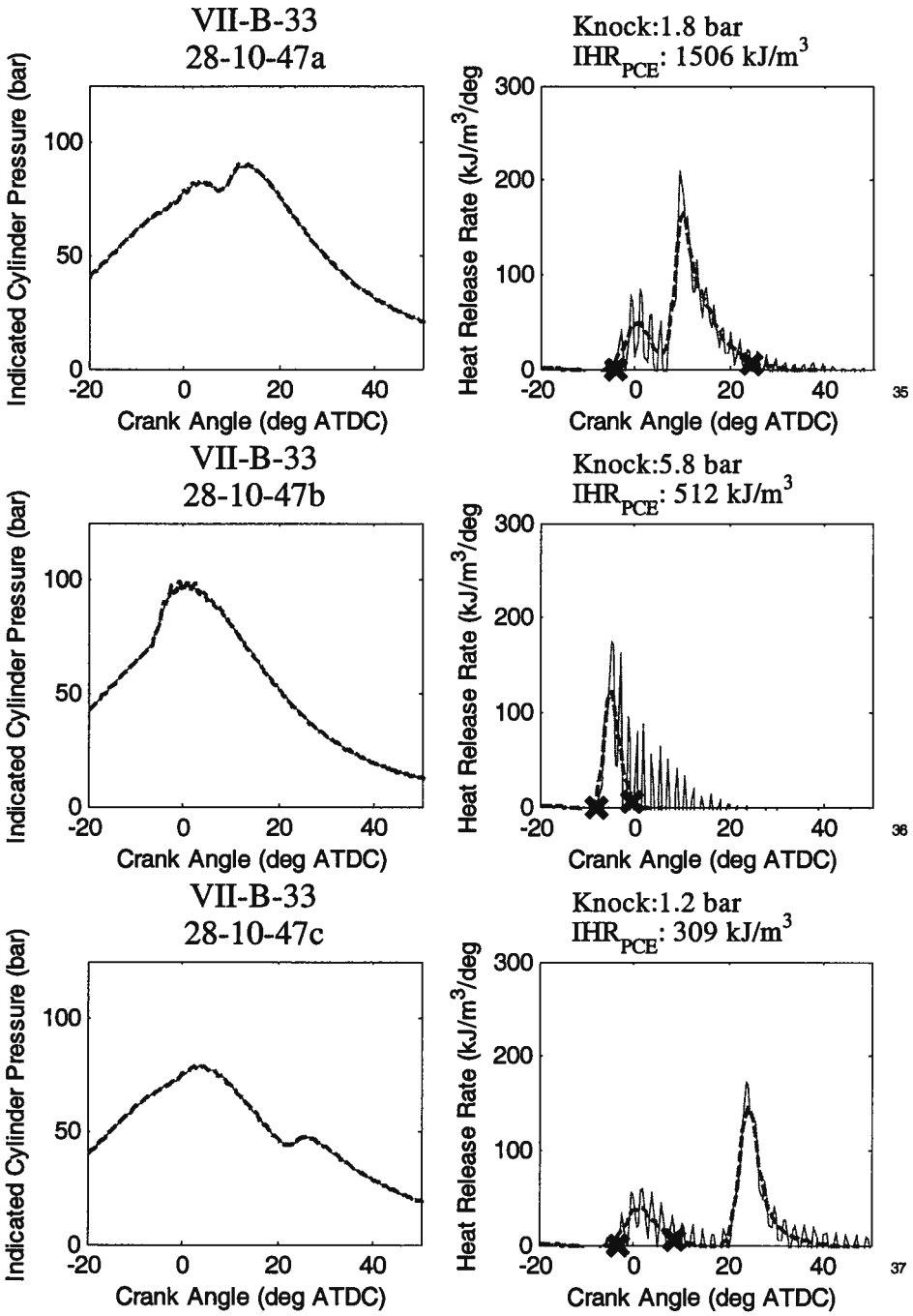

Figures E.4.35 to E.4.37 : Diesel flowrate: 11.4 mg/inj
IHR$_{ratio}$: 0.60 Knock Ratio: 0.21 Ignition Offset: 4.77 deg

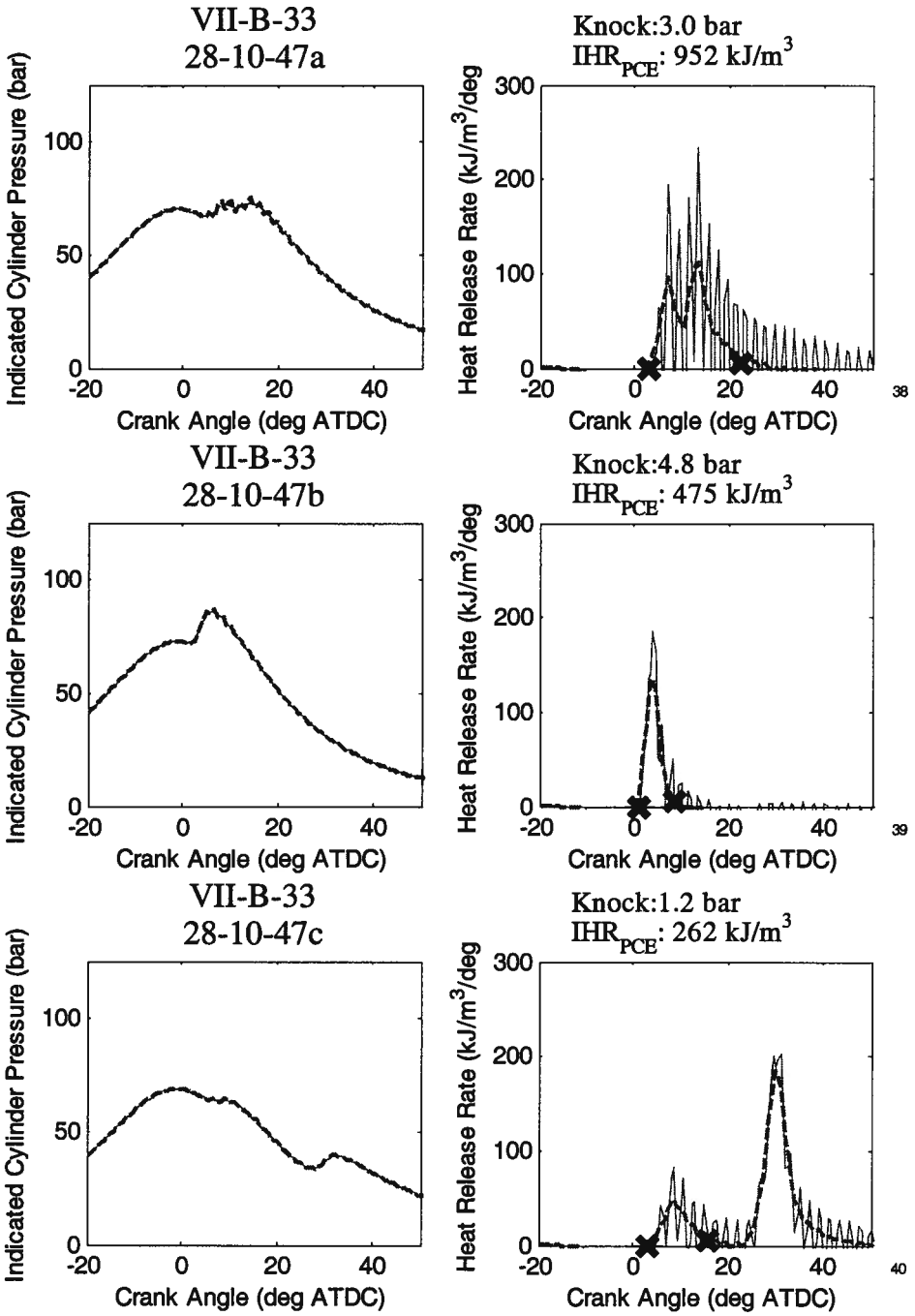

Figures E.4.38 to E.4.40 : Diesel flowrate: 21.1 mg/inj
IHR$_{ratio}$: 0.55 Knock Ratio: 0.25 Ignition Offset: 2.29 deg

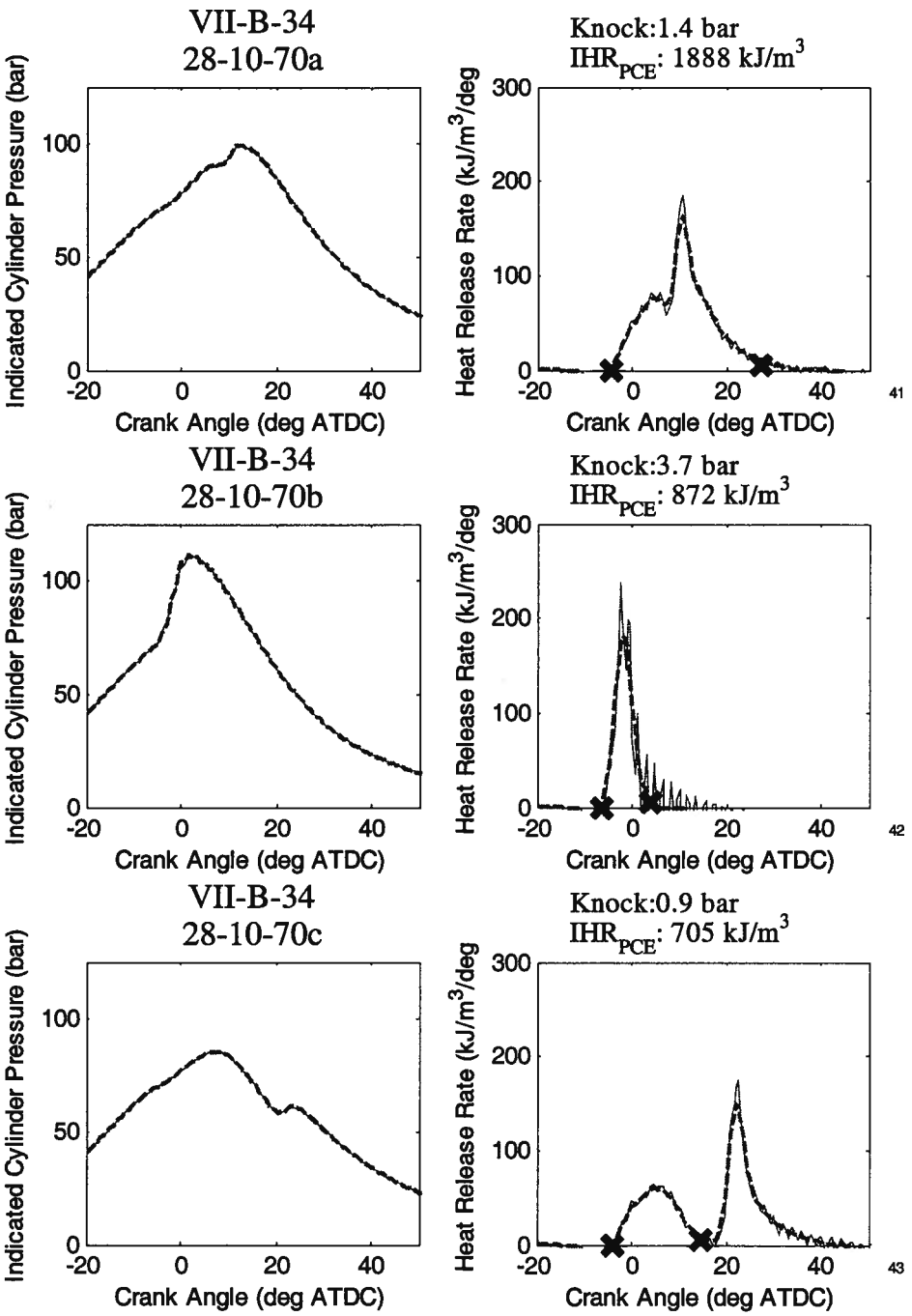

Figures E.4.41 to E.4.43 : Diesel flowrate: 12.3 mg/inj
IHR$_{ratio}$: 0.81 Knock Ratio: 0.24 Ignition Offset: 2.24 deg

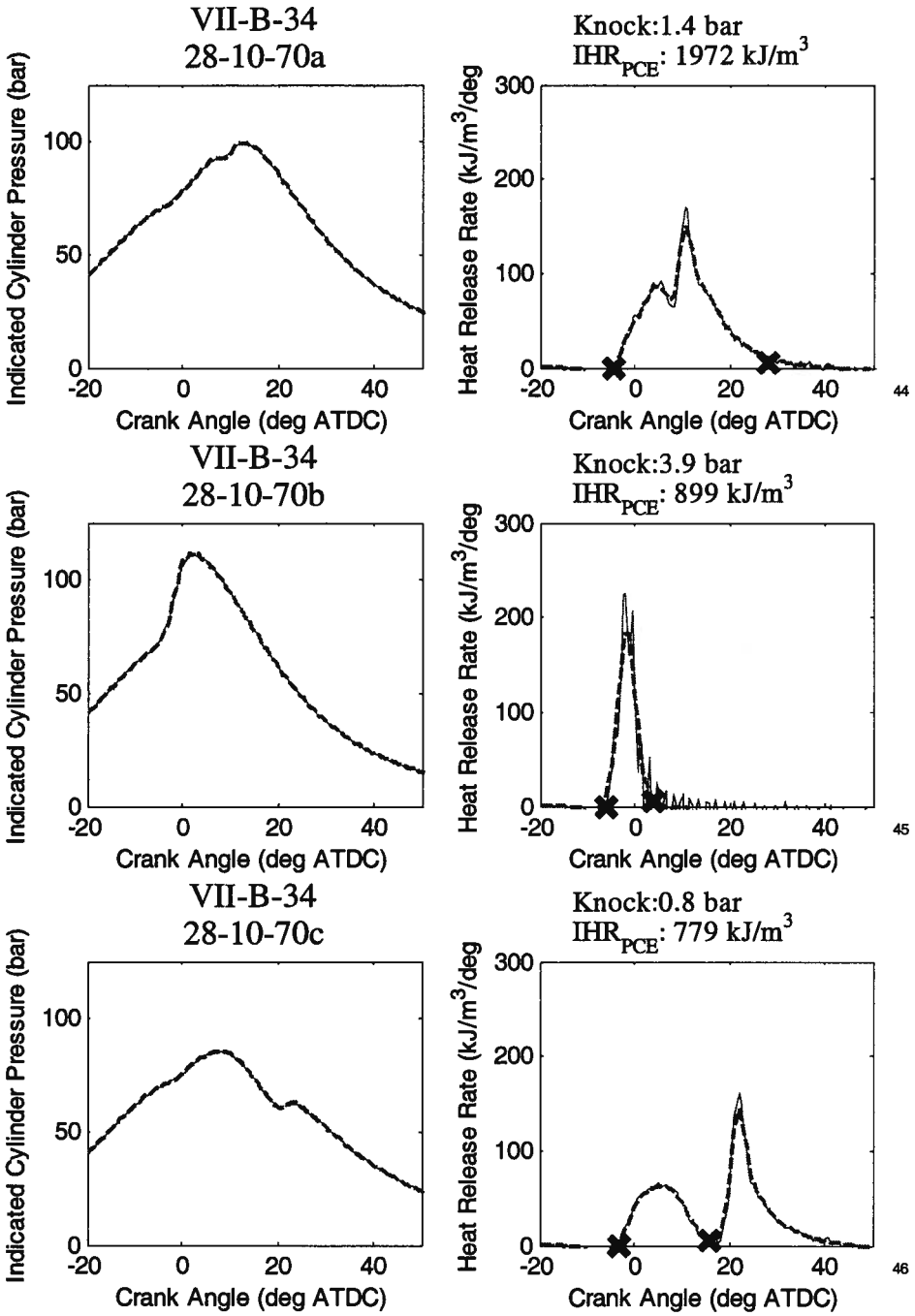

Figures E.4.44 to E.4.46 : Diesel flowrate: 13.3 mg/inj
IHR_{ratio}: 0.87 Knock Ratio: 0.21 Ignition Offset: 2.83 deg

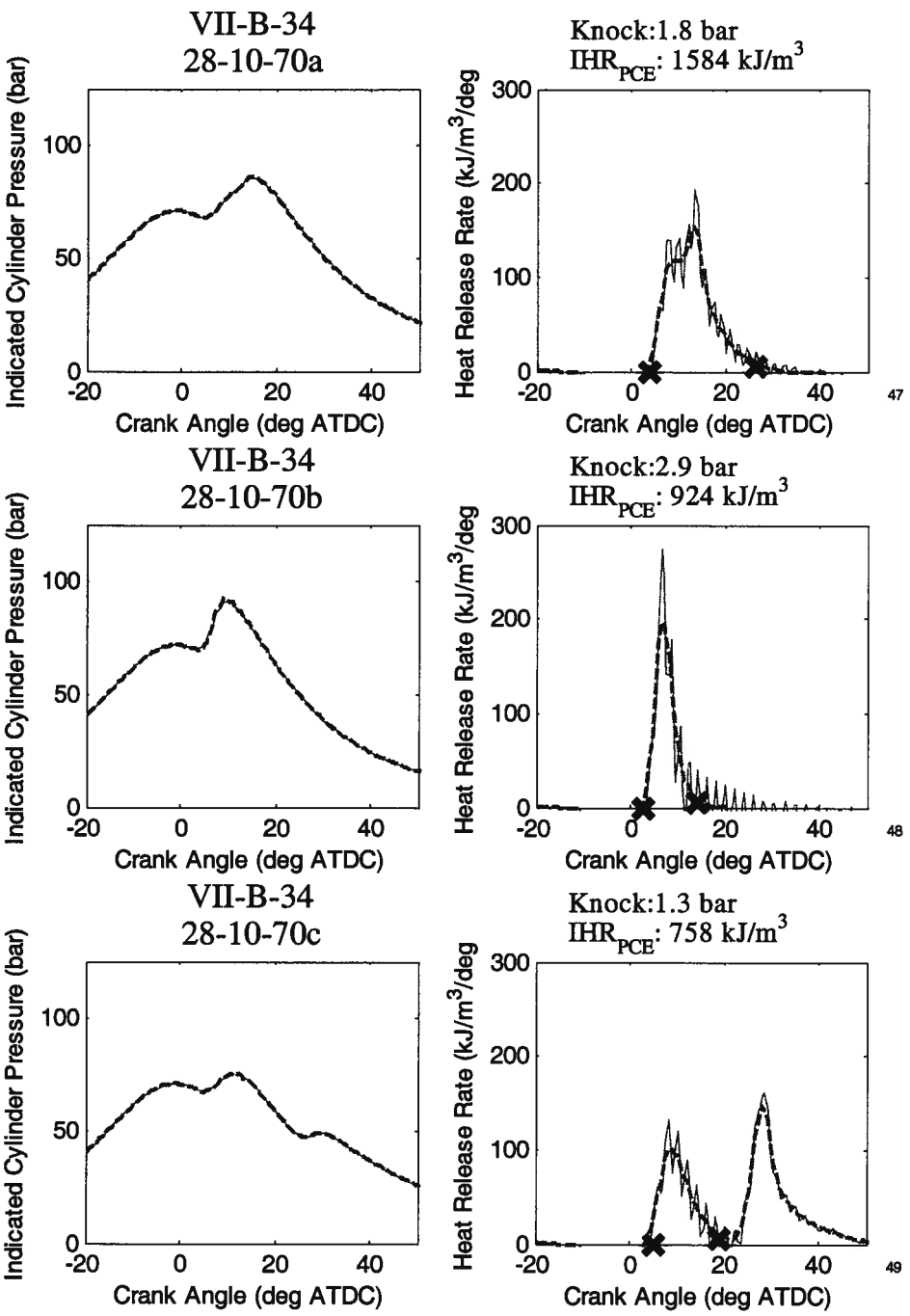

Figures E.4.47 to E.4.49 : Diesel flowrate: 19.9 mg/inj
IHR$_{ratio}$: 0.82 Knock Ratio: 0.44 Ignition Offset: 2.17 deg

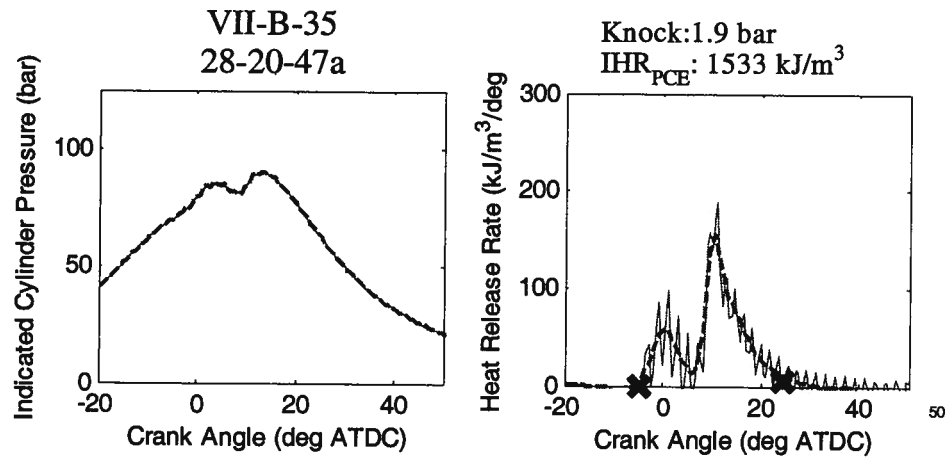

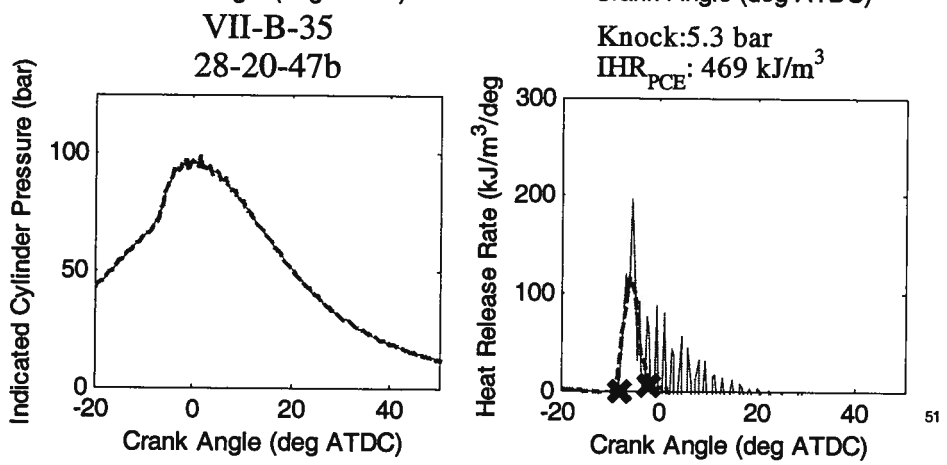

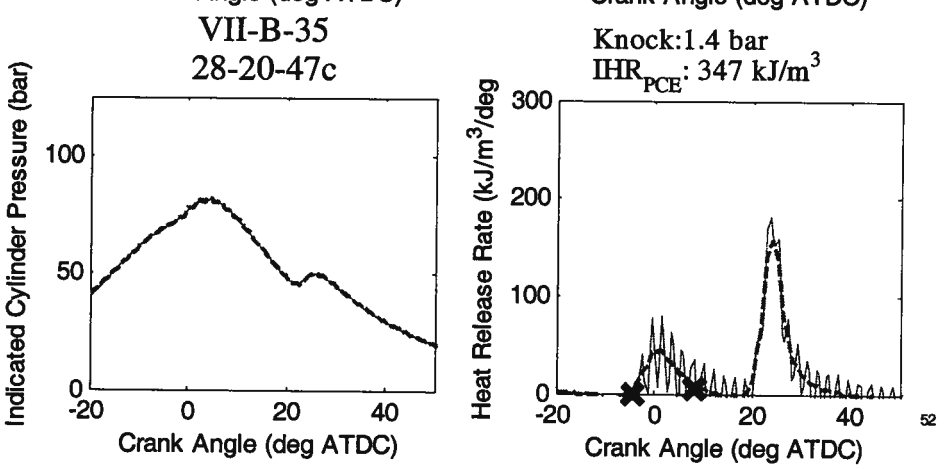

Figures E.4.50 to E.4.52 : Diesel flowrate: 15.7 mg/inj
IHR_{ratio}: 0.74 Knock Ratio: 0.27 Ignition Offset: 3.58 deg

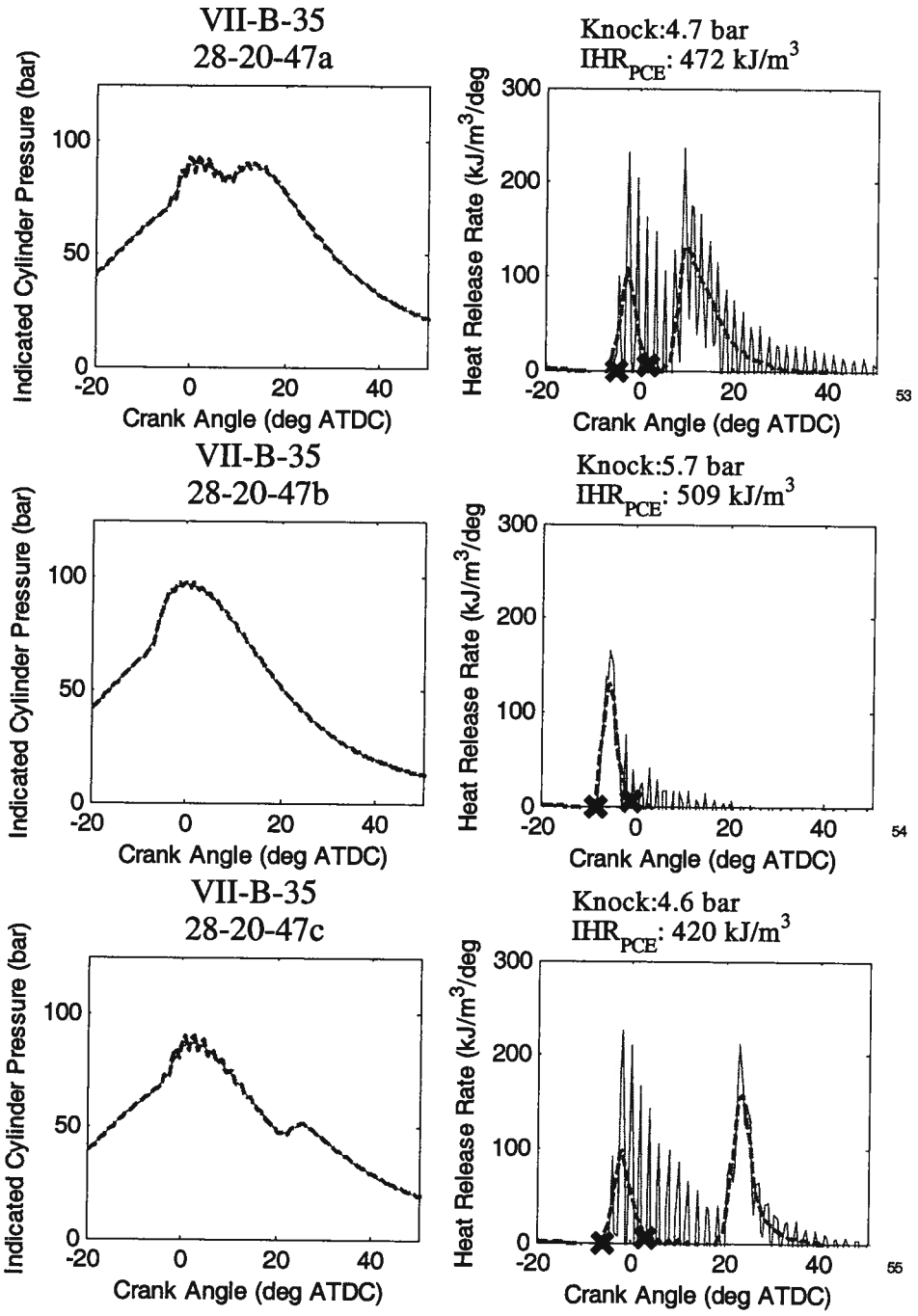

Figures E.4.53 to E.4.55 : Diesel flowrate: 18.4 mg/inj
IHR_{ratio}: 0.82 Knock Ratio: 0.81 Ignition Offset: 2.65 deg

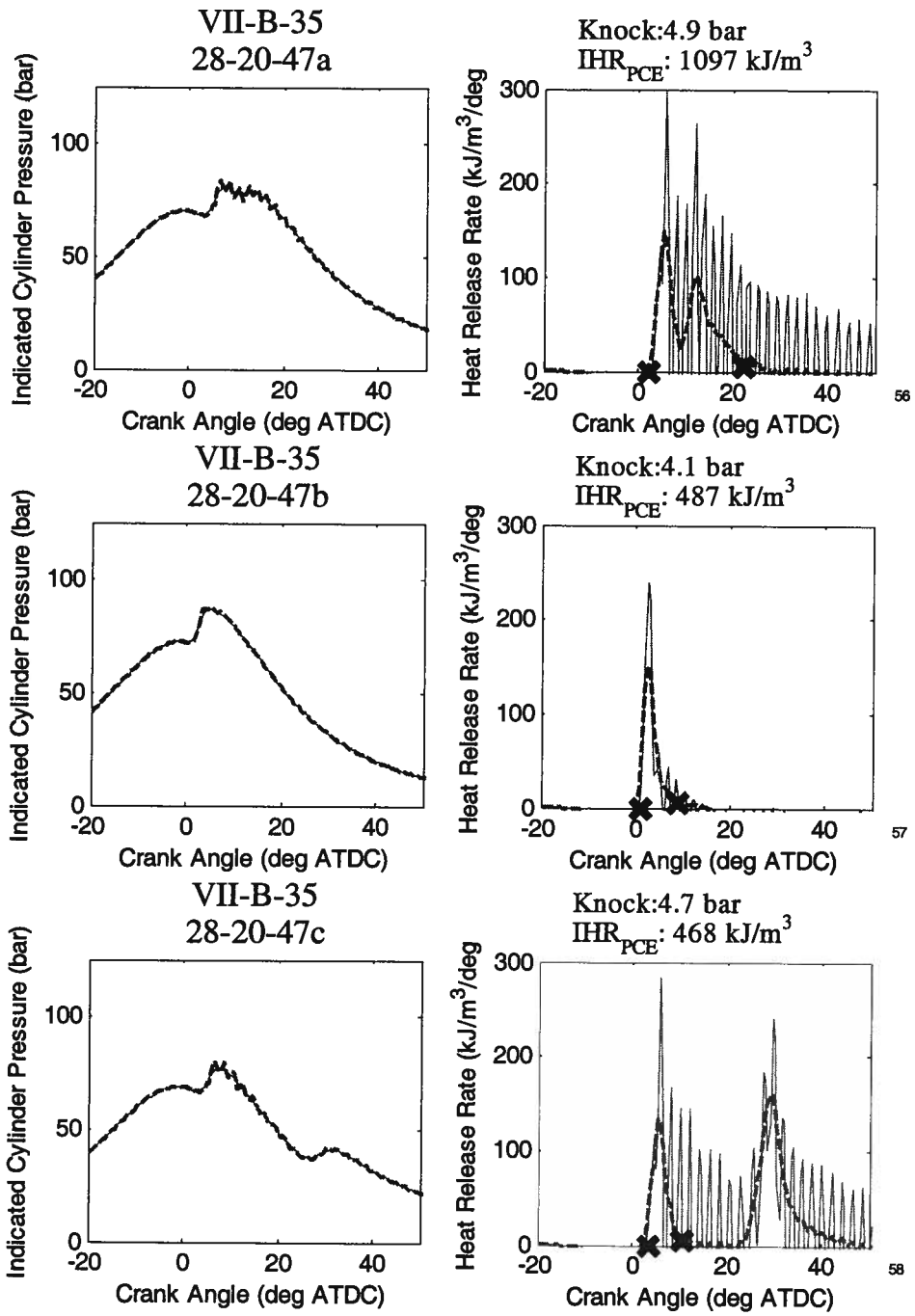

Figures E.4.56 to E.4.58 : Diesel flowrate: 15.9 mg/inj
IHR_{ratio}: 0.96 Knock Ratio: 1.13 Ignition Offset: 2.50 deg

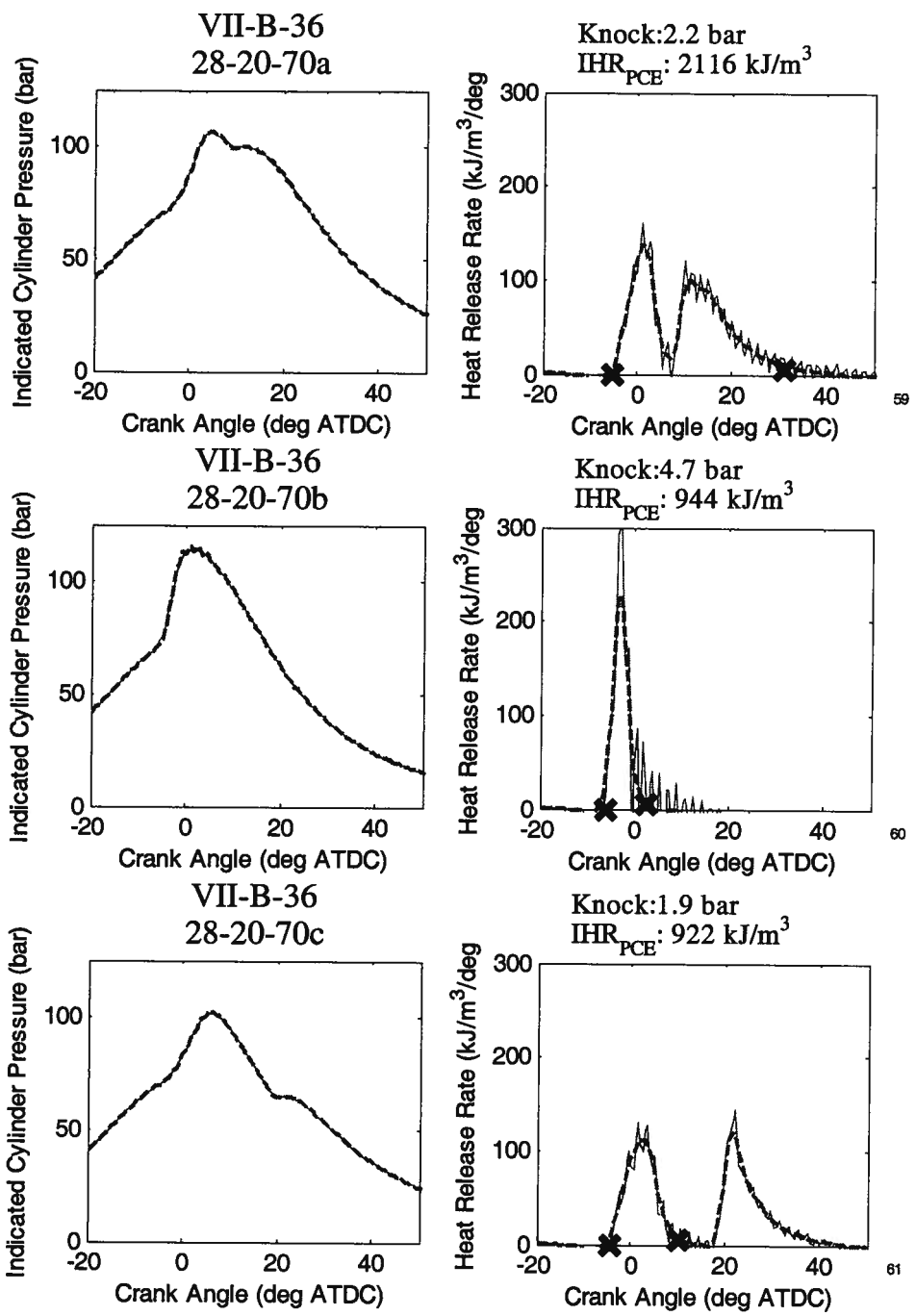

Figures E.4.59 to E.4.61 : Diesel flowrate: 15.2 mg/inj
IHR$_{ratio}$: 0.98 Knock Ratio: 0.40 Ignition Offset: 1.43 deg

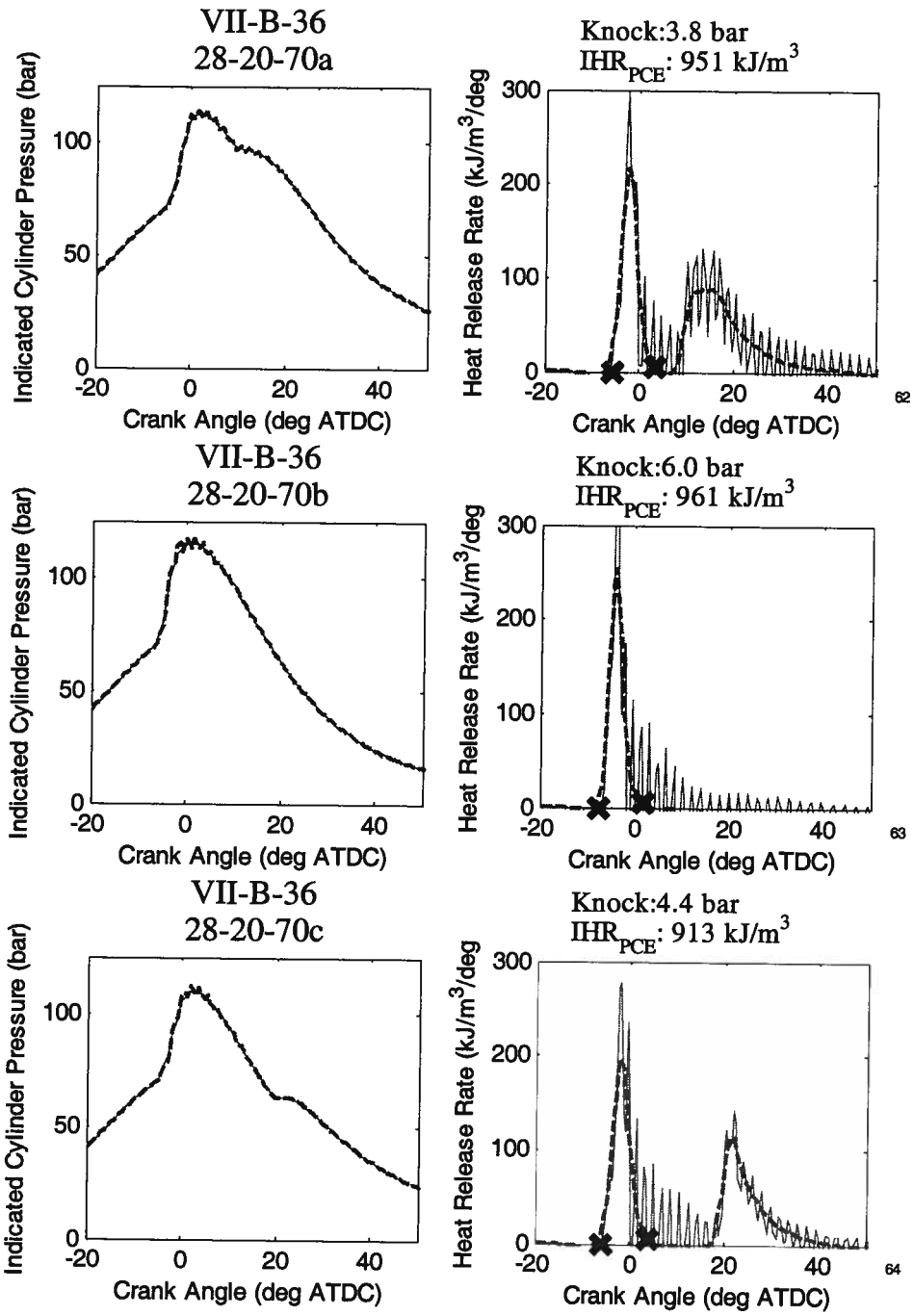

Figures E.4.62 to E.4.64 : Diesel flowrate: 15.9 mg/inj
IHR$_{ratio}$: 0.95 Knock Ratio: 0.73 Ignition Offset: 1.27 deg

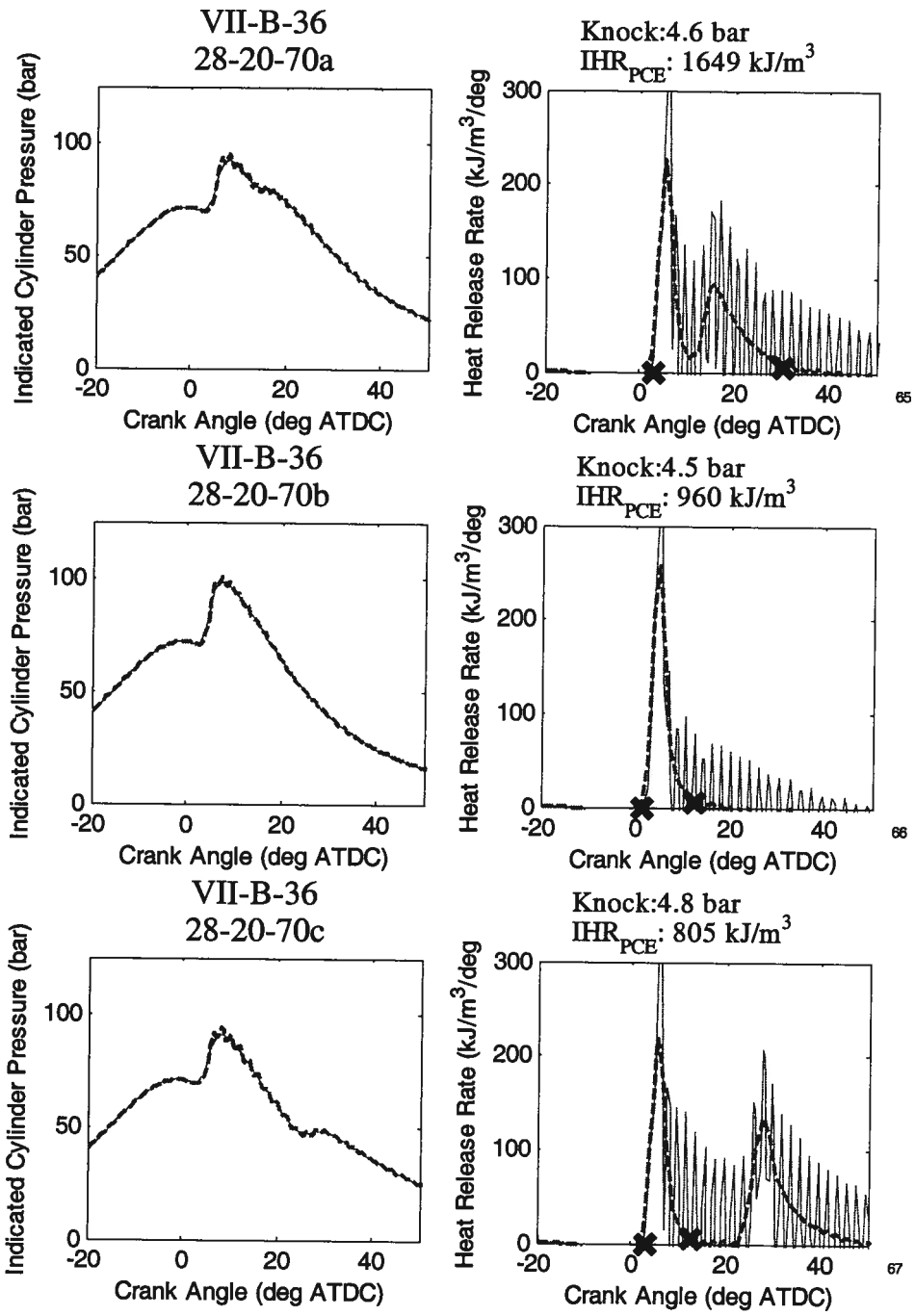

Figures E.4.65 to E.4.67 : Diesel flowrate: 19.8 mg/inj
IHR_{ratio}: 0.84 Knock Ratio: 1.07 Ignition Offset: 1.37 deg

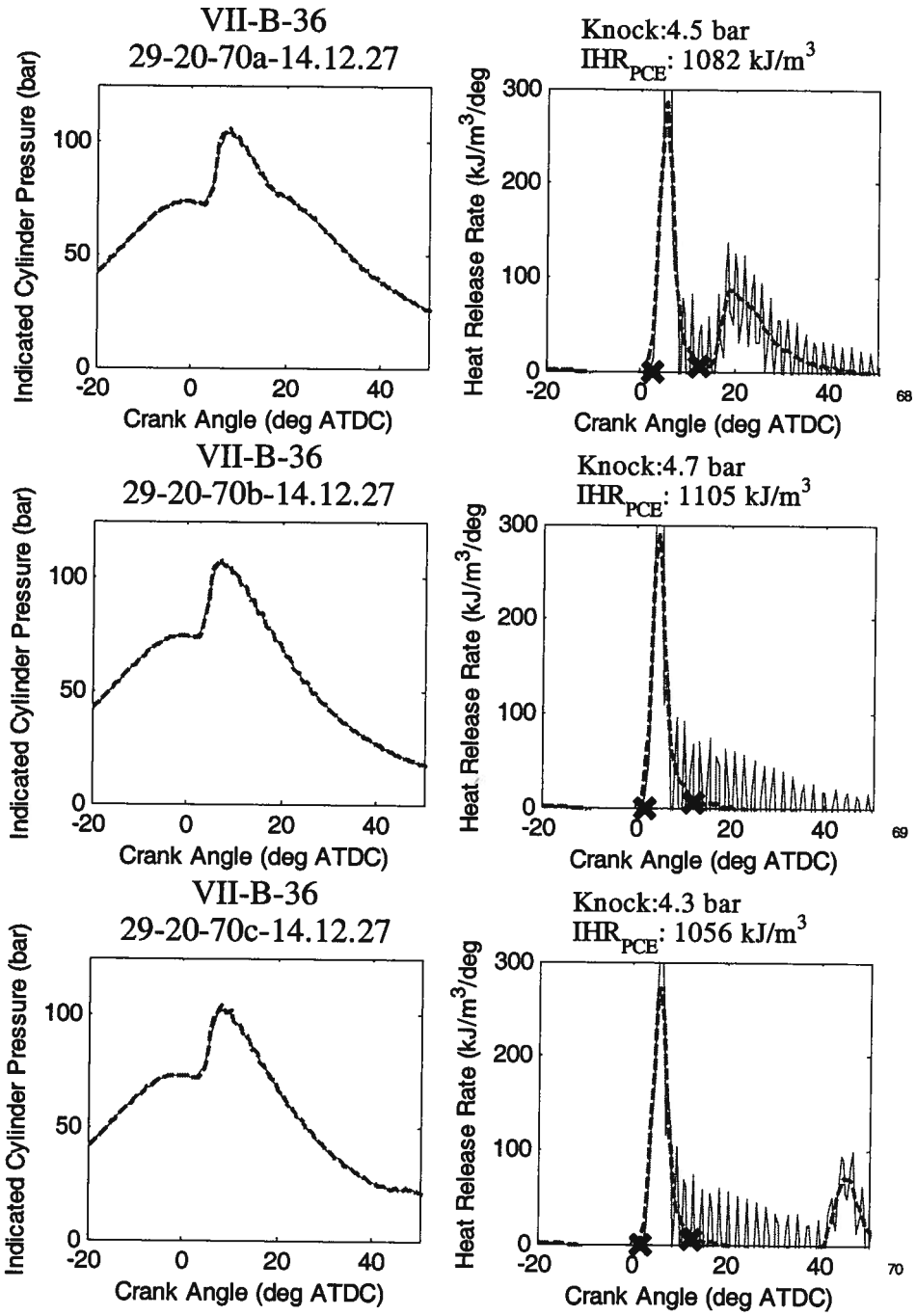

Figures E.4.68 to E.4.70 : Diesel flowrate: 17.1 mg/inj
IHR_{ratio}: 0.96 Knock Ratio: 0.90 Ignition Offset: 0.02 deg

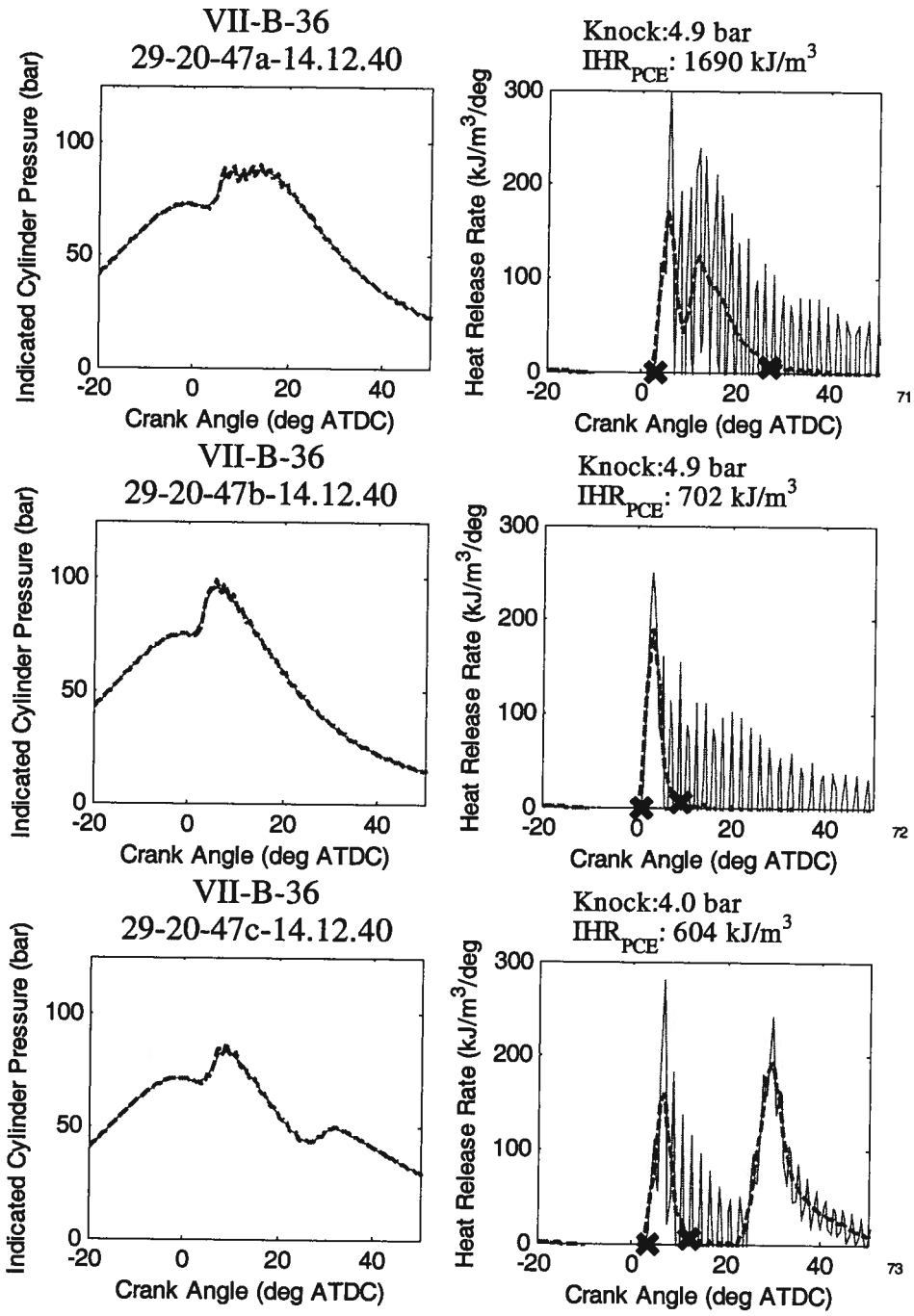

Figures E.4.71 to E.4.73 : Diesel flowrate: 15.0 mg/inj
IHR$_{ratio}$: 0.86 Knock Ratio: 0.83 Ignition Offset: 2.50 deg

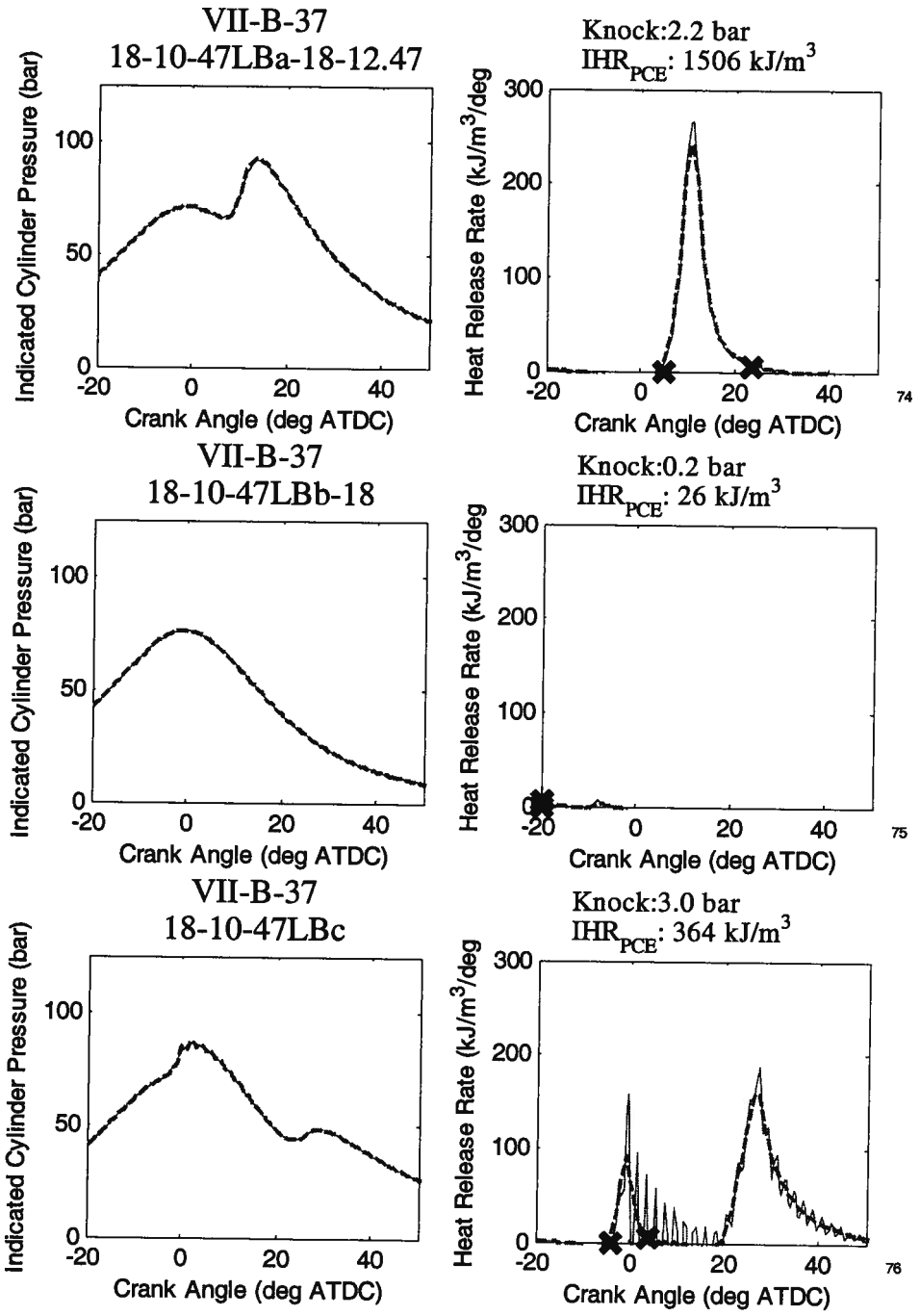

Figures E.4.74 to E.4.76 : Diesel flowrate: 11.6 mg/inj
IHR_{ratio}: 14.18 Knock Ratio: 12.38 Ignition Offset: 16.15 deg

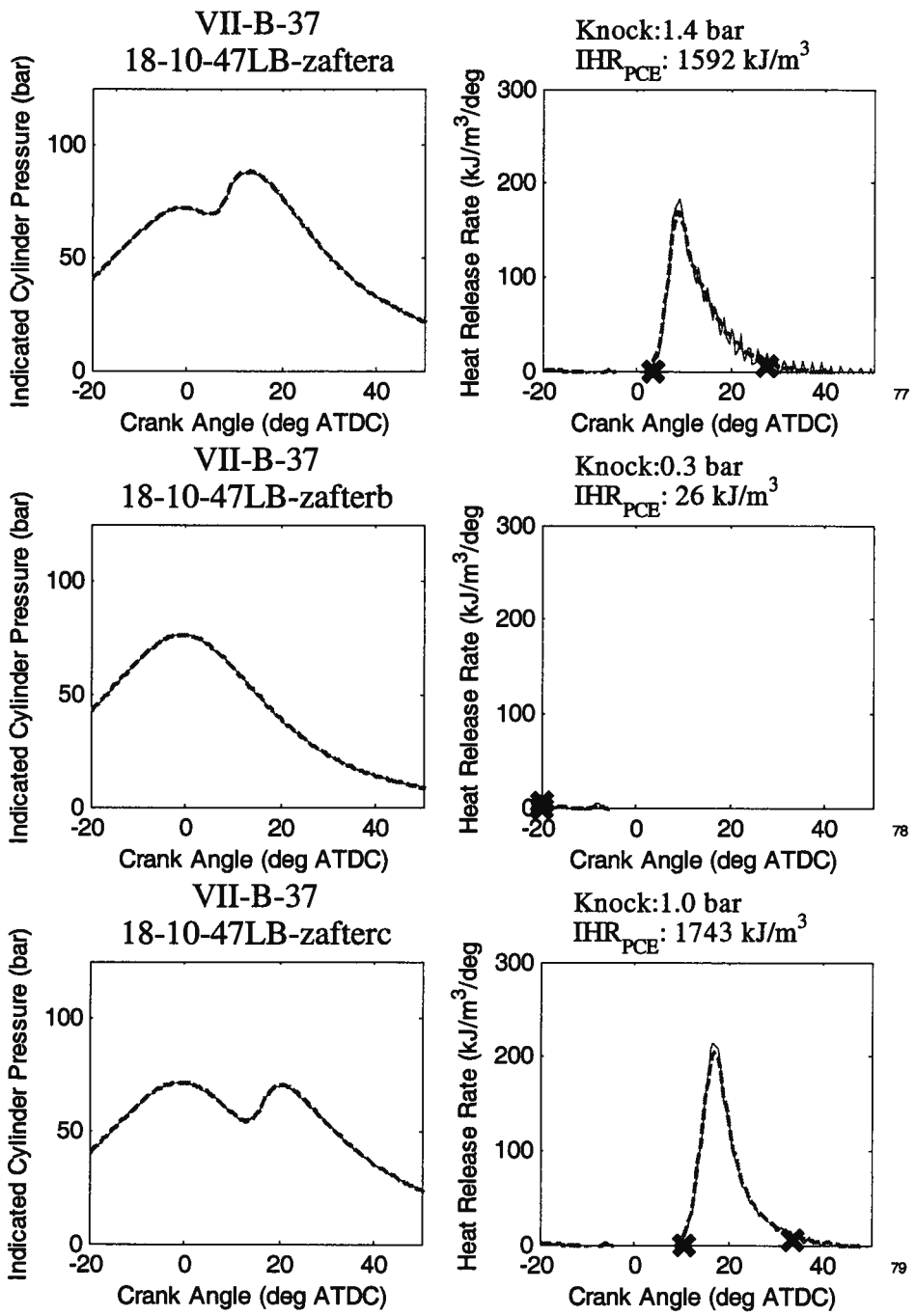

Figures E.4.77 to E.4.79 : Diesel flowrate: 13.5 mg/inj
IHR$_{ratio}$: 66.81 Knock Ratio: 4.08 Ignition Offset: 30.50 deg

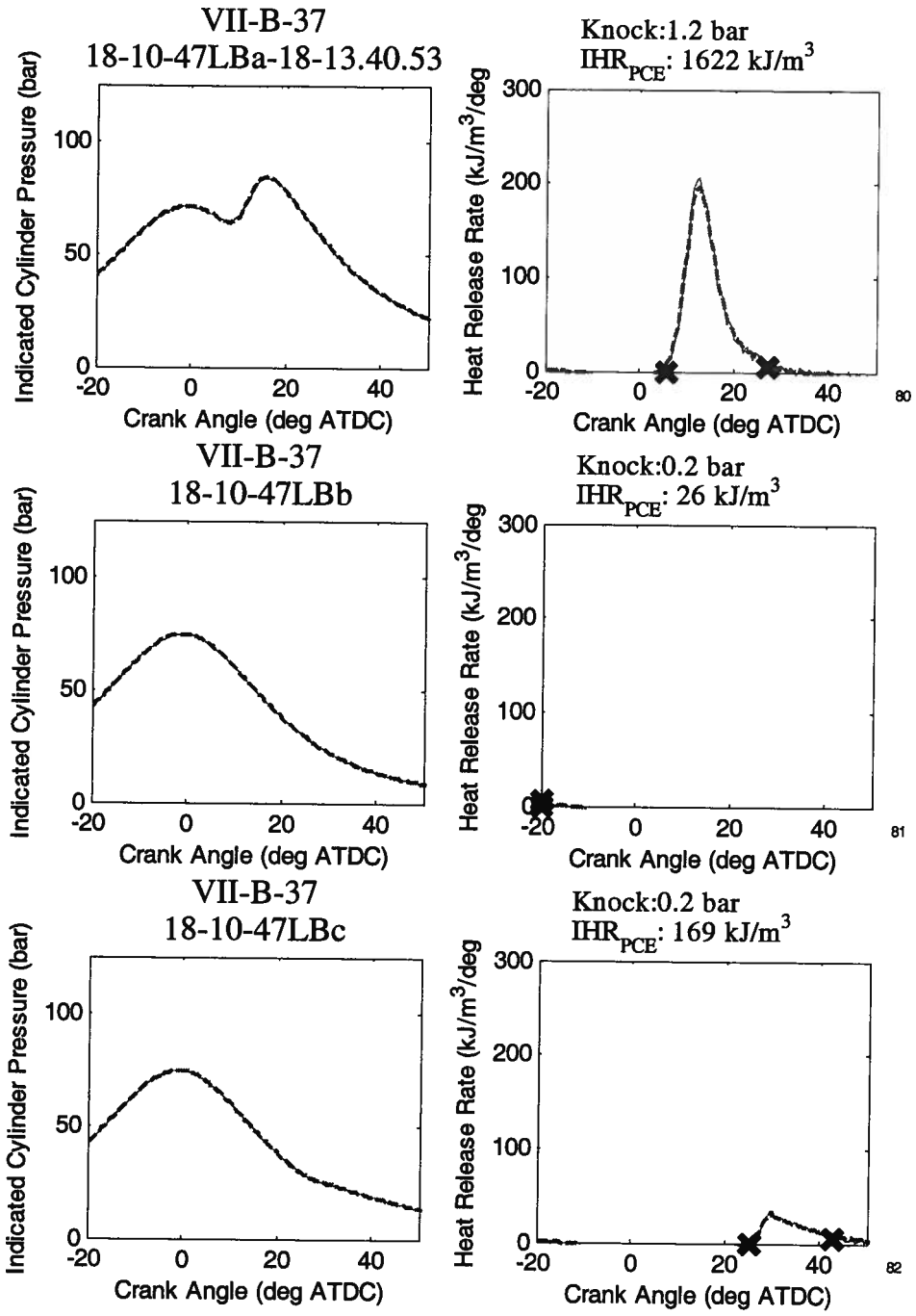

Figures E.4.80 to E.4.82 : Diesel flowrate: 7.8 mg/inj
IHR$_{ratio}$: 6.39 Knock Ratio: 1.18 Ignition Offset: 45.15 deg

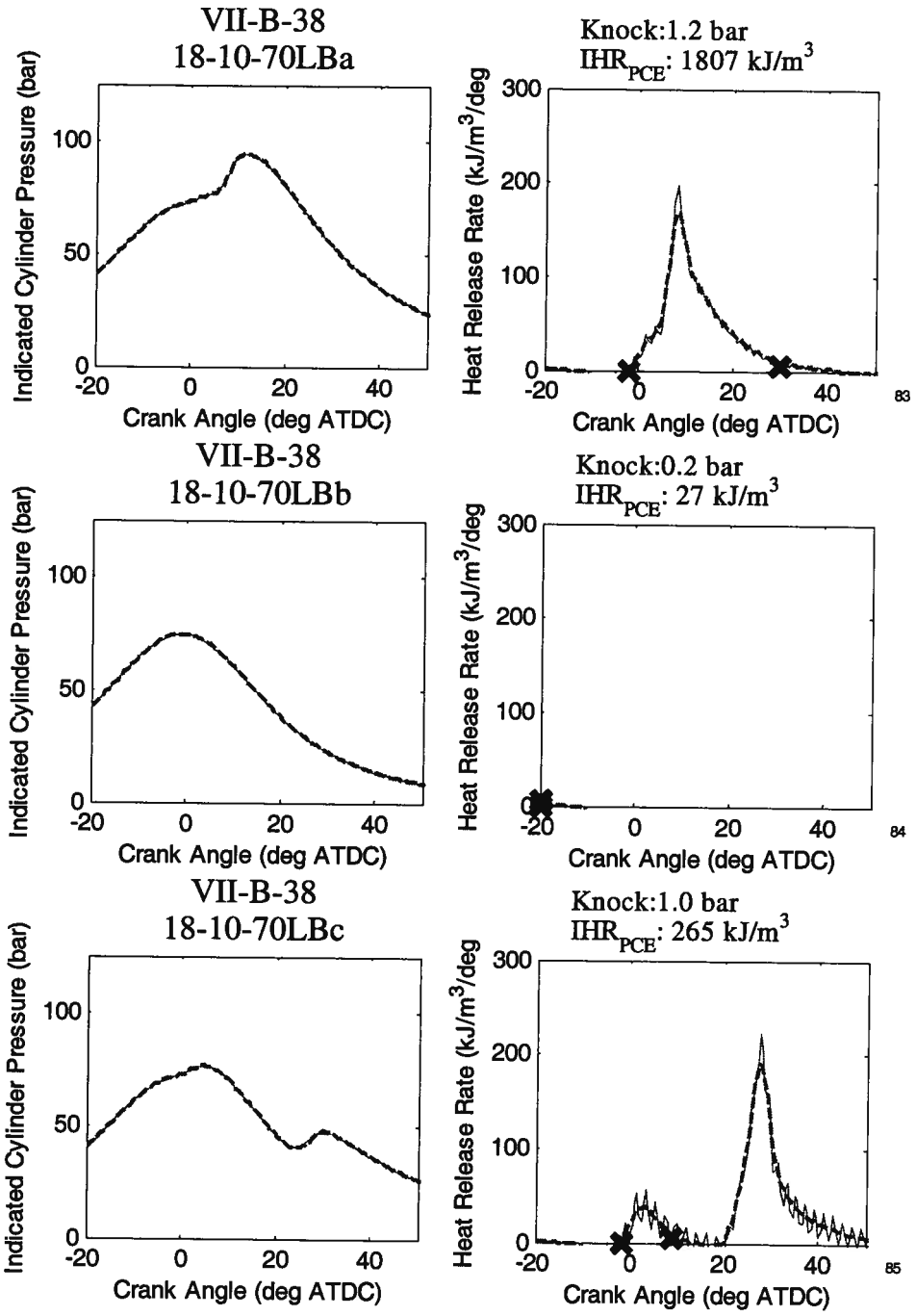

Figures E.4.83 to E.4.85 : Diesel flowrate: 8.0 mg/inj
IHR_{ratio}: 9.85 Knock Ratio: 6.21 Ignition Offset: 18.58 deg

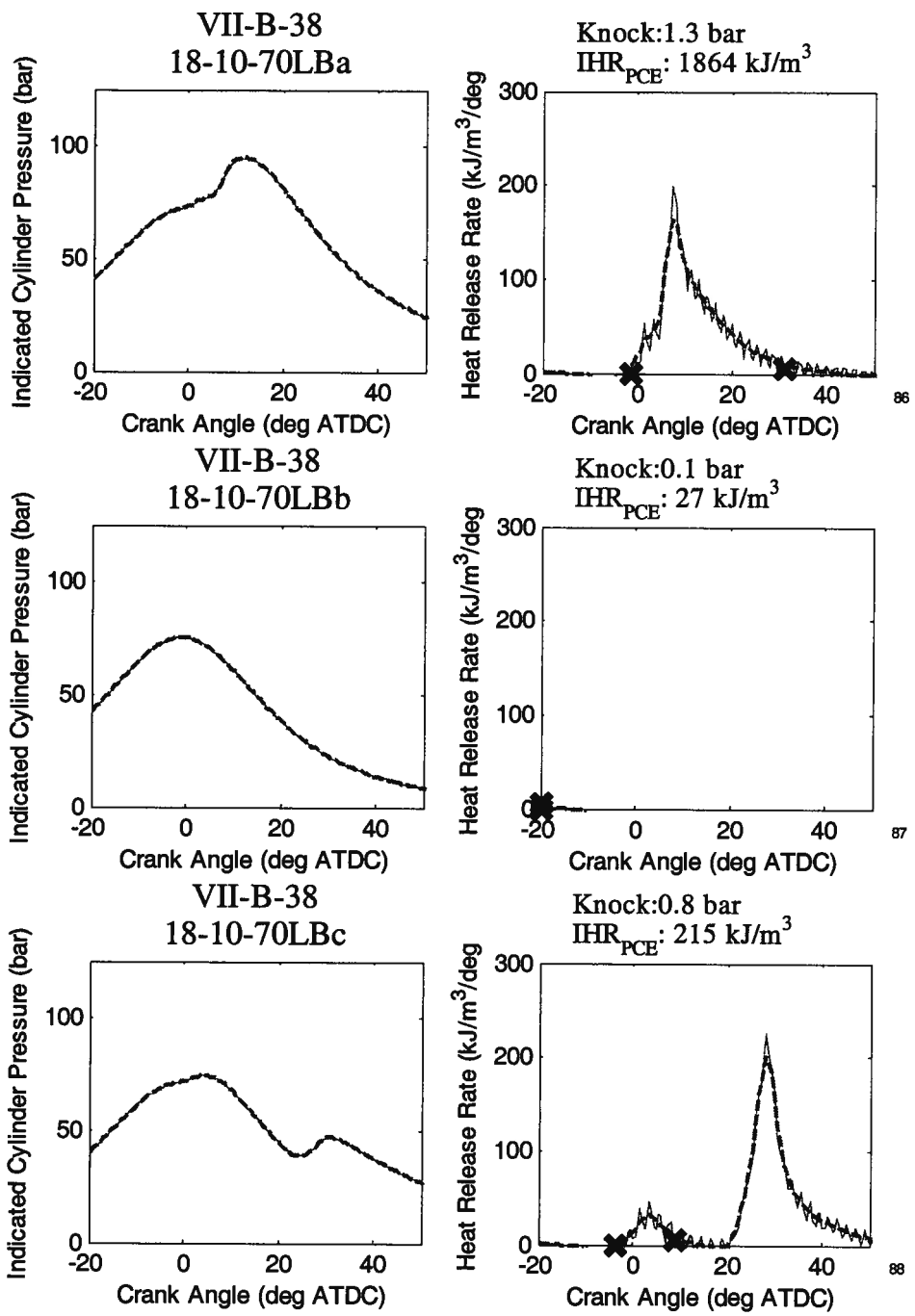

Figures E.4.86 to E.4.88 : Diesel flowrate: 8.7 mg/inj
IHR$_{ratio}$: 7.92 Knock Ratio: 5.62 Ignition Offset: 16.45 deg

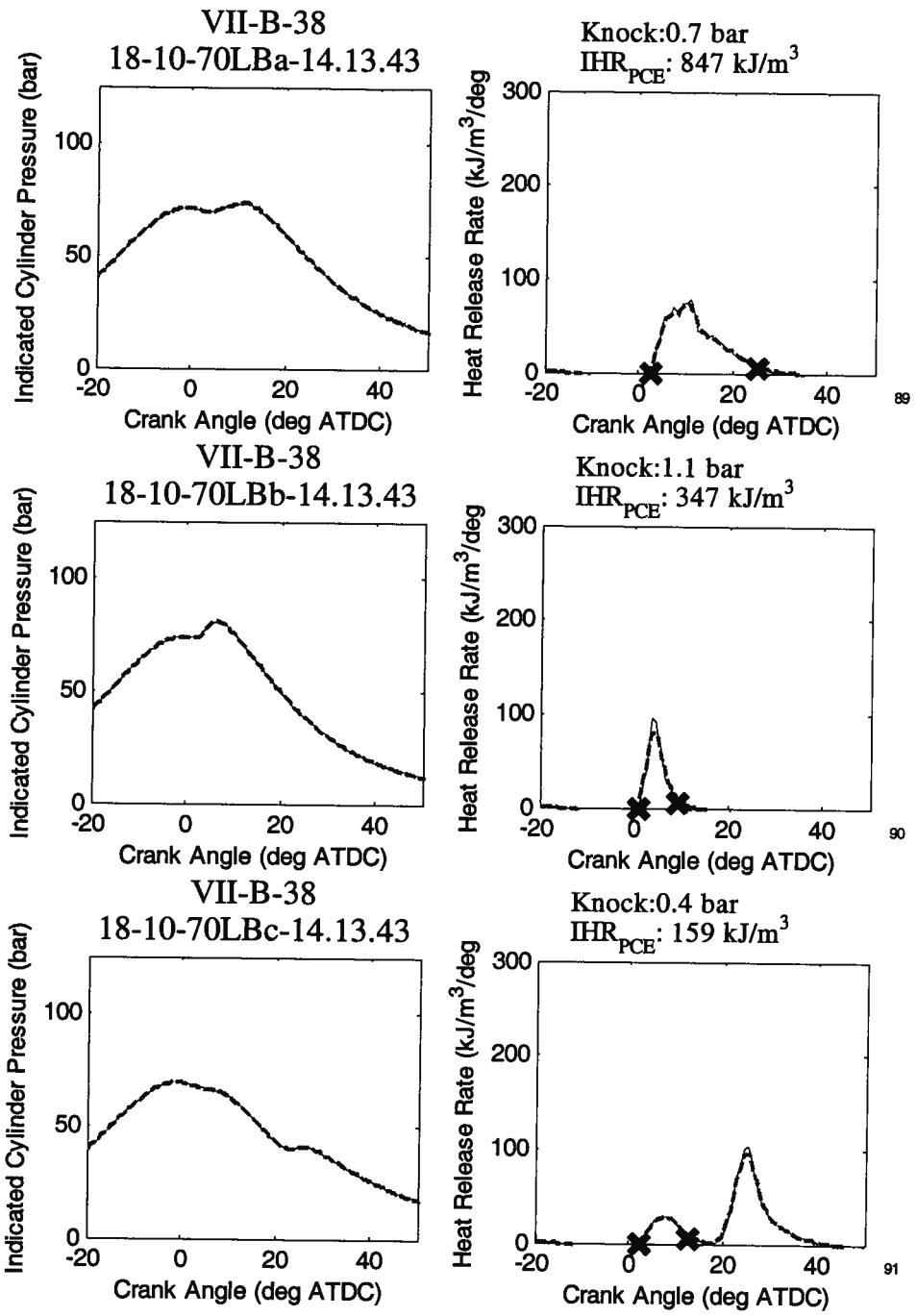

Figures E.4.89 to E.4.91 : Diesel flowrate: 9.9 mg/inj
IHR$_{ratio}$: 0.46 Knock Ratio: 0.34 Ignition Offset: 1.32 deg

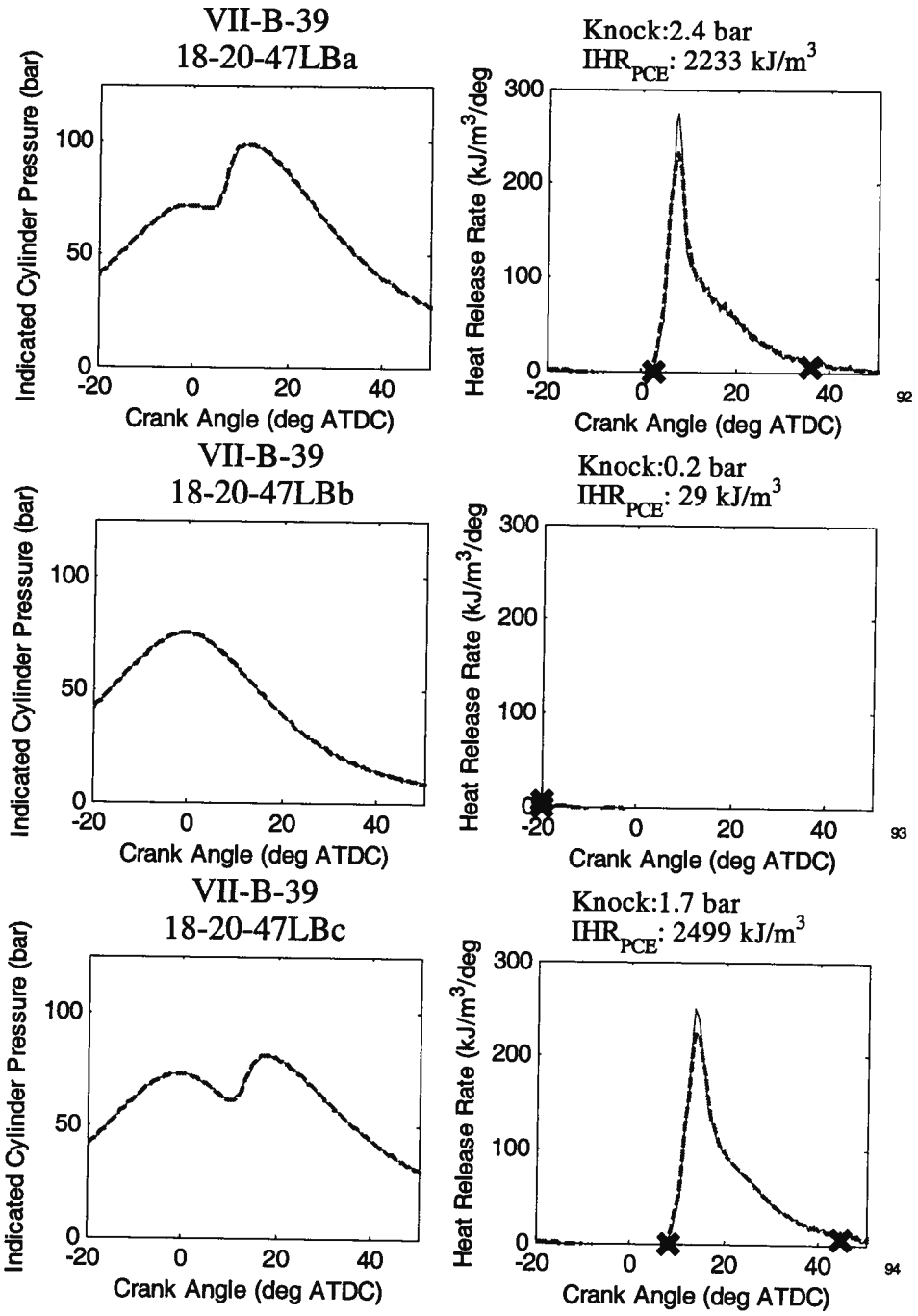

Figures E.4.92 to E.4.94 : Diesel flowrate: 13.8 mg/inj
IHR$_{ratio}$: 85.50 Knock Ratio: 8.68 Ignition Offset: 28.16 deg

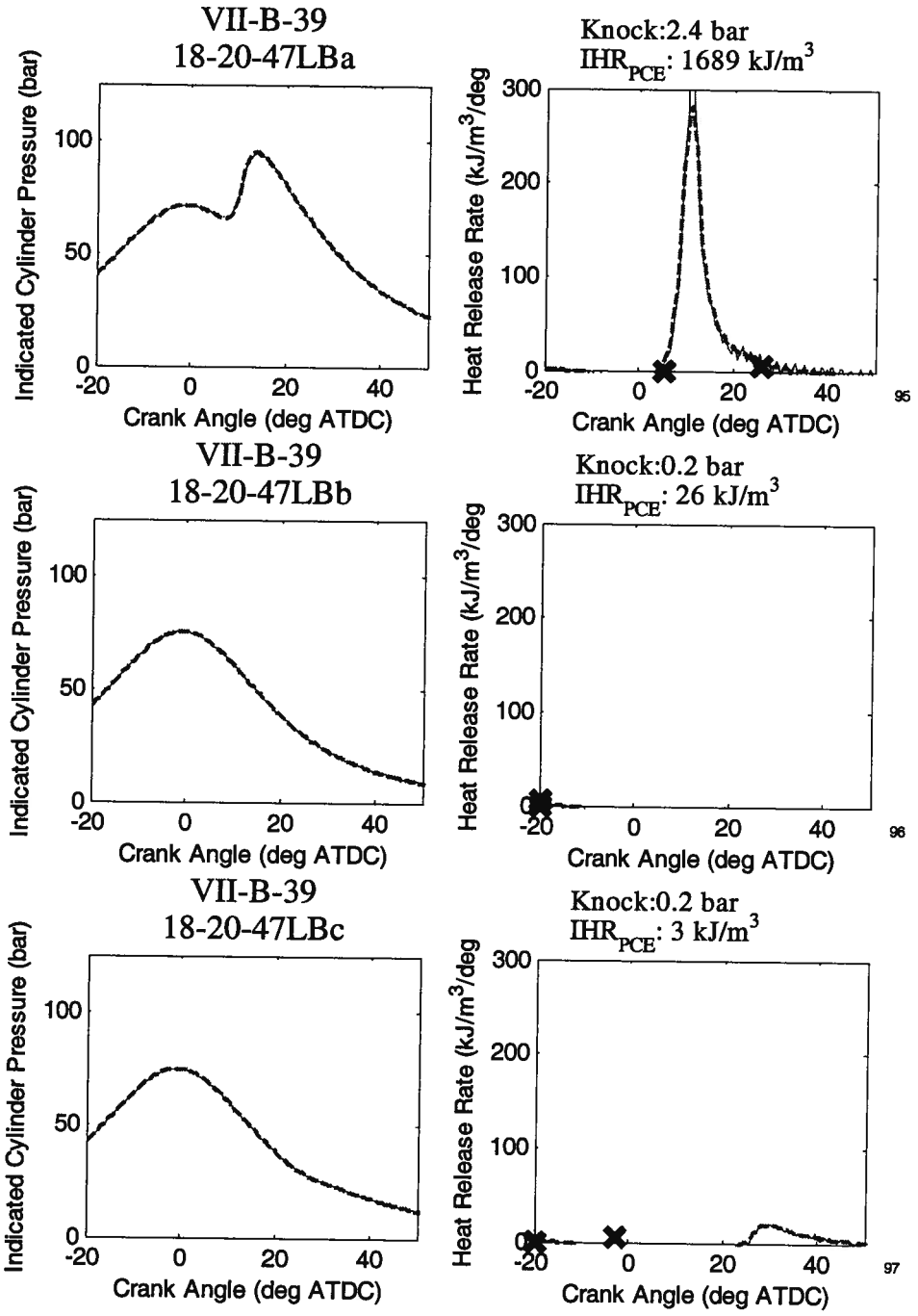

Figures E.4.95 to E.4.97 : Diesel flowrate: 15.9 mg/inj
IHR$_{ratio}$: 0.12 Knock Ratio: 1.07 Ignition Offset: 0.00 deg

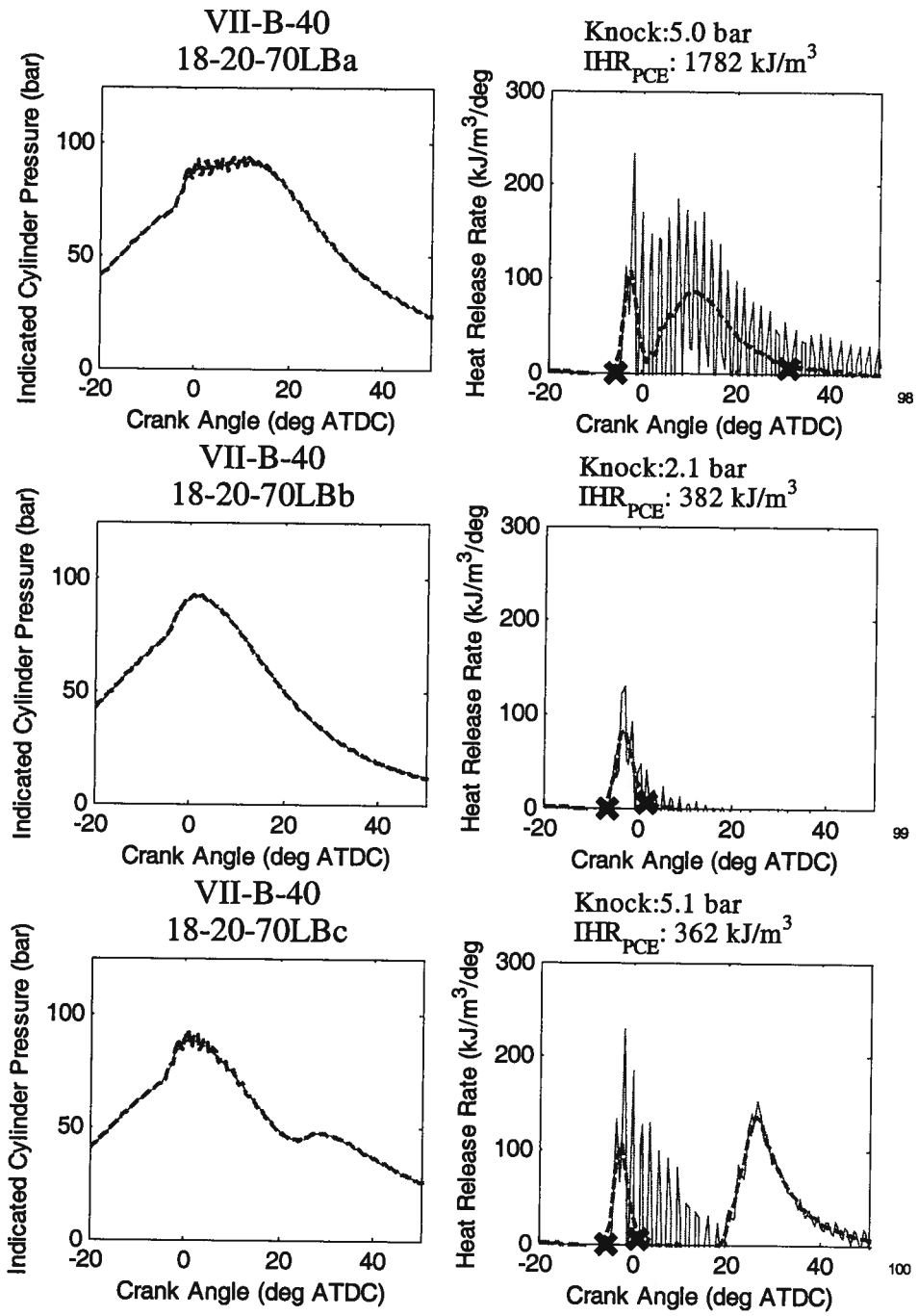

Figures E.4.98 to E.4.100 : Diesel flowrate: 13.4 mg/inj
IHR$_{ratio}$: 0.95 Knock Ratio: 2.44 Ignition Offset: 0.98 deg

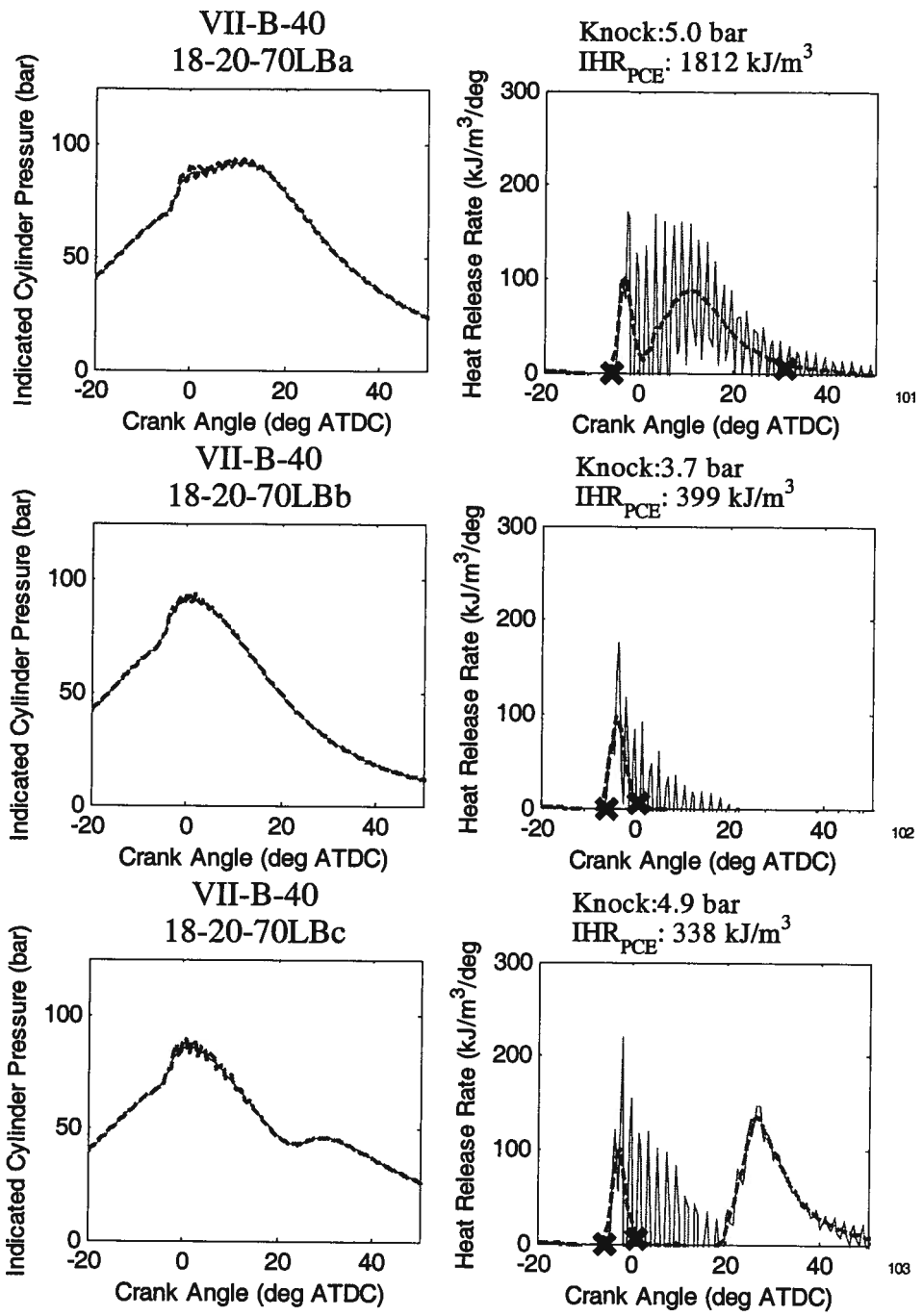

Figures E.4.101 to E.4.103 : Diesel flowrate: 16.2 mg/inj
IHR$_{ratio}$: 0.85 Knock Ratio: 1.32 Ignition Offset: 0.45 deg

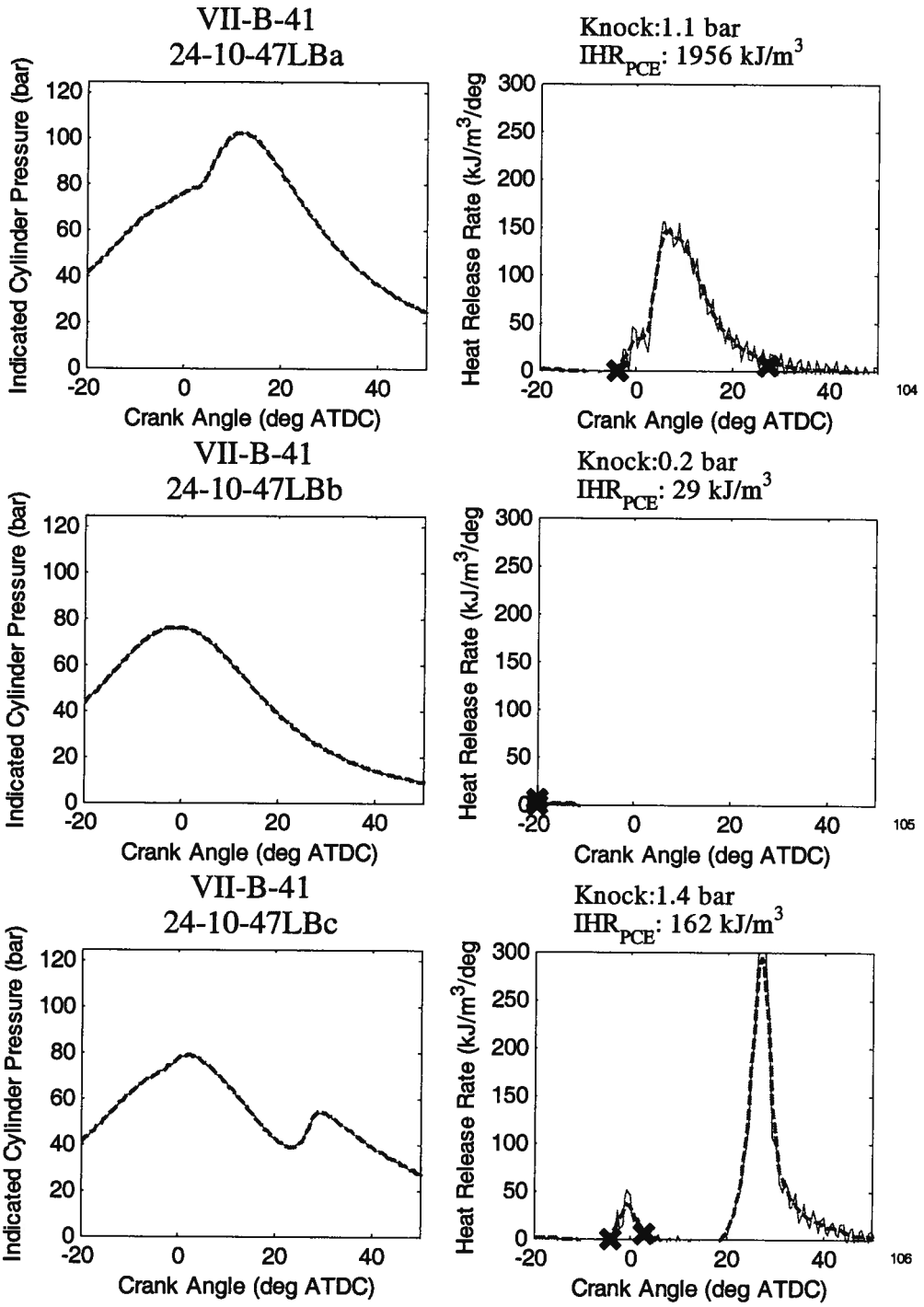

Figures F.4.104 to F.4.106 : Diesel flowrate: 4.7 mg/inj
IHR_{ratio}: 5.56 Knock Ratio: 6.53 Ignition Offset: 16.22 deg

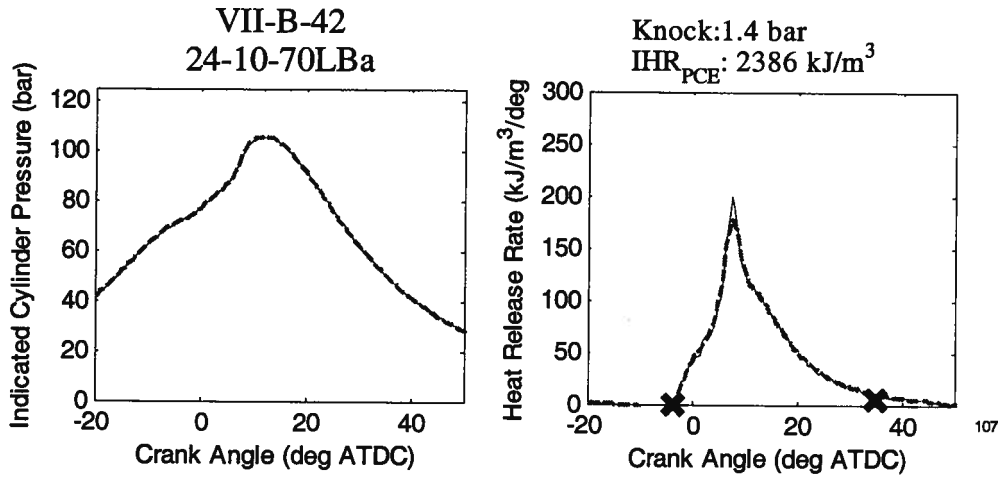
VII-B-42
24-10-70LBa
Knock:1.4 bar
IHR$_{PCE}$: 2386 kJ/m^3
Indicated Cylinder Pressure (bar)
Heat Release Rate (kJ/m^3/deg
Crank Angle (deg ATDC)
Crank Angle (deg ATDC)
107

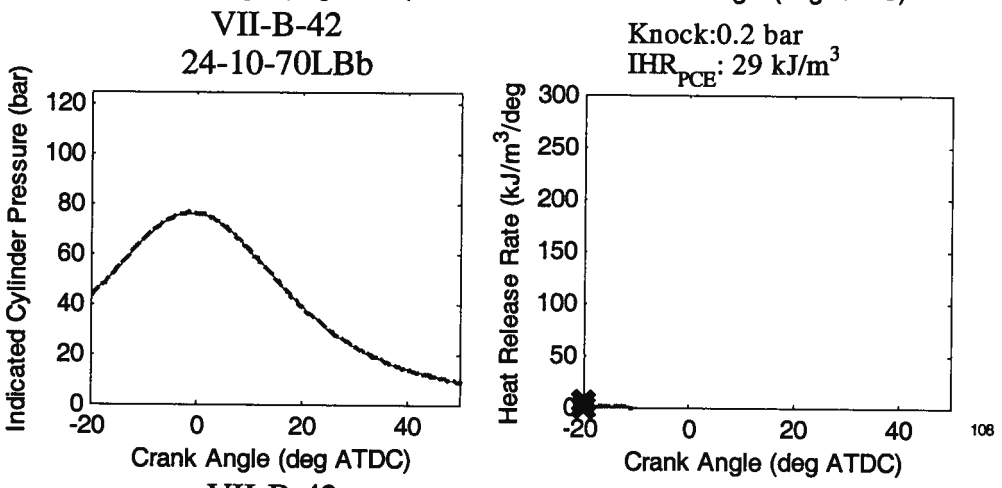
VII-B-42
24-10-70LBb
Knock:0.2 bar
IHR$_{PCE}$: 29 kJ/m^3
Indicated Cylinder Pressure (bar)
Heat Release Rate (kJ/m^3/deg
Crank Angle (deg ATDC)
Crank Angle (deg ATDC)
108

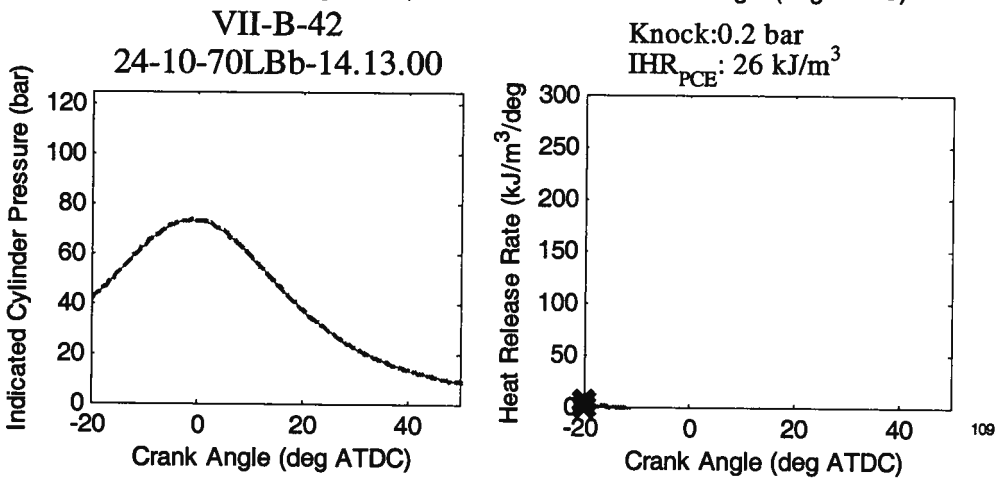
VII-B-42
24-10-70LBb-14.13.00
Knock:0.2 bar
IHR$_{PCE}$: 26 kJ/m^3
Indicated Cylinder Pressure (bar)
Heat Release Rate (kJ/m^3/deg
Crank Angle (deg ATDC)
Crank Angle (deg ATDC)
109

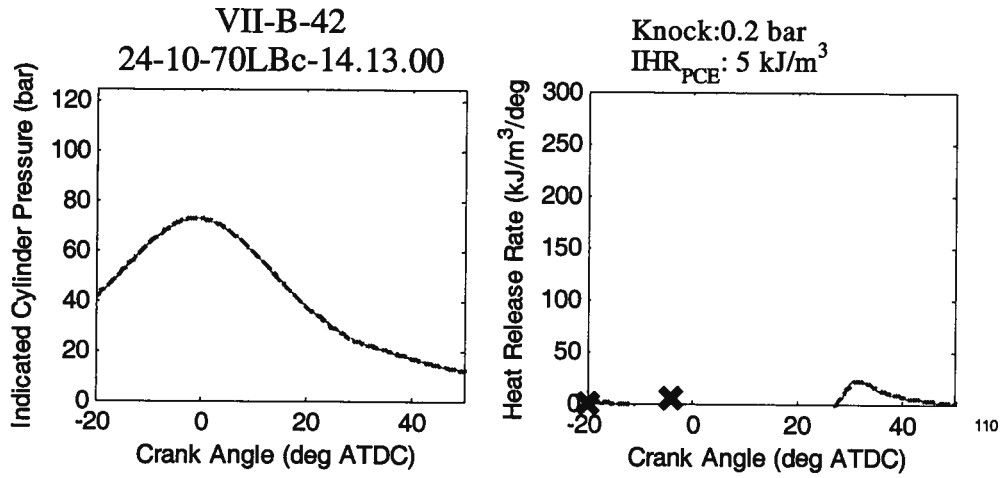

Figures F.4.108 to F.4.110 : Diesel flowrate: -7.4 mg/inj
IHR_{ratio}: 0.19 Knock Ratio: 0.95 Ignition Offset: 0.00 deg

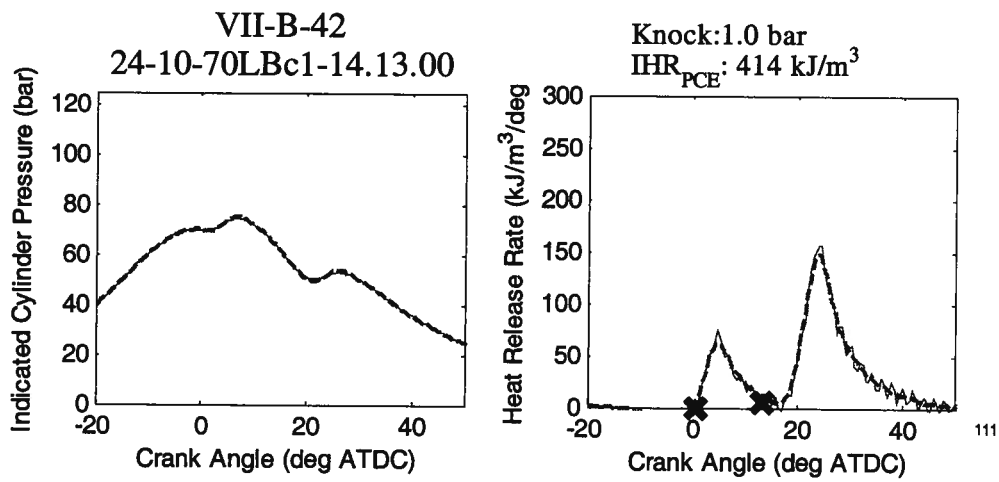

Figures F.4.109 to F.4.111 : Diesel flowrate: 39.6 mg/inj
IHR_{ratio}: 84.17 Knock Ratio: 5.60 Ignition Offset: 20.98 deg

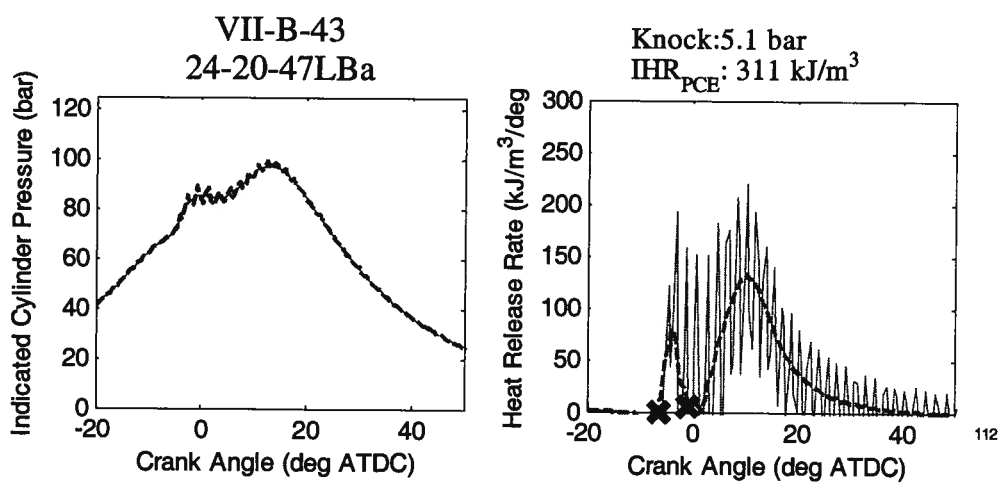

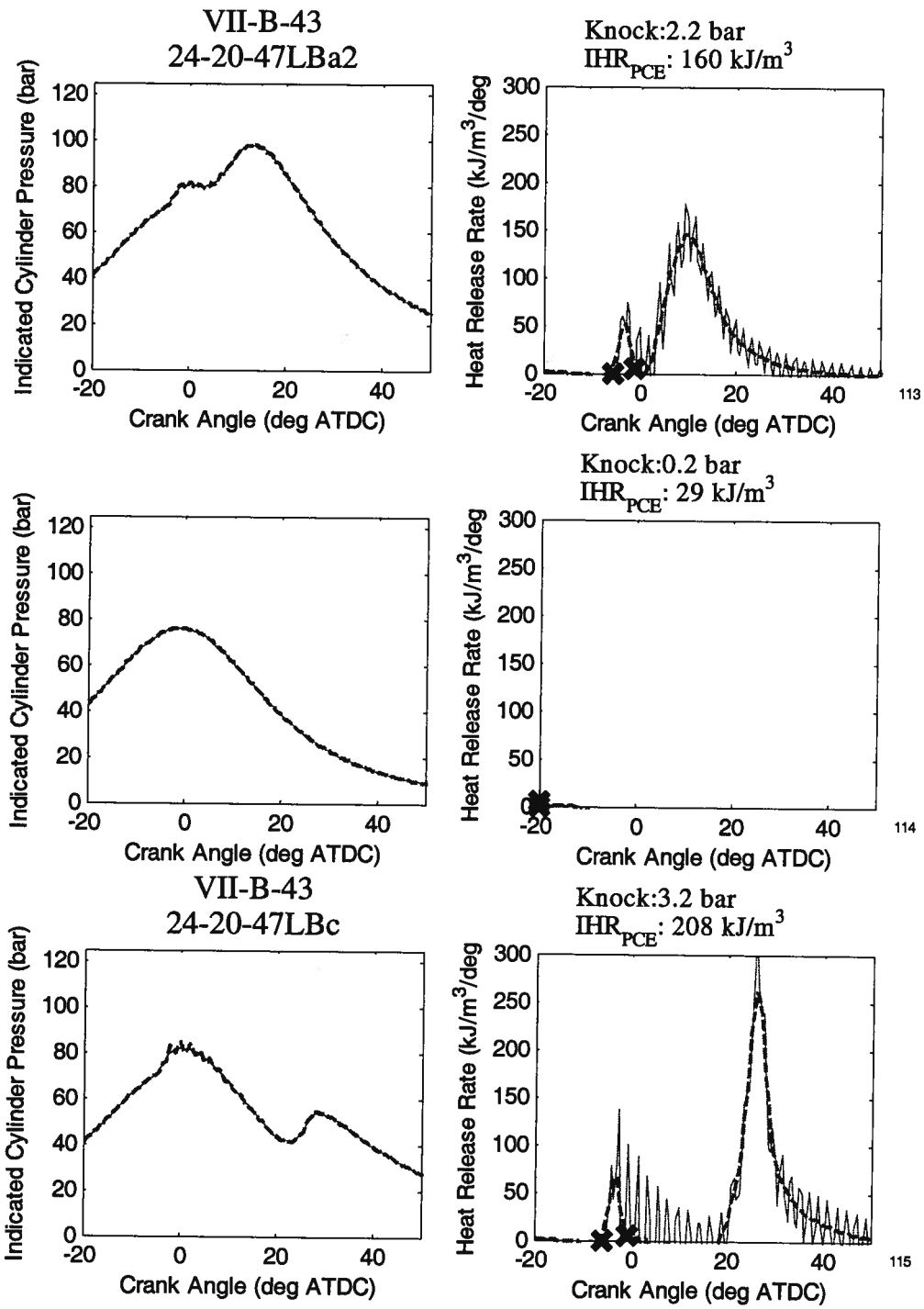

Figures F.4.113 to F.4.115 : Diesel flowrate: 17.6 mg/inj
IHR_{ratio}: 7.13 Knock Ratio: 13.93 Ignition Offset: 14.32 deg

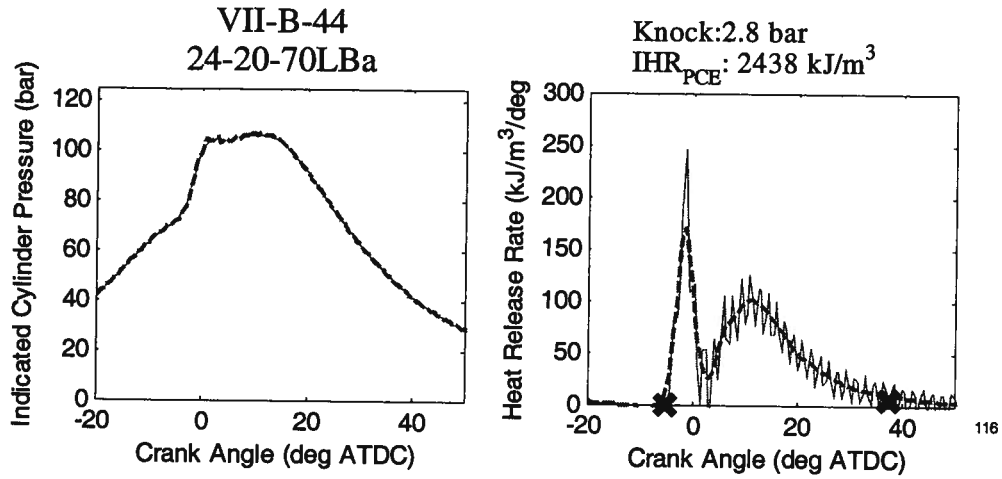
VII-B-44
24-20-70LBa
Knock:2.8 bar
IHR$_{PCE}$: 2438 kJ/m^3
Indicated Cylinder Pressure (bar)
Heat Release Rate (kJ/m^3/deg
Crank Angle (deg ATDC)
116

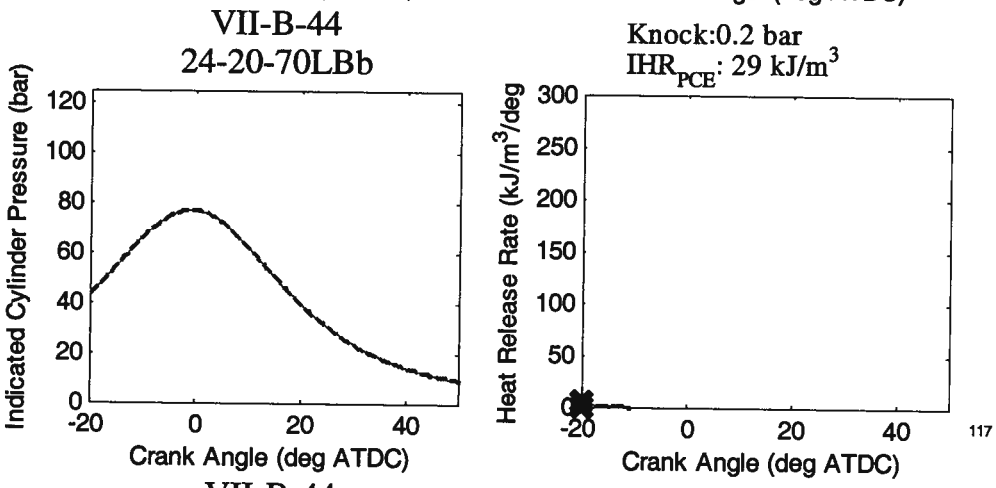
VII-B-44
24-20-70LBb
Knock:0.2 bar
IHR$_{PCE}$: 29 kJ/m^3
Indicated Cylinder Pressure (bar)
Heat Release Rate (kJ/m^3/deg
Crank Angle (deg ATDC)
117

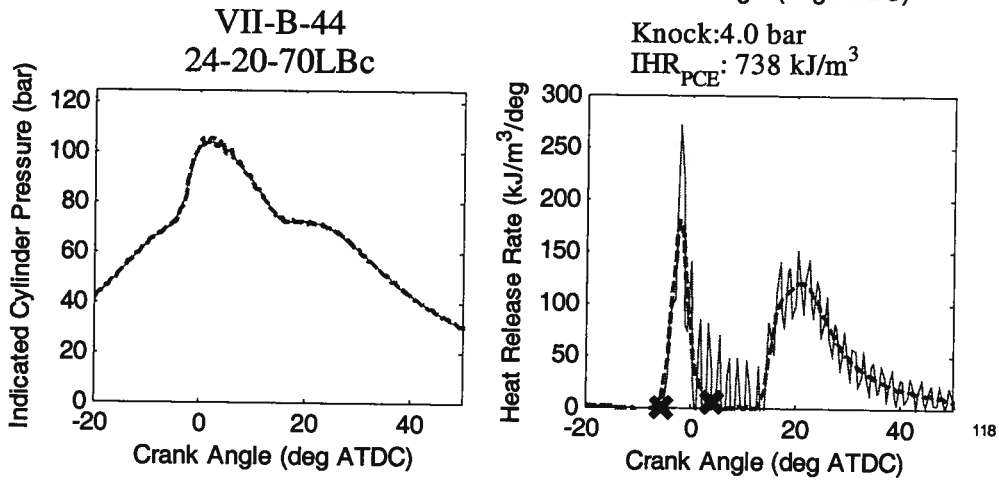
VII-B-44
24-20-70LBc
Knock:4.0 bar
IHR$_{PCE}$: 738 kJ/m^3
Indicated Cylinder Pressure (bar)
Heat Release Rate (kJ/m^3/deg
Crank Angle (deg ATDC)
118

Figures F.4.116 to F.4.118 : Diesel flowrate: 14.5 mg/inj
IHR_{ratio}: 25.11 Knock Ratio: 25.17 Ignition Offset: 14.51 deg

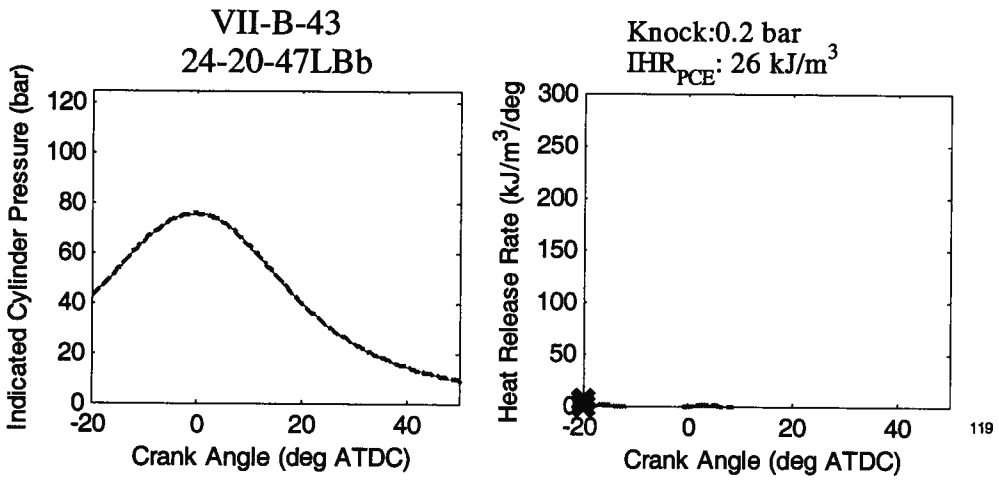

Appendix F.5- Test Series VIII-A Pressure and HRR Curves

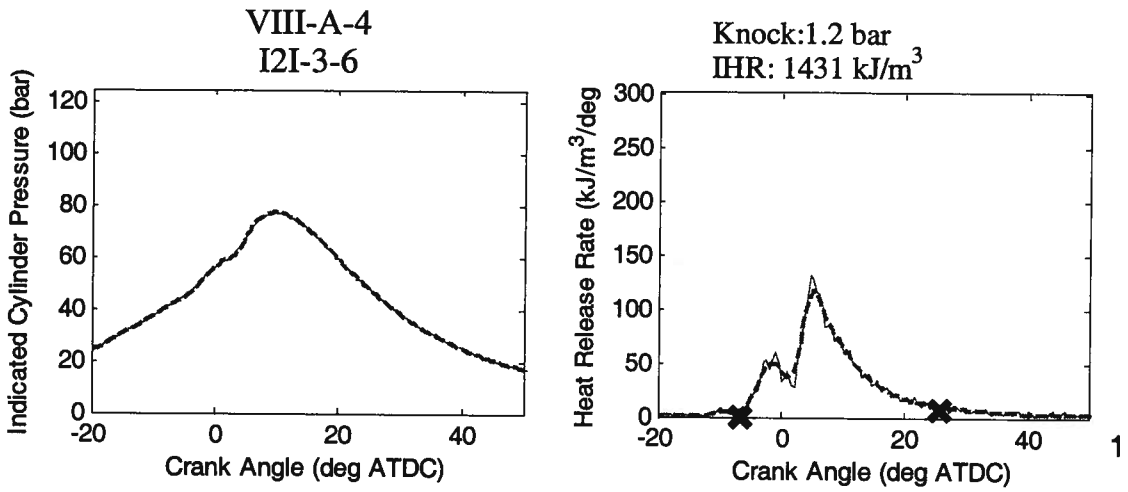

Figure F.5.1 : Diesel flowrate: 13.8 mg/inj

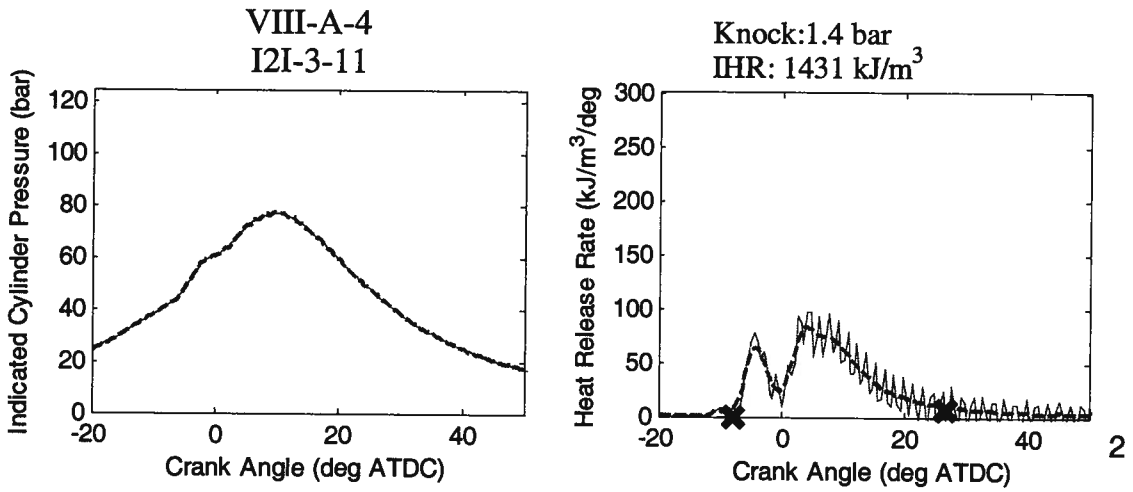

Figure F.5.2 : Diesel flowrate: 19.9 mg/inj

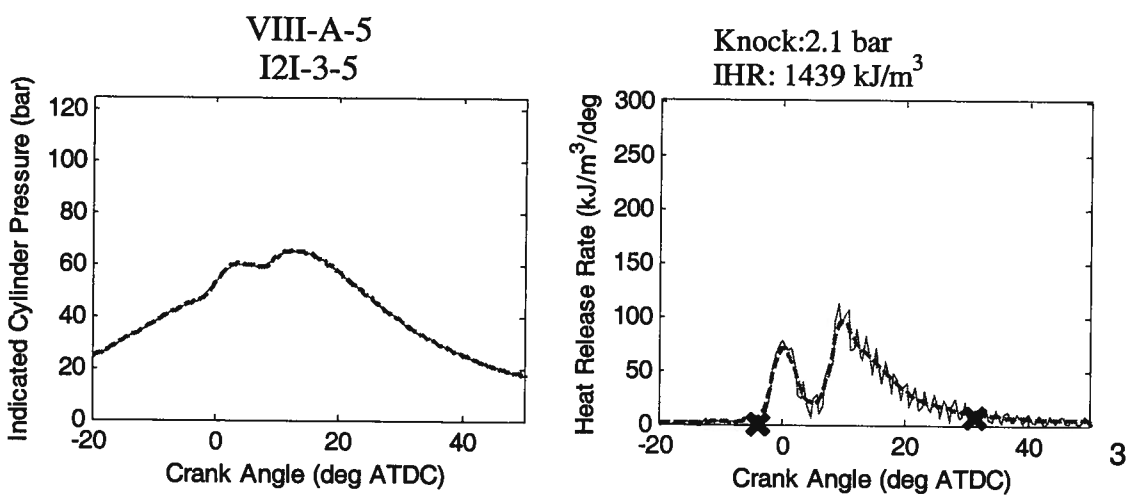

Figure F.5.3 : Diesel flowrate: 14.5 mg/inj

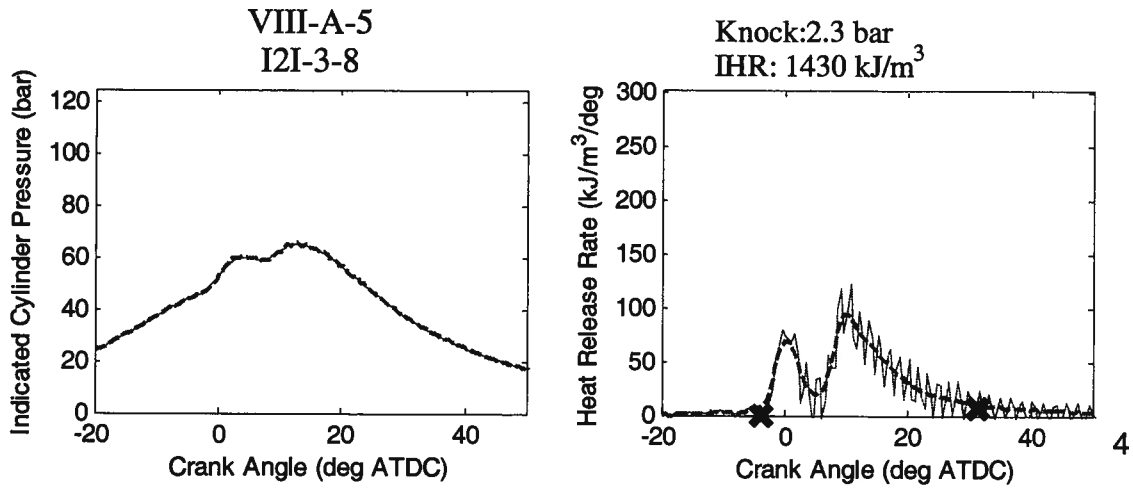

Figure F.5.4 : Diesel flowrate: 14.9 mg/inj

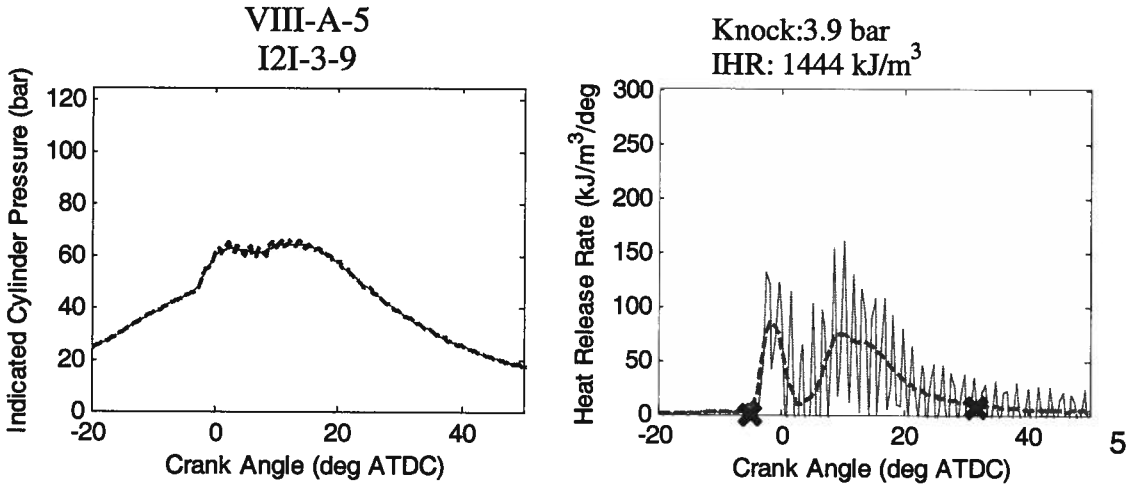

Figure F.5.5 : Diesel flowrate: 23.1 mg/inj

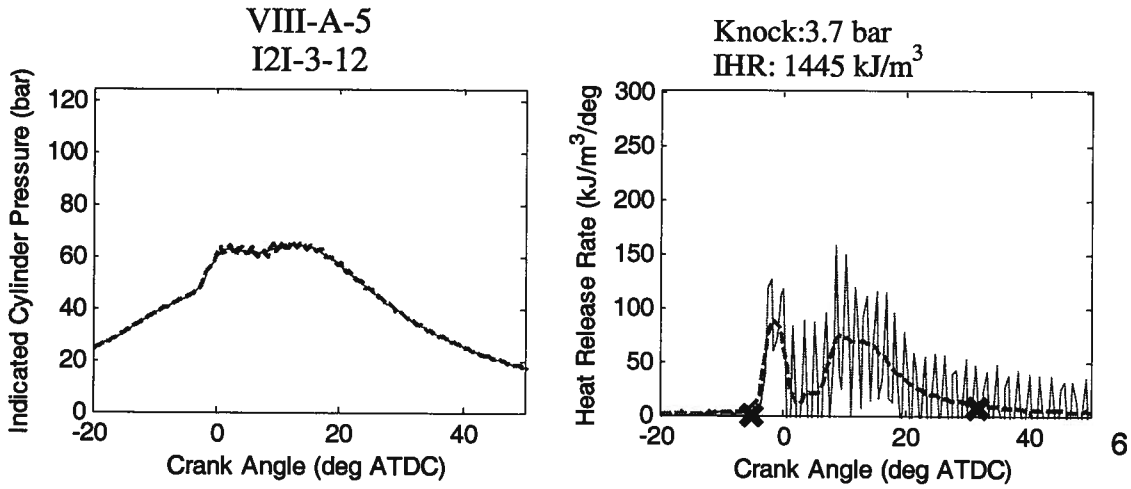

Figure F.5.6 : Diesel flowrate: 22.1 mg/inj

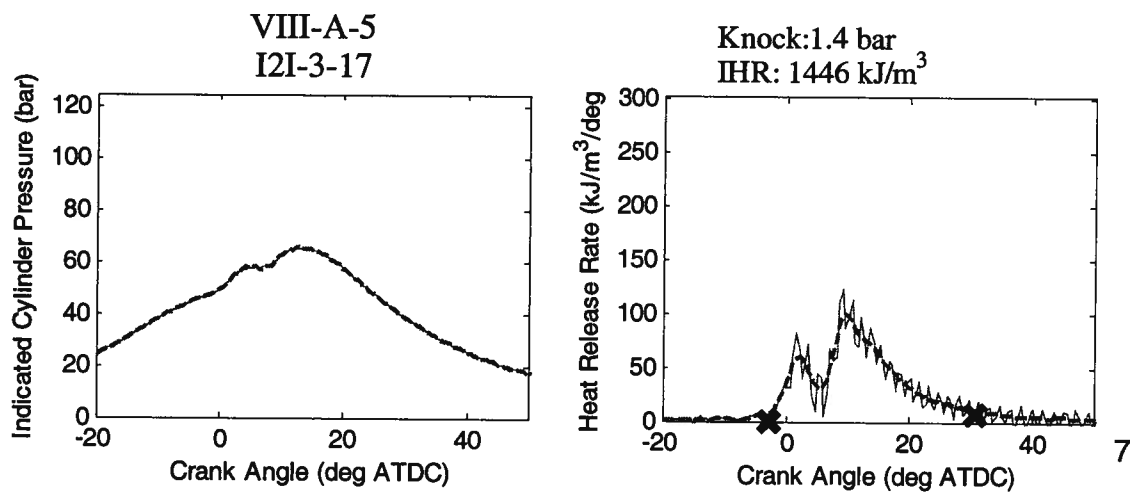

Figure F.5.7 : Diesel flowrate: 16.3 mg/inj

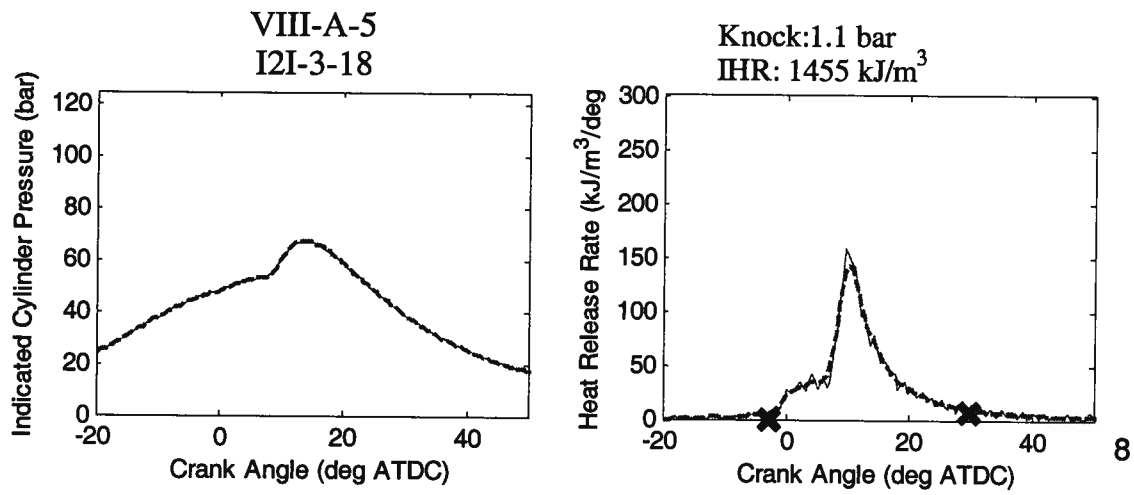

Figure F.5.8 : Diesel flowrate: 14.2 mg/inj

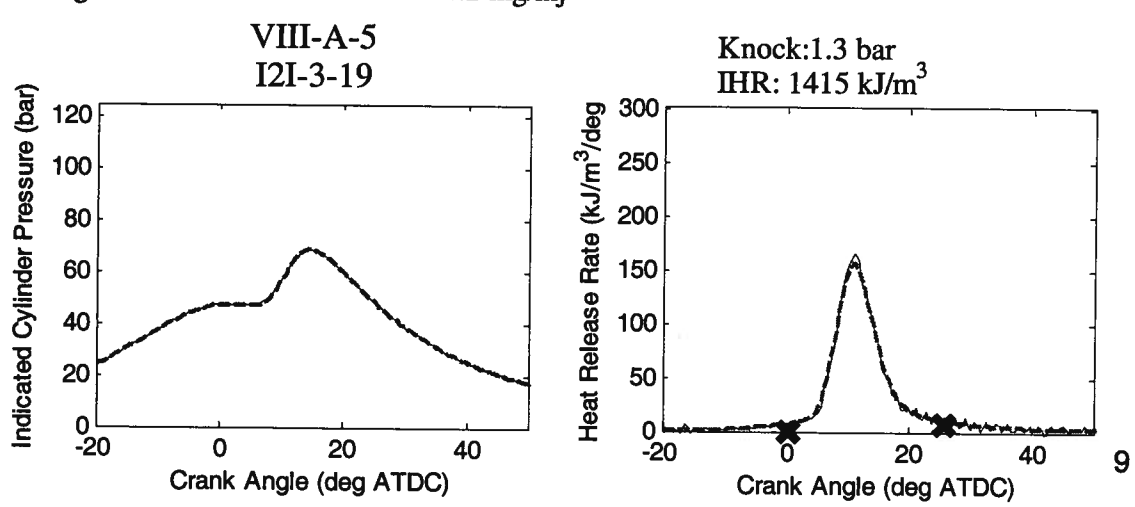

Figure F.5.9 : Diesel flowrate: 18.4 mg/inj

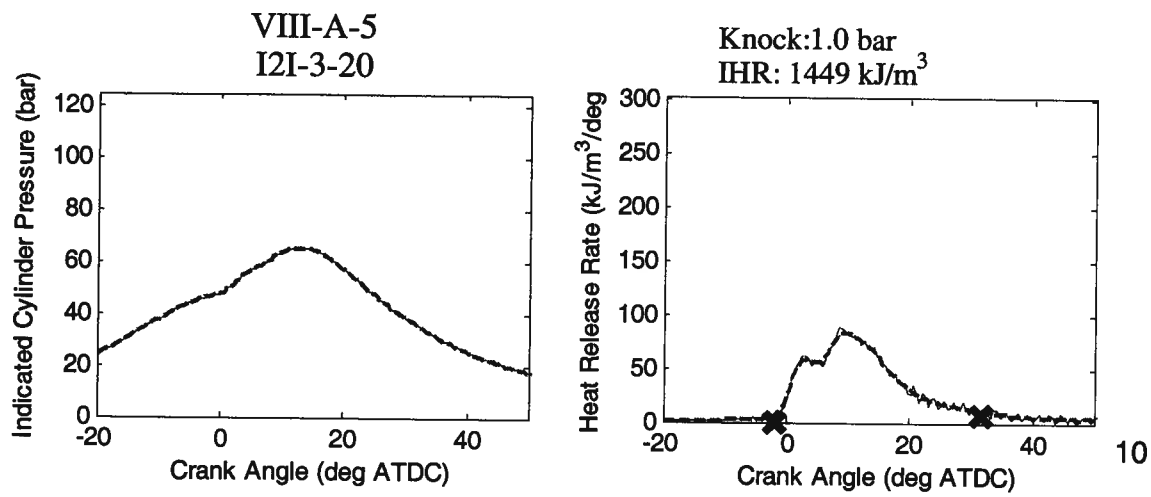

Figure F.5.10 : Diesel flowrate: 18.9 mg/inj

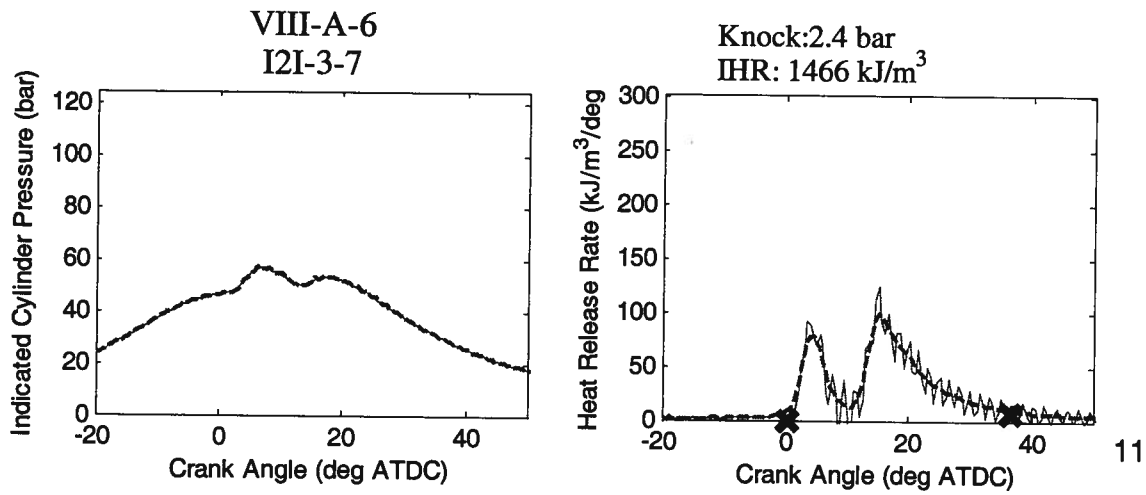

Figure F.5.11 : Diesel flowrate: 11.9 mg/inj

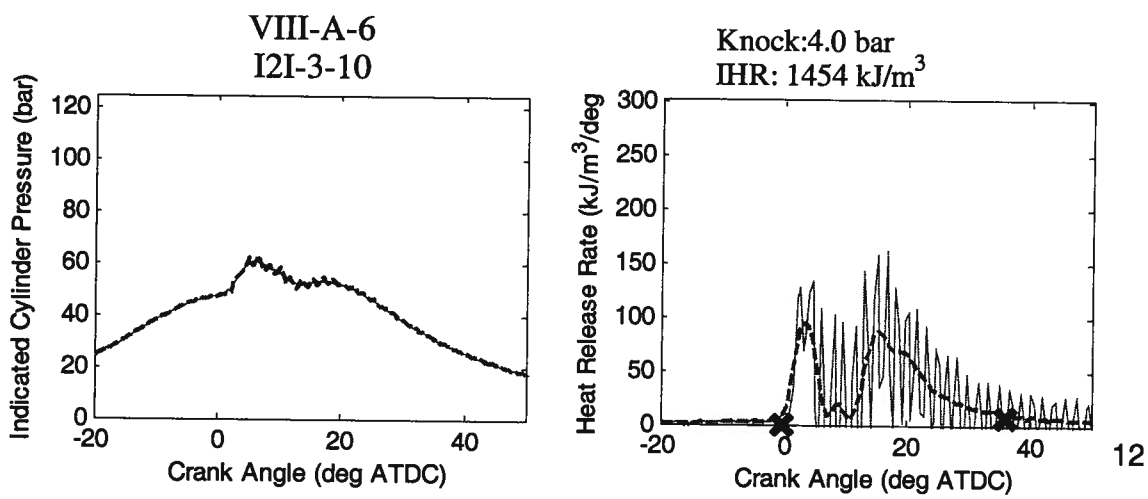

Figure F.5.12 : Diesel flowrate: 21.2 mg/inj

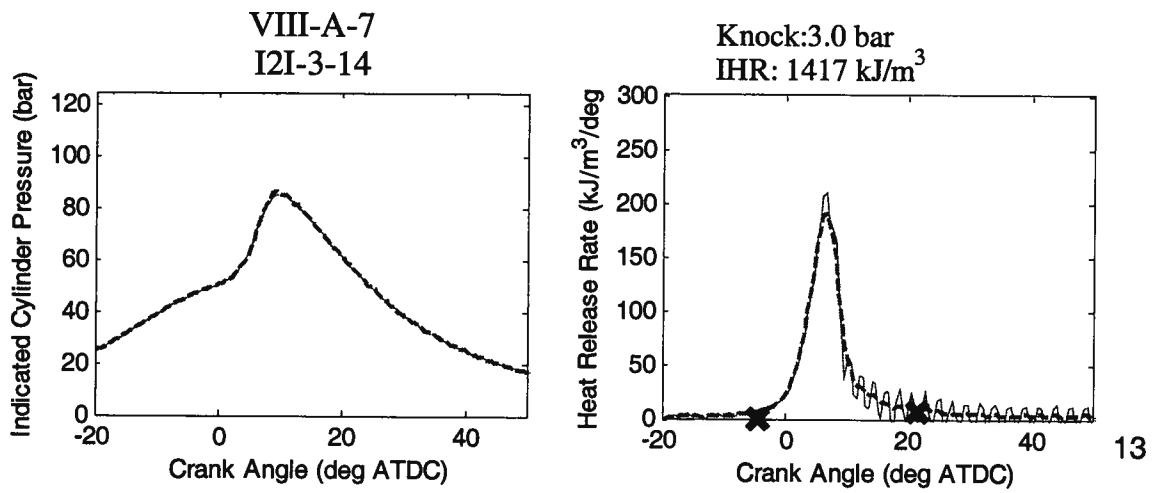

Figure F.5.13 : Diesel flowrate: 16.8 mg/inj

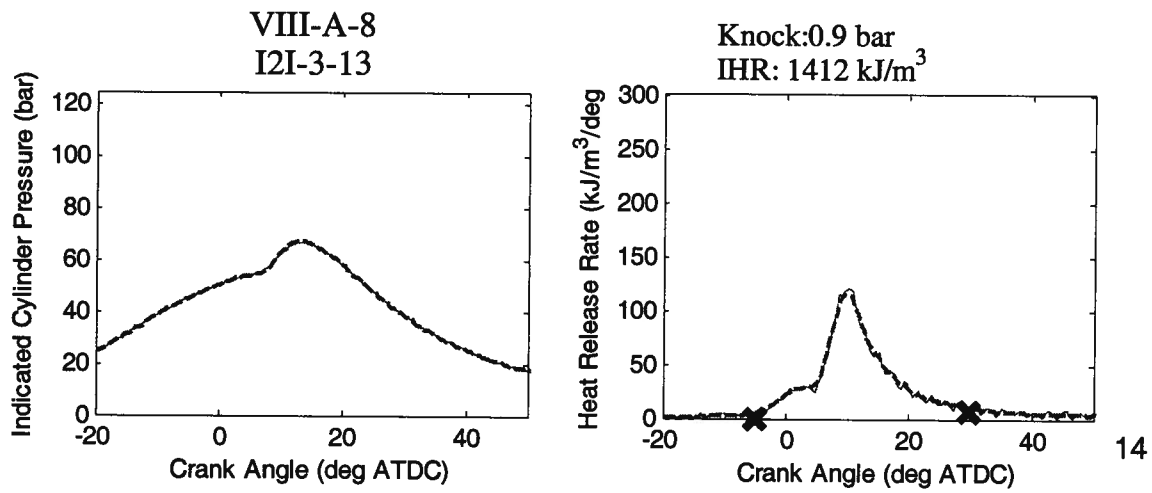

Figure F.5.14 : Diesel flowrate: 15.3 mg/inj

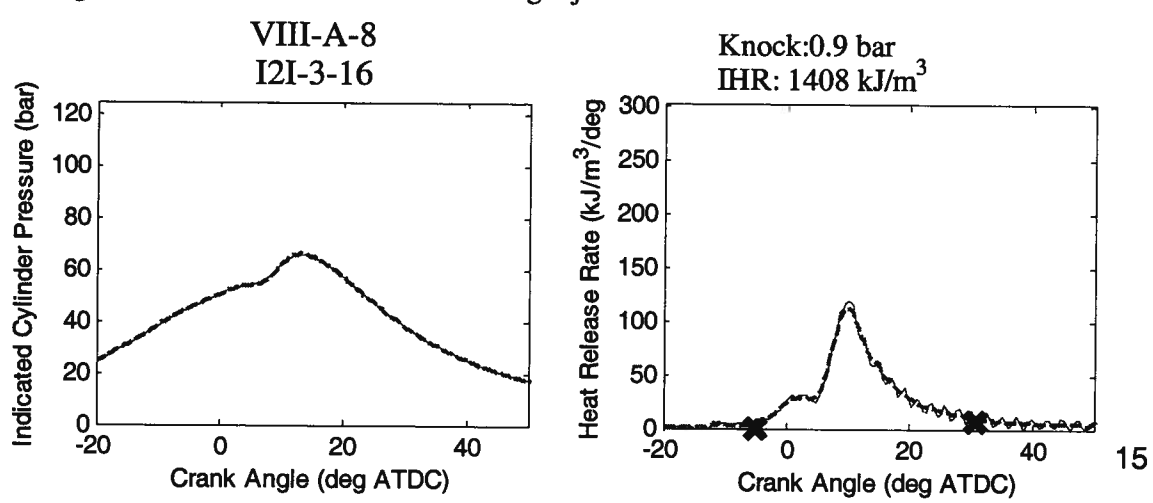

Figure F.5.15 : Diesel flowrate: 13.9 mg/inj

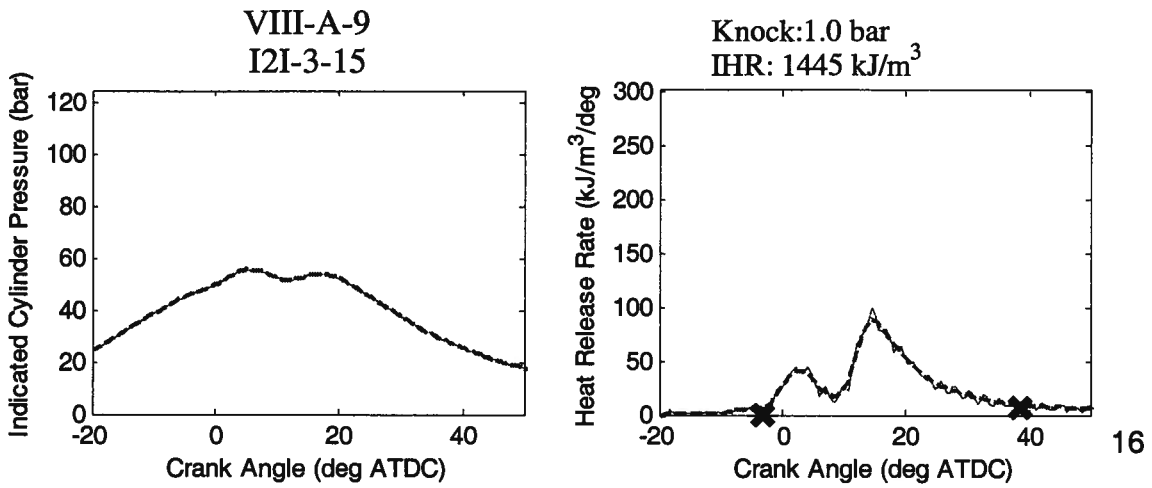

Figure F.5.16 : Diesel flowrate: 11.3 mg/inj

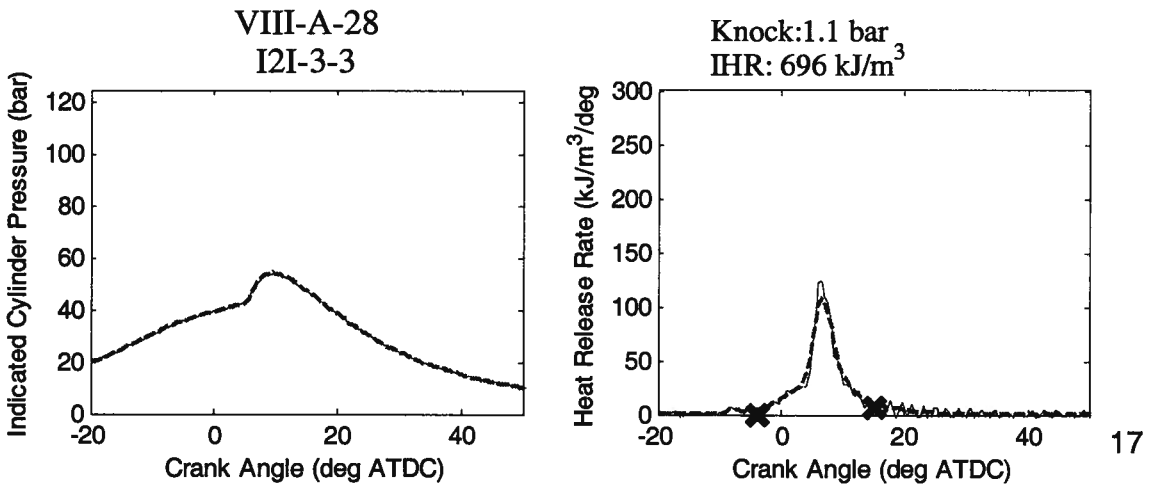

Figure F.5.17 : Diesel flowrate: 12.4 mg/inj

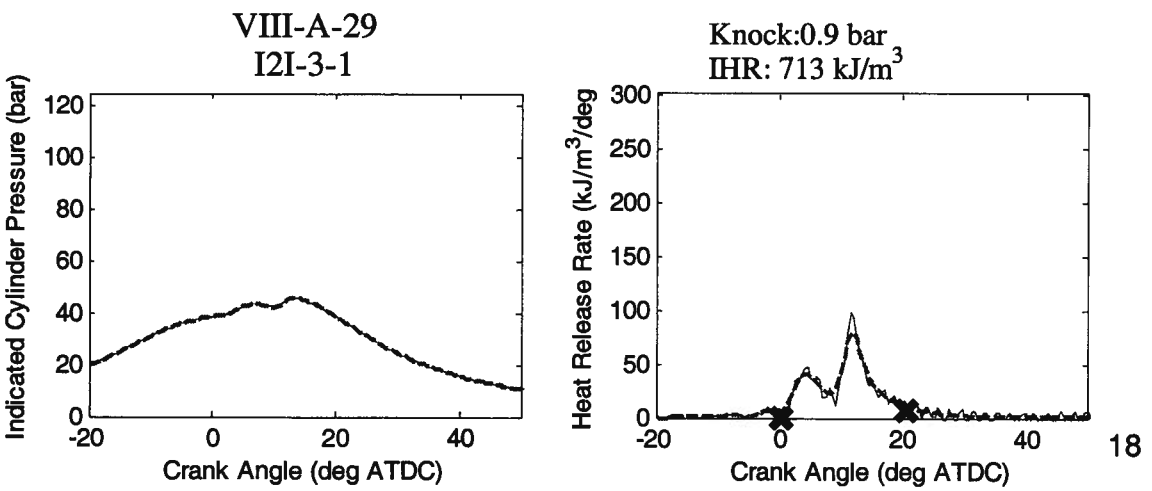

Figure F.5.18 : Diesel flowrate: 13.9 mg/inj

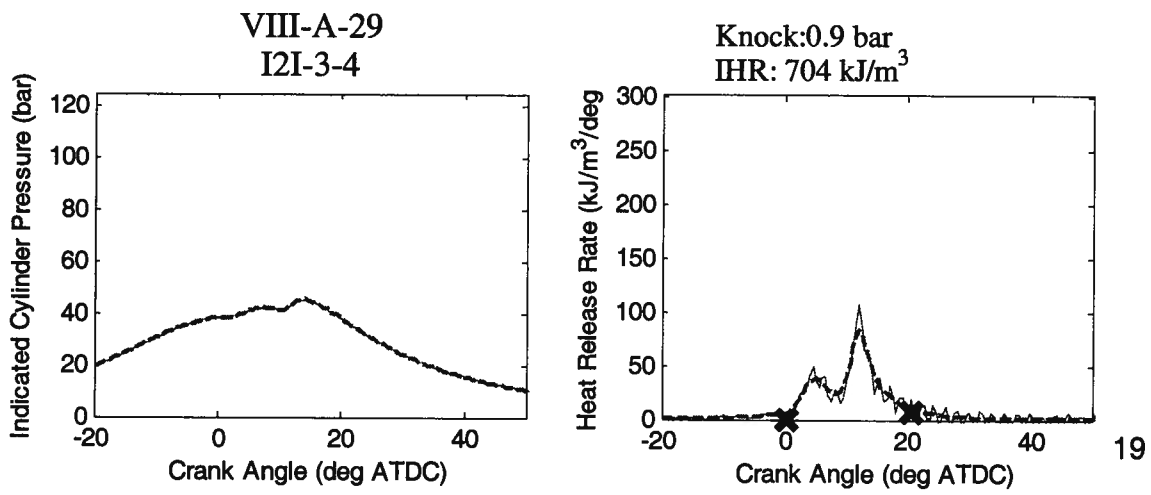

Figure F.5.19 : Diesel flowrate: 16.6 mg/inj

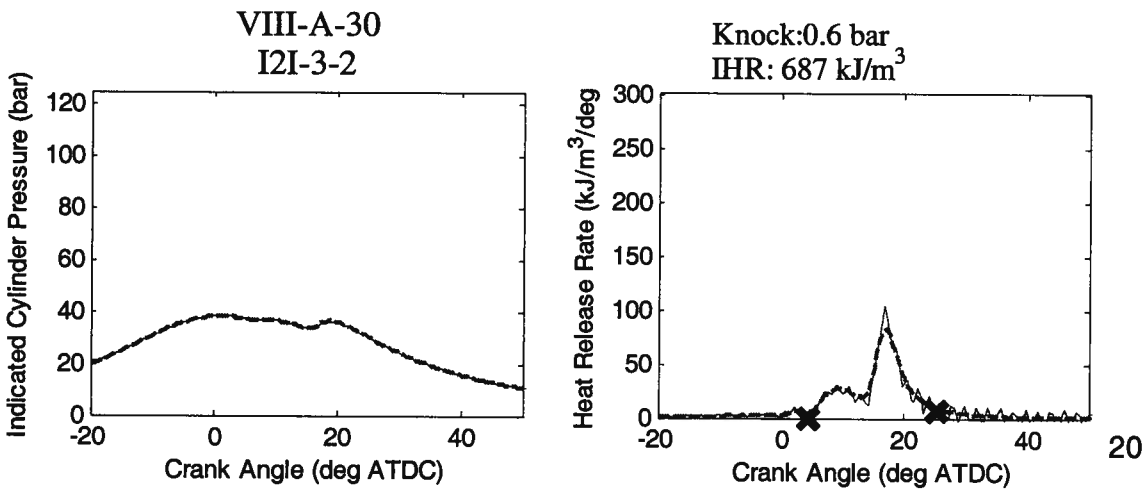

Figure F.5.20 : Diesel flowrate: 15.2 mg/inj

Appendix F.6- Test Series VIII-B Pressure and HRR Curves

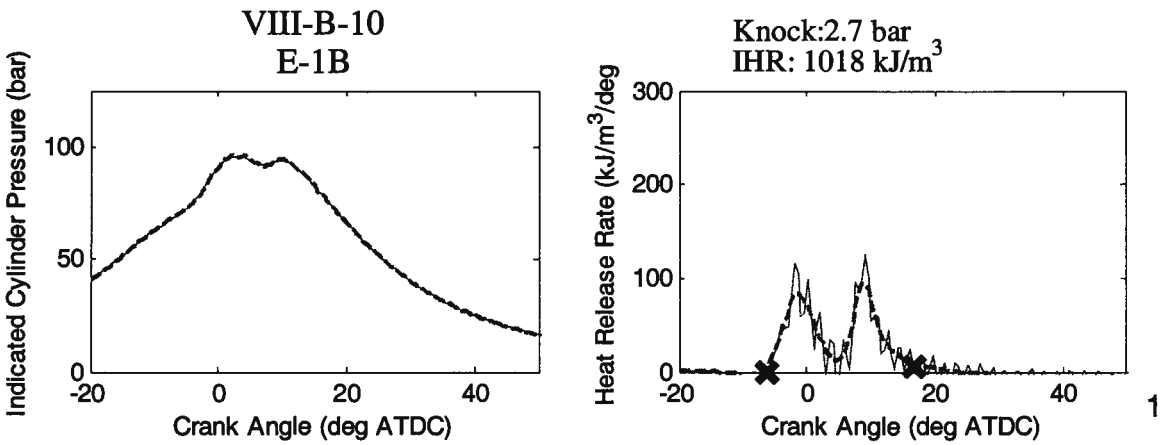

Figure F.6.1 : Diesel flowrate: 13.4 mg/inj

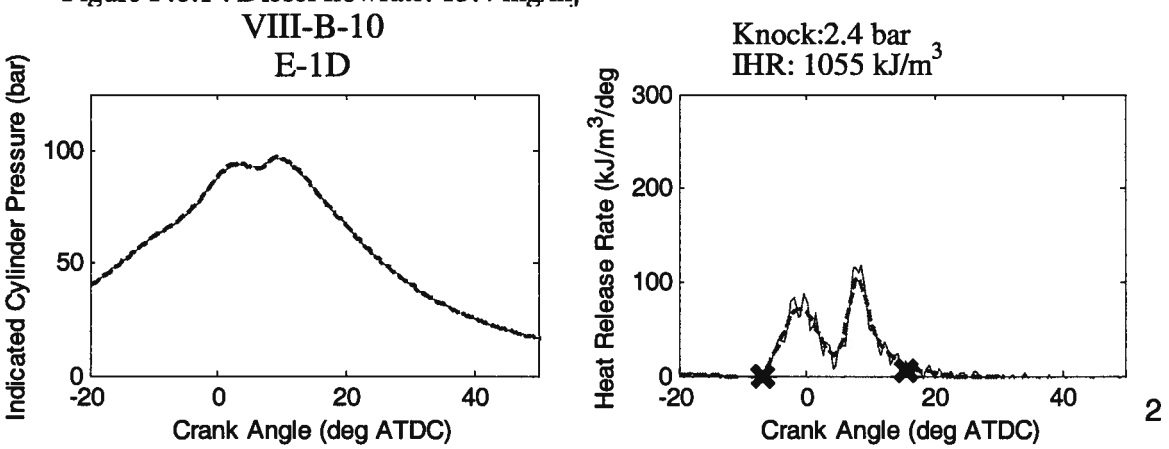

Figure F.6.2 : Diesel flowrate: 12.7 mg/inj

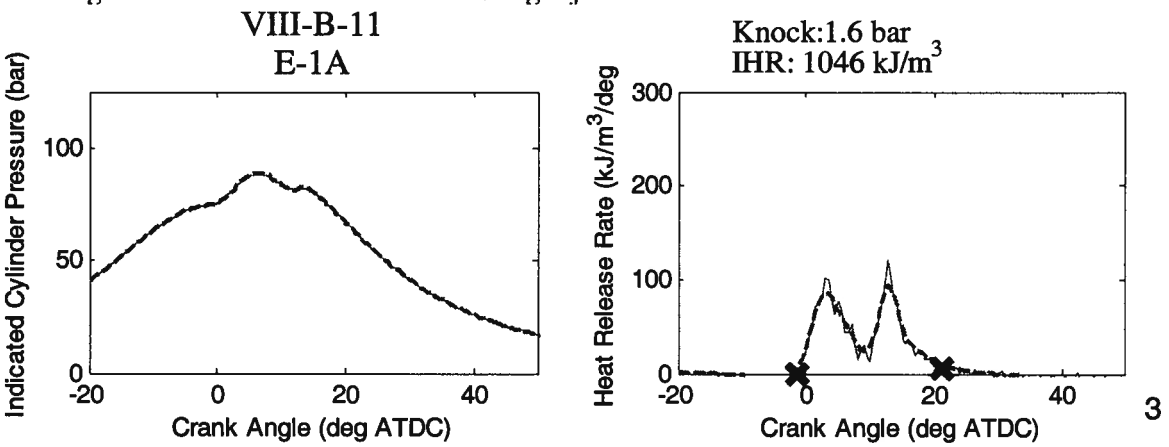

Figure F.6.3 : Diesel flowrate: 14.1 mg/inj

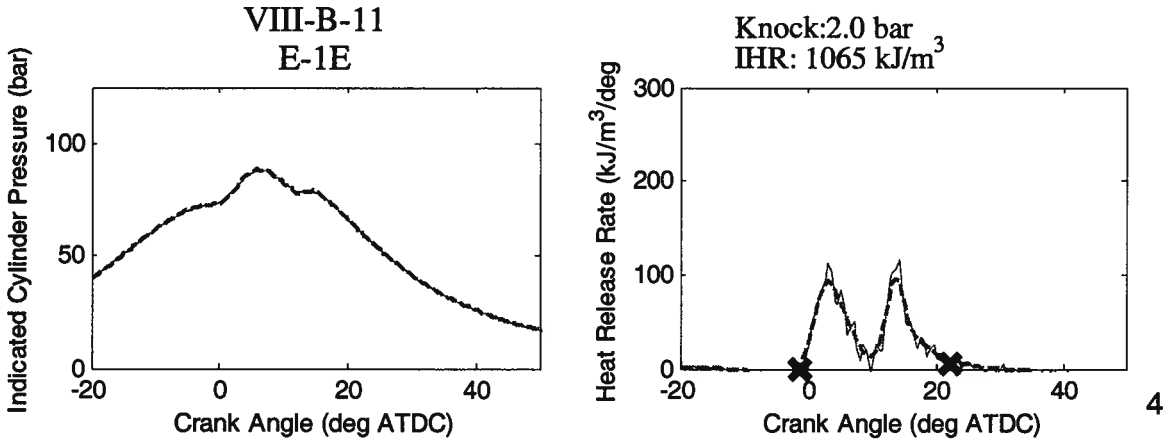

Figure F.6.4 : Diesel flowrate: 13.0 mg/inj

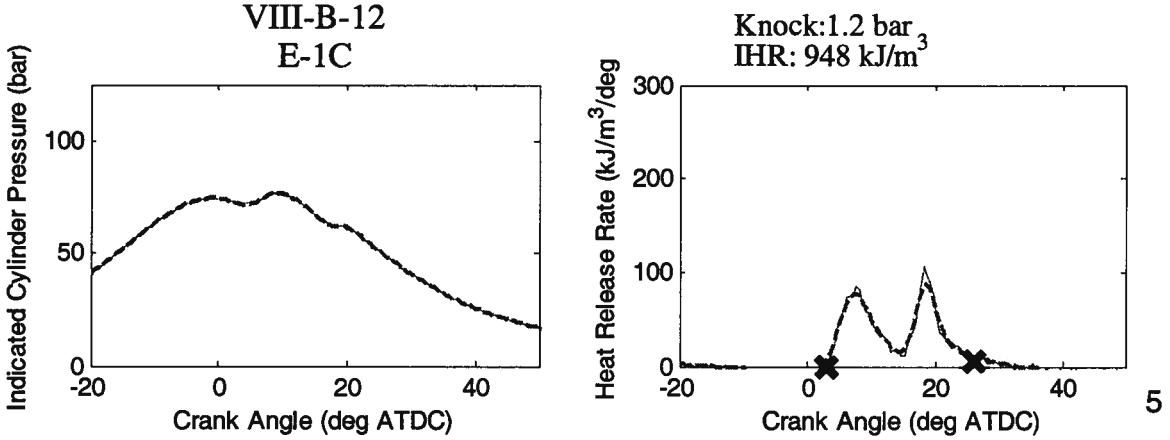

Figure F.6.5 : Diesel flowrate: 12.6 mg/inj

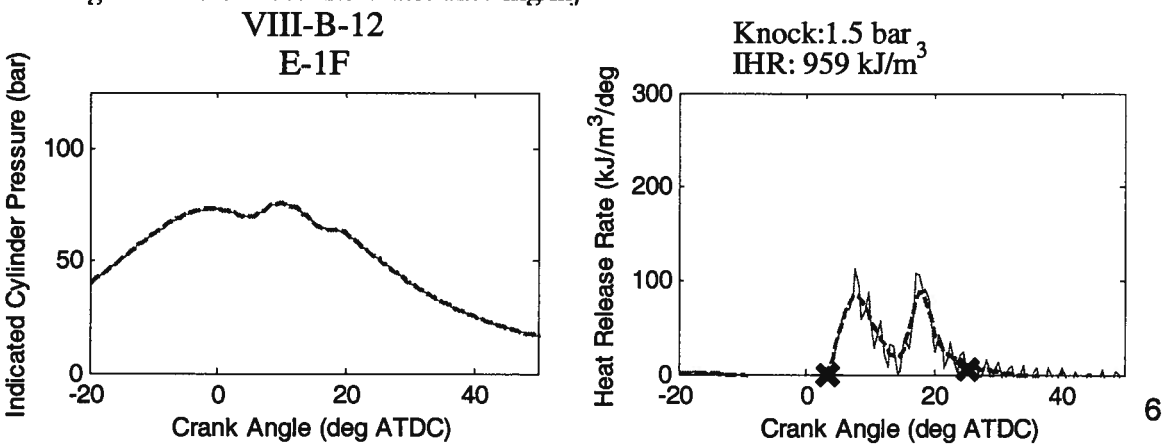

Figure F.6.6 : Diesel flowrate: 14.9 mg/inj

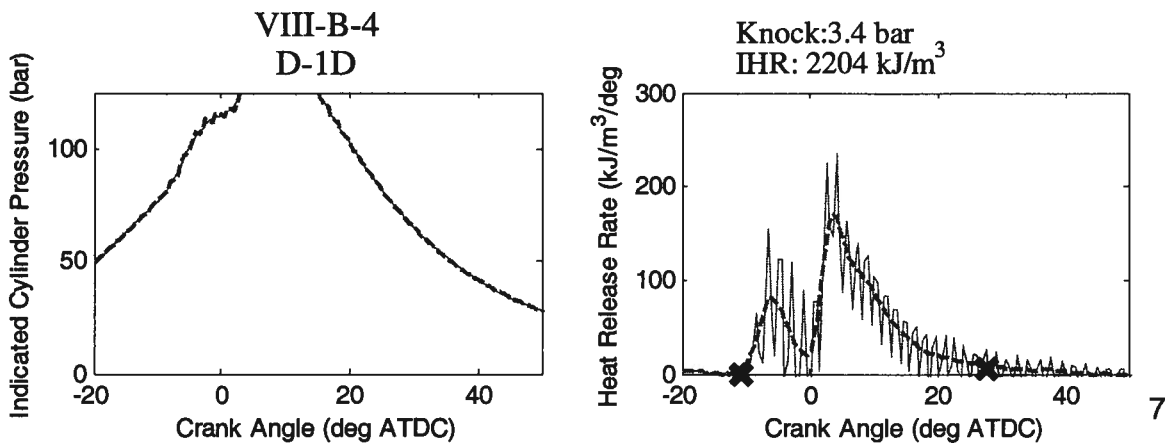

Figure F.6.7 : Diesel flowrate: 14.4 mg/inj

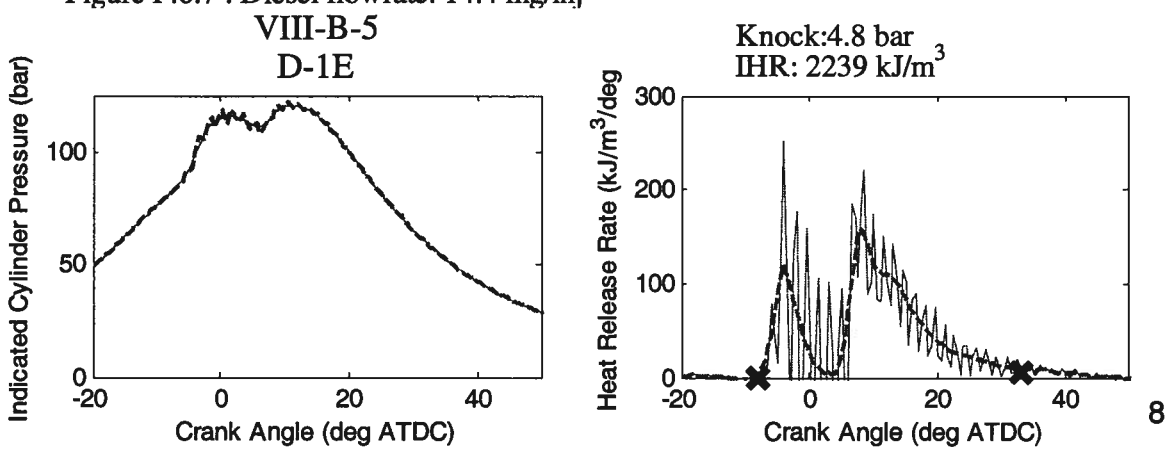

Figure F.6.8 : Diesel flowrate: 15.5 mg/inj

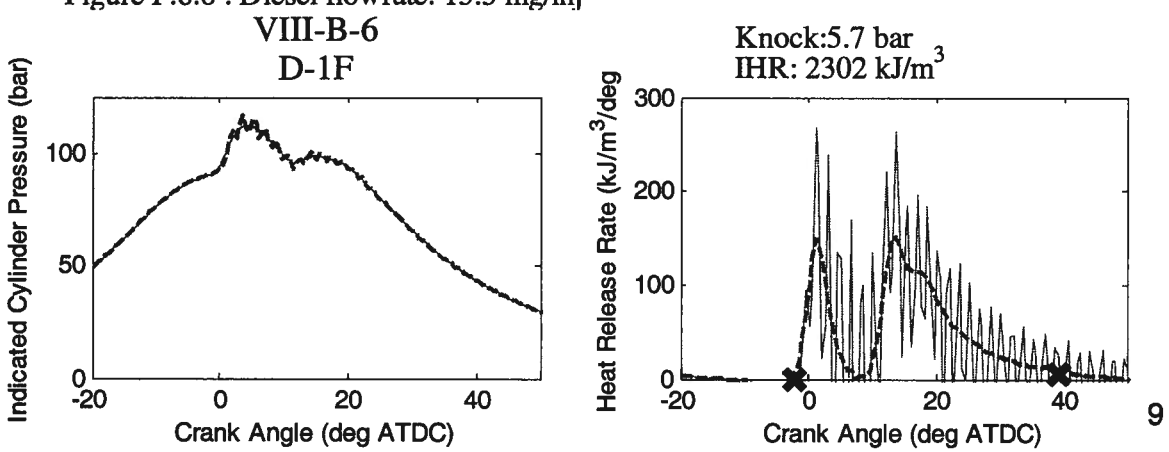

Figure F.6.9 : Diesel flowrate: 15.0 mg/inj

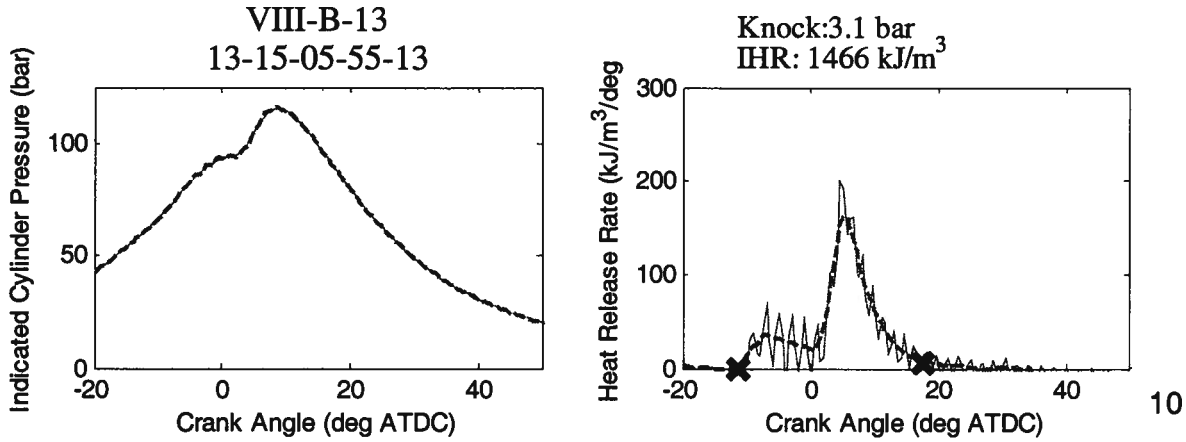

Figure F.6.10 : Diesel flowrate: 17.0 mg/inj

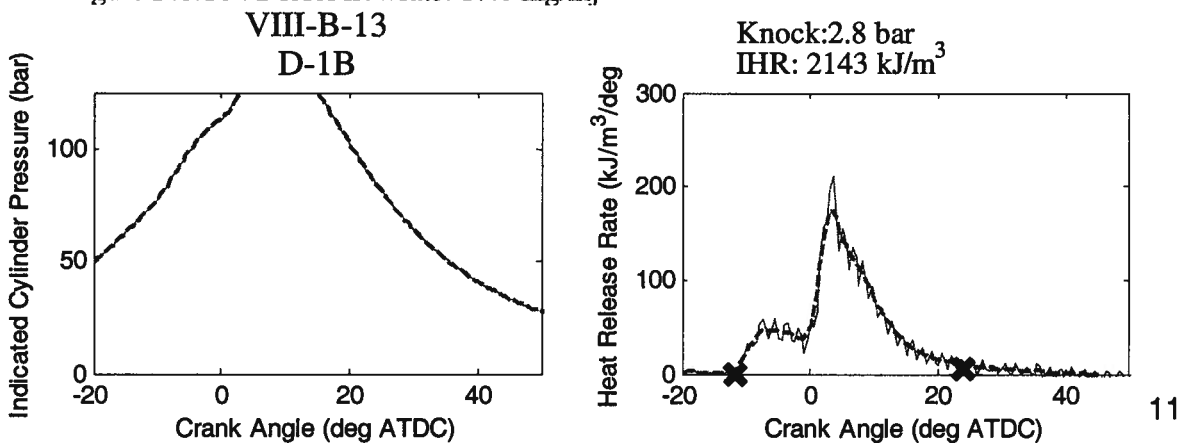

Figure F.6.11 : Diesel flowrate: 11.4 mg/inj

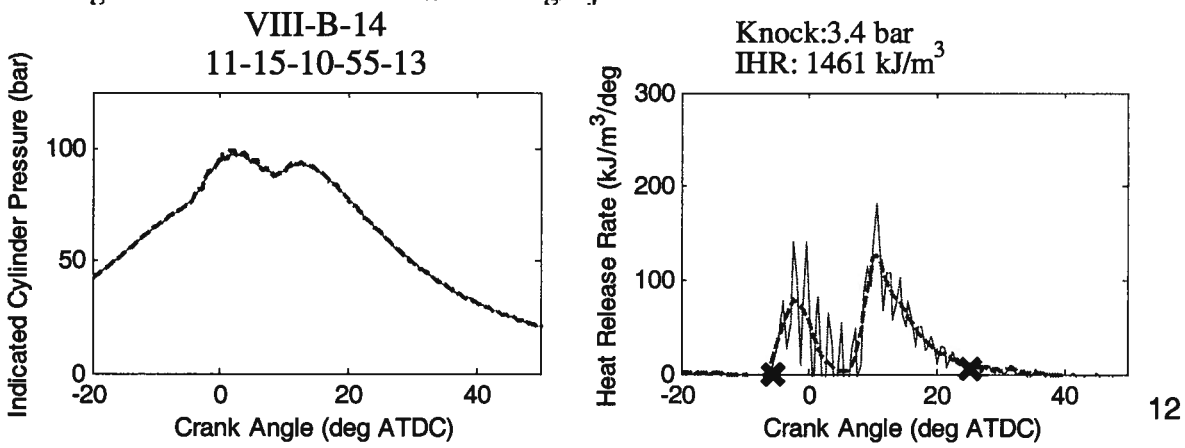

Figure F.6.12 : Diesel flowrate: 17.2 mg/inj

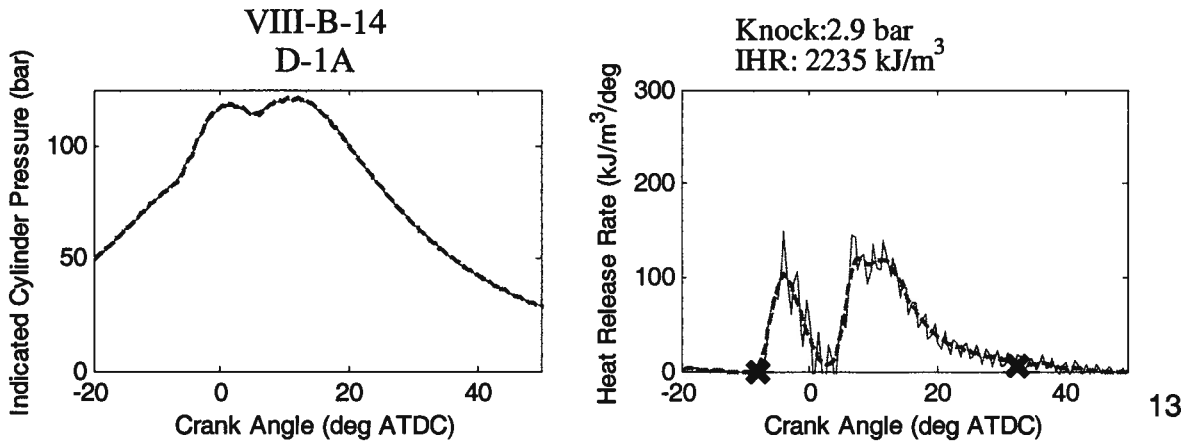

Figure F.6.13 : Diesel flowrate: 18.4 mg/inj

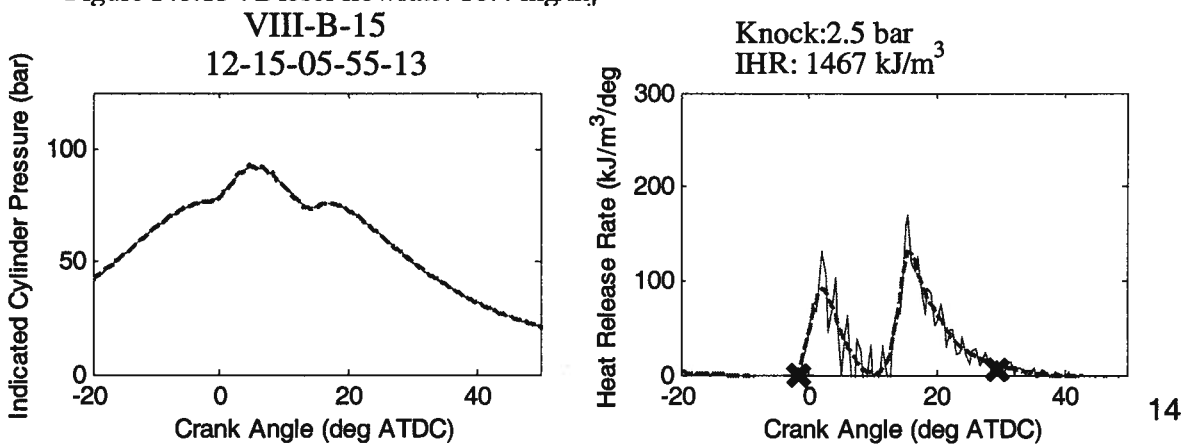

Figure F.6.14 : Diesel flowrate: 15.5 mg/inj

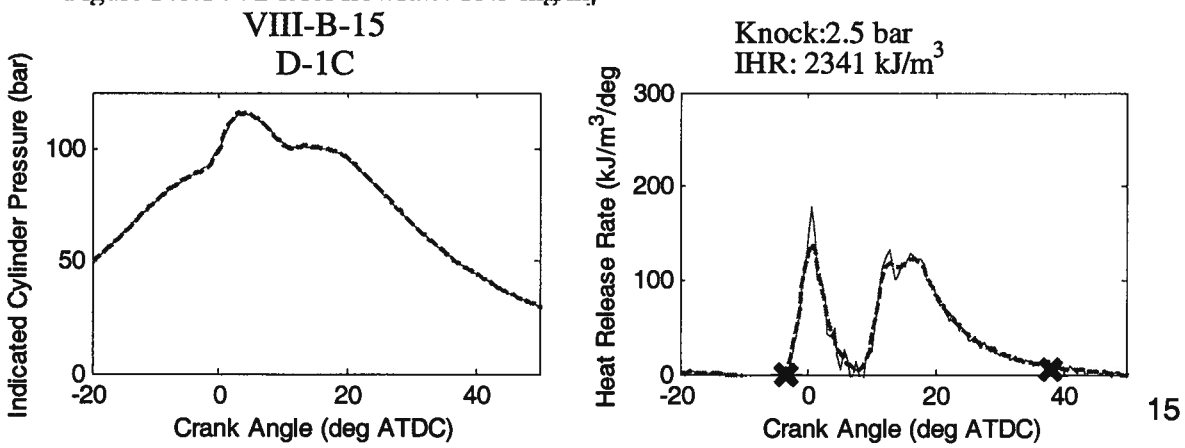

Figure F.6.15 : Diesel flowrate: 11.8 mg/inj

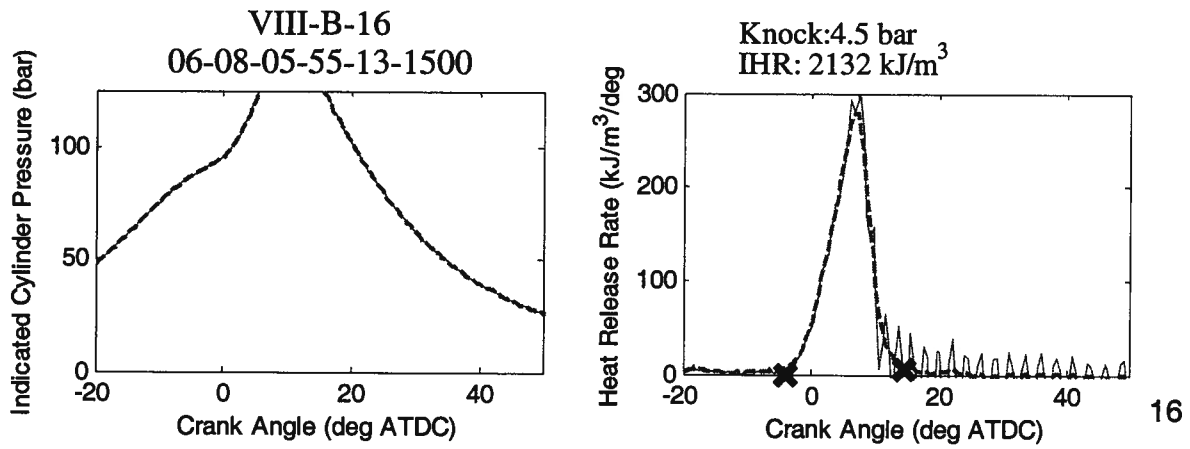

Figure F.6.16 : Diesel flowrate: 16.3 mg/inj

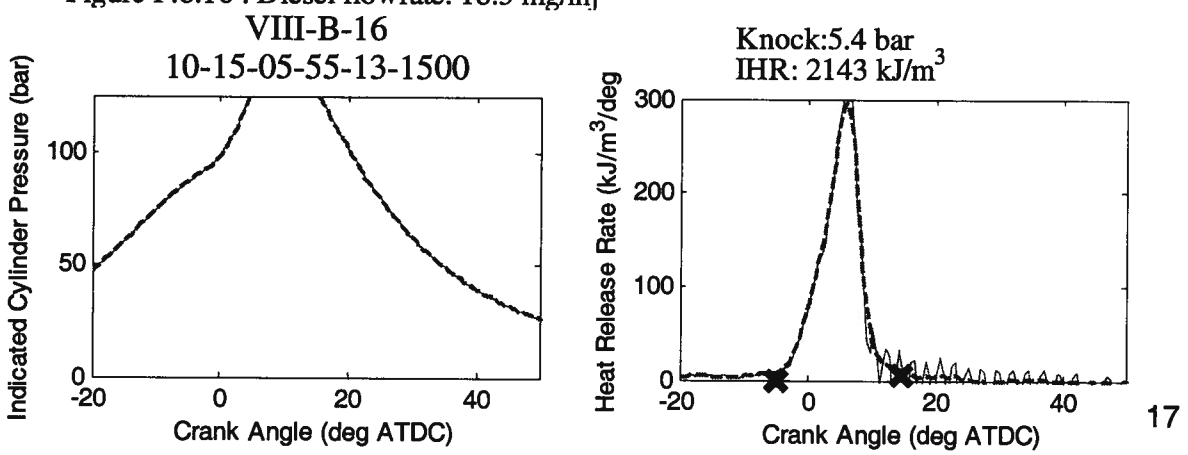

Figure F.6.17 : Diesel flowrate: 14.3 mg/inj

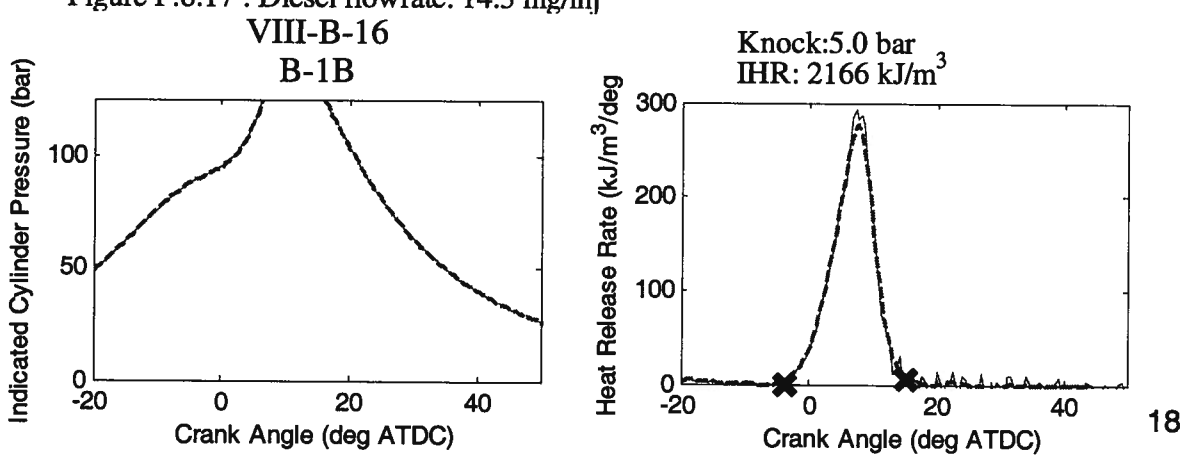

Figure F.6.18 : Diesel flowrate: 15.2 mg/inj

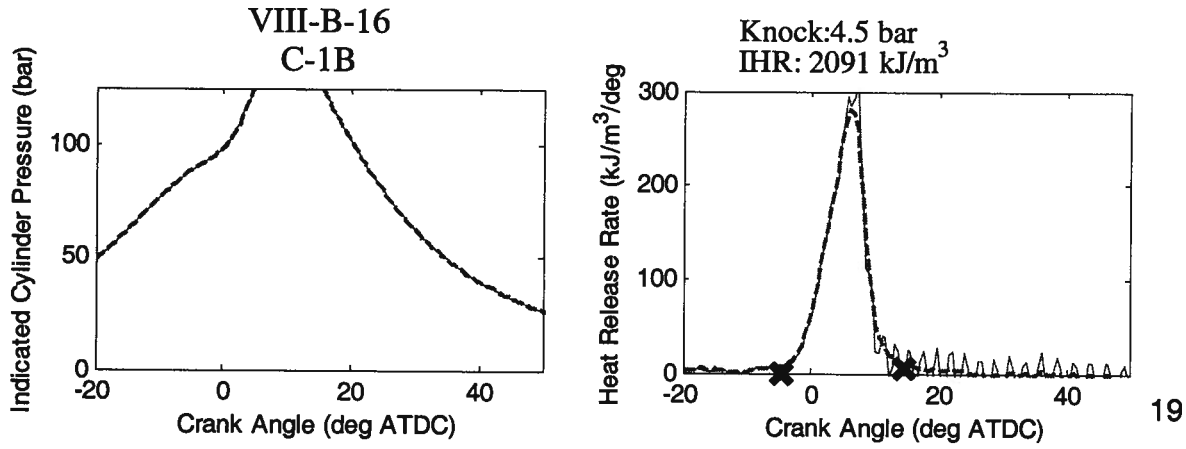

Figure F.6.19 : Diesel flowrate: 18.2 mg/inj

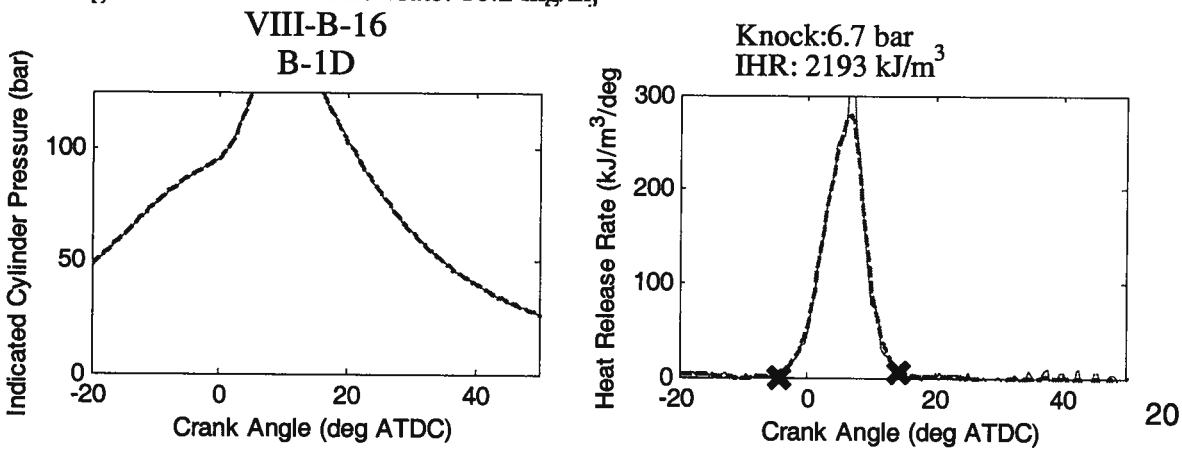

Figure F.6.20 : Diesel flowrate: 15.3 mg/inj

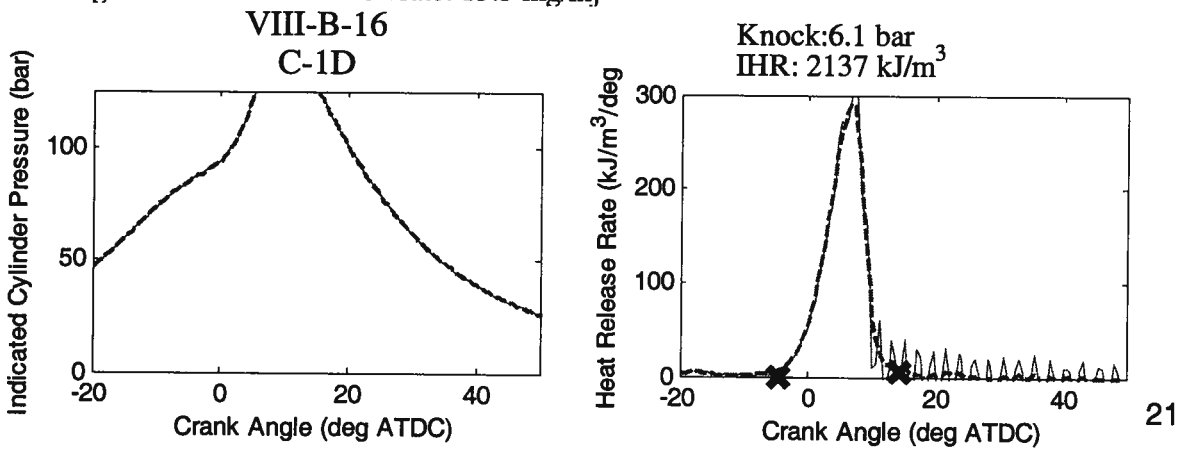

Figure F.6.21 : Diesel flowrate: 17.8 mg/inj

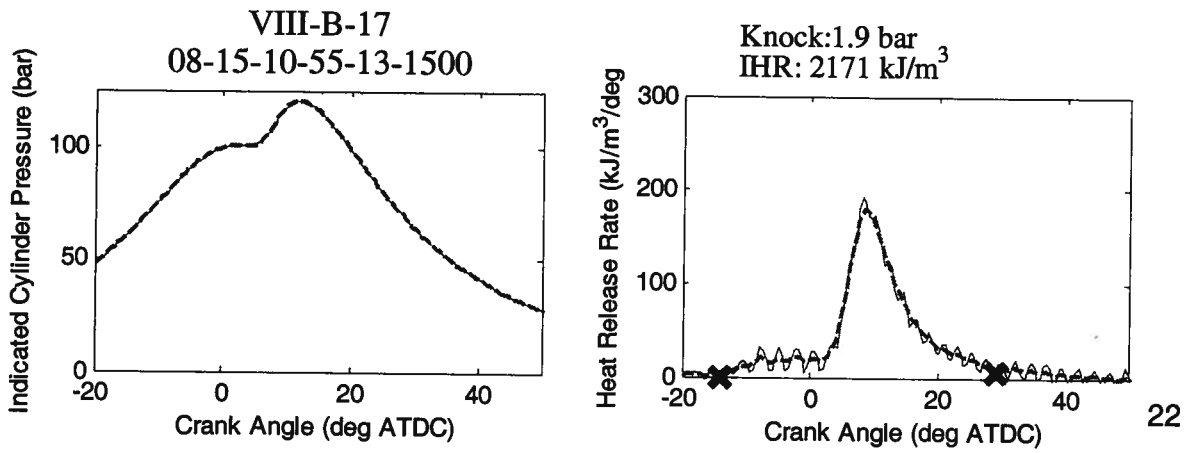

Figure F.6.22 : Diesel flowrate: 14.0 mg/inj

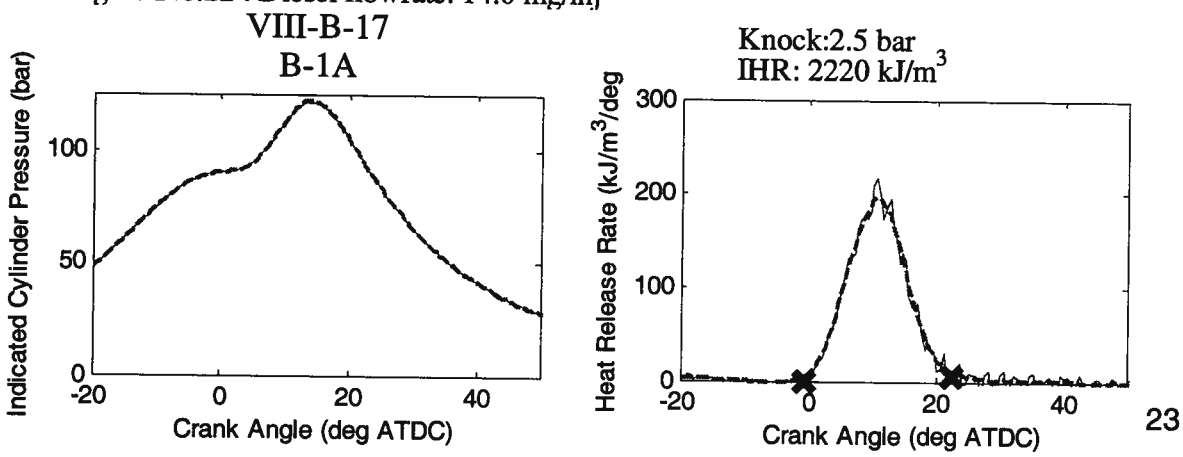

Figure F.6.23 : Diesel flowrate: 14.8 mg/inj

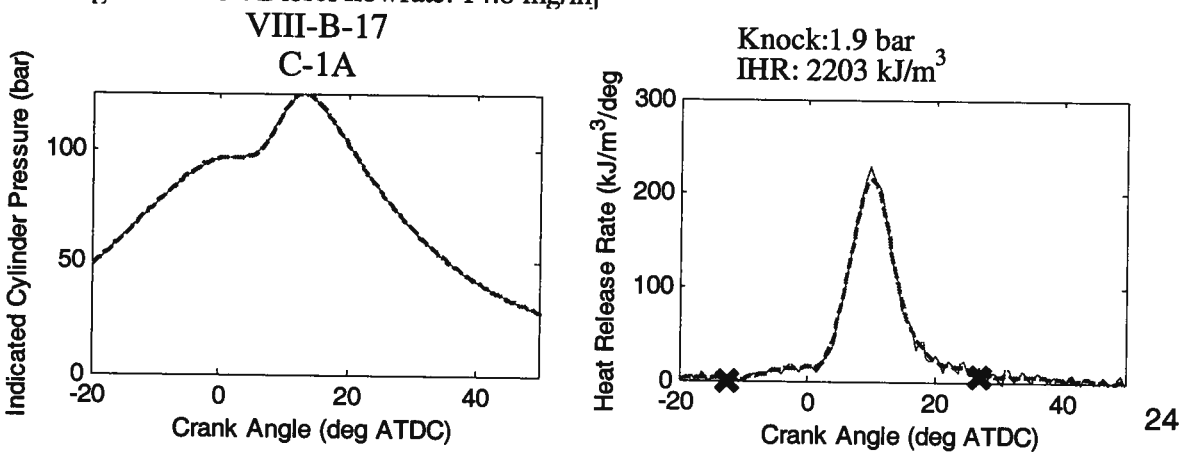

Figure F.6.24 : Diesel flowrate: 17.9 mg/inj

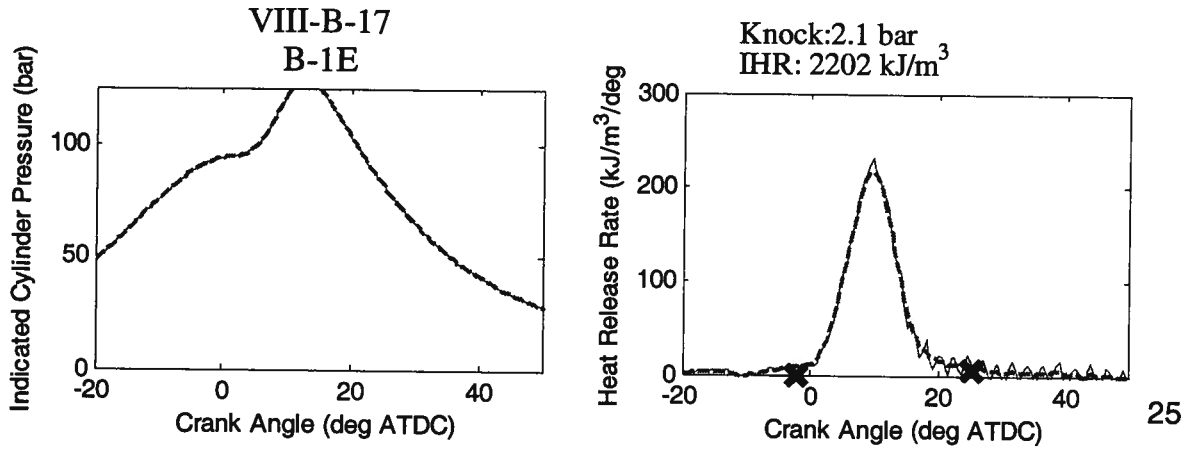

Figure F.6.25 : Diesel flowrate: 16.5 mg/inj

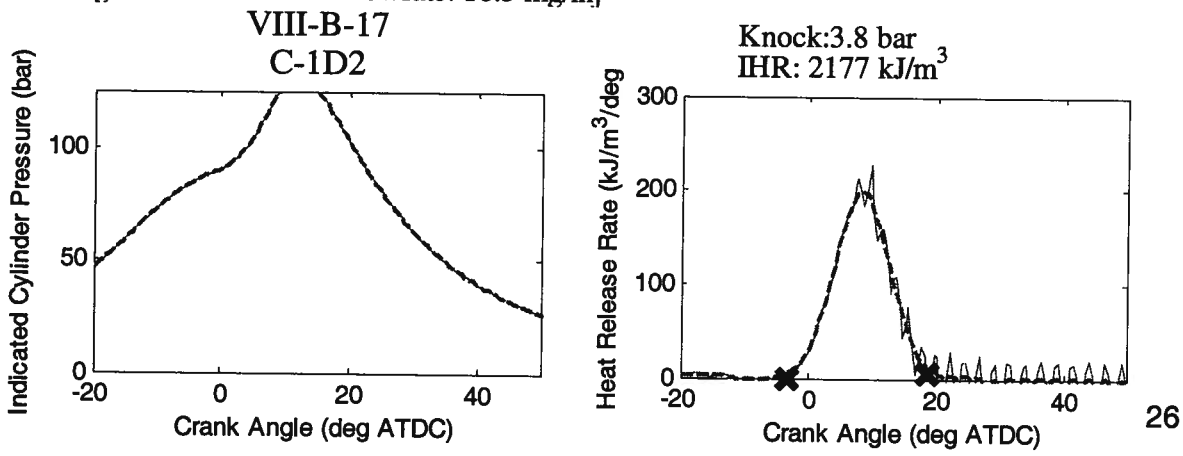

Figure F.6.26 : Diesel flowrate: 16.3 mg/inj

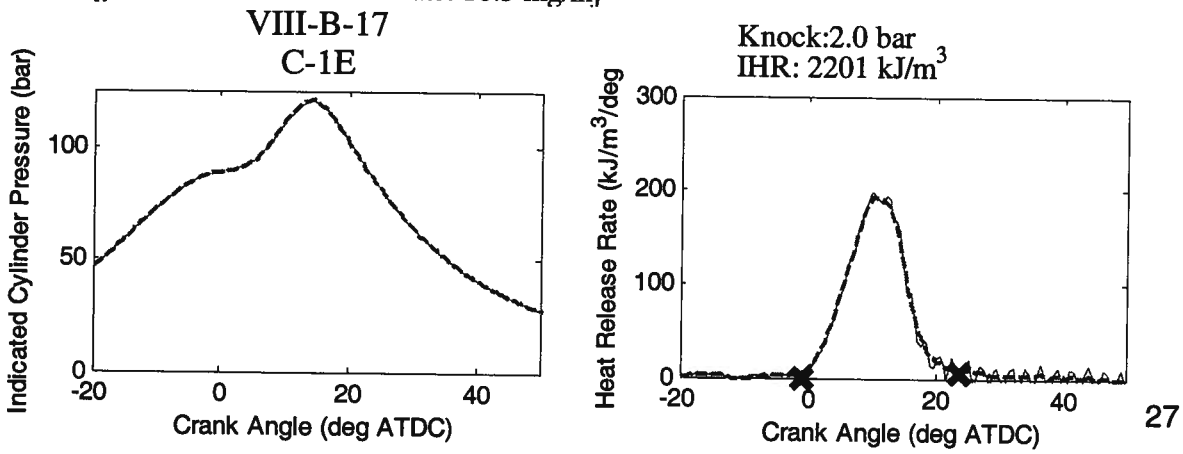

Figure F.6.27 : Diesel flowrate: 16.5 mg/inj

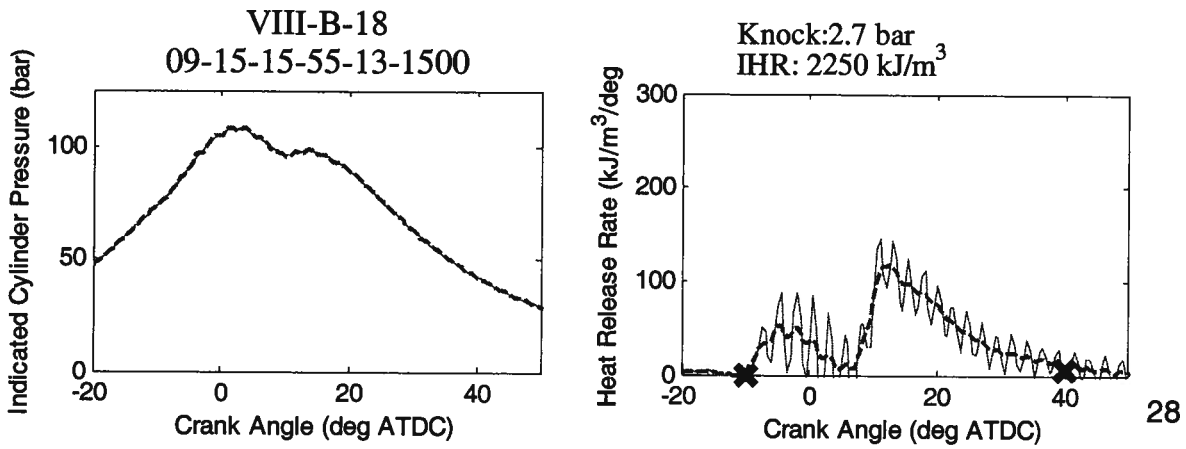

Figure F.6.28 : Diesel flowrate: 14.0 mg/inj

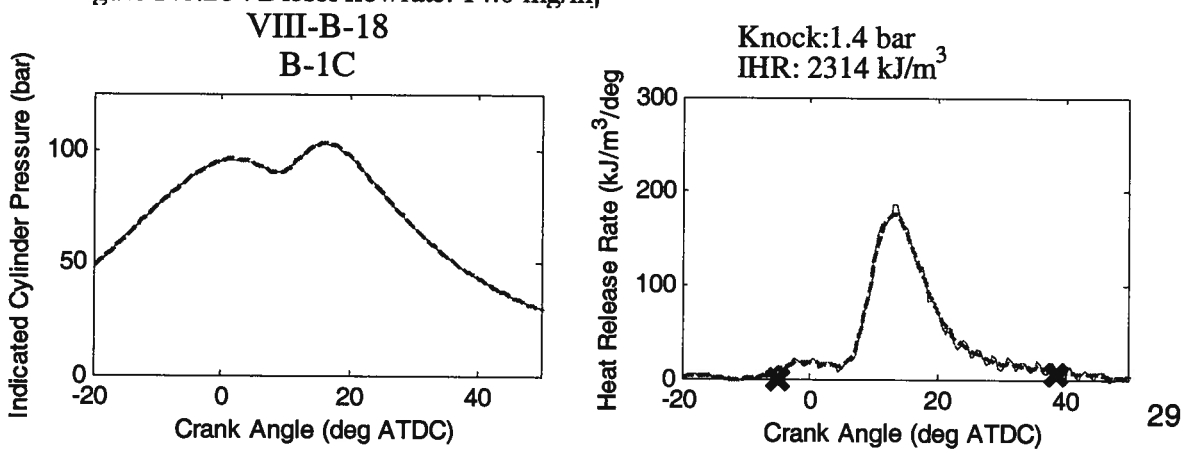

Figure F.6.29 : Diesel flowrate: 15.8 mg/inj

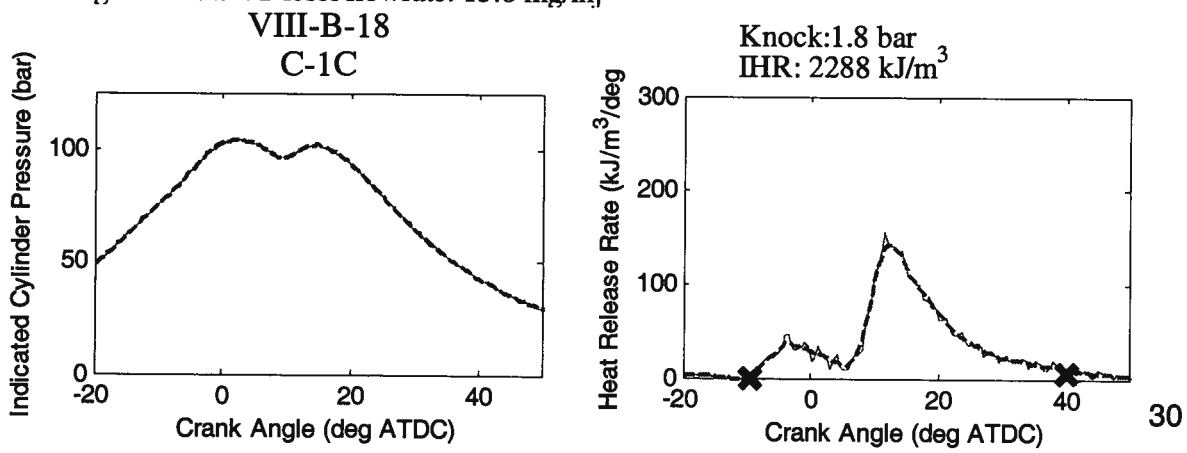

Figure F.6.30 : Diesel flowrate: 17.5 mg/inj

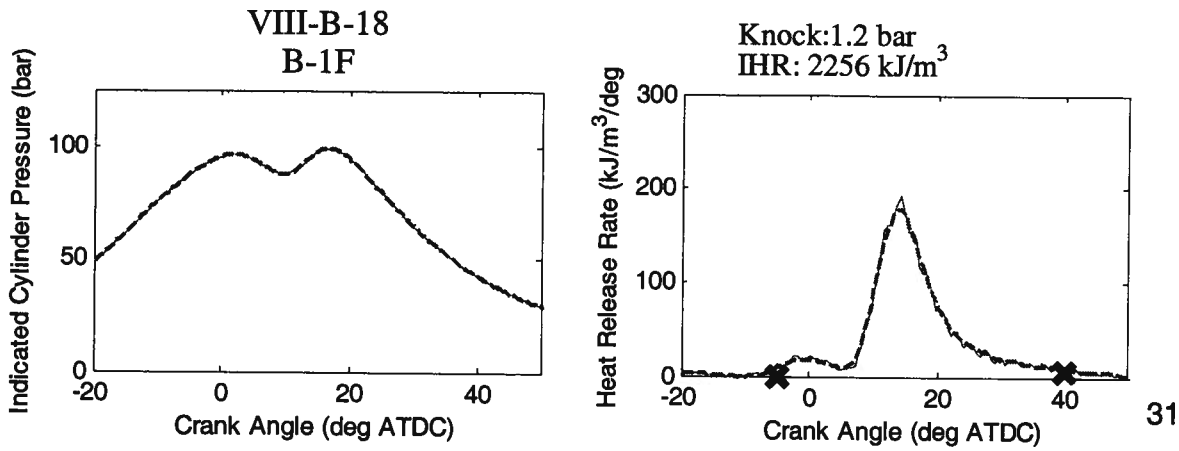

Figure F.6.31 : Diesel flowrate: 14.2 mg/inj

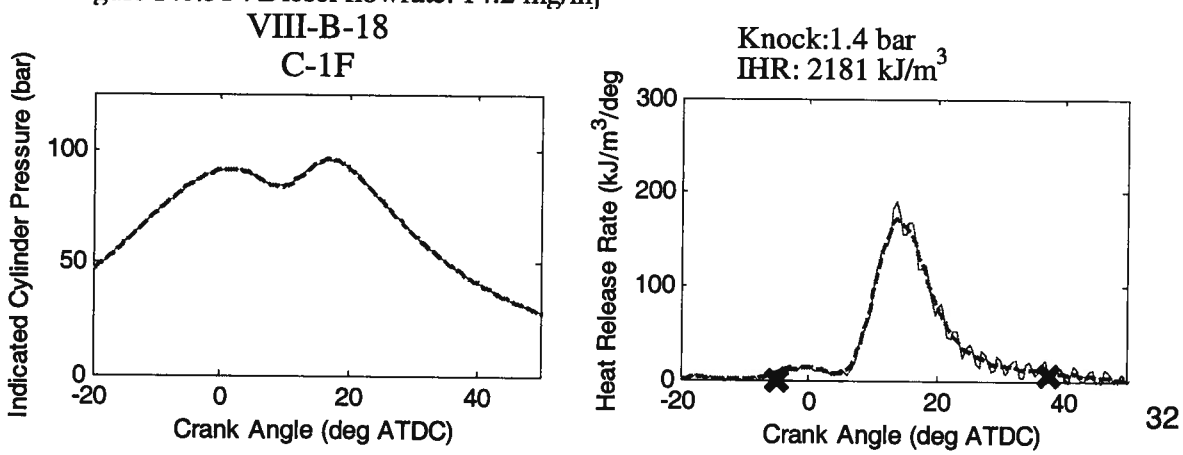

Figure F.6.32 : Diesel flowrate: 15.5 mg/inj

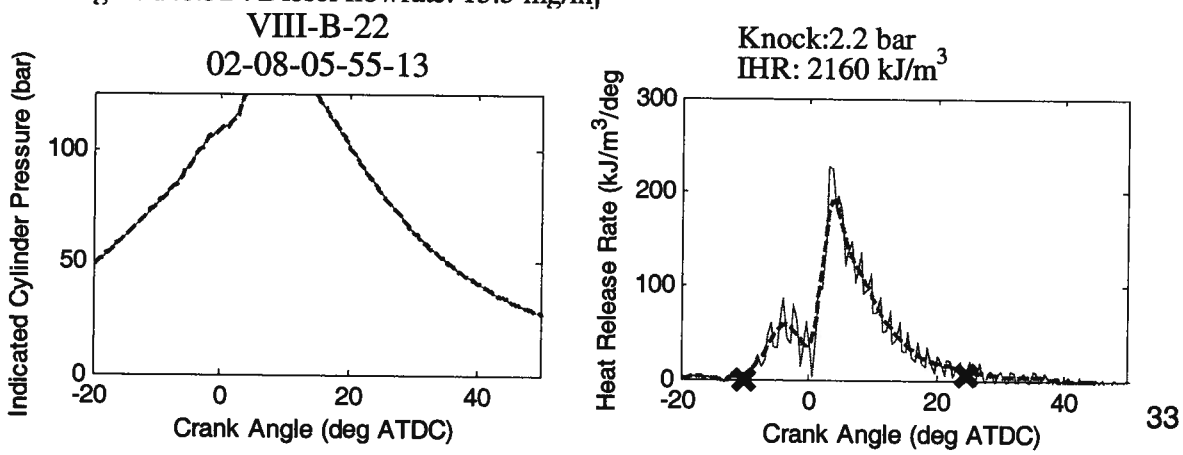

Figure F.6.33 : Diesel flowrate: 6.3 mg/inj

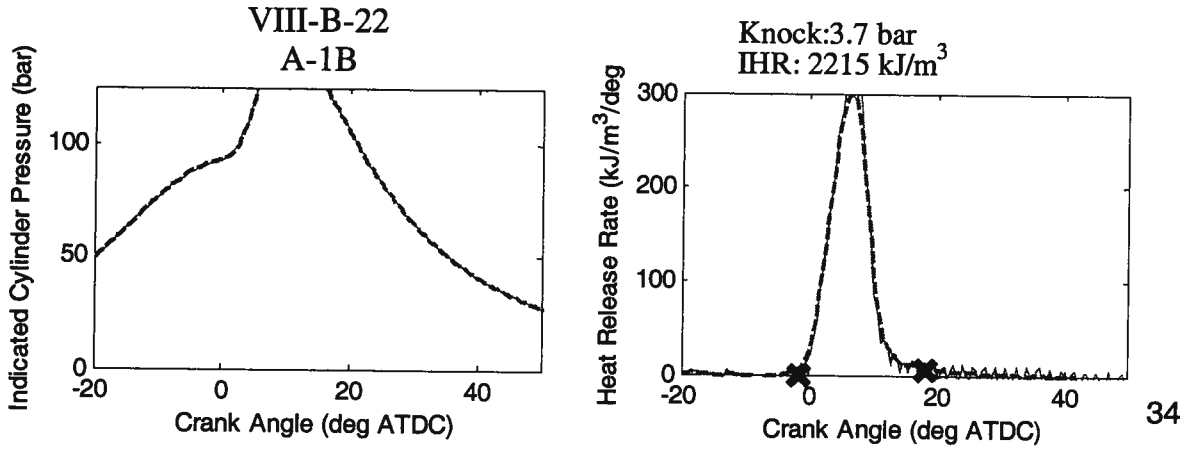

Figure F.6.34 : Diesel flowrate: 6.9 mg/inj

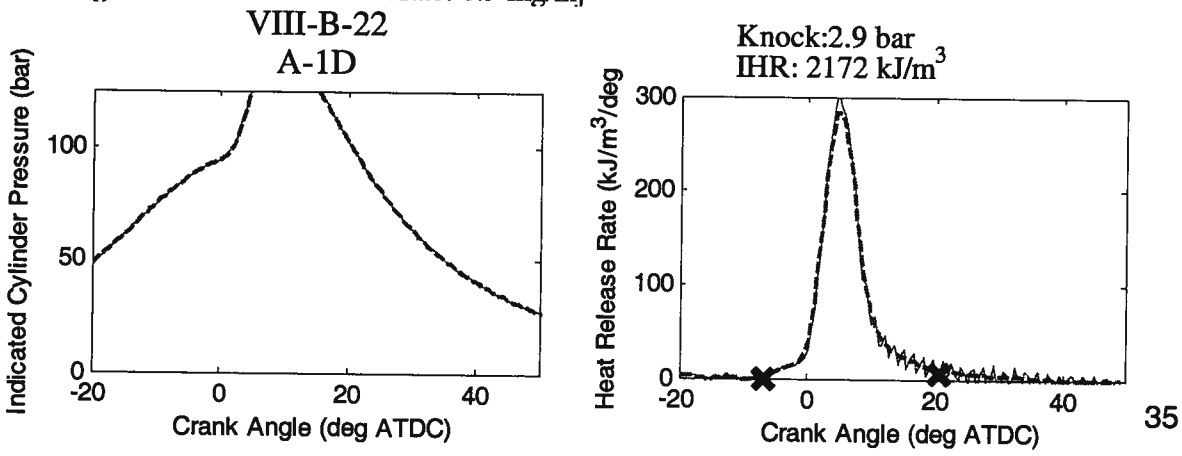

Figure F.6.35 : Diesel flowrate: 8.9 mg/inj

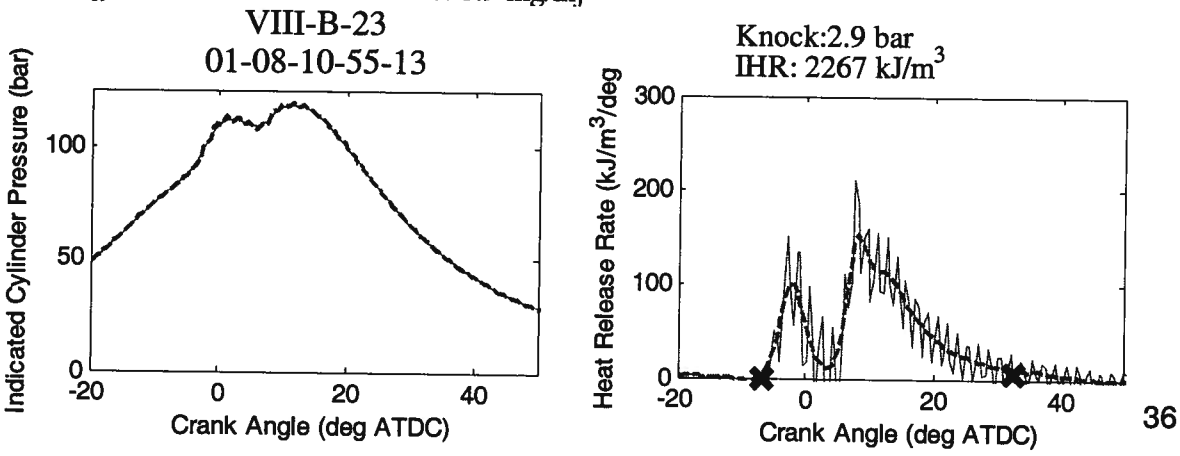

Figure F.6.36 : Diesel flowrate: 8.6 mg/inj

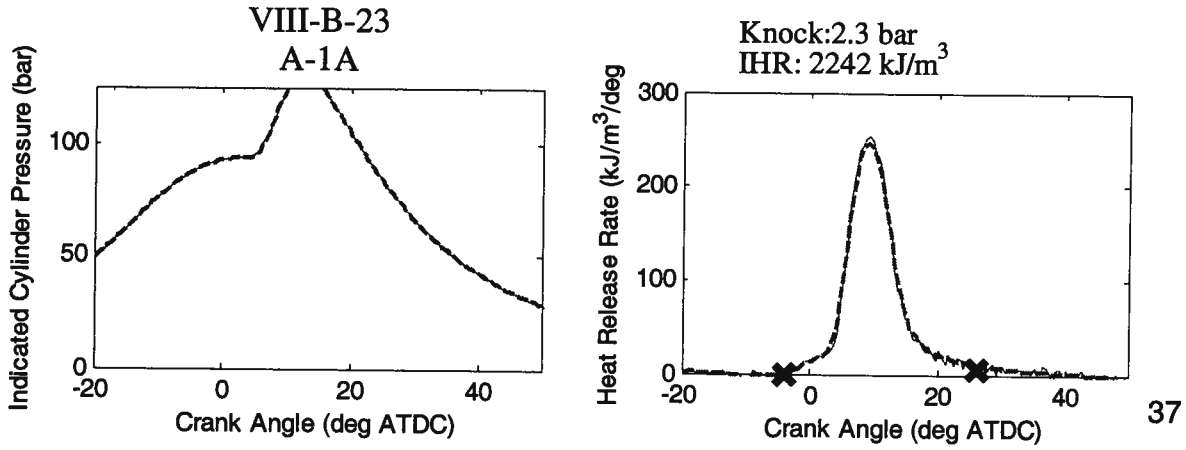

Figure F.6.37 : Diesel flowrate: 7.4 mg/inj

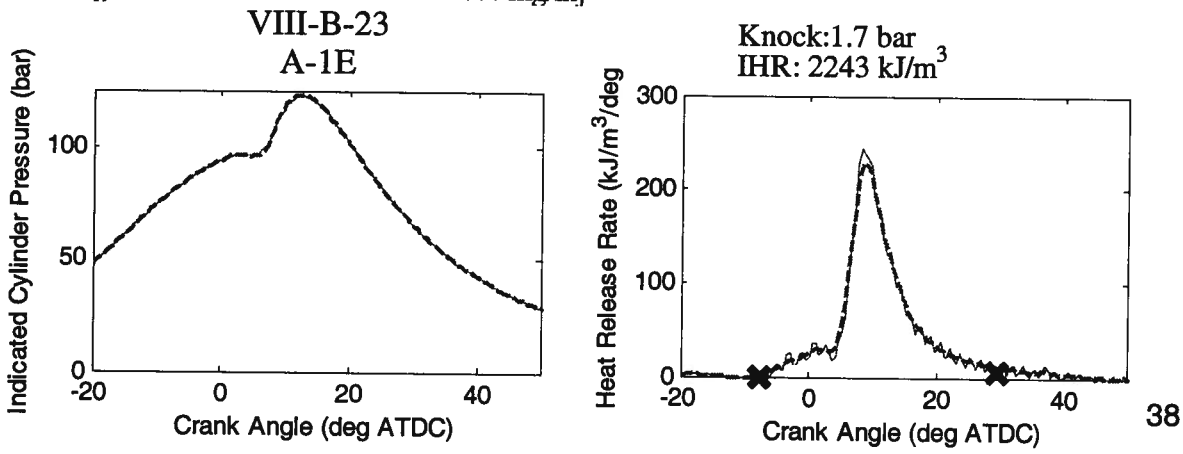

Figure F.6.38 : Diesel flowrate: 9.6 mg/inj

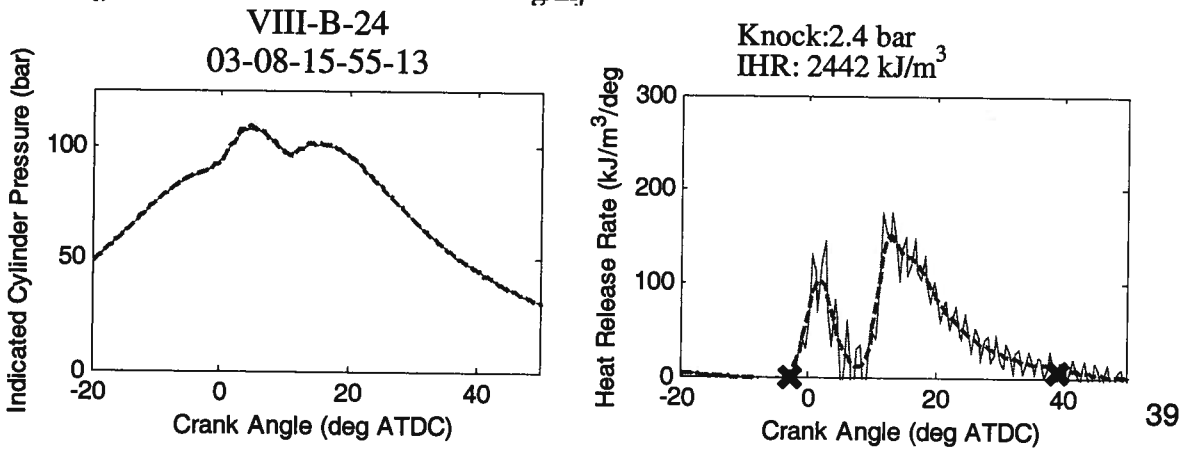

Figure F.6.39 : Diesel flowrate: 7.0 mg/inj

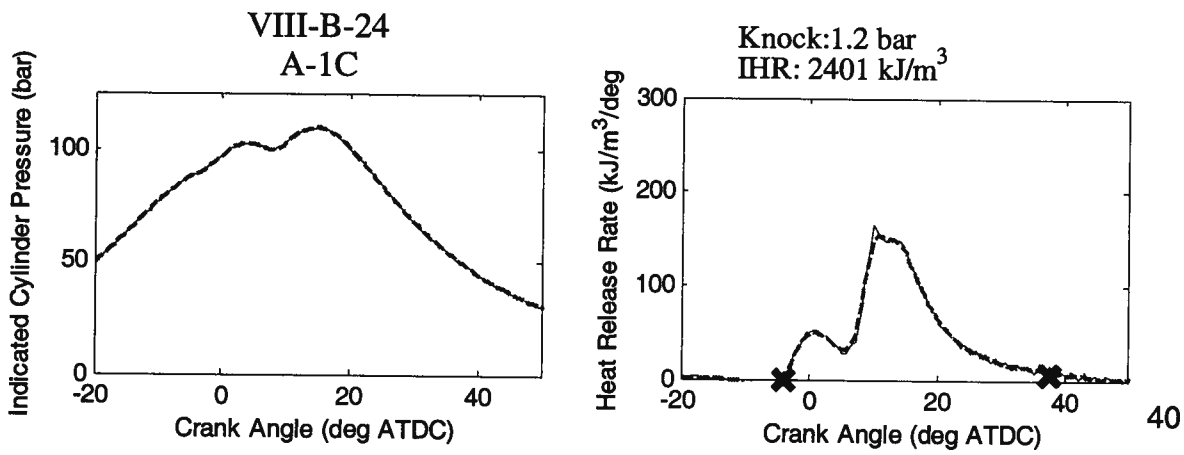

Figure F.6.40 : Diesel flowrate: 11.0 mg/inj

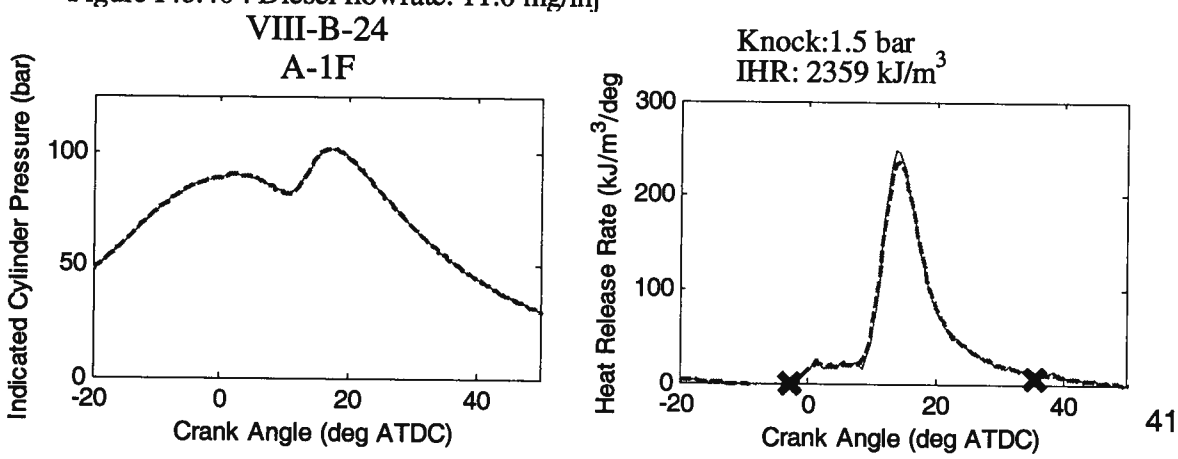

Figure F.6.41 : Diesel flowrate: 10.7 mg/inj

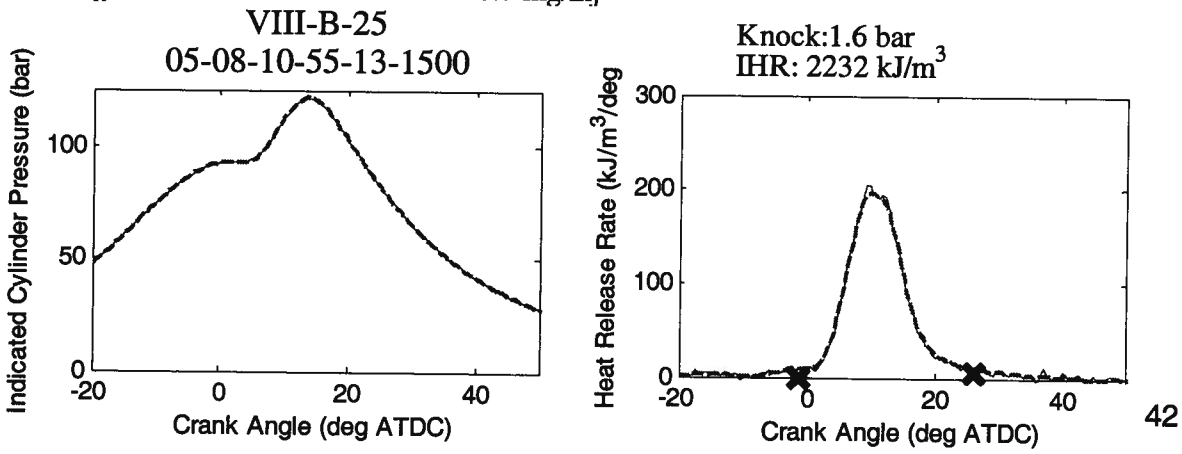

Figure F.6.42 : Diesel flowrate: 13.1 mg/inj

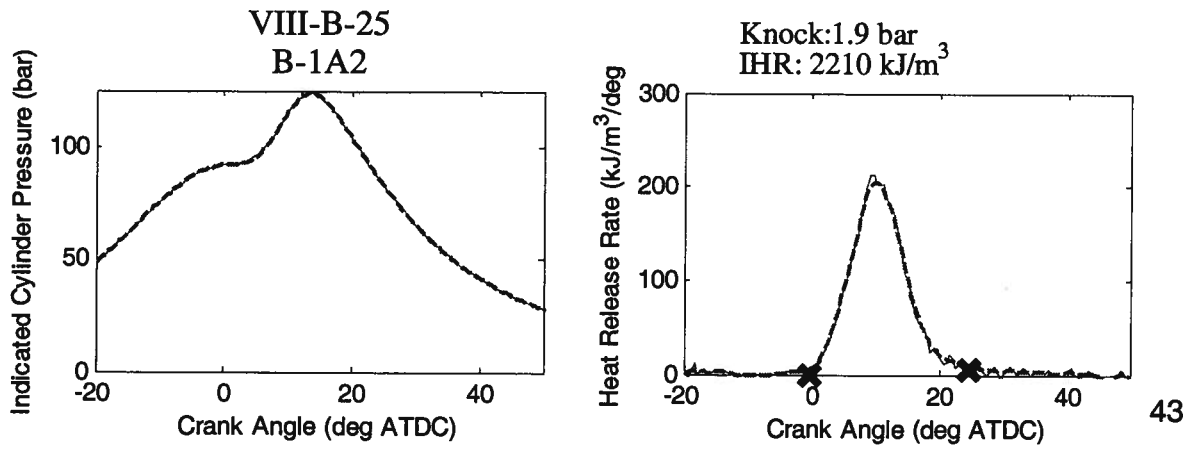

Figure F.6.43 : Diesel flowrate: 13.7 mg/inj

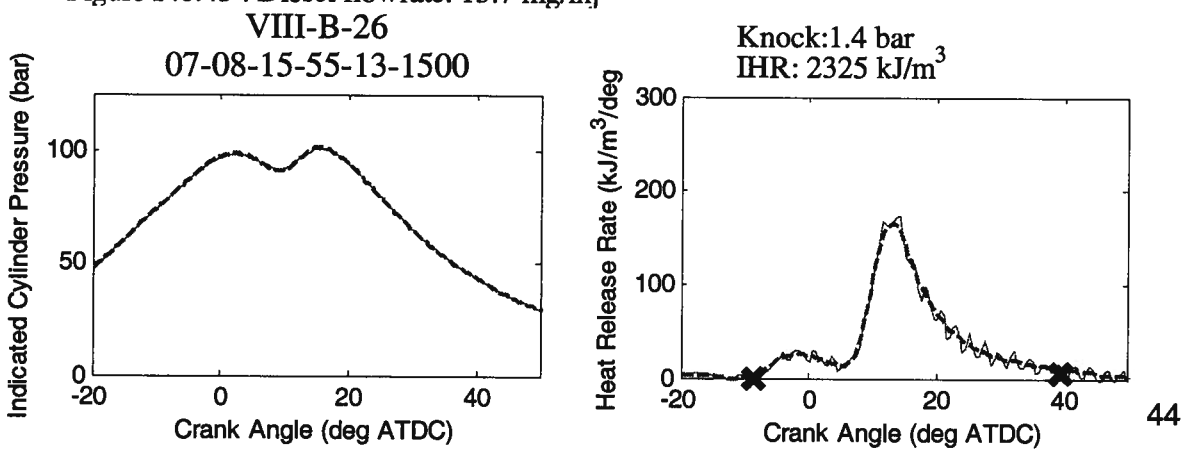

Figure F.6.44 : Diesel flowrate: 11.1 mg/inj

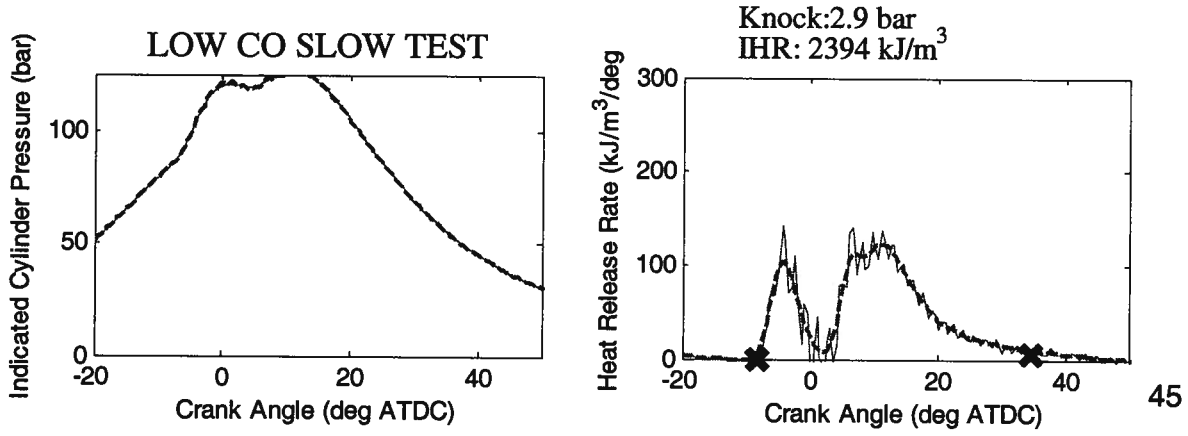

Figure F.6.45 : Diesel flowrate: 11.4 mg/inj

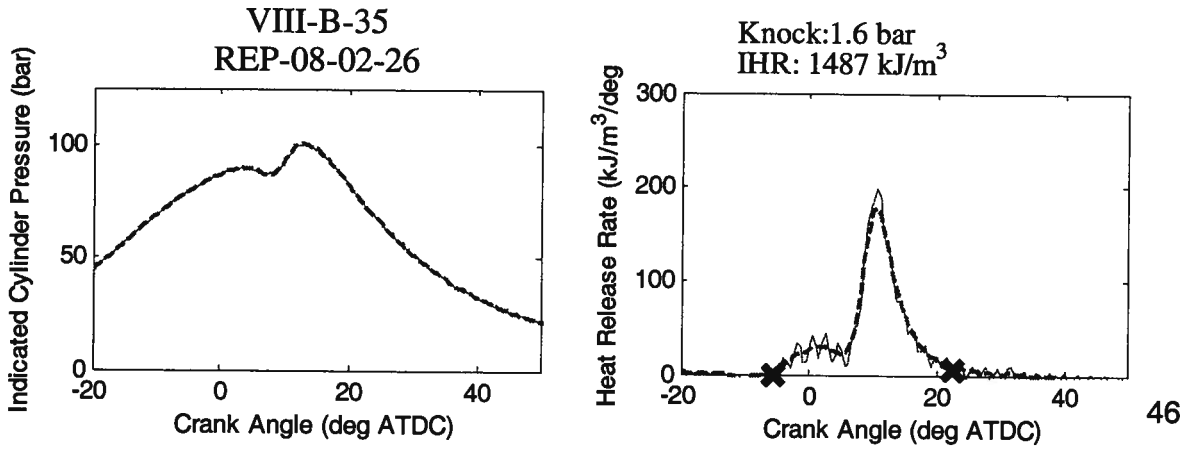

Figure F.6.46 : Diesel flowrate: 12.4 mg/inj

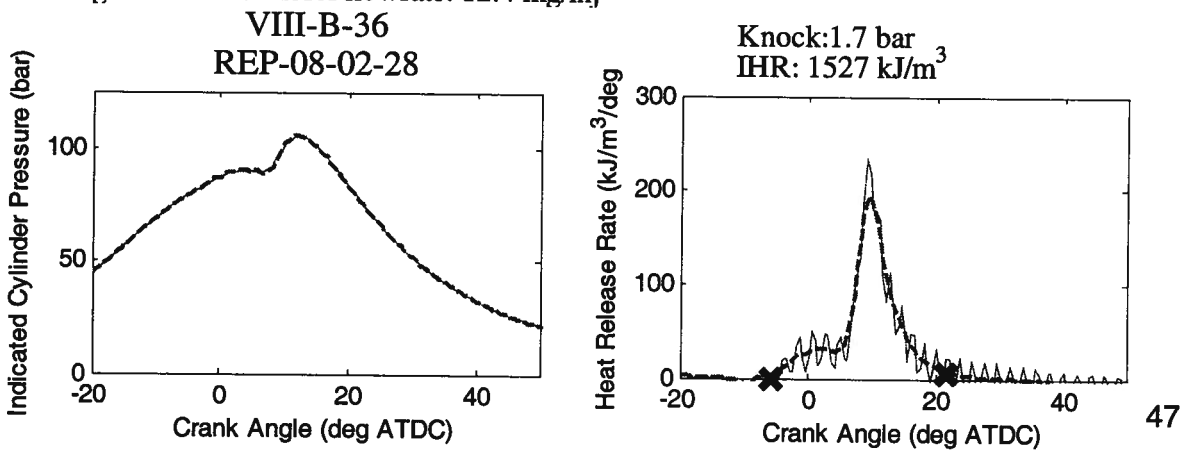

Figure F.6.47 : Diesel flowrate: 13.3 mg/inj

Appendix F.7- Test Series VIII-B2
Pressure and HRR Curves

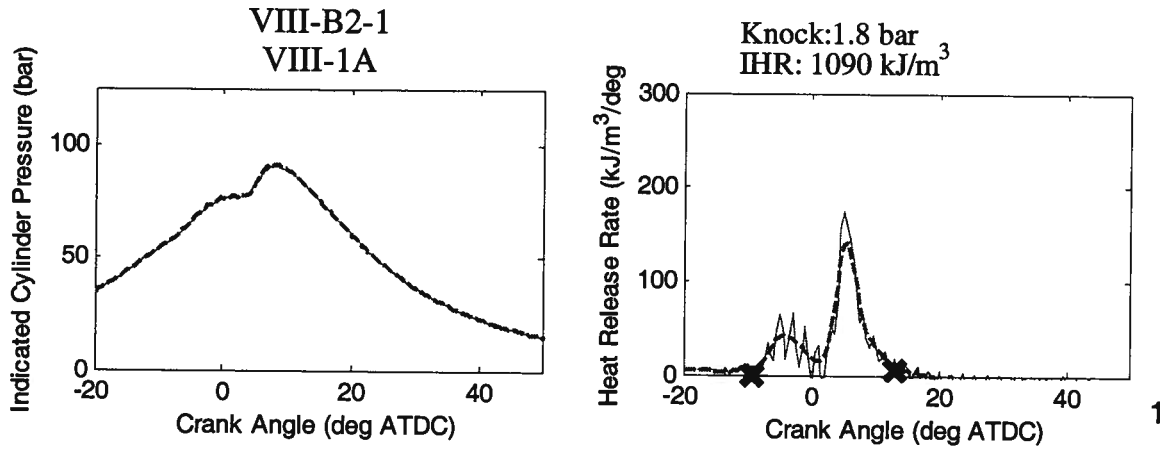

Figure F.7.1 : Diesel flowrate: 14.2 mg/inj

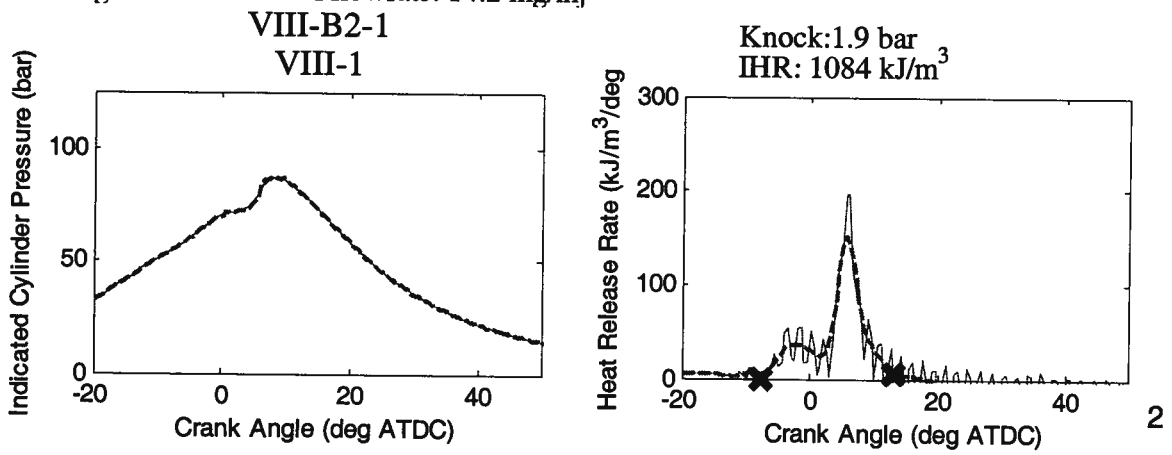

Figure F.7.2 : Diesel flowrate: 14.4 mg/inj

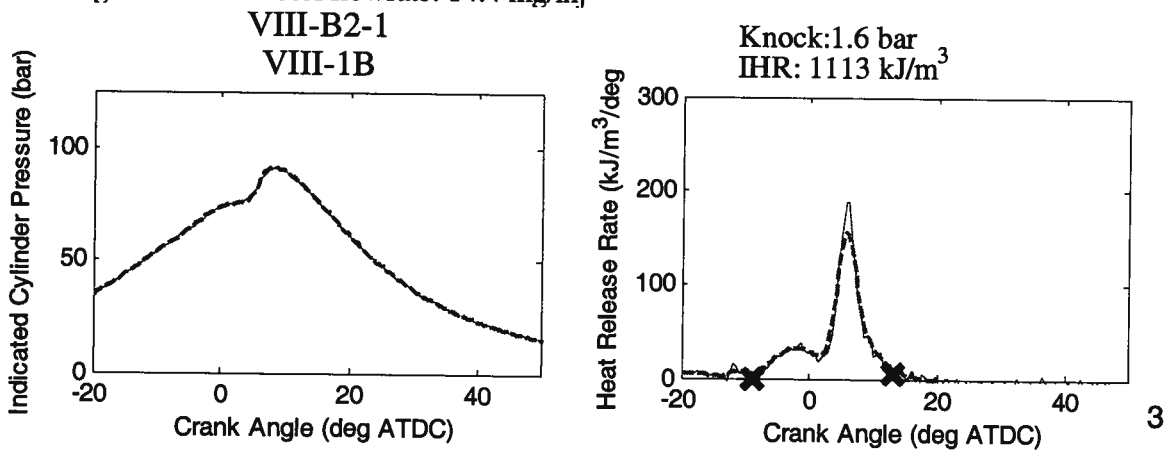

Figure F.7.3 : Diesel flowrate: 15.3 mg/inj

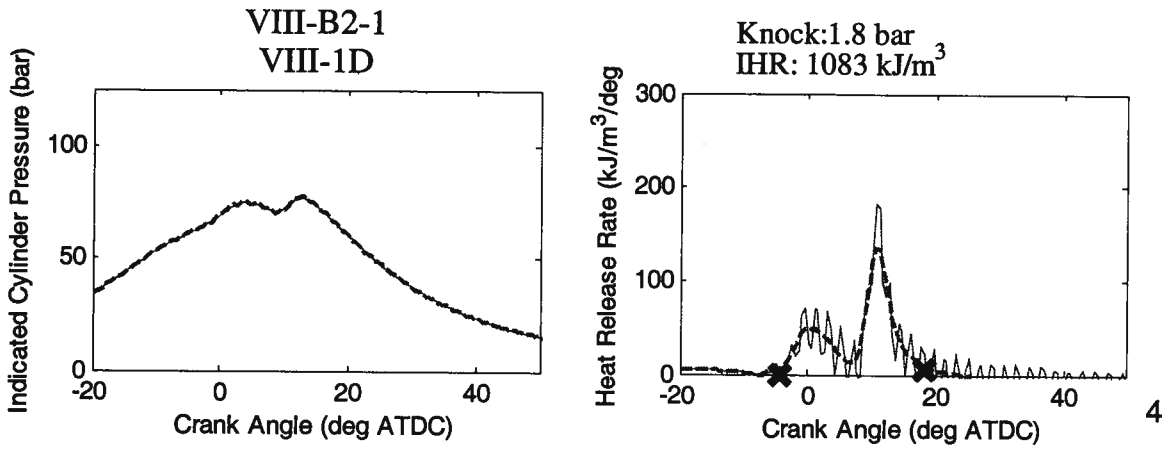

Figure F.7.4 : Diesel flowrate: 14.2 mg/inj

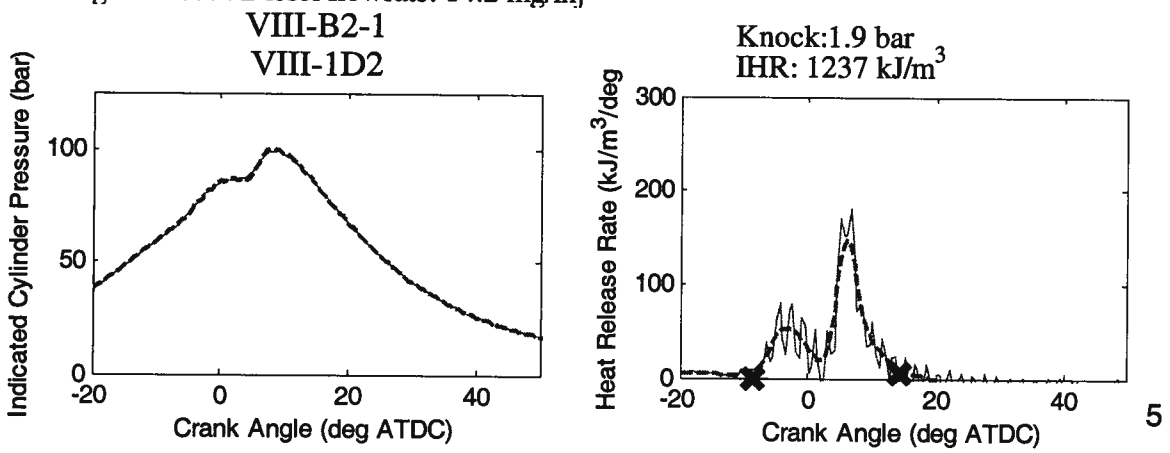

Figure F.7.5 : Diesel flowrate: 14.6 mg/inj

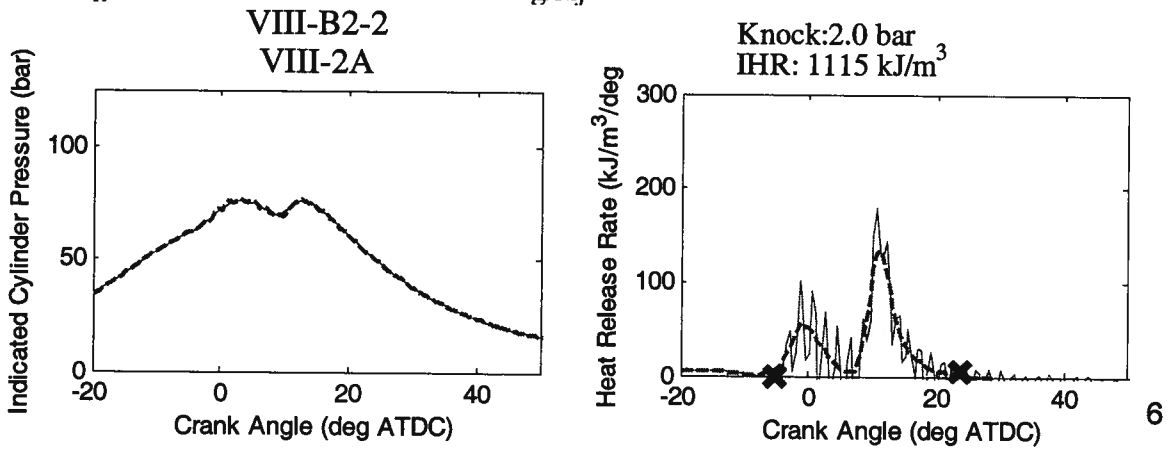

Figure F.7.6 : Diesel flowrate: 14.1 mg/inj

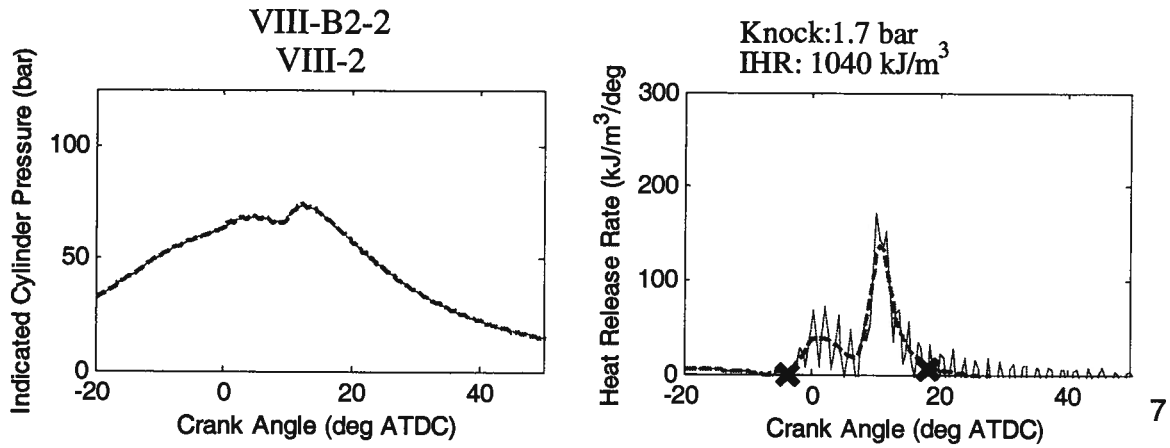

Figure F.7.7 : Diesel flowrate: 14.3 mg/inj

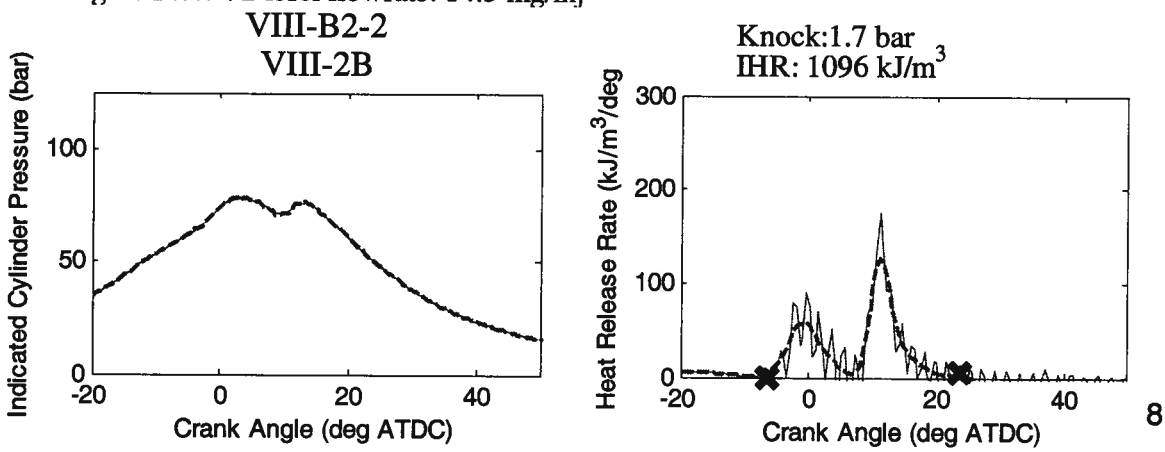

Figure F.7.8 : Diesel flowrate: 14.6 mg/inj

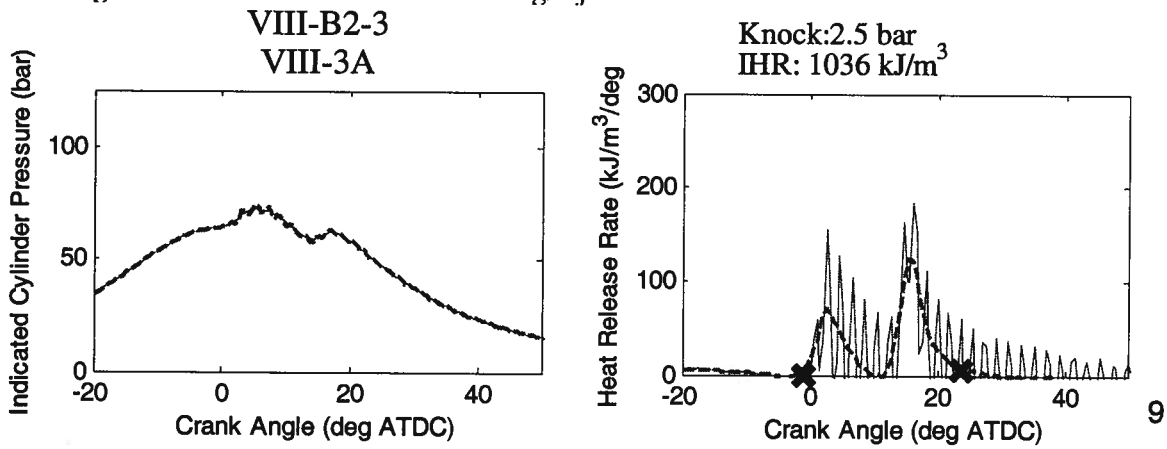

Figure F.7.9 : Diesel flowrate: 14.5 mg/inj

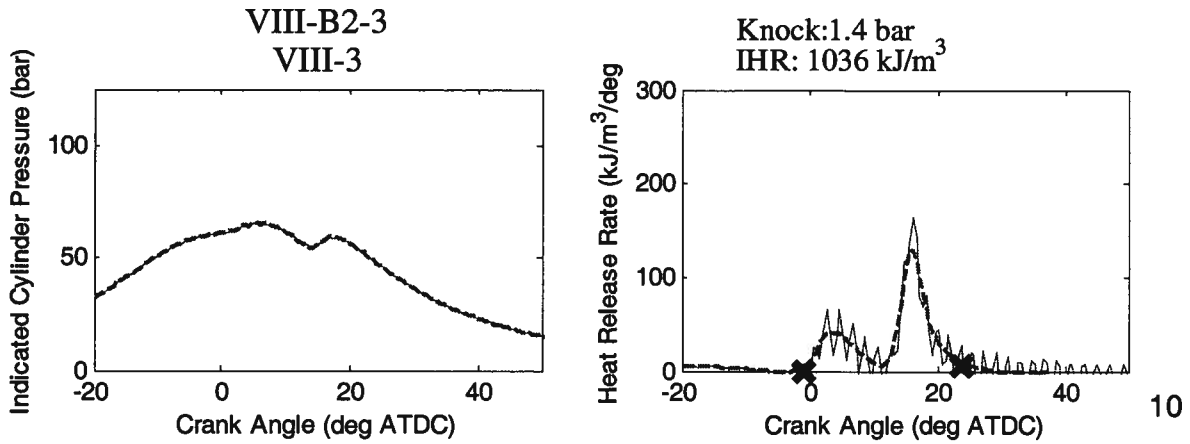

Figure F.7.10 : Diesel flowrate: 14.0 mg/inj

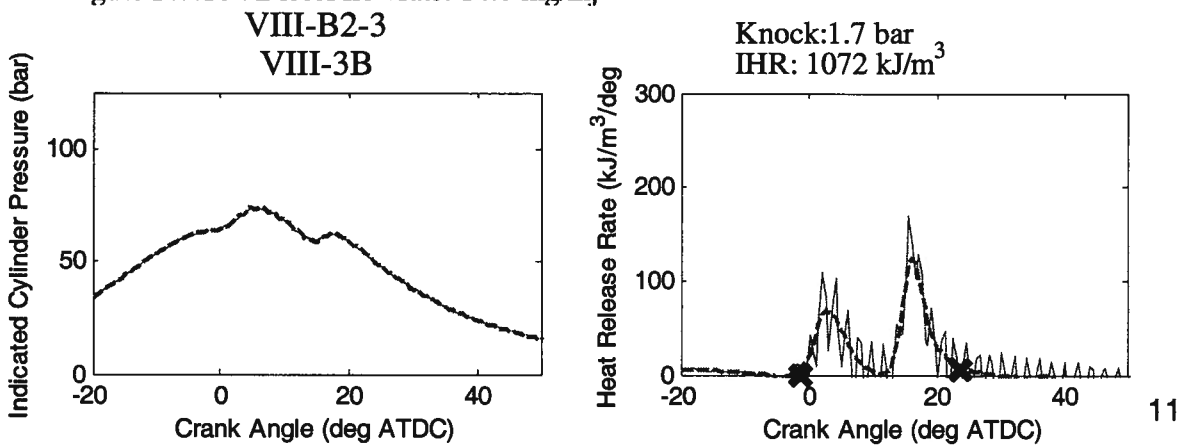

Figure F.7.11 : Diesel flowrate: 15.3 mg/inj

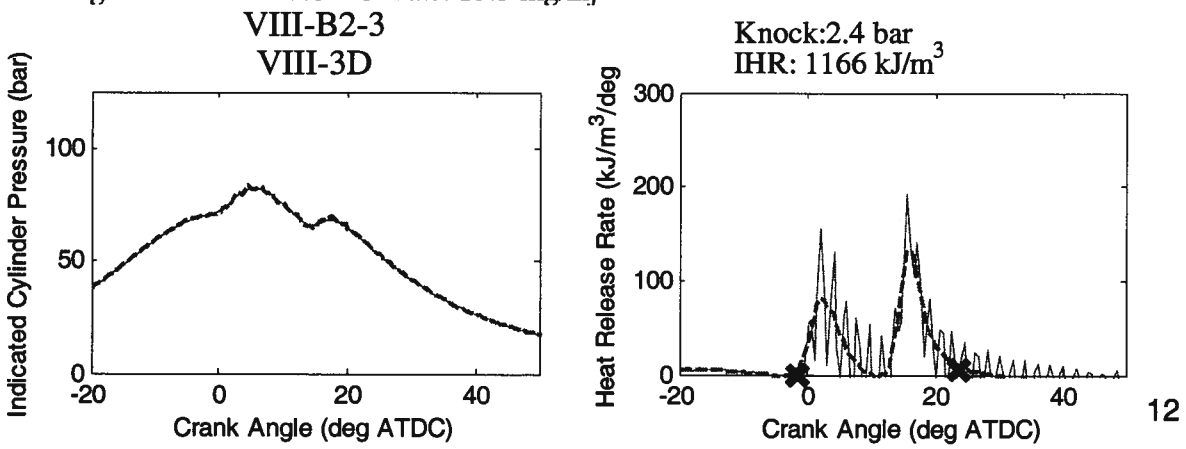

Figure F.7.12 : Diesel flowrate: 14.8 mg/inj

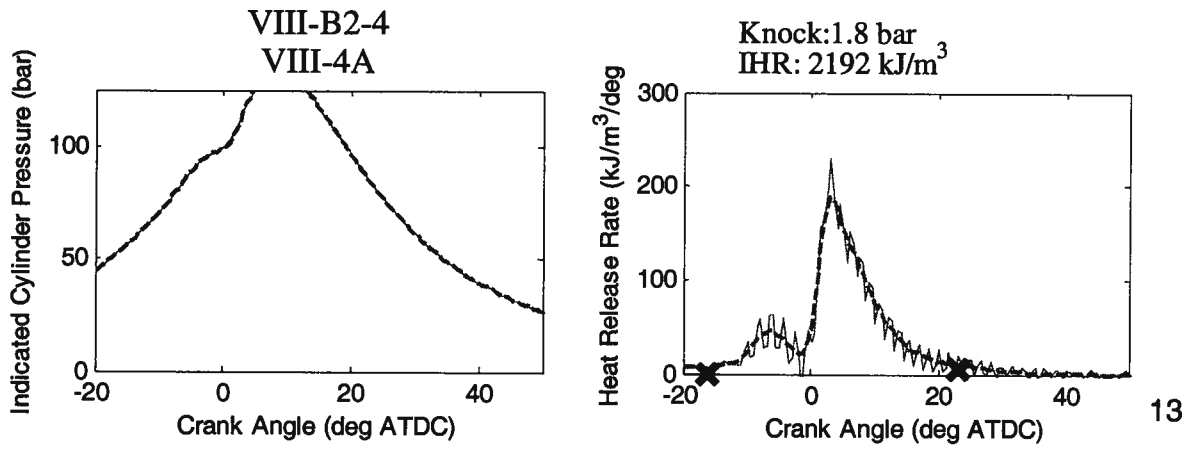

Figure F.7.13 : Diesel flowrate: 15.1 mg/inj

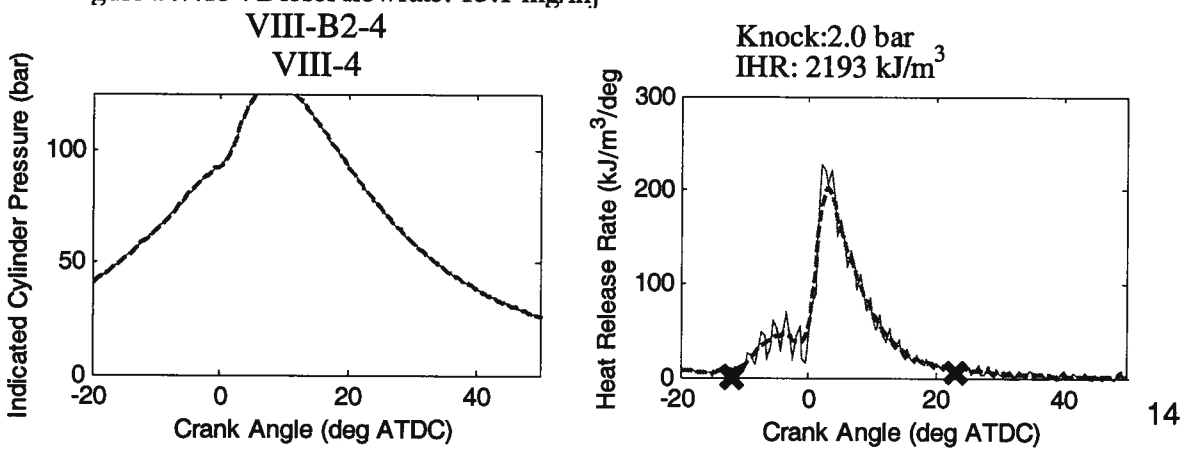

Figure F.7.14 : Diesel flowrate: 16.0 mg/inj

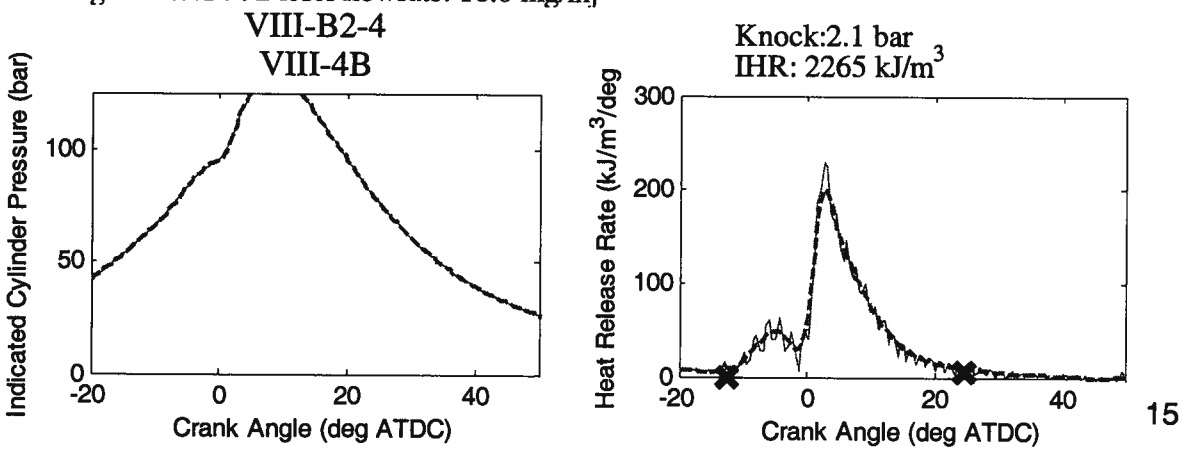

Figure F.7.15 : Diesel flowrate: 15.8 mg/inj

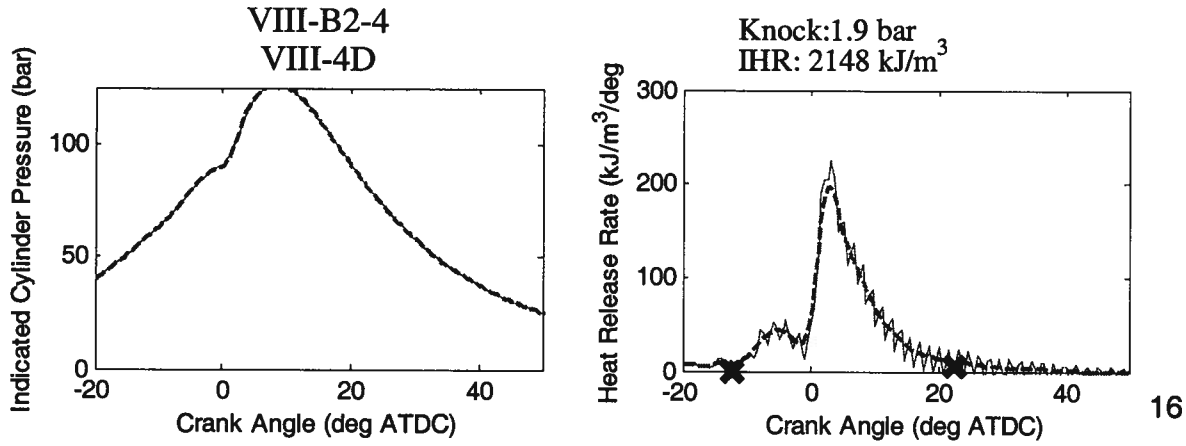

Figure F.7.16 : Diesel flowrate: 15.2 mg/inj

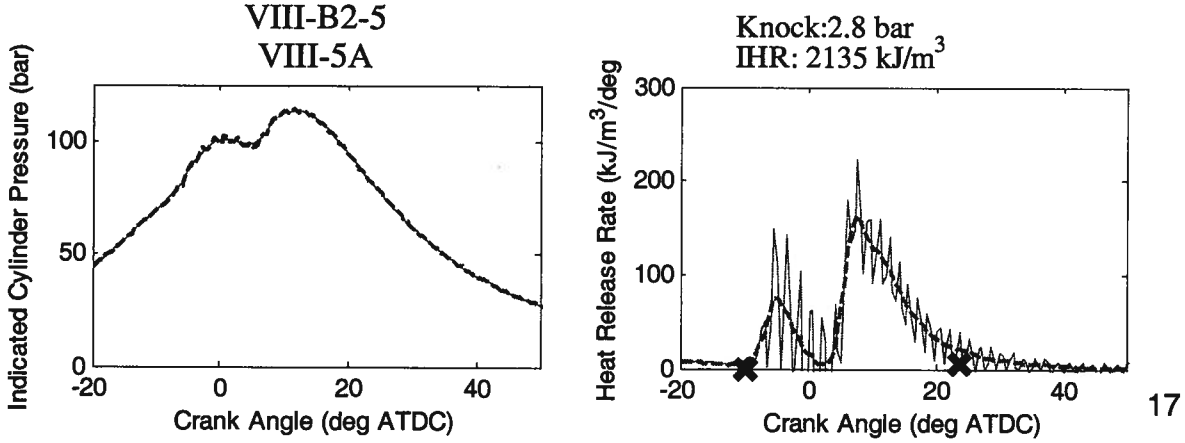

Figure F.7.17 : Diesel flowrate: 14.9 mg/inj

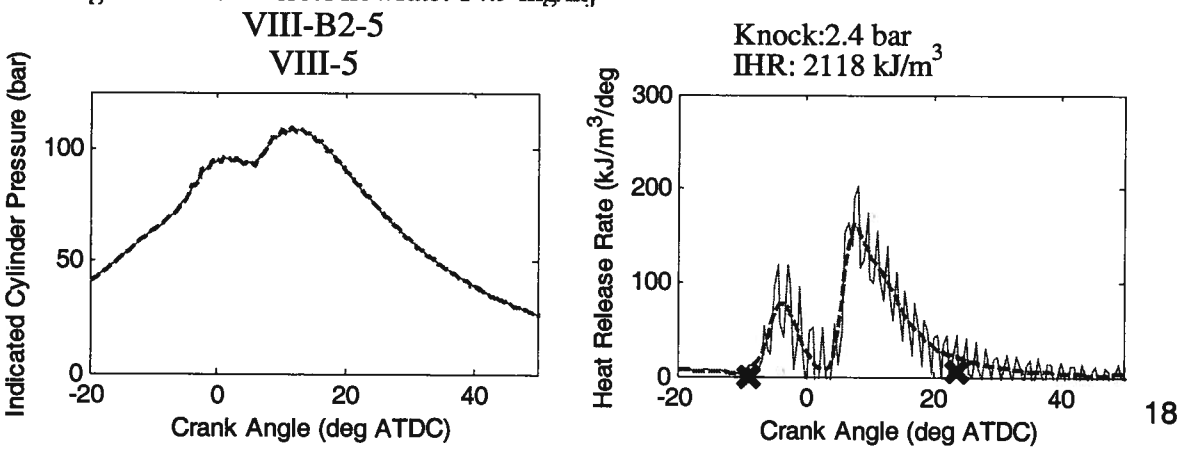

Figure F.7.18 : Diesel flowrate: 15.7 mg/inj

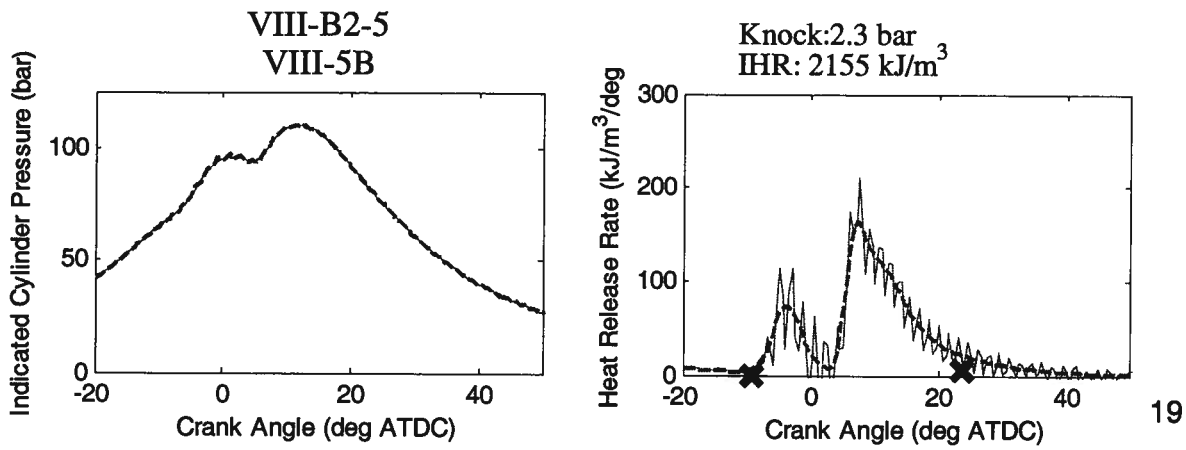

Figure F.7.19 : Diesel flowrate: 16.1 mg/inj

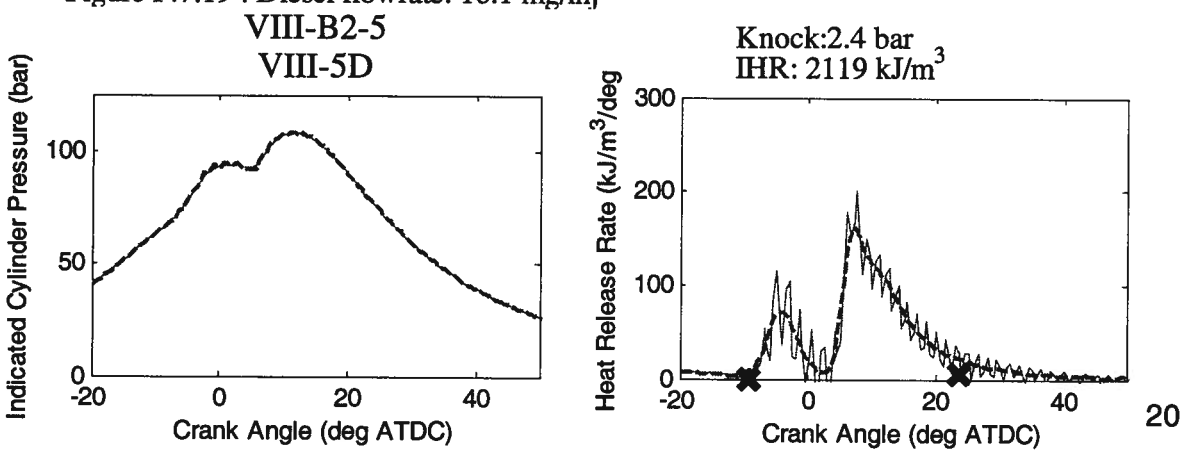

Figure F.7.20 : Diesel flowrate: 15.2 mg/inj

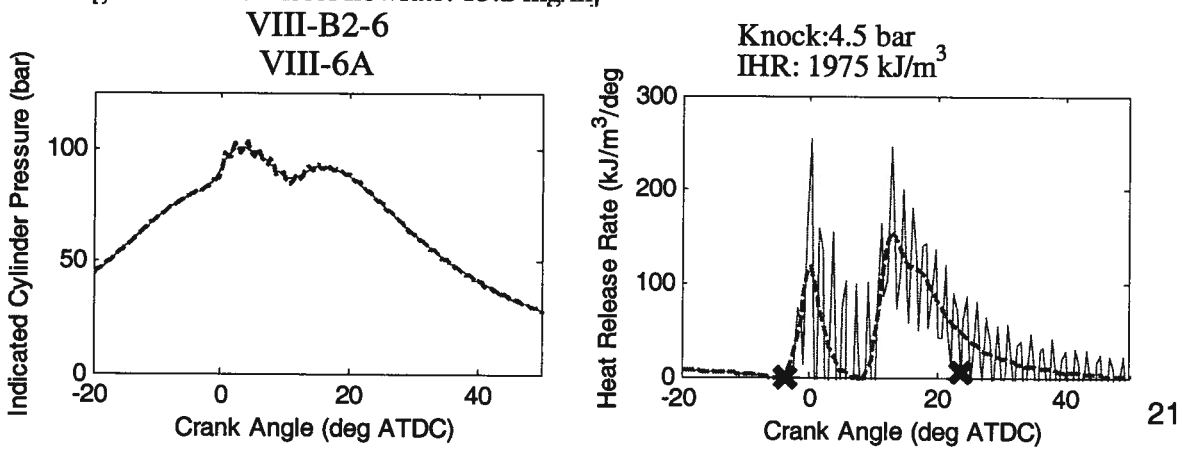

Figure F.7.21 : Diesel flowrate: 15.2 mg/inj

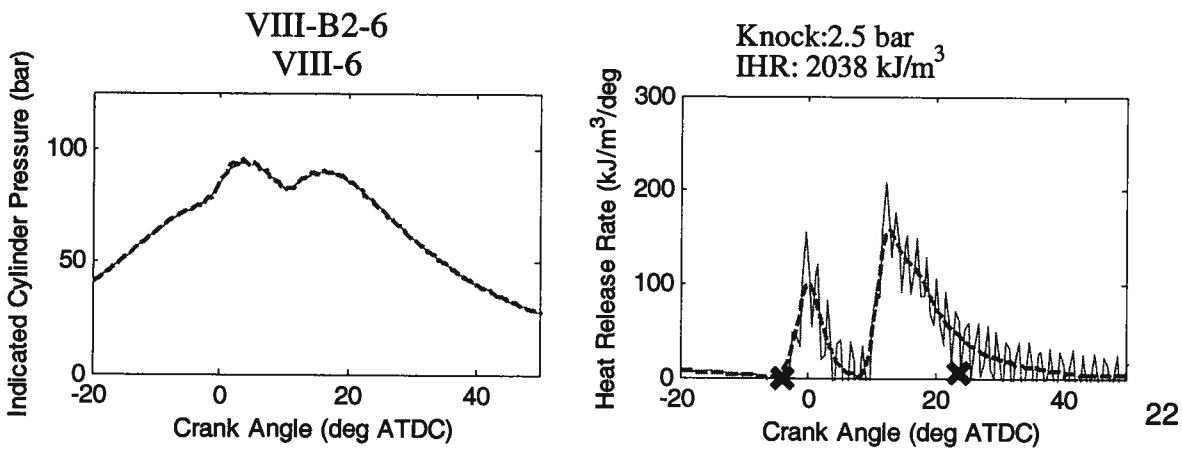

Figure F.7.22 : Diesel flowrate: 15.7 mg/inj

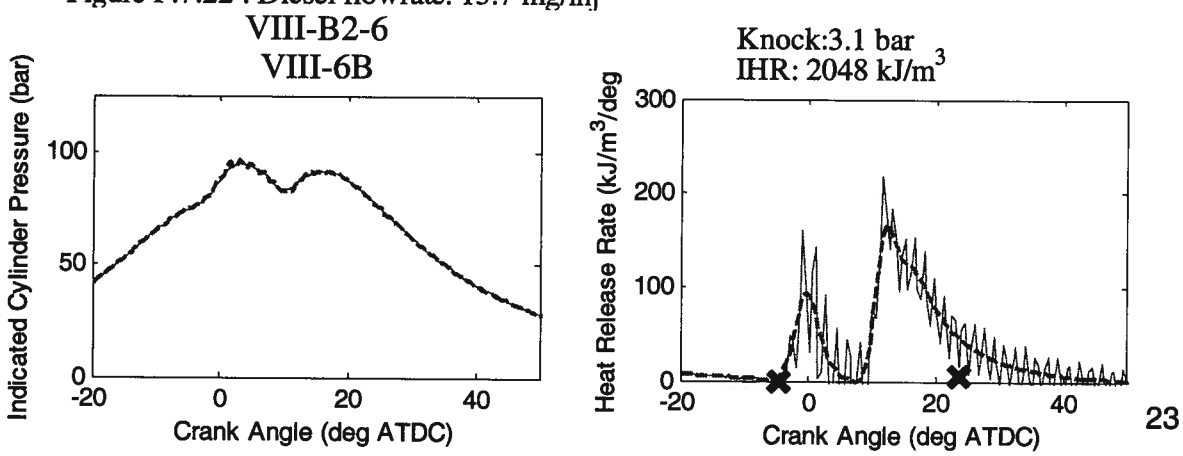

Figure F.7.23 : Diesel flowrate: 15.5 mg/inj

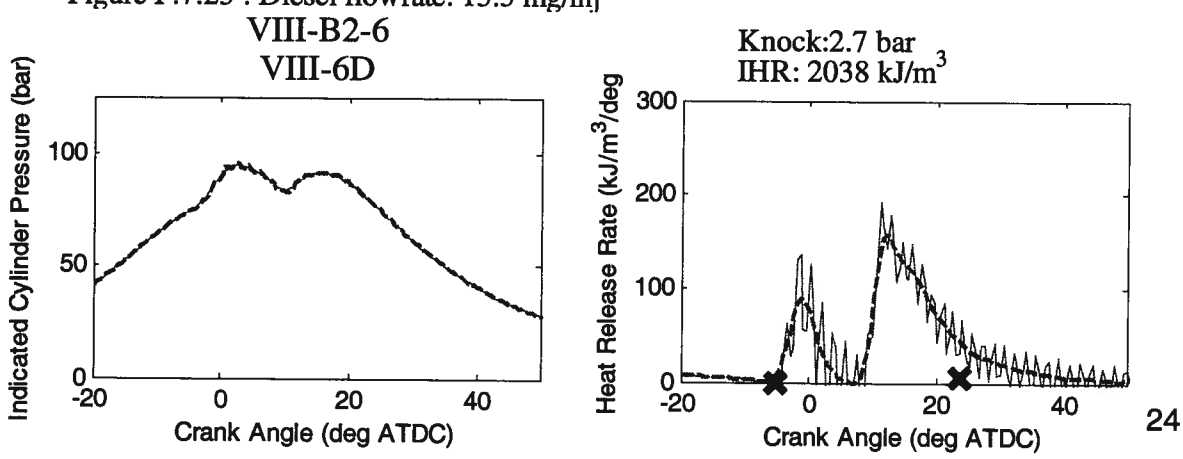

Figure F.7.24 : Diesel flowrate: 14.9 mg/inj

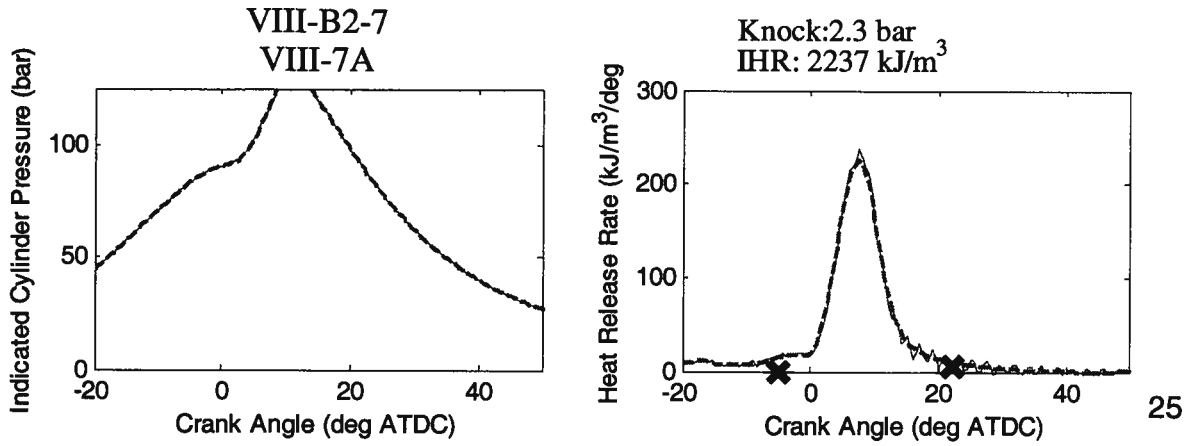

Figure F.7.25 : Diesel flowrate: 14.5 mg/inj

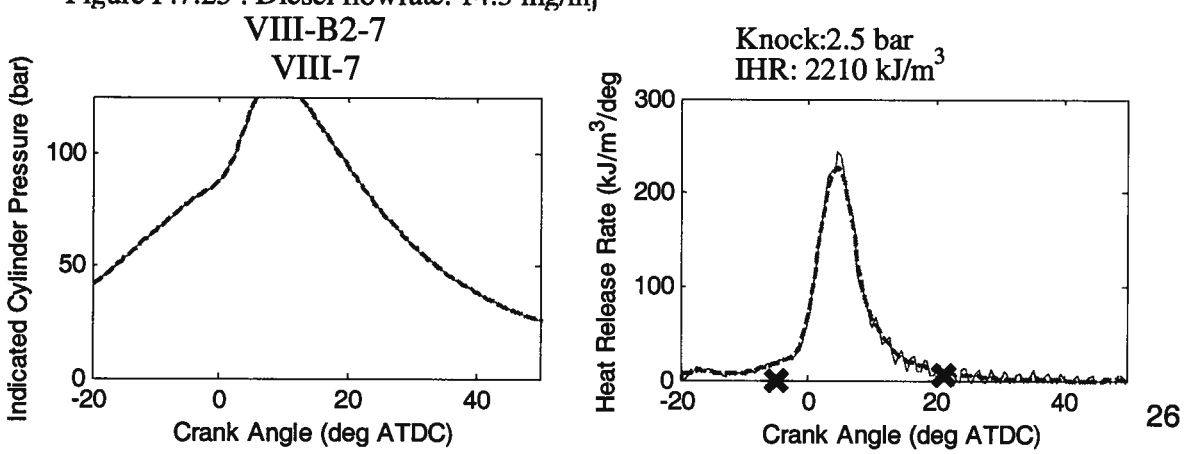

Figure F.7.26 : Diesel flowrate: 14.5 mg/inj

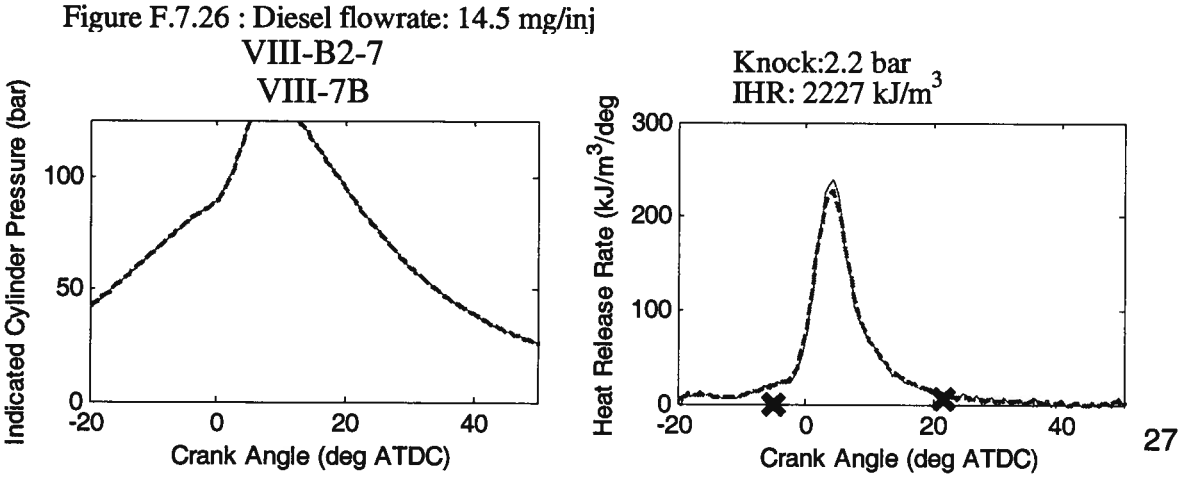

Figure F.7.27 : Diesel flowrate: 14.5 mg/inj

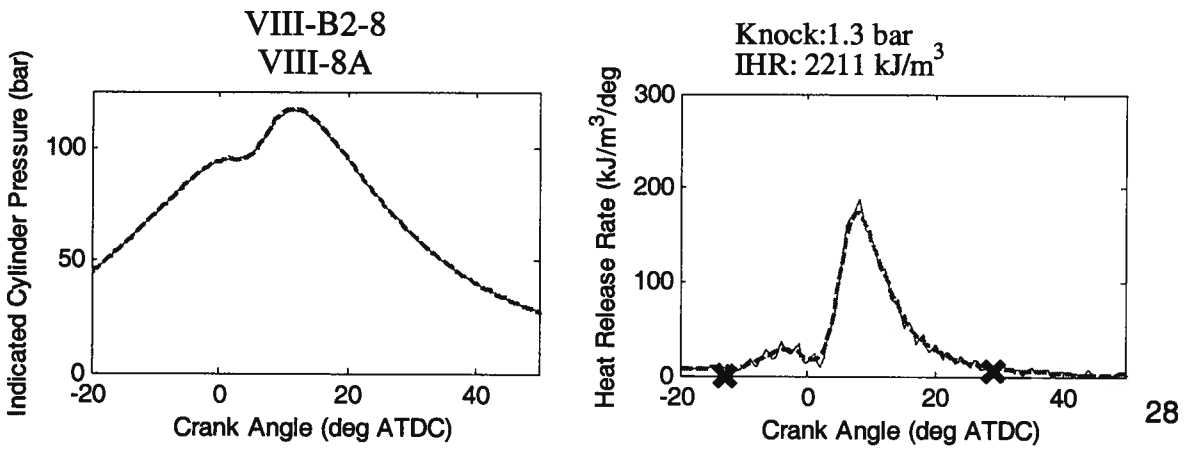

Figure F.7.28 : Diesel flowrate: 14.7 mg/inj

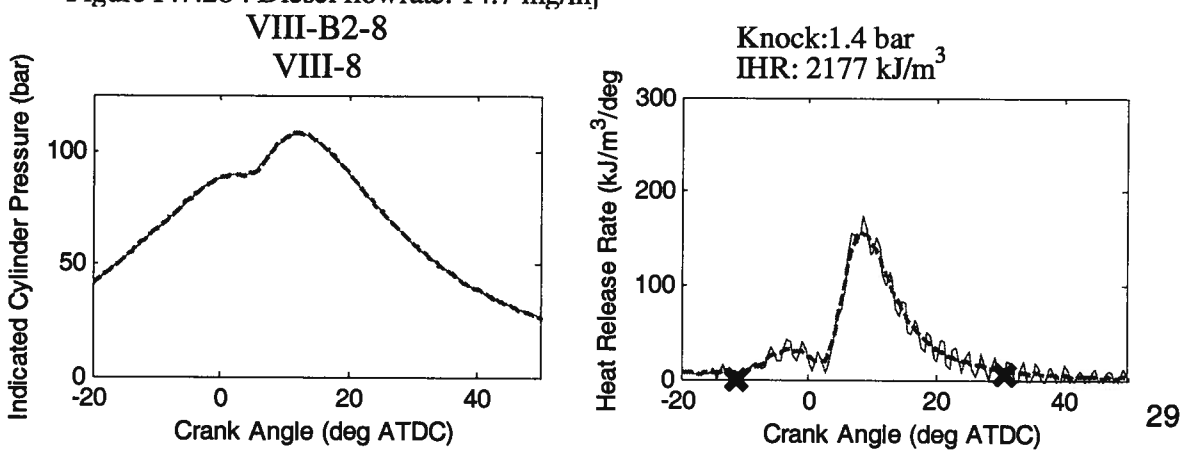

Figure F.7.29 : Diesel flowrate: 14.7 mg/inj

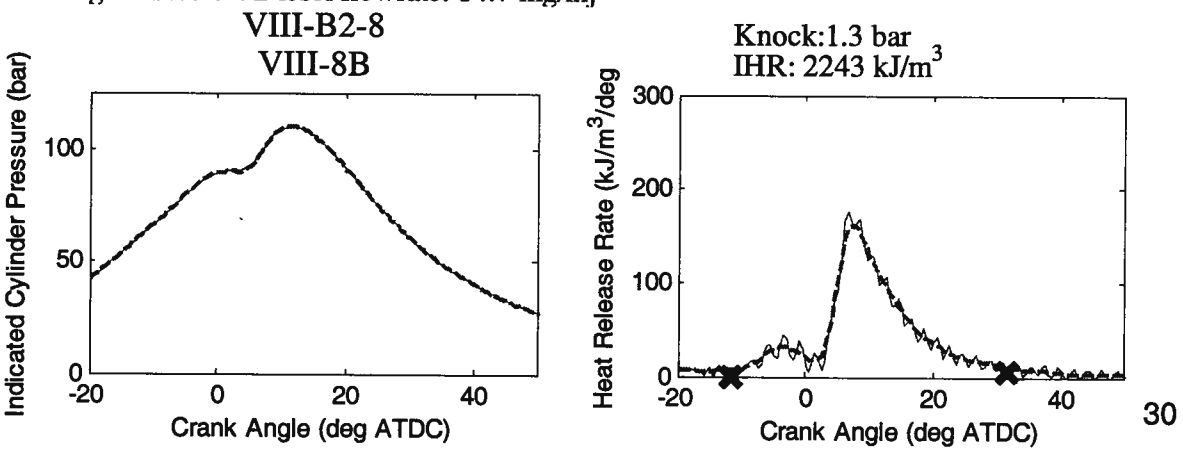

Figure F.7.30 : Diesel flowrate: 14.5 mg/inj

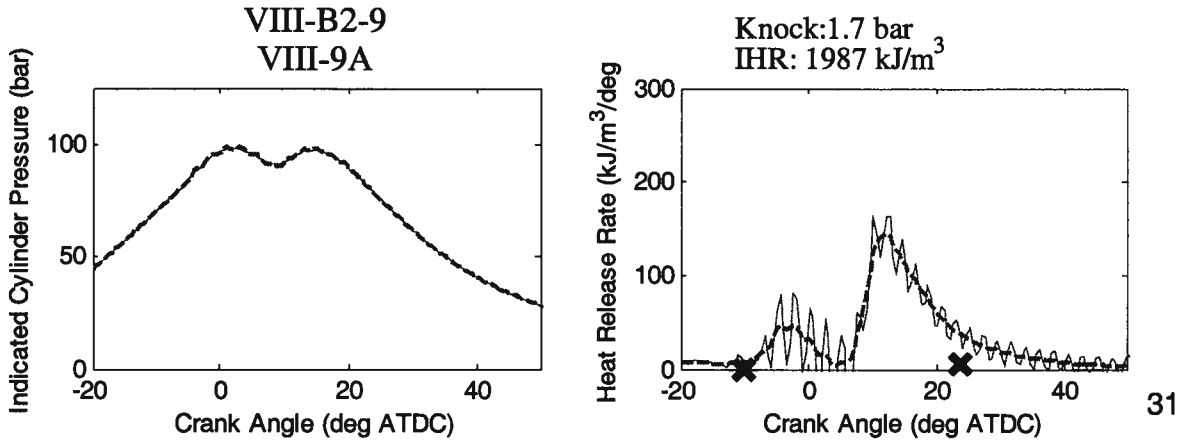

Figure F.7.31 : Diesel flowrate: 14.0 mg/inj

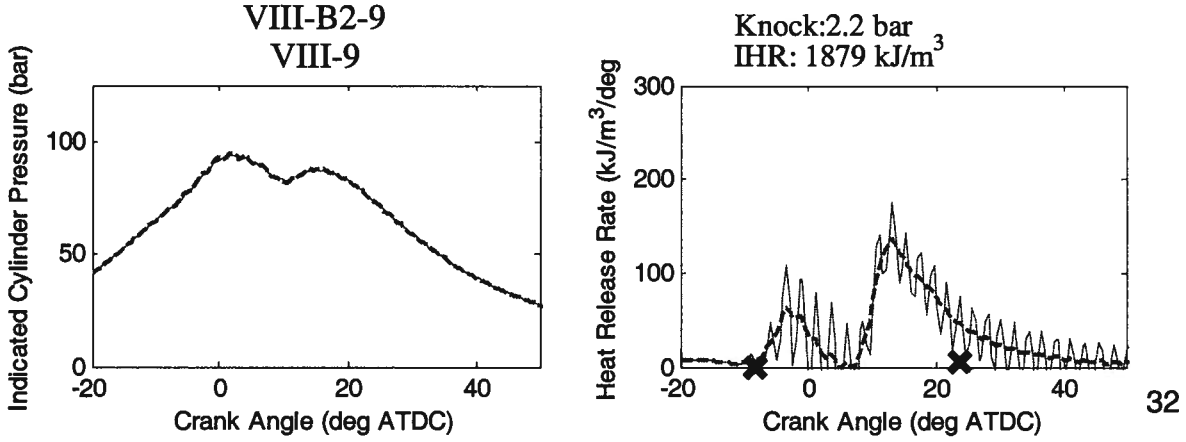

Figure F.7.32 : Diesel flowrate: 15.2 mg/inj

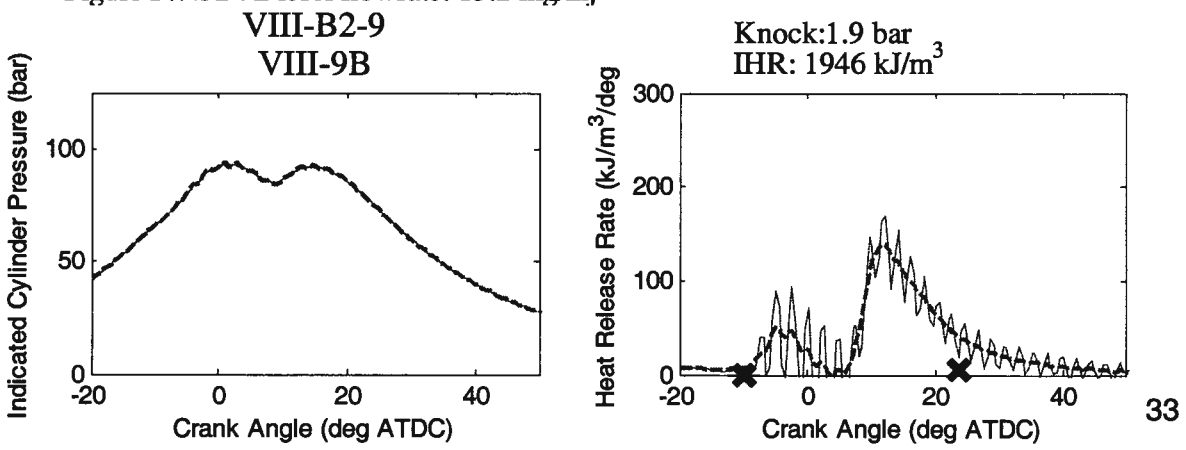

Figure F.7.33 : Diesel flowrate: 14.8 mg/inj

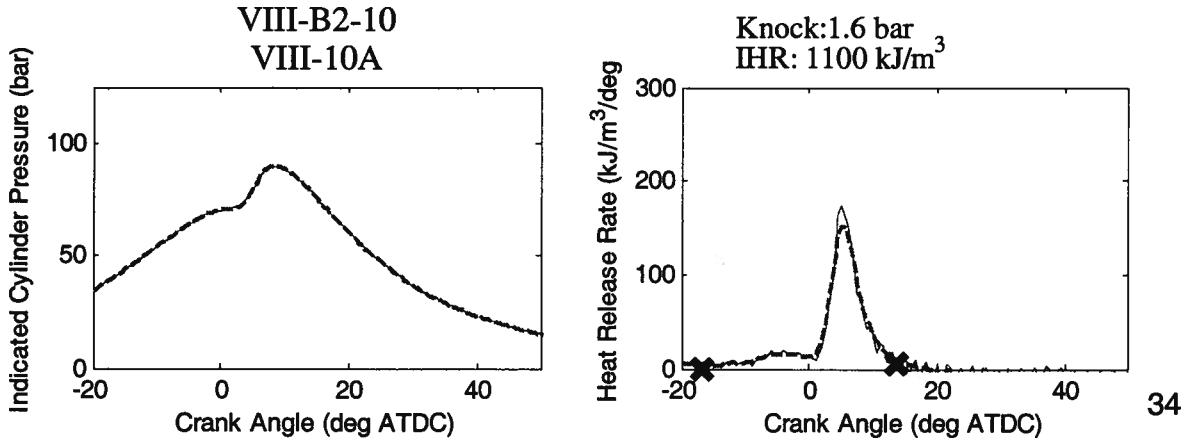

Figure F.7.34 : Diesel flowrate: 15.4 mg/inj

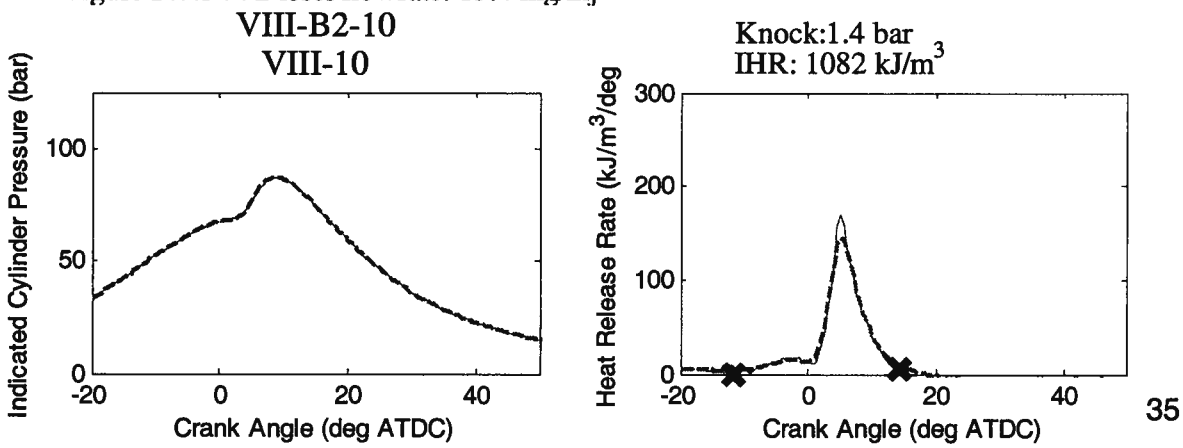

Figure F.7.35 : Diesel flowrate: 16.0 mg/inj

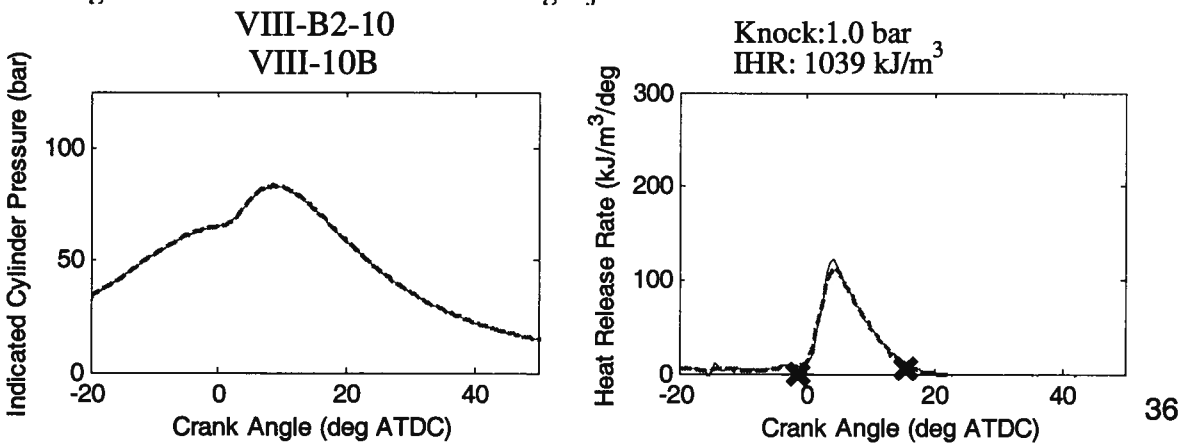

Figure F.7.36 : Diesel flowrate: 14.8 mg/inj

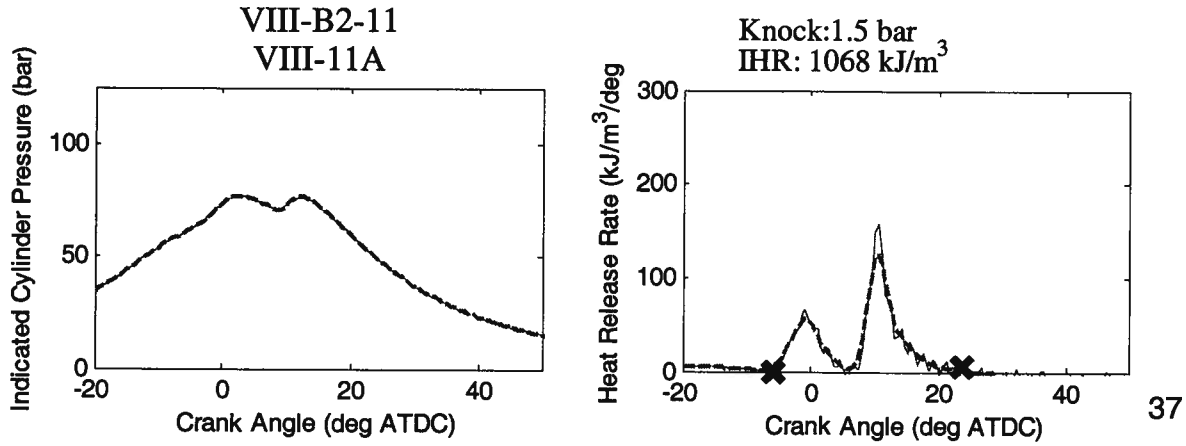

Figure F.7.37 : Diesel flowrate: 16.0 mg/inj

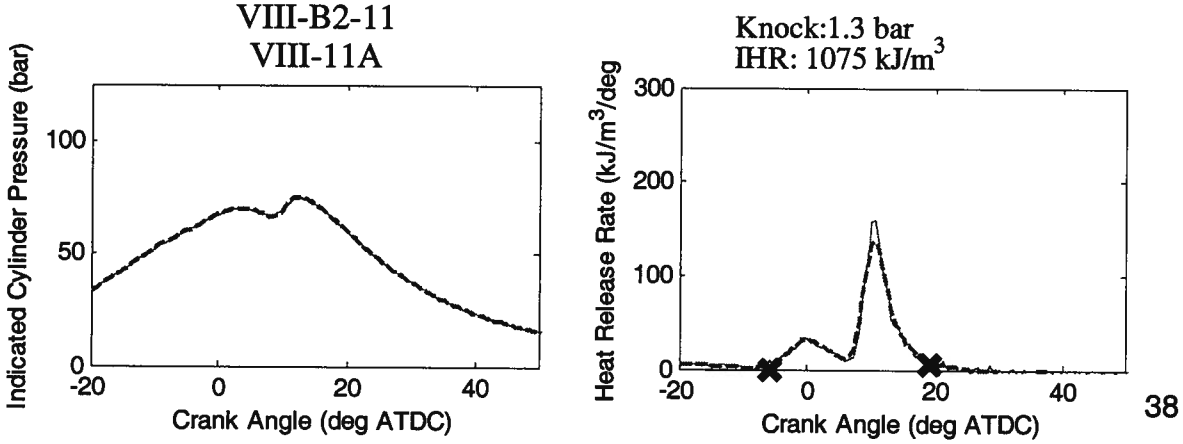

Figure F.7.38 : Diesel flowrate: 16.0 mg/inj

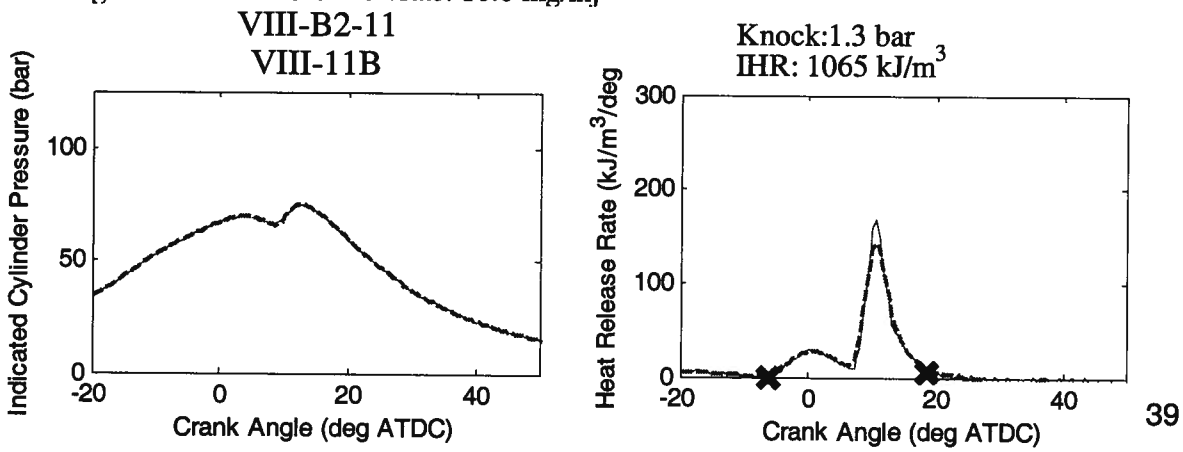

Figure F.7.39 : Diesel flowrate: 15.0 mg/inj

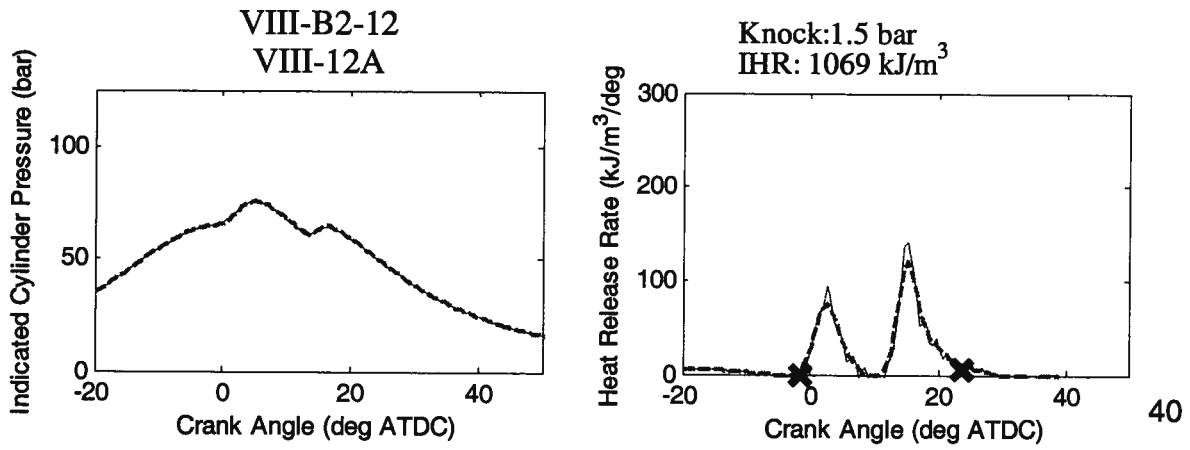

Figure F.7.40 : Diesel flowrate: 16.1 mg/inj

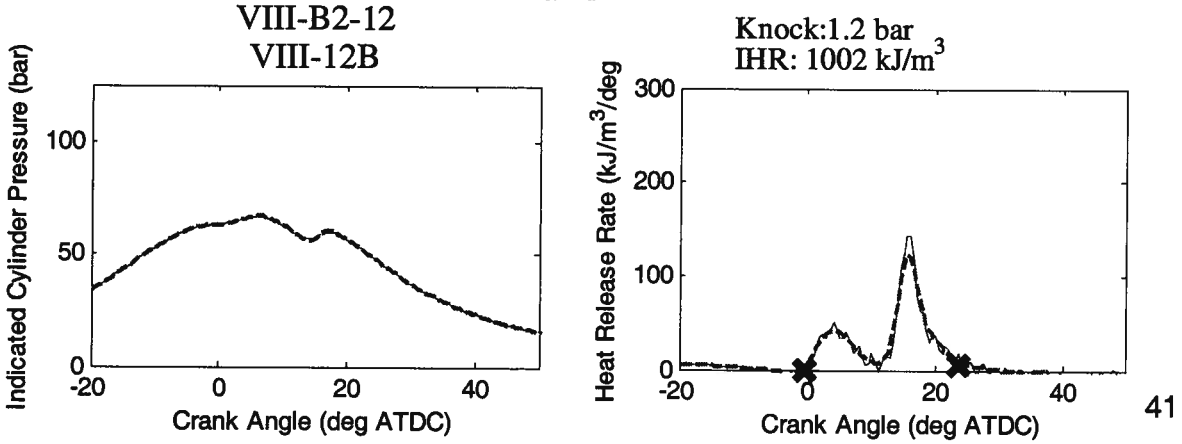

Figure F.7.41 : Diesel flowrate: 14.8 mg/inj

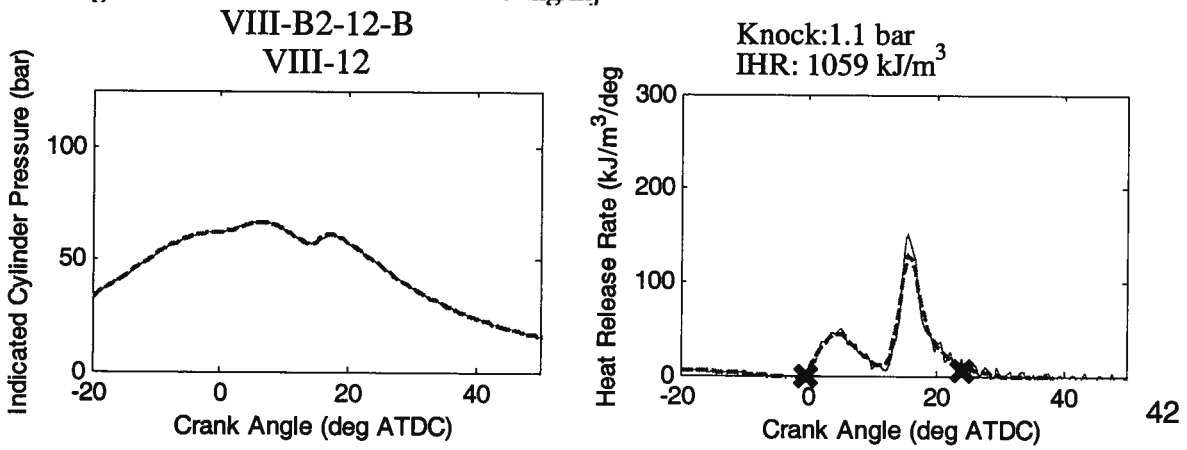

Figure F.7.42 : Diesel flowrate: 15.6 mg/inj

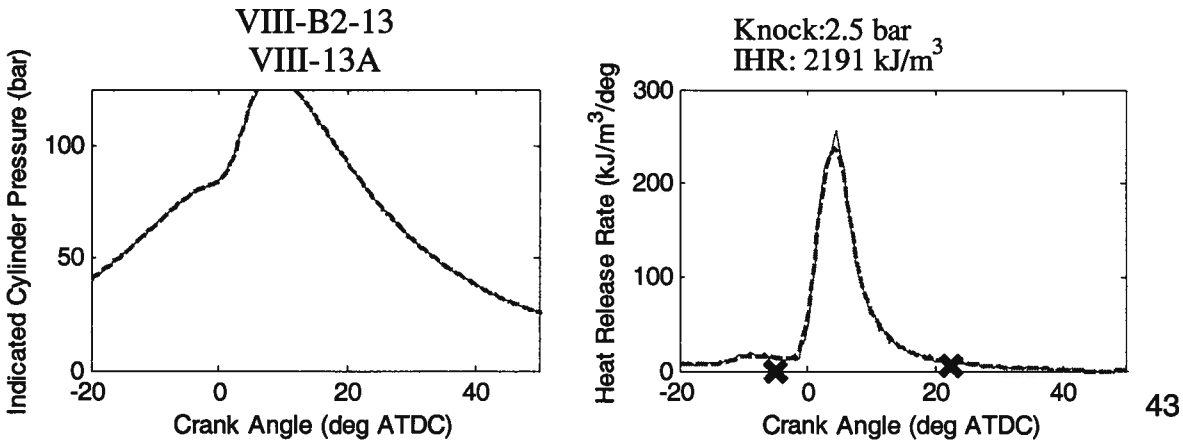

Figure F.7.43 : Diesel flowrate: 16.6 mg/inj

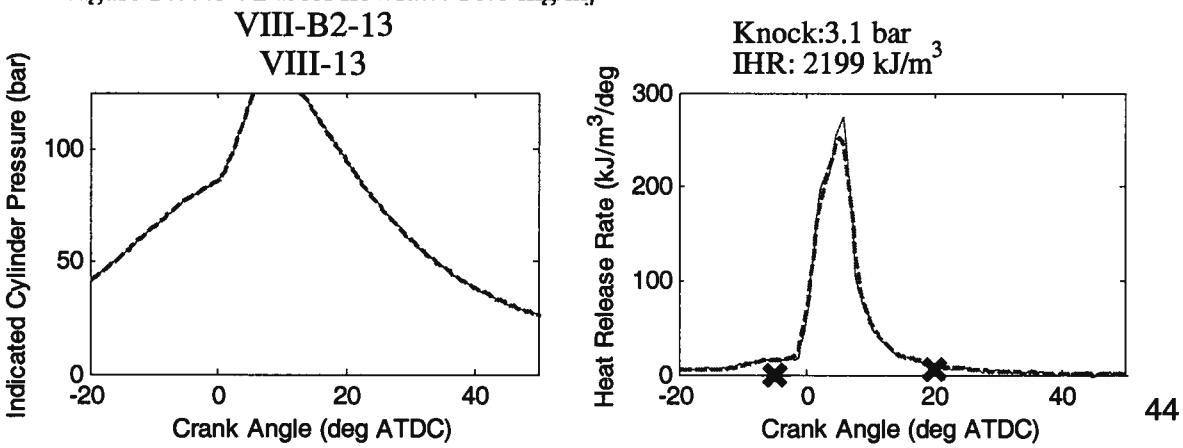

Figure F.7.44 : Diesel flowrate: 16.2 mg/inj

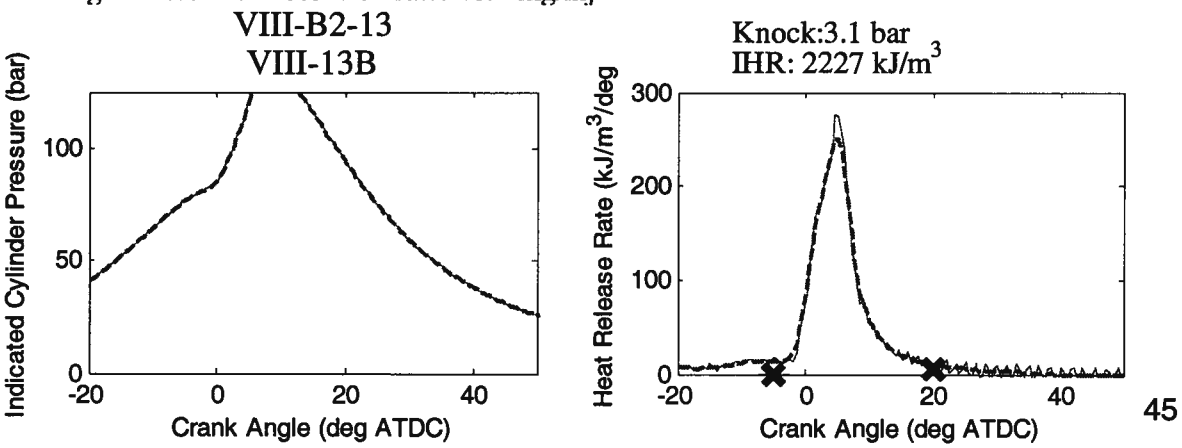

Figure F.7.45 : Diesel flowrate: 16.3 mg/inj

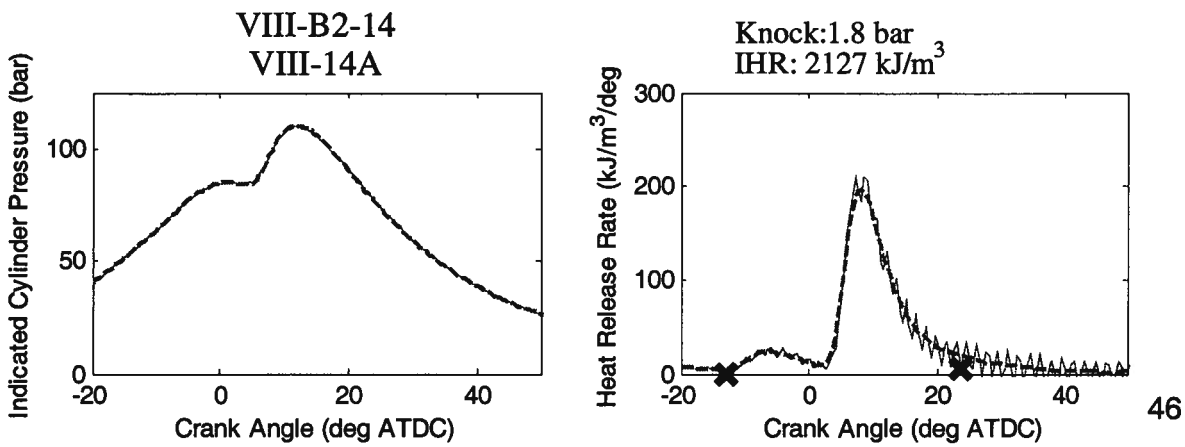

Figure F.7.46 : Diesel flowrate: 16.7 mg/inj

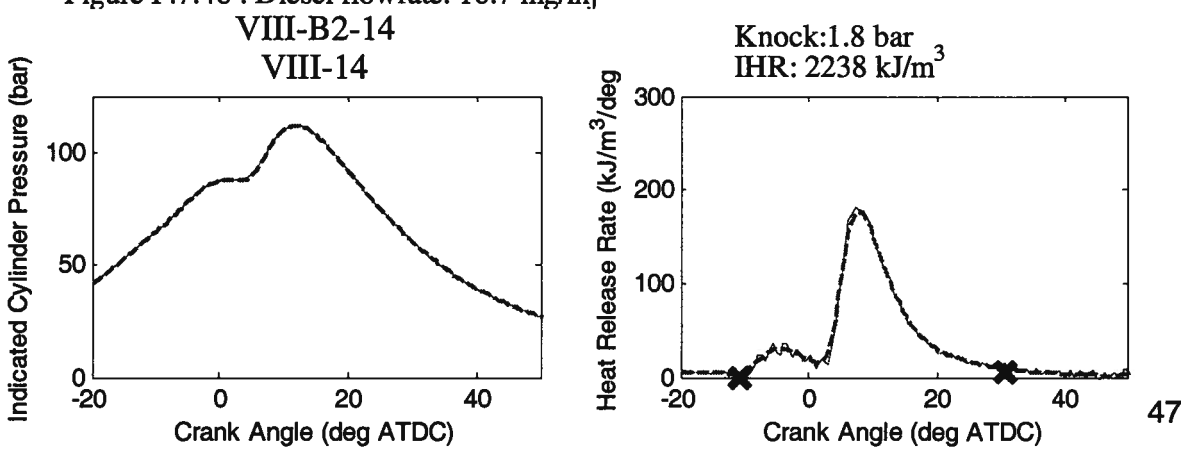

Figure F.7.47 : Diesel flowrate: 15.8 mg/inj

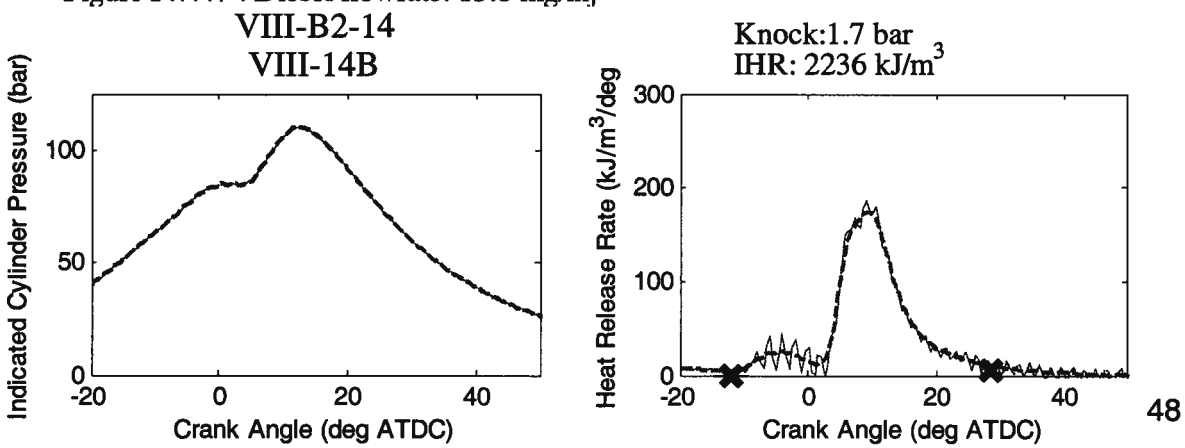

Figure F.7.48 : Diesel flowrate: 16.5 mg/inj

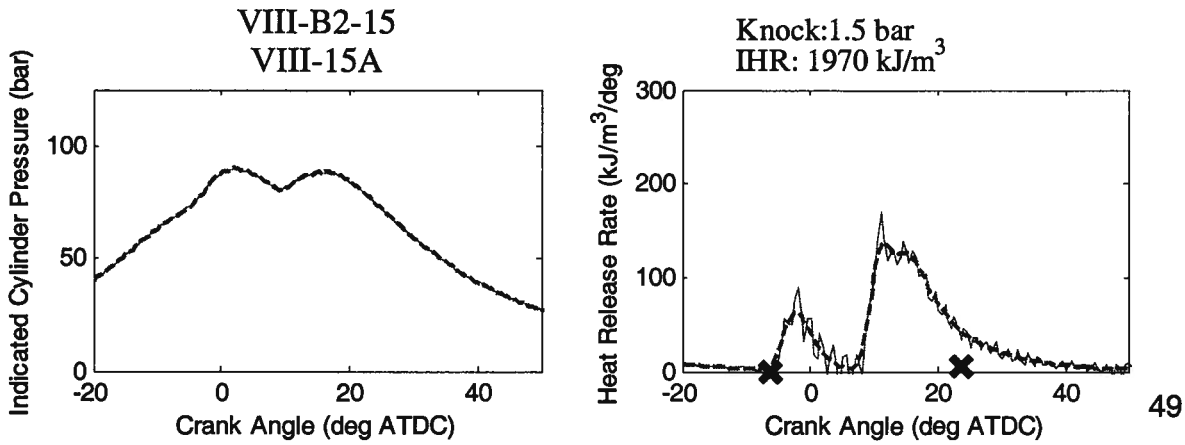

Figure F.7.49 : Diesel flowrate: 16.9 mg/inj

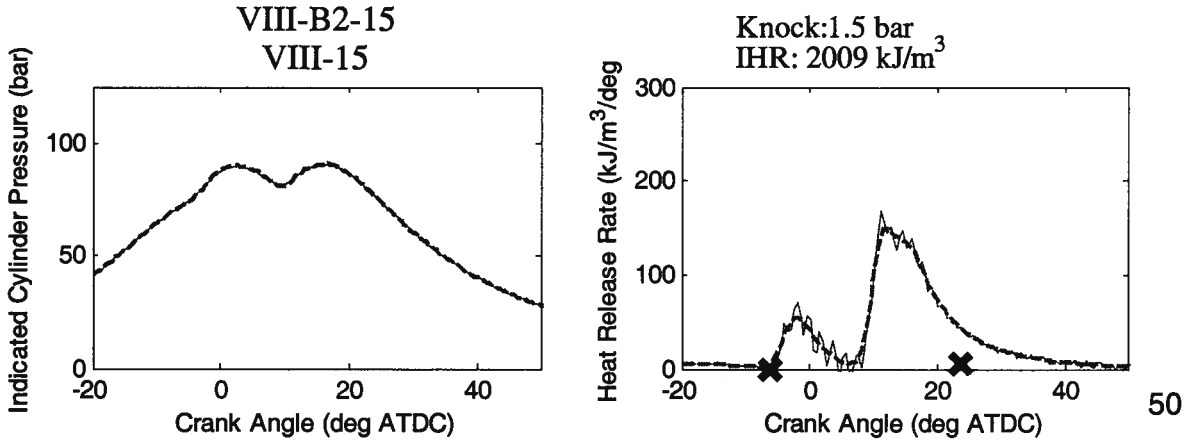

Figure F.7.50 : Diesel flowrate: 16.4 mg/inj

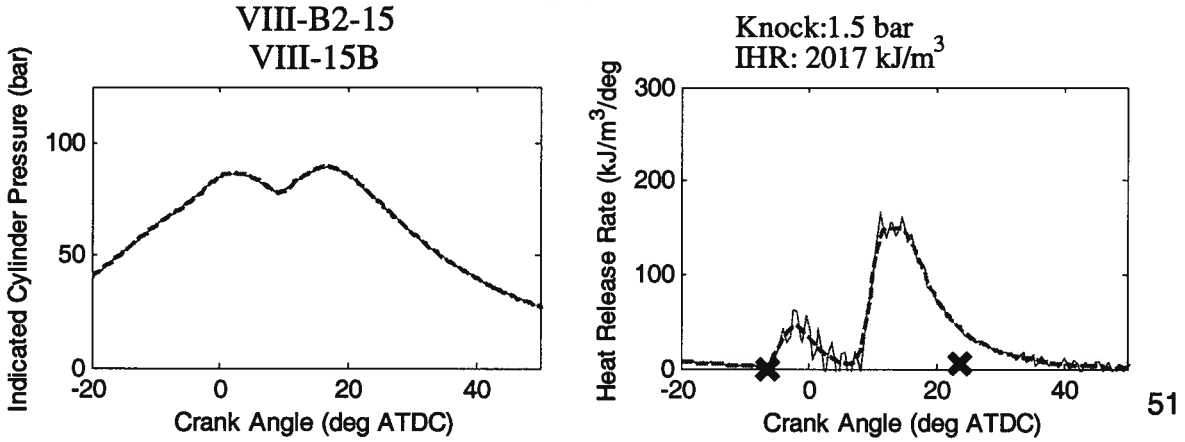

Figure F.7.51 : Diesel flowrate: 16.8 mg/inj

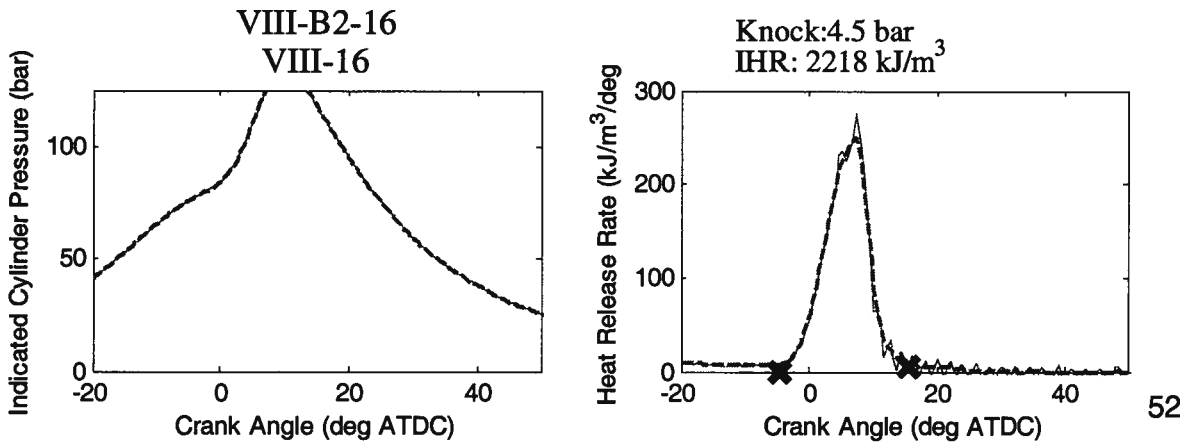

Figure F.7.52 : Diesel flowrate: 17.9 mg/inj

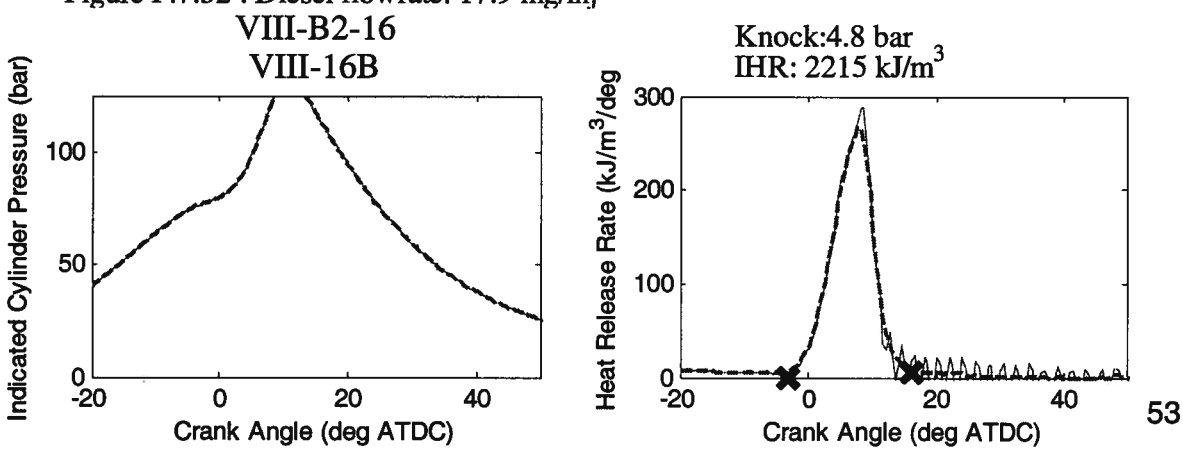

Figure F.7.53 : Diesel flowrate: 17.9 mg/inj

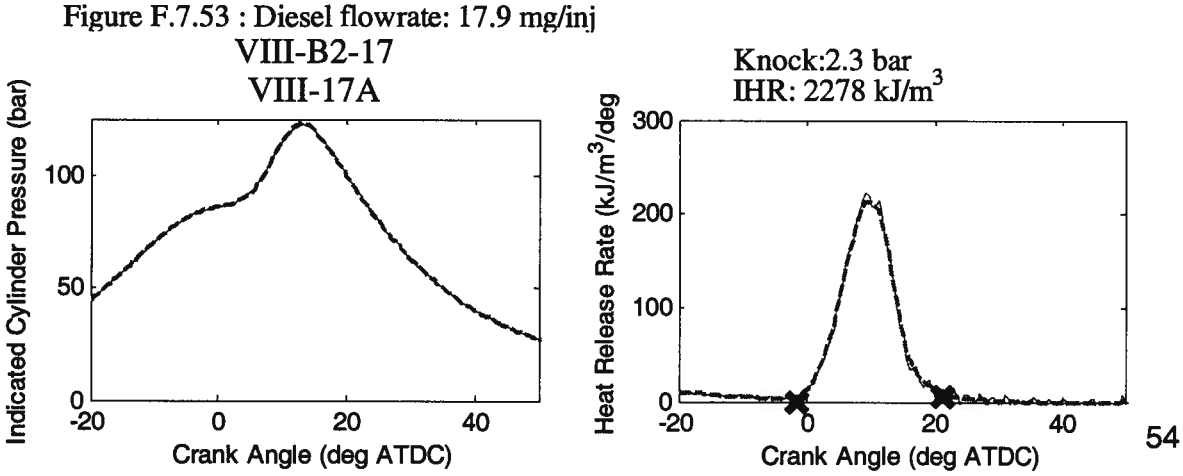

Figure F.7.54 : Diesel flowrate: 16.0 mg/inj

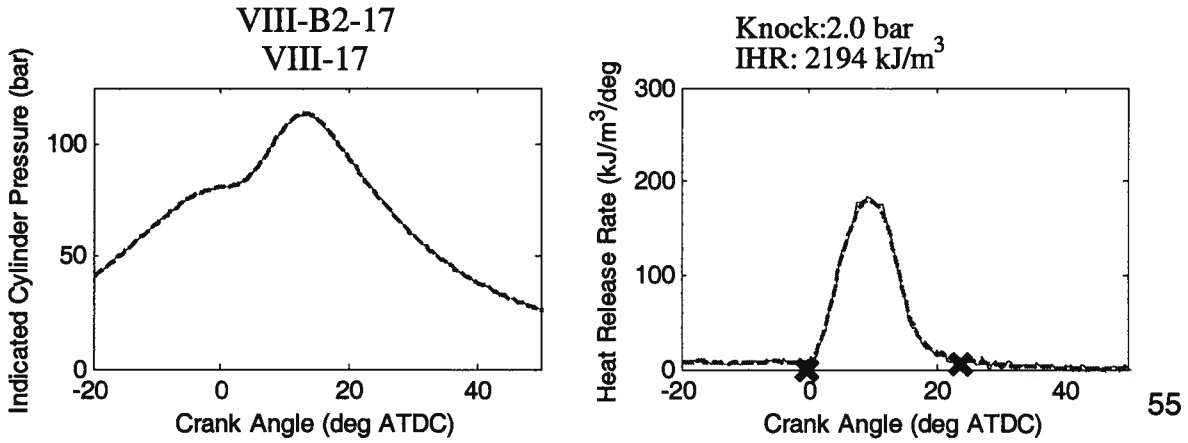

Figure F.7.55 : Diesel flowrate: 17.5 mg/inj

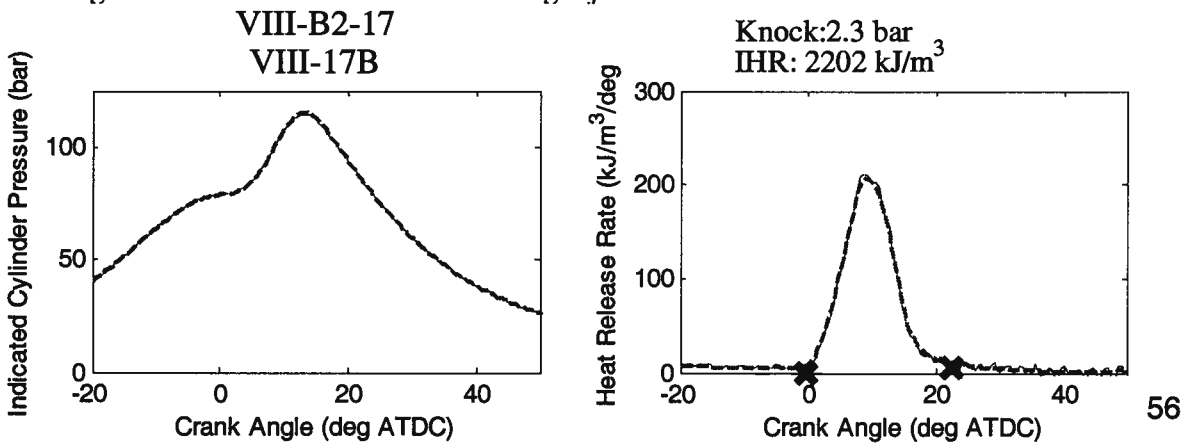

Figure F.7.56 : Diesel flowrate: 17.0 mg/inj

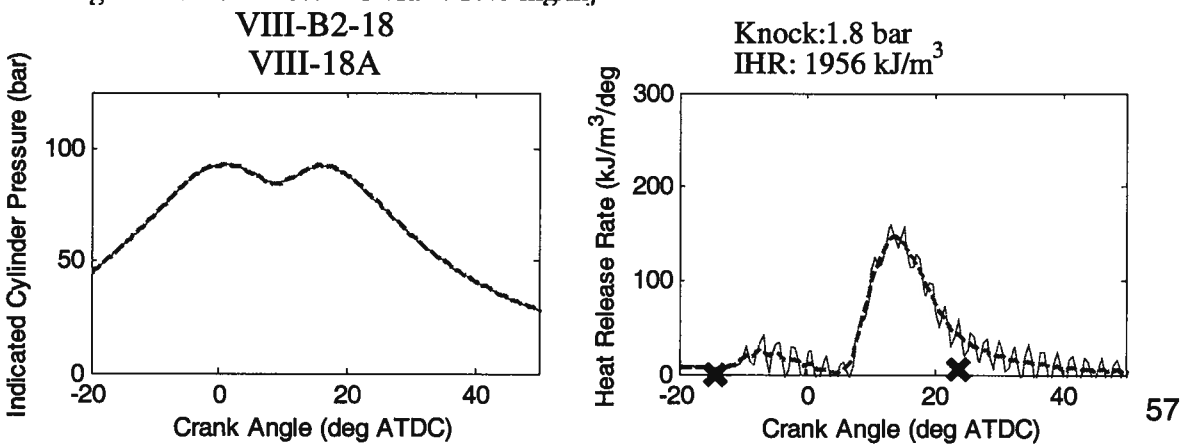

Figure F.7.57 : Diesel flowrate: 18.3 mg/inj

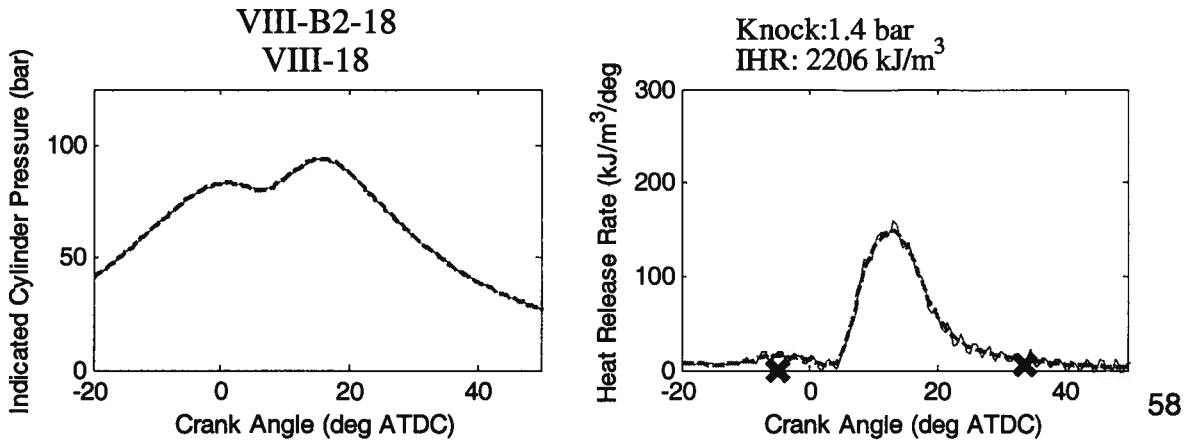

Figure F.7.58 : Diesel flowrate: 17.1 mg/inj

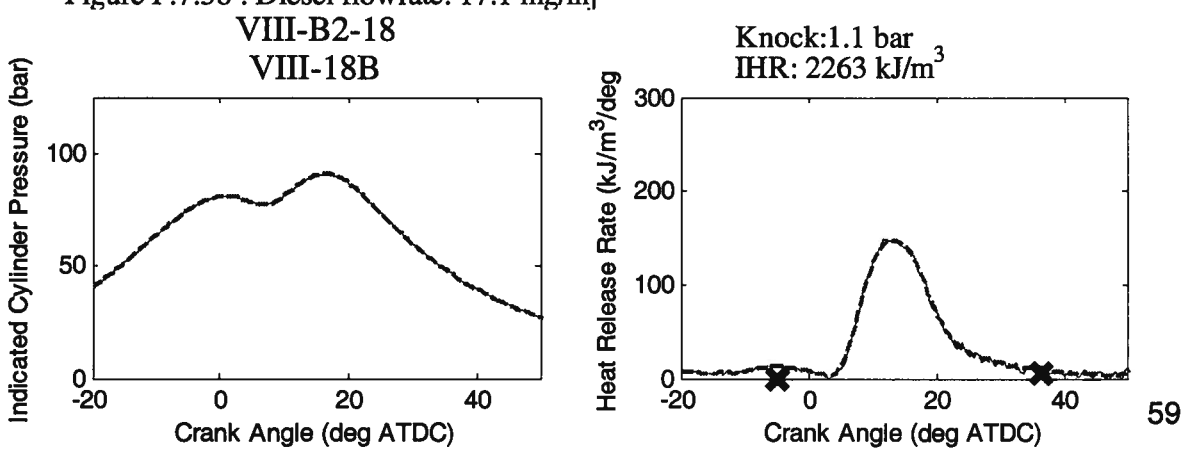

Figure F.7.59 : Diesel flowrate: 16.5 mg/inj

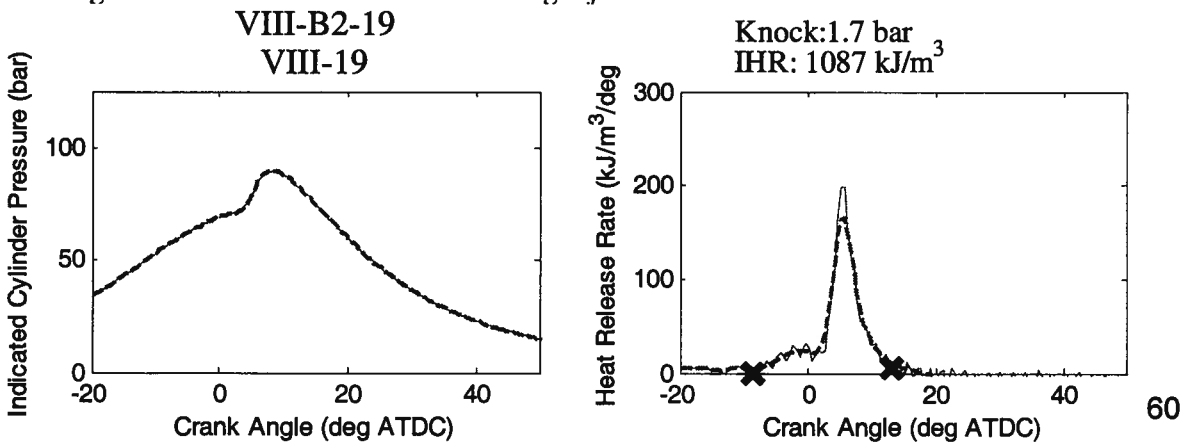

Figure F.7.60 : Diesel flowrate: 13.9 mg/inj

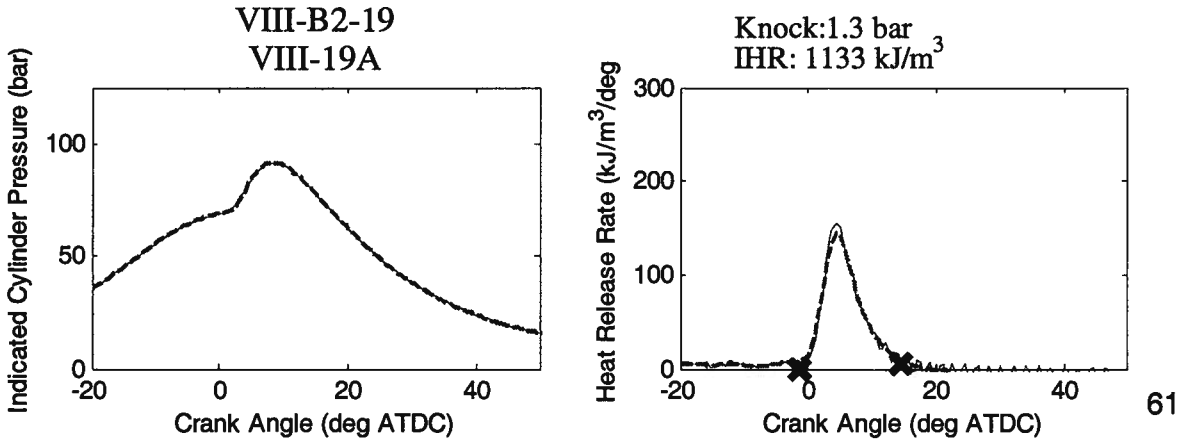

Figure F.7.61 : Diesel flowrate: 12.2 mg/inj

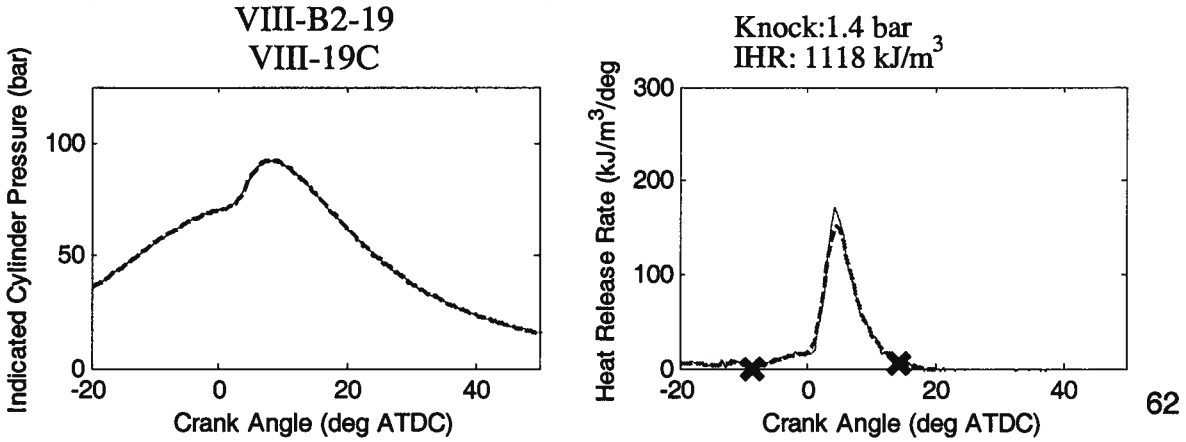

Figure F.7.62 : Diesel flowrate: 12.1 mg/inj

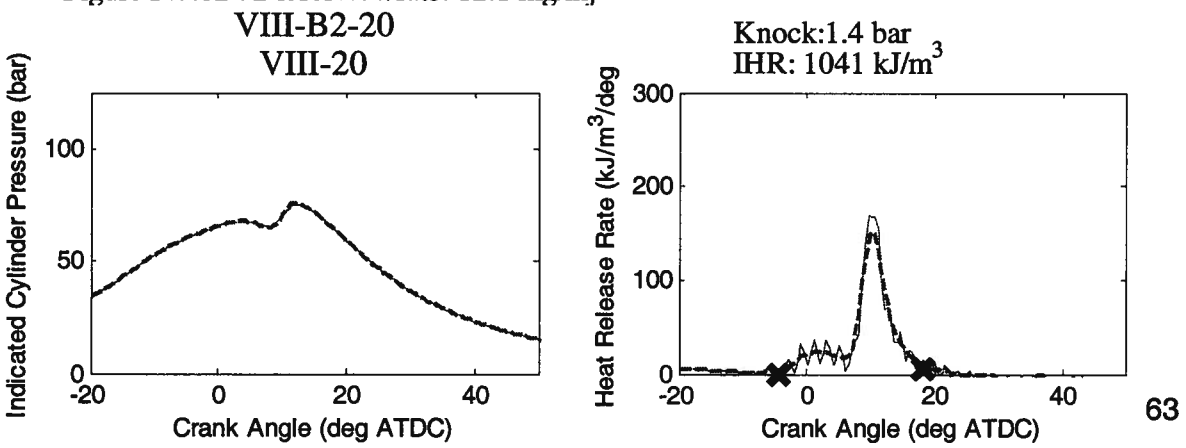

Figure F.7.63 : Diesel flowrate: 12.3 mg/inj

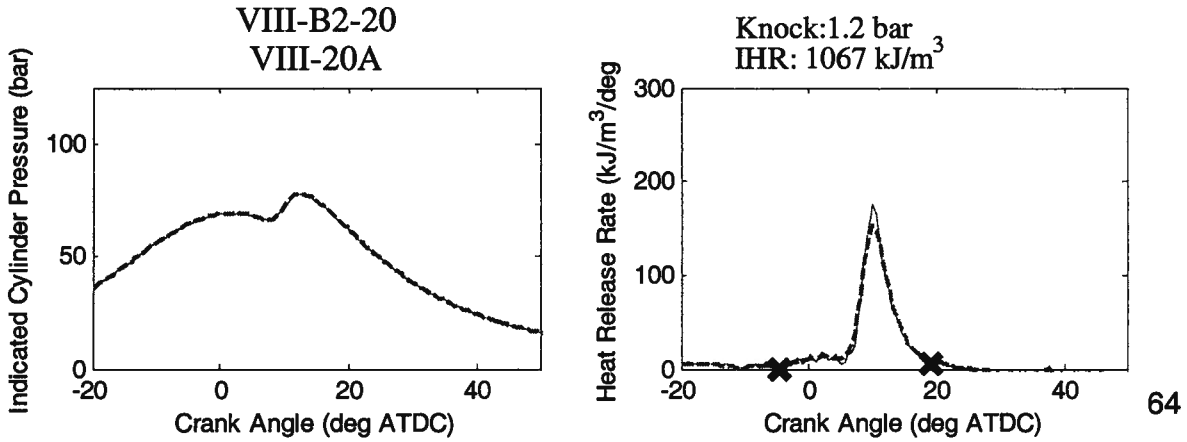

Figure F.7.64 : Diesel flowrate: 11.6 mg/inj

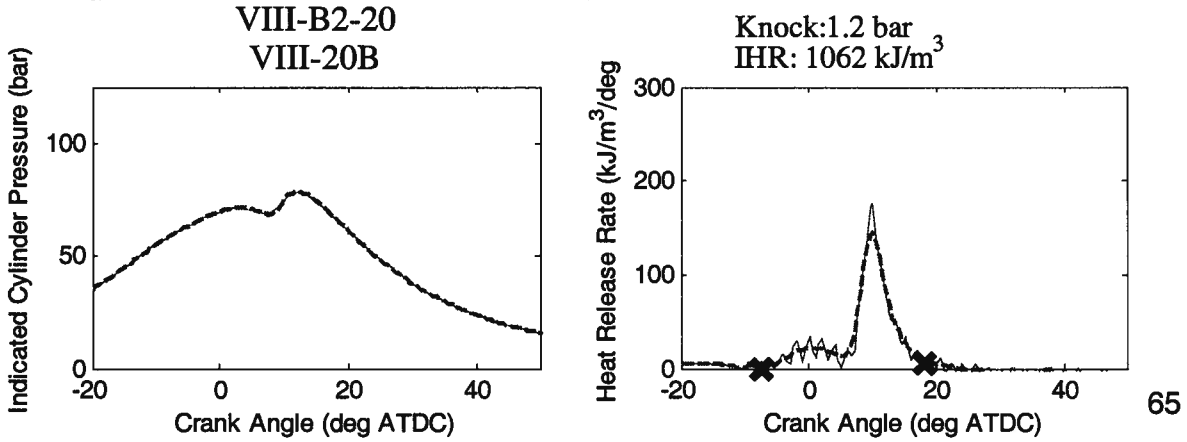

Figure F.7.65 : Diesel flowrate: 12.8 mg/inj

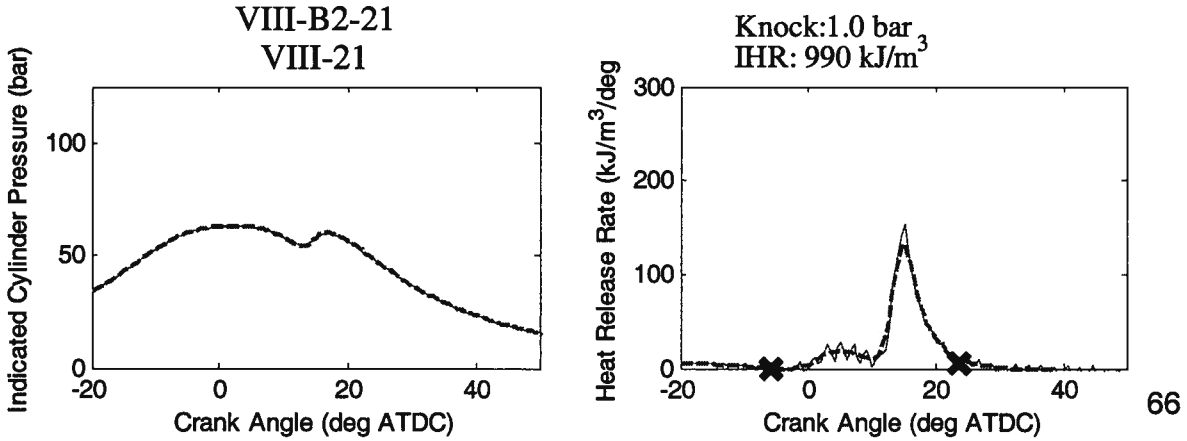

Figure F.7.66 : Diesel flowrate: 12.0 mg/inj

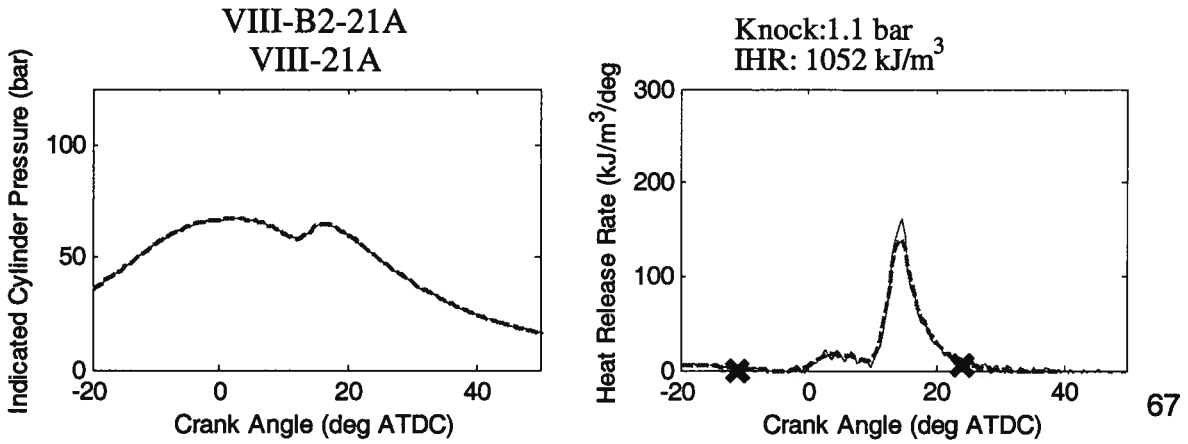

Figure F.7.67 : Diesel flowrate: 11.8 mg/inj

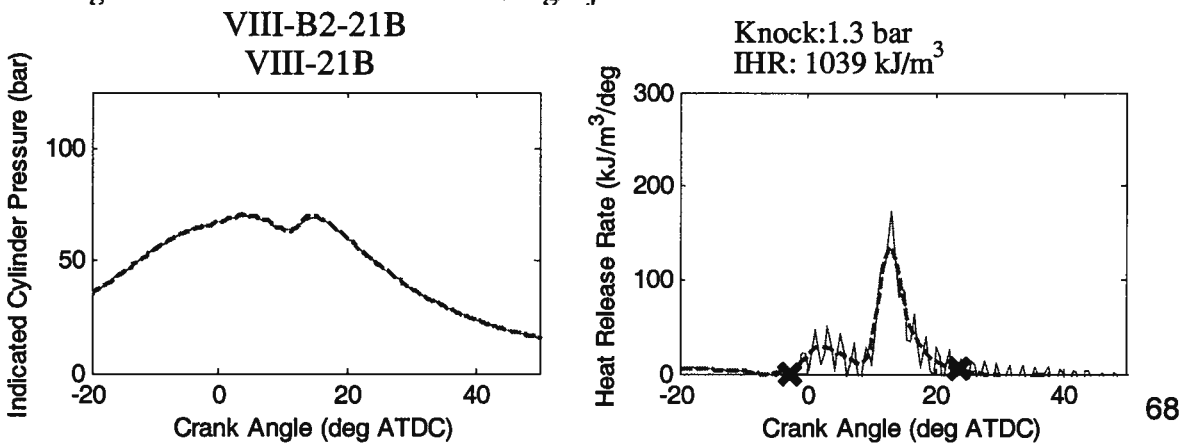

Figure F.7.68 : Diesel flowrate: 12.2 mg/inj

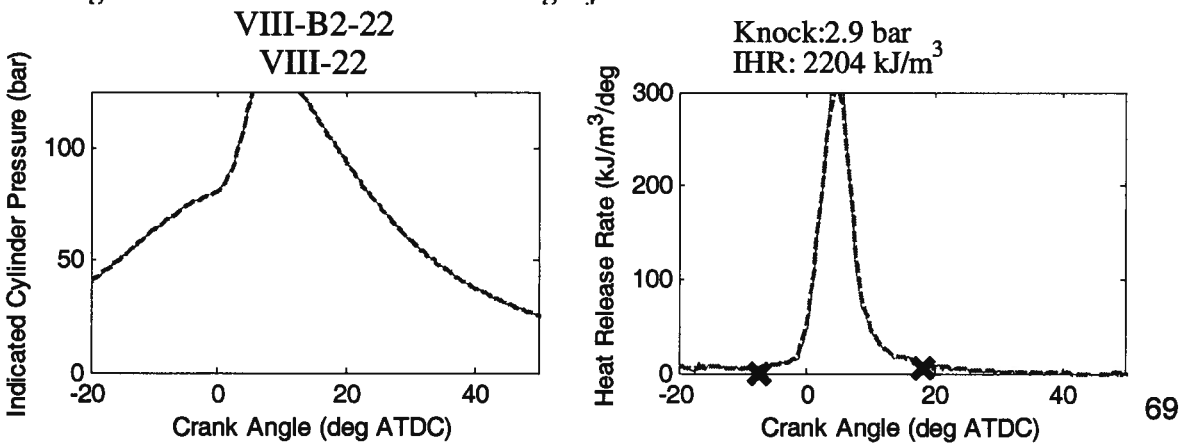

Figure F.7.69 : Diesel flowrate: 12.4 mg/inj

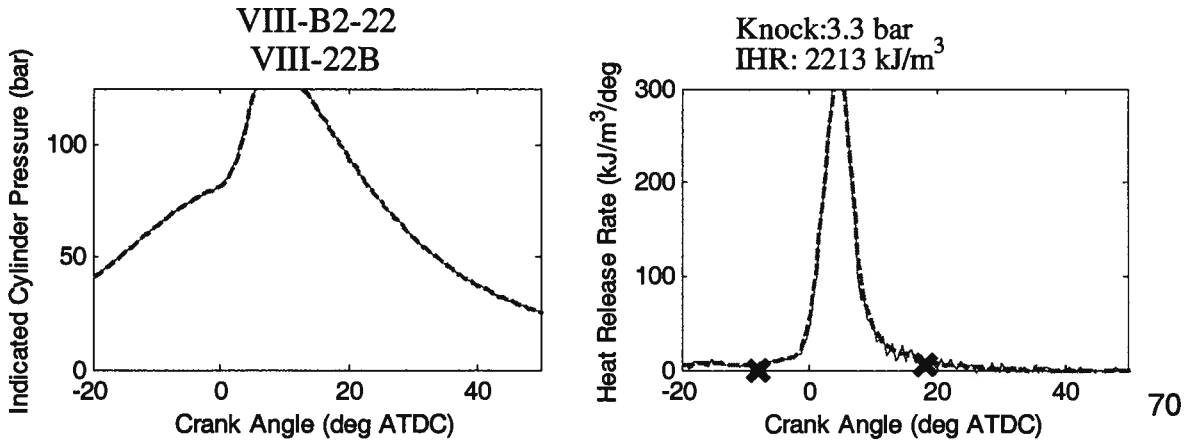

Figure F.7.70 : Diesel flowrate: 11.7 mg/inj

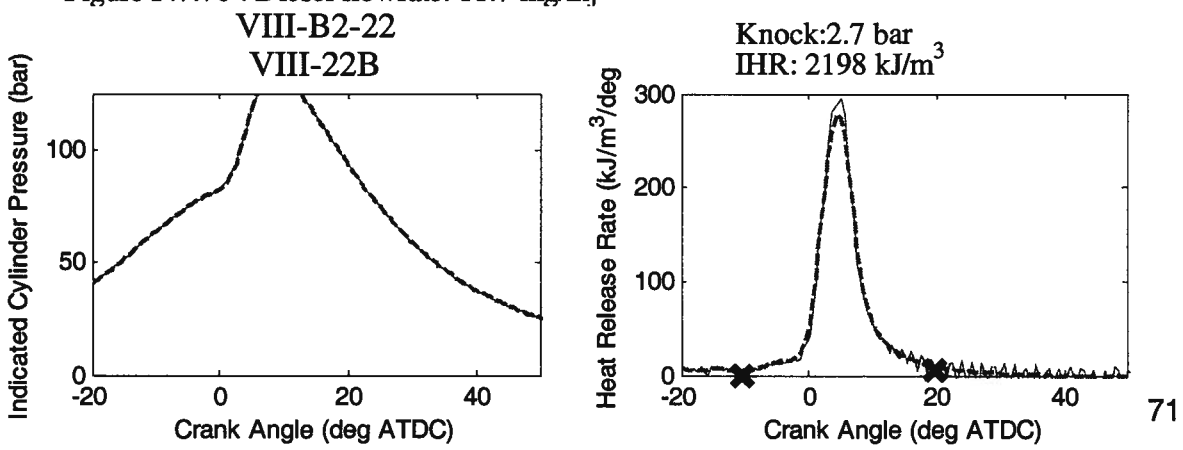

Figure F.7.71 : Diesel flowrate: 12.0 mg/inj

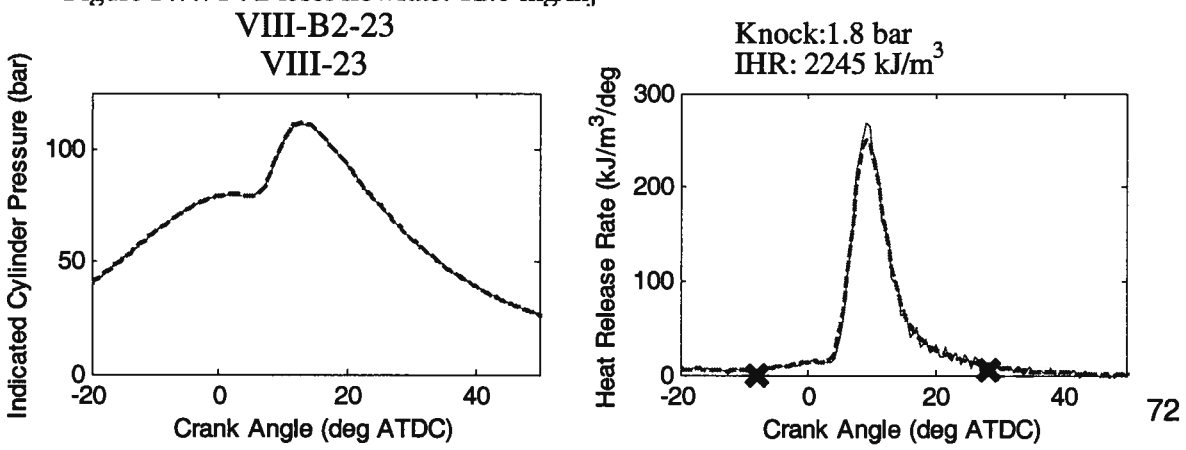

Figure F.7.72 : Diesel flowrate: 11.9 mg/inj

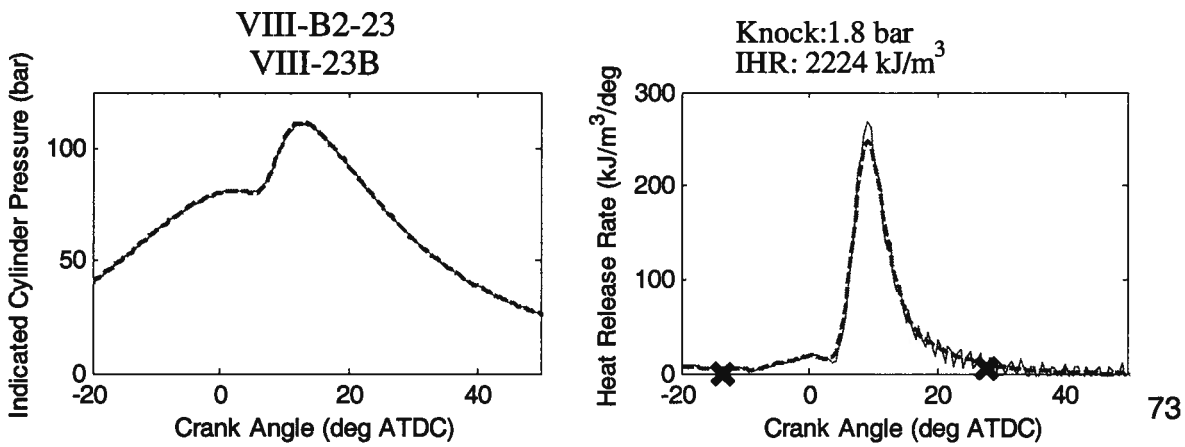

Figure F.7.73 : Diesel flowrate: 12.0 mg/inj

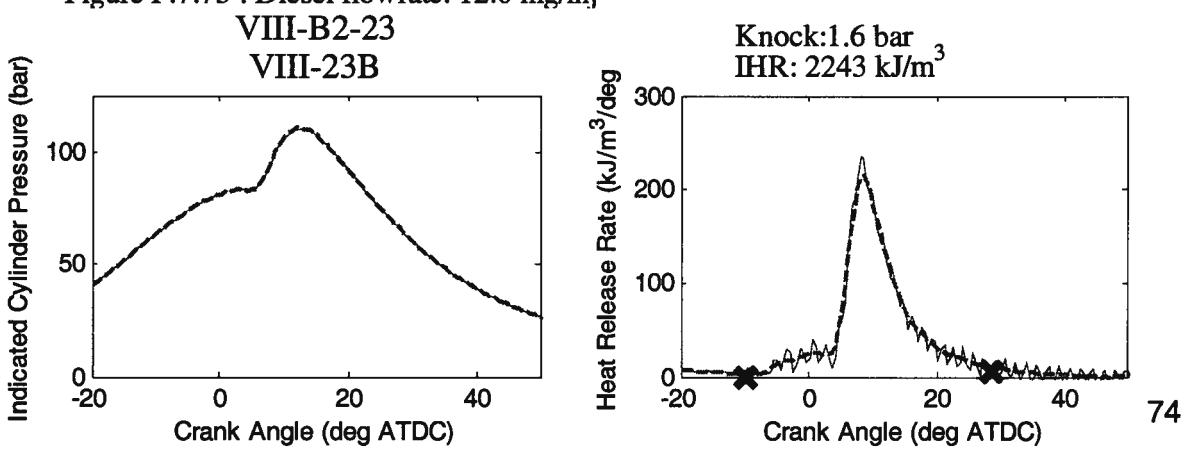

Figure F.7.74 : Diesel flowrate: 11.6 mg/inj

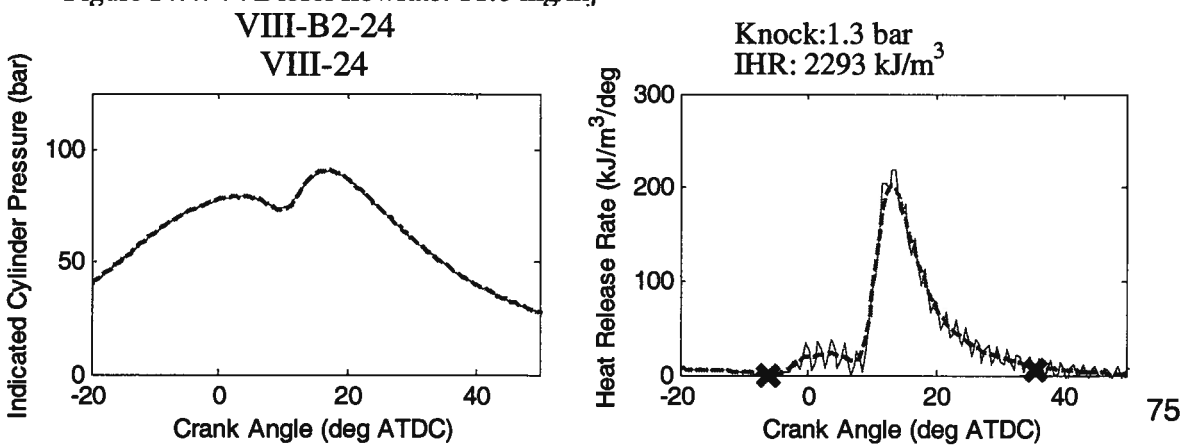

Figure F.7.75 : Diesel flowrate: 12.4 mg/inj

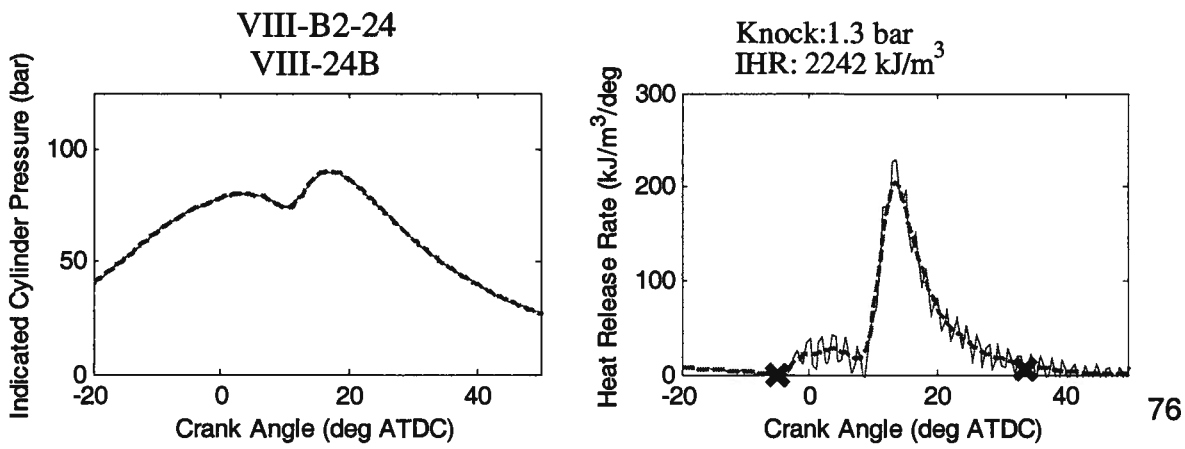

Figure F.7.76 : Diesel flowrate: 11.9 mg/inj

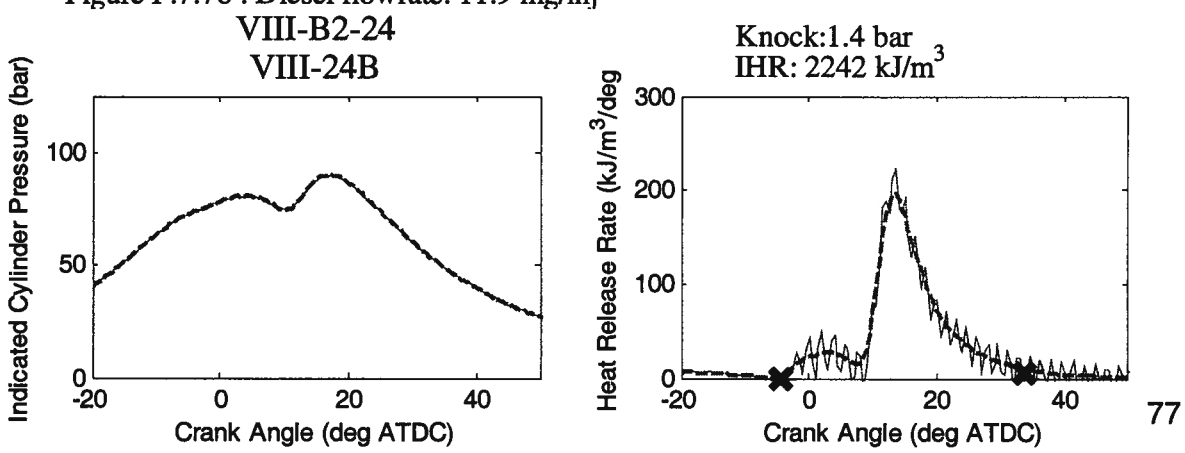

Figure F.7.77 : Diesel flowrate: 11.6 mg/inj

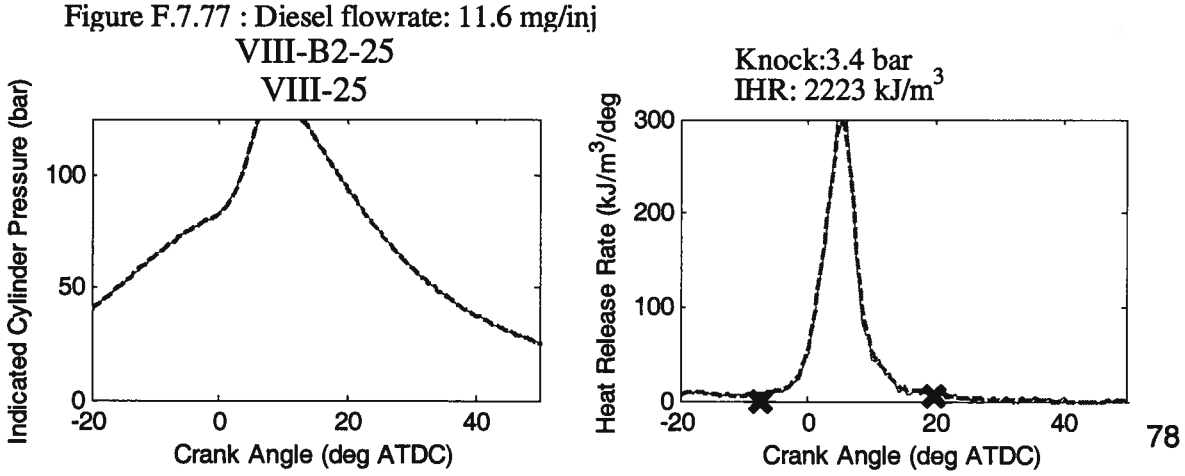

Figure F.7.78 : Diesel flowrate: 13.3 mg/inj

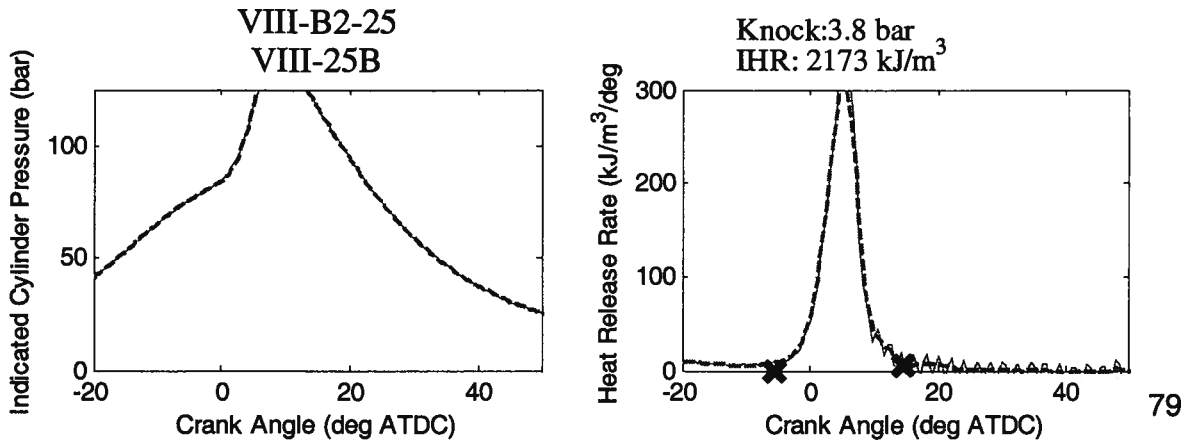

Figure F.7.79 : Diesel flowrate: 12.6 mg/inj

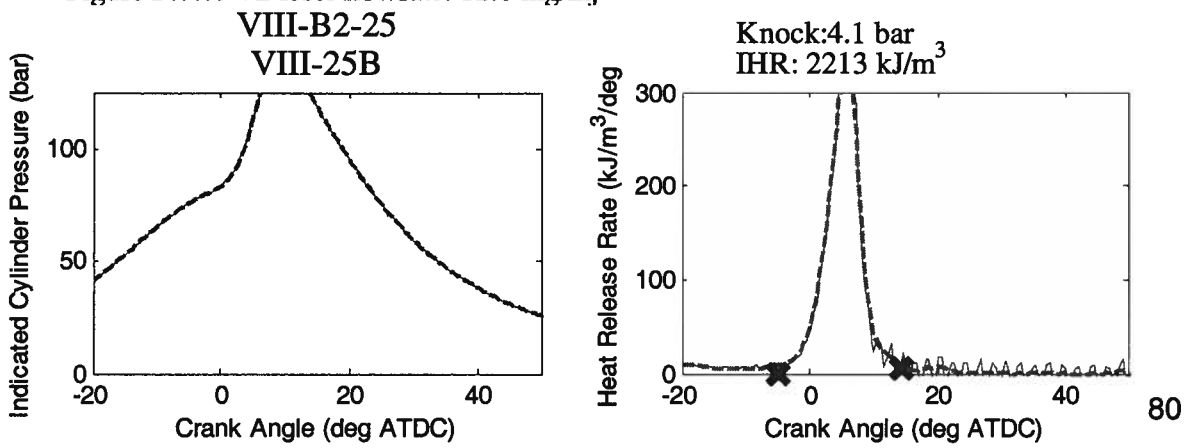

Figure F.7.80 : Diesel flowrate: 12.2 mg/inj

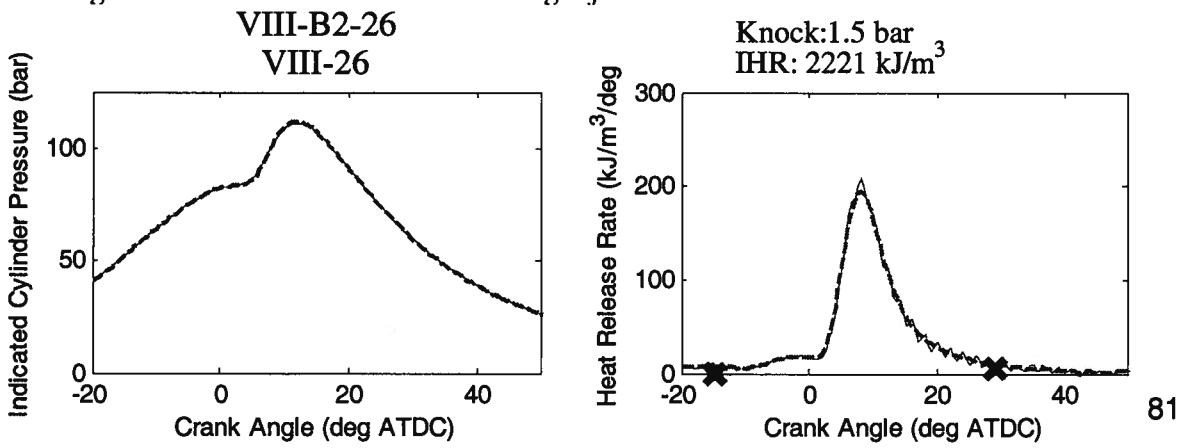

Figure F.7.81 : Diesel flowrate: 13.4 mg/inj

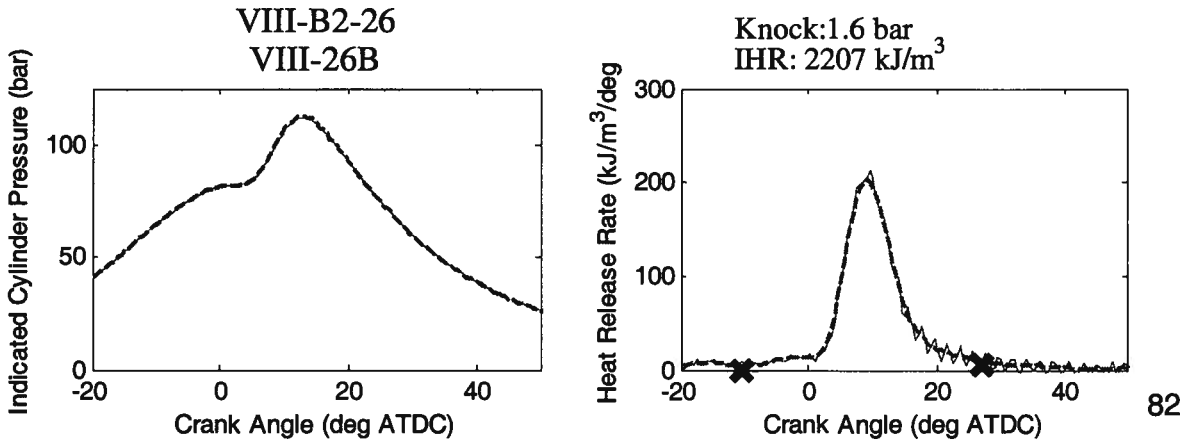

Figure F.7.82 : Diesel flowrate: 12.4 mg/inj

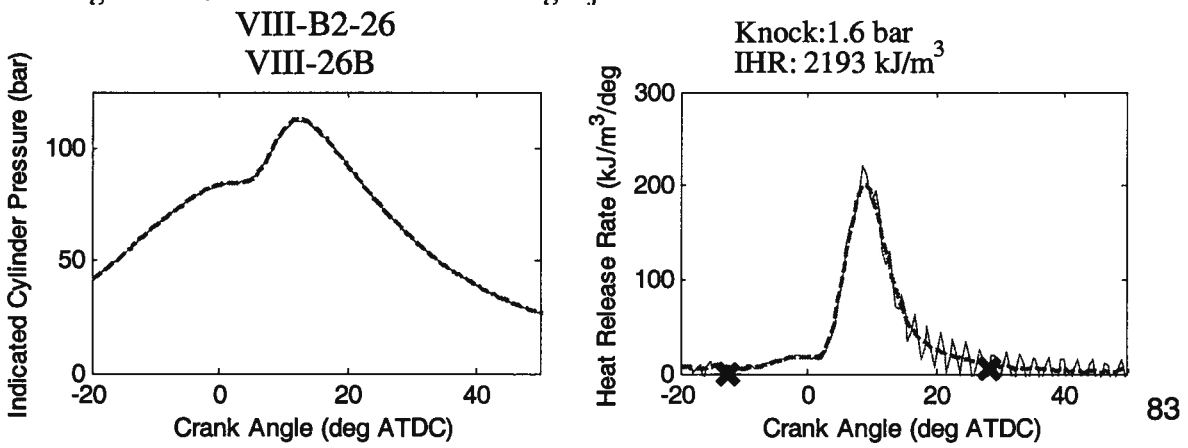

Figure F.7.83 : Diesel flowrate: 12.6 mg/inj

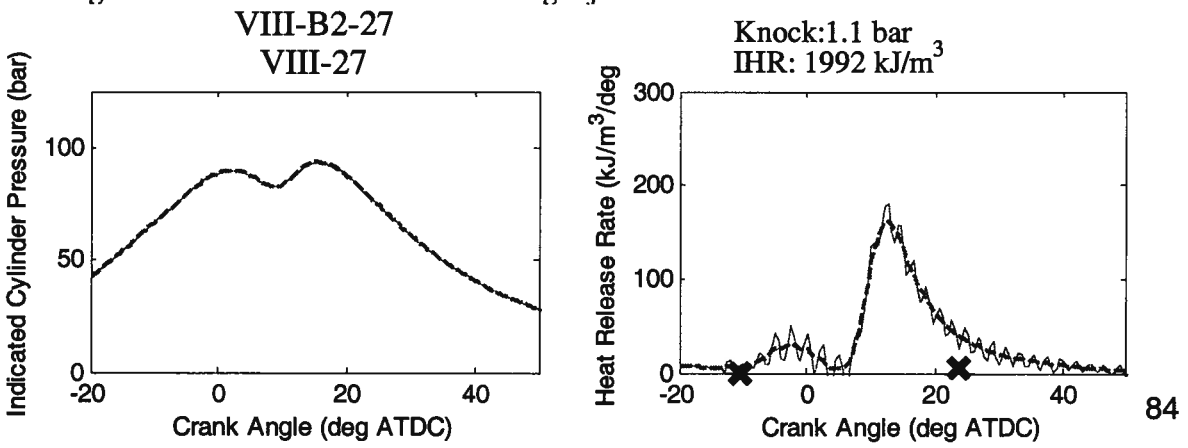

Figure F.7.84 : Diesel flowrate: 13.3 mg/inj

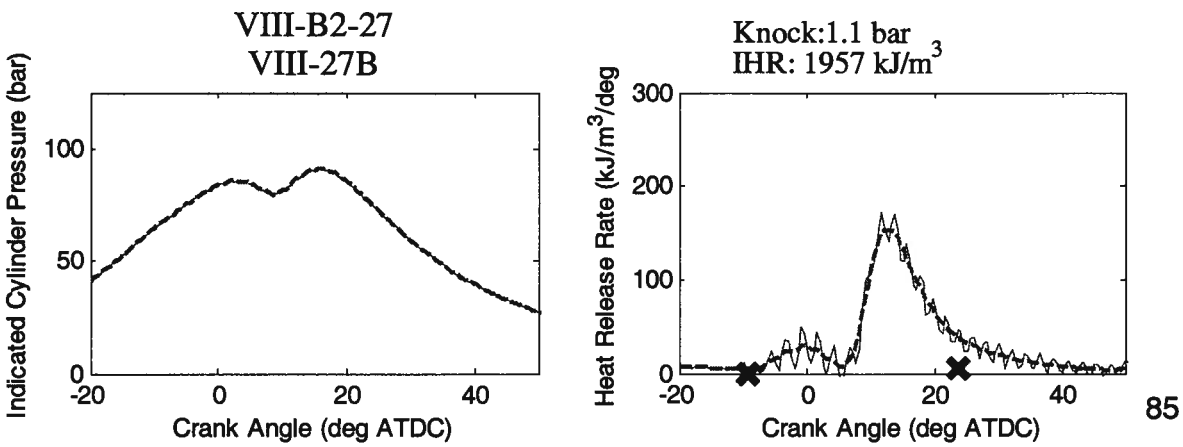

Figure F.7.85 : Diesel flowrate: 12.3 mg/inj

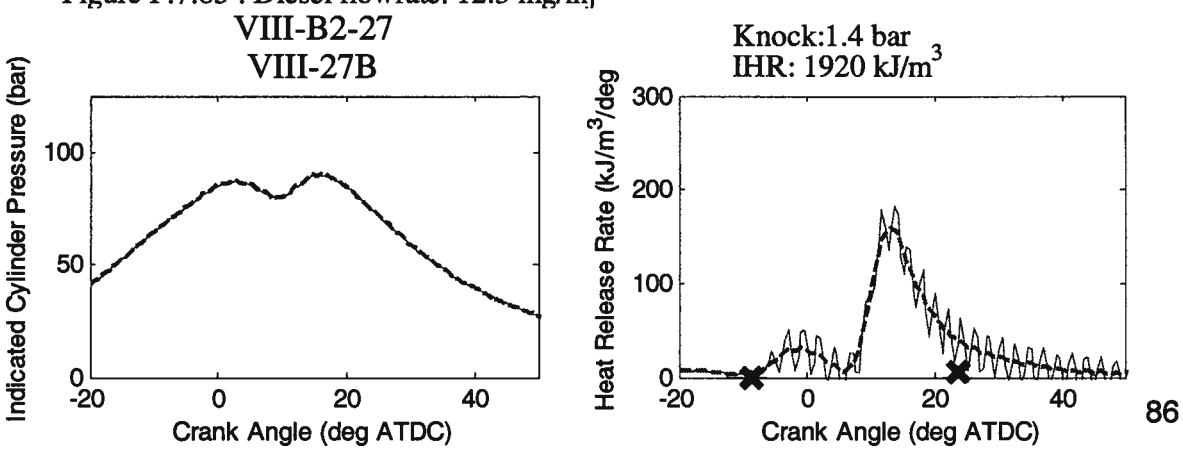

Figure F.7.86 : Diesel flowrate: 12.1 mg/inj

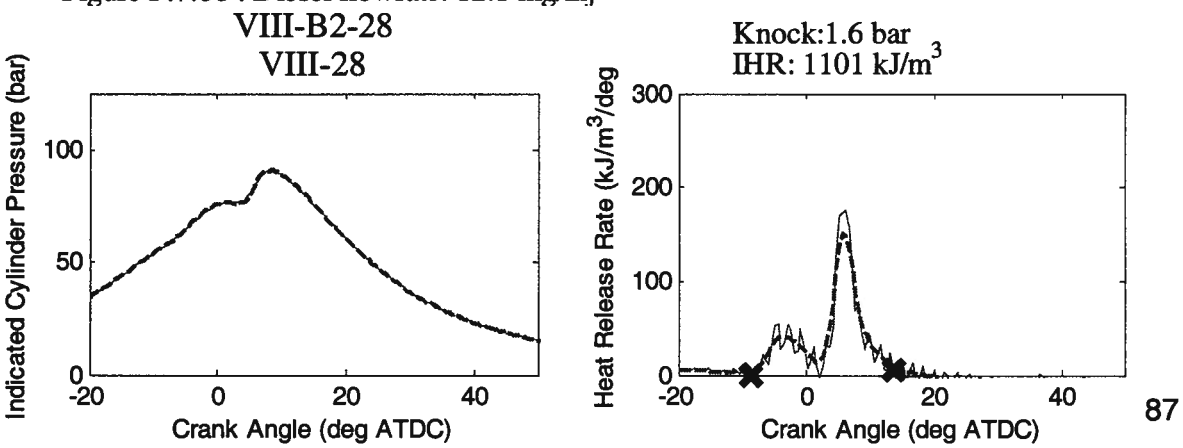

Figure F.7.87 : Diesel flowrate: 15.8 mg/inj

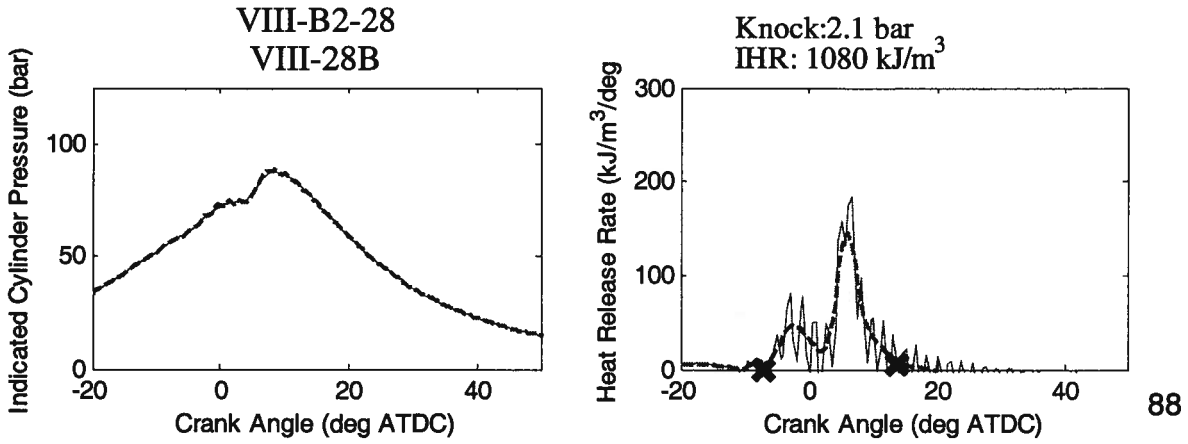

Figure F.7.88 : Diesel flowrate: 14.8 mg/inj

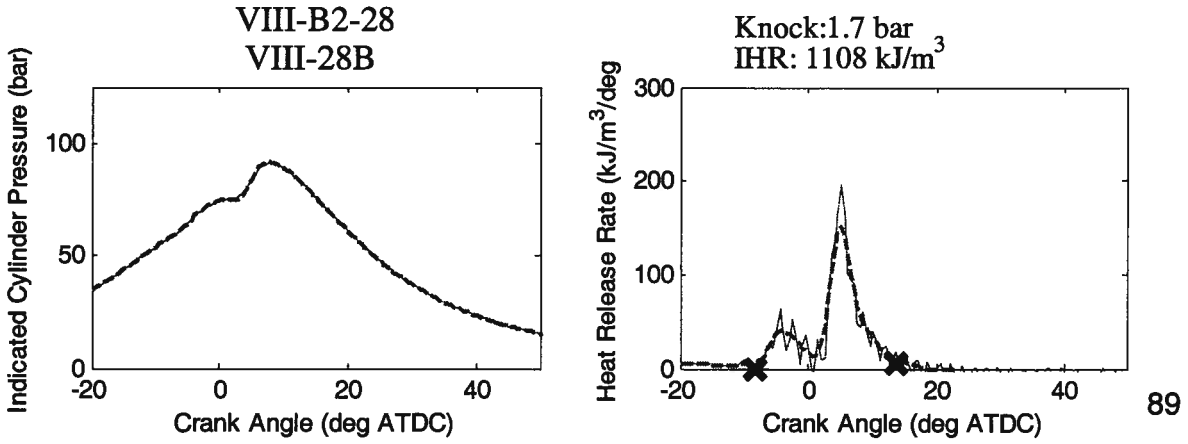

Figure F.7.89 : Diesel flowrate: 14.6 mg/inj

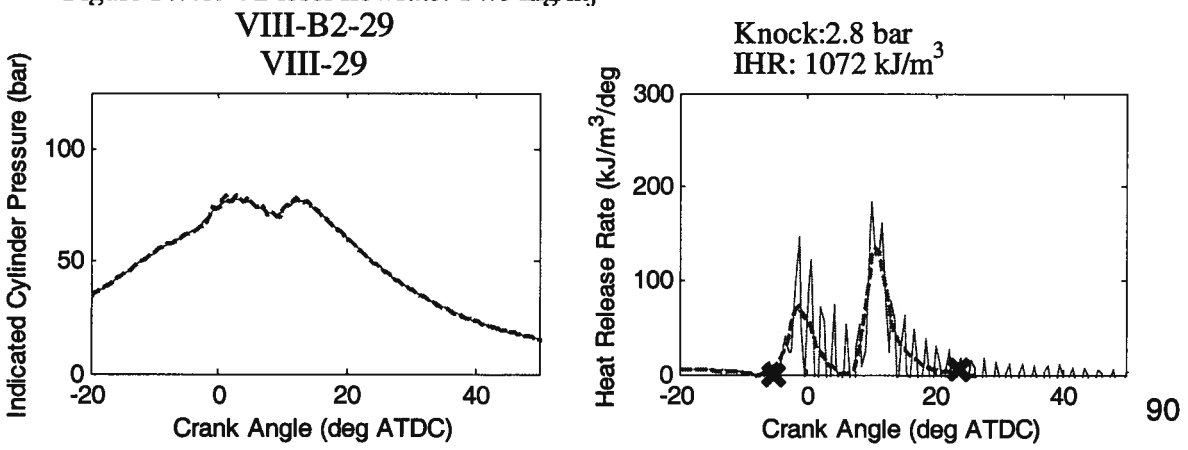

Figure F.7.90 : Diesel flowrate: 15.5 mg/inj

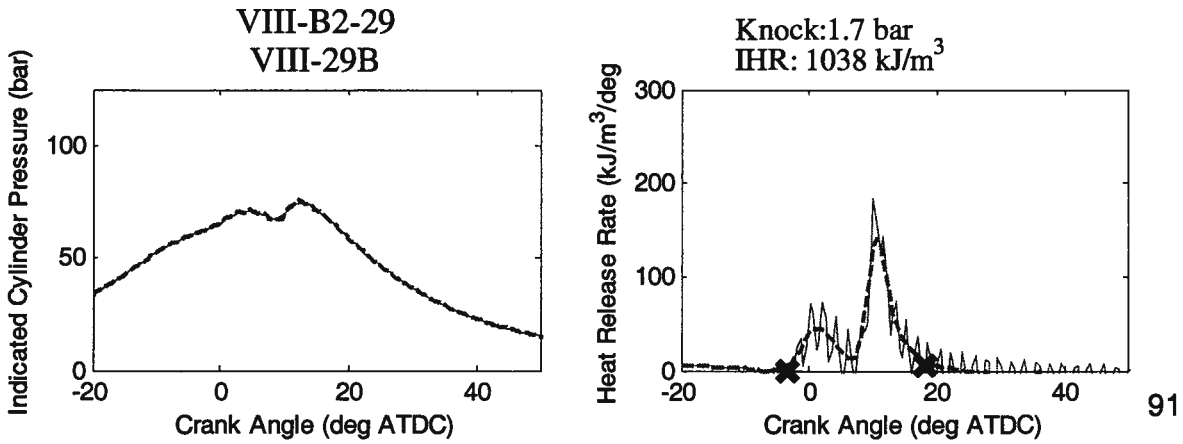

Figure F.7.91 : Diesel flowrate: 13.7 mg/inj

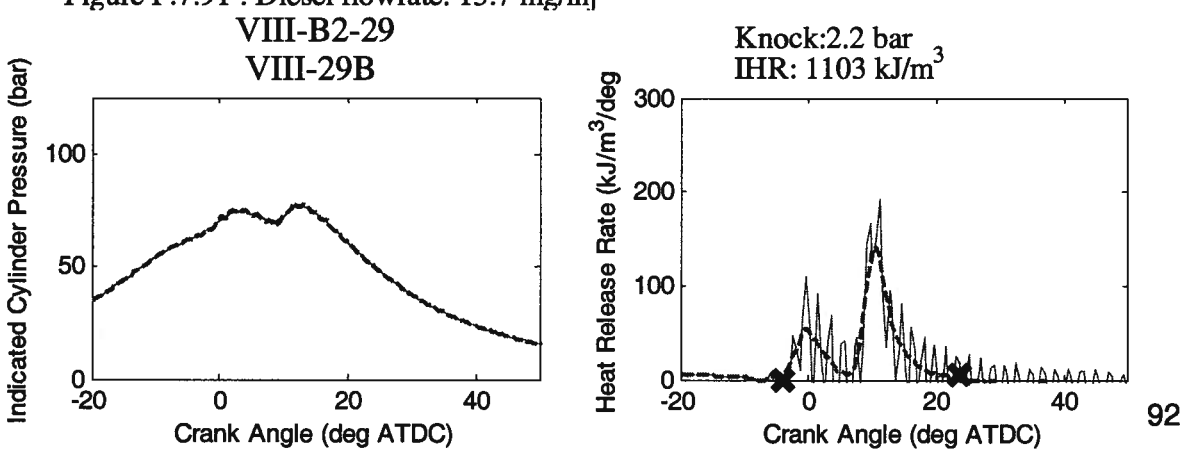

Figure F.7.92 : Diesel flowrate: 13.5 mg/inj

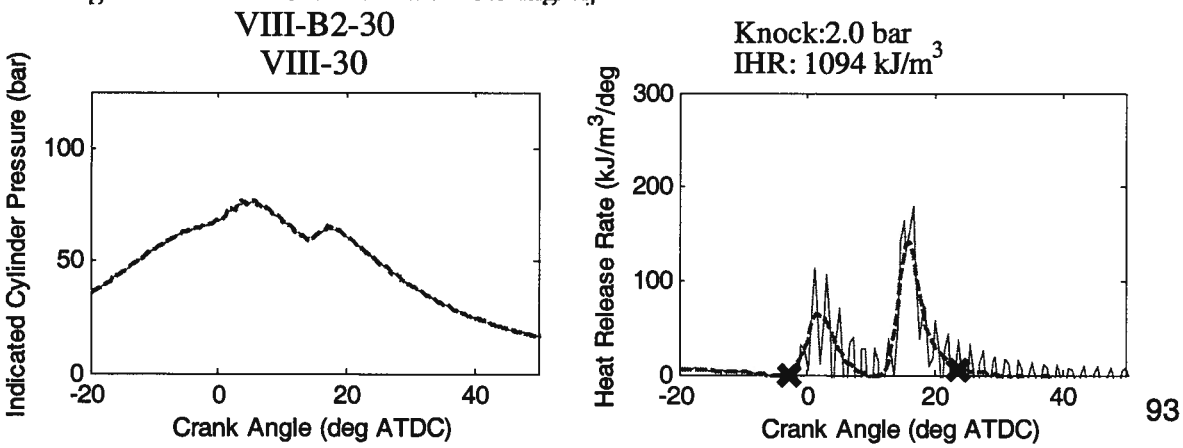

Figure F.7.93 : Diesel flowrate: 15.5 mg/inj

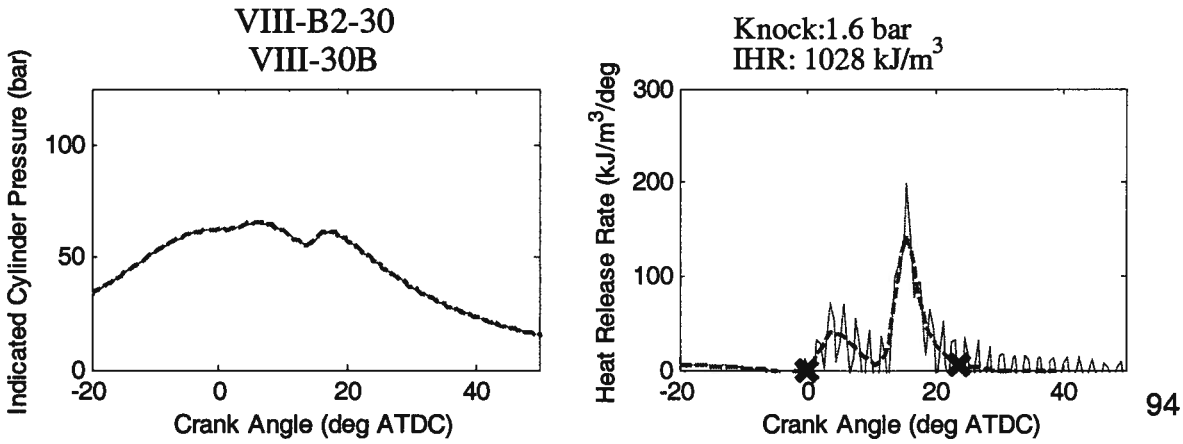

Figure F.7.94 : Diesel flowrate: 13.6 mg/inj

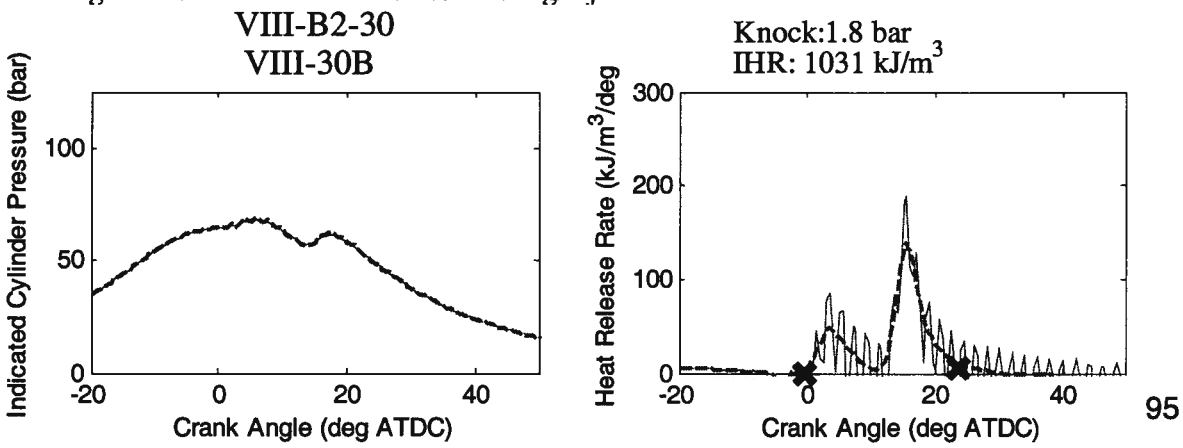

Figure F.7.95 : Diesel flowrate: 14.4 mg/inj

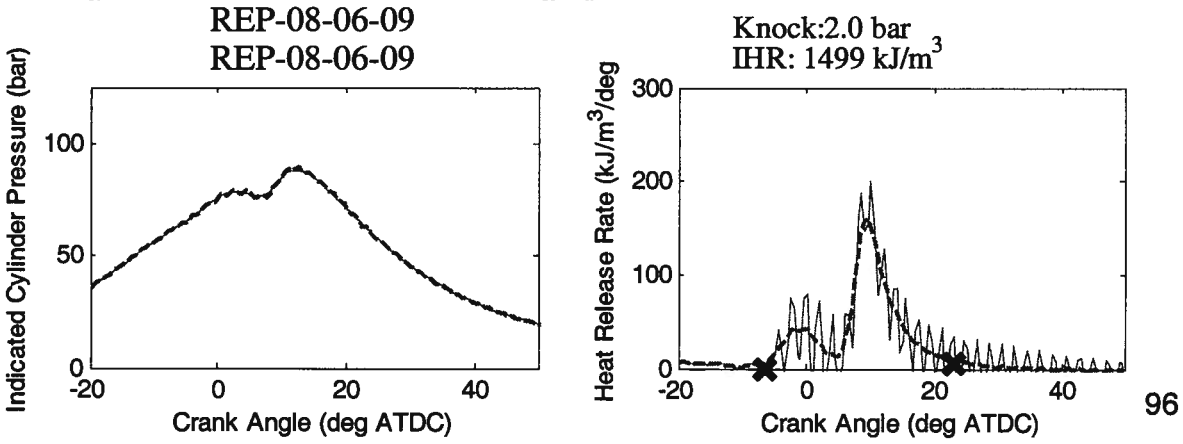

Figure F.7.96 : Diesel flowrate: 13.8 mg/inj

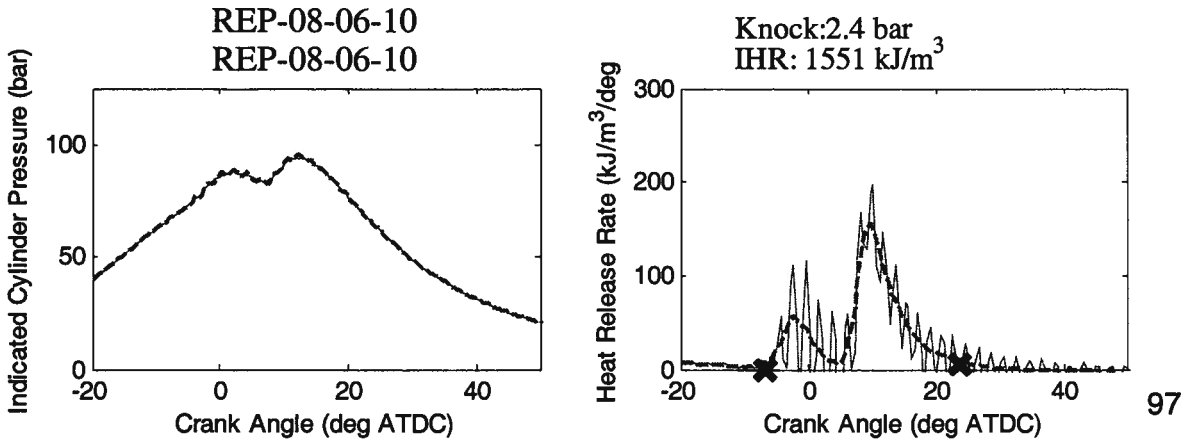

Figure F.7.97 : Diesel flowrate: 14.2 mg/inj

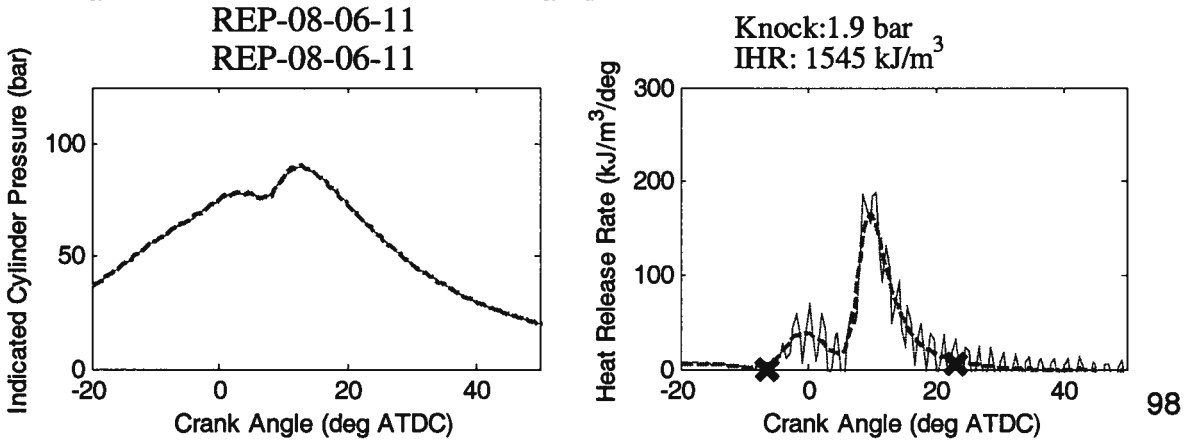

Figure F.7.98 : Diesel flowrate: -278527.0 mg/inj

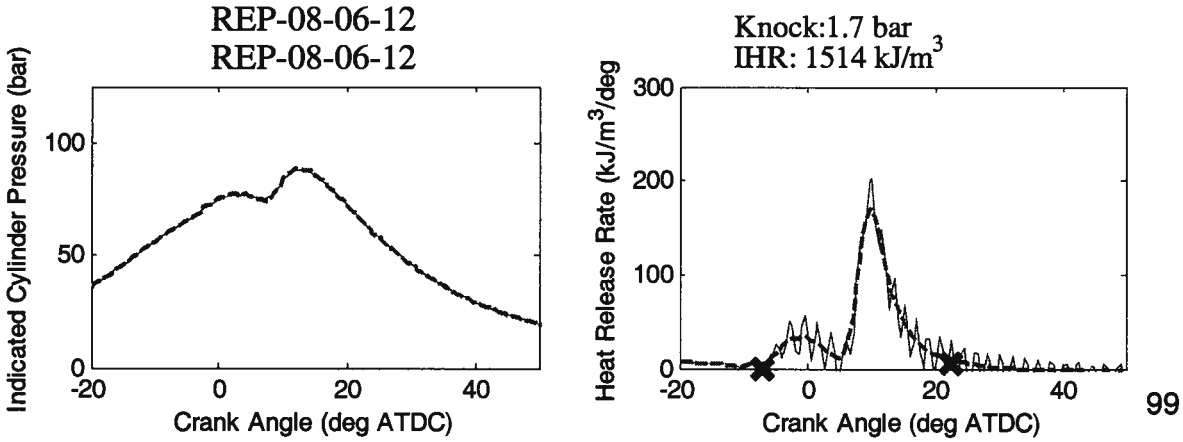

Figure F.7.99 : Diesel flowrate: 13.6 mg/inj

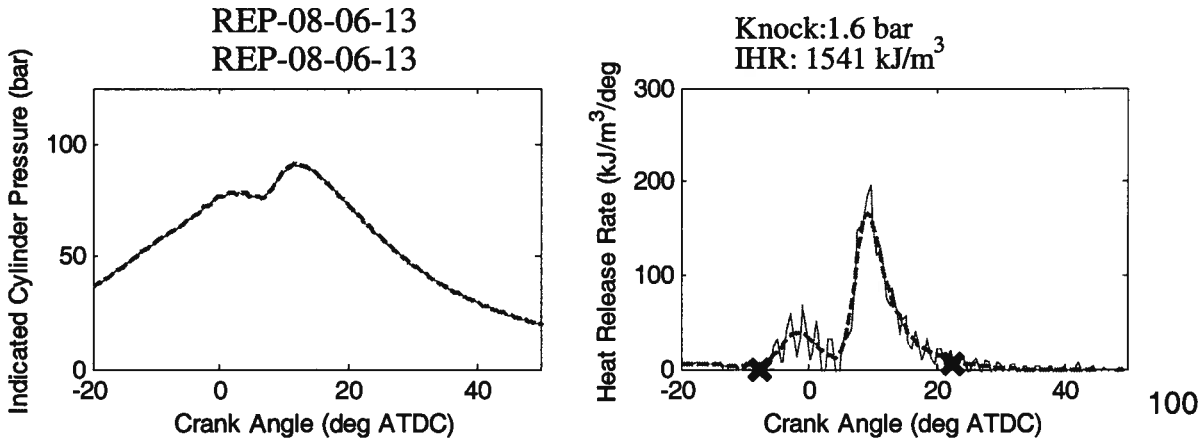

Figure F.7.100 : Diesel flowrate: 13.6 mg/inj

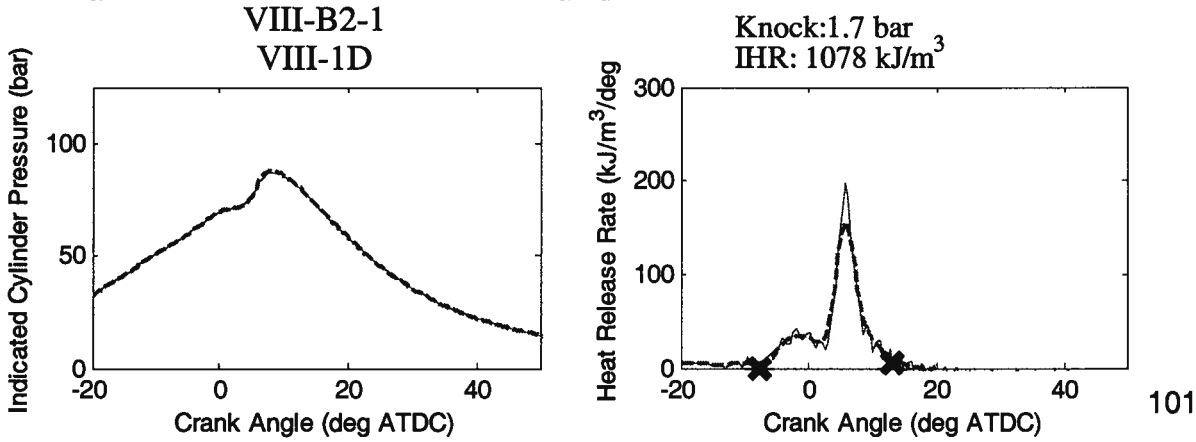

Figure F.7.101 : Diesel flowrate: 14.5 mg/inj

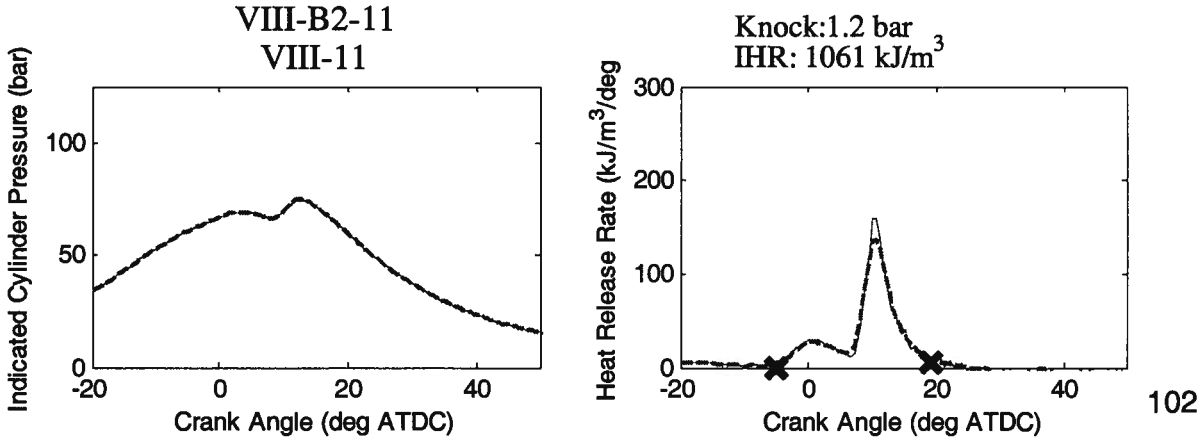

Figure F.7.102 : Diesel flowrate: 14.6 mg/inj

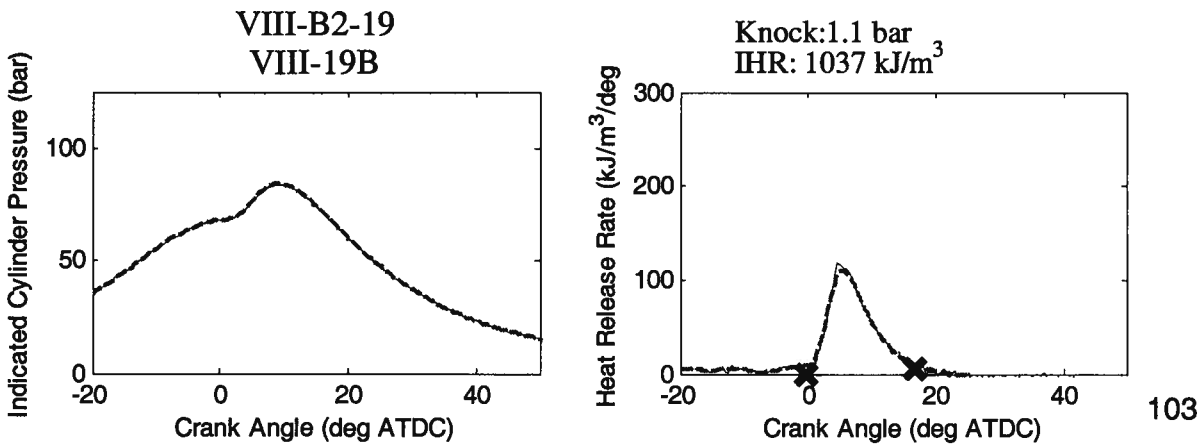

Figure F.7.103 : Diesel flowrate: 11.7 mg/inj

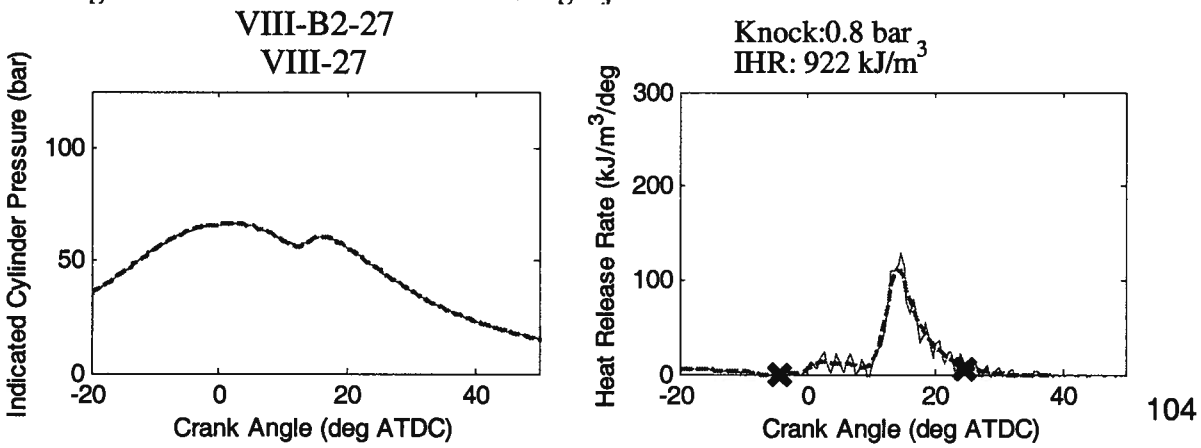

Figure F.7.104 : Diesel flowrate: 13.3 mg/inj